FREDERICO CARNEVALLI DE MIRANDA

PRELIMINARY DESIGN OF AN EXPERIMENTAL BIPLANE AIRCRAFT, BIPLANE CANARD AND PUSHER THRUST, FOR TWO OCCUPANTS IN TANDEM



UNIVERSIDADE FEDERAL DE UBERLÂNDIA

FACULDADE DE ENGENHARIA MECÂNICA

2017

FREDERICO CARNEVALLI DE MIRANDA

PRELIMINARY DESIGN OF AN EXPERIMENTAL BIPLANE AIRCRAFT, BIPLANE CANARD AND PUSHER THRUST, FOR TWO OCCUPANTS IN TANDEM

Undergraduate thesis submitted to the Course of Aeronautical Engineering from the Federal University of Uberlândia as a part of requirement for obtaining the BACHELORS DEGREE ON AERONAUTICAL ENGINEERING.

Tutor: Prof. Dr. Odenir de Almeida

UBERLÂNDIA – MG

2017

FREDERICO CARNEVALLI DE MIRANDA

PRELIMINARY DESIGN OF AN EXPERIMENTAL BIPLANE AIRCRAFT, BIPLANE CANARD AND PUSHER THRUST, FOR TWO OCCUPANTS IN TANDEM

Undergraduate thesis **APROVED** by the Course of Aeronautical Engineering from the Faculty of Mechanical Engineering of the Federal University of Uberlândia.

Thesis Committee Composition:

_____

Prof. Dr Odenir de Almeida

_____

Prof. Msc Giuliano Gardolinski Venson

_____

Prof. Dr Thiago Augusto Machado Guimarães

Uberlândia, 13 December 2017

ACKNOLEGEMENTS

To undergraduate in aeronautical engineering and to design a new airplane always was a dream that I was able to perform with the help of the Federal University of Uberlândia (UFU), so I would like to thank all the staff of masters that supplied me with the necessary technical knowledge to realize this work.

I thank the design engineer from Sensenich, Mr. Jon Bristol for provide the propeller technical data that I needed for conduct some important parts of this work. I immensely thank Prof. Dr. Odenir de Almeida to accept my proposal of work and his counseling.

MIRANDA, F. C. **Preliminary Design of an Experimental Biplane Aircraft, Biplane Canard and Pusher Thrust, for two Occupants in Tandem.** 2017. 443 f. Projeto de Conclusão de Curso, Universidade Federal de Uberlândia, Uberlândia.

RESUMO

A concepção e desenvolvimento de uma nova aeronave é naturalmente uma atividade multidisciplinar envolvendo tecnologias relacionadas à aerodinâmica, estruturas e diversas outras relacionadas aos diversos sistemas sejam eles mecânicos, elétricos, eletrônicos entre outros. Dessa característica resulta uma sequência de trabalho extremamente complexa. Quando a aeronave em questão é caracterizada por uma configuração extremamente peculiar e para a qual as fontes de referência técnica são bastante limitadas, esse trabalho se torna ainda mais desafiador e complexo, já nas fases iniciais de concepção essas dificuldades foram sentidas. As atividades relacionadas ao projeto preliminar tiveram como ponto de partida a ergonomia do “cockpit”, adotando a filosofia de projeto de dentro para fora. À medida que as tarefas de engenharia se desenvolviam e considerando as características particulares da aeronave, modificações na teoria existente e proposições de novas abordagens surgiram inevitavelmente, uma vez que a teoria disponível na literatura se mostrou limitada. Conforme os resultados relacionados à aerodinâmica foram sendo obtidos verificou-se que o desempenho da aeronave com relação às velocidades de voo superou em muito os valores inicialmente assumidos para a operação da mesma. Com respeito às características de controle os resultados obtidos podem ser considerados bastante satisfatórios, exceto aqueles relacionados com a corrida de decolagem devido à pouca eficiência dos “canards” nessa fase do voo. Com relação à estabilidade os resultados indicam que a aeronave está com comportamento marginalmente positivo em alguns aspectos e marginalmente negativo em outros aspectos.

Palavras-chave: Projeto preliminar de aeronaves; Biplano; Canard biplano; Pusher; Campo de wash global.

MIRANDA, F. C. **Preliminary Design of an Experimental Biplane Aircraft, Biplane Canard and Pusher Thrust, for two Occupants in Tandem.** 2017. 443 f. Projeto de Conclusão de Curso, Universidade Federal de Uberlândia, Uberlândia.

ABSTRACT

The conception and development of a new aircraft is naturally a multidisciplinary activity that involves technologies related to the aerodynamics, structures, and technologies related to several systems as mechanical, electrical, electronic among others. Due this characteristic, was resulted an extremely complex sequence of work. When the aircraft to be developed is characterized by a very peculiar configuration and for which the sources of technical reference are quite limited, this work turn even more challenger and complex, already in the earlier conceptual phases these difficulties were faced. The activities related to the preliminary design had as start point the ergonomics of the cockpit, adopting for the aircraft the design philosophy from the inside to the outside. As the engineering activities were developed and considering the particular characteristics of the aircraft, were proposed modifications on the existing theory and new theory approach necessarily emerged, once the available theory on the bibliography proved insufficient. As the results related to the aerodynamics were being obtained, was verified that the performance relative to the flight speeds far exceeded the values initially defined for the operation of the aircraft. With respect to the in flight control characteristics, the results obtained may be considered very satisfactory, except that related to the take-off runway rolling due the few canards efficiency. With respect to the stability behavior the results indicate that the aircraft is marginally positive in some aspects and is marginally negative relative to other aspects.

Key-words : Aircraft preliminary design; Biplane; Biplane canard; Pusher; Global wash field.

LIST OF FIGURES

Figure 1.1 - 14Bis flight on October 23th, 1906. (Available in: <https://www.google.com.br/search?q=14bis&tbm=isch&tbo=u&source=univ&sa=X&ved=0ahUKEwic5f-T6NfWAhXFFpAKHas-B2kQsAQIQA&biw=1366&bih=651>. Access in november 11, 2017) 7

Figure 1.2 - Airplane UFU-1 initial sketch. 7

Figure 1.3 - Airplane UFU-1 initial sketch. 8

Figure 1.4 - Airplane UFU-1 final drawing. 9

Figure 1.5 - 14bis at flight. (Available in: <https://www.google.com.br/search?q=14bis&tbm=isch&tbo=u&source=univ&sa=X&ved=0ahUKEwic5f-T6NfWAhXFFpAKHas-B2kQsAQIQA&biw=1366&bih=651>. Access in november 11, 2017) 10

Figure 1.6 - Wright brothers's Flyer I. (Available in: <https://www.google.com.br/search?biw=1366&bih=651&tbm=isch&sa=1&q=FLYER+I+WRITE+BROTHERS&oq=FLYER+I+WRITE+BROTHERS&gs_l=psy-ab.3...185598.208467.0.209760.30.27.2.0.0.0.428.3789.2j16j4j0j1.23.0....0...1.1.64.psy-ab..6.9.1538...0j0i67k1.0.OHOkrI57P7A#imgrc=_&spf=1507149400162>. Access in november 11, 2017) 10

Figure 1.7 - Red baron airplane, Fokker Dr.I. (Available in: <https://www.google.com.br/search?q=bar%C3%A3o+vermelho+avi%C3%A3o&tbm=isch&tbo=u&source=univ&sa=X&ved=0ahUKEwi9ksj169fWAhUCP5AKHTZIAIIQsAQIRA&biw=1366&bih=651#imgrc=_&spf=1507150197293>. Access in november 11, 2017) 11

Figure 1.8 - Airplane Spad 13, first great war. (Available in: <https://www.google.com.br/search?q=Airplane+Spad+13&tbm=isch&tbo=u&source=univ&sa=X&ved=0ahUKEwicsYP87NfWAhXDE5AKHbaHCMYQsAQIQA&biw=1366&bih=651#imgrc=_&spf=1507150916189>. Access in november 11, 2017) 11

Figure 1.9 - Airliner Fokker F-10, from 1927. (Available in: <https://en.wikipedia.org/wiki/Fokker_F.10>. Access in november 11, 2017) 12

Figure 1.10 - Douglas DC-3, introduction in service in 1936. (Available in: <https://pt.wikipedia.org/wiki/Douglas_DC-3>. Access in november 11, 2017) 12

Figure 1.11 - North American XB-70 Valkyrie, before first flight on September 21th, 1964. (Available in: <https://en.wikipedia.org/wiki/North_American_XB-70_Valkyrie>. Access in november 11, 2017) 13
Figure 1.12 - Beechcraft Starship, executive airplane. (Available in: <https://en.wikipedia.org/wiki/Beechcraft_Starship>. Access in november 11, 2017) 13
Figure 2.1 - Wings with various taper ratios: (a) Rectangle (λ = 1); (b) Trapezoid 0 < λ < 1 16
Figure 2.2 - Mean aerodynamic chord (Raymer, 2006). 17
Figure 2.3 - Five wings with different sweep angles (Sadraey, 2013). 17
Figure 2.4 - Dihedral and anhedral angles (Sadraey, 2013). 18
Figure 2.5 - Oswald factor for straight and trapezoidal wings (After Venson, 2015). 23
Figure 2.6 - Typical mission profile for a civil airplane. 25
Figure 2.7 - Generic Payload-Range Diagram. 35
Figure 2.8 - Tail sizing geometric scheme (Raymer, 2006). 37
Figure 2.9 - Weight-CG envelope. 43
Figure 2.10 - Height variation for male and female and for different ethnic (Sadraey, 2013). 45
Figure 2.11 - Linear body dimensions (cm) (Sadraey, 2013). 45
Figure 2.12 - Dimensions for a cockpit of a light aircraft with stick control (Torenbeek, 1976). .. 46
Figure 2.13 - Dimensions for a cockpit of a fighter aircraft (Sadraey, 2013). 46
Figure 2.14 - Airfoil lift curve slope (Sadraey, 2013). 48
Figure 2.15 - Plain flap geometry (Roskam, 2000). 50
Figure 2.16 - Lift effectiveness of a plain flap (Roskam, 2000). 50
Figure 2.17 - Correction factor for nonlinear lift behavior of a plain flap (Roskam, 2000). 51
Figure 2.18 - Correction factor for plain flap lift (Roskam, 2000). 51
Figure 2.19 - Basic airfoil maximum lift increment due to trailing edge flap (Roskam, 2000). 52
Figure 2.20 - Flap chord correction factor (Roskam, 2000). 53
Figure 2.21 - Flap angle correction factor (Roskam, 2000). 53
Figure 2.22 - Flap motion correction factor (Roskam, 2000). 54
Figure 2.23 - Biplane interference factor (Raymer, 2006). 57
Figure 2.24 - Positive and negative stagger representation (Rodrigues, 2011). 59
Figure 2.25 - Effect of taper ratio and flap span to wing span ratio on kb (Roskam, 2000). 62
Figure 2.26 - Effect of aspect ratio and flap chord ratio on the three dimensional flap effectiveness (Roskam, 2000). 63
Figure 2.27 - Definition of flapped wing area (Roskam, 2000). 64

Figure 2.28 - Effect of sweep on planform correction factor (Roskam, 2000). 64
Figure 2.29 - Control surface effectiveness parameter (Sadraey, 2013). 66
Figure 2.30 - Wing fuselage interference factor (Roskam and Lan, 1997). 70
Figure 2.31 - Lifting surface correction factor (Roskam and Lan, 1997). 70
Figure 2.32 - Turbulent mean skin friction coefficient (After Roskam and Lan, 1997). 71
Figure 2.33 - Airfoil thickness location parameter (Roskam and Lan, 1997). 72
Figure 2.34 - Ratio of drag coefficient of a circular cylinder in function of the body fineness (Roskam, 2000). 75
Figure 2.35 - Steady state cross-flow drag coefficient for two-dimensional circular cylinder (Roskam, 2000). 75
Figure 2.36 - Downwash and upwash fields (Brandt). 77
Figure 2.37 - Parameters for downwash and upwash prediction (Brandt). 77
Figure 2.38 - Sidewash due the wing (Nelson, 1998). 79
Figure 2.39 - Fuselage division for wing aerodynamic center shift estimative (Roskam, 2000). 83
Figure 2.40 - Effect of fuselage segment location on upwash gradient (Roskam, 2000). 83
Figure 2.41 - Airplane projected side area segments (Sadraey, 2013). 84
Figure 2.42 - Canard airplane CG location (After Sadraey, 2013). 87
Figure 2.43 - Pitch moment curves (Nelson, 1998). 89
Figure 2.44 - Fuselage segmentation (Nelson, 1998). 93
Figure 2.45 - Fuselage fineness ratio (Nelson, 1998). 94
Figure 2.46 - Forces and moments during the take-off rotation (Sadraey, 2013). 96
Figure 2.47 - Typical variation of elevator deflection versus aircraft speed (Sadraey, 2013). 98
Figure 2.48 - Static roll stability (Nelson, 1998). 99
Figure 2.49 - Tip shape and aspect ratio effect on Cl_β (Nelson, 1998). 99
Figure 2.50 - Aileron guidelines (Raymer, 2006). 100
Figure 2.51 - Geometry of aileron (a) top view; (b) side view (Sadraey, 2013). 101
Figure 2.52 - Incremental change in lift and drag in generating a rolling motion (Sadraey, 2013). 102
Figure 2.53 - Static directional stability (Nelson, 1998). 104
Figure 2.54 - Wing body interference factor (Nelson, 1998). 105
Figure 2.55 - Reynolds number correction factor (Nelson, 1998). 106
Figure 2.56 - Possible geometries for a rudder (After Sadraey, 2013). 107
Figure 2.57 - Directional control and rudder deflection (Sadraey, 2013). 109

Figure 2.58 - Forces and angles in cross-wind crabbed landing (Sadraey, 2013). 110
Figure 2.59 - Empirical factor for $Cn\delta A$ estimate (Nelson, 1998). 114
Figure 2.60 - Variation of roots with damping ratio (Nelson, 1998). 115
Figure 2.61 -The spiral motion (Nelson, 1998). 121
Figure 2.62 - The roll motion (Nelson, 1998). 122
Figure 2.63 - The Dutch-roll motion (Nelson, 1998). 122
Figure 2.64 - Definition of FAR 23 take-off distance (After Roskam, 1991). 129
Figure 2.65 - Definition of FAR 23 landing distance (Roskam, 1997). 132
Figure 2.66 - FAR 23.333 combined V-n diagram. 133
Figure 2.67 - Multi-rib wing structure example (Megson, 2010). 136
Figure 2.68 - Multi-spar wing structure example (Megson, 2010). 136
Figure 2.69 - Fuselage structural layout (Niu, 1995). 137
Figure 2.70 - Fuselage structural layout (Megson, 2010). 138
Figure 2.71 - Castoring wheel geometry (Raymer, 2006). 140
Figure 2.72 - Wheel load geometry (Raymer, 2006). 141
Figure 3.1 - Payload-range Diagram for the airplane UFU-1. 149
Figure 3.2 - Estimated CG-Weight envelope for the airplane UFU-1. 154
Figure 3.3 - Standard pilot standing dimensioning. 161
Figure 3.4 - Standard pilot sitting position. 161
Figure 3.5 - Airplane seat. 162
Figure 3.6 - Pilots seats positioning inside the cockpit. 163
Figure 3.7 - Cockpit frames drawings. 163
Figure 3.8 - Equipped avionics panel. 164
Figure 3.9 - Cockpit assembly. 164
Figure 3.10 - Aerodynamic data for the airfoils NACA 65-415. 170
Figure 3.11 - Aerodynamic data for the airfoils NACA 65-418. 170
Figure 3.12 - Aerodynamic data for the airfoils NACA 66-218. 171
Figure 3.13 - *Aerodynamic data for the airfoils NACA 66-418.* 171
Figure 3.14 - Aerodynamic data for the airfoils with mean camber line "a-0". 172
Figure 3.15 - Aerodynamic data for the airfoils with mean camber line "a-1". 172
Figure 3.16 - Airfoil NACA 65-418 "a0". 173
Figure 3.17 - Aerodynamic data for the airfoils with chord equal to 0.61m. 175
Figure 3.18 - Aerodynamic data for the airfoils with chord equal to 0.40m. 175

Figure 3.19 - Airfoil NACA 0009. 176
Figure 3.20 - Aerodynamic data for the airfoil NACA 0012. 177
Figure 3.21 - Airfoil NACA 0012. 177
Figure 3.22 - Fuselage division for the lower wing. 180
Figure 3.23 - Fuselage division for the lower wing. 181
Figure 3.24 - Fuselage division for the upper wing. 183
Figure 3.25 - Fuselage division for the upper wing. 184
Figure 3.26 - Fuselage division for the lower canard. 187
Figure 3.27 - Fuselage division for the lower canard. 187
Figure 3.28. Complete airplane side segmentation. 193
Figure 3.29 - Airplane UFU-1 lift curve slope. 194
Figure 3.30 - Drag polar for W=473.9 Kgf, FL080 and V = 235 [km/h]. 196
Figure 3.31 - Drag polar for W=478.9 Kgf, FL080 and V = 235 [km/h]. 197
Figure 3.32 - CG-Weight envelopes comparison. 201
Figure 3.33 - Longitudinal static stability for the configuration 12. 203
Figure 3.34 - Longitudinal static stability for the configuration 27. 203
Figure 3.35 - Take-off rotation moment for the configuration 20. 205
Figure 3.36 - Take-off rotation moment for the configuration 30. 206
Figure 3.37 - Directional static stability for the configuration 12. 210
Figure 3.38 - Directional static stability for the configuration 27. 211
Figure 3.39 - Short period response for the configuration 12. 214
Figure 3.40 - Short period response for the configuration 27. 214
Figure 3.41 - Phugoid response for the configuration 12. 215
Figure 3.42 - Phugoid response for the configuration 27. 215
Figure 3.43 - Roll response for the configuration 12. 217
Figure 3.44 - Roll response for the configuration 27. 217
Figure 3.45 - Spiral response for the configuration 12. 218
Figure 3.46 - Spiral response for the configuration 27. 218
Figure 3.47 - Dutch-roll response for the configuration 12. 219
Figure 3.48 - Dutch-roll response for the configuration 27. 219
Figure 3.49 - Excess of power for the configuration 12 and engine power at 70%. 221
Figure 3.50 - Excess of thrust for the configuration 12 and engine power at 70%. 221
Figure 3.51 - Excess of power for the configuration 12 and engine power at 100%. 222

Figure 3.52 - Excess of thrust for the configuration 12 and engine power at 100%. 222
Figure 3.53 - Excess of power for the configuration 27 and engine power at 70%. 223
Figure 3.54 - Excess of thrust for the configuration 27 and engine power at 70%. 223
Figure 3.55 - Excess of power for the configuration 27 and engine power at 100%. 224
Figure 3.56 - Excess of thrust for the configuration 27 and engine power at 100%. 224
Figure 3.57 - Airplane UFU-1 maneuvering V-n diagram. 230
Figure 3.58 - Wings structural layout with skin. 231
Figure 3.59 - Wings structural layout. 232
Figure 3.60 - Canards structural layout with skin. 233
Figure 3.61 - Canards structural layout. 233
Figure 3.62 - Vertical tail structural layout with skin. 234
Figure 3.63 - Vertical tail structural layout. 234
Figure 3.64 - Fuselage structural layout with skin. 236
Figure 3.65 - Fuselage structural layout, nose gear compartment detail. 236
Figure 3.66 - Fuselage structural layout. 237
Figure 3.67 - Landing gear geometric parameters. 238
Figure 3.68 - Nose wheel steering study. 241
Figure 3.69 - Engine pusher positioning on the airplane. 242
Figure 3.70 - Approximate propeller efficiency curve. 243
Figure 3.71 - Garmin suite architecture (Garmin G3X pilot's guide). 244
Figure 3.72 - Avionic panel layout. 247
Figure 4.1 - Airplane UFU-1 views. 255
Figure 4.2 - Airplane isometric view. 255
Figure 4.3 - Airplane bottom view. 256
Figure 4.4 - Airplane internal compartments. 256

LIST OF TABLES

Table 2.1 - Historical tendencies data for wing aspect ratio and taper ratio (After Venson, 2013). 18
Table 2.2 - Historical tendencies data for wing dihedral (After Venson, 2013). 19
Table 2.3 - Historical tendencies data for horizontal tail aspect ratio and taper ratio (After Venson, 2013). 19
Table 2.4 - Historical tendencies data for vertical tail aspect ratio and taper ratio (After Venson, 2013). 20
Table 2.5 - Historical tendencies data for airplane wetted area (After Venson, 2015). 21
Table 2.6 - Reference friction coefficient values (After Venson, 2015). 22
Table 2.7 - Historical tendencies values for the empty-to-take-off weight ratio constants (After Venson, 2015). 24
Table 2.8 - Historical tendencies data for flight phase weight fraction (After Venson, 2015). 26
Table 2.9 - Historical tendencies data for wing loading (After Venson, 2015). 27
Table 2.10 - Constants for empirical estimative for the wing loading (After Venson, 2015) 28
Table 2.11 - Constants for empirical estimative for the power-to-weight ratio (After Venson, 2015). 30
Table 2.12 - Historical tendencies data for power-to-weight ratio (After Venson, 2015). 30
Table 2.13 - Constants for empirical estimative for the thrust-to-power ratio (After Venson, 2015). 31
Table 2.14 - Historical tendencies data for thrust-to-disc loading ratio (After Venson, 2015). 32
Table 2.15 - Historical tendencies data for thrust-to-weight ratio (After Venson, 2015). 32
Table 2.16 - Historical tendencies data for take-off runway (After Venson, 2015). 33
Table 2.17 - Historical tendencies data for landing runway (After Venson, 2015). 34
Table 2.18 - Historical tendencies data for fuselage sizing (After Venson, 2015). 36
Table 2.19 - Historical tendencies for cockpit sizing (After Venson, 2014). 37
Table 2.20 - Historical tendencies data for tail volume coefficient (After Venson, 2015). 38
Table 2.21 - Historical tendencies data for primary control surfaces (After Venson, 2015). 39
Table 2.22 - Historical tendencies data for moment of inertia (After Venson, 2015). 40
Table 2.23 - Stability requirements values (Sadraey, 2013). 85
Table 2.24 - Typical values for geometry of control surfaces (Sadraey, 2013). 85

Table 2.25 - Take-off rotational acceleration for various aircraft (Sadraey, 2013). 97
Table 2.26 - Rudder design requirements (Sadraey, 2013). 108
Table 2.27 - Variation of response with damping ratio (Nelson, 1998). 116
Table 2.28 - Aircraft classes (Sadraey, 2013). 119
Table 2.29 - Flight phase categories (Sadraey, 2013). 120
Table 2.30 - Levels of acceptability (Sadraey, 2013). 120
Table 2.31 - Short-period mode damping ratio specification (Sadraey, 2013). 120
Table 2.32 - Phugoid mode requirement (Sadraey, 2013). 121
Table 2.33 - Roll control requirements (Sadraey, 2013). 126
Table 2.34 - Roll mode specification maximum value (Sadraey, 2013). 126
Table 2.35 - Time to double amplitude in spiral mode (Sadraey, 2013). 127
Table 2.36 - Dutch-roll mode handling qualities (Sadraey, 2013). 127
Table 2.37 - Take-off parameters. 129
Table 2.38 - Wheel-ground rolling friction coefficient. 129
Table 2.39 - Aircrafts flight ceilings. 131
Table 3.1 - Total range estimated for the airplane UFU-1. 149
Table 3.2 - CG positioning for some weights configurations. 153
Table 3.3 - Airfoils stall characteristics. 166
Table 3.4 - Airfoils drag polar bottom and pitch moment. 167
Table 3.5 - Lift increment due the global wash fields, comparison. 194
Table 3.6 - Mass configurations for dynamics of flight assessing. 198
Table 3.7 - Mass configurations for dynamics of flight assessing continuation. 199
Table 3.8 - Trimmed cruise flight configuration for dynamics of flight assessing. 200
Table 3.9 - Trimmed cruise flight configuration for dynamics of flight assessing continuation. . 200
Table 3.10 - Longitudinal static stability results. 202
Table 3.11 - Longitudinal static stability results continuation. 202
Table 3.12 - Longitudinal static stability results continuation. 202
Table 3.13 - Longitudinal control dimensioning parameters and results. 205
Table 3.14 - Longitudinal control dimensioning parameters and results continuation. 205
Table 3.15 - Lateral control dimensioning parameters and results. 208
Table 3.16 - Lateral control dimensioning parameters and results continuation. 208
Table 3.17 - Directional static stability results. 210
Table 3.18 - Directional control dimensioning parameters. 212

Table 3.19 - Directional control dimensioning parameters and results. 212
Table 3.20 - Longitudinal dynamic stability results. 213
Table 3.21 - Longitudinal dynamic stability results continuation. 214
Table 3.22 - Lateral-directional dynamic stability results. 216
Table 3.23 - Lateral-directional dynamic stability results continuation. 216
Table 3.24 - Take-off estimative airplane setting. 225
Table 3.25 - Take-off estimative setting and runway parameters. 225
Table 3.26 - Take-off estimative results. 226
Table 3.27 - Climb estimative airplane setting. 226
Table 3.28 - Climb estimative airplane setting continuation. 226
Table 3.29 - Climb estimative results. 227
Table 3.30 - Descent estimative airplane setting. 228
Table 3.31 - Descent estimative results. 228
Table 3.32 - Landing estimative airplane setting. 228
Table 3.33 - Landing estimative airplane setting continuation. 229
Table 3.34 - Landing estimative results. 229
Table 3.35 - Electrical & Electronic devices electrical characteristics. 248

LIST OF SYMBOLS

Roman Symbols

a_0	Airfoil lift curve slope
b	Aerodynamic surface span
b_A	Aileron span
b_{Ai}	Location of the inner chord of the aileron along the y axis
b_{CAN}	Canard span
b_{CAN_B}	Biplane canard span
b_{CAN_LOW}	Lower canard span
b_{CAN_UP}	Upper canard span
b_E	Elevator span
b_{E_i}	Elevator inner position along the canard span
b_F	Flap span
b_{F_i}	Location of the inner chord of the flap along the y axis
b_{long}	Longest wing or canard span
b_R	Rudder span
b_{R_i}	Rudder inner position along the vertical tail span
b_{VT}	Vertical tail span
b_{VT_LEF}	Left vertical tail span
b_{VT_RIG}	Right vertical tail span
b_W	Wing span
b_{W_B}	Biplane wing span
b_{W_LOW}	Lower wing span

b_{W_UP}	Upper wing span
cd	Airfoil drag coefficient
c_{d_c}	Experimental steady state cross-flow drag coefficient of a circular cylinder
cd_{CAN}	Canard airfoil drag coefficient
cd_p	Airfoil pressure drag coefficient
cd_{VT}	Vertical tail airfoil drag coefficient
cd_w	Airfoil wave drag coefficient
cd_W	Wing airfoil drag coefficient
cd_0	Airfoil zero lift drag coefficient
cl	Airfoil lift coefficient
$cl_{vt_{max}}$	Vertical tail airfoil maximum lift coefficient
cl_α	Airfoil lift curve slope
$cl_{\alpha_{can}}$	Canards airfoil lift curve slope
$cl_{\alpha_{vt}}$	Vertical tails airfoil lift curve slope
cl_{α_w}	Wings airfoil lift curve slope
$(cl_\delta)_{theory}$	Parameter based on flap size and on profile thickness ratio
cm	Airfoil pitch moment coefficient
cm_{CAN_LOW}	Lower canard airfoil pitch moment coefficient
cm_{CAN_UP}	Upper canard airfoil pitch moment coefficient
cm_W	Wing airfoil pitch moment coefficient
d	Main landing gear tire diameter
d_c	Distance between the aircraft CG and the aerodynamic center of the airplane Projected side area
d_{cg-mg}	Distance between the airplane CG and the contact point of the main landing

	gear leg to the ground
d_f	Fuselage equivalent diameter for maximum cross section area
e	Aerodynamic surface span efficiency factor
e_{CAN}	Canard span efficiency factor
e_{CAN_B}	Biplane canard span efficiency factor
e_{VT}	Vertical tail span efficiency factor
e_{VT_LEF}	Left vertical tail span efficiency factor
e_{VT_RIG}	Right vertical tail span efficiency factor
e_W	Wing span efficiency factor
e_{W_B}	Biplane wing span efficiency factor
e_{wing}	Wing Oswald efficiency factor obtained from graphic
e_o	Aerodynamic surface Oswald efficiency factor
g	Gravity acceleration
h	Maximum fuselage depth
h_{AC_W}	Wing aerodynamic center location relative to the leading edge of its own $\bar{C}_W$
h_{TO}	Take-off obstacle height
i_{CAN_LOW}	Lower canard incidence angle
i_{CAN_UP}	Upper canard incidence angle
i_f	Incidence of the fuselage camber line relative to the fuselage reference line at the center of each fuselage increment. The incidence angle is defined as negative for nose droop and aft upsweep.
i_{HT}	Horizontal tail incidence angle
i_{VT_LEF}	Left vertical tail incidence angle
i_{VT_RIG}	Right vertical tail incidence angle
i_W	Wing incidence angle

i_{W_LOW}	Lower wing incidence angle
i_{W_UP}	Upper wing incidence angle
k_{long}	Longitudinal oscillation stiffness constant
k_{wf}	Wing-fuselage interference factor
k_1	Factor which accounts for flap chord to airfoil chord ratio different from 25%
k_2	Factor which accounts for the "actual flap" angle different from the "reference flap" angle
k_3	Factor which accounts for flap motion as a function of the flap deflection
k'	Correction factor that accounts nonlinearities at high flap deflections
l	Component or part moment arm
l_{CAN}	Canard tail moment arm
l_f	Fuselage length
l_{HT}	Horizontal tail moment arm
l_{VT}	Vertical tail moment arm
m	Mass of the airplane
n_P	Number of blades of the propeller
p	Airplane roll rate due the ailerons deflection
p_{ss}	Airplane constant rolling rate
$\dot{p}$	Temporal differential rate $(\partial/\partial t)$ of p
q	Dynamic pressure of the air
q_{VT}	Dynamic pressure at the vertical tail
r	Airplane yaw rate due the rudder deflection
r	Ratio between the aerodynamic area of the shorter aerodynamic surface and the longer aerodynamic surface
r_{CAN}	Ratio between the aerodynamic area of the shorter canard and the longer canard

r_W	Ratio between the aerodynamic area of the shorter wing and the longer wing
$t_{doub-halve}$	Time for halving the amplitude of an oscillatory motion
t_{TO}	Time to the airplane take-off from the start to the obstacle position
t/c	Airfoil thickness
t/c_{HT}	Horizontal tail thickness
t/c_{VT}	Vertical tail thickness
t/c_W	Wing thickness
w	Main landing gear tire width
w_f	Fuselage maximum width
x_i	Distance between the center of the projected side area of the i-th segment of the airplane and the reference line
y_A	Location of the aileron aerodynamic center along the y axis
y_D	Mean distance of the point of application of the rolling drag (drag generated) by the ailerons, wings, tails, fuselage; applied normally at 40% of the semi-span of the wing from the root chord)
AC	Aerodynamic center location of an aerodynamic body
AC_{CAN_LOW}	Aerodynamic center location of the lower canard
AC_{CAN_UP}	Aerodynamic center location of the upper canard
AC_{VT_LEF}	Aerodynamic center location of the left vertical tail
AC_{VT_RIG}	Aerodynamic center location of the right vertical tail
AC_{W_B}	Aerodynamic center location of the biplane wing
AC_{W_LOW}	Aerodynamic center location of the lower wing
AC_{W_UP}	Aerodynamic center location of the upper wing
A_i	i-th segment of the projected side area of the complete airplane
AR	Aerodynamic surface aspect ratio

AR_B	Biplane aspect ratio
AR_{CAN}	Canard aspect ratio
AR_{CAN_B}	Biplane canard aspect ratio
AR_{CAN_LOW}	Lower canard aspect ratio
AR_{CAN_UP}	Upper canard aspect ratio
AR_{HT}	Horizontal tail aspect ratio
AR_{VT}	Vertical tail aspect ratio
AR_{VT_LEF}	Left vertical tail aspect ratio
AR_{VT_RIG}	Right vertical tail aspect ratio
AR_W	Wing aspect ratio
AR_{W_B}	Biplane wing aspect ratio
AR_{W_LOW}	Lower wing aspect ratio
AR_{W_UP}	Upper wing aspect ratio
BEW	Basic empty weight
C	Damping of an oscillatory motion
C_{cr}	Critical damping of an oscillatory motion
C_{fe}	Surface friction coefficient
Cf_{fus}	Turbulent flat plate skin-friction coefficient of the fuselage
C_{f_W}	Turbulent flat plate friction coefficient of the wing
$C_{f_{W_{lam}}}$	Wing laminar friction coefficient
$C_{f_{W_{turb}}}$	Wing turbulent friction coefficient
Cl_{CG}	Airplane rolling moment coefficient at the CG
$Cl_{\beta_{CG}}$	Airplane rolling moment coefficient curve slope at the CG
$C_{l_{\delta A}}$	Coefficient of rolling moment rate due the ailerons deflection

Cm	Airplane pitch moment coefficient
Cm_{CG}	Airplane pitch moment coefficient applied on the CG of the own airplane
$Cm_{CG_{CAN\_LOW}}$	Lower canard pitch moment coefficient applied on the CG of the airplane
$Cm_{CG_{CAN\_UP}}$	Upper canard pitch moment coefficient applied on the CG of the airplane
$Cm_{CG_{FUS}}$	Fuselage pitch moment coefficient applied on the CG of the airplane
$Cm_{CG_{HT}}$	Horizontal tail pitch moment coefficient applied on the CG of the airplane
$Cm_{CG_{W}}$	Wing pitch moment coefficient applied on the CG of the airplane
$Cm_{CG_{W\_LOW}}$	Lower wing pitch moment coefficient applied on the CG of the airplane
$Cm_{CG_{W\_UP}}$	Upper wing pitch moment coefficient applied on the CG of the airplane
$Cm_{\alpha_{CG}}$	Airplane pitch moment coefficient curve slope at CG
$Cm_{\alpha_{CAN\_LOW}}$	Lower canard pitch moment coefficient curve slope
$Cm_{\alpha_{CAN\_UP}}$	Upper canard pitch moment coefficient curve slope
$Cm_{\alpha_{FUS}}$	Fuselage pitch moment coefficient curve slope
$Cm_{\alpha_{HT}}$	Horizontal tail pitch moment coefficient curve slope
$Cm_{\alpha_{W}}$	Wing pitch moment coefficient curve slope
$C_{m_{\delta E}}$	Coefficient of pitch moment rate due the elevator deflection
$Cm_{0_{CG}}$	Airplane zero lift pitch moment coefficient at CG
$Cm_{0_{CAN\_LOW}}$	Lower canard zero lift pitch moment coefficient
$Cm_{0_{CAN\_UP}}$	Upper canard zero lift pitch moment coefficient
$Cm_{0_{FUS}}$	Fuselage zero lift pitch moment coefficient
$Cm_{0_{HT}}$	Horizontal tail zero lift pitch moment coefficient
$Cm_{0_{W}}$	Wing zero lift pitch moment coefficient
Cn_{CG}	Airplane yawing moment coefficient at the CG

$Cn_{\beta_{CG}}$	Airplane yaw moment coefficient curve slope at the CG
$Cn_{\beta_{dyn}}$	Airplane dynamic yaw moment coefficient curve slope at the CG
$Cn_{\beta_{VT}}$	Vertical tail yaw moment coefficient curve slope
$Cn_{\beta_{VT\_LEF}}$	Left verticl tail yaw moment coefficient curve slope
$Cn_{\beta_{VT\_RIG}}$	Right verticl tail yaw moment coefficient curve slope
$Cn_{\beta_{W\_B-FUS}}$	Biplane wing-fuselage yaw moment coefficient curve slope
$C_{n_{\delta R}}$	Coefficient of yaw moment rate due the rudder deflection
C_{root}	Aerodynamic surface root chord
C_{root_A}	Aileron root chord
$C_{root_{CAN\_LOW}}$	Lower canard root chord
$C_{root_{CAN\_UP}}$	Upper canard root chord
C_{root_E}	Elevator root chord
C_{root_F}	Flap root chord
C_{root_R}	Rudder root chord
$C_{root_{VT\_LEF}}$	Left vertical tail root chord
$C_{root_{VT\_RIG}}$	Right vertical tail root chord
$C_{root_{W\_B}}$	Biplane wing root chord
$C_{root_{W\_LOW}}$	Lower wing root chord
$C_{root_{W\_UP}}$	Upper wing root chord
C_{tip}	Aerodynamic surface tip chord
C_{tip_A}	Aileron tip chord
$C_{tip_{CAN\_LOW}}$	Lower canard tip chord
$C_{tip_{CAN\_UP}}$	Upper canard tip chord

C_{tip_E}	Elevator tip chord
C_{tip_F}	Flap tip chord
C_{tip_R}	Rudder tip chord
$C_{tip_{VT\_LEF}}$	Left vertical tail tip chord
$C_{tip_{VT\_RIG}}$	Right vertical tail tip chord
$C_{tip_{W\_LOW}}$	Lower wing tip chord
$C_{tip_{W\_UP}}$	Upper wing tip chord
C_A	Aileron chord
C_{CAN}	Canard chord
CD	Airplane or body drag coefficient
CD_{CAN}	Canard drag coefficient
$CD_{CAN\_fair\_lef}$	Canards left fairing drag coefficient
$CD_{CAN\_fair\_rig}$	Canards right fairing drag coefficient
CD_{CAN_LOW}	Lower canard drag coefficient
CD_{CAN_UP}	Upper canard drag coefficient
CD_{FAIR_CAN}	Canards fairing drag coefficient
CD_{FUS}	Fuselage drag coefficient
CD_i	Airplane or body induced drag coefficient
$CD_{i_{CAN}}$	Canard induced drag coefficient
$CD_{i_{CAN\_LOW}}$	Lower canard induced drag coefficient
$CD_{i_{CAN\_UP}}$	Upper canard induced drag coefficient
$CD_{i_{VT}}$	Vertical tail induced drag coefficient
$CD_{i_{VT\_LEF}}$	Left vertical tail induced drag coefficient
$CD_{i_{VT\_RIG}}$	Right vertical tail induced drag coefficient

CD_{i_W}	Wing induced drag coefficient
$CD_{i_{W\_LOW}}$	Lower wing induced drag coefficient
$CD_{i_{W\_UP}}$	Upper wing induced drag coefficient
$CD_{L_{fus}}$	Fuselage induced drag coefficient
CD_{LGEAR}	Landing gear drag coefficient
CD_{PROP}	Propeller drag coefficient
C_{D_R}	Airplane drag coefficient at rolling condition (between 0.7 and 1.2)
CD_{VT}	Vertical tail drag coefficient
CD_{VT_BOOM}	Vertical tail booms drag coefficient
CD_{VT_LEF}	Left vertical tail drag coefficient
CD_{VT_RIG}	Right vertical tail drag coefficient
CD_W	Wing drag coefficient
CD_{W_LOW}	Lower wing drag coefficient
CD_{W_UP}	Upper wing drag coefficient
C_{D_y}	Airplane side drag coefficient (typical values for conventional shape airplane are between 0.5 and 0.8)
CD_0	Airplane or body equivalent profile drag coefficient
$CD_{0_{CAN}}$	Canard airfoil drag coefficient
$CD_{0_{CAN\_LOW}}$	Lower canard airfoil drag coefficient
$CD_{0_{CAN\_UP}}$	Upper canard airfoil drag coefficient
$CD_{0_{fus}}$	Fuselage equivalent profile drag coefficient
$CD_{0_{VT}}$	Vertical tail airfoil drag coefficient
$CD_{0_{VT\_LEF}}$	Left vertical tail airfoil drag coefficient
$CD_{0_{VT\_RIG}}$	Right vertical tail airfoil drag coefficient

CD_{0_W}	Wing airfoil drag coefficient
$CD_{0_{W\_LOW}}$	Lower wing airfoil drag coefficient
$CD_{0_{W\_UP}}$	Upper wing airfoil drag coefficient
C_E	Elevator chord
C_F	Flap chord
C_{HT}	Horizontal tail chord
CL	Airplane or body lift coefficient
CL_{CAN}	Canard lift coefficient
CL_{CAN_LOW}	Lower canard lift coefficient
CL_{CAN_UP}	Upper canard lift coefficient
$C_{L_{CAN\_LOW_{\delta E}}}$	Lower canard lift coefficient increment due the elevator deflection
$C_{L_{CAN\_UP_{\delta E}}}$	Upper canard lift coefficient increment due the elevator deflection
CL_{FUS}	Fuselage lift coefficient
CL_{HT}	Horizontal tail lift coefficient
$CL_{HT_{\delta E}}$	Horizontal tail lift coefficient rate due the elevator deflection
CL_{max}	Airplane maximum lift coefficient
$CL_{max_{TO}}$	Airplane maximum lift coefficient at the Take-off phase
$CL_{take-off}$	Airplane takeoff lift coefficient
CL_{VT}	Vertical tail lift coefficient
$C_{L_{VT\_LEF_{\delta R}}}$	Left vertical tail lift coefficient increment due the rudder deflection
$C_{L_{VT\_RIG_{\delta R}}}$	Right vertical tail lift coefficient increment due the rudder deflection
CL_W	Wing lift coefficient
CL_{W_LOW}	Lower wing lift coefficient

CL_{W_UP}	Upper wing lift coefficient
$CL_{\alpha_{AP}}$	Airplane lift coefficient curve slope
$CL_{\alpha_{CAN}}$	Canard lift coefficient curve slope
$CL_{\alpha_{CAN\_LOW}}$	Lower canard lift coefficient curve slope
$CL_{\alpha_{CAN\_UP}}$	Upper canard lift coefficient curve slope
CL_{α_F}	Fuselage lift coefficient curve slope
$CL_{\alpha_{HT}}$	Horizontal tail lift coefficient curve slope
$CL_{\alpha,surface}$	Aerodynamic surface lift coefficient curve slope
$CL_{\alpha_{VT}}$	Vertical tail lift coefficient curve slope
$CL_{\alpha_{VT\_LEF}}$	Left vertical tail lift coefficient curve slope
$CL_{\alpha_{VT\_RIG}}$	Right vertical tail lift coefficient curve slope
CL_{α_W}	Wing lift coefficient curve slope
$CL_{\alpha_{W\_B}}$	Biplane wing lift coefficient curve slope
$CL_{\alpha_{W-F}}$	Wing-fuselage lift coefficient curve slope
$CL_{\alpha_{W\_LOW}}$	Lower wing lift coefficient curve slope
$CL_{\alpha_{W\_UP}}$	Upper wing lift coefficient curve slope
$CL_{\alpha=0_{AP}}$	Airplane lift coefficient for angle of attack equal to zero
$CL_{\alpha=0_{CAN\_LOW}}$	Lower canard lift coefficient for angle of attack equal to zero
$CL_{\alpha=0_{CAN\_UP}}$	Upper canard lift coefficient for angle of attack equal to zero
$CL_{\alpha=0_W}$	Wing lift coefficient for angle of attack equal to zero
$CL_{\alpha=0_{W\_LOW}}$	Lower wing lift coefficient for angle of attack equal to zero
$CL_{\alpha=0_{W\_UP}}$	Upper wing lift coefficient for angle of attack equal to zero
$CL_{\delta E}$	Airplane lift coefficient rate due the elevator deflection

CL_0	Airplane or body lift coefficient for angle of attack equal to zero
C_R	Rudder chord
C_{VT}	Vertical tail chord
$\bar{C}$	Mean aerodynamic chord
$\bar{C}_{CAN}$	Canard mean aerodynamic chord
$\bar{C}_{CAN\_LOW}$	Lower canard mean aerodynamic chord
$\bar{C}_{CAN\_UP}$	Upper canard mean aerodynamic chord
$\bar{C}_{HT}$	Horizontal tail mean aerodynamic chord
$\bar{C}_{VT}$	Vertical tail mean aerodynamic chord
$\bar{C}_{VT\_LEF}$	Left vertical tail mean aerodynamic chord
$\bar{C}_{VT\_RIG}$	Right vertical tail mean aerodynamic chord
$\bar{C}_W$	Wing mean aerodynamic chord
$\bar{C}_{W\_B}$	Biplane wing mean aerodynamic chord
$\bar{C}_{W\_LOW}$	Lower wing aerodynamic chord
$\bar{C}_{W\_UP}$	Upper wing aerodynamic chord
D	Drag generated by the airplane
Di	Induced drag generated by the airplane
Di_{A_left}	Induced drag due the left aileron deflection
Di_{A_right}	Induced drag due the right aileron deflection
D_P	Propeller diameter
E	Flight endurance
F_{A_y}	Airplane aerodynamic side force
FL	Flight level
F_W	Aerodynamic load generated by the cross wind

GAP_{CAN_B}	Biplane canard gap
GAP_{W_B}	Biplane wing gap
GAS_{TOF}	Fuel consumption during the take-off phase
H_{HT}	Horizontal tail height above fuselage
H_{HT}/H_{VT}	0.0 for conventional tail; 1.0 for "T" tail
H_{VT}	Vertical tail height above fuselage
$I_{xx_{cg}}$	Airplane moment of inertia at the CG around the X axis
$I_{yy_{mg}}$	Airplane moment of inertia at the main landing gear leg around the Y axis
$I_{yy_{cg}}$	Airplane moment of inertia at the CG around the Y axis
$I_{zz_{cg}}$	Airplane moment of inertia at the CG around the Z axis
ISA	International standard atmosphere
K_{f2}	Parameter of the fuselage contribution to the directional stability, that depends Of the fuselage shape and its projected side area (Typical between 1.3 to 1.4)
K_{STAT}	Static margin of the airplane
$K_2 - K_1$	Correction factor for the body (fuselage) fineness ratio
L	Lift generated by the airplane
L_m	Extended length of main landing gear
L_n	Extended length of nose landing gear
L_{ref}	Body reference length
L_A	Rolling moment due the ailerons deflection
LSA	Light sport airplane
L_{VT}	Lift generated by the vertical tail
L/D	Airplane aerodynamic efficiency
L'	Airfoil thickness location parameter

M	Flight Mach number
M_a	Pitch moment due the inercial force
M_{ac_h}	Horizontal tail pitch moment
$M_{ac_{wf}}$	Wing-Fuselage pitch moment
M_{mg}	Pitch moment at the main landing gear leg
M_{CAN_LOW}	Lower canard pitch moment
M_{CAN_UP}	Upper canard pitch moment
M_{FUS}	Fuselage canard pitch moment
M_{W_LOW}	Lower wing pitch moment
M_{W_UP}	Upper wing pitch moment
M_D	Airplane pitch moment due the drag
$M_{D_{CAN\_LOW}}$	Lower canard pitch moment due its own drag
$M_{D_{CAN\_UP}}$	Upper canard pitch moment due its own drag
$M_{D_{FUS}}$	Fuselage pitch moment due its own drag
$M_{D_{W\_LOW}}$	Lower wing pitch moment due its own drag
$M_{D_{W\_UP}}$	Upper wing pitch moment due its own drag
$M_{D_{VT\_LEF}}$	Left vertical tail pitch moment due its own drag
$M_{D_{VT\_RIG}}$	Right vertical tail pitch moment due its own drag
M_L	Airplane pitch moment due the lift
$M_{L_{CAN\_LOW}}$	Lower canard pitch moment due its own lift
$M_{L_{CAN\_UP}}$	Upper canard pitch moment due its own lift
$M_{L_{FUS}}$	Fuselage pitch moment due its own lift
M_{L_h}	Horizontal tail pitch moment due its own lift

$M_{L_{wf}}$	Wing-Fuselage pitch moment due its own lift
$M_{L_{W\_LOW}}$	Lower wing pitch moment due its own lift
$M_{L_{W\_UP}}$	Upper wing pitch moment due its own lift
M_T	Pitch moment due the propeller thrust
$MTOW$	Maximum take-off weight
M_W	Pitch momet due the airplane weight
N_{crew}	Number of crew
$N_{doub-halve}$	Number of cycles for doubling or halving the amplitude of an oscillatory motion
N_{eng}	Number of engines
N_{gear}	Landing load factor
N_t	Number of fuel tanks
N_y	Limit in flight load factor
N_A	Airplane yawing moment at the CG
$N_{L.U}$	Ultimate landing load factor
N_U	Ultimate in flight load factor
OEW	Operational empty weight
P	Period of an oscillatory motion
P_{climb}	Climb engine power
P_{TO}	Take-off power available corrected by the propeller efficiency
$P_{S_{TO}}$	Engine shaft power at the take-off phase
R	Range of cruise flight
R_{cf}	Canard-fuselage interference factor
Re	Reynolds number
R_{vtf}	Vertical tail-fuselage interference factor

R_{wf}	Wing-fuselage interference factor
R_{A_left}	Left aileron turning radius
R_{A_right}	Right aileron turning radius
R_{LS}	Lifting surface correction factor
R_T	Take-off runway distance
S	Aerodynamic surface reference area
S_{aero}	Surface or body aerodynamic area
$S_{aero_{CAN}}$	Canard aerodynamic area
$S_{aero_{CAN\_BIP}}$	Biplane total canard aerodynamic area
$S_{aero_{CAN\_LOW}}$	Lower canard aerodynamic area
$S_{aero_{CAN\_UP}}$	Upper canard aerodynamic area
$S_{aero_{VT}}$	Vertical tail aerodynamic area
$S_{aero_{VT\_LEF}}$	Left vertical tail aerodynamic area
$S_{aero_{VT\_RIG}}$	Right vertical tail aerodynamic area
$S_{aero_{W}}$	Wing aerodynamic area
$S_{aero_{W\_BIP}}$	Biplane total wing aerodynamic area
$S_{aero_{W\_LOW}}$	Lower wing aerodynamic area
$S_{aero_{W\_UP}}$	Upper wing aerodynamic area
S_{ail}	Total aileron area
$S_{b_{fus}}$	End of the fuselage cross section area
S_{fus}	Fuselage wetted area
S_p	Propeller disc loading area
$S_{pl_{fus}}$	Fuselage planform area on the plan xy

S_{rud}	Total rudder area
$S_{wet_{ap}}$	Airplane total wetted area
$S_{wet_{CAN\_fair\_lef}}$	Canards left fairing wetted area
$S_{wet_{CAN\_fair\_rig}}$	Canards right fairing wetted area
$S_{wet-fus}$	Fuselage wetted area
$S_{wet_{VT\_boom}}$	Vertical tail boom wetted area
$S_{wet_{LGEAR}}$	Landing gear wetted area
S_A	Aileron area
S_{CAN}	Canard reference area
S_{CAN_BIP}	Biplane canard reference area
S_{CAN_LOW}	Lower canard reference area
S_{CAN_UP}	Upper canard reference area
S_E	Total elevator area
SEP	Shaft engine power
SHP_{rated}	Shaft horse power for the actual flight condition
SFC	Specific fuel consumption
SFC_{CRU}	Specific fuel consumption during the cruise phase
SFC_{TO}	Specific fuel consumption during the take-off phase
$S_{F_{max-cs}}$	Fuselage maximum cross section area
S_{Flap}	Total area of flaps extended
S_{F_s}	Fuselage projected side area
S_{HT}	Horizontal tail reference area
S_R	Rudder area
S_S	Total airplane projected side area

S_T	Total biplane wing or canard reference area
S_{TO}	Total take-off distance
S_{TO_A}	Airborne take-off distance
S_{TO_G}	Ground take-off distance
S_{VT}	Vertical tail reference area
S_{VT_LEF}	Left vertical tail reference area
S_{VT_RIG}	Right vertical tail reference area
S_W	Wing reference area
S_{W_BIP}	Biplane wing reference area
S_{W_LOW}	Lower wing reference area
S_{W_UP}	Upper wing reference area
S_{W_f}	Wing flapped area
$S_{W_{wet}}$	Wing wetted area
$S_{W_{wet_{lam}}}$	Wing wetted area part exposed to laminar flow
T	Thrust generated by the propeller
TFW	Total fuel weight
TOP	Take-off parameter (used for estimate the take-off runway distance)
TOW	Take-off weight
$\bar{T}$	Mean thrust ratio at the speed $0.707 \cdot V_{LOF}$
U_0	Freestream velocity
U_1	Airplane landing speed
$V_{f.t}$	Total fuel tanks volume, gallon
V_{fu}	Total fuel volume, gallon
V_{max}	Airplane maximum flight speed

V_{A_left}	Aerodynamic speed at the left aileron
V_{A_right}	Aerodynamic speed at the right aileron
V_{CAN}	Canard volume coefficient
V_{CAN_LOW}	Lower canard volume coefficient
V_{CAN_UP}	Upper canard volume coefficient
V_{HT}	Horizontal tail volume coefficient
V_{MC}	Airplane minimum control speed
V_R	Airplane rotation speed during the take-off running
V_S	Stall speed
$V_{S_{TO}}$	Stall speed in the take-off configuration
V_{SO}	Stall speed at landing configuration
V_T	Airplane total speed or relative wind
V_{TD}	Airplane touch down speed
V_{TO}	Take-off speed
V_{VT}	Vertical tail volume coefficient
V_W	Cross wind speed
V_0	Cruise or Loiter phase flight speed
V_3	Speed at the obstacle
W	Airplane actual weight
$W_{Control.Surf}$	Primary flight control surfaces weight
W_e	Airplane weight at the end of the cruise flight
W_{empty}	Airplane operational empty weight
W_{eng}	Engine gross weight
W_{fuel}	Fuel weight

$W_{fuel.syst}$	Fuel system weight
W_{fus}	Fuselage weight
W_i	Airplane weight at the beginning of the cruise flight
W_l	Airplane landing gross weight
$W_{oil.syst}$	Oil system weight
$W_{payload}$	Payload weight
W_{pilot}	Pilot weight
W_{prop}	Propeller weight
W_{tire}	Weight carried by each main landing gear tire
W_{Elect_mod}	Avionics electronic modulus weight
$W_{Flap.cont.syst}$	Flap control system weight
$W_{Flig.cont.syst}$	Flight control system weight
W_{HT}	Horizontal tail weight
W_{MLG}	Main landing gear weight
W_{NLG}	Nose landing gear weight
W_{Seat_pil}	Pilot seat weight
W_{VT}	Vertical tail weight
W_W	Wing weight
W_0	Airplane Take-off gross weight
X_{fus}	Length of the fuselage
$X_{AC_{W\_B}}$	Location of the aerodynamic center of the biplane wing related its own leading edge
X_C	Length of the cockpit
X_{CG}	Airplane CG location along the x axis

$X_{LE_{mac_W}}$	Location along the x axis of the leading edge of the mean aerodynamic chord of the wing
$X_{LE_{\bar{C}_{W\_B}}}$	Location along the x axis of the leading edge of the mean aerodynamic chord of the biplane wing
X_N	Length of the fuselage nose
X_{NP}	Airplane neutral point location along the x axis
X_T	Length of the fuselage tail
X_{Thrust}	Negative for the propeller disc plane behind the CG
Y_C	Width of the cockpit (maximum fuselage width)
Z_{Thrust}	Negative for the propeller axis line above the CG
Z_W	Distance parallel to the z axis, from wing 25% of the chord point to the fuselage centerline

Greek Symbols

α	Angle of attack
$\alpha_{cl=0_{can}}$	Canards airfoil angle of attack for zero lift
$\alpha_{cl=0_{vt}}$	Vertical tail airfoil angle of attack for zero lift
$\alpha_{cl=0_{w}}$	Wings airfoil angle of attack for zero lift
α_{CAN_LOW}	Lower canard effective angle of attack
α_{CAN_UP}	Upper canard effective angle of attack
$\alpha_{CL=0_{CAN\_LOW}}$	Lower canard angle of attack for zero lift
$\alpha_{CL=0_{CAN\_UP}}$	Upper canard angle of attack for zero lift
$\alpha_{CL=0_{W\_LOW}}$	Lower wing angle of attack for zero lift
$\alpha_{CL=0_{W\_UP}}$	Upper wing angle of attack for zero lift

α_{HT}	Horizontal tail effective angle of attack
α_W	Wing effective angle of attack
α_{0_W}	Wing zero-lift angle relative to the fuselage reference line
β	Sideslip angle
δ_A	Aileron deflection
$\delta_{A.max}$	Aileron maximum deflection
δ_E	Elevator deflection
$\delta_{E.max}$	Elevator maximum deflection
δ_f	Flap deflection
$\delta_{flap.max}$	Maximum flaps deflection
δ_R	Rudder deflection
$\delta_{R.max}$	Rudder maximum deflection
δ_T	Thrust rate
ε	Downwash or upwash angle
ε_u	Upwash angle
ε_{CAN_LOW}	Lower canard downwash or upwash angle
ε_{CAN_UP}	Upper canard downwash or upwash angle
ε_{W_LOW}	Lower wing downwash or upwash angle
ε_0	Downwash or upwash angle for angle of attack equal to zero
$\varepsilon_{0_{CAN\_LOW}}$	Lower canard downwash or upwash angle for angle of attack equal to zero
$\varepsilon_{0_{CAN\_UP}}$	Upper canard downwash or upwash angle for angle of attack equal to zero
$\varepsilon_{0_{W\_LOW}}$	Lower wing downwash or upwash angle for angle of attack equal to zero
η	Governing factor of the damping of an oscillatory motion
η_{fus}	Ratio of the drag of a finite cylinder to the drag of an infinite cylinder

η_{CAN}	Canard efficiency factor (dynamic pressure rate on the canard)
η_{CAN_LOW}	Lower canard efficiency factor
η_{CAN_UP}	Upper canard efficiency factor
η_P	Propeller aerodynamic efficiency
η_{HT}	Horizontal tail efficiency factor (dynamic pressure rate between the horizontal tail and the wing); normally between 0.8 and 1.2
η_{VT}	Vertical tail efficiency factor (dynamic pressure rate on the vertical tail)
θ_0	Airplane initial pitch angle
$\ddot{\theta}$	Pitch moment angular acceleration
λ	Aerodynamic surface planform taper ratio
λ_{CAN}	Canard taper ratio
λ_{CAN_B}	Biplane canard taper ratio
λ_{CAN_LOW}	Lower canard taper ratio
λ_{CAN_UP}	Upper canard taper ratio
λ_{HT}	Horizontal tail taper ratio
λ_{VT}	Vertical tail taper ratio
λ_{VT_LEF}	Left vertical tail taper ratio
λ_{VT_RIG}	Right vertical tail taper ratio
λ_W	Wing taper ratio
λ_{W_B}	Biplane wing taper ratio
λ_{W_LOW}	Lower wing taper ratio
λ_{W_UP}	Upper wing taper ratio
μ	Dynamic viscosity of the fluid
μ	Ratio between the shorter span and the longer span of a biplane

μ_g	Wheel-ground rolling friction coefficient
μ_{CAN}	Ratio between the shorter span and the longer span of the biplane canard
μ_W	Ratio between the shorter span and the longer span of the biplane wing
μ'	Corrected wheel-ground rolling friction coefficient
ξ	Damping ratio of an oscillatory motion
π	Trigonometric ratio of the circumference
ρ_{cruise}	Air density at cruise altitude
ρ_{FL}	Air density at actual flight level
ρ_0	Air density at sea level
σ	Air density ratio
σ	Biplane Prandtl interference factor
σ	Airplane crab angle
σ	Sidewash angle
σ_{CAN}	Canard biplane Prandtl interference factor
σ_W	Wing biplane Prandtl interference factor
τ_A	Aileron effectiveness
τ_E	Elevator effectiveness
τ_R	Rudder effectiveness
$\emptyset_{prop}$	Propeller diameter
$\emptyset_{fus}$	Fuselage equivalent diameter
ω	Angular speed
ω	Damped natural frequency of an oscillatory motion
ω_n	Undamped natural frequency of an oscillatory motion
Δ_{cl}	Airfoil lift coefficient increment

$\left(\Delta_{cl_{max}}\right)_{base}$	Parameter based on a 25% “reference flap” chord to airfoil chord ratio
ΔAC_{CAN_LOW}	Shift on the aerodynamic center of the lower canard
ΔAC_{CAN_UP}	Shift on the aerodynamic center of the upper canard
ΔAC_{W_LOW}	Shift on the aerodynamic center of the lower wing
ΔAC_{W_UP}	Shift on the aerodynamic center of the upper wing
ΔCl_{β}	Airplane increment of the rolling moment rate coefficient
$\Delta CL_{\alpha_{CAN\_LOW}}$	Lower canard increment or decrement on the lift curve sole due the global wash field
$\Delta CL_{\alpha_{CAN\_UP}}$	Upper canard increment or decrement on the lift curve sole due the global wash field
$\Delta CL_{\alpha_{W\_LOW}}$	Lower wing increment on the lift curve sole due the global wash field
$\Delta CL_{\alpha_{W\_UP}}$	Upper wing increment on the lift curve sole due the global wash field
ΔL_A	Wing lift increment or decrement due the ailerons deflection
E	Global wash filed angle
E_{CAN_LOW}	Lower canard global wash field angle
E_{CAN_UP}	Upper canard global wash field angle
E_0	Global wash field angle for angle of attack equal to zero
φ	Bank angle
Γ	Aerodynamic surface dihedral angle
Γ_{CAN}	Canard dihedral angle
Γ_{CAN_B}	Biplane canard dihedral anlge
Γ_{CAN_LOW}	Lower canard dihedral angle
Γ_{CAN_UP}	Upper canard dihedral angle
Γ_{VT_LEF}	Left vertical tail dihedral angle

Γ_{VT_RIG}	Right vertical tail dihedral angle
Γ_{W}	Wing dihedral angle
Γ_{W_B}	Biplane wing dihedral angle
Γ_{W_LOW}	Lower wing dihedral angle
Γ_{W_UP}	Upper wing dihedral angle
Λ	Aerodynamic surface sweep angle
$\Lambda_{t_{max}}$	Sweep angle of the line connecting the point of maximum thickness on each airfoil of the wing.
Λ_{CAN}	Canard sweep angle at 25% of $\bar{C}_{CAN}$
Λ_{CAN_LOW}	Lower Canard sweep angle at 25% of $\bar{C}_{CAN\_LOW}$
Λ_{CAN_UP}	Upper Canard sweep angle at 25% of $\bar{C}_{CAN\_UP}$
Λ_{HT}	Horizontal tail sweep angle at 25% of $\bar{C}_{HT}$
$\Lambda_{L.E}$	Aerodynamic surface leading edge sweep angle
Λ_{VT}	Vertical tail sweep angle at 25% of $\bar{C}_{VT}$
Λ_{VT_LEF}	Left vertical tail sweep angle at 25% of $\bar{C}_{VT\_LEF}$
Λ_{VT_RIG}	Right vertical tail sweep angle at 25% of $\bar{C}_{VT\_RIG}$
Λ_{W}	Wing sweep angle at 25% of $\bar{C}_{W}$
Λ_{W_B}	Biplane wing sweep angle at 25% of $\bar{C}_{W\_B}$
Λ_{W_LOW}	Lower wing sweep angle at 25% of $\bar{C}_{W\_LOW}$
Λ_{W_UP}	Upper wing sweep angle at 25% of $\bar{C}_{W\_UP}$

SUMMARY

CHAPTER 1 - INTRODUCTION.....6
1.1. ABOUT THE NEW AIRPLANE..... 6
1.2. BRIEF HISTORICAL PERSPECTIVE 9
1.3. BIBLIOGRAPHIC REVIEW 14
CHAPTER 2 - AIRPLANE DESIGN THEORY.....15
2.1. CONCEPTUAL DESIGN..... 15
2.1.1. General configuration..... 16
2.1.2. Drag polar estimate 20
2.1.3. Weight estimate 23
2.1.4. Performance estimate 27
2.1.5. Sizing estimate 35
2.1.6. Parts weights estimate 41
2.1.7. CG-Weight envelope diagram estimate..... 42
2.2. SELECTION OF MATERIALS..... 43
2.3. ERGONOMICS..... 44
2.4. AERODYNAMICS..... 47
2.4.1. 2D – Aerodynamics..... 47
2.4.1.1. Airfoil lift..... 47
2.4.1.2. Airfoil drag..... 54
2.4.1.3. Airfoil pitch moment..... 55
2.4.1.4. Reynolds number..... 56
2.4.2. 3D – Aerodynamics..... 56
2.4.2.1. Biplane configuration..... 56
2.4.2.2. Canard configuration 59
2.4.2.3. Pusher configuration..... 60
2.4.2.4. Lift 61
2.4.2.5. Drag..... 67
2.4.2.6. Pitch moment 76

2.4.2.7. Wash fields 77
2.4.2.8. Aerodynamic centers 82
2.5. DYNAMICS OF FLIGHT 85
2.5.1. Longitudinal static stability 89
2.5.1.1. Wings contribution 90
2.5.1.2. Canards contribution 90
2.5.1.3. Fuselage contribution 93
2.5.1.4. Stick fixed neutral point & Static margin 94
2.5.2. Longitudinal control 94
2.5.2.1. Elevator dimensioning considerations 95
2.5.2.2. Longitudinal control derivatives 95
2.5.2.3. Take-off rotation 96
2.5.2.4. Longitudinal trim 97
2.5.3. Lateral static stability 98
2.5.4. Lateral control 100
2.5.4.1. Aileron dimensioning considerations 100
2.5.4.2. Rolling estimate 102
2.5.4.3. Lateral stability and control derivatives 103
2.5.5. Directional static stability 104
2.5.5.1. Wing-Fuselage contribution 105
2.5.5.2. Vertical tails contribution 106
2.5.6. Directional control 106
2.5.6.1. Rudder dimensioning considerations 107
2.5.6.2. Yawing estimate 108
2.5.6.3. Directional stability and control derivatives 111
2.5.7. Lateral-Directional static stability & control coupling 113
2.5.8. Longitudinal dynamic stability 114
2.5.8.1. Longitudinal characteristic equation 115
2.5.8.2. Longitudinal state equation 116
2.5.8.3. Longitudinal stability and control derivatives 117
2.5.8.4. Longitudinal flying qualities considerations 119

2.5.9. Lateral-Directional dynamic stability 121
2.5.9.1. Lateral-Directional characteristic equation 123
2.5.9.2. Lateral-Directional state equation 124
2.5.9.3. Lateral-Directional stability and control derivatives 125
2.5.9.4. Lateral-Directional flying qualities considerations 126
2.6. PERFORMANCE 127
2.6.1. Excess of power and thrust 128
2.6.2. Take-off performance 128
2.6.3. Climb performance 130
2.6.3.1. Rate of climb 130
2.6.3.2. Climb gradient 130
2.6.3.3. Flight ceiling 131
2.6.4. Cruise performance 131
2.6.5. Descent performance 131
2.6.6. Landing performance 132
2.7. LOADS 132
2.7.1. Maneuver V-n diagram 133
2.7.1.1. Design airspeeds 133
2.7.1.2. Limit maneuvering load factors 134
2.8. STRUCTURAL LAYOUT 135
2.8.1. Wing structural layout 135
2.8.2. Horizontal & Vertical tail structural layout 137
2.8.3. Fuselage structural layout 137
2.9. LANDING GEAR SYSTEM 138
2.9.1. Main landing gear leg considerations 139
2.9.2. Nose landing gear leg considerations 139
2.9.2.1. Castoring wheel geometry 139
2.9.3. Tire sizing 140
CHAPTER 3 - DESIGN, DIMENSIONING & SPECIFICATION 142
3.1. CONCEPTUAL DESIGN 142
3.1.1. General configuration 143

3.1.2. Drag polar estimate 144
3.1.3. Weight estimate 145
3.1.4. Performance estimate 147
3.1.5. Sizing estimate 149
3.1.6. Parts weights estimate 152
3.1.7. CG-Weight envelope diagram estimate 153
3.2. SELECTION OF MATERIALS 154
3.2.1. Selected material 154
3.2.2. Material properties 156
3.3. ERGONOMICS 158
3.3.1. Human body 159
3.3.2. Cockpit design 162
3.4. AERODYNAMICS 165
3.4.1. 2D – Aerodynamics 165
3.4.1.1. Airfoils preselection 165
3.4.1.2. Wings airfoil 168
3.4.1.3. Canards airfoil 174
3.4.1.4. Vertical tails airfoil 177
3.4.2. 3D – Aerodynamics 178
3.4.2.1. Biplane wing 178
3.4.2.2. Lower Wing 179
3.4.2.3. Upper Wing 183
3.4.2.4. Biplane canard 185
3.4.2.5. Lower canard 186
3.4.2.6. Upper canard 189
3.4.2.7. Vertical tails 190
3.4.2.8. Fuselage 192
3.4.2.9. Complete airplane 192
3.5. DYNAMICS OF FLIGHT 198
3.5.1. Longitudinal static stability 201
3.5.2. Longitudinal control 204

3.5.2.1. Elevators parameters 206
3.5.3. Lateral static stability 207
3.5.4. Lateral control 207
3.5.4.1. Ailerons parameters 208
3.5.5. Directional static stability 209
3.5.6. Directional control 211
3.5.6.1. Rudders parameters 212
3.5.7. Lateral-Directional static stability & control coupling 213
3.5.8. Longitudinal dynamic stability 213
3.5.9. Lateral-Directional dynamic stability 216
3.6. PERFORMANCE 220
3.6.1. Excess of power and thrust 220
3.6.2. Take-off performance 225
3.6.3. Climb performance 226
3.6.4. Cruise performance 227
3.6.5. Descent performance 228
3.6.6. Landing performance 228
3.7. LOADS 229
3.8. STRUCTURAL LAYOUT 230
3.8.1. Wing structural layout 230
3.8.2. Canards & Vertical tail structural layout 232
3.8.2.1. Canards structural layout 232
3.8.2.2. Vertical tails structural layout 233
3.8.3. Fuselage structural layout 235
3.9. LANDING GEAR SYSTEM 237
3.9.1. Landing gear legs locations & considerations 237
3.9.2. Tires dimensioning 239
3.9.3. Shock absorber considerations 240
3.9.4. Steering considerations 240
3.9.5. Breaking system 241
3.10. FUEL SYSTEM 241

3.11. PROPULSIVE SYSTEM 242
3.11.1. Engine 242
3.11.2. Propeller 242
3.12. AVIONIC SYSTEM 243
3.12.1. Main suite 244
3.12.2. Redundancy suite 246
3.12.3. Communication suite 246
3.12.4. Avionic panel layout 247
3.13. ELECTRICAL SYSTEM 248
CHAPTER 4 - TECHNICAL DESCRIPTION 250
4.1. External dimensions 250
4.1.1. Wings 250
4.1.1.1. Biplane wing 250
4.1.1.2. Lower wing 251
4.1.1.3. Upper wing 251
4.1.2. Canards 252
4.1.2.1. Biplane canard 252
4.1.2.2. Lower canard 252
4.1.2.3. Upper canard 253
4.1.3. Vertical tails 253
4.1.3.1. Left vertical tail 253
4.1.3.2. Right vertical tail 254
4.1.4. Fuselage 254
4.2. Airplane views 255
4.3. Airplane internal compartments 256
CHAPTER 5 - CONCLUSION 257
REFERENCES 261
APPENDIX A 265
APPENDIX B 271
APPENDIX C 288
APPENDIX D 387

APPENDIX E **390**
APPENDIX F **391**
APPENDIX G **392**
APPENDIX H **396**
APPENDIX I **398**

INTRODUCTION

CHAPTER I

1.1. ABOUT THE NEW AIRPLANE

The development of a complete new airplane always was the intention for the conclusion of the undergraduation in aeronautical engineering, evolving for what is presented in this work.

The intention was to develop an airplane that it would have a very specific mission, involving theoretical and practical aspects and with an unconventional configuration.

The mission of the aircraft here developed is to serve as a technical platform for the development of studies on the aeronautical engineering, being used at the undergraduation as well as on the post-graduation levels, what would involve activities since its design, manufacturing and flying. Its main purpose is to be a flying laboratory, so as can be noted, the primary mission of this airplane do not consider basic characteristics as the flight altitude, cruise speed, range, etc, though these characteristics had been defined below.

$$V_{cruise} = 170\ [k\,m/h]$$

$$FL_{cruise} = 8000\ [ft]$$

$$R = 600.0\ [km]$$

As complementary specification, this aircraft should be easy and safe to pilot, it should be able to receive flight test instrumentation. The airplane UFU-1 will be certified for at the experimental categories, but, complying the FAR 23 when possible.

Quickly the intention of developing this airplane evolved for to be a tribute to the Alberto Santo Dumont and his 14bis presented on the Figure 1.1. At this moment the configuration of the airplane was decided, it should be a biplane equipped with canard and one pusher engine as presented on the Figure 1.2 and Figure 1.3, and its designation should be UFU-1 due the fact this airplane to be the first to be built at the Universidade Federal de Uberlândia.

The intent of this work was to develop the preliminary design of the airplane UFU-1 considering the ergonomics, aerodynamics, dynamics of flight and performance, the other

technical aspects were developed as required just to support these four technologies described here. Was considered convenient to present the theory and results obtained during the conceptual design phase, intending to show how the airplane was conceived.

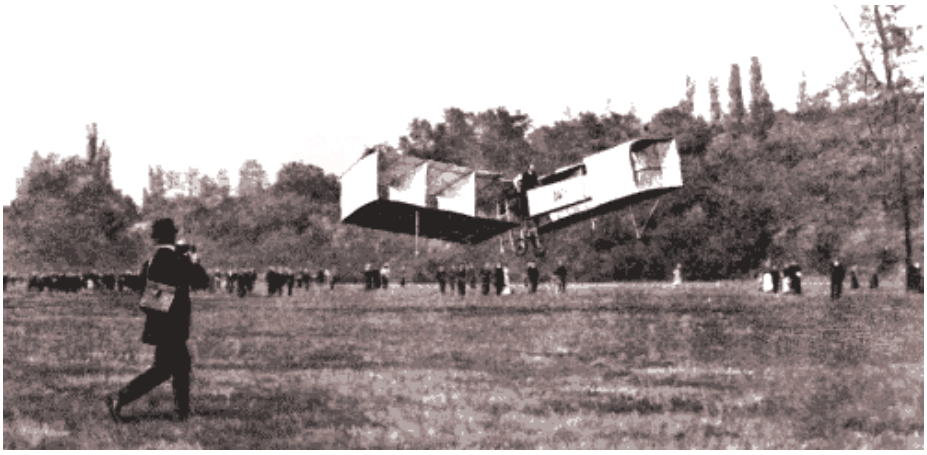


Figure 1.1 - 14Bis flight on October 23th, 1906. (Available in: <https://www.google.com.br/search?q=14bis&tbm=isch&tbo=u&source=univ&sa=X&ved=0ahUKEwic5f-T6NfWAhXFFpAKHas-B2kQsAQIQA&biw=1366&bih=651>. Access in november 11, 2017)

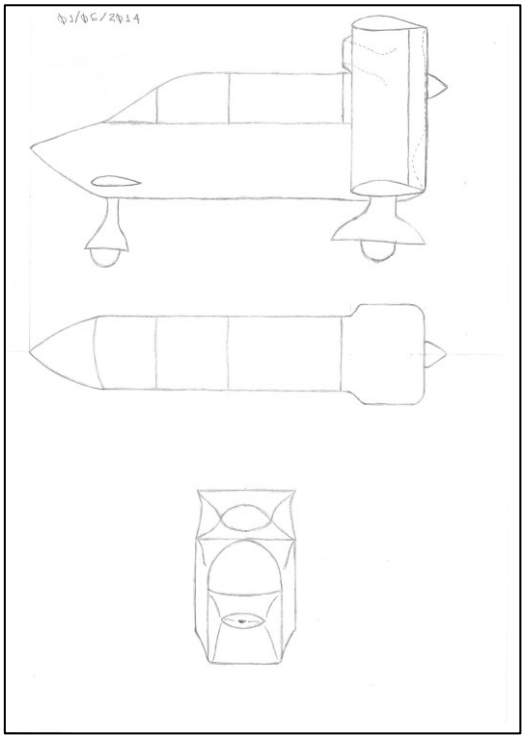


Figure 1.2 - Airplane UFU-1 initial sketch.

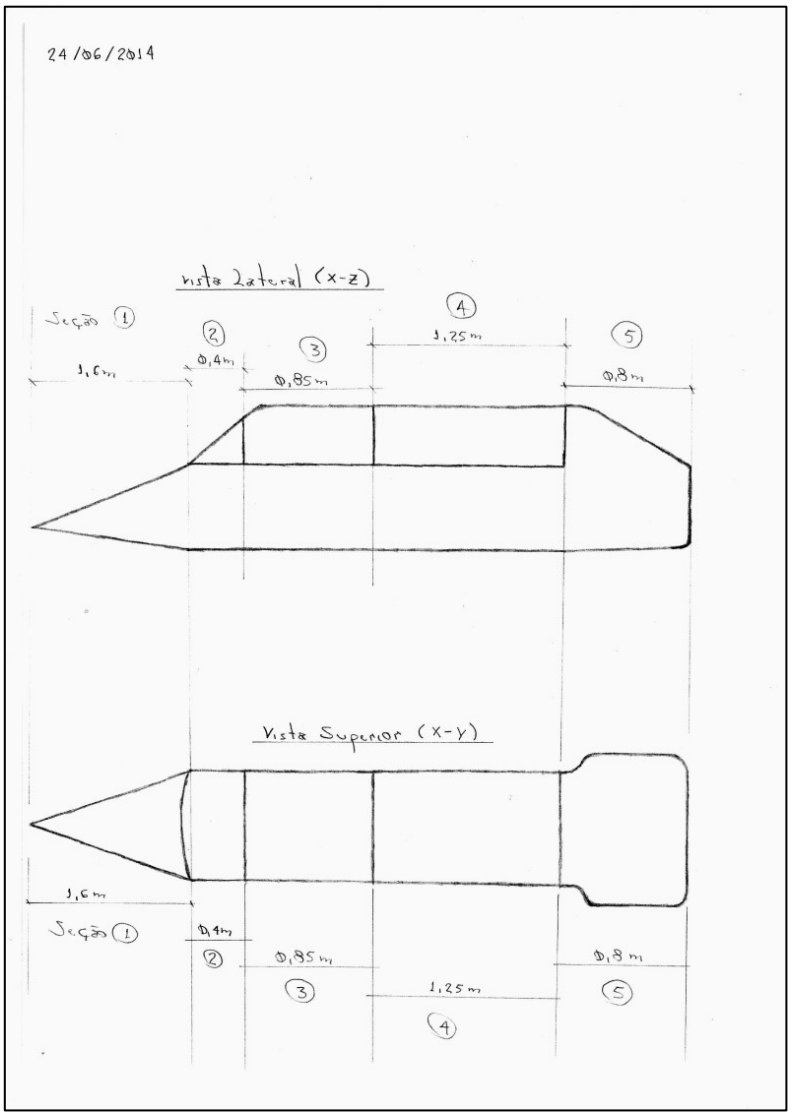


Figure 1.3 - Airplane UFU-1 initial sketch.

After this decision and with the initial activities initiated, was noted one obvious detail that had been escaped, the 14bis conceived by Santos Dumont was equipped with a two planes canard as is the wing, what was incorporated on the design of the airplane UFU-1 which has its final design presented on the Figure 1.4. Additionally the project should be cheap and easy to build having for example the same wing body for both lower and upper wing, and the same being valid for both canards and both vertical tails.

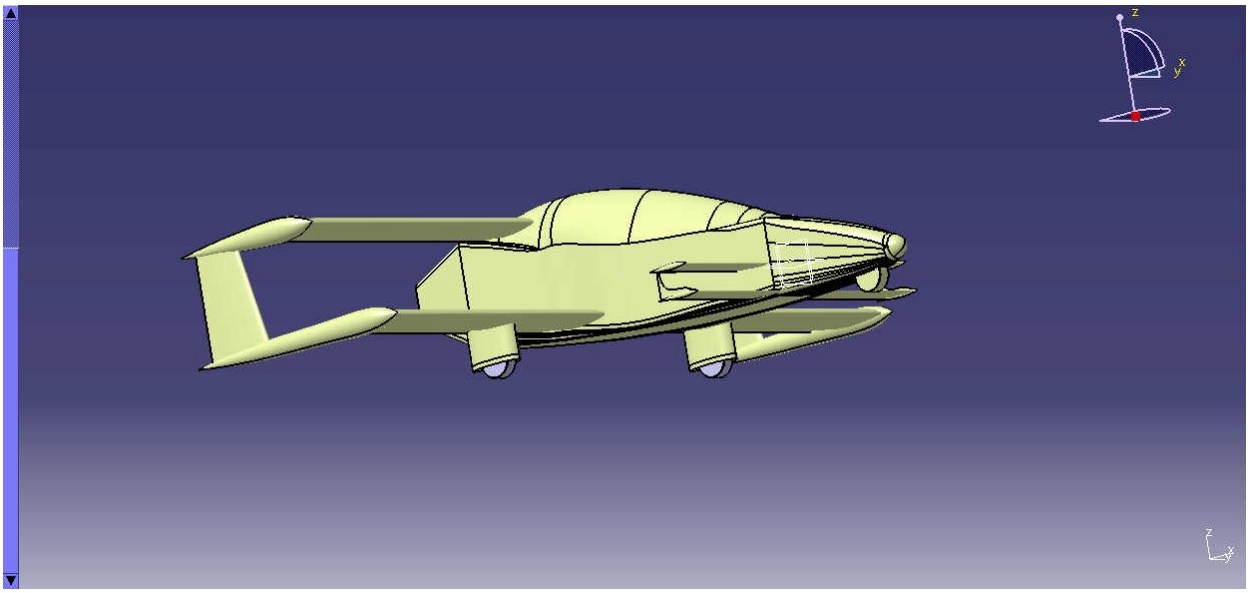


Figure 1.4 - Airplane UFU-1 final drawing.

1.2. BRIEF HISTORICAL PERSPECTIVE

The dawn of the aviation is characterized by aircrafts that employed the biplane wing configuration as the 14bis showed on the Figure 1.5, and the Wright brothers's Flyer I showed on the Figure 1.6 that probably were the two more iconic airplanes of this historical moment.

This configuration was the standard until the time of the first Great War, when practically all the airplane models conceived were biplane wing as showed on the Figure 1.8 or even triplane as the famous Fokker Dr.I piloted by the red baron and showed on the Figure 1.7.

During the beginning of the period between wars the aeronautical engineering evolved for airplane configurations characterized by only one wing located high on the fuselage with strut-braced or parasol configuration as showed on the Figure 1.9, and at the end of this period the airplanes had already evolved for configuration monoplane with low wing many times cantilever as showed on the Figure 1.10, this evolution was possible due the aeronautical material development with the employment of metal alloys basically the aluminum.

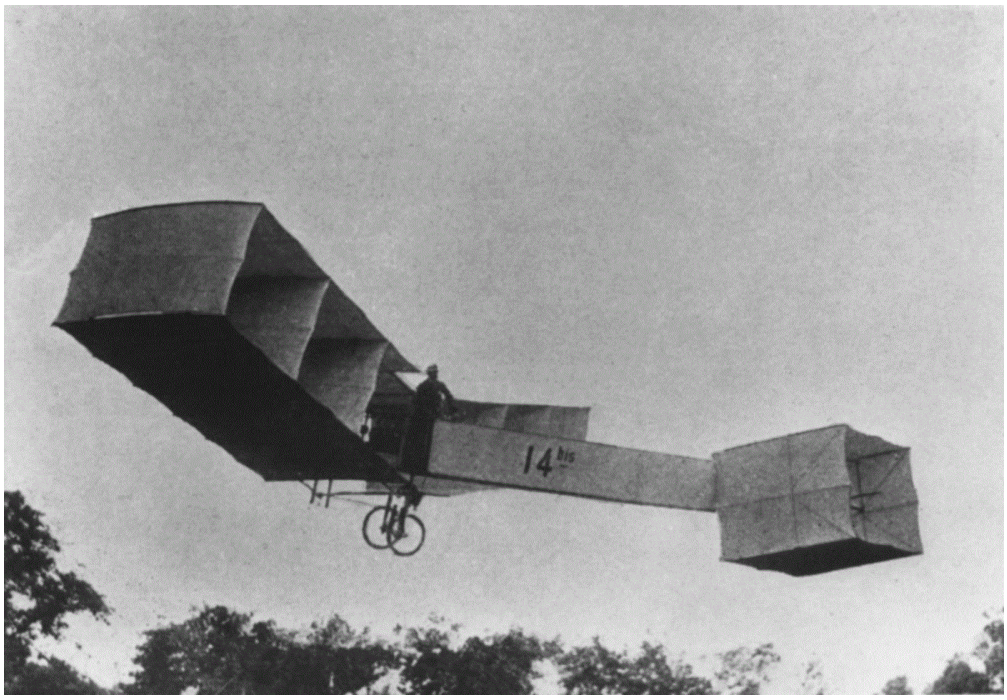


Figure 1.5 - 14bis at flight. (Available in:

<https://www.google.com.br/search?q=14bis&tbm=isch&tbo=u&source=univ&sa=X&ved=0ahUKEwic5f-T6NfWAhXFFpAKHas-B2kQsAQIQA&biw=1366&bih=651>. Access in november 11, 2017)

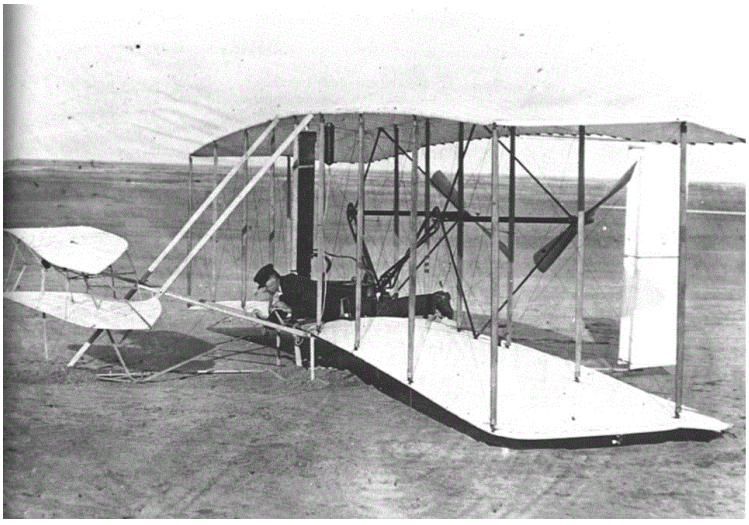


Figure 1.6 - Wright brothers's Flyer I. (Available in:

<https://www.google.com.br/search?biw=1366&bih=651&tbm=isch&sa=1&q=FLYER+I+WRITE+BROTHERS&oq=FLYER+I+WRITE+BROTHERS&gs_l=psy-ab.3...185598.208467.0.209760.30.27.2.0.0.0.428.3789.2j16j4j0j1.23.0....0...1.1.64.psy-ab..6.9.1538...0j0i67k1.0.OHOkrI57P7A#imgrc=_&spf=1507149400162>. Access in november 11, 2017)

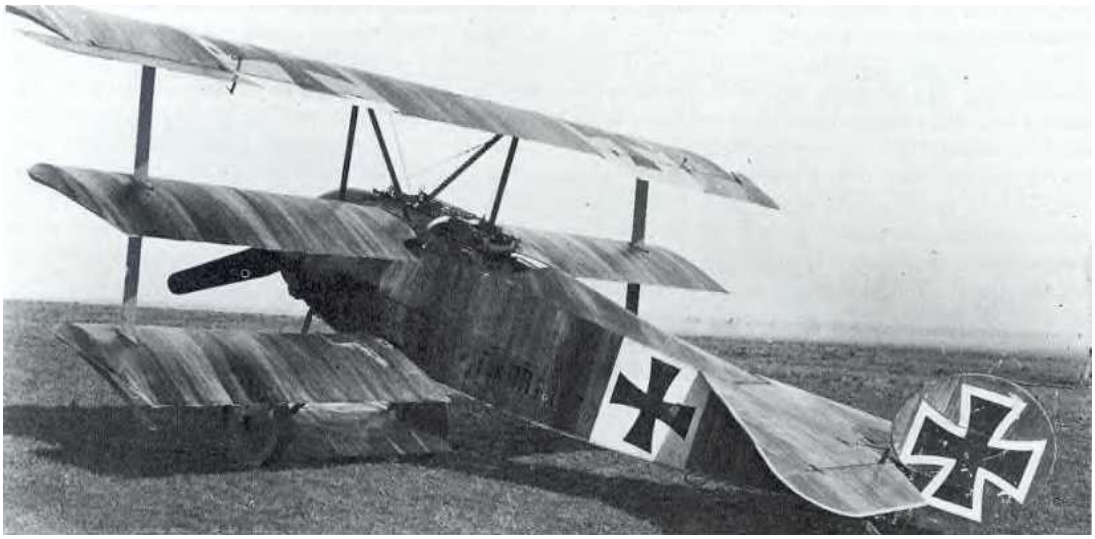


Figure 1.7 - Red baron airplane, Fokker Dr.I. (Available in:

<https://www.google.com.br/search?q=bar%C3%A3o+vermelho+avi%C3%A3o&tbm=isch&tbo=u&source=univ&sa=X&ved=0ahUKEwi9ksj169fWAhUCP5AKHTZIAIIQsAQIRA&biw=1366&bih=651#imgrc=_&spf=1507150197293>. Access in november 11, 2017)



Figure 1.8 - Airplane Spad 13, first great war. (Available in:

<https://www.google.com.br/search?q=Airplane+Spad+13&tbm=isch&tbo=u&source=univ&sa=X&ved=0ahUKEwicsYP87NfWAhXDE5AKHbaHCMYQsAQIQA&biw=1366&bih=651#imgrc=_&spf=1507150916189>. Access in november 11, 2017)



Figure 1.9 - Airliner Fokker F-10, from 1927. (Available in: <https://en.wikipedia.org/wiki/Fokker_F.10>. Access in november 11, 2017)



Figure 1.10 - Douglas DC-3, introduction in service in 1936. (Available in: <https://pt.wikipedia.org/wiki/Douglas_DC-3>. Access in november 11, 2017)

Despite the canard had its origin in the dawn of the aviation, such configuration stood practically forgotten until the 60th decade of the twentieth century, when the military

manufacturers revived this configuration as showed on the Figure 1.11. From the 70th decade such configuration started to be employed on civil airplanes of the general/executive and experimental/homebuilt categories as showed on the Figure 1.12, but, always as an exception much more than a trend. This is justified by its technical aspects related mainly to dynamics of flight, which if not treated adequately, is destabilizing.



Figure 1.11 - North American XB-70 Valkyrie, before first flight on September 21th, 1964. (Available in: <https://en.wikipedia.org/wiki/North_American_XB-70_Valkyrie>. Access in november 11, 2017)



Figure 1.12 - Beechcraft Starship, executive airplane. (Available in: <https://en.wikipedia.org/wiki/Beechcraft_Starship>. Access in november 11, 2017)

1.3. BIBLIOGRAPHIC REVIEW

The design of conventional configuration airplanes is well known and has a rich literature that provides a huge volume of theory, covering the different technologies involved on the design of an airplane.

As will be detailed along this work, due the very particular configuration of the aircraft conceived, probably unique considering the aeronautical engineering developed after the pioneers of the aviation, all the literature available for conventional and even unconventional configurations showed to be insufficient, thus, adaptations on that theory and suggestion of theory had to be proposed and applied on the development of the airplane UFU-1.

Besides all the bibliography indicated at the end of this work, were done surveys at internet sites dedicated to provide technical publications and sites of institutions dedicated to the aerospace field of the knowledge, and again, were not found airplanes with similar configuration or theory proposition as that done into this text.

AIRPLANE DESIGN THEORY

CHAPTER II

This chapter of the text presents the theory used and proposed on the development of the airplane UFU-1.

The development of a new aircraft is a multidisciplinary activity involving multiple technologies that can be classified in three groups, the first relative to aerodynamics, the second relative to structure and the third relative to the several systems that are present on an aircraft.

As all these technologies are dependent from each other and impacts each other, such development must conduct activities relative to each of these technologies at the same time, turning this, a very complex and hard work. This chapter was organized in a way that, the sequence of disciplines was considered intuitive, logical and didactic.

2.1. CONCEPTUAL DESIGN

The first activities done when a new airplane is conceived are related to its mission, it is necessary define for what this airplane is been developed. The airplane will transport passengers, cargo, or will be employed on aeromedical service or yet, will be employed on military activities, for example. Therefore some design parameter known as technical specification must be defined as, the number of crew, passengers, load to be carried, speed and altitude of cruise flight, range and endurance, distance of take-off and landing and others.

Initially the conceptual design was developed using the theory which apply statistical historical parameters along the classes activities of the discipline *"Projeto de aeronaves I"*, during this phase, were selected parameters that most approximates to the configuration of the airplane here proposed. A succinct presentation of this theory is showed on this topic.

During this phase there is defined the basic configuration of the airplane as number and geometry of the wing, geometry of the tail and fuselage. There is defined to, the propulsion system, as for example, propelled or jet; there are specified the avionic system, and landing gear system. Finally there are defined the materials to be employed on construction of the airplane.

2.1.1. General configuration

Regarding the aerodynamic configuration, some parameters are defined during the conceptual design as aerodynamic surfaces span, chord, aspect ratio, planform taper ratio, mean aerodynamic chord, sweep angle, dihedral angle and incidence angle, some of these parameters are presented on Figure 2.1 to Figure 2.4.

$$AR = \frac{b^2}{S} \tag{2.1}$$

$$\lambda = \frac{C_{tip}}{C_{root}} \tag{2.2}$$

$$\bar{C} = \frac{2}{3} \cdot C_{root} \cdot \left(\frac{1+\lambda+\lambda^2}{1+\lambda}\right) \tag{2.3}$$

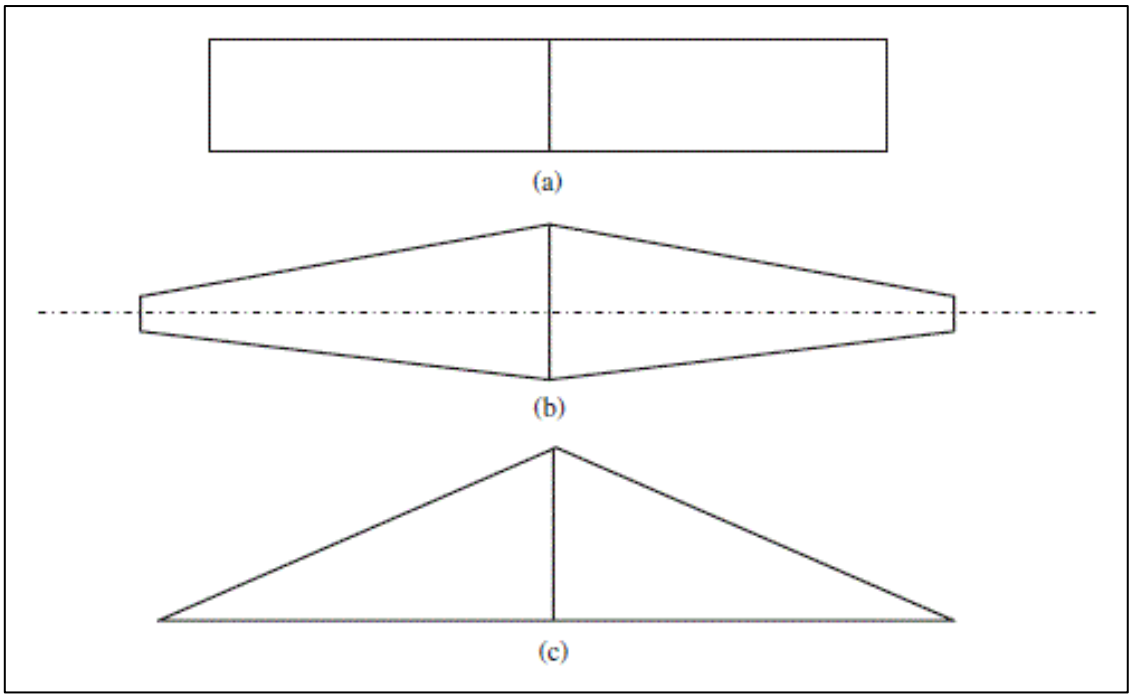


Figure 2.1 - Wings with various taper ratios: (a) Rectangle (λ = 1); (b) Trapezoid 0 < λ < 1 (straight tapered); and (c) Triangle (delta) λ = 0 (Sadraey, 2013).

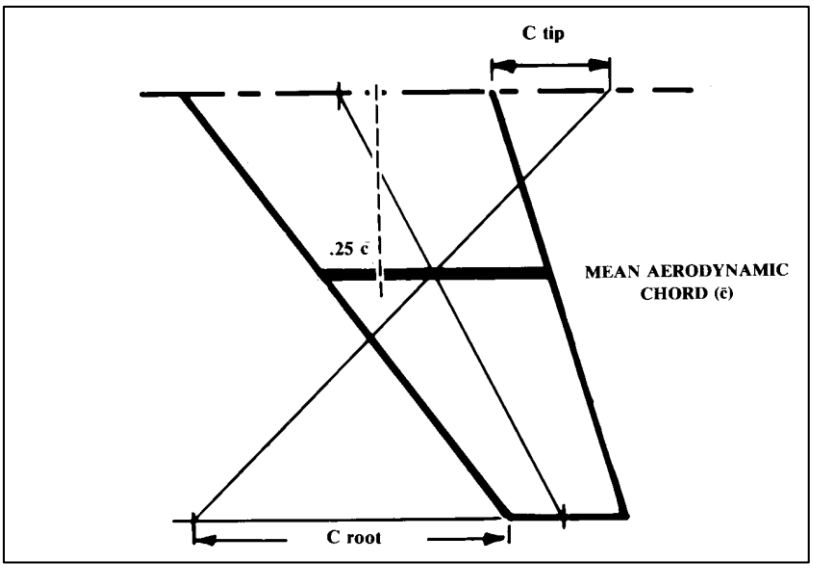


Figure 2.2 - Mean aerodynamic chord (Raymer, 2006).

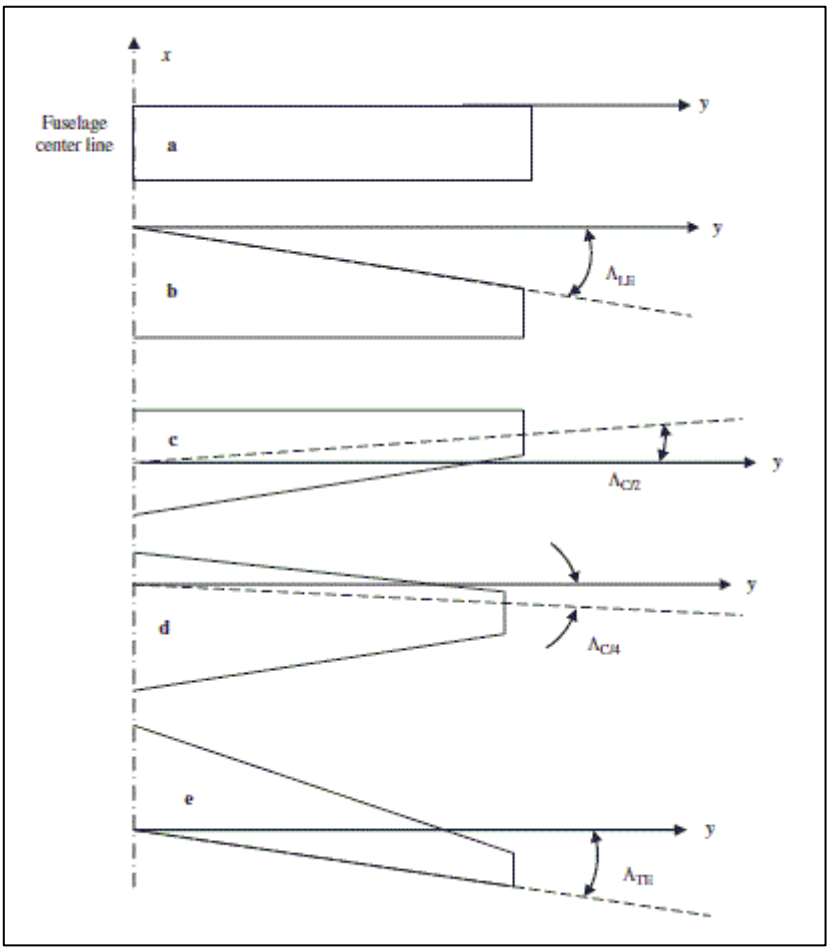


Figure 2.3 - Five wings with different sweep angles (Sadraey, 2013).

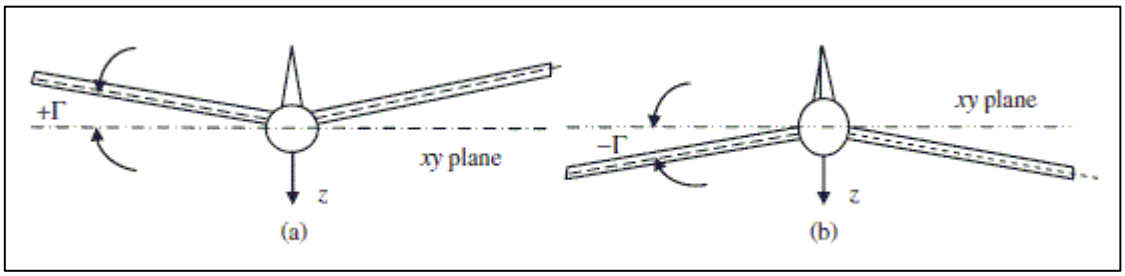


Figure 2.4 - Dihedral and anhedral angles (Sadraey, 2013).

For the parameter above, there are some historical values presented on the Table 2.1 to Table 2.4.

Table 2.1 - Historical tendencies data for wing aspect ratio and taper ratio (After Venson, 2013).

Airplane Category	***AR***	***λ***
Glider	19.8 ± 4.4	0.2 to 0.5
Motorglider	21.2 ± 8.0	0.2 to 0.5
LSA or Homebuilt	6.4 ± 2.1	0.5 to 1.0
General aviation and utility single-engine piston	7.2 ± 1.2	0.5 to 1.0
General aviation and utility single-engine turboprop	8.4 ± 2.1	0.5 to 1.0
General aviation and utility multi-engine piston	7.8 ± 0.7	0.5 to 1.0
General aviation and utility multi-engine turboprop	9.1 ± 1.4	0.5 to 1.0
Acrobatic airplane	5.6 ± 1.4	0.3 to 0.8
Agricultural airplane	6.9 ± 1.3	0.5 to 1.0
Amphibious airplane single-engine or multi-engine	7.1 ± 1.7	0.5 to 0.8
II WW fighter propeller	6.2 ± 0.8	0.5 to 0.8
Training jet airplane	5.7 ± 1.0	0.3 to 0.6
Fighter jet airplane	3.9 ± 1.5	0.3 to 0.5
Cargo or bomber propeller	9.6 ± 1.5	0.5 to 0.8
Cargo or bomber jet	7.3 ± 1.6	0.3 to 0.5
Passenger airplane propeller	10.1 ± 1.5	0.5 to 0.8
Passenger airplane jet	8.3 ± 1.0	0.3 to 0.5
Executive jet	8.0 ± 1.3	0.3 to 0.5

Table 2.2 - Historical tendencies data for wing dihedral (After Venson, 2013).

Airplane Category	***Low wing***	***Medium wing***	***High wing***
Wing without sweep	5º to 7º	2º to 4º	0º to 2º
Subsonic airplane with sweep	3º to 7º	-2º to 2º	-5º to -2º
Supersonic airplane with sweep	0º to 5º	-5º to 0º	-5º to -0º

Table 2.3 - Historical tendencies data for horizontal tail aspect ratio and taper ratio (After Venson, 2013).

Airplane Category	***AR***	***λ***
Glider and Motorglider	3.5 ± 0.8	0.2 to 0.5
LSA or Homebuilt	3.2 ± 1.1	0.5 to 1.0
General aviation and utility single-engine propeller, Conventional tail	3.9 ± 0.6	0.5 to 1.0
General aviation and utility single-engine propeller, T tail	4.1 ± 0.6	0.5 to 1.0
General aviation and utility multi-engine propeller, Conventional tail	4.3 ± 1.1	0.5 to 1.0
General aviation and utility multi-engine propeller, T tail	4.4 ± 1.1	0.5 to 1.0
Acrobatic airplane	2.8 ± 0.7	0.3 to 0.8
Agricultural airplane	3.5 ± 0.7	0.5 to 1.0
Amphibious airplane single-engine or multi-engine	3.6 ± 0.9	0.5 to 0.8
II WW fighter propeller	3.1 ± 0.4	0.5 to 1.0
Training jet airplane	2.9 ± 0.5	0.3 to 0.8
Fighter jet airplane	2.5 ± 1.0	0.3 to 0.8
Cargo or bomber propeller, Conventional tail	4.8 ± 0.8	0.4 to 0.6
Cargo or bomber propeller, T tail	5.0 ± 0.8	0.4 to 0.6
Cargo or bomber jet, Conventional tail	3.9 ± 0.5	0.3 to 0.5
Cargo or bomber jet, T tail	4.9 ± 0.2	0.3 to 0.5
Passenger airplane propeller, Conventional tail	5.2 ± 0.7	0.4 to 0.7
Passenger airplane propeller, T tail	5.5 ± 0.4	0.4 to 0.7
Passenger airplane jet, Conventional tail	4.3 ± 0.6	0.3 to 0.5
Passenger airplane jet, T tail	4.4 ± 0.7	0.3 to 0.5
Executive jet, Conventional tail	4.6 ± 0.7	0.4 to 0.6
Executive jet, T tail	4.8 ± 0.9	0.4 to 0.6

Table 2.4 - Historical tendencies data for vertical tail aspect ratio and taper ratio (After Venson, 2013).

Airplane Category	***AR***	***λ***
Glider and Motorglider	1.1 ± 0.2	0.2 to 0.5
LSA or Homebuilt	1.3 ± 0.3	0.3 to 0.6
General aviation and utility single-engine propeller, Conventional tail	1.5 ± 0.3	0.5 to 1.0
General aviation and utility single-engine propeller, T tail	1.2 ± 0.2	0.5 to 1.0
General aviation and utility multi-engine propeller, Conventional tail	1.4 ± 0.3	0.4 to 0.7
General aviation and utility multi-engine propeller, T tail	1.0 ± 0.2	0.4 to 0.7
Acrobatic airplane	1.2 ± 0.3	0.4 to 0.7
Agricultural airplane	1.4 ± 0.2	0.4 to 0.7
Amphibious airplane single-engine or multi-engine	1.6 ± 0.3	0.4 to 0.7
II WW fighter propeller	0.9 ± 0.2	0.4 to 0.7
Training jet airplane	0.9 ± 0.4	0.2 to 0.6
Fighter jet airplane	0.6 ± 0.3	0.2 to 0.6
Cargo or bomber propeller, Conventional tail	1.5 ± 0.3	0.3 to 0.5
Cargo or bomber propeller, T tail	1.2 ± 0.3	0.5 to 0.7
Cargo or bomber jet, Conventional tail	1.5 ± 0.3	0.3 to 0.5
Cargo or bomber jet, T tail	1.2 ± 0.1	0.7 to 0.9
Passenger airplane propeller, Conventional tail	1.4 ± 0.5	0.4 to 0.6
Passenger airplane propeller, T tail	1.4 ± 0.4	0.5 to 0.7
Passenger airplane jet, Conventional tail	1.6 ± 0.3	0.3 to 0.5
Passenger airplane jet, T tail	1.0 ± 0.2	0.5 to 0.7
Executive jet, Conventional tail	1.6 ± 0.4	0.3 to 0.5
Executive jet, T tail	1.0 ± 0.2	0.5 to 0.7

2.1.2. Drag polar estimate

The drag polar is a graph that shows the variation of the drag as the lift of the airplane is changed, it is most common to present the drag polar in terms of the aerodynamic coefficients CL and CD. When there is not enough information about the geometry and aerodynamic

properties of an airplane, as at the beginning of the development of a new airplane, as typically, at the conceptual design phase, the following estimation for the drag polar is taken.

The drag polar has two components, one relative to parasite drag end the other is related to the induced drag, this relation between lift and drag is defined by the Equation 2.4 presented next.

$$CD = CD_0 + CD_i = CD_0 + K_2 \cdot CL^2 \quad (2.4)$$

$$CD_0 = C_{fe} \cdot \frac{S_{wet_{ap}}}{S_W} \quad (2.5)$$

For the estimative of the total wetted area of the airplane, there are used the historical tendencies data presented on the Table 2.5.

Table 2.5 - Historical tendencies data for airplane wetted area (After Venson, 2015).

Airplane Category	***SWET_ap/Sw***	***Standard Deviation***
Glider	4.0	± 1.0
Motorglider	4.0	± 1.0
LSA or Homebuilt	3.0	± 1.0
General aviation and utility single-engine piston	4.5	± 1.0
General aviation and utility single-engine turboprop	5.5	± 1.5
General aviation and utility multi-engine piston	4.0	± 0.5
General aviation and utility multi-engine turboprop	5.5	± 1.0
Acrobatic airplane	3.0	± 0.5
Agricultural airplane	4.0	± 1.0
Amphibious airplane single-engine or multi-engine	4.0	± 1.0
II WW fighter propeller	4.0	± 0.5
Training jet airplane	6.0	± 1.0
Fighter jet airplane	5.0	± 1.5
Cargo or bomber propeller	5.0	± 1.0
Cargo or bomber jet	5.5	± 1.0
Passenger airplane propeller	5.5	± 1.0
Continues on the next page		

Passenger airplane jet	6.0	± 1.0
Executive jet	5.5	± 1.0

This method of estimation for the parasite drag, is based at the theory of flat plate, which consider the friction coefficient for an equivalent surface. The Table 2.6 provides some values of the friction coefficient for some kinds of surfaces and airplane categories. To estimate the total wetted area of the airplane, historical values not presented here may be taken, or may be estimated from the drawings of the airplane, if available.

Table 2.6 - Reference friction coefficient values (After Venson, 2015).

Airplane Category	***C_{fe}***
Light airplane*, with corrugated structure	0.0150
Light airplane*, with cloth skin, strut-braced wing and fixed landing gear	0.0100
Light airplane*, with aluminum skin, strut-braced wing and fixed landing gear	0.0080
Light airplane*, with aluminum skin, no strut-braced wing and fixed landing gear	0.0070
Light airplane*, with aluminum skin, no strut-braced wing and retractable landing gear	0.0055
Amphibious airplane single-engine or multi-engine propeller	0.0065
Military training jet airplane	0.0040
Fighter jet airplane	0.0035
Cargo or bomber propeller	0.0045
Cargo or bomber jet	0.0040
Passenger airplane propeller	0.0035
Passenger airplane jet	0.0030
Supersonic airplane	0.0015

The Oswald factor used for solution of the Equation 2.7 may be obtained from the Figure 2.5 below, that is valid for straight and trapezoidal wings.

$$CD_i = K_2 \cdot CL^2 \tag{2.6}$$

$$K_2 = \frac{1}{\pi \cdot AR_W \cdot e_{wing}} \tag{2.7}$$

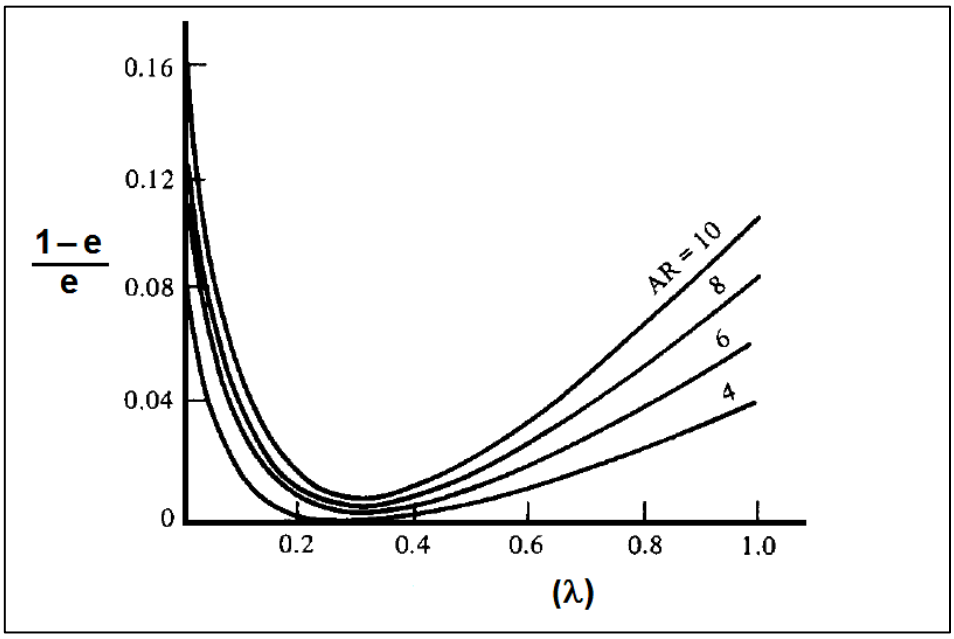


Figure 2.5 - Oswald factor for straight and trapezoidal wings (After Venson, 2015).

Despite the common development of new airplanes uses the Figure 2.5 above for estimate the Oswald factor, the bibliography (Brandt) presents an equation obtained from wind tunnel tests that provide the Oswald efficiency factor for the estimation of the induced drag for a complete airplane, as showed on Equation 2.8.

$$e_o = 4{,}61(1 - 0{,}045AR^{0{,}68})(\cos \Lambda_{L.E})^{0{,}15} - 3{,}1 \quad (2.8)$$

2.1.3. Weight estimate

During the initial conception phase of a new airplane, some weights important for the development must be estimated, as takeoff weight, operational empty weight, payload weight and fuel weight. These parameters impact significantly the whole development of the new airplane and must be estimated early at the conceptual design phase.

In order to obtain the values for these four weights, is employed a well-known method commonly called as fraction weight method, this method is based on historical tendencies values and iterative calculation. Next will be presented a resumed description of the fraction weight method. The Equation 2.9 is the basis for obtain the main weights mentioned above.

$$W_0 = W_{empty} + W_{payload} + W_{fuel} \tag{2.9}$$

Developing this equation is obtained de relation for the take-off weight on the form showed on Equation 2.10. From this moment, the method of the fraction weight must to be employed.

$$W_0 = W_{payload} + \frac{W_{empty}}{W_0} \cdot W_0 + \frac{W_{fuel}}{W_0} \cdot W_0 = \frac{W_{payload}}{1 - \frac{W_{empty}}{W_0} - \frac{W_{fuel}}{W_0}} \tag{2.10}$$

The ratio between the empty weight and the take-off weight may be found applying the historical tendency data from Table 2.7 at the empirical Equation 2.11, where $K = 1$ for wings with fixed sweep and $K = 1.04$ for wings with variable sweep.

$$\frac{W_{empty}}{W_0} = a \cdot W_0^C \cdot K \tag{2.11}$$

Table 2.7 - Historical tendencies values for the empty-to-take-off weight ratio constants (After Venson, 2015).

Airplane Category	***a***	***C***
Glider	2.743 ± 0.772	-0.187
Motorglider	0.086 ± 0.022	0.235
LSA or Homebuilt	0.222 ± 0.041	0.103
General aviation and utility single-engine piston	0.925 ± 0.138	-0.047
General aviation and utility single-engine turboprop	0.925 ± 0.138	-0.047
General aviation and utility multi-engine piston	0.766 ± 0.175	-0.020
General aviation and utility multi-engine turboprop	0.766 ± 0.175	-0.020
Acrobatic airplane	1.036 ± 0.316	-0.047
Agricultural airplane	2.919 ± 0.732	-0.167
Amphibious airplane single-engine or multi-engine	0.865 ± 0.161	-0.032
II WW fighter propeller	2.394 ± 0.839	-0.117
Training jet airplane	1.364 ± 0.556	-0.079
Continues on the next page		

Fighter jet airplane	2.388 ± 0.839	-0.126
Cargo or bomber propeller	3.013 ± 1.051	-0.132
Cargo or bomber jet	0.706 ± 0.439	-0.034
Passenger airplane propeller	0.713 ± 0.105	-0.014
Passenger airplane jet	1.385 ± 0.141	-0.070
Executive jet	0.786 ± 0.129	-0.028

At this point is necessary to estimate the ratio of fuel weight, which is dependent of the phases of the flight that are based on the mission of the airplane. The Figure 2.6 presents a typical mission profile for a civil airplane where the phases of a flight may be classified as taxi and take-off (0 → 1), climb (1 → 2), cruise (2 → 3), descent (3 → 4), loiter and approach (4 → 5), landing and taxi (5 → 6).

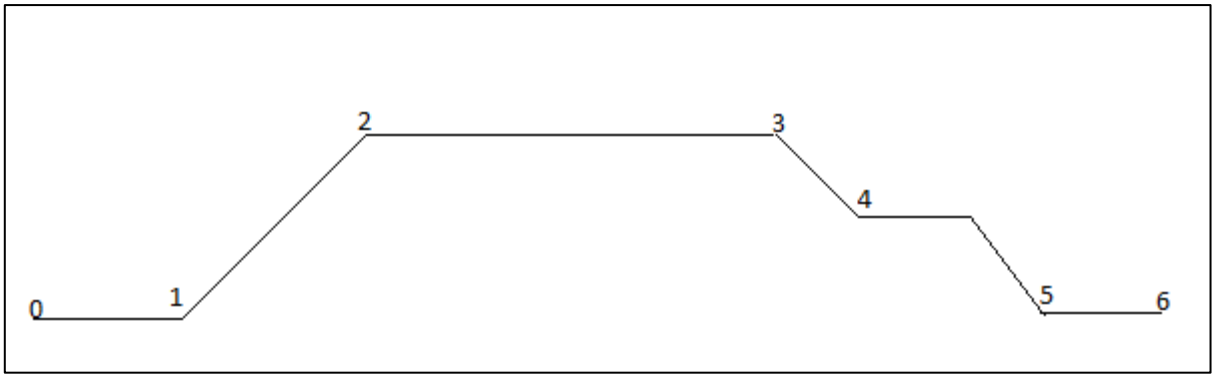


Figure 2.6 - Typical mission profile for a civil airplane.

$$W_{fuel} = W_0 - W_6 \tag{2.12}$$

$$\frac{W_{fuel}}{W_0} = \frac{W_0 - W_6}{W_0} = 1 - \frac{W_6}{W_0} \tag{2.13}$$

$$\frac{W_6}{W_0} = \frac{W_1}{W_0} \cdot \frac{W_2}{W_1} \cdot \frac{W_3}{W_2} \cdot \frac{W_4}{W_3} \cdot \frac{W_5}{W_4} \cdot \frac{W_6}{W_5} \tag{2.14}$$

$$\frac{W_{fuel}}{W_0} = 1 - \frac{W_1}{W_0} \cdot \frac{W_2}{W_1} \cdot \frac{W_3}{W_2} \cdot \frac{W_4}{W_3} \cdot \frac{W_5}{W_4} \cdot \frac{W_6}{W_5} \tag{2.15}$$

Some of the fractions that make up the Equation 2.15 may be obtained from historical tendencies, which are presented on Table 2.8.

Table 2.8 - Historical tendencies data for flight phase weight fraction (After Venson, 2015).

Airplane Category	***W1/W0***	***W2/W1***	***W4/W3***	***W6/W5***
Glider	1.000	1.000	1.000	1.000
Motorglider	0.998	0.995	1.000	1.000
LSA or Homebuilt	0.994	0.995	0.995	0.995
General aviation and utility single-engine piston	0.990	0.992	0.993	0.993
General aviation and utility single-engine turboprop	0.990	0.992	0.993	0.993
General aviation and utility multi-engine piston	0.984	0.990	0.992	0.992
General aviation and utility multi-engine turboprop	0.981	0.985	0.985	0.995
Acrobatic airplane	0.990	0.992	0.993	0.993
Agricultural airplane	0.987	0.998	0.998	0.998
Amphibious airplane single-engine or multi-engine	0.978	0.985	0.990	0.990
II WW fighter propeller	0.985	0.980	0.990	0.990
Training jet airplane	0.970	0.980	0.990	0.995
Fighter jet airplane	0.970	0.930	0.990	0.995
Cargo or bomber propeller	0.975	0.980	0.990	0.992
Cargo or bomber jet	0.975	0.980	0.990	0.992
Passenger airplane propeller	0.970	0.985	0.985	0.995
Passenger airplane jet	0.970	0.985	0.985	0.995
Executive jet	0.980	0.985	0.990	0.995

For estimate the fractions of cruise and loiter are used the Breguet equations. Note that for the cruise phase the fraction is in function of the cruise flight range as showed by Equation 2.16, and for the loiter phase the equation is in function of the endurance as showed by Equation 2.17.

$$\frac{W_3}{W_2} = e^{-\frac{g \cdot R \cdot SFC_{cruise}}{\eta_P \cdot (L/D)_{cruise}}} \tag{2.16}$$

$$\frac{W_5}{W_4} = e^{-\frac{g \cdot E \cdot V_0 \cdot SFC_{loiter}}{\eta_P \cdot (L/D)_{loiter}}} \tag{2.17}$$

$$\left(\frac{L}{D}\right)_{cruise} = \frac{1}{2 \cdot \sqrt{K_2 \cdot C_{D0}}} \tag{2.18}$$

$$\left(\frac{L}{D}\right)_{loiter} = \frac{3}{4 \cdot \sqrt{3 \cdot K_2 \cdot C_{D0}}} \quad (2.19)$$

All the development presented above must be implemented on an iterative algorithm in which a null residual value for W_0 must be achieved. The value of aerodynamic efficiency at cruise condition must be corrected inside the final iterative logical of the algorithm using the Equation 2.21.

2.1.4. Performance estimate

This topic aims to estimate the stall speed of the airplane, its wing loading, power-to-weight ratio, take-off distance, landing distances, range and the Payload-Range diagram. To estimate these parameters, iterative calculus must be done at the same algorithm where the weight estimative is implemented, once, there are influences between these parameters.

The wing loading impact directly the stall speed, climb ratio, maneuverability and take-off and landing distances. Commonly the wing loading is defined in terms of MTOW or W_0. The Table 2.9 presents the historical tendencies for this parameter, and may be used for an initial guess.

Table 2.9 - Historical tendencies data for wing loading (After Venson, 2015).

Airplane Category	***W/S (N/m^2)***	***W/S (Kg/m^2)***
Glider	370 ± 110	38 ± 11
Motorglider	380 ± 85	39 ± 9
LSA or Homebuilt	430 ± 120	43 ± 12
General aviation and utility single-engine piston	760 ± 230	78 ± 23
General aviation and utility single-engine turboprop	1720 ± 490	175 ± 50
General aviation and utility multi-engine piston	1260 ± 260	128 ± 27
General aviation and utility multi-engine turboprop	2100 ± 470	215 ± 48
Acrobatic airplane	700 ± 160	71 ± 16
Agricultural airplane	990 ± 340	100 ± 35
Amphibious airplane single-engine or multi-engine	1200 ± 480	122 ± 49
Continues on the next page		

II WW fighter propeller	2000 ± 500	203 ± 51
Training jet airplane	2950 ± 880	291 ± 90
Fighter jet airplane	4730 ± 1790	483 ± 183
Cargo or bomber propeller	3430 ± 1220	350 ± 125
Cargo or bomber jet	5940 ± 1530	605 ± 157
Passenger airplane propeller	2600 ± 760	265 ± 78
Passenger airplane jet	5600 ± 1290	570 ± 131
Executive jet	3470 ± 900	354 ± 92

Other way to estimate the wing loading is employing the empirical Equation 2.20, the constants of this equation are presented on Table 2.10.

$$\frac{W_0}{S} = a \cdot W_0^C \tag{2.20}$$

Table 2.10 - Constants for empirical estimative for the wing loading (After Venson, 2015) .

Airplane Category	***a***	***C***
Glider	0.808 ± 0,32	0.721
Motorglider	5.809 ± 2,12	0.487
LSA or Homebuilt	0.049 ± 0,03	1.06
General aviation and utility single-engine piston	0.408 ± 0,14	0.804
General aviation and utility single-engine turboprop	0.408 ± 0,14	0.804
General aviation and utility multi-engine piston	1.512 ± 0,48	0.664
General aviation and utility multi-engine turboprop	1.512 ± 0,48	0.664
Acrobatic airplane	1.178 ± 0,84	0.705
Agricultural airplane	7.321 ± 4,11	0.48
Amphibious airplane single-engine or multi-engine	46.0 ± 12,4	0.284
II WW fighter propeller	37.4 ± 13,1	0.363
Training jet airplane	0.188 ± 0,09	0.883
Fighter jet airplane	12.3 ± 4,5	0.482
Cargo or bomber propeller	53.2 ± 12,2	0.324
Cargo or bomber jet	91.5 ± 25,2	0.288
Continues on the next page		

Passenger airplane propeller	59.6 ± 16,2	0.313
Passenger airplane jet	329.6 ± 62,6	0.206
Executive jet	142.3 ± 46,9	0.268

It is important to note that the weight of the airplane during the cruise changes, due the fuel consumption, then the aerodynamic efficiency at cruise may be estimated iteratively using the Equation 2.21 and the Equation 2.22.

$$\left(\frac{L}{D}\right)_{cruise} = \frac{CL_{cruise}}{CD_{cruise}} = \frac{CL_{cruise}}{C_{D0}+K_2 \cdot CL_{cruise}^2} = \frac{1}{\frac{C_{D0}}{CL_{cruise}}+K_2 \cdot CL_{cruise}} \tag{2.21}$$

$$CL_{cruise} = \frac{2 \cdot W_{cruise}}{\rho_{cruise} \cdot S_W \cdot V_0^2} \tag{2.22}$$

As the wing loading changes during the iterative process, the values of wet and reference area changes either, therefore, these parameter should be calculated iteratively too.

The stall speed occur for the maximum lift coefficient, once, reached this value the wing will lost lift due the flow separation over its upper surface, note that the stall speed depends directly of the airplane actual weight, for the airplane developed on this work, the maximum lift coefficient may be estimated as being $CL_{max} = 1.8$. The Equation 2.23 is used for estimate the stall speed.

$$V_S = \sqrt{\frac{2 \cdot L}{\rho_{FL} \cdot S_W \cdot CL_{max}}} = \sqrt{\frac{2 \cdot W}{\rho_{FL} \cdot S_W \cdot CL_{max}}} = \sqrt{\frac{2}{\rho_{FL} \cdot CL_{max}} \cdot \left(\frac{W}{S_W}\right)} \tag{2.23}$$

The power-to-weight ratio is based on the shaft engine power. For an initial guess is common use the take-off gross weight or MTOW for the maximum speed expected for the airplane, as showed on the empirical Equation 2.24 whose constants are presented on Table 2.11, or may be estimated based on historical tendencies data presented on Table 2.12.

$$\frac{SEP}{W_0} = a \cdot V_{max}^C \tag{2.24}$$

Table 2.11 - Constants for empirical estimative for the power-to-weight ratio (After Venson, 2015).

Airplane Category	***a***	***C***
Motorglider	0.0047 ± 0.001	0.5345
LSA or Homebuilt	0.1170 ± 0.015	0.0662
General aviation and utility single-engine piston	0.0116 ± 0.002	0.4789
General aviation and utility single-engine turboprop	0.0030 ± 0.001	0.7255
General aviation and utility multi-engine piston	0.0116 ± 0.002	0.4789
General aviation and utility multi-engine turboprop	0.0030 ± 0,001	0.7255
Acrobatic airplane	0.0039 ± 0.001	0.7434
Agricultural airplane	0.0146 ± 0.002	0.4601
Amphibious airplane single-engine or multi-engine	0.0969 ± 0.025	0.096
II WW fighter single-engine propeller	0.0059 ± 0.001	0.6288
II WW fighter multi-engine propeller	0.0059 ± 0.001	0.6288
Cargo or bomber propeller	0.0443 ± 0.004	0.2437
Cargo or bomber turboprop	0.0385 ± 0.010	0.3105
Passenger airplane propeller	0.0443 ± 0.002	0.2437
Passenger airplane turboprop	0.0385 ± 0.005	0.3105

Table 2.12 - Historical tendencies data for power-to-weight ratio (After Venson, 2015).

Airplane Category	***sep/W (shp/Kg)***	***W/sep (Kg/shp)***
Motorglider	0.096 ± 0.04	10.5 ± 4.0
LSA or Homebuilt	0.165 ± 0.03	6.0 ± 1.5
General aviation and utility single-engine piston	0.167 ± 0.03	6.0 ± 1.0
General aviation and utility single-engine turboprop	0.264 ± 0.07	4.0 ± 1.0
General aviation and utility multi-engine piston	0.206 ± 0.02	5.0 ± 0.5
General aviation and utility multi-engine turboprop	0.303 ± 0.05	3.5 ± 0.5
Acrobatic airplane	0.289 ± 0.08	3.5 ± 1.0
Agricultural airplane	0.183 ± 0.03	5.5 ± 1.0
Amphibious airplane single-engine or multi-engine	0.175 ± 0.05	6.0 ± 3.5
II WW fighter single-engine propeller	0.350 ± 0.07	3.0 ± 0.5
Continues on the next page		

II WW fighter multi-engine propeller	0.275 ± 0.06	3.5 ± 1.0
Cargo or bomber propeller	0.203 ± 0.05	5.0 ± 1.0
Cargo or bomber turboprop	0.296 ± 0.06	3.5 ± 1.0
Passenger airplane propeller	0.200 ± 0.03	5.0 ± 1.0
Passenger airplane turboprop	0.267 ± 0.04	4.0 ± 0.5

Now it is possible to estimate the dimensioning of the propeller to be installed on the engine of the airplane, that is done based on the thrust generated by the propeller at static condition.

Knowing the SEP of the engine, the thrust may be estimated by the thrust-to-power ratio that can be found by Equation 2.25 whose constants are presented on Table 2.13.

$$\frac{T}{SEP} = a \cdot SEP_{eng}^{C} \tag{2.25}$$

Table 2.13 - Constants for empirical estimative for the thrust-to-power ratio (After Venson, 2015).

Airplane Category	***Number of blades***	***a***	***C***
Motorglider	2-blades prop	34.94	-0.068
LSA or Homebuilt	2 or 3-blades prop	39.23	-0.175
General aviation and utility single-engine piston	2 or 3-blades prop	33.19	-0.122
General aviation and utility single-engine turboprop	2 or 3-blades prop	21.58	-0.052
General aviation and utility multi-engine piston	3 or 4-blades prop	23.13	-0.089
General aviation and utility multi-engine turboprop	3 or 4-blades prop	18.02	-0.048
Acrobatic airplane	3 or 4-blades prop	14.87	0.028
Agricultural airplane	2 or 3-blades prop	27.24	-0.057
Amphibious airplane single-engine or multi-engine	3 or 4-blades prop	42.75	-0.184
II WW fighter single-engine propeller	3 or 4-blades prop	37.11	-0.089
II WW fighter multi-engine propeller	3 or 4-blades prop	35.15	-0.089
Cargo or bomber propeller	3 or 4-blades prop	53.84	-0.136
Cargo or bomber turboprop	4 or more blades	26.44	-0.039
Passenger airplane propeller	3 or 4-blades prop	25.21	-0.095
Passenger airplane turboprop	4 or more blades	19.07	-0.066

The diameter of the propeller is obtained by the thrust-to-disc loading ratio T/S_p given by the historical tendencies presented on Table 2.14.

Table 2.14 - Historical tendencies data for thrust-to-disc loading ratio (After Venson, 2015).

Engine Type	***Propeller Blades***	***T/Sp (N/m^2)***
Piston	2-blades prop	1000
Piston and Turboprop	3-blades prop	1500
Piston and Turboprop	4-blades prop	2000
Advanced Turboprop	5 or more blades prop	2500

Once the thrust had been estimated, it is possible to define an approximation for the thrust-to weight ratio and compare to the historical data presented on the Table 2.15.

Table 2.15 - Historical tendencies data for thrust-to-weight ratio (After Venson, 2015).

Airplane Category	***Number of blades***	***T/W***
Motorglider	2-blades prop	0.26 ± 0.11
LSA or Homebuilt	2 or 3-blades prop	0.33 ± 0.05
General aviation and utility single-engine piston	2 or 3-blades prop	0.30 ± 0.04
General aviation and utility single-engine turboprop	2 or 3-blades prop	0.40 ± 0.10
General aviation and utility multi-engine piston	3 or 4-blades prop	0.30 ± 0.03
General aviation and utility multi-engine turboprop	3 or 4-blades prop	0.40 ± 0.07
Acrobatic airplane	3 or 4-blades prop	0.52 ± 0.17
Agricultural airplane	2 or 3-blades prop	0.36 ± 0.09
Amphibious airplane single-engine or multi-engine	3 or 4-blades prop	0.23 ± 0.03
II WW fighter single-engine propeller	3 or 4-blades prop	0.68 ± 0.13
II WW fighter multi-engine propeller	3 or 4-blades prop	0.60 ± 0.11
Cargo or bomber propeller	3 or 4-blades prop	0.41 ± 0.11
Cargo or bomber turboprop	4 or more blades	0.57 ± 0.13
Passenger airplane propeller	3 or 4-blades prop	0.25 ± 0.03
Passenger airplane turboprop	4 or more blades	0.32 ± 0.05

At this point the take-off and landing performance can be estimated. For the take-off runway distance estimative, the historical tendencies data presented on Table 2.16 are inserted on the empirical Equation 2.26.

$$R_T = a \cdot TOP \tag{2.26}$$

$$TOP = \frac{\left(\frac{W}{S_W}\right)_{take-off}}{\sigma \cdot CL_{take-off} \cdot \left(\frac{SEP}{W}\right)_{take-off}} \tag{2.27}$$

$$\sigma = \frac{\rho_{FL}}{\rho_0} \tag{2.28}$$

Table 2.16 - Historical tendencies data for take-off runway (After Venson, 2015).

Airplane Category	***Takeoff condition***	***a***
Motorglider	Without obstacle	5.14 ± 0.51
LSA or Homebuilt	Without obstacle	8.00 ± 0.80
General aviation and utility single-engine piston	Without obstacle	8.23 ± 1.23
	With obstacle (50ft)	9.30 ± 1.39
General aviation and utility multi-engine piston	Without obstacle	9.68 ± 1.45
	With obstacle (50ft)	10.51 ± 1.58
Acrobatic airplane	Without obstacle	7.89 ± 0.79
Agricultural airplane	Without obstacle	7.40 ± 0.74
	With obstacle (50ft)	8.25 ± 0.82
Amphibious airplane single-engine or multi-engine	With obstacle (50ft)	8.19 ± 0.82
II WW fighter propeller	With obstacle (50ft)	7.98 ± 0.80
Cargo or bomber propeller	Without obstacle	6.67 ± 0.67
	With obstacle (50ft)	6.94 ± 0.69
Passenger airplane propeller two-engine	With obstacle (50ft)	11.58 ± 1.16
	Balanced takeoff	17.57 ± 1.76
Passenger airplane propeller four-engine	With obstacle (50ft)	11.56 ± 1.16
	Balanced takeoff	13.82 ± 1.38

The landing runway distance may be estimated by the empirical Equation 2.29, and the historical tendencies data used on this equation are presented on Table 2.17.

$$R_L = a \cdot \frac{1}{\rho_{FL} \cdot CL_{max}} \cdot \left(\frac{W}{S_W}\right)_{landing} \quad (2.29)$$

Table 2.17 - Historical tendencies data for landing runway (After Venson, 2015).

Airplane Category	***Landing condition***	***a***
Glider	Without obstacle	0.878 ± 0.005
Motorglider	Without obstacle	0.869 ± 0.008
LSA or Homebuilt	Without obstacle	1.136 ± 0.017
General aviation and utility single-engine piston	With obstacle (50ft)	1.524 ± 0.023
General aviation and utility single-engine turboprop	With obstacle (50ft)	1.524 ± 0.023
General aviation and utility multi-engine piston	With obstacle (50ft)	1.463 ± 0.016
General aviation and utility multi-engine turboprop	With obstacle (50ft)	1.463 ± 0.016
Acrobatic airplane	Without obstacle	1.035 ± 0.026
Agricultural airplane	Without obstacle	1.053 ± 0.010
Amphibious airplane single-engine or multi-engine	Without obstacle	1.062 ± 0.015
II WW fighter propeller	Without obstacle	1.061 ± 0.008
Training jet airplane	With obstacle (50ft)	0.834 ± 0.017
Fighter jet airplane	With obstacle (50ft)	0.676 ± 0.011
Cargo or bomber propeller	With obstacle (50ft)	1.358 ± 0.021
Cargo or bomber jet	With obstacle (50ft)	0.830 ± 0.006
Passenger airplane propeller	With obstacle (50ft)	1.437 ± 0.015
Passenger airplane jet	With obstacle (50ft)	0.860 ± 0.004
Executive jet	With obstacle (50ft)	0.946 ± 0.011

In order to estimate the total range of the airplane there are employed the weight fraction defined earlier, the values that must to be used are that obtained on the last iteration calculated on the algorithm. The Equation 2.30 provides an approximation the total range of the new airplane.

$$R_{total} = -\frac{\eta_P \cdot \ln\left(\frac{W_3}{W_2}\right) \cdot \left(\frac{L}{D}\right)_{cruise}}{g \cdot SFC_{cruise}} \quad (2.30)$$

Considering that different combinations of payload and fuel weight may occur during the operational life of an airplane, the Equation 2.30 will provide a wide variation of values that may be visually resumed graphically on the Payload-range Diagram. This diagram is formed by the following parts: point 1 (maximum payload and zero fuel), point 2 (maximum payload and fuel enough for MTOW), point 3 (maximum fuel weight and payload enough for MTOW) and point 4 (maximum fuel weight and zero payload). The Figure 2.7 shows a generic Payload-range Diagram.

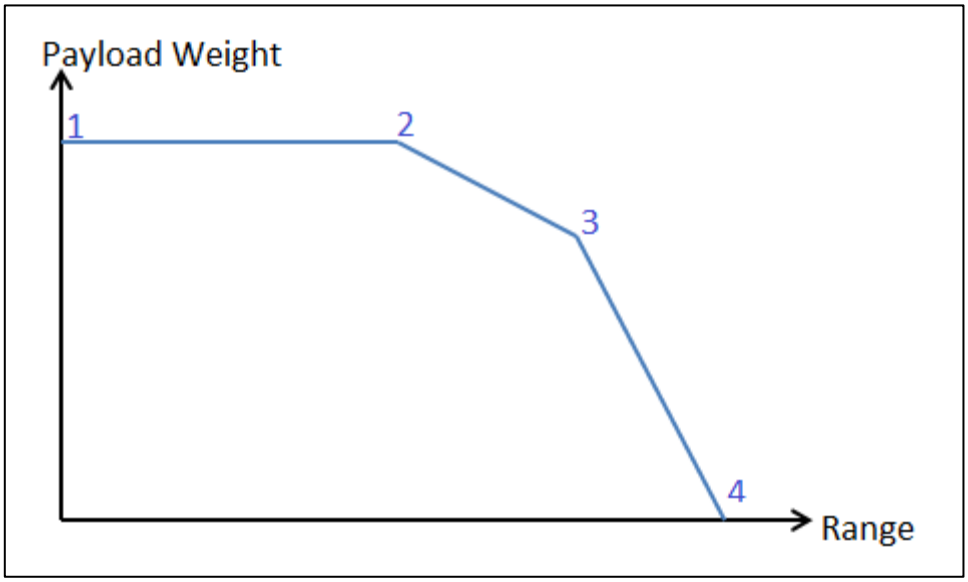


Figure 2.7 - Generic Payload-Range Diagram.

Finally it is necessary to say that, all the lift coefficient mentioned above as CL, CL_{max} and $CL_{takeoff}$ may be considered as the wing lift coefficient for its actual aerodynamic configuration, once, at this phase of the development of the airplane, enough information is not available or produced.

2.1.5. Sizing estimate

Continuing the conception of the new airplane it is necessary proceeding to the sizing of the fuselage length, cockpit, tail, primary control surfaces and positioning these structural parts, landing gear and engines. Concluding this topic, after the work of initial sizing done it is possible to estimate de moment of inertia on the three axis.

The initial sizing of the fuselage is done using the empirical Equation 2.31 that is based on the MTOW or W_0, and historical data presented on Table 2.18.

$$X_{fus} = a \cdot W_0^C \tag{2.31}$$

Table 2.18 - Historical tendencies data for fuselage sizing (After Venson, 2015).

Airplane Category	***a***	***C***
Glider	2.1763	0.1437
Motorglider		
LSA or Homebuilt	0.4431	0.3063
General aviation and utility single-engine piston	0.4088	0.3140
General aviation and utility single-engine turboprop		
General aviation and utility multi-engine piston		
General aviation and utility multi-engine turboprop		
Acrobatic airplane	0.265	0.3549
Agricultural airplane	0.7888	0.2371
Amphibious airplane single-engine or multi-engine	0.2373	0.3752
II WW fighter propeller	0.2111	0.3592
Training jet airplane	0.615	0.2647
Fighter jet airplane	0.2683	0.3396
Cargo or bomber propeller	0.0576	0.4678
Cargo or bomber jet		
Passenger airplane propeller	0.3115	0.3539
Passenger airplane jet	0.4546	0.3321
Executive jet	0.226	0.3739

For estimating the dimension of the cockpit for the actual airplane, there are applied the historical tendencies data resumed on the Table 2.19.

Table 2.19 - Historical tendencies for cockpit sizing (After Venson, 2014).

Airplane Category		
General aviation and utility single-engine piston	X_{fus}/Y_C	X_N/X_{fus}
	5.9 ± 0.4	0.23 ± 0.03
	X_C/X_{fus}	X_T/X_{fus}
	0.38 ± 0.03	0.40 ± 0.05

The initial sizing of the tail surfaces is done based on the concept of tail volume coefficient, that is a relation involving tail arm, and the main geometric properties of the wing and the tail surfaces itself. The tail moment arms are the distance between the position at 25% of the tail mean aerodynamic chord and the position at 25% of the wing mean aerodynamic chord. The horizontal empennage and vertical empennage are estimated by the tail volume coefficient Equation 2.32 and Equation 2.33 respectively, the Figure 2.8 shows the geometric scheme for the sizing of the tail surfaces. As reference, the Table 2.20 presents historical tendencies data for the tail volume coefficients.

$$V_{HT} = \frac{l_{HT} \cdot S_{HT}}{\bar{C}_W \cdot S_W} \tag{2.32}$$

$$V_{VT} = \frac{l_{VT} \cdot S_{VT}}{b_W \cdot S_W} \tag{2.33}$$

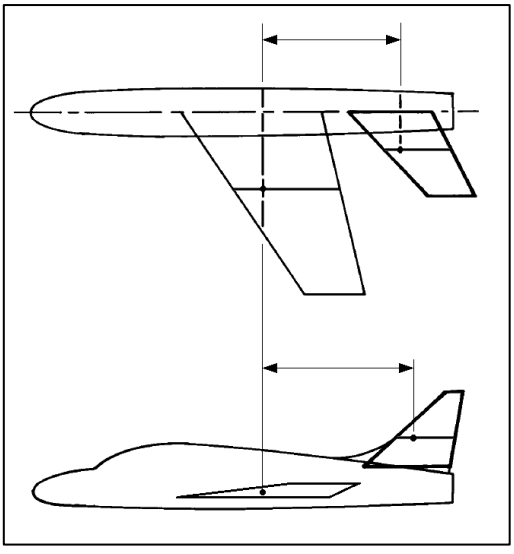


Figure 2.8 - Tail sizing geometric scheme (Raymer, 2006).

Table 2.20 - Historical tendencies data for tail volume coefficient (After Venson, 2015).

Airplane Category	V_{HT}	V_{VT}
Glider and Motorglider	0.50 ± 0.05	0.020 ± 0.005
LSA or Homebuilt	0.50 ± 0.05	0.020 ± 0.005
General aviation and utility single-engine propeller, conventional tail	0.45 ± 0.11	0.030 ± 0.004
General aviation and utility single-engine propeller, T tail	0.60 ± 0.15	0.030 ± 0.005
General aviation and utility multi-engine propeller, conventional tail	0.84 ± 0.19	0.050 ± 0.015
General aviation and utility multi-engine propeller, T tail	0.96 ± 0.17	0.071 ± 0.011
Acrobatic airplane	0.35 ± 0.08	0.030 ± 0.003
Agricultural airplane	0.46 ± 0.09	0.028 ± 0.004
Amphibious airplane single-engine or multi-engine	0.50 ± 0.14	0.060 ± 0.005
Training jet airplane	0.70 ± 0.11	0.060 ± 0.005
Fighter jet airplane	0.40 ± 0.14	0.070 ± 0.006
Cargo or bomber two engine, conventional tail	1.23 ± 0.22	0.089 ± 0.015
Cargo or bomber two engine, T tail	0.96 ± 0.12	0.088 ± 0.022
Cargo or bomber four engine, conventional tail	0.88 ± 0.18	0.058 ± 0.014
Cargo or bomber four engine, T tail	0.98 ± 0.06	0.064 ± 0.011
Passenger airplane two engine, conventional tail	1.07 ± 0.23	0.077 ± 0.019
Passenger airplane two engine, T tail	1.08 ± 0.16	0.093 ± 0.021
Passenger airplane four engine, conventional tail	0.87 ± 0.11	0.069 ± 0.011
Passenger airplane four engine, T tail	0.97 ± 0.12	0.076 ± 0.012
Executive jet two engine, conventional tail	0.80 ± 0.16	0.070 ± 0.009
Executive jet two engine, T tail	0.77 ± 0.17	0.064 ± 0.017
Executive jet three engine, conventional tail	0.72 ± 0.03	0.059 ± 0.002

Once the wing and tail had been sized the next step is to estimate the size of the three flight primary control surfaces which are aileron, elevator and rudder. During the conceptual design phase these three surfaces may be pre-sized employing the three relations called aileron wing ratio, elevator tail ratio and rudder tail ratio, that are respectively provided by Equation 2.34, Equation 2.35 and Equation 2.36, straight from the historical tendencies data showed on the Table 2.21.

$$Ail_{rate} = \frac{S_{ail}}{S_W} \quad (2.34)$$

$$Elev_{rate} = \frac{S_E}{S_{HT}} \quad (2.35)$$

$$Rud_{rate} = \frac{S_{rud}}{S_{VT}} \quad (2.36)$$

Table 2.21 - Historical tendencies data for primary control surfaces (After Venson, 2015).

Airplane Category	***Ail-wing Ratio***	***Elev-HT Ratio***	***Rud-VT Ratio***
Glider and Motorglider	0.07 ± 0.02	0.29 ± 0.03	0.43 ± 0.04
LSA or Homebuilt	0.06 ± 0.01	0.38 ± 0.09	0.39 ± 0.05
General aviation and utility single-engine propeller	0.07 ± 0.01	0.41 ± 0.04	0.36 ± 0.04
General aviation and utility multi-engine propeller	0.05 ± 0.01	0.44 ± 0.20	0.38 ± 0.06
Acrobatic airplane	0.11 ± 0.01	0.50 ± 0.06	0.50 ± 0.09
Agricultural airplane	0.09 ± 0.03	0.47 ± 0.08	0.53 ± 0.09
Amphibious airplane single-engine or multi-engine	0.06 ± 0.03	0.42 ± 0.13	0.37 ± 0.06
Training jet airplane	0.08 ± 0.02	0.24 ± 0.04	0.31 ± 0.02
Fighter jet airplane	0.15 ± 0.03	0.60 ± 0.14	0.32 ± 0.04
Cargo or bomber two engine propeller	0.06 ± 0.01	0.31 ± 0.03	0.32 ± 0.03
Cargo or bomber four engine propeller		0.37 ± 0.10	0.36 ± 0.07
Cargo or bomber two engine jet	0.04 ± 0.02	0.30 ± 0.04	0.22 ± 0.02
Cargo or bomber four engine jet			0.25 ± 0.02
Passenger airplane two engine propeller	0.05 ± 0.02	0.42 ± 0.05	0.42 ± 0.05
Passenger airplane four engine propeller		0.37 ± 0.11	0.37 ± 0.11
Passenger airplane two engine jet	0.03 ± 0.01	0.27 ± 0.05	0.31 ± 0.05
Passenger airplane three engine jet			0.22 ± 0.06
Passenger airplane four engine jet			0.29 ± 0.03
Executive jet two engine	0.05 ± 0.02	0.33 ± 0.05	0.32 ± 0.08
Executive jet three engine		0.26 ± 0.04	0.12 ± 0.02

After conclude the activities above, the positioning of the main structural parts will be already pre-defined, once the distances of the horizontal tail and vertical tail relative to the wing were defined and the positioning of the wing relative to the fuselage also. It is necessary to pre-

define the positioning of the landing gears and engines on the airplane, trying keep the CG position between the nose and main legs of the landing gear, preferably near the main landing gear leg, what provide a good behavior of the airplane during take-off rotate. The positioning of the engines must be done on a way that its position contribute to keep the airplane CG on position that do not degrade the flight behavior, that is, ahead of the aerodynamic center of the airplane.

Finally it is necessary to estimate the moment of inertia on the three axis, for the initial assess of dynamics of flight. These parameters are obtained from the three empirical relations given by the Equation 2.37, Equation 2.38 and Equation 2.39, based on the historical tendencies data showed on the Table 2.22.

$$I_{XX} = \frac{b_W^2 \cdot W_0 \cdot R_X^2}{4 \cdot g} \tag{2.37}$$

$$I_{YY} = \frac{X_{fus}^2 \cdot W_0 \cdot R_Y^2}{4 \cdot g} \tag{2.38}$$

$$I_{ZZ} = \left(\frac{b_W + X_{fus}}{2}\right)^2 \cdot \frac{W_0 \cdot R_Z^2}{4 \cdot g} \tag{2.39}$$

Table 2.22 - Historical tendencies data for moment of inertia (After Venson, 2015).

Airplane Category	***Rx***	***Ry***	***Rz***
Glider and Motorglider	0.28	0.34	0.44
General aviation and utility single-engine propeller	0.25	0.38	0.39
General aviation and utility multi-engine propeller	0.34	0.29	0.44
Amphibious airplane single-engine or multi-engine	0.25	0.32	0.41
Training jet airplane	0.22	0.14	0.25
Fighter jet airplane	0.23	0.38	0.52
Cargo or bomber two engine	0.33	0.31	0.47
Cargo or bomber four engine	0.35	0.29	0.46
Passenger airplane turboprop	0.22	0.34	0.38
Passenger airplane two engine jet on fuselage	0.24	0.36	0.44
Passenger airplane two engine jet on wing	0.25	0.38	0.46
Passenger airplane four engine jet on wing	0.31	0.33	0.45
Continues on the next page			

Executive jet	0.3	0.3	0.43
Flying Wing	0.32	0.32	0.51

Once the moments of inertia were defined, this work proposes to consider that the airplane mass is concentrated in a single point, based on it and having the values of the moment of inertia obtained earlier, it is possible to estimate the values of the product of inertia applying the next six equations provided at the bibliography (Hibbeler, 2005).

Therefore, inserting the results of the Equation 2.37 to the Equation 2.39 into the Equation 2.40 to the Equation 2.42 it is possible to obtain the values for the variables x, y and z, that are employed to estimate the products of inertia by solving the Equation 2.43 to the Equation 2.45.

$$I_{XX} = \int_m r_x^2 \cdot dm = \int_m (y^2 + z^2) \cdot dm \quad (2.40)$$

$$I_{YY} = \int_m r_y^2 \cdot dm = \int_m (x^2 + z^2) \cdot dm \quad (2.41)$$

$$I_{ZZ} = \int_m r_z^2 \cdot dm = \int_m (x^2 + y^2) \cdot dm \quad (2.42)$$

$$I_{XY} = I_{YX} = \int_m x \cdot y \cdot dm \quad (2.43)$$

$$I_{YZ} = I_{ZY} = \int_m y \cdot z \cdot dm \quad (2.44)$$

$$I_{XZ} = I_{ZX} = \int_m x \cdot z \cdot dm \quad (2.45)$$

2.1.6. Parts weights estimate

This subsection is dedicated to estimate the weight of each component of an airplane, employing for this, statistical equations. Although these equations provide approximated values for the weight of each component, as stated by (Raymer, 2006), it is necessary keep in mind that there are no “right” answers in weights estimation until the first flight. The following equations are used for estimation of the weights of the parts of the airplane and are in pounds, some equations relative to avionics and electrical system for example, were omitted because they were not used on the development of the airplane. These equations were simplified when necessary, eliminating terms that may be omitted for the airplane which was developed on this work.

$$W_W = 0.036 \cdot S_W^{0.758} \cdot \left(\frac{AR_W}{cos^2 \Lambda_W}\right)^{0.6} \cdot q^{0.006} \cdot \lambda_W^{0.04} \cdot \left(\frac{100 \cdot t/c_W}{\cos \Lambda_W}\right)^{-0.3} \cdot (N_U \cdot W_0)^{0.49};$$

$$N_U = N_y \times 1.5 \quad (2.46)$$

$$W_{HT} = 0.016 \cdot (N_U \cdot W_0)^{0.414} \cdot q^{0.168} \cdot S_{HT}^{0.896} \cdot \left(\frac{100 \cdot t/c_{HT}}{\cos \Lambda_{HT}}\right)^{-0.12} \cdot \left(\frac{AR_{HT}}{cos^2 \Lambda_{HT}}\right)^{0.043} \cdot \lambda_{HT}^{-0.02} \quad (2.47)$$

$$W_{VT} = 0.073 \cdot \left(1 + 0.2 \cdot \frac{H_{HT}}{H_{VT}}\right) \cdot (N_U \cdot W_0)^{0.376} \cdot q^{0.122} \cdot S_{VT}^{0.873} \cdot \left(\frac{100 \cdot t/c_{VT}}{\cos \Lambda_{VT}}\right)^{-0.49}$$

$$\cdot \left(\frac{AR_{VT}}{cos^2 \Lambda_{VT}}\right)^{0.357} \cdot \lambda_{VT}^{-0.039} \quad (2.48)$$

$$W_{fus} = 0.052 \cdot S_{fus}^{1.086} \cdot (N_U \cdot W_0)^{0.177} \cdot l_{HT}^{-0.051} \cdot \left(L/D_{cruise}\right)^{-0.072} \cdot q^{0.241} \quad (2.49)$$

$$W_{MLG} = 0.095 \cdot (N_{L.U} \cdot W_l)^{0.768} \cdot (L_m/12)^{0.409}; \quad N_{L.U} = N_{gear} \times 1.5 \quad (2.50)$$

$$W_{NLG} = 0.125 \cdot (N_{L.U} \cdot W_l)^{0.566} \cdot (L_n/12)^{0.845} \quad (2.51)$$

$$W_{Control.Surf} = 0.053 \cdot X_{fus}^{1.536} \cdot b_W^{0.371} \cdot (N_U \cdot W_0 \cdot 10^{-4})^{0.80} \quad (2.52)$$

$$W_{oil.syst} = \left(0.01 \cdot N_{eng} \cdot W_{eng}\right) \cdot 2.204623 \quad (2.53)$$

$$W_{fuel.syst} = 2.49 \cdot V_{fu}^{0.726} \cdot \left(\frac{1}{1+(V_{f.t}/V_{fu})}\right)^{0.363} \cdot N_t^{0.242} \cdot N_{eng}^{0.157} \quad (2.54)$$

$$W_{Flig.cont.syst} = (0.154 \cdot W_0^{0.67}) \cdot 2.204623 \quad (2.55)$$

$$W_{Flap.cont.syst} = \left(5.569 \cdot \left(S_{Flap} \cdot \sin \delta_{flap.max}\right)^{0.92}\right) \cdot 2.204623 \quad (2.56)$$

2.1.7. CG-Weight envelope diagram estimate

The weight of the airplane changes during the flight and depending of the characteristics of a flight, as for example, the number of passengers and its weight, the weight of the cargo and weighs of the crew members. The weight of the airplane may changes even due the variation of the fuel consumption.

All these variation on the airplane weight affects directly the control and stability of the airplane in a way that the actual weight and its corresponding CG position may not exceed certain limits.

The estimative of the CG position of the airplane may be done by the Equation 2.57 to Equation 2.59. The CG position is related to the Datum reference, which is normally located on the nose of the airplane.

$$X_{CG} = \frac{\sum l_{x\_i} \cdot W_i}{W_i} \tag{2.57}$$

$$Y_{CG} = \frac{\sum l_{y\_i} \cdot W_i}{W_i} \tag{2.58}$$

$$Z_{CG} = \frac{\sum l_{z\_i} \cdot W_i}{W_i} \tag{2.59}$$

For resuming all the weights and CG positions allowed for an airplane operation even in ground as in flight, were developed a diagram called weight-CG envelope, presented generically on the Figure 2.9.

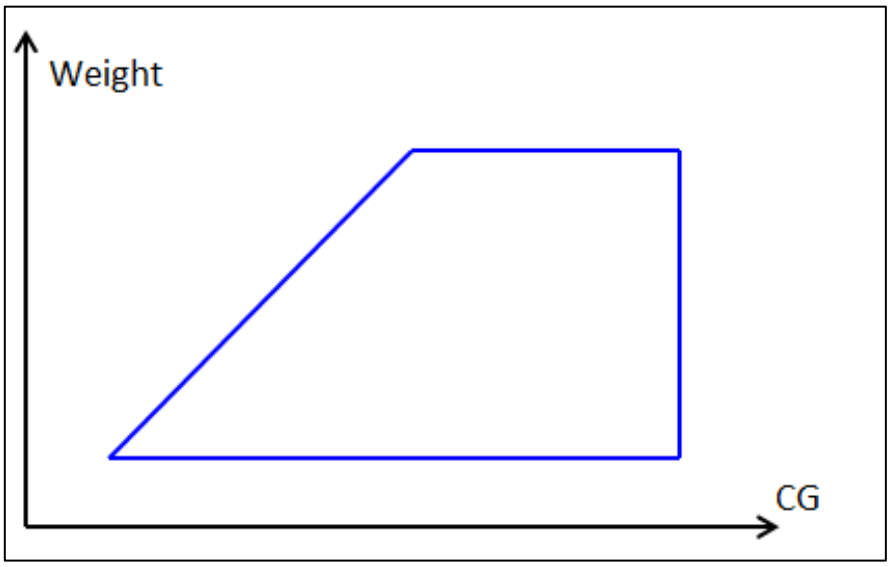


Figure 2.9 - Weight-CG envelope.

2.2. SELECTION OF MATERIALS

The selection or definition of materials to be employed on the manufacturing of a new airplane is not trivial and represents many impacts on its final characteristics.

Once an airplane have obviously to takes off and fly, the materials used on its manufacturing must to be lite for turn easier these acts, and strong enough for resists the flight loads. As the two main characteristics that one aeronautical material must present were already described, is now convenient to talk about some of them.

The most common materials employed on the structure of the airplanes are the aeronautical aluminum alloys, once these materials are at the same time lite and strong. Some steel alloys are used on the manufacturing of mechanical components and on the landing gear legs.

Recently on the aeronautical industry a new class of material has been introduced in substitution to the aluminum alloys on the structural elements, they are the composite materials, basically based on glass, carbon and aramid fiber.

In addition to these ones there is a wide variety of materials, as polymeric alloys that are employed on the manufacturing of interior components, cabin components, and other metallic alloys for engines and its systems for example.

Finally, during the initial phase of the development of a new airplane, it is necessary to do a comparative analysis of the potential materials to be employed on its manufacturing, in order to define the most appropriate to be used considering its mechanical, thermal and chemical properties and costs, having in mind the mission for which the airplane is been conceived.

2.3. ERGONOMICS

The cockpit and passenger cabin of an aircraft must be conceived considering the characteristics of the human body. Statistical anthropometric studies collected data of the dimensions of the human body and its parts, organizing these data in groups of gender and sizing dispersion. Ergonomics studies also were developed with the purpose of identifying the positions of the human body more comfortable, and that avoid muscular and orthopedic diseases, these studies resulted in angular positions for the members of the body. The results of these studies are presented next on the Figure 2.10 to Figure 2.13.

On the beginning of the design of a new airplane these parameters have to be considered, and more, they must be applied in order to avoid wrong internal dimensioning of the cockpit and passengers cabin, as for example, insufficient space for accommodate all the

members of the crew and passengers, what if noted late on the development could cause serious impact on the chronogram and on the budget available.

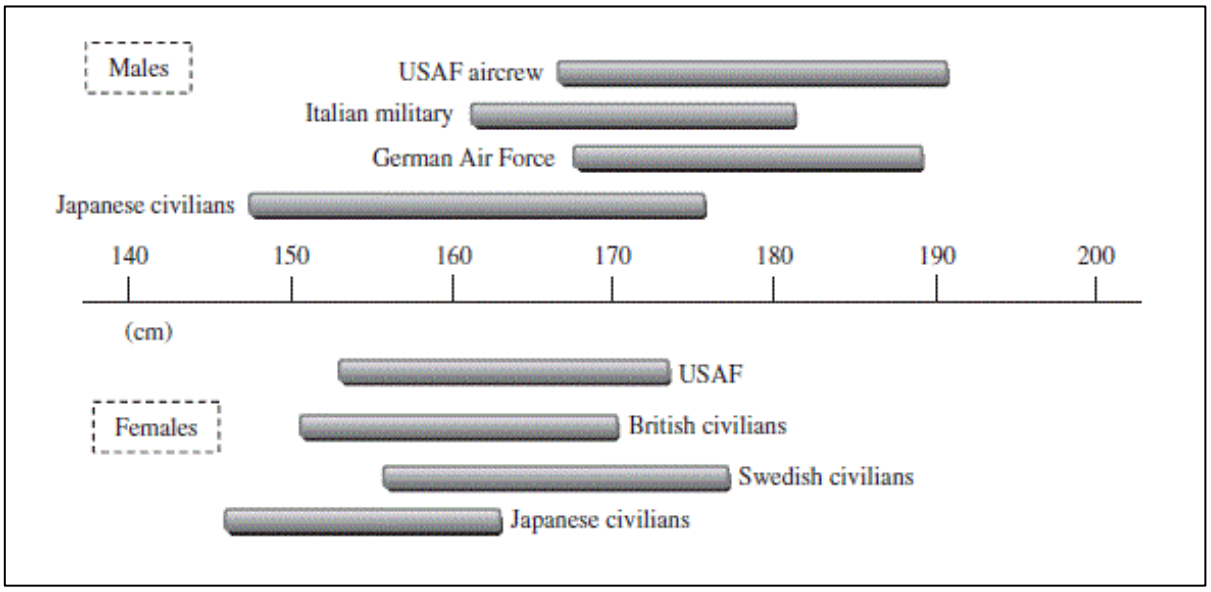


Figure 2.10 - Height variation for male and female and for different ethnic (Sadraey, 2013).

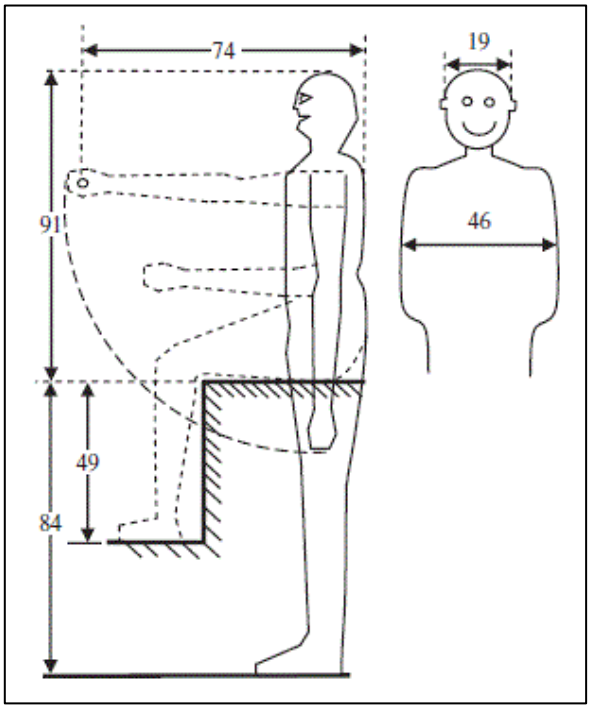


Figure 2.11 - Linear body dimensions (cm) (Sadraey, 2013).

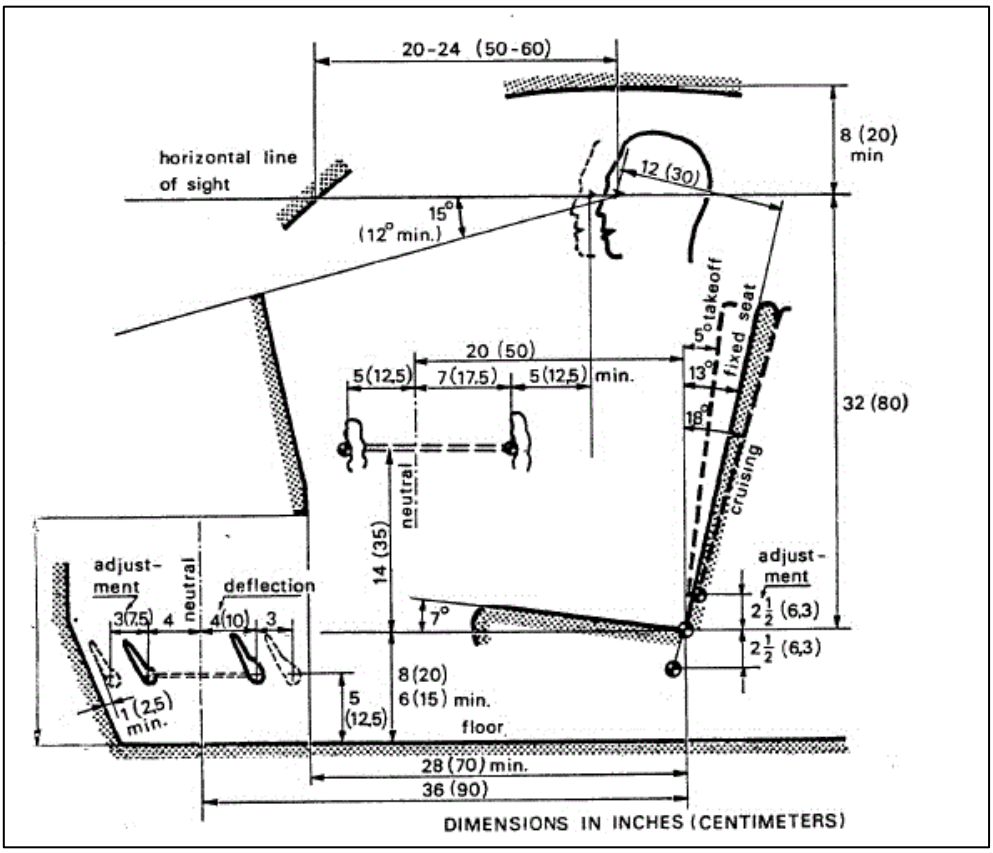


Figure 2.12 - Dimensions for a cockpit of a light aircraft with stick control (Torenbeek, 1976).

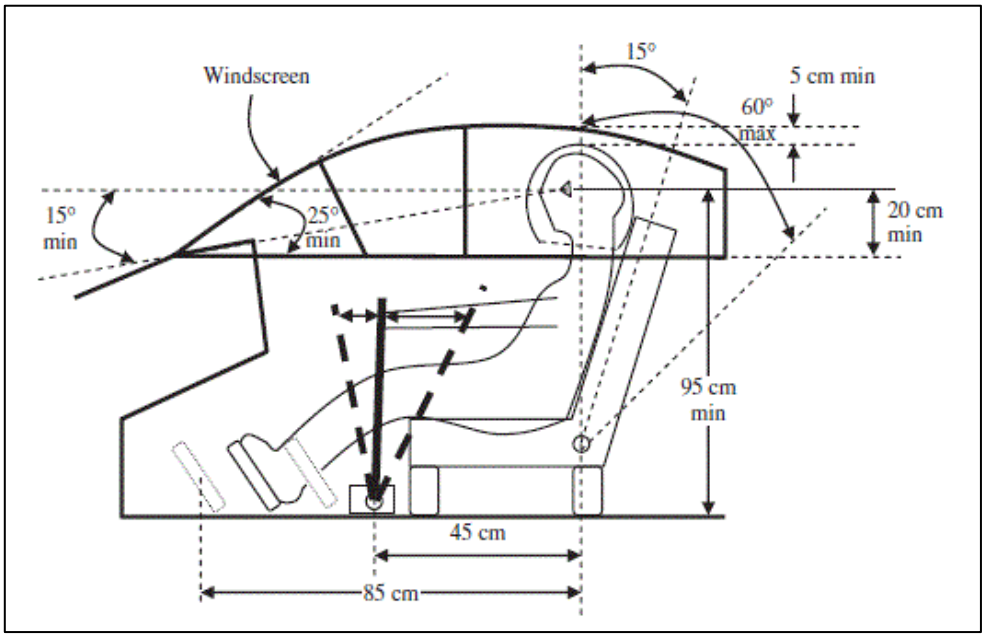


Figure 2.13 - Dimensions for a cockpit of a fighter aircraft (Sadraey, 2013).

2.4. AERODYNAMICS

The aerodynamics theory employed on the development of the aircraft is described, sharing it in two parts, the first considering the 2D theory that treats essentially of the airfoil aerodynamics, and the second considering the 3D theory that applies for the aircraft parts that are exposed to the air flow.

2.4.1. 2D – Aerodynamics

The 2D aerodynamics basically consider the loads and moment resulted of the air flow over an airfoil, which are, one normal force related to de air flow known as lift, one force parallel to the air flow known as drag and a moment called pitch moment. The intent of this topic is not explains from the fundamentals how this aerodynamics forces and moment are generated, it will be just presented the formulation that applies on the design of the airplane proposed on this work. The same approach is valid for the 3D aerodynamics topic.

Airfoils are aerodynamic two-dimensional geometry which resemble a drop of water, and give shape for the transversal section of the aerodynamic surfaces as wing and tails for example.

There are many airfoils geometry that were developed along the aeronautical history, as the necessities were occurring, as for example, applications for low and high speeds, small or high drag generation and the same for lift. These airfoils were developed under families that present similar aerodynamic characteristics. The most famous are the profiles of the NACA families, which were designed for different applications. It is not the objective of this text present these airfoils and its characteristics, for this purpose, there is available a vast bibliography.

2.4.1.1. Airfoil lift

The lift generated by an airfoil is commonly considered as a result from the difference of pressure between its lower and upper surface, and explained with the help of the Bernoulli's equation, actually there is other physical effect that contributes to the lift and knowns as Coanda effect, which was observed by Henry Coanda and explained with the help of the Newton's third law. The lift of an airfoil is normally expressed in the form of a coefficient denoted by cl.

In fact the lift generated by an airfoil is dependent on the angle which it is placed in relation to the air flow, the called attack angle. As the attack angle increases the lift generated by the profile increases either. When the profile reach a determined attack angle the lift generated is suddenly broken, for understanding this phenomenon it is necessary to introduce two concepts, the first is related to the viscosity, such property generates over the surface of the airfoil what is known as boundary layer, that is essentially a film of air that adhere on its surface and turn possible the air flow contour the profile, the other is the concept of pressure gradient, but it is not the intent to explain here its theory, it is enough says that, for a given value of attack angle, this boundary layer separates from the upper surface of the airfoil due changes on the local pressure gradient, causing the brake of the lift, this phenomenon is known as stall.

A very common way to visualize the change of the lift with respect to the attack angle is by the graphical showed on the Figure 2.14. The slope of the lift curve is defined by the Equation 2.60, and may be measured by performing experimental methods as running wind tunnel tests or estimated with the help of computational numerical methods.

$$a_0 = \frac{dcl}{d\propto} = cl_\alpha \tag{2.60}$$

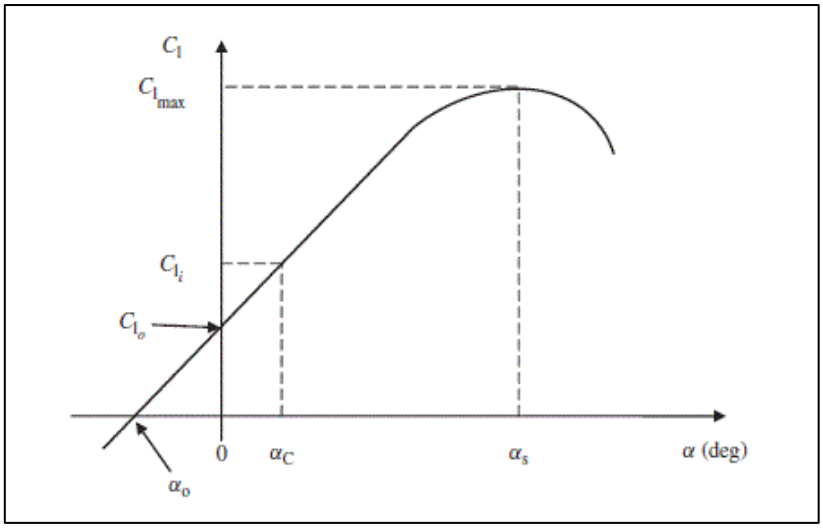


Figure 2.14 - Airfoil lift curve slope (Sadraey, 2013).

There are some kinds of stall, and they depend on the airfoil geometry. Next is presented a brief description about them.

Leading edge stall: occurs in airfoils of medium thickness, around 10% and 15% of the chord length. When the angle of attack reaches a determined value the boundary layer suddenly separates of the entire upper surface of the airfoil starting from some point over the leading edge. The occurrence of this phenomenon is normally due the geometry of the leading edge of the profile that has small ray. This condition characterizes an abrupt stall, in which few buffeting occur.

Trailing edge stall: is characteristic of thick airfoils, which the thickness is bigger than 15% of the chord length. For a given value of angle of attack the boundary layer starts its separation over the upper surface from the trailing edge of the profile, and as the angle of attack continues increase the separation of the boundary layer advances for the leading edge. This behavior is due the geometry of the leading edge which is on these profiles, normally more rounded and less sharp then that observed at airfoil with medium thickness. This stall is characterized by a clear buffeting of the wing as the separation of the boundary layer propagates, that turn this, a smooth and gradual stall.

Thin profile stall: due the small thickness of these airfoils, for very low angles of attack the boundary layer separates at the leading edge, once its ray is too small, as the angle of attack suffer a small increase the boundary layer re-attach generating a recirculation bubble over the upper surface of the profile, which grows with the increase on the angle of attack until cover the complete upper surface, when the angle of attack increase over this value, the bubble breaks causing the separation of the boundary layer from the trailing edge for the leading edge, causing the stall that is smooth and gradual as that observed on thick airfoils.

Lift increment

It is well known that the lift generated by an profile is dependent of its geometry, but, it is possible to change the geometry of the airfoil intending to improve the lift generated, the three most famous ways to do this is by flapping or slotting the profile, when the flapping is done on the leading edge of the airfoil it is called slat. Next will be describes a method based on experimental data that provides the increment on the lift generated by a profile due the flapping of its trailing edge.

The lift increment Δ_{cl} generated at an airfoil due the flap depends first of all, of the type of flap that is used. For a plain flap with sealed gap as showed on the Figure 2.15, the lift increment for a given profile is determined by the Equation 2.61.

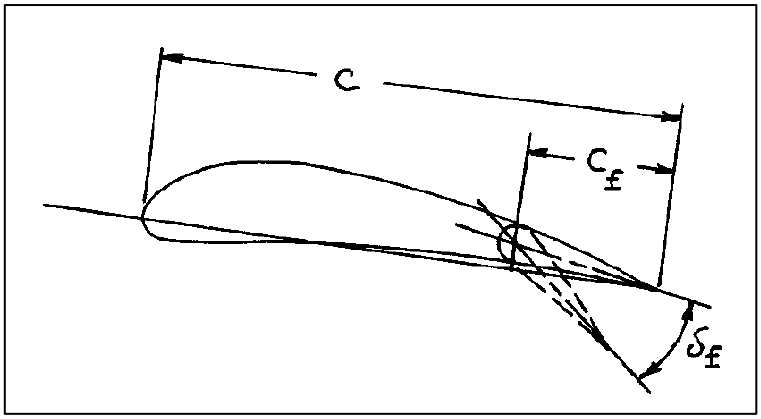


Figure 2.15 - Plain flap geometry (Roskam, 2000).

$$\Delta_{cl} = \delta_f \cdot \left\{\frac{cl_\delta}{(cl_\delta)_{theory}}\right\} \cdot (cl_\delta)_{theory} \cdot k' \tag{2.61}$$

The parameters $(cl_\delta)_{theory}$; k' and $\frac{cl_\delta}{(cl_\delta)_{theory}}$ may be found by the Figure 2.16 to Figure 2.18 respectively presented next.

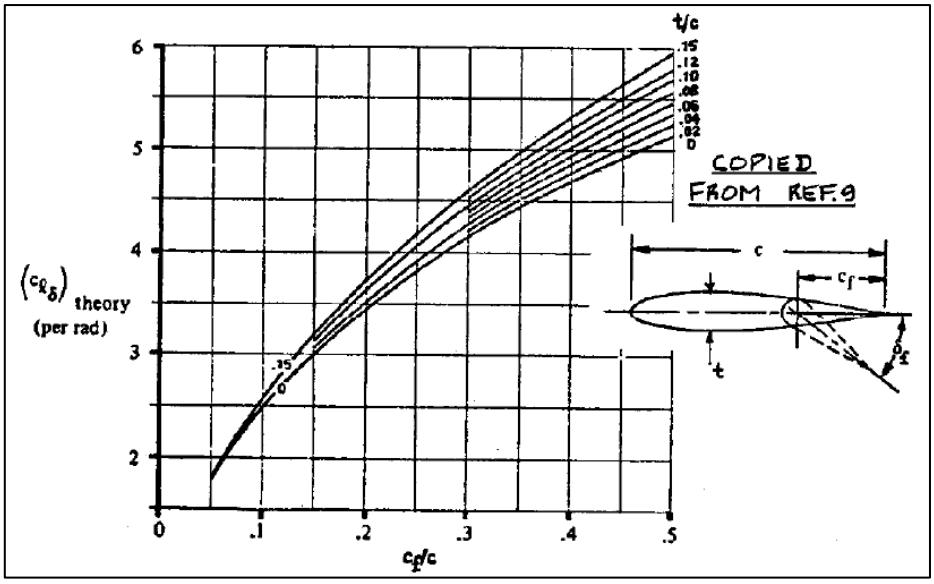


Figure 2.16 - Lift effectiveness of a plain flap (Roskam, 2000).

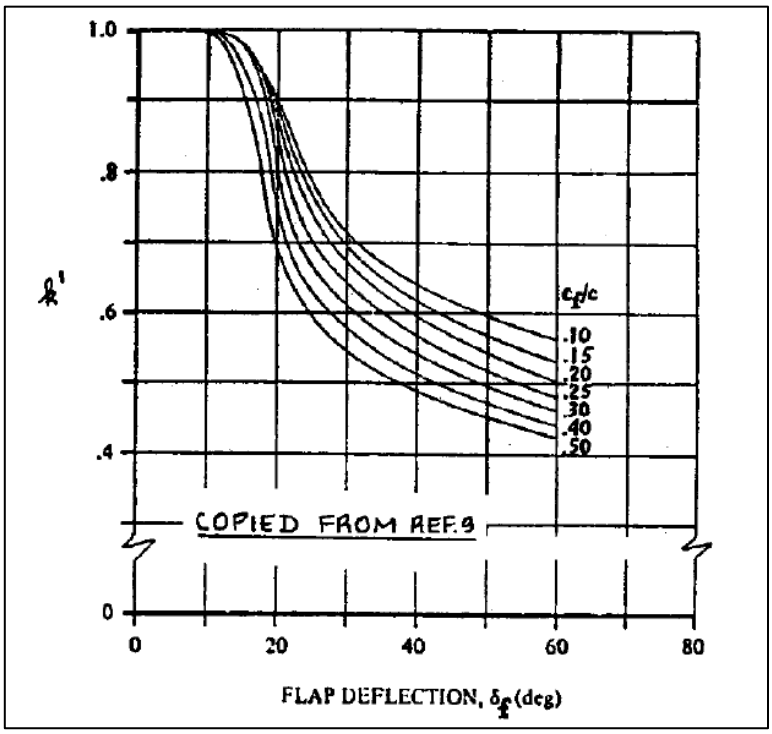


Figure 2.17 - Correction factor for nonlinear lift behavior of a plain flap (Roskam, 2000).

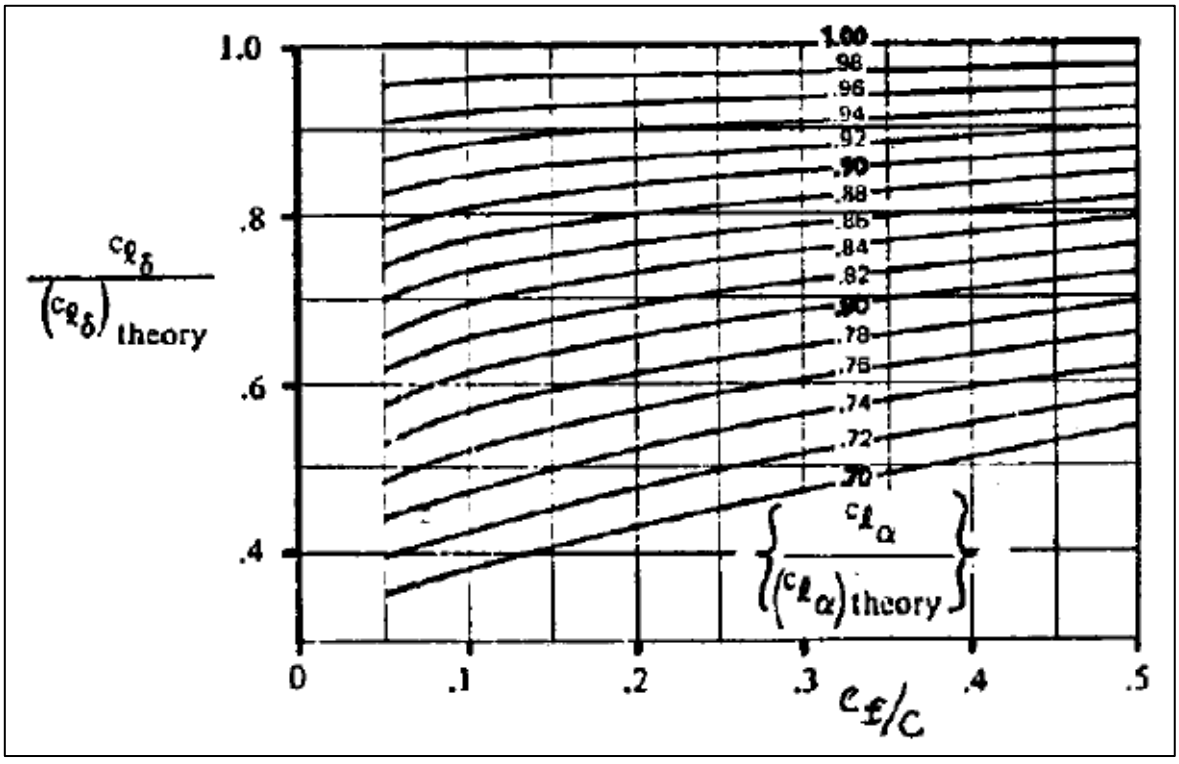


Figure 2.18 - Correction factor for plain flap lift (Roskam, 2000).

For the Figure 2.18, cl_α is the well known airfoil lift curve slope, that may be estimated by wind tunnel experimental data or by estimations on computational codes; the other parameter may be assumed as: $(cl_\alpha)_{theory} = 2\pi$.

The maximum increment on the lift coefficient of an airfoil $\Delta_{cl_{max}}$ can be obtained by the Equation 2.62, and its parameters are given by the Figure 2.19 to Figure 2.22.

$$\Delta_{cl_{max}} = k_1 k_2 k_3 \left(\Delta_{cl_{max}}\right)_{base} \tag{2.62}$$

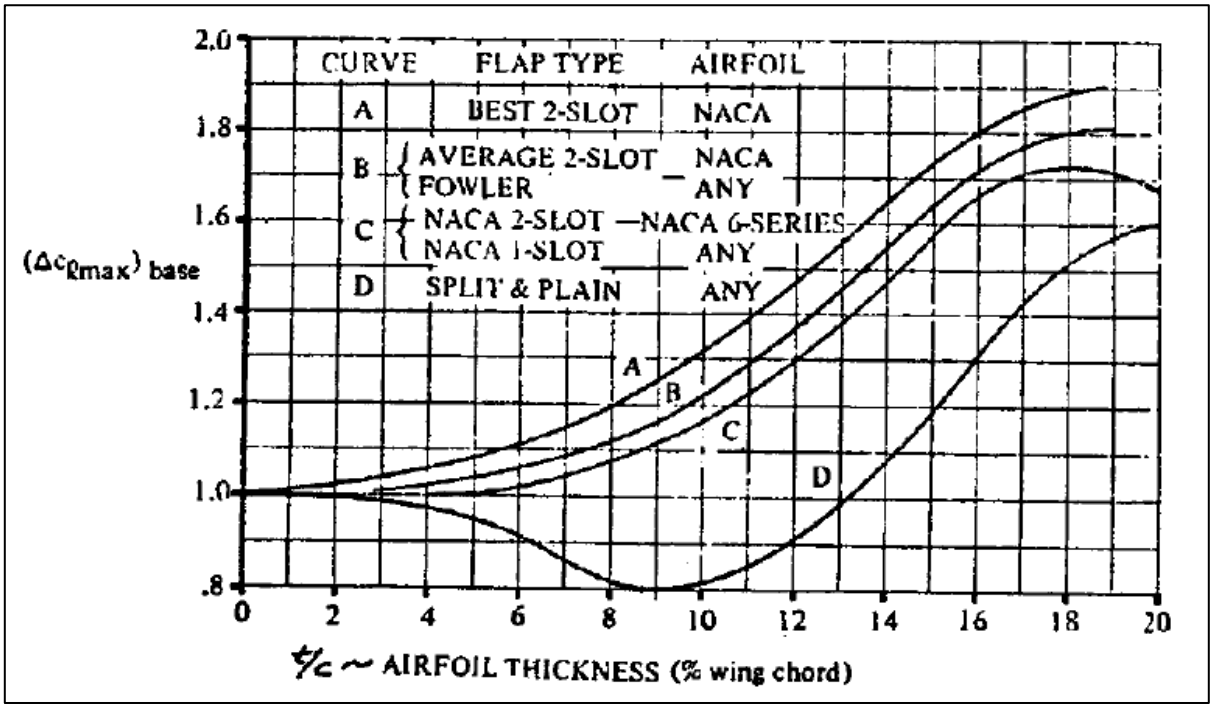


Figure 2.19 - Basic airfoil maximum lift increment due to trailing edge flap (Roskam, 2000).

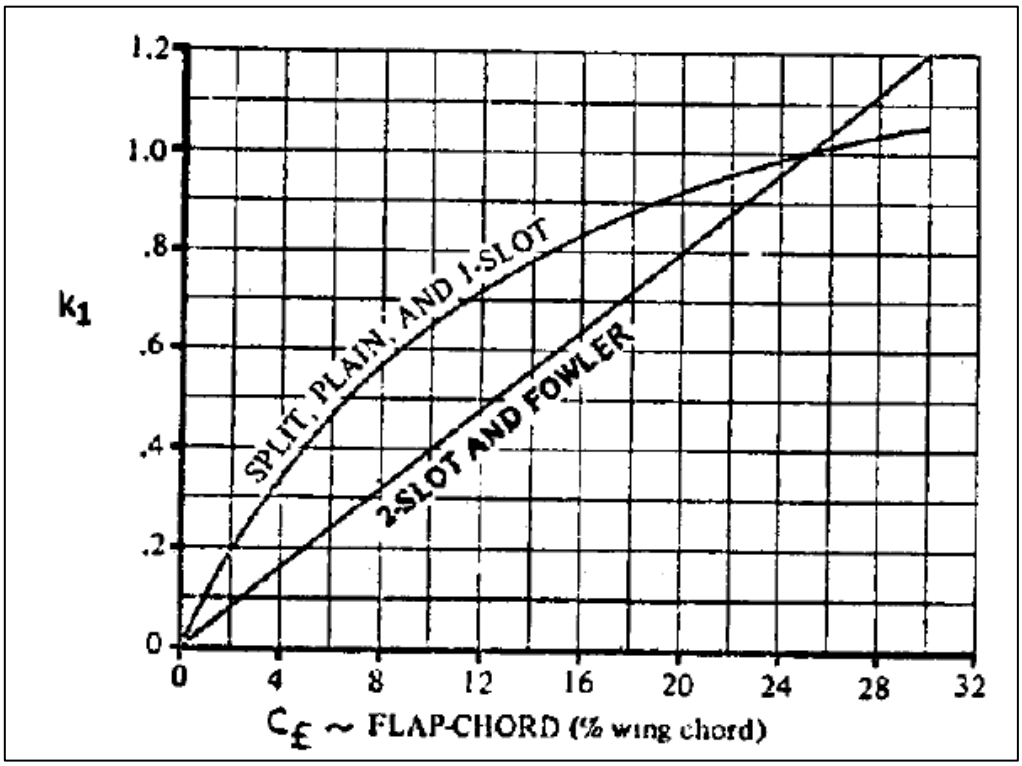


Figure 2.20 - Flap chord correction factor (Roskam, 2000).

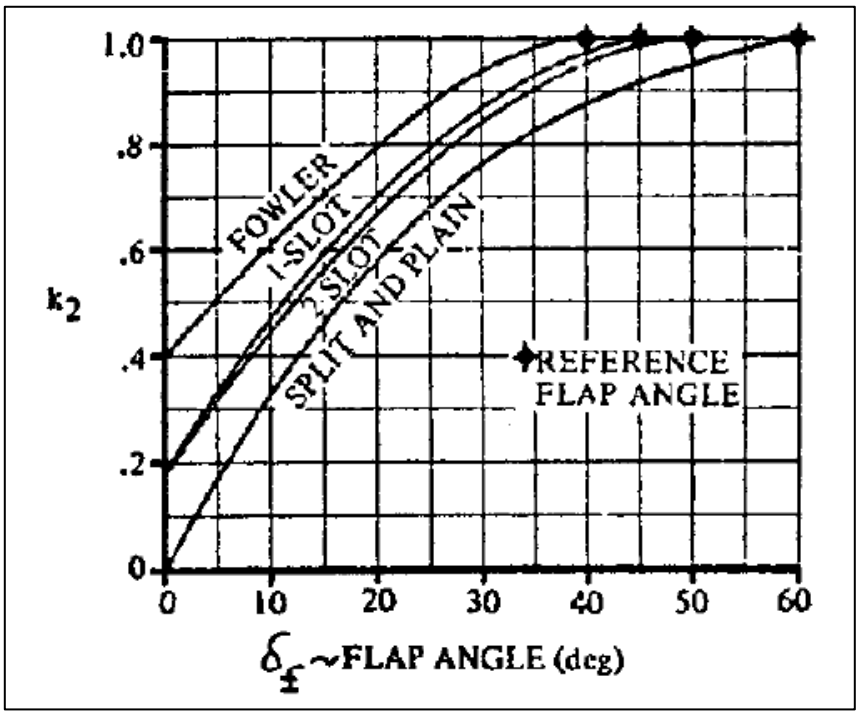


Figure 2.21 - Flap angle correction factor (Roskam, 2000).

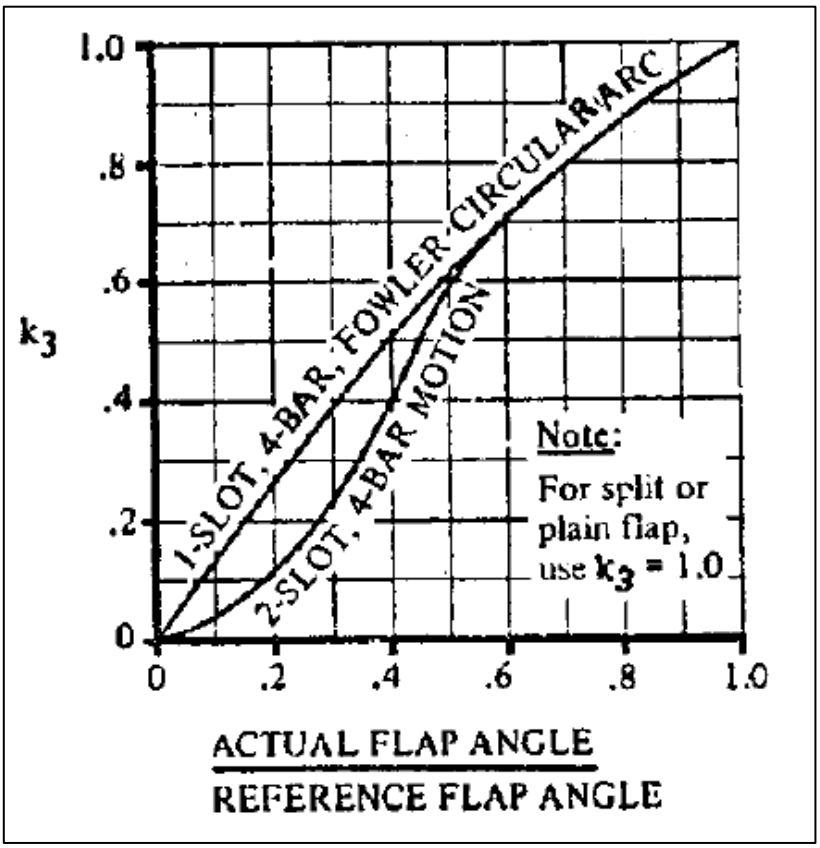


Figure 2.22 - Flap motion correction factor (Roskam, 2000).

2.4.1.2. Airfoil drag

Drag is the aerodynamic resistance imposed by the air flow that surrounds a given body, this force is parallel and opposed to the direction of the movement of the body, and is normally expressed in the form of a coefficient denoted by cd.

The drag generated by an airfoil is normally composed by two parcels one called skin friction drag and other called pressure drag, if the airfoil is subjected to a transonic flow or higher, appears a third parcel called wave drag. The composition of the drag generated by an airfoil may be described as on the Equation 2.63.

$$cd = cd_0 + cd_p + cd_w \tag{2.63}$$

The friction drag is due the friction of the air molecules of the boundary layer over the amount of the surface of the airfoil in which is attached, and it is strongly dependent of the viscosity of the air and its velocity inside the boundary layer and depends too of the geometry of the profile. The boundary layer may be laminar or turbulent what affects the parcel of the friction drag, on a way that, for laminar boundary layers the drag will be lower than that observed for turbulent one.

The pressure drag is the parcel that depends of the air pressure distribution around the surface of the airfoil, which in turn depends on the amount of the profile surface which has the boundary layer attached to it, in a way that, the more the boundary layer is attached to the airfoil surface, lower will be the pressure drag. The physical process that explains this phenomenon will not be described here, it is enough says that this is dependent of the pressure gradient along the profile surface.

As is done for the lift, the measurement of the drag generated by an airfoil may be done by experimental methods or by computational numerical methods.

2.4.1.3. Airfoil pitch moment

The pitch moment generated by an airfoil is consequence of the pressure distribution around it and is dependent of its chord length.

The air pressure distributed around the profile may be considered applied on a single point called pressure center of the airfoil, and its positioning along the chord varies as the angle of attack changes resulting in different values for the pitch moment, however, was observed that for a point localized at around 25% of the airfoil chord, the value for the pitch moment keeps reasonably constant as angle of attack changes, this point was called aerodynamic center of the airfoil, and it is the position considered for the pitch moment calculus at the development of an aircraft.

As well as for the lift and drag, the measurement of the pitch moment is done at the same way, and it is normally expressed in the form of a coefficient denoted by cm.

2.4.1.4. Reynolds number

The Reynolds number is a dimensionless parameter that relates inertial and viscous forces in a flow. This parameter affects directly the lift, the drag, the pitch moment and the stall of an airfoil, once it is related to the phenomenon that causes the separation of the boundary layer and in consequence, it is related to the characterization of laminar and turbulent flows. The Equation 2.64 defines the Reynolds number.

$$\mathrm{Re} = \frac{\rho_{FL} \cdot U_0 \cdot L_{ref}}{\mu} \tag{2.64}$$

2.4.2. 3D – Aerodynamics

This topic will only address the theory related to the aerodynamic configuration of the aircraft developed on this work, considering first the theories about the biplane configuration, the canard configuration and the pusher configuration, on the sequence, the theories related to the fundamental aerodynamic forces and moments.

2.4.2.1. Biplane configuration

This configuration is advantageous wen are desired low stall speeds, other advantages are short span, lower wing loading and lower structural weight when compared to a single wing configuration, its disadvantage is aerodynamics efficiency penalties. The theory (Raymer, 2006) indicates that biplane wings theoretically produces half of the induced drag produced by a monoplane of same span, however, the aerodynamic interference between each wing of the biplane reducing this advantage regarding induced drag to about 30% instead 50%, when well designed.

The span efficiency factor for a biplane may be estimated by the Equation 2.65 that is based on an interference factor developed by Prandtl, which is showed on the Figure 2.23. For a conventional configuration, basing on an extensive data from experimental wind tunnel tests using a wide variety of wing shape, was obtained the following empirical expression for the span efficiency factor given by the Equation 2.66.

$$e = \frac{\mu^2 \cdot (1+r^2)}{\mu^2 + 2 \cdot \sigma \cdot \mu \cdot r + r^2} \tag{2.65}$$

$$e = \frac{2}{2 - AR + \sqrt{4 + AR^2 \cdot (1 + tan^2 \Lambda_{t_{max}})}} \tag{2.66}$$

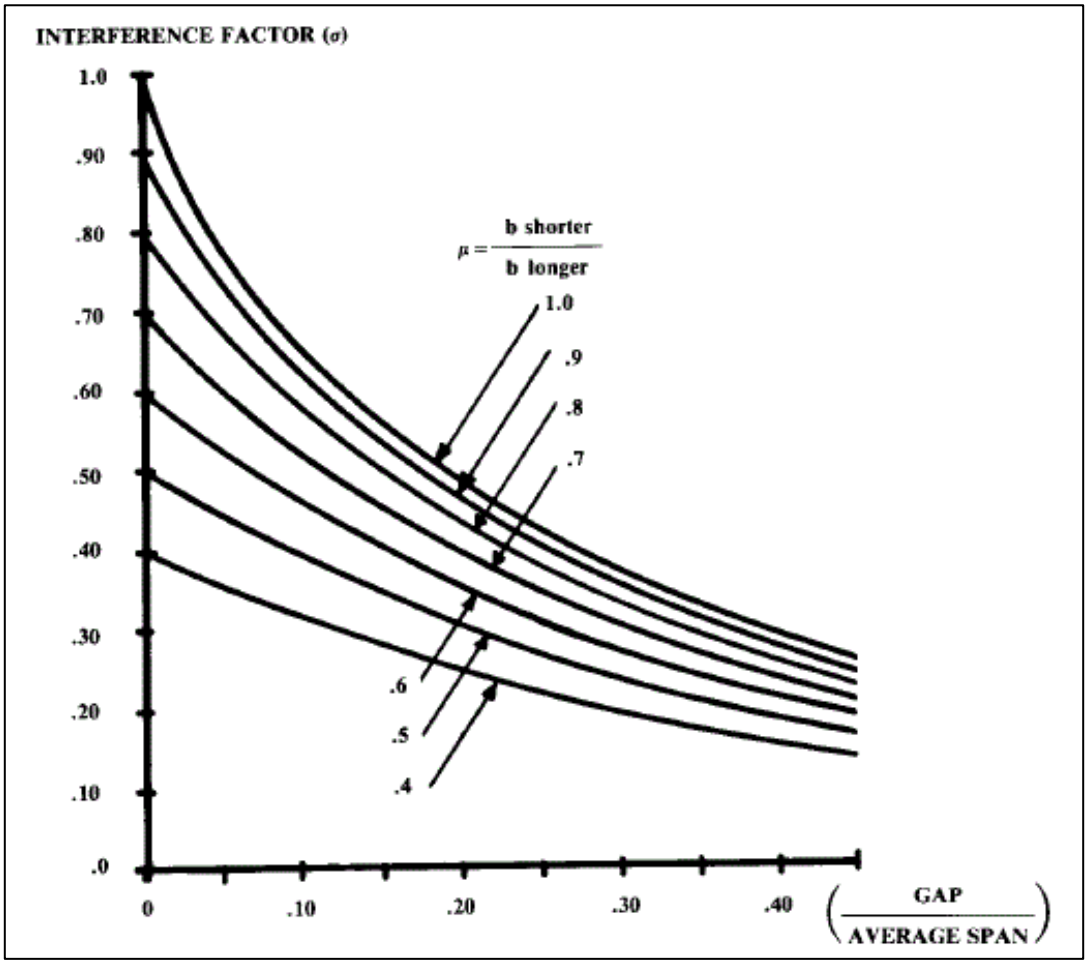


Figure 2.23 - Biplane interference factor (Raymer, 2006).

Some geometrical parameters for the biplane configuration have to be defined on a different manner, as biplane AR where on the Equation 2.1, the span is the longest between both wings and the area is sum of the lower and upper wings reference areas as presented on the Equation 2.67.

$$AR_B = \frac{b_{long}^2}{S_T} \tag{2.67}$$

Other parameter is the $\bar{C}_{W\_B}$ that may be obtained by calculating the weighted average of the mean aerodynamic chord of the lower and upper wings weighted by the relative areas of both wings. For the aerodynamic assess will be considered the $\bar{C}$ of each wing separately, and for dynamics of flight will be considered the $\bar{C}_{W\_B}$ or the $\bar{C}$ of each wing depending on the application.

The AC of a biplane is normally considered at 23% instead 25% of the $\bar{C}$ due the wings aerodynamic interference (Raymer, 2006). But for this airplane the AC of each wing will be considered at 25% once the stagger between both wings is too large, and the GAP bigger than one wing chord, what as a preliminary approach is considered that the change on the AC position may be neglected. The biplane configuration is characterized by four parameters that are described next.

Gap

It is the vertical distance between the wings, on the ideal condition where the gap is infinite, the induced drag will be the half compare to an equivalent monoplane. The closer the wings been from each other, that is, the smaller be the gap, bigger will be the interference between the wings. It is common the gap has the dimension of the chord of the wing.

Span ratio

It is the ratio between the smallest and the biggest span. For a ratio equal to one there is obtained the smallest induced drag.

Stagger

It is the displacement on x axis between the two wings, it is positive when the upper wing is located ahead the lower one. This parameter is measured by an angle, which is defined by a vertical line starting on the leading edge of the lower wing and other line between the leading edges of both wings. When negative, helps to reduce the negative pitch moment generated by the lower wing when equipped whit flaps. When positive the stagger helps the inferior visibility of the pilot. The Figure 2.24 shows a representation of the stagger.

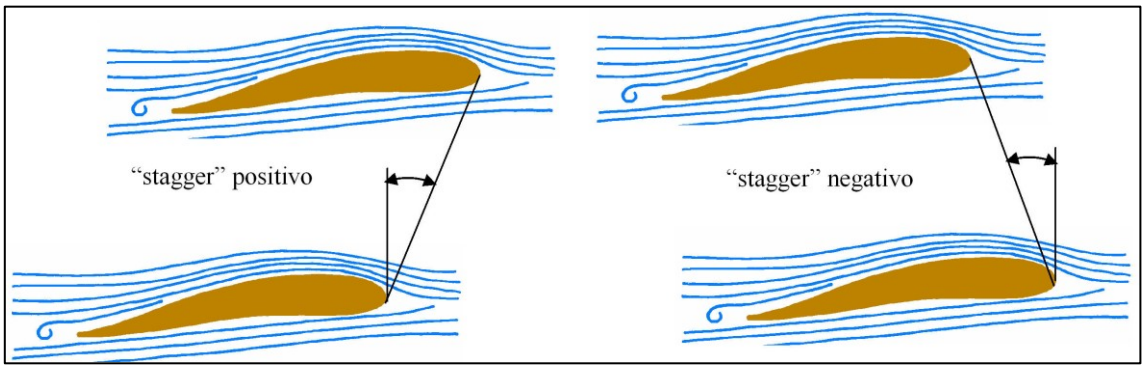


Figure 2.24 - Positive and negative stagger representation (Rodrigues, 2011).

Decalage

It is the relative incidence angle between the two wings, and is considered positive when the upper wing has incidence bigger the lower one.

2.4.2.2. Canard configuration

The canard configuration is that in which the horizontal stabilizer is located ahead of the wing. One of the advantages of this configuration is that the horizontal stabilizer is located out of the turbulent flow generated by the wing. There are two types of canard, the lifting canard and the control canard, the control characteristics related to canards will be described on the topic relative to dynamics of flight.

The canard in opposition to the conventional horizontal tail, generates positive lift for trimming the airplane, in consequence contributes to reduce the induced drag generated by the wing, therefore, less lift generated by it will be necessary, consequently, the angle of attack will be lower.

One important question related to the canard design is the wake generated by it on the wing, along a length of the wing span equal to the canard span; in other words, the problem is the downwash field over the wing. As consequence, the incidence of the wing will have to be increased, and how the lift is perpendicular to the local flow, will appear a drag parcel due the downwash angle on the wing region, turning lower the effective lift generated by it. The downwash over the wing is proportional to the canard to wing area ratio, to the canard to wing span ratio, to the horizontal and vertical distances between both and the angle of attack of the aircraft. This condition degrades the induced drag generated by the wing and increases the

bending moment on the wing root. All these effects may be reduced by positioning the canard well ahead and below the wing; other aspect that helps reduce these effects is to define an airfoil to the wing region affected by the canard wake with opposite camber.

When designing an airplane with canard configuration it is very important keep in mind that for safety, it is mandatory that the canard stalls first relative to the wing. By ensuring this, the airplane nose will go down avoiding the wing stall. For the canard stalls first, its aspect ratio must be bigger than the wing's one, and the CG position of the airplane must be located ahead when compared to the CG position of a conventional aircraft.

When the canard stalls, it is generated a pitch down moment and the wing lift increases due the reduction of the downwash over it, what contributes to the pitch down moment.

In addition, other very important design decision is related to the airfoil to be used on the canard, once it impacts significantly the behavior of the airplane, mainly during the stall. It is necessary have in mind that as the canard must stall first, the choice of designing of the airfoil have to consider the Reynolds number, once it affects the stall characteristics of the profile as for example, the main parameter to be considered, the angle of attack for maximum lift, or stall. If a laminar airfoil is selected, particular attention should be paid to the transition from laminar to turbulent flow, as in rain condition, once this may affects the lifting generated by the canard and the premature boundary layer separation may happens, what must be avoided.

Concluding, after all these considerations, if an airplane is designed for the canard stalls first relative to the wing, this airplane will never face a condition of deep stall, on other words, the aircraft will never to depart.

2.4.2.3. Pusher configuration

The pusher thrust configuration from the aspect of aerodynamics, has the advantage of have the wing and stabilizers out of vortex wake generated by the propeller, avoiding degrading the drag of the airplane. This configuration still has the advantage of reducing the noise and vibration on the cabin interior and clean the pilot visibility, once the propeller will not interfere to the vision of the pilot.

The disadvantage is that in this configuration the propeller will be immersed on the airplane wake, what obviously degrades its efficiency, other problem is related to the engine refrigeration that is penalized either.

2.4.2.4. Lift

The Equation 2.68 gives the general physic relation that governs the lift generated by an aerodynamic body. As well as presented on the 2D theory, it is possible define the lift curve slope for a 3D body, as showed by the Equation 2.69, and based on this equation is possible to obtain the lift coefficient for the angle of attack equal zero, which will be necessary for the aerodynamic characterization of the airplane, this relation is presented on Equation 2.70.

$$L = \frac{1}{2} \cdot CL \cdot \rho_{FL} \cdot U_0 \cdot S_{aero} \tag{2.68}$$

$$CL_\alpha = \frac{Cl_\alpha}{\left(1+\left(\frac{Cl_\alpha}{\pi \cdot e \cdot AR}\right)\right)} = \frac{dCL}{d\propto} \tag{2.69}$$

$$CL_{\alpha=0} = CL_\alpha \cdot (0 - \alpha_{CL=0}) \tag{2.70}$$

For the airplane that is the work object of this text, the formulation presented now considers its configuration particularities.

The lift generated by the complete airplane in flight may be estimated by sum of the lift generated by the main aerodynamic components as presented on the Equation 2.71. On this equation the lift parcel due the lower wing is incremented by the contribution of the flaps, the lift parcel of the upper wing is incremented by the contribution of the ailerons, the lift parcel of both canards are incremented by the contribution of the elevators, and the lift parcel of the fuselage is based on the lift generated by the wings. The lift generated by both vertical tails don't contribute to the lift generated by the airplane as a whole, due the direction of application of these forces, but, it is necessary says that, they are obtained the same way as is the lift generated by the canards, applying the same equations. For each one of these parcels occurs a lift increment due the contribution of the wash fields that will be detailed in a posterior topic.

$$L = L_{W\_LOW} + L_{W\_UP} + L_{CAN\_LOW} + L_{CAN\_UP} + L_{FUS} \tag{2.71}$$

Lower wing

The lift generated by the lower wing is first estimated in terms of lift coefficient by the Equation 2.72, and applying this result on the Equation 2.68 above, is obtained the value for the lift.

$$CL_{W_{LOW}} = \left(\left(\left(CL_{\alpha_{W_{LOW}}} + \Delta CL_{\alpha_{W_{LOW}}}\right) \cdot \left(\left(\alpha - \alpha_{CL=0_{W_{LOW}}}\right) + i_{W_{LOW}}\right)\right) \cdot \cos\left(\Gamma_{W_{LOW}}\right)\right)$$

$$+\Delta CL_{FLAP} \tag{2.72}$$

The lift increment due the trailing edge plain flaps deflection is obtained by the formulation presented on the Equation 2.73, which applies the parameters obtained by the graphics of the Figure 2.25, the Figure 2.26 and the parameter obtained from Equation 2.61.

$$\Delta CL_{FLAP} = k_b \cdot \Delta_{cl} \cdot \left(\frac{CL_{\alpha_{W\_LOW}}}{cl_\alpha}\right) \cdot \left[\frac{(\alpha_\delta)_{CL}}{(\alpha_\delta)_{cl}}\right] \tag{2.73}$$

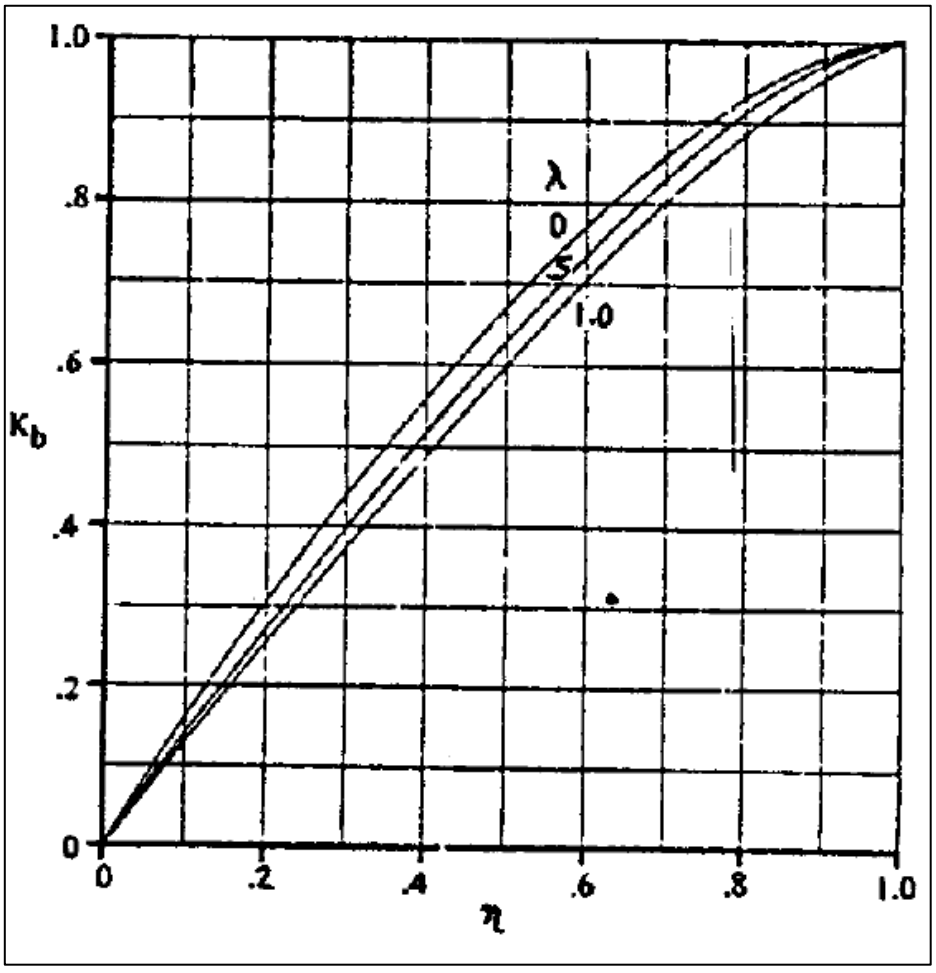


Figure 2.25 - Effect of taper ratio and flap span to wing span ratio on k_b (Roskam, 2000).

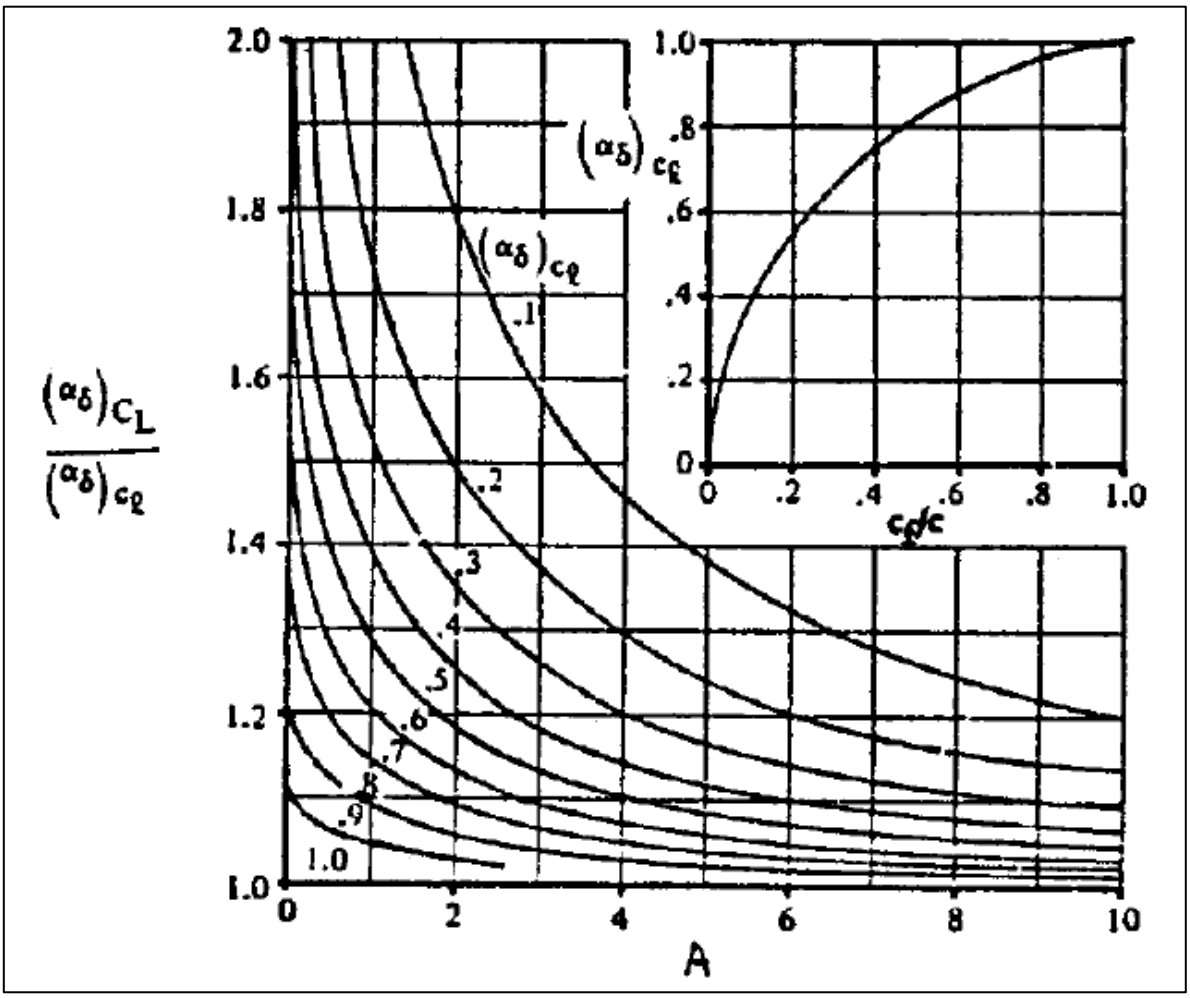


Figure 2.26 - Effect of aspect ratio and flap chord ratio on the three dimensional flap effectiveness (Roskam, 2000).

Concluding the flaps dimensioning, now the maximum lift increment due to trailing edge plain flaps deflection can be estimated by the Equation 2.74, which uses the parameter obtained from the Equation 2.62, Figure 2.27 and the Figure 2.28. Substituting this equation solved on the Equation 2.72 it is obtained the maximum lift generated by the lower wing, which is valid just for the stall condition.

$$\Delta CL_{FLAP\_max} = \Delta_{cl_{max}} \cdot \left(\frac{S_{W_f}}{S_{aero_{W\_LOW}}}\right) \cdot k_\Lambda \tag{2.74}$$

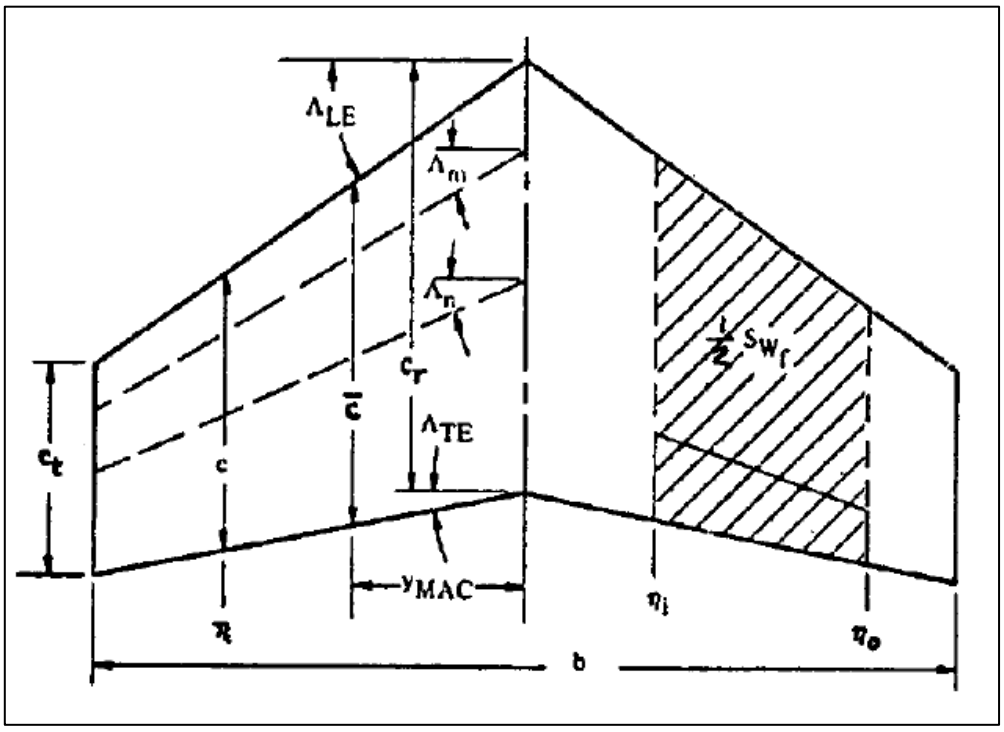


Figure 2.27 - Definition of flapped wing area (Roskam, 2000).

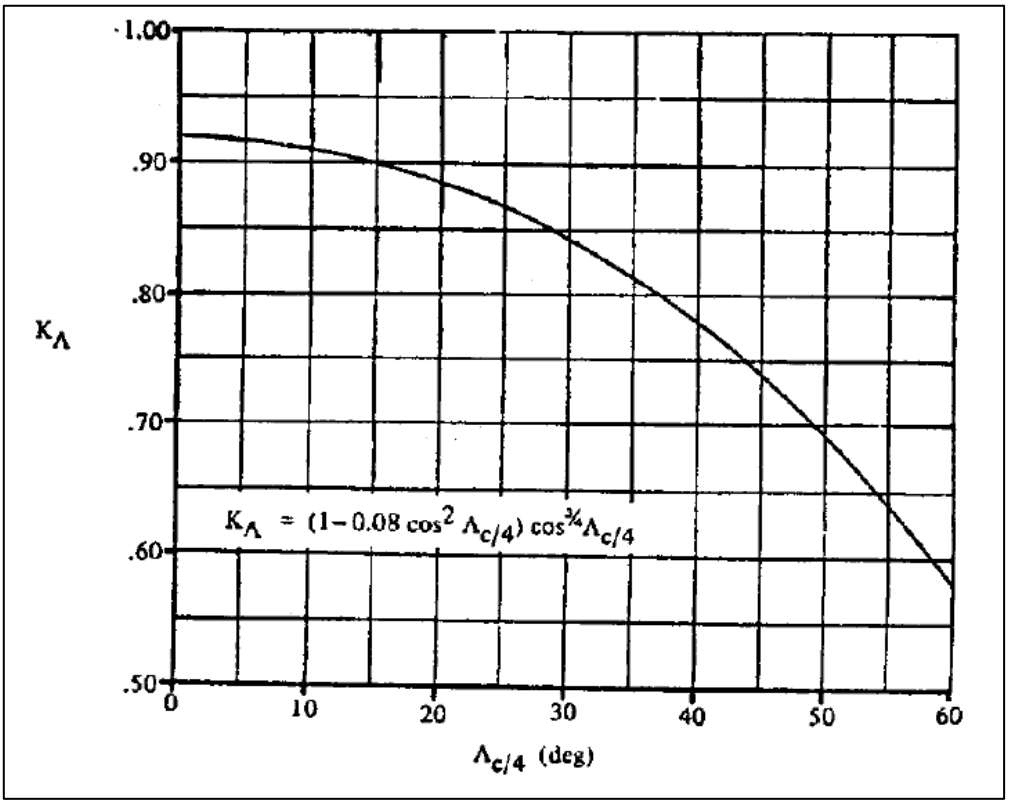


Figure 2.28 - Effect of sweep on planform correction factor (Roskam, 2000).

Upper wing

The lift generated by the upper wing is first estimated in terms of lift coefficient by the Equation 2.75, and applying this result on the Equation 2.68 above, it is obtained the value for the lift.

$$CL_{W\_UP} = \left(\left(\left(CL_{\alpha_{W\_UP}} + \Delta CL_{\alpha_{W\_UP}}\right) \cdot \left(\left(\alpha - \alpha_{CL=0_{W\_UP}}\right) + i_{W\_UP}\right)\right) \cdot \cos\left(\Gamma_{W\_UP}\right)\right) + \Delta CL_{AIL\_LEF} + \Delta CL_{AIL\_RIG} \quad (2.75)$$

For the lift increment due the ailerons deflection, this work proposes to apply the theory of lift increment for the primary control surfaces (Sadraey, 2013) as defined on the Equation 2.76 and on the Equation 2.77 which applies the parameter obtained by the graphic of the Figure 2.29.

$$\Delta CL_{AIL} = C_{L_{W_{\delta A}}} \cdot \delta_A \quad (2.76)$$

$$C_{L_{W_{\delta A}}} = \frac{\partial C_{L_W}}{\partial \delta_A} = \frac{\partial C_{L_W}}{\partial \alpha_W} \cdot \frac{\partial \alpha_W}{\partial \delta_A} = C_{L_{\alpha_{W\_UP}}} \cdot \tau_A \quad (2.77)$$

Despite the lift increment due the primary control surfaces is provided above, this work propose another manner to estimates the lift increment due the primary control surfaces deflection, that is simply to apply the flap theory (Roskam, 2000), but, as can be observed in the graphs of the 2D part of the theory, negative deflections for the flaps panels are not predicted, what open way for some new studies about this theme. Due this reason, the lift increment due the three primary control surfaces estimates were based on the Equation 2.76 and Equation 2.77.

Canards

The lift generated by each canard is obtained the same way that was done before for the wings, first estimated in terms of lift coefficient by the Equation 2.78 and Equation 2.79 and on the sequence applying these results on the Equation 2.68 above, it is obtained the value for the lift generated by each canard.

$$CL_{CAN\_LOW} = \left(\left(\left(CL_{\alpha_{CAN\_LOW}} + \Delta CL_{\alpha_{CAN\_LOW}}\right) \cdot \left(\left(\alpha - \alpha_{CL=0_{CAN\_LOW}}\right) + i_{CAN\_LOW}\right)\right) \cdot \cos\left(\Gamma_{CAN\_LOW}\right)\right) + \Delta CL_{E\_LOW} \quad (2.78)$$

$$CL_{CAN\_UP} = \left(\left(\left(CL_{\alpha_{CAN\_UP}} + \Delta CL_{\alpha_{CAN\_UP}}\right) \cdot \left(\left(\alpha - \alpha_{CL=0_{CAN\_UP}}\right) + i_{CAN\_UP}\right)\right) \cdot \cos\left(\Gamma_{CAN\_UP}\right)\right) + \Delta CL_{E\_UP} \quad (2.79)$$

The lift increment due the elevator deflection which is the last term on the Equation 2.78 and on the Equation 2.79, is obtained by the formulation presented on the Equation 2.80 and on the Equation 2.81 which applies the parameters obtained by the graphic of the Figure 2.29.

$$\Delta CL_{ELEV} = CL_{CAN_{\delta E}} \cdot \delta_E \quad (2.80)$$

$$CL_{CAN_{\delta E}} = \frac{\partial C_{L_{CAN}}}{\partial \delta_E} = \frac{\partial C_{L_{CAN}}}{\partial \alpha_{CAN}} \cdot \frac{\partial \alpha_{CAN}}{\partial \delta_E} = CL_{\alpha_{CAN}} \cdot \tau_E \quad (2.81)$$

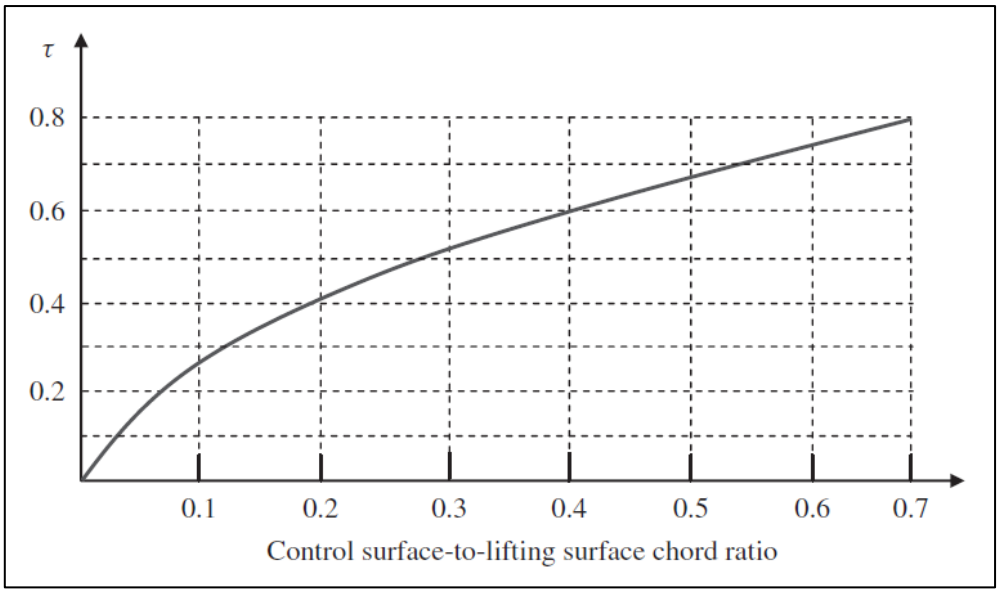


Figure 2.29 - Control surface effectiveness parameter (Sadraey, 2013).

Fuselage

The theory presented on the bibliography (Roskam, 2000) predicts the lift generated by the set wing-fuselage, given by the Equation 2.82 to the Equation 2.84, but, on this work it is proposed to estimates the fuselage alone lift as presented on the Equation 2.85 and on the

Equation 2.86, which are based on the Equation 2.82, Equation 2.72 and on the Equation 2.75. Note that, once more, the lift parcel for the fuselage was defined in terms of aerodynamic coefficient. To obtain the value for the lift generated by the fuselage, just apply this result on the Equation 2.68. Note that on the Equation 2.82 the lift curve slope of the wing is assumed as being the lift curve slope for the biplane equivalent wing.

$$CL_{\alpha_{W-F}} = k_{wf} \cdot CL_{\alpha_{W\_B}} \tag{2.82}$$

$$k_{wf} = 1 + 0.025 \cdot \left(d_f / b_W\right) - 0.25 \cdot \left(d_f / b_W\right)^2 \tag{2.83}$$

$$d_f = \sqrt{\frac{4}{\pi} \cdot S_{F_{max-cs}}} \tag{2.84}$$

$$CL_{\alpha_F} = CL_{\alpha_{W-F}} - \frac{\left(CL_{\alpha_{W\_LOW}} + CL_{\alpha_{W\_UP}}\right)}{2} \tag{2.85}$$

$$CL_{FUS} = CL_{\alpha_F} \cdot \alpha \tag{2.86}$$

Airplane lift curve slope

The theory do not provide a manner to estimate the lift of the airplane in terms of aerodynamic coefficient and its curve slope, so, this work proposes the following method.

Considering the Equation 2.71 in terms of aerodynamic coefficients, by parametrizing each parcel by the aerodynamic area of the biplane wing, and applying it to the right side of the Equation 2.69 it become the airplane lift curve slope.

2.4.2.5. Drag

To estimate the drag produced by an airplane in flight, first it is necessary to estimate the drag generated by each part of this airplane that is in contact to the air flow. However, on the real flight condition occurs interaction between the flows that surrounds these parts, causing interferences between them. The theory presented here is simplified and don't accounts these interferences.

In practical terms considering the development of an airplane, it is recommended to make the interface areas with ninety degrees between the parts to be joined, for minimize what

is known as interference drag. One way to turn smooth the flow on these regions and in consequence reduces the drag is fairing it.

Before beginning the description of the drag formulation for the airplane, it is necessary to explicit one type of drag that is present in all flight condition where a body produces lift, this is known as induced drag and is directly related to the lift generated by this body, such drag is defined by the Equation 2.87.

$$CD_i = \frac{CL^2}{\pi \cdot e \cdot AR} \tag{2.87}$$

Done the preliminary considerations above, the drag generated by the whole aircraft may be defined by the Equation 2.88 that is known as the airplane drag polar. This mathematical relation is very important on the assessing of an airplane, once it is related to its performance. The equation was adapted for the particularities of the aerodynamic configuration of the aircraft UFU-1, and again it is developed in terms of aerodynamic coefficients. One important note must be done before the drag formulation itself, that is, all the drag parcels of the Equation 2.88 are parametrized in function of the total aerodynamic area of the biplane wing.

$$CD = CD_{W\_LOW} + CD_{W\_UP} + CD_{CAN\_LOW} + CD_{CAN\_UP} + CD_{FAIR\_CAN} + CD_{VT\_LEF} + CD_{VT\_RIG} + CD_{VT\_BOOM} + CD_{FUS} + CD_{LGEAR} + CD_{PROP} \tag{2.88}$$

Wings

The method developed here is valid for both wings. The theory (Roskam, 2000) proposes the Equation 2.89 for estimate the drag generated by the wing, in this equation the first term developed in the Equation 2.90 is related to the condition of zero lift and the second term developed in the Equation 2.91 is the induced drag.

$$CD_W = CD_{0_W} + CD_{i_W} \tag{2.89}$$

$$CD_{0_W} = R_{wf} \cdot R_{LS} \cdot C_{f_W} \cdot [1 + L' \cdot (t/c) + 100 \cdot (t/c)^4] \cdot \frac{S_{W_{wet}}}{S_W} \tag{2.90}$$

$$CD_{i_W} = \frac{CL_W^2}{\pi \cdot e_W \cdot AR_W} \tag{2.91}$$

The solution above is valid for a conventional airfoil that produces a turbulent boundary layer over almost all its surface, however, if a laminar airfoil is employed on the design of the wing, this equation must be substituted by the Equation 2.92.

$$CD_{0_W} = R_{wf} \cdot R_{LS} \cdot [1 + L' \cdot (t/c) + 100 \cdot (t/c)^4] \cdot \frac{\left[\left(C_{f_{W_{lam}}} - C_{f_{W_{turb}}}\right) \cdot S_{W_{wet_{lam}}} + C_{f_{W_{turb}}} \cdot S_{W_{wet}}\right]}{S_W} \quad (2.92)$$

As defined on the theory (Roskam, 2000) the first term of the Equation 2.89 is due the zero lift condition, but, it is function of the airfoil geometric parameters as its thickness, what may be associated to the pressure drag, and the friction coefficient what may be associated to the skin friction drag. So, it is observed that this first term is valid for estimates when the airfoil was not specified yet.

This work proposes that the first term of the Equation 2.89 is indeed, the characterization of the aerodynamic properties of the airfoil employed on the design of the wing, and once this profile is known and is possible to obtain its aerodynamic coefficient data, the first term of the wing drag equation may be considered for any lift condition. Based on this, it is proposed the Equation 2.93 in substitution of the Equation 2.90 and of the Equation 2.92.

$$CD_{0_W} = R_{wf} \cdot R_{LS} \cdot cd_W \quad (2.93)$$

The parameters R_{wf}, R_{LS}, C_{f_W} and L' may be obtained by the Figure 2.30 to Figure 2.33.

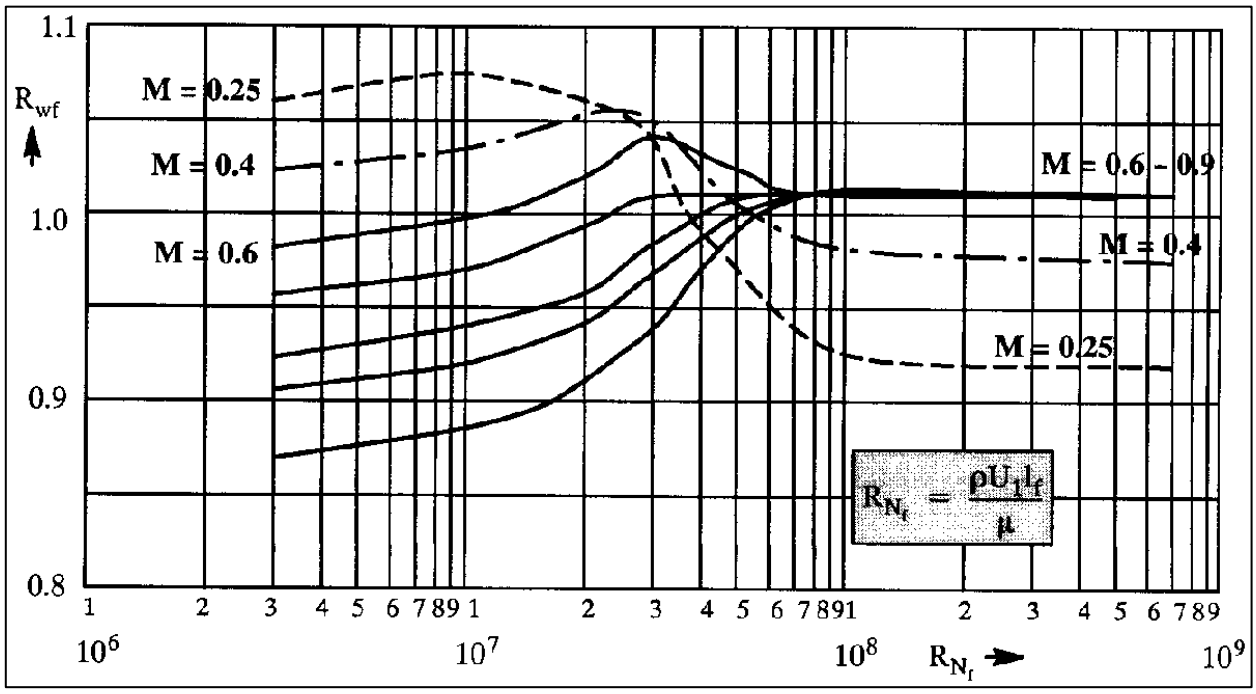


Figure 2.30 - Wing fuselage interference factor (Roskam and Lan, 1997).

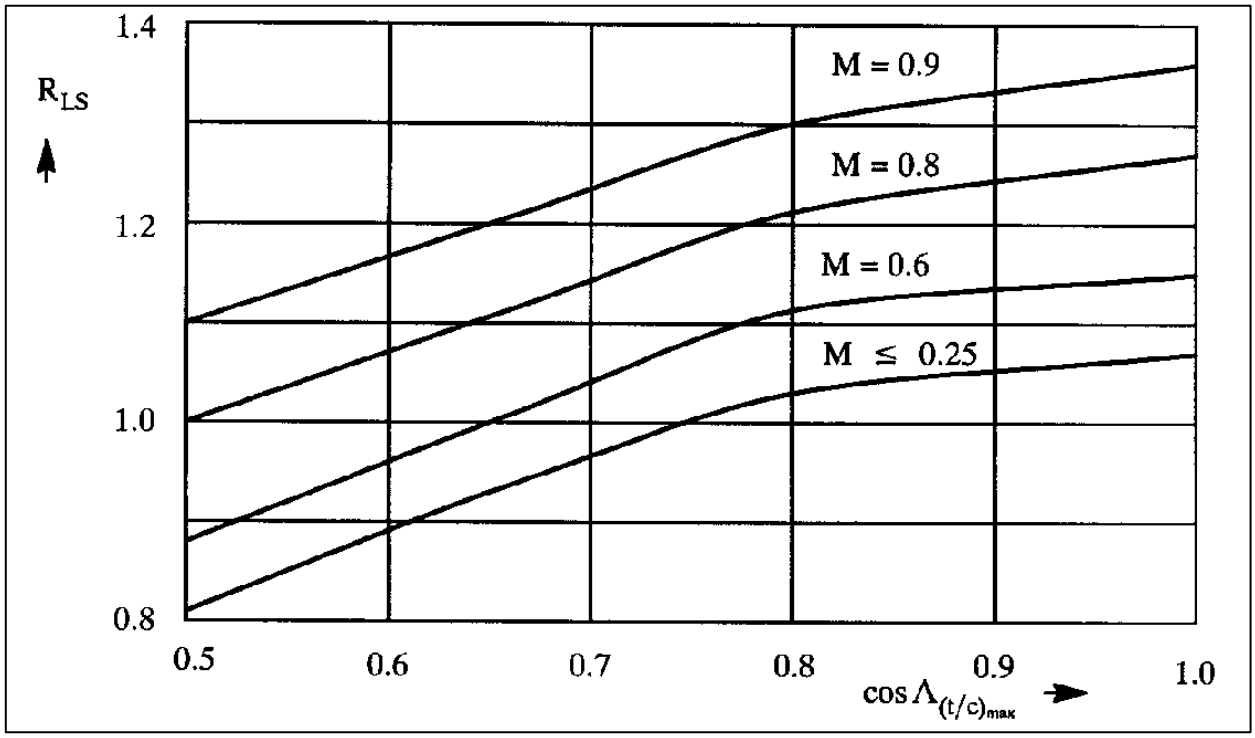


Figure 2.31 - Lifting surface correction factor (Roskam and Lan, 1997).

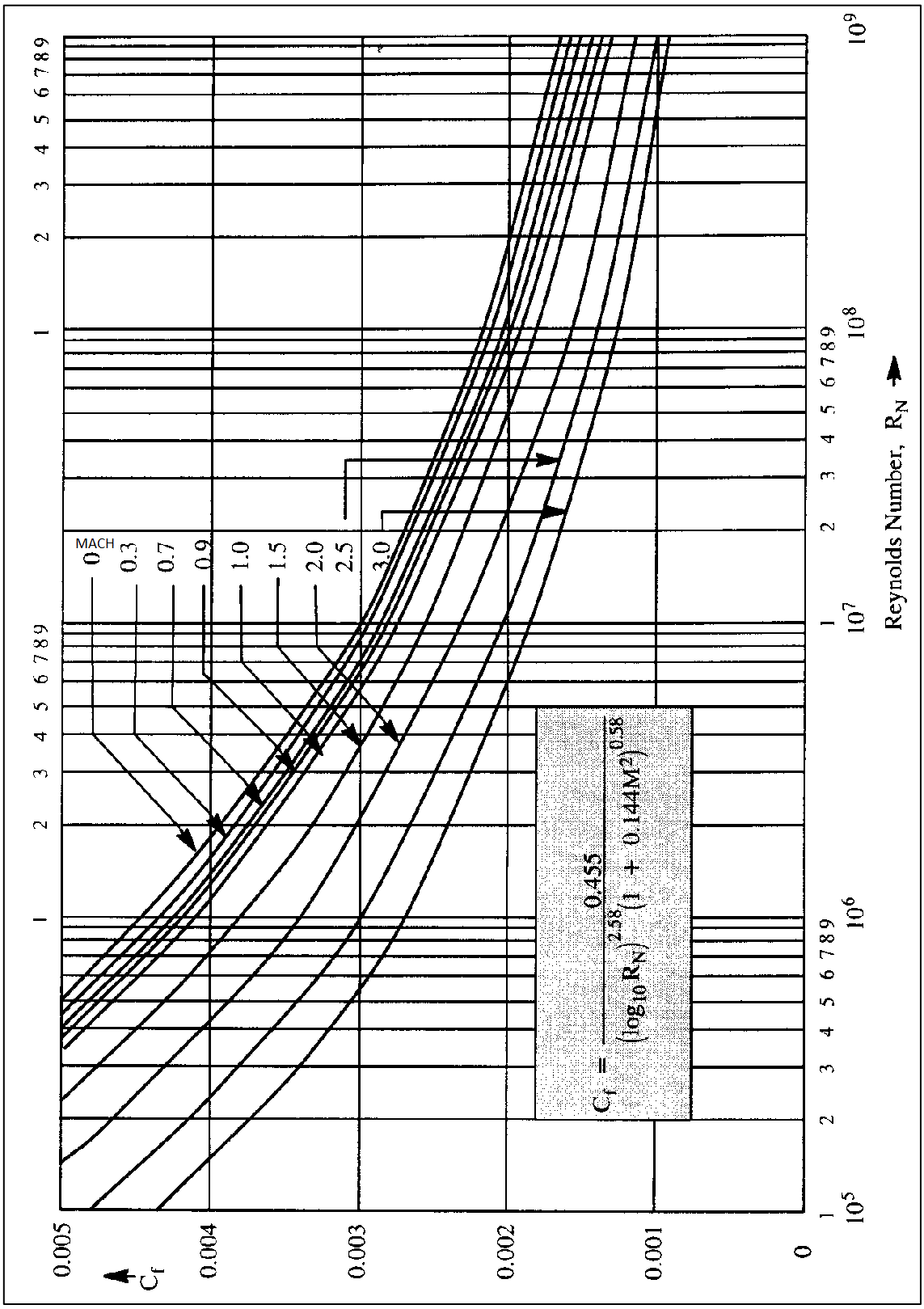


Figure 2.32 - Turbulent mean skin friction coefficient (After Roskam and Lan, 1997).

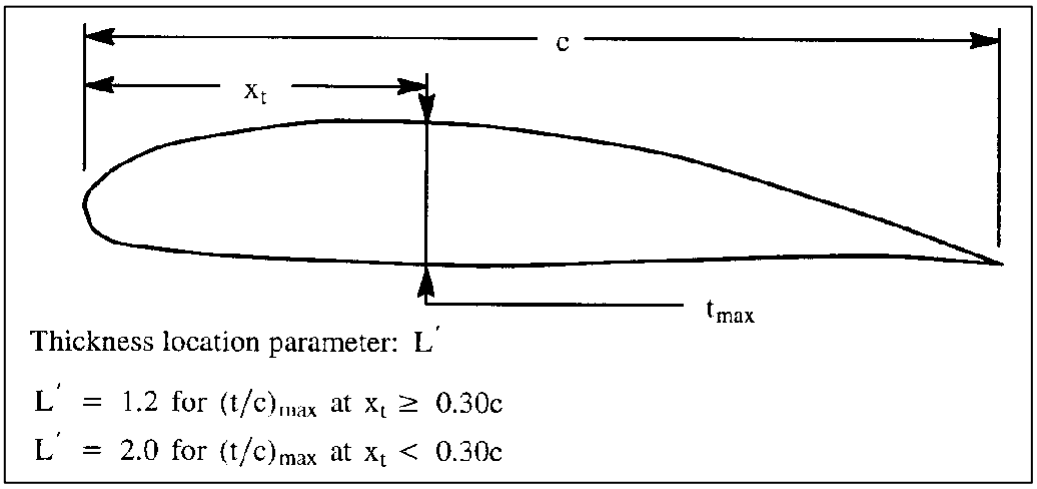


Figure 2.33 - Airfoil thickness location parameter (Roskam and Lan, 1997).

Finally, once the development above was done for a generic wing, and the airplane developed here is a biplane, the Equation 2.89 is modified related to the theory by parametrizing it for an aerodynamic area ratio, considering the total aerodynamic area of the biplane wing which is the sum of the aerodynamic areas of the lower and upper wings, resulting in the Equation 2.94 and in the Equation 2.95. To estimate the induced drag for each wing, was applied the span efficiency factor defined by the Equation 2.65.

$$CD_{W\_LOW} = \left(CD_{0_{W\_LOW}} + CD_{i_{W\_LOW}}\right) \cdot \frac{S_{aero_{W\_LOW}}}{S_{aero_{W\_BIP}}} \tag{2.94}$$

$$CD_{W\_UP} = \left(CD_{0_{W\_UP}} + CD_{i_{W\_UP}}\right) \cdot \frac{S_{aero_{W\_UP}}}{S_{aero_{W\_BIP}}} \tag{2.95}$$

Canards

The drag generated by both canard surfaces are obtained at the same way that were obtained for the wings, and is presented by the Equation 2.96 to Equation 2.100. To estimate the induced drag for each canard, was applied the span efficiency factor defined by the Equation 2.65.

One important note must be done, the lift estimative for the canards presented on the topic related to the lift consider the parcel due the elevator deflection, therefore it is not necessary to estimate the parcel related to the trimming drag, due the fact that it is computed on the parcel of the induced drag of both canards.

$$CD_{CAN} = CD_{0_{CAN}} + CD_{i_{CAN}} \quad (2.96)$$

$$CD_{0_{CAN}} = R_{cf} \cdot R_{LS} \cdot cd_{CAN} \quad (2.97)$$

$$CD_{i_{CAN}} = \frac{CL_{CAN}^2}{\pi \cdot e_{CAN} \cdot AR_{CAN}} \quad (2.98)$$

$$CD_{CAN\_LOW} = \left(CD_{0_{CAN\_LOW}} + CD_{i_{CAN\_LOW}}\right) \cdot \frac{S_{aero_{CAN\_LOW}}}{S_{aero_{W\_BIP}}} \quad (2.99)$$

$$CD_{CAN\_UP} = \left(CD_{0_{CAN\_UP}} + CD_{i_{CAN\_UP}}\right) \cdot \frac{S_{aero_{CAN\_UP}}}{S_{aero_{W\_BIP}}} \quad (2.100)$$

This aircraft has boomed fairings on the tips of the canards, and they are considered for turn the computation of the whole airplane drag more realistic and in consequence the drag polar. For simplification the drag will be considered as just that of the friction type. The drag for each fairing is obtained by the Equation 2.101 and the Equation 2.102.

$$CD_{CAN\_fair\_lef} = C_{fe} \cdot \frac{S_{wet_{CAN_{fair_{lef}}}}}{S_{aero_{W_{BIP}}}} \quad (2.101)$$

$$CD_{CAN\_fair\_rig} = C_{fe} \cdot \frac{S_{wet_{CAN\_fair\_rig}}}{S_{aero_{W\_BIP}}} \quad (2.102)$$

Vertical tails

The method used to estimate the drag generated by both vertical tails is the same that was employed before, for the wings and canards. The formulation is defined on the Equation 2.103 to Equation 2.107. To estimate the induced drag for each vertical tail, was applied the span efficiency factor defined by the Equation 2.66.

$$CD_{VT} = CD_{0_{VT}} + CD_{i_{VT}} \quad (2.103)$$

$$CD_{0_{VT}} = R_{vtf} \cdot R_{LS} \cdot cd_{VT} \quad (2.104)$$

$$CD_{i_{VT}} = \frac{CL_{VT}^2}{\pi \cdot e_{VT} \cdot AR_{VT}} \quad (2.105)$$

$$CD_{VT\_LEF} = \left(CD_{0_{VT\_LEF}} + CD_{i_{VT\_LEF}}\right) \cdot \frac{S_{aero_{VT\_LEF}}}{S_{aero_{W\_BIP}}} \quad (2.106)$$

$$CD_{VT\_RIG} = \left(CD_{0_{VT\_RIG}} + CD_{i_{VT\_RIG}}\right) \cdot \frac{S_{aero_{VT\_RIG}}}{S_{aero_{W\_BIP}}} \tag{2.107}$$

The drag generated by the booms that support the vertical tails surfaces are obtained as being just the friction drag, how there are four booms, the Equation 2.108 was defined in a generic form and is applicable for all the booms, therefore the parameters as areas for example, must be changed as the necessity. For the total drag generated for the airplane this equation must be applied four times and added as the term related to the boom on the Equation 2.88.

$$CD_{VT\_BOOM} = C_{fe} \cdot \frac{S_{wet_{VT\_boom}}}{S_{aero_{W\_BIP}}} \tag{2.108}$$

Fuselage

The theory (Roskam, 2000) predicts that to estimate the fuselage drag, there is a component due the area of the cross section of the end of the fuselage called fuselage base-drag, however, for this aircraft it will not be computed due its configuration characteristics, once on this region is installed the engine plus the propeller, what changes completely the pressure distribution on this region.

The formulation adapted for this airplane is presented on the Equation 2.109 to Equation 2.111, that are solved with the help of the Figure 2.30, Figure 2.32, Figure 2.34 and the Figure 2.35.

$$CD_{0_{fus}} = R_{wf} \cdot Cf_{fus} \cdot \left[1 + \frac{60}{\left(l_f/d_f\right)^3} + 0.0025 \cdot \frac{l_f}{d_f}\right] \cdot \left(\frac{S_{wet-fus}}{S_{aero_{W\_BIP}}}\right) \tag{2.109}$$

$$CD_{L_{fus}} = \frac{2 \cdot \alpha^2 \cdot S_{b_{fus}}}{S_{aero_{W\_BIP}}} + \frac{\eta_{fus} \cdot c_{d_c} \cdot |\alpha|^3 \cdot S_{pl_{fus}}}{S_{aero_{W\_BIP}}} \tag{2.110}$$

$$d_f = \sqrt{\frac{4}{\pi} \cdot S_{F_{max-cs}}} \tag{2.111}$$

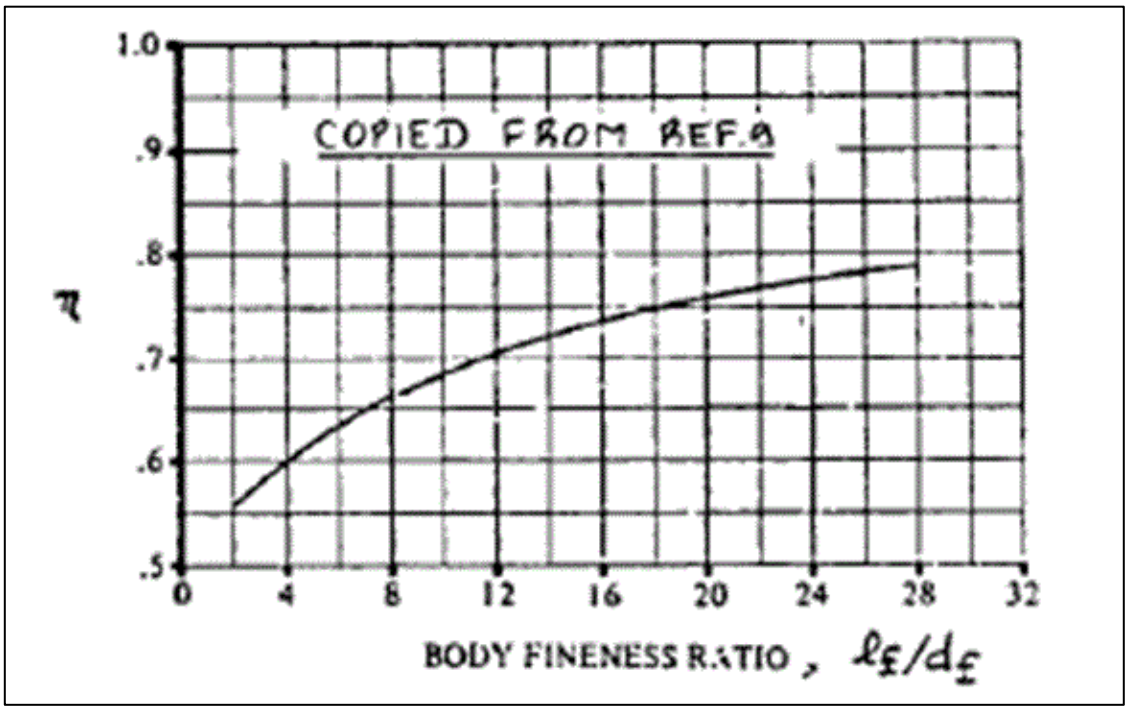


Figure 2.34 - Ratio of drag coefficient of a circular cylinder in function of the body fineness (Roskam, 2000).

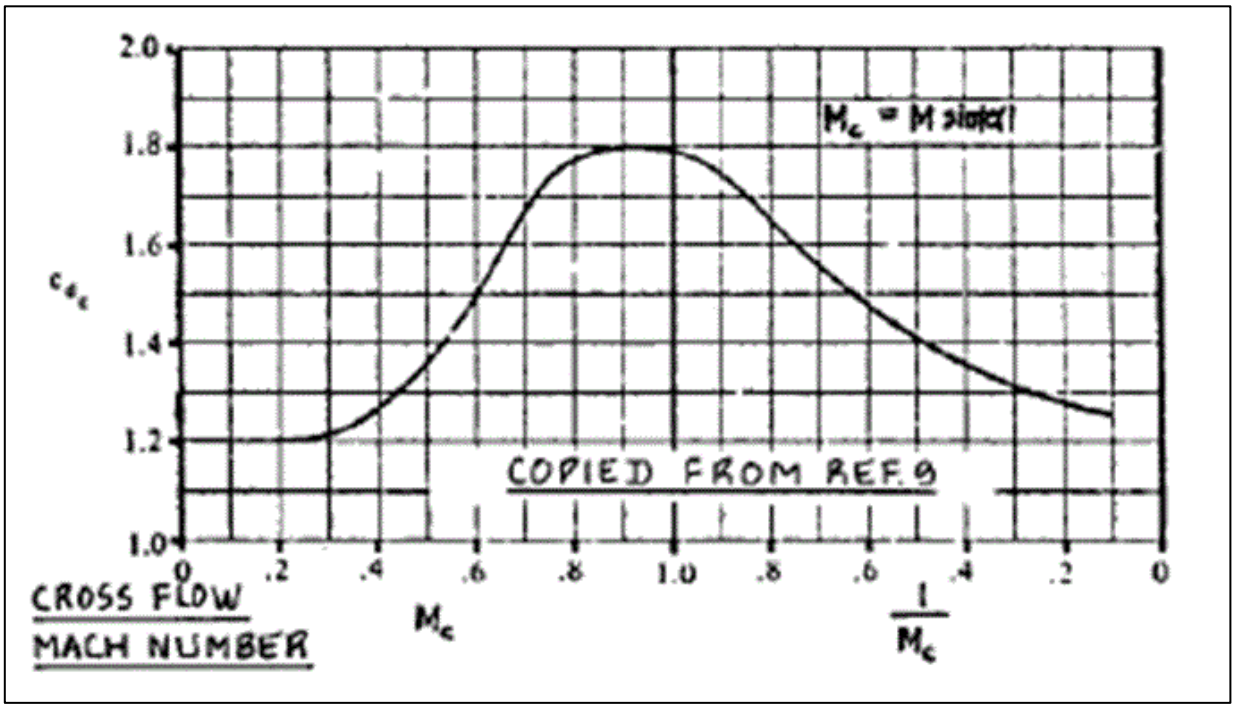


Figure 2.35 - Steady state cross-flow drag coefficient for two-dimensional circular cylinder (Roskam, 2000).

Once the canopy is integrated to the fuselage and its profile is smooth, the CD due the canopy was not determined, and the CD calculated for the fuselage is considered for the whole fuselage plus canopy.

Landing gear

This work proposes that the drag generated by the landing gear legs may be estimated considering just the skin friction drag as showed by the Equation 2.112, which is applicable for the three legs, remembering that it is necessary to calculate the drag generated by each leg and to sum on the Equation 2.88.

$$CD_{LGEAR} = C_{fe} \cdot \frac{S_{wet_{LGEAR}}}{S_{aero_{W\_BIP}}} \tag{2.112}$$

Propeller

The theory (Roskam, 2000) predicts that for a propeller that is spinning, the drag may be estimated by the Equation 2.113, and for a stopped propeller the drag may be estimated by the Equation 2.114, both equations are given in English units.

$$CD_{PROP} = 33 \cdot \frac{1}{\left(q \cdot S_{aero_{W\_BIP}}\right)} \cdot \frac{SHP_{rated}}{U_0} \tag{2.113}$$

$$CD_{PROP} = 0.00125 \cdot n_P \cdot \frac{D_P^2}{S_{aero_{W\_BIP}}} \tag{2.114}$$

2.4.2.6. Pitch moment

There are two basic conditions in which the pitch moment of the airplane must be obtained, the first is for the take-off rolling and the second must be defined for each flight condition as cruise for example, for to trimming the airplane.

The estimates for the pitch moment will be done in the chapter related to dynamics of flight, once it is part of its formulation.

2.4.2.7. Wash fields

When in flight, some parts of the aircraft are under the influence of flow field generated by other components of the own aircraft. Considering a wing for example, it perturbs the air flow ahead and behind itself, deflecting the air up and down respectively. This angular deflection or inclination of the air flow is called upwash for the ahead airflow and is called downwash for the airflow behind the wing, as showed on the Figure 2.36. Actually it is valid for any aerodynamic surface besides the wing as canard, horizontal tail and vertical tail. The bibliography commonly presents this as a rate in function of the angle of attack. The upwash or the downwash are represented by the symbols ε and ε_u respectively. The Figure 2.37 show the parameters used on the estimative of the downwash and upwash fields.

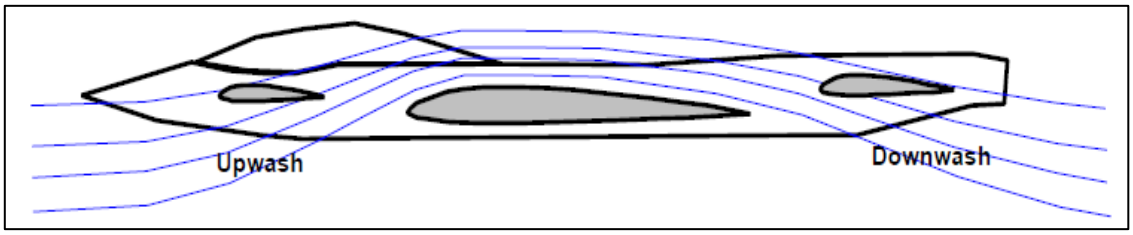


Figure 2.36 - Downwash and upwash fields (Brandt).

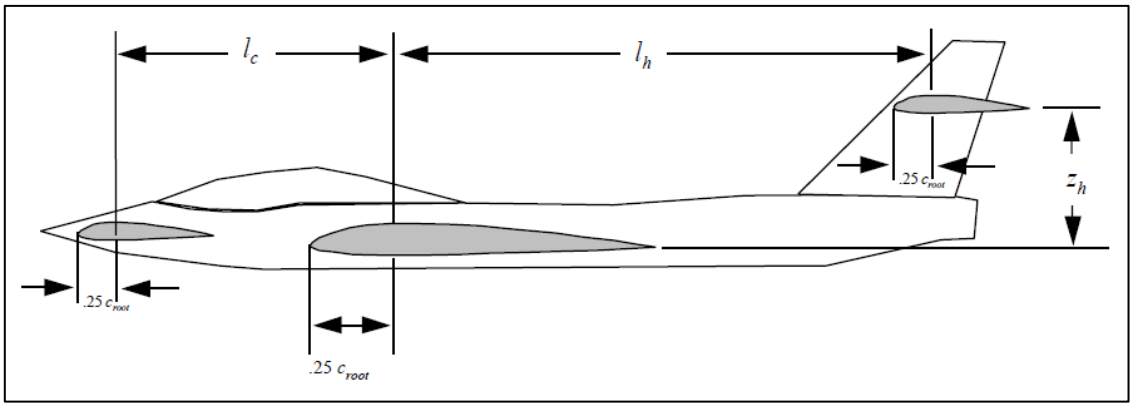


Figure 2.37 - Parameters for downwash and upwash prediction (Brandt).

<u>*Downwash field*</u>

There are some formulations for these fields, the most common and simple is that showed on the Equation 2.115. As described on the theory (Brandt), for an airplane equipped with a conventional horizontal tail, the downwash gradient can be estimated by the empirical

Equation 2.116 obtained from a curve fit of experimental data in wind tunnel. This downwash field leads to a contribution to the airplane lift curve slope given by the Equation 2.117, if the obtainment of the lift increment related to the horizontal tail itself is intended, it is possible to be obtained by the modified Equation 2.118.

$$\frac{d\varepsilon}{d\alpha} = \frac{2 \cdot CL_{\alpha}}{\pi \cdot AR} \tag{2.115}$$

$$\frac{d\varepsilon}{d\alpha} = \frac{21^{\circ} C_{L_{\alpha_W}}}{AR_W^{0.725}} \cdot \frac{\bar{C}_W}{l_h} \cdot \frac{10-3\lambda_W}{7} \cdot \left(1 - \frac{z_h}{b_W}\right) \tag{2.116}$$

$$\Delta CL_{\alpha_{HT}} = CL_{\alpha_{HT}} \cdot \left(1 - \frac{d\varepsilon}{d\alpha}\right) \cdot \frac{S_{HT}}{S_W} \tag{2.117}$$

$$\Delta CL_{\alpha_{HT}} = CL_{\alpha_{HT}} \cdot \left(1 - \frac{d\varepsilon}{d\alpha}\right) \tag{2.118}$$

Upwash field

For an airplane equipped with a canard horizontal tail as described on the theory (Brandt), the upwash gradient can be estimated by the empirical Equation 2.119 obtained from a curve fit of experimental data in wind tunnel for wings with $\Lambda_{25\%} < 35^{\circ}$. This upwash field leads to a contribution to the airplane lift curve slope given by the Equation 2.120, if the obtainment of the lift increment related to the canard itself is intended, it is possible to be obtained by the modified Equation 2.121.

$$\frac{d\varepsilon_u}{d\alpha} = (0.3 \cdot AR_W^{0.3} - 0.33) \cdot \left(\frac{l_c}{\bar{C}_W}\right)^{-\left(1.04+6 \cdot AR_W^{-1.7}\right)} \tag{2.119}$$

$$\Delta CL_{\alpha_{CAN}} = CL_{\alpha_{CAN}} \cdot \left(1 + \frac{d\varepsilon_u}{d\alpha}\right) \cdot \frac{S_{CAN}}{S_W} \tag{2.120}$$

$$\Delta CL_{\alpha_{CAN}} = CL_{\alpha_{CAN}} \cdot \left(1 + \frac{d\varepsilon_u}{d\alpha}\right) \tag{2.121}$$

Sidewash field

The sidewash field is similar to the downwash and upwash, it is generated due distortions on the air flow that surrounds the vertical tail due the wing and fuselage, the symbol which designates the sidewash is σ.

The theory (Nelson, 1998) predicts that the sidewash gradient may be estimated by applying the Equation 2.122, which is function of the vertical tail efficiency. Note by the Figure 2.38 that the sidewash occurs when the airplane is in a sideslip condition.

$$\eta_{VT} \cdot \left(1 + \frac{d\sigma}{d\beta}\right) = 0.724 + 3.06 \cdot \frac{S_{VT}/S_W}{1+\cos \Lambda_W} + 0.4 \cdot \frac{Z_W}{h} + 0.009 \cdot AR_W \quad (2.122)$$

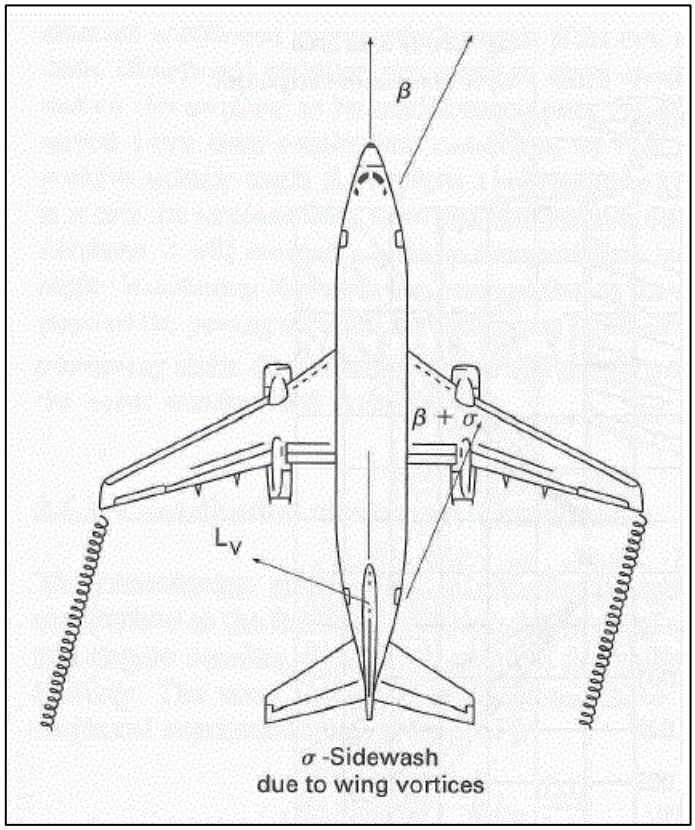


Figure 2.38 - Sidewash due the wing (Nelson, 1998).

For the airplane UFU-1 it is assumed that the vertical tail efficiency is equal to one, and the areas considered are the aerodynamic, so the equation for the sidewash gradient was modified to the Equation 2.123.

$$\frac{d\sigma}{d\beta} = 0.724 + 3.06 \cdot \frac{S_{aero_{VT}}/S_{aero_W}}{1+\cos \Lambda_W} + 0.4 \cdot \frac{Z_W}{h} + 0.009 \cdot AR_W - 1 \quad (2.123)$$

Global wash field

The bibliography consider the downwash and the upwash fields separately, for conventional airplanes and canard aircraft respectively, however, for the airplane UFU-1 it must be reassessed, once there are many aerodynamic surfaces in tandem disposition between them.

This work proposes a new theory named "*global wash field",* that is a specific flow condition in which one determined surface may be immersed. It happens when any aerodynamic surface is immersed in a region that is under the effect of more than one downwash or upwash fields at the same time, as occurs for the configuration of the airplane UFU-1.

For example, considering the lower canard, it is immersed on a wash field that is a composition of the upwash due the upper canard and the upwash due the lower wing, the upwash due the upper wing may be ignored due its distance from the lower canard.

Considering the upper canard, it is immersed on a wash field that is a composition of the downwash due the lower canard and the upwash due the lower wing, the upwash due the upper wing may be ignored due its distance from the upper canard.

Now, considering the lower wing, it is immersed on a wash field that is a composition of the downwash due the upper canard and the upwash due the upper wing, the downwash due the lower canard may be ignored due a combination between its vertical and horizontal distances from the lower wing, and its area ratio.

Finally considering the upper wing, it is immersed on a pure downwash field due the lower wing, and the wash field due both canards may be ignored.

If an ideal prediction is desired, all the wash fields generated by each aerodynamic surface must be considered, intending to obtain the global wash field in which an aerodynamic surface could be.

Therefore, is proposed the Equation 2.124 that may be used to estimate the lift curve slope increment due the global wash field that surrounds any aerodynamic surface. Note that there is a correction term which is a span ratio for the aerodynamic surfaces, given by the Equation 2.125 and the Equation 2.126. For these equations, if the span of the surface i or j is bigger than the span of the surface immersed on the wash field the equation must assume the value equal to one, once the affected surface will be completely immersed on the wash field generated by this surface i or j. This lift curve slope increment Equation 2.124 is valid for each one of the equations related to the lift generated by the wings and canards presented earlier on this text.

$$\Delta CL_{\alpha_{surface}} = \sum_{i=1}^{n} CL_{\alpha,surface-i} \cdot \left(1 - \frac{d\varepsilon_i}{d\alpha}\right) \cdot A_\varepsilon + \sum_{j=1}^{m} CL_{\alpha,surface-j} \cdot \left(1 + \frac{d\varepsilon_{u_j}}{d\alpha}\right) \cdot B_\varepsilon \quad (2.124)$$

$$A_\varepsilon = \frac{b_{surface-i}}{b_{surface}} \quad (2.125)$$

$$B_\varepsilon = \frac{b_{surface-j}}{b_{surface}} \quad (2.126)$$

From the Equation 2.124 it is possible to define the expression for the gradient of the global wash field, given by the Equation 2.127.

$$\frac{dE}{d\alpha} = \sum_{i=1}^{n} -\frac{d\varepsilon_i}{d\alpha} \cdot A_\varepsilon + \sum_{j=1}^{m} \frac{d\varepsilon_{u_j}}{d\alpha} \cdot B_\varepsilon \quad (2.127)$$

Integrating the left hand side of the equation above for an angle of attack equal to zero, it is obtained the angle of wash for the aerodynamic surface that is immersed in the global wash field, as presented on the Equation 2.128.

$$E = \frac{dE}{d\alpha} \cdot \alpha + E_0 \quad (2.128)$$

The angle of downwash for angle of attack equal to zero is defined in the theory (Nelson, 1998) as given by the Equation 2.129, which is obtained from the Equation 2.115.

$$\varepsilon_0 = \frac{2 \cdot CL_0}{\pi \cdot AR} \quad (2.129)$$

Assuming that this equation is valid for upwash either, it is proposed the Equation 2.130 that provides the global wash field angle for angle of attack equal to zero, for a given surface immersed in this field.

$$E_0 = \sum_{i=1}^{n} -\frac{2 \cdot CL_{0_i}}{\pi \cdot AR_i} \cdot A_\varepsilon + \sum_{j=1}^{m} \frac{2 \cdot CL_{0_j}}{\pi \cdot AR_j} \cdot B_\varepsilon \quad (2.130)$$

2.4.2.8. Aerodynamic centers

During the development of a new aircraft, several aerodynamics and dynamics of flight calculus are dependent from the location of the aerodynamic center of the main aerodynamic components as wings and tail surfaces, as well as the lateral area of the complete airplane. Next are presented methods to estimate the location of these aerodynamic centers.

Wings AC

The aerodynamic center position of a wing is changed due the fuselage interference as predicted by the theory (Roskam, 2000) that in this case divided the fuselage in 13 segments, but it is not necessary to respect this number of segments. Such aerodynamic center shift is given by the Equation 2.131 which was modified substituting the wing reference area for the wing aerodynamic area, this equation is solved with the help of the Equation 2.132 and the Figure 2.39. The Figure 2.40 is valid for the fuselage segments forward the wing, for the segments behind the wing, it is valid the Equation 2.133. As can be observed, this last equation is function of the downwash generated by the own wing, therefore, for the downwash gradient estimative will be applied the Equation 2.115.

$$\Delta x_{AC_W} = -\frac{dM/d\alpha}{q \cdot S_{aero_W} \cdot \bar{C}_W \cdot C_{L_{\alpha_W}}} \tag{2.131}$$

$$\frac{dM}{d\alpha} = \frac{q}{36.5} \cdot \frac{C_{L_{\alpha_W}}}{0.08} \cdot \sum_{i=1}^{i=13} \left(w_f^2\right)_i \cdot \left(\frac{d\bar{\varepsilon}}{d\alpha}\right)_i \cdot \Delta x_i \tag{2.132}$$

$$\left(\frac{d\bar{\varepsilon}}{d\alpha}\right)_i = \frac{x_i}{x_h} \cdot \left(1 - \frac{d\varepsilon}{d\alpha}\right) \tag{2.133}$$

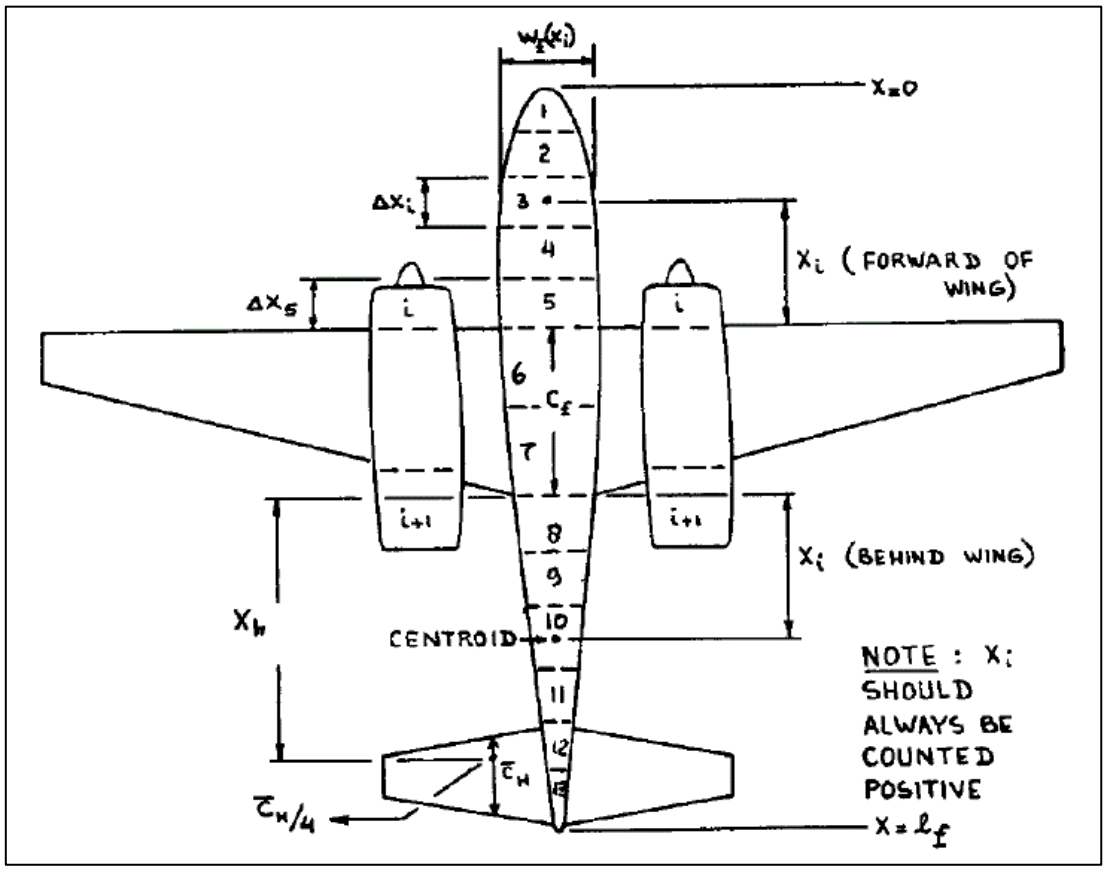


Figure 2.39 - Fuselage division for wing aerodynamic center shift estimative (Roskam, 2000).

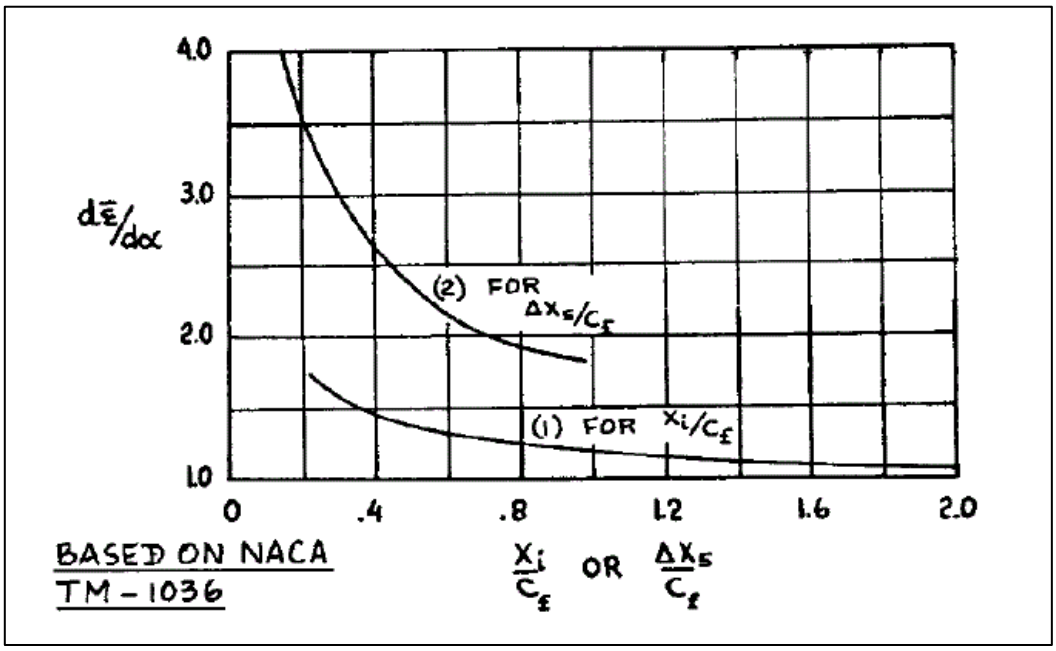


Figure 2.40 - Effect of fuselage segment location on upwash gradient (Roskam, 2000).

The procedure describe above must be repeated for both wings, defining the position of the aerodynamic center for each wing, based on these positions the location of the aerodynamic center for the equivalent wing may be defined as been the average between both position.

Canards AC

Assuming that the canards are aerodynamic surfaces as are the wings and that they are installed on the fuselage as well as the wings are installed, it is reasonable that the method used for estimate the shift on the aerodynamic center of the wings may be employed to estimate the shift on the aerodynamic center of the canards either.

Vertical tails AC

As the vertical tail surfaces are not under the interference of the fuselage, there are no shifts on its aerodynamic center.

Lateral area of the complete airplane AC

For estimate the position of the aerodynamic center of the aircraft projected side area, the following procedure can be used based on the Figure 2.41, drawing a reference line on the nose of the aircraft and dividing de side area into n segments of simple geometry, as square, rectangle, circle or triangle.

The position of the aerodynamic center of the side area of the complete aircraft is given by the Equation 2.134.

$$AC_{AP\_SIDE} = \frac{\sum_{i=1}^{n} A_i \cdot x_i}{\sum_{i=1}^{n} A_i} \tag{2.134}$$

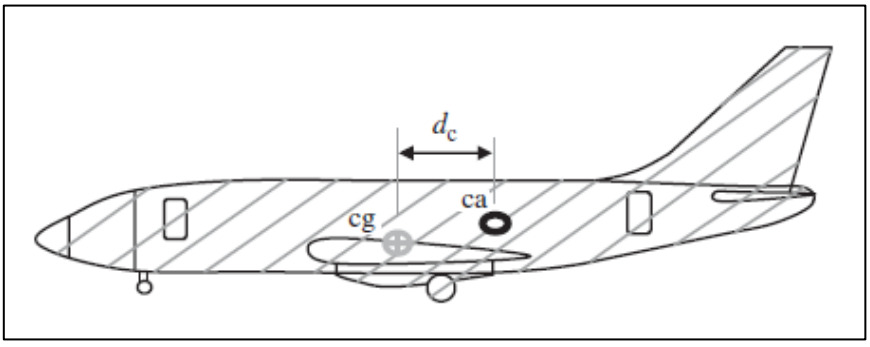


Figure 2.41 - Airplane projected side area segments (Sadraey, 2013).

2.5. DYNAMICS OF FLIGHT

This chapter is dedicated to develop the theory necessary for the estimative of the flight behavior of the aircraft on the three axes, as the static stability, control and the dynamic stability. The Table 2.23 presents some reference values for the stability assessing.

Table 2.23 - Stability requirements values (Sadraey, 2013).

No.	Requirements	Stability derivatives	Symbol	Typical value (1/rad)
1a	Static longitudinal stability	Rate of change of pitching moment coefficient with respect to angle of attack	C_{m_α}	−0.3 to −1.5
1b	Static longitudinal stability	Static margin	$h_{np}-h_{cg}$	0.1–0.3
2	Dynamic longitudinal stability	Rate of change of pitching moment coefficient with respect to pitch rate	C_{m_q}	−5 to −40
3	Static directional stability	Rate of change of yawing moment coefficient with respect to sideslip angle	C_{n_β}	+0.05 to +0.4
4	Dynamic directional stability	Rate of change of yawing moment coefficient with respect to yaw rate	C_{n_r}	−0.1 to −1

The primary control surfaces are designed considering its dynamic effectivity, and there are considered too the structural flexibility and the system effects as mechanical losses for example. The Table 2.24 presents the reference values for the main parameters used on the design of the three primary control surfaces.

Table 2.24 - Typical values for geometry of control surfaces (Sadraey, 2013).

Control surface	Elevator	Aileron	Rudder
Control surface area/lifting surface area	$S_E/S_h = 0.15–0.4$	$S_A/S = 0.03–0.12$	$S_R/S_V = 0.15–0.35$
Control surface span/lifting surface span	$b_E/b_h = 0.8–1$	$b_A/b = 0.2–0.40$	$b_R/b_V = 0.7–1$
Control surface chord/lifting surface chord	$C_E/C_h = 0.2–0.4$	$C_A/C = 0.15–0.3$	$C_R/C_V = 0.15–0.4$
Control surface maximum deflection (negative)	−25 deg (up)	25 deg (up)	−30 deg (right)
Control surface maximum deflection (positive)	+20 deg (down)	20 deg (down)	+30 deg (left)

The parameters that indicate the effectiveness of a control surface are the control derivatives, these parameters provide the rate of the aerodynamic loads and moments expressed in terms of coefficients, and they are proportional to the control surfaces deflection.

The greater be the value of a given control derivative, the bigger will be the command power of the corresponding control surface. The main control derivatives related to the ailerons, elevator and rudder are respectively $C_{l_{\delta A}}$, $C_{m_{\delta E}}$ and $C_{n_{\delta R}}$. Finally as the control authority is smaller for low speeds, the design of the primary control surfaces is done considering the take-off and landing conditions.

All the dynamics of flight of an aircraft is directly dependent of several aerodynamic coefficients which are obtained from the flight aerodynamic forces and moments. Therefore, despite the bibliography generally to apply the reference areas of the wings and tails on the formulation of the dynamics of flight, during the development of this work it was decided to apply the aerodynamic areas of these aerodynamic surfaces, once it is much more reasonable, considering that actually the aerodynamic forces and moments are generated by the aerodynamic areas, having in mind that the region inside the fuselage of these reference areas do not generate aerodynamic forces nor moments. The changes between the reference areas and the aerodynamic ones will be indicated along the text of this chapter. All the stability derivatives and all the control derivatives that are function of the airplane wing parameters had such parameters substituted by the parameters of the equivalent biplane wing.

As the dynamics of flight is directly affected by the aircraft configuration, next are presented the principal concepts related to the configuration adopted on the conception of the airplane UFU-1.

Biplane configuration

Assuming that for a given design weight and consequently a given wing area, a biplane airplane will have wings with a smaller span when compared to a monoplane airplane. This smaller span leads to a greater rolling maneuver capacity, as bigger angular speeds and accelerations, due its smaller moment of inertia on the x axis.

For the airplane developed here, specifically considering the dynamics of flight, the mean aerodynamic chord of the biplane is considered as the length between the leading edge of the lower wing and the trailing edge of upper wing, due its large stagger. The mean aerodynamic chord is assumed this way once it is important to know the actual positon of the CG relative to the mac during the estimative of the longitudinal static margin of the airplane.

Canard configuration

There are basically two kinds of canards one called lift canard and the other is known as control canard as mentioned above in the aerodynamics theory.

For airplanes in which the canard assumes just the control purpose, the wing is responsible for the whole lift generated, and in this case the canard is located very ahead of the wing what tend to turn this configuration longitudinally unstable, what in many times requires a closed control system. For control canards the dynamic stability can be guaranteed keeping its area smaller than 10% of the area of the wing.

There are many considerations that must be done for the canard configuration, related to the in-flight operation and the take-off condition.

Considering the take-off operation it is normal to occur some difficulty in generate enough lift for lifting the nose of the airplane during the rotation phase. This condition is aggravated when the flaps are deflected, what increase the pitch down moment of the wing, in this way the canard must be designed for generates enough lift to oppose this bigger negative pitch moment.

The Figure 2.42 shows that for a canard configuration, when the CG is located behind the AC of the airplane, it produces a positive pitch moment and for oppose this, the canard should genertate negative lift, and for the CG located ahead of the AC it produces a negative pitch moment which is nullified by a positive lift generated by the canard for trimming the airplane.

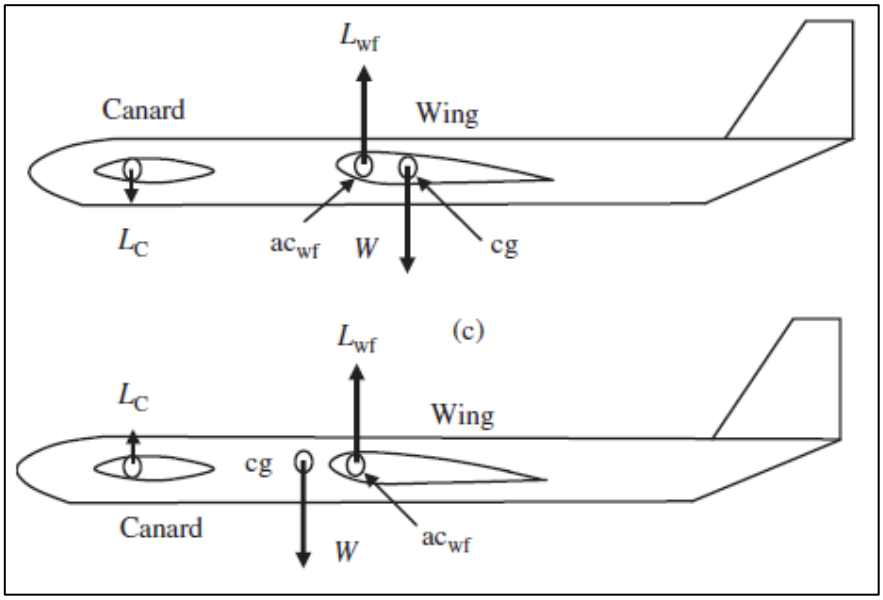


Figure 2.42 - Canard airplane CG location (After Sadraey, 2013).

Considering in flight conditions, the trimming drag is normally smaller than that observed on a conventional airplane what lead to a higher L/D ratio, once the canard generally produces positive lift. The static margin related to the longitudinal stability tends to be smaller than that observed in conventional airplanes, what lead to a smaller longitudinal stability. Therefore, a challenge on the designing of a canard aircraft is to define the location of the fuel tank, which preferably should be located near the CG intending avoid its broad movement during the aircraft operation.

During the pitch up maneuvers, canard aircrafts faces another challenge that is its longitudinal destabilization, once the canard surface has its lift increased while the angle of attack increase and the effective lift generate by the wing decreases due the downwash produced by the canard, what produces a pitch up movement of the airplane. For avoid this condition the airplane must be designed on a way that the canard stalls first than the wing, obtaining a longitudinal stable and safe configuration, which leads to a good pitch break behavior, preventing the aircraft to have a divergent pitch movement. Therefore, is recommended that in a canard aircraft the wing be placed behind the CG, what will produces a stabilizing pitch moment compared to that produced by the canard, but it is necessary to ensure that the canard will always stalls first than the wing, intending avoid the called deep stall, a catastrophic flight condition.

To conclude, it is interesting make two more considerations, the first is that for a complete movable canard surface deflected down around 45°, it may put down the airplane nose practically in any flight condition, but in this case it is required a complex control system. The second is that airplanes with canard configuration normally have lighter structure, due the canard contribution for a positive lift, what turn the structure of the wing a bit smaller and lighter.

Pusher configuration

The literature indicates that such a configuration tend to increases the longitudinal and directional stability, compared to the tractor configuration.

One disadvantage is the back shift on the CG location, what decreases the longitudinal stability of the aircraft. Specifically related to the longitudinal static stability, the more behind of the CG to be located the propeller, better will be this stability behavior.

2.5.1. Longitudinal static stability

For an aircraft to be longitudinal statically stable it must produce a restoring moment when disturbed from an equilibrium flight condition. The Figure 2.43 shows the pitch curve for two distinct aircrafts, the airplane one present a stable behavior once its pitch moment is a restoring one, while the airplane two presents an unstable behavior due its divergent pitch moment. Analyzing these two curves, it is observed that for an airplane to be longitudinal statically stable it would have a negative pitch moment curve slope as given by the Equation 2.135, the Table 2.23 present typical values for this static stability derivative.

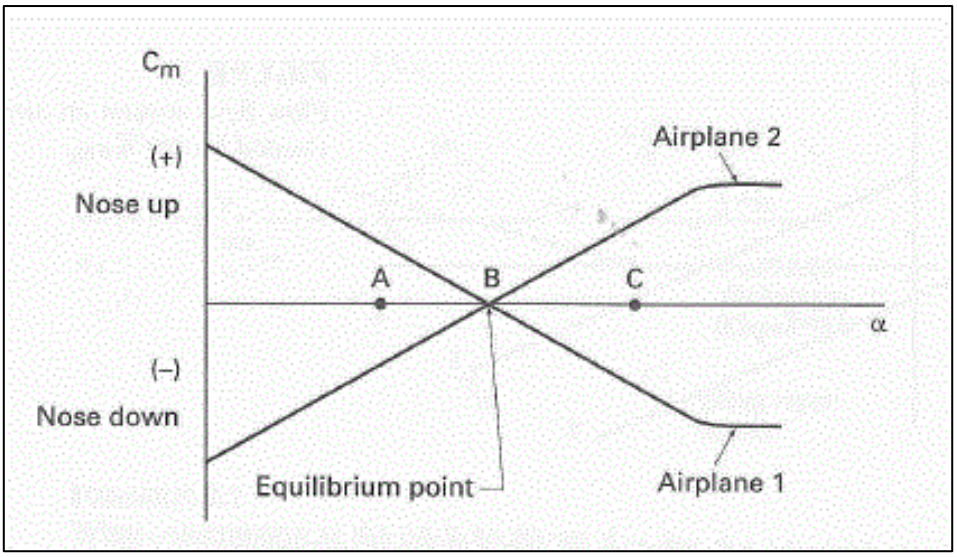


Figure 2.43 - Pitch moment curves (Nelson, 1998).

$$\frac{dCm}{d\alpha} < 0 \tag{2.135}$$

The longitudinal static stability of an aircraft is usually measured at its CG, leading to the Equation 2.136, which was defined specifically for the airplane UFU-1.

$$Cm_{CG} = Cm_{CG_{W\_LOW}} + Cm_{CG_{W\_UP}} + Cm_{CG_{CAN\_LOW}} + Cm_{CG_{CAN\_UP}} + Cm_{CG_{FUS}} \tag{2.136}$$

2.5.1.1. Wings contribution

The contribution of each wing for the longitudinal static stability is obtained by applying the following formulation for both, lower and upper wings.

$$Cm_{0_W} = cm_W + CL_{\alpha=0_W} \cdot \left(h_W - h_{AC_W}\right) \quad (2.137)$$

$$h_W = \frac{X_{CG} - X_{LE_{mac_W}}}{\bar{C}_W} \quad (2.138)$$

$$Cm_{\alpha_W} = CL_{\alpha_W} \cdot \left(h_W - h_{AC_W}\right) \quad (2.139)$$

$$Cm_{CG_W} = Cm_{0_W} + Cm_{\alpha_W} \cdot \alpha \quad (2.140)$$

2.5.1.2. Canards contribution

Conventional tail theory

The bibliography (Nelson, 1998) defines the contribution of a conventional horizontal tail to the longitudinal static stability as described on the formulation showed below. The Equation 2.141 is the effective angle of attack of the horizontal tail, the Equation 2-5-9 provides the pitch moment coefficient on the CG of the aircraft. After some mathematical manipulation there are obtained the Equation 2.144 and the Equation 2.145 that are the two parcels of the pitch moment coefficient at the CG of the aircraft. Note that the ratio $d\varepsilon/d\alpha$ denotes the rate of the downwash field produced by the wing, in which the horizontal tail is immersed, and ε_0 is the angle of downwash for the wing at angle of attack equal to zero.

$$\alpha_{HT} = \alpha - i_W - \varepsilon + i_{HT} \quad (2.141)$$

$$CL_{HT} = CL_{\alpha_{HT}} \cdot \alpha_{HT} \quad (2.142)$$

$$Cm_{CG_{HT}} = -\eta_{HT} \cdot V_{HT} \cdot CL_{HT} = Cm_{0_{HT}} + Cm_{\alpha_{HT}} \cdot \alpha \quad (2.143)$$

$$Cm_{0_{HT}} = \eta_{HT} \cdot V_{HT} \cdot CL_{\alpha_{HT}} \cdot (\varepsilon_0 + i_W - i_{HT}) \quad (2.144)$$

$$Cm_{\alpha_{HT}} = -\eta_{HT} \cdot V_{HT} \cdot CL_{\alpha_{HT}} \cdot \left(1 - \frac{d\varepsilon}{d\alpha}\right) \quad (2.145)$$

Lower canard contribution

For the contribution of the lower canard to the longitudinal static stability, some modification on the theory of the conventional horizontal tail had to be proposed as described below.

The Equation 2.146 is the effective angle of attack of the lower canard, note that the terms of the angles of incidence of both wings and of the upper canard are not considered due the fact of these aerodynamic surfaces to be located behind the lower canard. The Equation 2.148 provides the pitch moment coefficient on the CG of the aircraft. As done above, proceeding some mathematical manipulation the parcels of the pitch moment coefficient equation of the lower canard were obtained and presented on the Equation 2.149 and on the Equation 2.150.

The ratio $d\varepsilon_{W\_LOW}/d\alpha$ denotes the rate of the upwash field produced by the lower wing and the ratio $d\varepsilon_{CAN\_UP}/d\alpha$ denotes the rate of the upwash field produced by the upper canard, the sum of both represents the rate of the global wash field surrounding the lower canard. The term $\varepsilon_{0_{W\_LOW}}$ is the angle of upwash for the lower wing at angle of attack equal to zero and the term $\varepsilon_{0_{CAN\_UP}}$ is the angle of upwash for the upper canard at angle of attack equal to zero. Note that the lower canard volume coefficient is negative due its position ahead the location of the CG of the aircraft, the equations as presented here do not account for its negative sign. The obtainment of the lower canard volume coefficient may be done applying the Equation 2.32 replacing the reference areas by the aerodynamic ones. The tail arm l_{HT} in the Equation 2.32 is correctly obtained as being the distance between the point at 25% of the canard mean aerodynamic chord and the CG location of the airplane.

$$\alpha_{CAN\_LOW} = \alpha + \varepsilon_{W\_LOW} + \varepsilon_{CAN\_UP} + i_{CAN\_LOW} \tag{2.146}$$

$$CL_{CAN\_LOW} = CL_{\alpha_{CAN\_LOW}} \cdot \alpha_{CAN\_LOW} \tag{2.147}$$

$$Cm_{CG_{CAN_{LOW}}} = -\eta_{CAN_{LOW}} \cdot V_{CAN_{LOW}} \cdot CL_{CAN_{LOW}} = Cm_{0_{CAN_{LOW}}} + Cm_{\alpha_{CAN\_LOW}} \cdot \alpha \tag{2.148}$$

$$Cm_{0_{CAN_{LOW}}} = cm_{CAN_{LOW}} - \eta_{CAN_{LOW}} \cdot V_{CAN_{LOW}} \cdot CL_{\alpha_{CAN_{LOW}}} \cdot \left(\varepsilon_{0_{W\_LOW}} + \varepsilon_{0_{CAN\_UP}} + i_{CAN\_LOW}\right) \tag{2.149}$$

$$Cm_{\alpha_{CAN_{LOW}}} = -\eta_{CAN_{LOW}} \cdot V_{CAN_{LOW}} \cdot \left(CL_{\alpha_{CAN_{LOW}}} + \Delta CL_{\alpha_{CAN_{LOW}}}\right) \cdot \left(1 + \frac{d\varepsilon_{W\_LOW}}{d\alpha} + \frac{d\varepsilon_{CAN\_UP}}{d\alpha}\right) \tag{2.150}$$

Upper canard contribution

Applying the same procedure used on the development of the contribution of the lower canard, it is defined the contribution of the upper canard for the longitudinal static stability.

The Equation 2.151 is the effective angle of attack of the upper canard, note that again, the terms of the angles of incidence of both wings are not considered due the fact of these aerodynamic surfaces to be located behind the upper canard. The Equation 2.153 provides the pitch moment coefficient on the CG of the aircraft. The same mathematical manipulation was done, obtaining the two parcels of the pitch moment coefficient equation of the upper canard, presented on the Equation 2.154 and on the Equation 2.155.

The ratio $d\varepsilon_{W\_LOW}/d\alpha$ denotes the rate of the upwash field produced by the lower wing and the ratio $d\varepsilon_{CAN\_LOW}/d\alpha$ denotes the rate of the downwash field produced by the lower canard, the sum of both represents the rate of the global wash field surrounding the upper canard. The term $\varepsilon_{0_{W\_LOW}}$ is the angle of upwash for the lower wing at angle of attack equal to zero and the term $\varepsilon_{0_{CAN\_LOW}}$ is the angle of downwash for the lower canard at angle of attack equal to zero. Note that as mentioned for the lower canard, the upper canard volume coefficient is negative due its position ahead the location of the CG of the aircraft, the equations as presented here do not account for its negative sign. The obtainment of the upper canard volume coefficient is done the same way that was performed for the lower canard.

$$\alpha_{CAN\_UP} = \alpha + \varepsilon_{W\_LOW} - i_{CAN\_LOW} - \varepsilon_{CAN\_LOW} + i_{CAN\_UP} \tag{2.151}$$

$$CL_{CAN\_UP} = CL_{\alpha_{CAN\_UP}} \cdot \alpha_{CAN\_UP} \tag{2.152}$$

$$Cm_{CG_{CAN\_UP}} = -\eta_{CAN\_UP} \cdot V_{CAN\_UP} \cdot CL_{CAN\_UP} = Cm_{0_{CAN\_UP}} + Cm_{\alpha_{CAN\_UP}} \cdot \alpha \tag{2.153}$$

$$Cm_{0_{CAN_{UP}}} = cm_{CAN_{UP}} - \eta_{CAN_{UP}} \cdot V_{CAN_{UP}} \cdot CL_{\alpha_{CAN_{UP}}} \cdot \left(\varepsilon_{0_{W_{LOW}}} - i_{CAN_{LOW}} - \varepsilon_{0_{CAN_{LOW}}} + i_{CAN\_UP}\right) \tag{2.154}$$

$$Cm_{\alpha_{CAN_{UP}}} = -\eta_{CAN_{UP}} \cdot V_{CAN_{UP}} \cdot \left(CL_{\alpha_{CAN_{UP}}} + \Delta CL_{\alpha_{CAN_{UP}}}\right) \cdot \left(1 + \frac{d\varepsilon_{W\_LOW}}{d\alpha} - \frac{d\varepsilon_{CAN\_LOW}}{d\alpha}\right) \tag{2.155}$$

2.5.1.3. Fuselage contribution

An estimative for the fuselage contribution to the longitudinal static stability may be done based on its shape, the procedure for this estimative is described below starting on the Equation 2.156 to the Equation 2.158. These equations are solved with the help of the Figure 2.39 and the Figure 2.40, with the help of the Figure 2.44 and the Figure 2.45 and with the Equation 2.133. These equations are given for the basic linear dimensions in foot.

$$Cm_{CG_{FUS}} = Cm_{0_{FUS}} + Cm_{\alpha_{FUS}} \cdot \alpha \tag{2.156}$$

$$Cm_{0_{FUS}} = \frac{K_2 - K_1}{36.5 \cdot S_{aero_{W\_BIP}} \cdot \bar{C}_{W\_B}} \cdot \sum_{x=0}^{x=l_f} w_f^2 \cdot \left(\alpha_{0_W} + i_f\right) \cdot \Delta x_i \tag{2.157}$$

$$Cm_{\alpha_{FUS}} = \frac{1}{36.5 \cdot S_{aero_{W\_BIP}} \cdot \bar{C}_{W\_B}} \cdot \sum_{x=0}^{x=l_f} w_f^2 \cdot \frac{\partial \varepsilon_U}{\partial \alpha} \cdot \Delta x_i \quad [1/°] \tag{2.158}$$

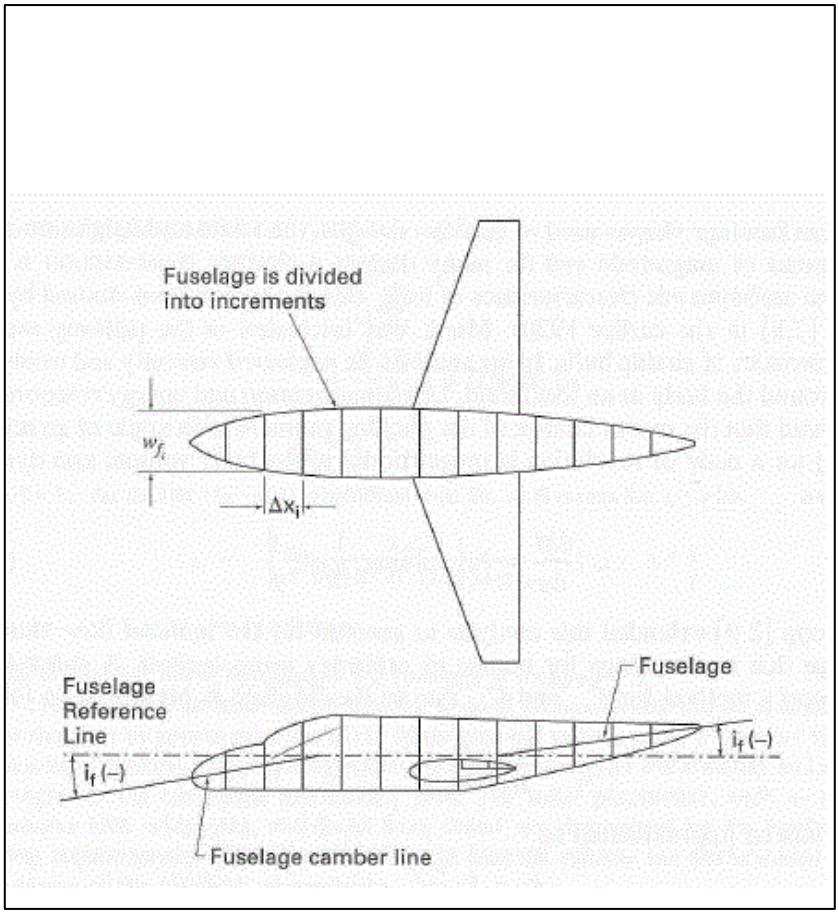


Figure 2.44 - Fuselage segmentation (Nelson, 1998).

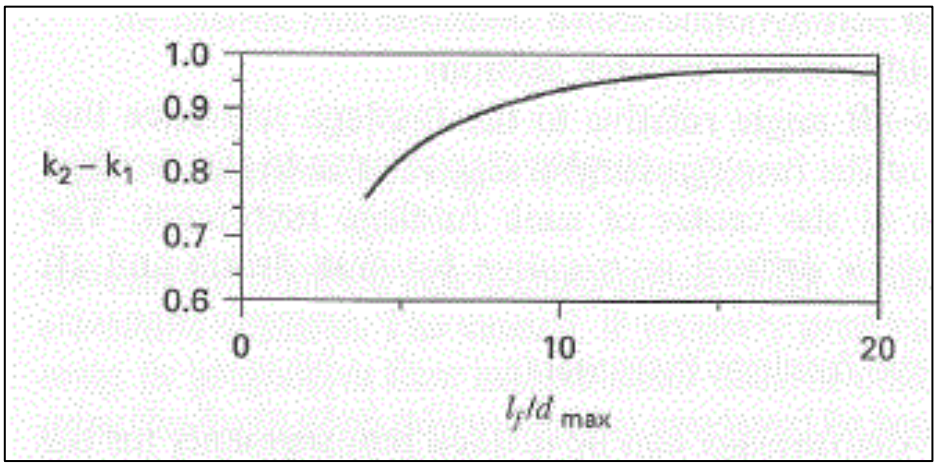


Figure 2.45 - Fuselage fineness ratio (Nelson, 1998).

2.5.1.4. Stick fixed neutral point & Static margin

The estimative of the neutral point for the airplane is proposed on the Equation 2.159, changing that defined on the bibliography (Nelson, 1998) for a conventional airplane.

On the Equation 2.159 the parcels $dE/d\alpha$ are the rate of the global wash field surrounding the lower canard and surrounding the upper canard, and there are considered the biplane wing mean aerodynamic chord. The static margin is obtained by the Equation 2.160.

$$\frac{X_{NP}}{\bar{C}_{W_B}} = \frac{X_{AC_{W_B}}}{\bar{C}_{W_B}} - \frac{Cm_{\alpha_{FUS}}}{CL_{\alpha_{W_B}}} + \eta_{CAN_{LOW}} \cdot V_{CAN_{LOW}} \cdot \frac{CL_{\alpha_{CAN_{LOW}}}}{CL_{\alpha_{W_B}}} \cdot \left(1 + \frac{dE_{CAN_{LOW}}}{d\alpha}\right) + \eta_{CAN_{UP}} \cdot V_{CAN_{UP}} \cdot \frac{CL_{\alpha_{CAN\_UP}}}{CL_{\alpha_{W\_B}}} \cdot \left(1 + \frac{dE_{CAN\_UP}}{d\alpha}\right) \quad (2.159)$$

$$K_{STAT} = X_{NP} - \frac{X_{CG} - X_{LE_{\bar{C}_{W\_B}}}}{\bar{C}_{W\_B}} \quad (2.160)$$

2.5.2. Longitudinal control

The control surface responsible for the longitudinal control, that is, responsible for the pitch change of the airplane is the elevator.

2.5.2.1. Elevator dimensioning considerations

This primary control surface normally has between 90% and 100% of the length of the trailing edge of the horizontal tail. Considering an airplane of the experimental/general category, the main relation of design and its reference value is $C_E/C_{HT} = 0{,}45$.

The design of the elevator is based in four main parameters which are S_E, C_E, b_E and its maximum positive and negative deflection $\pm\delta_{E.max}$, the positive deflection is that for which the elevator is deflected down and negative when deflected up. Typical values for these parameters are presented on the Table 2.24.

The control and trim of the airplane are the basic functions of the elevator, considering the longitudinal stability its influence is secondary. The effectivity of the elevator is dependent of its aerodynamic area and moment arm, another parameter relevant is the hinge moment that impacts directly the force that the pilot will apply for move this control surface. So, special attention must be payed to this, the aerodynamic balance and mass balance may be employed helping adjust the value of the hinge moment related to the elevator, what contribute yet, for aspects related to the aeroelasticity.

The maximum deflection of the elevator must be defined avoiding the boundary layer separation over the upper surface of the horizontal tail, and in consequence, inducing its premature stall. It is important keep in mind that for the horizontal tail near its stall angle, a small deflection of the elevator may be enough for cause the stall of the surface.

If during the designing of the elevator its chord surpass 50% of the chord of the horizontal tail, it is recommended change the design and use a comple movable horizontal tail, for avoid the premature stall of the surface.

2.5.2.2. Longitudinal control derivatives

The power of control of the elevator is defined basically by three control derivatives $Cm_{\delta E}$, $CL_{\delta E}$ and $CL_{HT_{\delta E}}$, this last one was already defined in the aerodynamic theory chapter by the Equation 2.81. The first two derivatives are defined by the Equation 2.161 and by the Equation 2.162. Note that for $Cm_{\delta E}$ it will assume a positive value due the fact that for the canards their volume coefficients are negative as explained before. These two equations are valid for both elevators that are installed on each canard. For airplanes equipped with

conventional horizontal tail the Equation 2.161 present commonly the $Cm_{\delta E} = -0.2\ to\ -0.4\ [1/rad]$ values.

$$Cm_{\delta E} = \frac{\partial C_m}{\partial \delta_E} = -CL_{\alpha_{CAN}} \cdot \eta_{CAN} \cdot V_{CAN} \cdot \frac{b_E}{b_{CAN}} \cdot \tau_E \tag{2.161}$$

$$CL_{\delta E} = \frac{\partial C_L}{\partial \delta_E} = CL_{\alpha_{CAN}} \cdot \eta_{CAN} \cdot \frac{S_{aero_{CAN}}}{S_{aero_{W\_BIP}}} \cdot \frac{b_E}{b_{CAN}} \cdot \tau_E \tag{2.162}$$

2.5.2.3. Take-off rotation

For an aircraft with landing gear of tricycle kind, during the take-off running with a weight configuration in which the CG location is the most ahead as possible, is recommended by regulation that the elevator must produce enough power to rotate the airplane at its main landing gear leg for a running speed of $V_R = 0{,}8 \cdot V_{TO}$.

The designing of the elevator considering the take-off rotation is done by summing all the moments produced by the components of the aircraft at the main landing gear leg as presented on the Figure 2.46, and given by the Equation 2.163. For the airplane UFU-1 is considered the Equation 2.164. Note that for all the moment equations it is not considered the sign of each moment parcel, which assume positive sign for clockwise direction and negative for counter clockwise.

$$\sum M_{mg} = I_{yy_{mg}} \cdot \ddot{\theta} = M_W + M_D + M_T + M_{L_{wf}} + M_{ac_{wf}} + M_{L_h} + M_{ac_h} + M_a \tag{2.163}$$

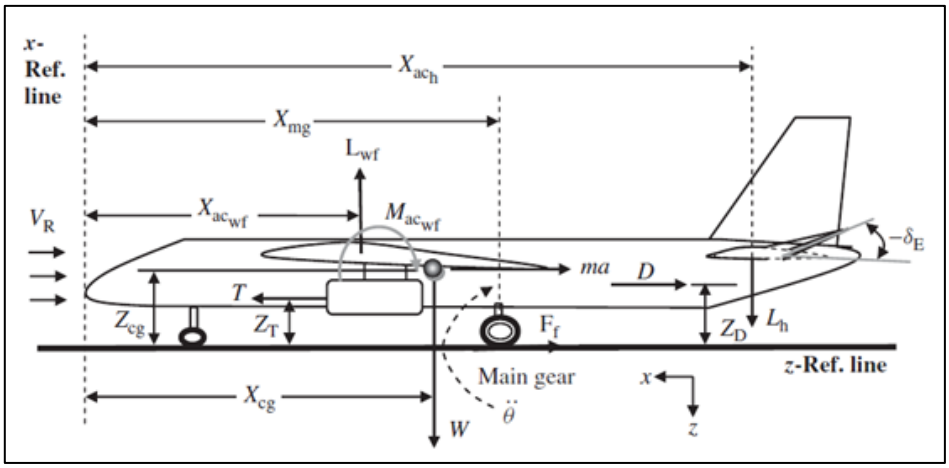


Figure 2.46 - Forces and moments during the take-off rotation (Sadraey, 2013).

$$\sum M_{mg} = I_{yy_{mg}} \cdot \ddot{\theta} = M_W + M_L + M_D + M_T + M_{W\_LOW} + M_{W\_UP} + M_{FUS} + M_{CAN\_LOW} + M_{CAN\_UP} + M_a \quad (2.164)$$

$$I_{yy_{mg}} = I_{yy_{cg}} + m \cdot \left(d_{cg-mg}\right)^2 \quad (2.165)$$

$$M_L = M_{L_{W\_LOW}} + M_{L_{W\_UP}} + M_{L_{FUS}} + M_{L_{CAN\_LOW}} + M_{L_{CAN\_UP}} \quad (2.166)$$

$$M_D = M_{D_{W\_LOW}} + M_{D_{W\_UP}} + M_{D_{FUS}} + M_{D_{CAN\_LOW}} + M_{D_{CAN\_UP}} + M_{D_{VT\_LEF}} + M_{D_{VT\_RIG}} \quad (2.167)$$

By solving the Equation 2.164, is obtained the pitch angular acceleration of the airplane, as reference, the Table 2.25 present typical values for some airplane categories.

Table 2.25 - Take-off rotational acceleration for various aircraft (Sadraey, 2013).

No.	Aircraft type	Take-off pitch angular acceleration $\ddot{\theta}$ (deg/s^2)
1	Highly maneuverable (e.g., acrobatic, fighter)	10–20
2	Utility, semi-acrobatic	10–15
3	Normal light general aviation	8–10
4	Small transport	6–8
5	Large transport	4–6

2.5.2.4. Longitudinal trim

Trim longitudinally the aircraft, is desired for some flight condition as cruise, climb and descent. The longitudinal trim is obtained when the summation of the moments at the CG of the aircraft is equal to zero.

The elevator must be capable to trim the airplane in any flight condition and for any CG location. For design purpose the cruise is the main flight condition considered, in which is desired to maintain the elevator at a deflection angle equal to zero. The Equation 2.168 and the Equation 2.169 are employed on the elevator design for trim purpose, and the Figure 2.47 show graphically the trim condition for a generic airplane at cruise flight.

$$\delta_E = -\frac{\left(\frac{T \cdot Z_{Thrust}}{q \cdot Saero_{W\_BIP} \cdot \bar{C}_{W\_B}} + Cm_{0_{AP}}\right) \cdot C_{L_{\alpha_{AP}}} + \left(C_{L_1} - CL_{\alpha=0_{AP}}\right) \cdot Cm_{\alpha_{CG}}}{C_{L_{\alpha_{AP}}} \cdot Cm_{\delta E} - Cm_{\alpha_{CG}} \cdot C_{L_{\delta E}}} \quad (2.168)$$

$$C_{L_1} = CL_{\alpha=0_{AP}} + C_{L_{\alpha_{AP}}} \cdot \alpha + C_{L_{\delta E}} \cdot \delta_E \quad (2.169)$$

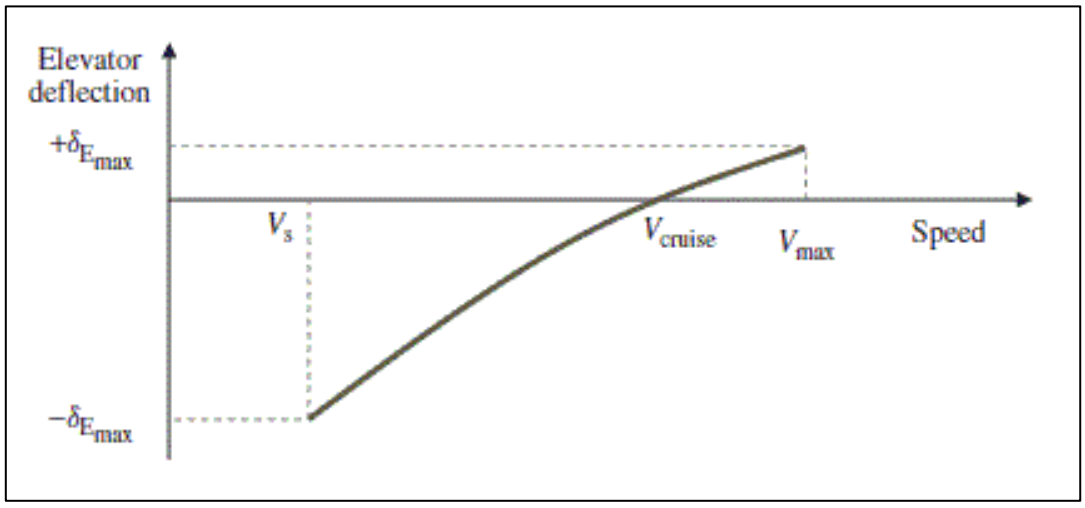


Figure 2.47 - Typical variation of elevator deflection versus aircraft speed (Sadraey, 2013).

Once the airplane is in the longitudinal trim condition, it is possible to obtain its angle of attack by the Equation 2.170.

$$\alpha = \frac{\left(\frac{T \cdot Z_{Thrust}}{q \cdot Saero_{W\_BIP} \cdot \bar{C}_{W\_B}} + Cm_{0_{AP}}\right) \cdot C_{L_{\delta E}} + \left(C_{L_1} - CL_{\alpha=0_{AP}}\right) \cdot Cm_{\delta E}}{C_{L_{\alpha_{AP}}} \cdot Cm_{\delta E} - Cm_{\alpha_{CG}} \cdot C_{L_{\delta E}}} \quad (2.170)$$

2.5.3. Lateral static stability

For an aircraft to present a lateral static stable behavior, it must produce a restoring rolling moment when disturbed from a leveled wing flight attitude. Due the coupling that exists between the lateral and the directional axis, the restoring rolling moment may be defined in term of a yawing disturb as presented on the Figure 2.48 which show two conditions, one for an aircraft with stable behavior and other for an aircraft with unstable behavior.

The lateral static stability is function of the wing parameters as dihedral, sweep, its location relative to the fuselage and also is dependent of the shape of the vertical tail. From all these parameters the one which most impact the lateral static stability is the wing dihedral.

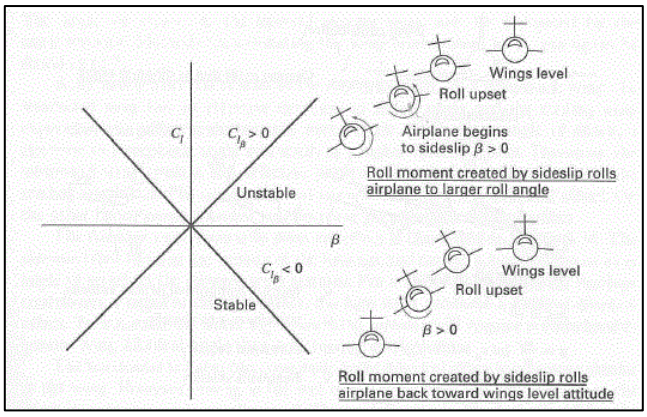


Figure 2.48 - Static roll stability (Nelson, 1998).

As can be observed by the figure, for an aircraft to present a stable behavior, it would have a negative rolling moment curve slope as given by the Equation 2.171. For to estimate the roll static stability of an airplane, considering that the wing dihedral is the parameter that most contribute to it, may be applied the Equation 2.172, with the help of the Figure 2.49.

$$\frac{dCl}{d\beta} < 0 \tag{2.171}$$

$$Cl_{\beta_{CG}} = \left(\frac{Cl_\beta}{\Gamma}\right) \cdot \Gamma_W + \Delta Cl_\beta \tag{2.172}$$

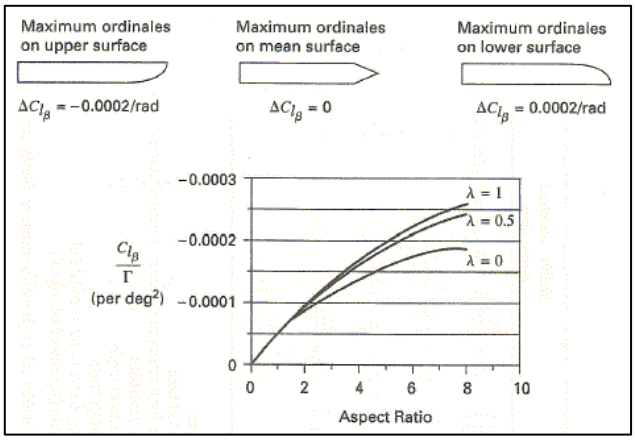


Figure 2.49 - Tip shape and aspect ratio effect on Cl_β (Nelson, 1998).

2.5.4. Lateral control

The control surface responsible for the lateral control, that is, responsible for rolling the airplane is the aileron.

2.5.4.1. Aileron dimensioning considerations

The chord of the aileron normally has between 15% and 25% of the chord of the wing. When positioning the aileron on the wing, it is recommended avoid coinciding its tip to the wing tip, once the wing tip vortex may decrease the aileron effectivity. The Figure 2.50 shows the historic tendency for the dimensions of the ailerons.

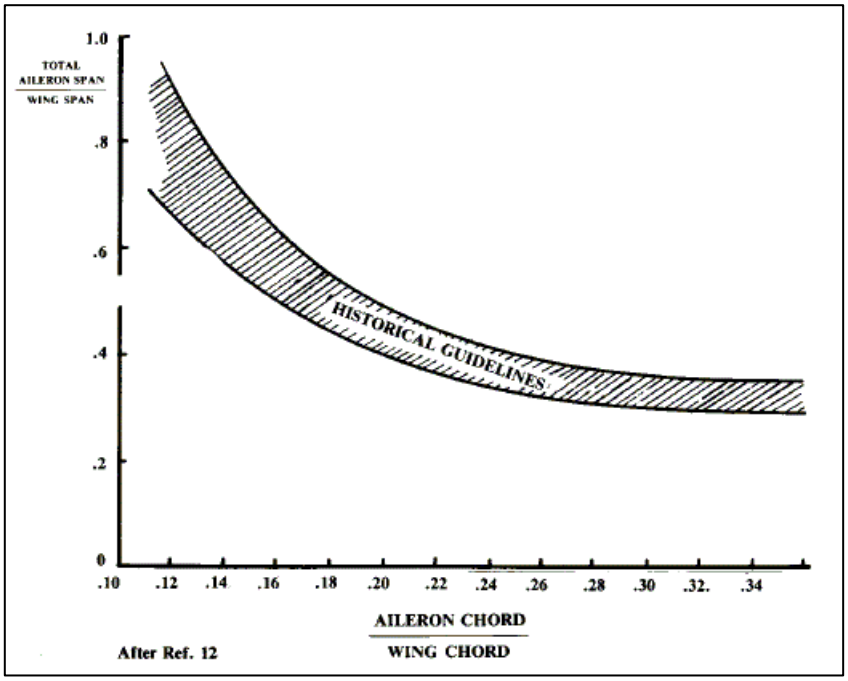


Figure 2.50 - Aileron guidelines (Raymer, 2006).

The rolling moment generated by the aileron is dependent of its size, deflection, and distance to the longitudinal axis of the aircraft. Different of the elevator and of the rudder which are displacement control surfaces, the aileron is a rate control. As well as for the elevator, the hinge moment related to the aileron will directly affect the force exercised by the pilot for move it.

There are four main parameters that must be considered during the design of the aileron S_A, b_A, C_A and $\pm\delta_{A.max}$, the typical values for these parameters are presented on the Table 2.24. Another reference relation is the ratio between the position of the internal chord of the aileron and the wing span given by $b_{Ai}/b_W = 0{,}6\ a\ 0{,}8$. The Figure 2.51 presents these basic geometric parameters.

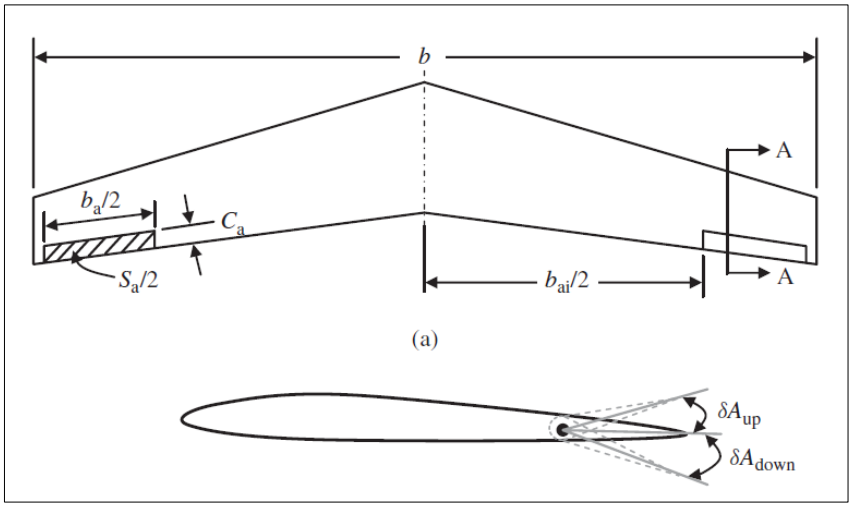


Figure 2.51 - Geometry of aileron (a) top view; (b) side view (Sadraey, 2013).

Due the existence of the coupling between the lateral and the directional axis, when the ailerons are deflected it may induce a yawing movement known as adverse yaw. For avoiding this movement during a turning maneuver, the aileron installed on the semi-wing that is, at the outside of the curve will need to be deflected down in an angle lower than that which will be deflected up by the aileron installed on the semi-wing which is at the inside of the curve. By ensuring this combined movement of both ailerons panels, the induced drag generated by them will have the same magnitude avoiding the adverse yaw. The flight conditions in which the adverse yaw must be avoided are that in low speed, which could induce a departure of the aircraft.

Considering the explanation above, it is concluded that the rolling moment generated by both ailerons panel must be the same in magnitude and direction, this condition is obtained by the relations showed on the Equation 2.173 to the Equation 2.176.

$$Di_{A\_left} = Di_{A\_right} \tag{2.173}$$

$$V_{A\_left} = \omega \cdot R_{A\_left} \tag{2.174}$$

$$V_{A\_right} = \omega \cdot R_{A\_right} \tag{2.175}$$

$$\frac{V_{A\_left}}{V_{A\_right}} = \frac{R_{A\_left}}{R_{A\_right}} \tag{2.176}$$

Therefore, considering for example a turning for the left, will be obtained the following relations $R_{A\_left} > R_{A\_right}$, which leads to $V_{A\_left} > V_{A\_right}$, which finally lead to $\delta_{A\_left} < \delta_{A\_right}$.

When the ailerons are deflected more than 20° or 25° in some cases, the air flow over it will tend to separate inducing its stall, and consequently decreasing drastically its effectivity. This condition is aggravated if the aircraft is at high angle of attack, on situations like this, small deflections are enough for induce the air flow separation.

2.5.4.2. Rolling estimate

The dimensioning of the ailerons for rolling is based on the Equation 2.177 to the Equation 2.180 which were obtained specifically for the airplane UFU-1, by modifying that showed on the bibliography (*Sadraey, 2013*) substituting the reference areas by the aerodynamic ones. The Figure 2.52 indicates the parameters employed in this dimensioning.

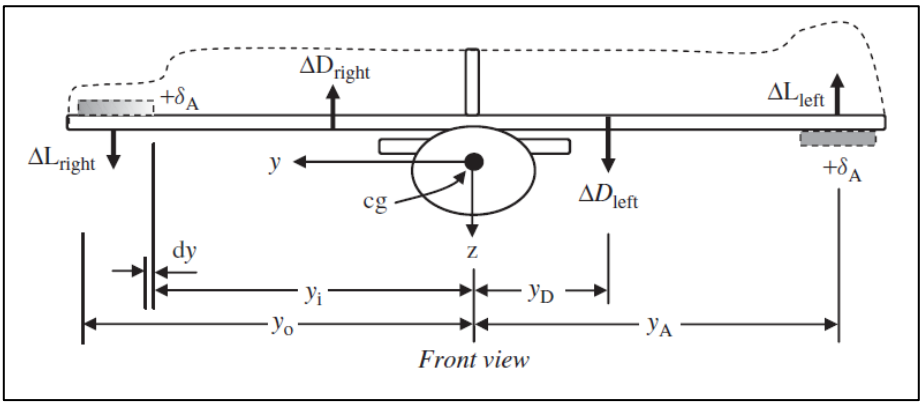


Figure 2.52 - Incremental change in lift and drag in generating a rolling motion (Sadraey, 2013).

$$L_A = 2 \cdot \Delta L_A \cdot y_A \tag{2.177}$$

$$\dot{p} = \frac{L_A}{I_{xx_{cg}}} \tag{2.178}$$

$$p_{ss} = \sqrt{\frac{2 \cdot L_A}{\rho_{FL} \cdot \left(S_{aero_{W\_BIP}} + S_{aero_{CAN\_BIP}} + S_{aero_{VT\_LEF}} + S_{aero_{VT\_RIG}}\right) \cdot C_{D_R} \cdot y_D^3}}} \quad (2.179)$$

$$\int_0^{\varphi} \dot{p} \cdot d\varphi = \int_0^{p_{ss}} p \cdot dp \quad (2.180)$$

2.5.4.3. Lateral stability and control derivatives

The rolling derivative of an aircraft is dependent of some other static stability and control derivatives that are relative to the aircraft aerodynamic configuration and its flight condition, as defined on the Equation 2.181.

$$Cl_{CG} = Cl_{\delta A} \cdot \delta_A + Cl_{p_{CG}} \cdot p_0 + Cl_{\delta R} \cdot \delta_R + Cl_{\beta_{CG}} \cdot \beta + Cl_{r_{CG}} \cdot r_0 \quad (2.181)$$

For an aircraft symmetric relative to the plane xz in a flight condition with no sideslip and no deflection of the rudder, the equation above may be reduced taking the form presented on the Equation 2.182.

$$Cl_{CG} = Cl_{\delta A} \cdot \delta_A \quad (2.182)$$

The control derivative relative to the aileron is obtained by the Equation 2.183 which is solved with the help of the Figure 2.29 and the help of the Figure 2.52. The aileron displacement is computed considering both panels as presented on the Equation 2.184. The Equation 2.183 was obtained by modifying the original equation given at the bibliography (Sadraey, 2013) to represent the geometric characteristics of the biplane wing, once these characteristics are different from that of both lower and upper wings.

$$Cl_{\delta A} = \frac{\partial Cl}{\partial \delta_A} = \frac{2 \cdot CL_{\alpha_{W\_B}} \cdot \tau_A \cdot C_{root_{W\_B}}}{S_{aero_{W\_BIP}} \cdot b_{W\_B}} \cdot \left[\frac{y^2}{2} + \frac{2}{3} \cdot \left(\frac{\lambda_{W\_B} - 1}{b_{W\_B}}\right) \cdot y^3\right]_{y_i}^{y_o} \quad (2.183)$$

$$\delta_A = 0{,}5 \cdot \left[\left|\delta_{A_{left}}\right| + \left|\delta_{A_{right}}\right|\right] \quad (2.184)$$

Related to the rolling speed of the airplane there is a derivative which contribute the lateral stability of the aircraft, given by the Equation 2.185, this derivative is the roll damping coefficient due the wing surface.

$$Cl_{p_{CG}} = -\frac{C_{L_{\alpha_{AP}}}}{12} \cdot \frac{1+3\cdot\lambda_{W\_B}}{1+\lambda_{W\_B}} \quad (2.185)$$

2.5.5. Directional static stability

An aircraft is said to be directional statically stable if when a yaw disturbed occur, the aircraft produce a restoring yawing moment, the Figure 2.53 presents two conditions for a generic aircraft when directionally disturbed. As can be observed, for an airplane to be directional statically stable it should have a positive yawing moment curve slope as given by the Equation 2.186, the Table 2.23 present typical values for this static stability derivative.

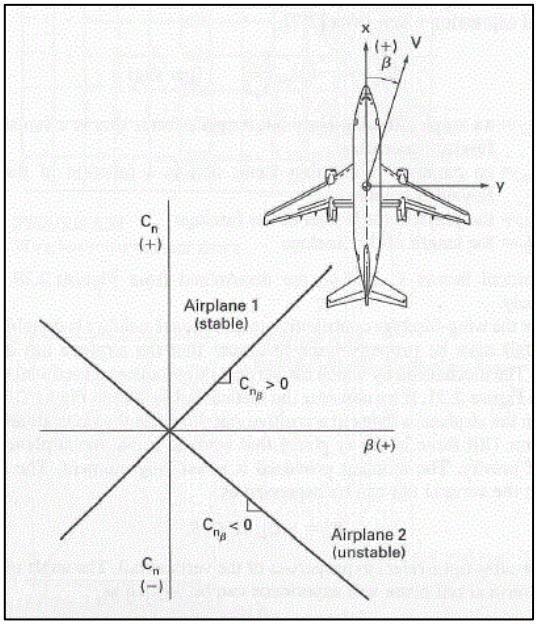


Figure 2.53 - Static directional stability (Nelson, 1998).

$$\frac{dCn}{d\beta} > 0 \quad (2.186)$$

The directional static stability curve slope of an aircraft is usually measured at its CG, leading to the derivative of stability presented on the Equation 2.187, which was defined specifically for the airplane UFU-1.

$$Cn_{\beta_{CG}} = Cn_{\beta_{W\_B-FUS}} + Cn_{\beta_{VT\_LEF}} + Cn_{\beta_{VT\_RIG}} \quad (2.187)$$

2.5.5.1. Wing-Fuselage contribution

Considering that the influence of the wings in the directional stability of an aircraft is neglectable, and the fuselage present a non neglectable influence, it is common to estimate the influence of them together, by applying an empirical formulation given by the bibliography (Nelson, 1998) and presented on the Equation 2.188. Such equation was adapted for the aerodynamic characteristics of the airplane here developed, considering the parameters of the biplane wing, this equation is solved with the help of the Figure 2.54 and the Figure 2.55.

As can be noted by the negative signal, this equation assume that the fuselage is directionally destabilizing, however, it is reasonable suppose that the fuselage will be destabilizing if the aerodynamic center of the projected side area is located ahead of the CG of the airplane, and will be stabilizing if such aerodynamic center is located behind the CG of the airplane, being necessary to change the signal of the Equation 2.188.

$$Cn_{\beta_{W\_B-FUS}} = -k_n \cdot k_{Rl} \cdot \frac{S_{F\_S} \cdot l_f}{S_{aero_{W\_BIP}} \cdot b_{W\_B}} \tag{2.188}$$

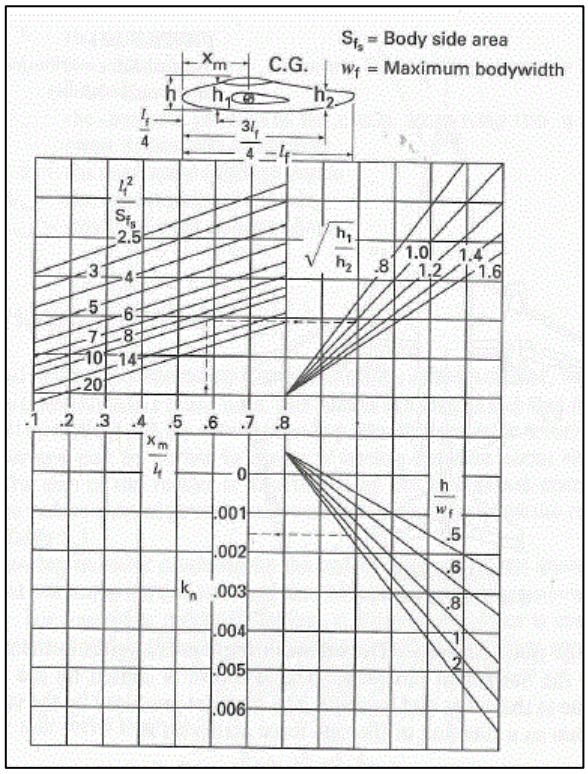


Figure 2.54 - Wing body interference factor (Nelson, 1998).

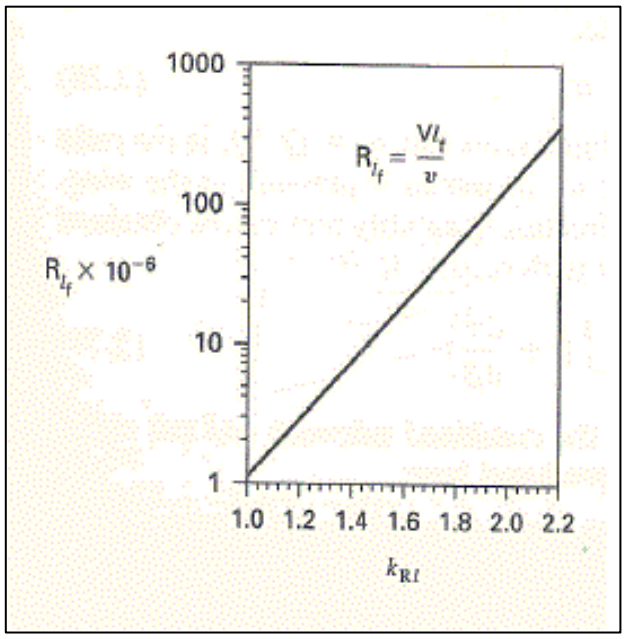


Figure 2.55 - Reynolds number correction factor (Nelson, 1998).

2.5.5.2. Vertical tails contribution

The vertical tail is the responsible for turn the aircraft directionally stable, this derivative of stability is estimated by the Equation 2.189 that may be applied for both vertical tail surfaces of the airplane UFU-1. The sidewash rate is given by the Equation 2.123.

The obtainment of the vertical tail volume coefficient may be done applying the Equation 2.33 replacing the reference areas by the aerodynamic areas. The tail arm l_{VT} in this equation is correctly obtained considering that it is the distance between the point at 25% of the vertical tail mean aerodynamic chord and the CG location of the airplane.

$$Cn_{\beta_{VT}} = V_{VT} \cdot \eta_{VT} \cdot CL_{\alpha_{VT}} \cdot \left(1 + \frac{d\sigma}{d\beta}\right) \tag{2.189}$$

2.5.6. Directional control

The control surface responsible for the directional control, that is, responsible for yawing the aircraft is the rudder.

2.5.6.1. Rudder dimensioning considerations

The span of the rudder in low performance aircrafts normally cover between 90% to 100% of the length of the trailing edge of the vertical tail, but, for aircrafts of high performance it has chord of big size and its span is reduced for length up to 50% of the span of the vertical tail, these geometric characteristics are defined intending to avoid the command reversal. Typical values for these parameters are presented on the Table 2.24. For an airplane of the experimental/general category the ratio between chords is around $C_R/C_{VT} = 0.4$.

The parameters of design of a rudder are based on the two basic functions that it exercises, directional control and directional trim. As the behavior of an aircraft due the deflection of ailerons and rudder are coupled, it is recommended that both be designed at the same time. Although the elevator and the rudder to be displacement control devices, the design of the rudder is more complex than that employed for elevators. The Figure 2.56 shows two possible geometry for the design of a rudder.

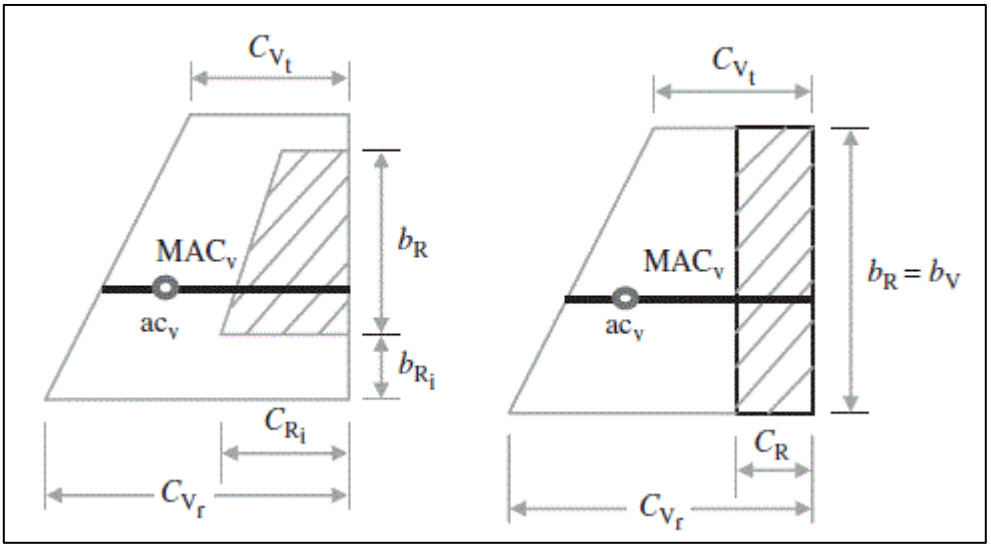


Figure 2.56 - Possible geometries for a rudder (After Sadraey, 2013).

The rudder must comply its function along all the flight phases, the six main functions of the rudder are presented on the Table 2.26.

Table 2.26 - Rudder design requirements (Sadraey, 2013).

No.	Requirements	Brief description	Aircraft
1	Asymmetric thrust	When one engine fails, the aircraft must be able to overcome the asymmetric thrust.	Multi-engine aircraft
2	Cross-wind landing	An aircraft must maintain alignment with the runway during a cross-wind landing.	All
3	Spin recovery	An aircraft must be able to oppose the spin rotation and to recover from a spin.	Spinnable aircraft
4	Coordinated turn	The aircraft must be able to coordinate a turn.	All
5	Adverse yaw	The rudder must be able to overcome the adverse yaw that is produced by the ailerons.	All
6	Glide slope adjustment	The aircraft must be able to adjust the glide slope by increasing aircraft drag using a rudder deflection.	Glider aircraft

As presented by the table above, for a multi-engine airplane asymmetric thrust is the most important parameter for the rudder design, for a single-engine the maximum cross wind at landing is the most important parameter, and so on. For a single-engine airplane it is suggested that the minimum control speed for rudder could be $V_{MC} = 0{,}8 \cdot V_S$, during the take-off run.

2.5.6.2. Yawing estimate

By convention, the positive rudder deflection is to the left and the negative deflection is to the right, considering the reference of the pilot. The positive deflection of the rudder generates a positive side force, which is the vertical tail lift L_{VT}, causing a positive yawing moment, aircraft nose for left side as showed by the Figure 2.57.

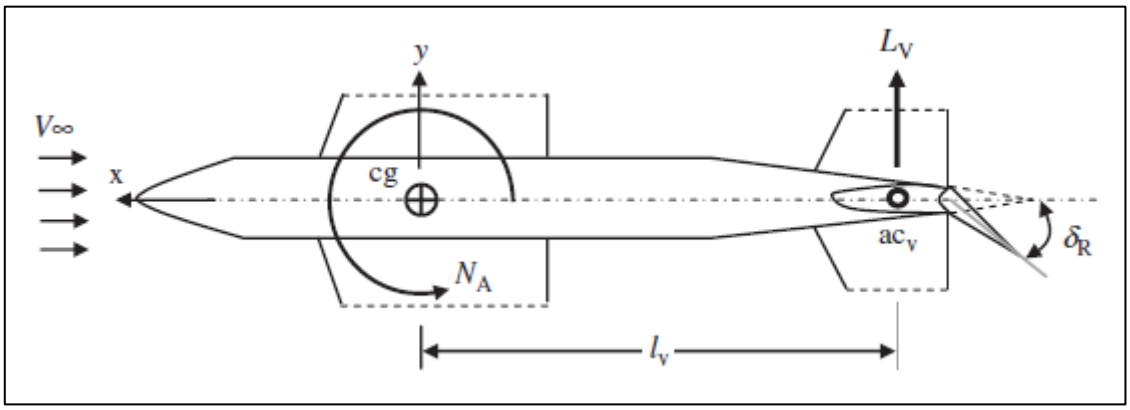


Figure 2.57 - Directional control and rudder deflection (Sadraey, 2013).

For a symmetric aircraft relative to the xz plane, in a flight configuration with no side slip angle and no deflection of ailerons, the yawing moment may be define by the Equation 2.190 given at the bibliography (*Sadraey, 2013*), which is valid for both vertical tails of the airplane here developed.

$$N_A = l_{VT} \cdot L_{VT} = q_{VT} \cdot S_{aero_{W\_BIP}} \cdot b_{W\_B} \cdot Cn_{CG_{VT}} \tag{2.190}$$

$$L_{VT} = q_{VT} \cdot S_{aero_{VT}} \cdot CL_{VT} \tag{2.191}$$

$$q_{VT} = \frac{1}{2} \cdot \rho_{FL} \cdot V_T^2 \tag{2.192}$$

As mentioned above, for a single-engine aircraft the most critical condition for rudder dimensioning is landing at cross wind condition. Pilots can conduce the landing in two ways, applying a maneuver called crabbing, where the wings are maintained leveled and a drift is generated by the rudder tracking the center line of the runway; or applying a maneuver called steady sideslip, where the fuselage is maintained aligned to the runway center line applying simultaneously the inner wind aileron and the opposite rudder deflection to correct the drift.

The dimensioning of the rudder for cross wind will be done considering the crabbing maneuver, which is shown on the Figure 2.58, and has its parameters presented on the Equation 2.193 to the Equation 2.195.

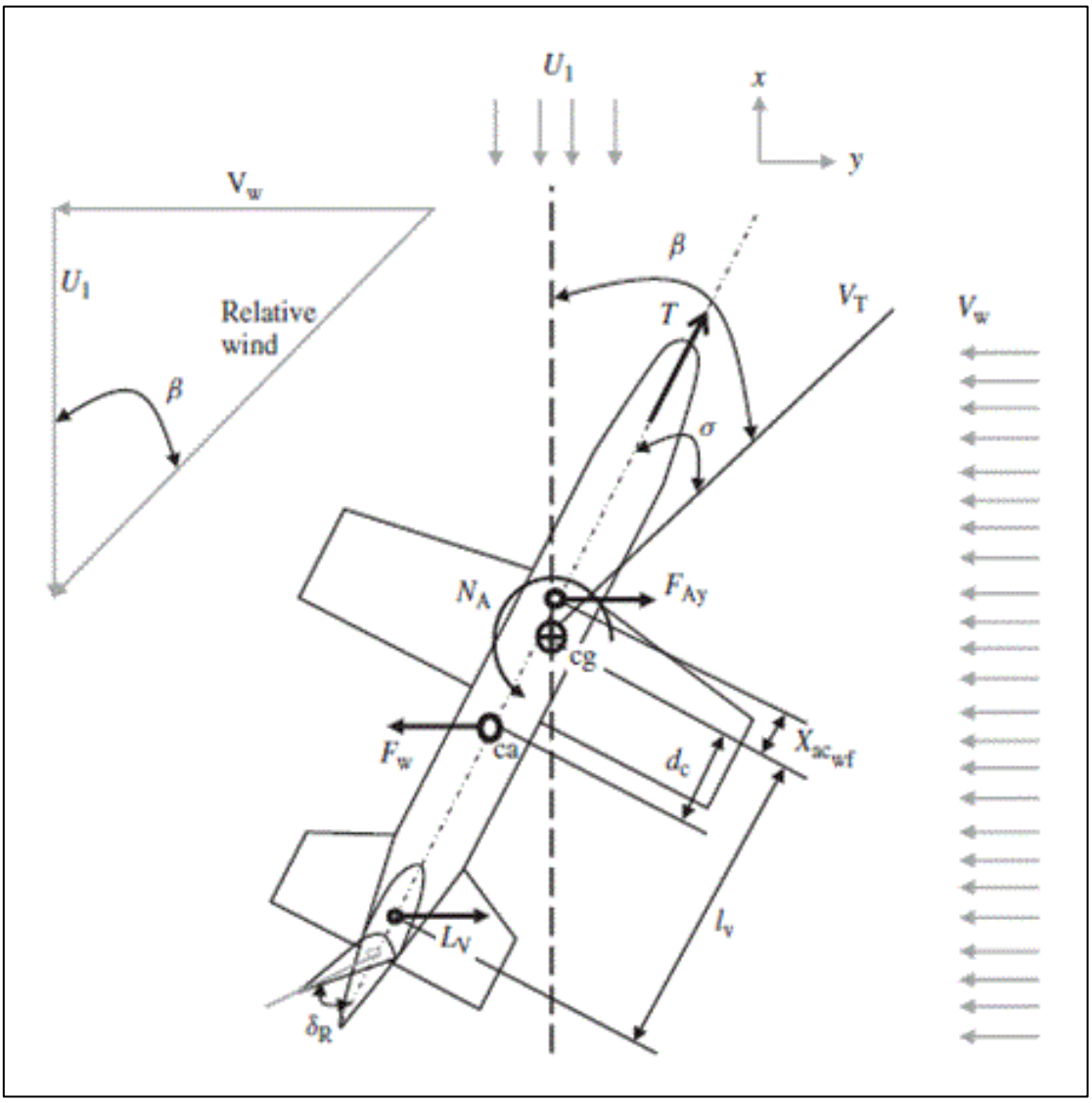


Figure 2.58 - Forces and angles in cross-wind crabbed landing (Sadraey, 2013).

$$\beta = tan^{-1}\left(\frac{V_W}{U_1}\right) \tag{2.193}$$

$$V_T = \sqrt{U_1^2 + V_W^2} \tag{2.194}$$

$$F_W = \frac{1}{2} \cdot \rho_{FL} \cdot V_W^2 \cdot S_S \cdot C_{D_y} \tag{2.195}$$

The sideslip angle is what generates the yawing moment N_A and the aerodynamic side force F_{Ay} at the aircraft. In order to react these force and moment, the rudder must be deflected

to align the aircraft flight direction to the runway center line, generating a “lift” L_{VT} on the vertical tail and a crab angle σ. The Equation 2.196 to the Equation 2.198 are the three governing ones.

$$\sum N_{cg} = 0 = N_A + F_W \cdot d_c \cdot \cos\sigma \tag{2.196}$$

$$\sum F_x = 0 \rightarrow T \cdot \cos\sigma = D \tag{2.197}$$

$$\sum F_y = 0 \rightarrow F_W = F_{A_y} \tag{2.198}$$

From the three equations above it is obtained a system of two equations and two unknowns δ_R and σ that provide the rudder deflection and crab angle, given by the Equation 2.199 and the Equation 2.200.

$$\frac{1}{2} \cdot \rho_{FL} \cdot V_T^2 \cdot S_{aero_{W_{BIP}}} \cdot b_{W_B} \cdot \left(Cn_0 + Cn_{\beta_{CG}} \cdot (\beta - \sigma) + Cn_{\delta R} \cdot \delta_R\right) + F_W \cdot d_c \cdot \cos\sigma = 0 \tag{2.199}$$

$$\frac{1}{2} \cdot \rho_{FL} \cdot V_W^2 \cdot S_S \cdot C_{D_y} - \frac{1}{2} \cdot \rho_{FL} \cdot V_T^2 \cdot S_{aero_{W_{BIP}}} \cdot \left(Cy_0 + Cy_{\beta_{CG}} \cdot (\beta - \sigma) + Cy_{\delta R} \cdot \delta_R\right) = 0 \tag{2.200}$$

Once the development of the theory for the rudder design was presented above, it is important use it together to the certification rules as for example that described by CS-VLA article 233, which determine that a very light aircraft should be able to land at a 90° cross wind up to $10\ kt$. Other important regulation regarding rudder dimensioning is FAR Part 23 section 233, which determine that the airplane of general aviation should be able to land at a 90° cross wind with velocity not less than $0{,}2 \cdot V_{SO}$.

2.5.6.3. Directional stability and control derivatives

For all the theory developed next, the terms developed for the generic vertical tail of a conventional airplane, are valid for both vertical tails of the airplane UFU-1.

The main static derivative related to the directional stability and control is that presented on the Equation 2.201, which is the yaw moment coefficient of the aircraft.

$$Cn_{CG} = Cn_0 + Cn_{\beta_{CG}} \cdot (\beta - \sigma) + Cn_{\delta R} \cdot \delta_R + Cn_{r_{CG}} \cdot r_0 + Cn_{\delta A} \cdot \delta_A \tag{2.201}$$

Note that for the aircraft developed in this work, the following derivatives must be applied for each vertical tail.

Yaw moment derivatives

On the Equation 2.201, the parcel $Cn_0 = 0$ for an airplane symmetric relative to the plane xz, as is the airplane UFU-1.

The Equation 2.202 is the directional control derivative due the rudder deflection and is solved with the help of the Figure 2.29, the Equation 2.203 is the directional derivative due the non-dimensional yaw speed, and the Equation 2.204 is the non-dimensional yaw speed, all defined on the bibliography (Nelson, 1998). By similarity the non-dimensional roll speed may be defined the same way as was defined the non-dimensional yaw speed, and is presented on the Equation 2.205. The derivative given by the Equation 2.203 is the one that most affect the dynamic characteristics, and it is strongly stabilizing when negative.

$$Cn_{\delta R} = \frac{\partial Cn}{\partial \delta_R} = -CL_{\alpha_{VT}} \cdot V_{VT} \cdot \eta_{VT} \cdot \tau_R \cdot \frac{b_R}{b_{VT}} \tag{2.202}$$

$$Cn_{r_{CG}} = \frac{\partial Cn}{\partial r} = -2 \cdot CL_{\alpha_{VT}} \cdot V_{VT} \cdot \eta_{VT} \cdot \frac{l_{VT}}{b_{W\_B}} \tag{2.203}$$

$$r_0 = \frac{r \cdot b_{W\_B}}{2 \cdot U_0} \tag{2.204}$$

$$p_0 = \frac{p \cdot b_{W\_B}}{2 \cdot U_0} \tag{2.205}$$

Yaw y-force derivatives

On the Equation 2.200, the parcel $Cy_0 = 0$ for an airplane symmetric relative to the plane xz, as is the airplane UFU-1.

The Equation 2.206 to the Equation 2.208 present the y-force derivatives related to the directional stability and control.

$$Cy_{\beta_{CG}} = \frac{\partial Cy}{\partial \beta} = -K_{f2} \cdot CL_{\alpha_{VT}} \cdot \left(1 - \frac{d\sigma}{d\beta}\right) \cdot \eta_{VT} \cdot \frac{S_{aero_{VT}}}{S_{aero_{W\_BIP}}} \tag{2.206}$$

$$Cy_{\delta R} = \frac{\partial Cy}{\partial \delta_R} = CL_{\alpha_{VT}} \cdot \eta_{VT} \cdot \tau_R \cdot \frac{b_R}{b_{VT}} \cdot \frac{S_{aero_{VT}}}{S_{aero_{W\_BIP}}} \tag{2.207}$$

$$Cy_{r_{CG}} = -2 \cdot Cy_{\beta_{CG}} \cdot \frac{l_{VT}}{b_{W\_B}} \quad (2.208)$$

2.5.7. Lateral-Directional static stability & control coupling

The aircrafts normally present coupling between the lateral and the directional axis because they are not symmetric relative to the xy plan, this fact is confirmed by inspecting the Equation 2.181 and the Equation 2.201, in these equations are found parcels that represent the coupling between these axis, that is, rolling derivative due the yaw and yawing derivative due the roll. Next are presented the equations for these stability and control derivatives.

Lateral derivatives

The derivatives to be presented here are responsible for to contribute to the rolling moment generated by the aircraft, and are produced or by the rudder deflection or by the yawing movement of the airplane.

$$Cl_{\delta R} = \frac{S_{aero_{VT}}}{S_{aero_{W\_BIP}}} \cdot \frac{Z_{VT}}{b_{W\_B}} \cdot \tau_R \cdot CL_{\alpha_{W\_B}} \quad (2.209)$$

$$Cl_{r_{CG}} = \frac{CL}{4} - 2 \cdot \frac{l_{VT}}{b_{W\_B}} \cdot \frac{Z_{VT}}{b_{W\_B}} \cdot Cy_{\beta_{CG}} \quad (2.210)$$

Directional derivatives

The derivatives presented here are responsible for to contribute to the yawing moment generated by the aircraft, and are produced or by the ailerons deflection or by the rolling movement of the aircraft. The Equation 2.211 that is the yaw moment coefficient due the ailerons deflection is solved with the help of the Figure 2.59.

$$Cn_{\delta A} = 2 \cdot K \cdot CL \cdot Cl_{\delta A} \quad (2.211)$$

$$Cn_{p_{CG}} = -\frac{CL}{8} \quad (2.212)$$

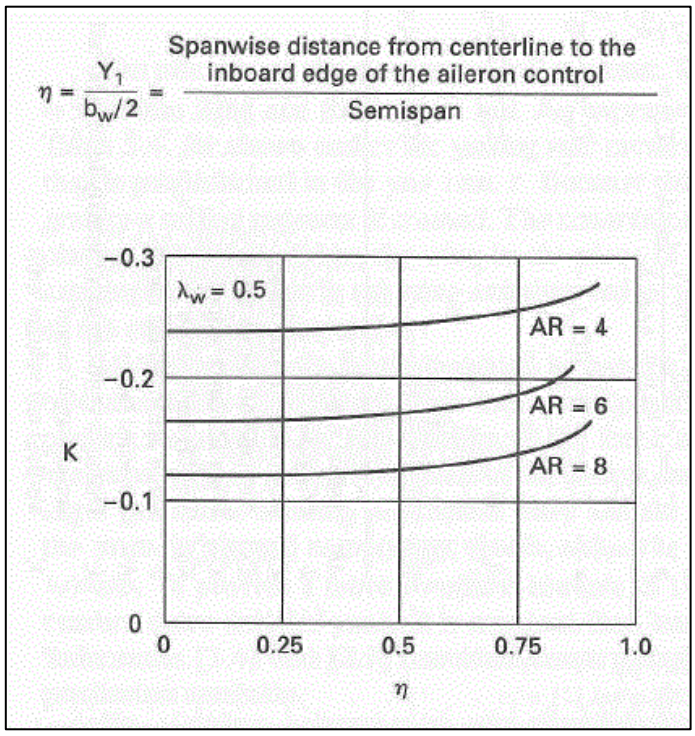


Figure 2.59 - Empirical factor for $Cn_{\delta A}$ estimate (Nelson, 1998).

2.5.8. Longitudinal dynamic stability

The longitudinal dynamic behavior of an aircraft is basically characterized by two distinct movements that are known as short period and phugoid, the first is defined by a short period and high frequency movement and the second is defined by a long period and low frequency movement.

Normally the short period movement is that of bigger interest in the assessing of the flying qualities of an aircraft. For assessing the dynamic longitudinal stability the weight configuration of the aircraft as presented in the Figure 2.9 is the most important parameter, being highly recommended that the lowest weight at the most behind CG should be evaluated, once in this weight configuration the airplanes tend to present a poor longitudinal stability characteristic.

Next is developed the theory necessary for estimate these two longitudinal movements of an aircraft.

2.5.8.1. Longitudinal characteristic equation

The longitudinal motion of an aircraft may be approximated by the characteristic second order differential Equation 2.213, which represents a damped oscillation of a given system that in this case, may be considered as being the aircraft in flight at the atmosphere. Its roots are given by the Equation 2.214, and are the mathematical model for both dynamic longitudinal motions, the short period and the phugoid. The elements of these two equations are given by the Equation 2.215 to the Equation 2.217.

$$\lambda^2 + 2 \cdot \xi \cdot \omega_n \cdot \lambda + \omega_n^2 = 0 \tag{2.213}$$

$$\lambda_{1,2} = \eta \pm i\omega \tag{2.214}$$

$$\eta = -\xi \cdot \omega_n \tag{2.215}$$

$$\omega = \omega_n \cdot \sqrt{1 - \xi^2} \tag{2.216}$$

$$\omega_n = \sqrt{\frac{k_{long}}{m}} \tag{2.217}$$

The term ξ is known as the damping ratio of the system. By varying it from $-\infty$ to $+\infty$ as presented in the Figure 2.60, the response of the system that in this case is the aircraft flying in the atmosphere, will present different behaviors, the Table 2.27 summarize it.

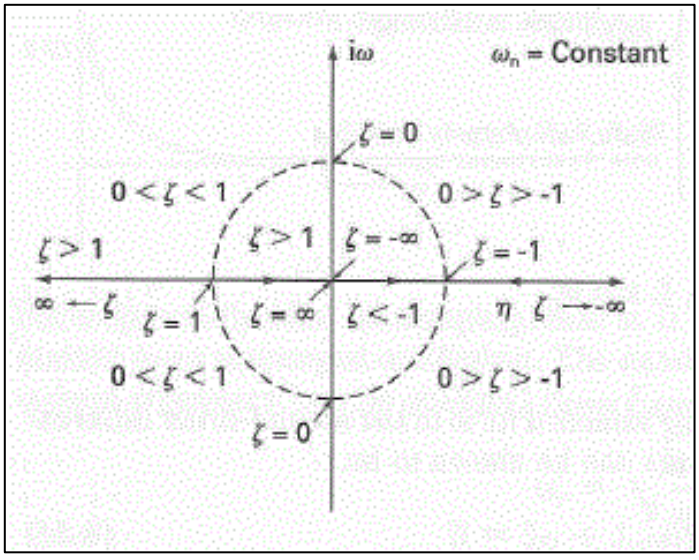


Figure 2.60 - Variation of roots with damping ratio (Nelson, 1998).

Table 2.27 - Variation of response with damping ratio (Nelson, 1998).

Magnitude of damping ratio	Type of root	Time response
$\zeta < -1$	Two positive real distinct roots	Exponentially growing motion
$0 > \zeta > -1$	Complex roots with a positive real part	Exponentially growing sinusoidal motion
$\zeta = 0$	Complex roots with a real part 0	Undamped sinusoidal motion Pure harmonic motion
$0 < \zeta < 1$	Complex roots with a real part negative	Underdamped exponentially decaying sinusoidal motion
$\zeta = 1$	Two negative equal real roots	Critically damped exponentially decaying motion
$\zeta > 1$	Two negative distinct real roots	Overdamped exponentially decaying motion

There are five other parameters that are employed for characterizes an oscillation motion, and they are presented on the Equation 2.218 to the Equation 2.222.

$$P = \frac{2 \cdot \pi}{\omega} \tag{2.218}$$

$$t_{doub-halve} = \frac{0.693}{|\eta|} \tag{2.219}$$

$$N_{doub-halve} = 0.110 \frac{|\omega|}{|\eta|} \tag{2.220}$$

$$C_{cr} = 2 \cdot \sqrt{k_{long} \cdot m} \tag{2.221}$$

$$C = \xi \cdot C_{cr} \tag{2.222}$$

2.5.8.2. Longitudinal state equation

The longitudinal dynamics behavior of an aircraft may be obtained by solving the first order differential Equation 2.223 that is known as state equation, and its coefficients A and B are matrices in which each element is a longitudinal stability or control derivative. In this equation x is the state vector and η is the control vector.

$$\dot{x} = A \cdot x + B \cdot \eta \tag{2.223}$$

$$A = \begin{bmatrix} X_U & X_W & 0 & -g \\ Z_U & Z_W & U_0 & 0 \\ M_U + M_{\dot{W}} \cdot Z_U & M_W + M_{\dot{W}} \cdot Z_W & M_q + M_{\dot{W}} \cdot U_0 & 0 \\ 0 & 0 & 1 & 0 \end{bmatrix} \quad (2.224)$$

$$B = \begin{bmatrix} X_{\delta E} & X_{\delta T} \\ Z_{\delta E} & Z_{\delta T} \\ M_{\delta E} + M_{\dot{W}} \cdot Z_U & M_{\delta T} + M_{\dot{W}} \cdot Z_{\delta T} \\ 0 & 0 \end{bmatrix} \quad (2.225)$$

$$\dot{X} = \begin{Bmatrix} \Delta\dot{U} \\ \Delta\dot{W} \\ \Delta\dot{q} \\ \Delta\dot{\theta} \end{Bmatrix} \quad (2.226)$$

$$X = \begin{Bmatrix} \Delta U \\ \Delta W \\ \Delta q \\ \Delta\theta \end{Bmatrix} \quad (2.227)$$

$$\eta = \begin{Bmatrix} \Delta\delta_E \\ \Delta\delta_T \end{Bmatrix} \quad (2.228)$$

By obtaining the eigenvalues of the Equation 2.224 will result in a vector of four elements, each of these elements has the form of the Equation 2.214, being the mathematical representation of the short period and of the phugoid for a condition of stick fixed motion.

For simplification, this work will not consider the stick free motion that is obtained by considering the Equation 2.225.

2.5.8.3. Longitudinal stability and control derivatives

Next are presented the stability and control derivatives that are employed in the building of the state matrix A.

X-force derivatives

$$CD_U = M \cdot \frac{\partial CD}{\partial M} \quad (2.229)$$

$$CT_U = -CD \quad (2.230)$$

$$CX_U = -(CD_U + 2 \cdot CD) + CT_U \quad (2.231)$$

$$CX_\alpha = \frac{\partial CX}{\partial \alpha} = \frac{\partial CX}{\partial (W/U_0)} = CL \cdot \left(1 - \frac{2 \cdot C_{L_{\alpha_{AP}}}}{\pi \cdot e_{W\_B} \cdot AR_{W\_B}}\right) \quad (2.232)$$

$$X_U = CX_U \cdot \left(\frac{1}{U_0}\right) \cdot \left(\frac{q \cdot S_{aero_{W\_BIP}}}{m}\right) \tag{2.233}$$

$$X_W = CX_\alpha \cdot \left(\frac{1}{U_0}\right) \cdot \left(\frac{q \cdot S_{aero_{W\_BIP}}}{m}\right) \tag{2.234}$$

Z-force derivatives

Note that some of the z-force derivatives are dependent of the parameters of the horizontal tail that in this case it is given for a generic canard, so, these derivatives must be applied for each canard of the airplane UFU-1.

$$CZ_U = \frac{\partial CZ}{\partial (U/U_0)} = -\left(\frac{M^2}{1-M^2}\right) \cdot CL - 2 \cdot CL \tag{2.235}$$

$$CZ_\alpha = \frac{\partial CZ}{\partial (W/U_0)} = -\left(C_{L_{\alpha_{AP}}} + CD\right) \tag{2.236}$$

$$CZ_{\dot{\alpha}} = \frac{\partial CZ}{\partial (\dot{W}/U_0)} = -2 \cdot CL_{\alpha_{CAN}} \cdot \eta_{CAN} \cdot V_{CAN} \cdot \frac{dE}{d\alpha} \tag{2.237}$$

$$CZ_q = \frac{\partial CZ}{\partial \left(q \cdot \bar{C}_{W\_B} / 2U_0\right)} = -2 \cdot CL_{\alpha_{CAN}} \cdot \eta_{CAN} \cdot V_{CAN} \tag{2.238}$$

$$Z_U = CZ_U \cdot \left(\frac{1}{U_0}\right) \cdot \left(\frac{q \cdot S_{aero_{W\_BIP}}}{m}\right) \tag{2.239}$$

$$Z_W = CZ_\alpha \cdot \left(\frac{1}{U_0}\right) \cdot \left(\frac{q \cdot S_{aero_{W\_BIP}}}{m}\right) \tag{2.240}$$

$$Z_{\dot{W}} = CZ_{\dot{\alpha}} \cdot \left(\frac{q \cdot S_{aero_{W\_BIP}}}{m}\right) \cdot \left(\frac{\bar{C}_{W\_B}}{2 \cdot U_0}\right) \tag{2.241}$$

$$Z_\alpha = U_0 \cdot Z_W \tag{2.242}$$

$$Z_{\dot{\alpha}} = U_0 \cdot Z_{\dot{W}} \tag{2.243}$$

$$Z_q = CZ_q \cdot \left(\frac{q \cdot S_{aero_{W\_BIP}}}{m}\right) \cdot \left(\frac{\bar{C}_{W\_B}}{2 \cdot U_0}\right) \tag{2.244}$$

Pitch moment derivatives

Note that as was done for the x-force derivatives, some of the z-force derivatives were defined in terms of the generic canard parameters.

$$CM_U = M \cdot \frac{\partial CM}{\partial M} \tag{2.245}$$

$$CM_{\dot{\alpha}} = CZ_{\dot{\alpha}} \cdot \frac{l_{CAN}}{\bar{C}_{W\_B}} \tag{2.246}$$

$$CM_q = CZ_q \cdot \frac{l_{CAN}}{\bar{C}_{W\_B}} \tag{2.247}$$

$$M_U = CM_U \cdot \left(\frac{1}{U_0}\right) \cdot \left(\frac{q \cdot S_{aero_{W\_BIP}} \cdot \bar{C}_{W\_B}}{I_Y}\right) \tag{2.248}$$

$$M_W = CM_\alpha \cdot \left(\frac{1}{U_0}\right) \cdot \left(\frac{q \cdot S_{aero_{W\_BIP}} \cdot \bar{C}_{W\_B}}{I_Y}\right) \tag{2.249}$$

$$M_{\dot{W}} = CM_{\dot{\alpha}} \cdot \left(\frac{1}{U_0}\right) \cdot \left(\frac{q \cdot S_{aero_{W\_BIP}} \cdot \bar{C}_{W\_B}}{I_Y}\right) \cdot \left(\frac{\bar{C}_{W\_B}}{2 \cdot U_0}\right) \tag{2.250}$$

$$M_\alpha = U_0 \cdot M_W \tag{2.251}$$

$$M_{\dot{\alpha}} = U_0 \cdot M_{\dot{W}} \tag{2.252}$$

$$M_q = CM_q \cdot \left(\frac{\bar{C}_{W\_B}}{2 \cdot U_0}\right) \cdot \left(\frac{q \cdot S_{aero_{W\_BIP}} \cdot \bar{C}_{W\_B}}{I_Y}\right) \tag{2.253}$$

2.5.8.4. Longitudinal flying qualities considerations

For assessing the longitudinal behavior of an aircraft, it is commonly employed a criterion based in the classification of the aircraft category and in flight phase categories specified in the military standard *MIL-F-8785C* as presented in the Table 2.28, Table 2.29 and in the Table 2.30.

Table 2.28 - Aircraft classes (Sadraey, 2013).

Class	Aircraft characteristics
I	Small, light aircraft (maximum take-off mass less than 6000 kg) with low maneuverability
II	Aircraft of medium weight and low-to-medium maneuverability (maximum take-off mass between 6000 and 30 000 kg)
III	Large, heavy, and low-to-medium maneuverability aircraft (maximum take-off mass more than 30 000 kg)
IV	Highly maneuverable aircraft, no weight limit (e.g., acrobatic, missile, and fighter)

Table 2.29 - Flight phase categories (Sadraey, 2013).

Category	Examples of flight operation
A	(i) Air-to-air combat (CO); (ii) ground attack (GA); (iii) weapon delivery/launch (WD); (iv) aerial recovery (AR); (v) reconnaissance (RC); (vi) in-flight refueling (receiver) (RR); (vii) terrain following (TR); (viii) anti-submarine search (AS); (xi) close formation flying (FF); and (x) low-altitude parachute extraction system (LAPES) delivery.
B	(i) Climb (CL); (ii) cruise (CR); (iii) loiter (LO); (iv) in-flight refueling in which the aircraft acts as a tanker (RT); (v) descent (D); (vi) emergency descent (ED); (vii) emergency deceleration (DE); and (viii) aerial delivery (AD).
C	(i) Take-off (TO); (ii) catapult take-off (CT); (iii) powered approach (PA); (iv) wave-off/go-around (WO); and (v) landing (L).

Table 2.30 - Levels of acceptability (Sadraey, 2013).

Level	Definition
1	Flying qualities clearly adequate for the mission flight phase.
2	Flying qualities adequate to accomplish the mission flight phase, but some increase in pilot workload or degradation in mission effectiveness, or both, exists.
3	Flying qualities such that the airplane can be controlled safely, but pilot workload is excessive or mission effectiveness is inadequate, or both. Category A flight phases can be terminated safely, and Category B and C flight phases can be completed.

After classify the aircraft in a given flight phase, it is possible to evaluate if the short period and the phugoid behavior are satisfactory, by comparing its results to the values obtained from the Table 2.31 and from the Table 2.32.

Table 2.31 - Short-period mode damping ratio specification (Sadraey, 2013).

Flight phase	Short-period damping ratio (ζ_s)					
	Level 1		Level 2		Level 3	
	Minimum	Maximum	Minimum	Maximum	Minimum	Maximum
A	0.35	1.3	0.25	2.0	0.15	No maximum
B	0.3	2.0	0.2	2.0	0.15	No maximum
C	0.35	1.3	0.25	2.0	0.15	No maximum

Table 2.32 - Phugoid mode requirement (Sadraey, 2013).

Level of acceptability	Requirement
1	Damping ratio of phugoid mode (ζ_{ph}) $\geq$ 0.04
2	Damping ratio of phugoid mode (ζ_{ph}) $\geq$ 0.0
3	Time to double the amplitude at least 55 seconds

2.5.9. Lateral-Directional dynamic stability

The lateral-directional dynamic behavior of an aircraft is basically characterized by three distinct movements that are known as rolling, spiral and Dutch-roll. The rolling mode is characterized by a highly damped convergent or divergent motion, the spiral mode is characterized by a coupled lightly damped convergent or divergent motion, and the Dutch-roll mode is characterized by a coupled lightly damped low frequency oscillatory motion. The Figure 2.61 to the Figure 2.63 shows these motions.

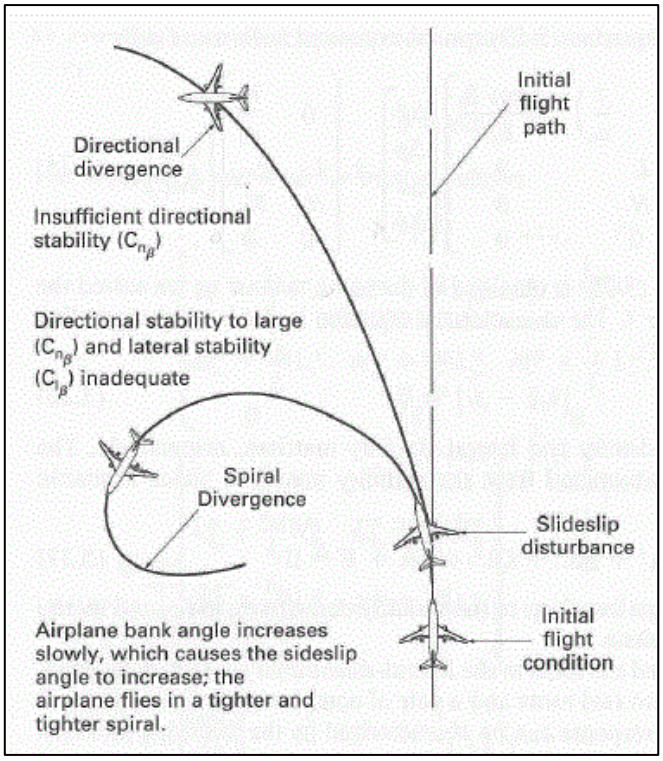


Figure 2.61 -The spiral motion (Nelson, 1998).

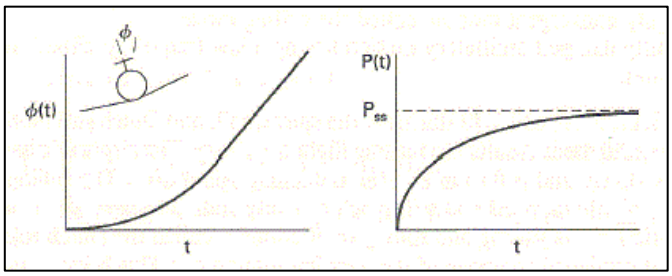


Figure 2.62 - The roll motion (Nelson, 1998).

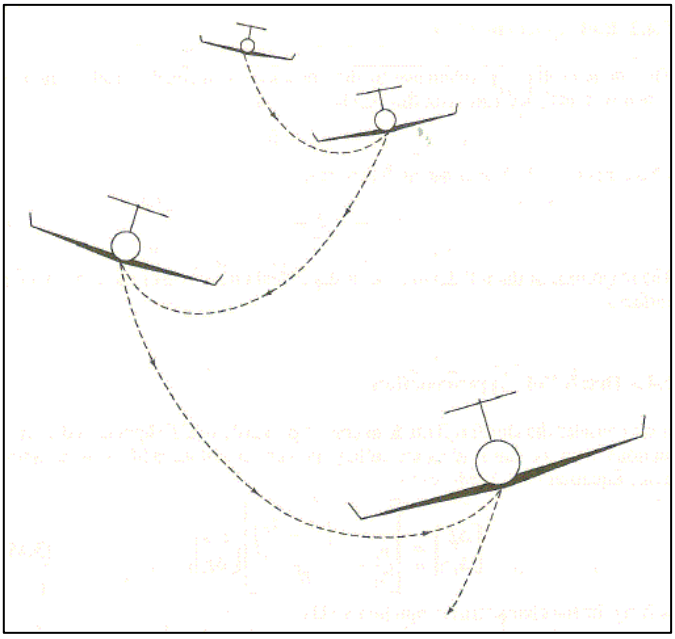


Figure 2.63 - The Dutch-roll motion (Nelson, 1998).

Normally the Dutch-roll and the spiral are the modes of bigger interest in the assessing of the flying qualities of an aircraft. The assessing of the Dutch-roll mode is necessary due the annoying movement that it produces, turning the flight very uncomfortable. The assessing of the spiral mode is mandatory once it impact the flight safety. Next is presented more details about the spiral mode and how to avoid this motion.

Spiral motion

When an aircraft reach its angle of stall, it is necessary that this aircraft present a resistant entering spiral mode behavior, with the objective to avoid the aircraft lateral-directional

departure. By applying the Equation 2.254, it is a manner to avoid the aircraft enter into a spiral mode.

$$Cn_{\beta_{dyn}} = \left\{Cn_{\beta_{CG}} - \left(\frac{I_{zz_{cg}}}{I_{xx_{cg}}}\right) \cdot Cl_{\beta_{CG}} \cdot \tan\alpha\right\} \cdot \cos\alpha > 0 \quad (2.254)$$

For this spiral equation normally it is necessary to perform wind tunnel tests to know how these derivatives varies as the angle of attack is changed. One way to avoid the aircraft to enter in the spiral mode is to limit its operation angle of attack by employing devices as shaker or pusher, or yet, write this limit in the flight manual.

2.5.9.1. Lateral-Directional characteristic equation

The lateral-directional motion of an aircraft may be approximated by the fourth-order characteristic Equation 2.255. Its roots are given by the Equation 2.256, and are the mathematical model for spiral mode, roll mode and Dutch-roll mode, its terms are defined in the Equation 2.215 and in the Equation 2.216.

When the root is a real pure, it will denote the spiral motion or the roll motion, and if the root is a pair of complex number it will denote the Dutch-roll motion.

For a pure real root, if the sign is negative it will characterize a convergent motion, and if its signal is positive the motion will be divergent. The spiral mode may be differed of the roll one by analyzing the modulus of the pure real roots, the biggest will characterize the roll mode and the other will characterize the spiral mode. As was explained for the two non-oscillatory modes, the Dutch-roll mode will be convergent if the real part of its root is negative.

The characterization of the three lateral-directional motions are done by applying the Equation 2.218 to the Equation 2.222, as was defined for the longitudinal motion.

$$a\lambda^4 + b\lambda^3 + c\lambda^2 + d\lambda + e = 0 \quad (2.255)$$

$$\lambda_{1,2,3} = \eta \pm i\omega \quad (2.256)$$

2.5.9.2. Lateral-Directional state equation

The lateral-directional dynamics behavior of an aircraft may be obtained by solving the first order differential Equation 2.257 that is the state equation of the lateral-directional motion, and its coefficients C and D are matrices in which each element is a lateral or directional stability or control derivative, note that many elements of these matrices evidence the coupling between the lateral and the directional axis. In this equation x is the state vector and η is the control vector.

$$\dot{x} = C \cdot x + D \cdot \eta \tag{2.257}$$

$$C = \begin{bmatrix} Y_v & Y_p & -(U_0 - Y_r) & g \cdot \cos\theta_0 \\ L_v^* + \frac{I_{xz_{cg}}}{I_{xx_{cg}}} \cdot N_v^* & L_p^* + \frac{I_{xz_{cg}}}{I_{xx_{cg}}} \cdot N_p^* & L_r^* + \frac{I_{xz_{cg}}}{I_{xx_{cg}}} \cdot N_r^* & 0 \\ N_v^* + \frac{I_{xz_{cg}}}{I_{zz_{cg}}} \cdot L_v^* & N_p^* + \frac{I_{xz_{cg}}}{I_{zz_{cg}}} \cdot L_p^* & N_r^* + \frac{I_{xz_{cg}}}{I_{zz_{cg}}} \cdot L_r^* & 0 \\ 0 & 1 & 0 & 0 \end{bmatrix} \tag{2.258}$$

$$D = \begin{bmatrix} 0 & Y_{\delta R} \\ L_{\delta A}^* + \frac{I_{xz_{cg}}}{I_{xx_{cg}}} \cdot N_{\delta A}^* & L_{\delta R}^* + \frac{I_{xz_{cg}}}{I_{xx_{cg}}} \cdot N_{\delta R}^* \\ N_{\delta A}^* + \frac{I_{xz_{cg}}}{I_{zz_{cg}}} \cdot L_{\delta A}^* & N_{\delta R}^* + \frac{I_{xz_{cg}}}{I_{zz_{cg}}} \cdot L_{\delta R}^* \\ 0 & 0 \end{bmatrix} \tag{2.259}$$

$$\dot{X} = \begin{Bmatrix} \Delta\dot{\beta} \\ \Delta\dot{p} \\ \Delta\dot{r} \\ \Delta\dot{\varphi} \end{Bmatrix} \tag{2.260}$$

$$X = \begin{Bmatrix} \Delta\beta \\ \Delta p \\ \Delta r \\ \Delta\varphi \end{Bmatrix} \tag{2.261}$$

$$\eta = \begin{Bmatrix} \Delta\delta_A \\ \Delta\delta_R \end{Bmatrix} \tag{2.262}$$

$$L_v^* = \frac{L_v}{\left[1 - \left(\frac{I_{xz_{cg}}^2}{I_{xx_{cg}} \cdot I_{zz_{cg}}}\right)\right]}; \quad L_p^* = \frac{L_p}{\left[1 - \left(\frac{I_{xz_{cg}}^2}{I_{xx_{cg}} \cdot I_{zz_{cg}}}\right)\right]}; \quad L_r^* = \frac{L_r}{\left[1 - \left(\frac{I_{xz_{cg}}^2}{I_{xx_{cg}} \cdot I_{zz_{cg}}}\right)\right]} \tag{2.263}$$

$$N_v^* = \frac{N_v}{\left[1 - \left(\frac{I_{xz_{cg}}^2}{I_{xx_{cg}} \cdot I_{zz_{cg}}}\right)\right]}; \quad N_p^* = \frac{N_p}{\left[1 - \left(\frac{I_{xz_{cg}}^2}{I_{xx_{cg}} \cdot I_{zz_{cg}}}\right)\right]}; \quad N_r^* = \frac{N_r}{\left[1 - \left(\frac{I_{xz_{cg}}^2}{I_{xx_{cg}} \cdot I_{zz_{cg}}}\right)\right]} \tag{2.264}$$

By obtaining the eigenvalues of the Equation 2.258 it will result in a vector of four elements, each of these elements has the form of the Equation 2.256, which is the mathematical representation of the spiral, roll and Dutch-roll for a condition of stick fixed motion.

As was done for the longitudinal motion, for simplification this work will not consider the stick free motion that is obtained by considering the Equation 2.259.

2.5.9.3. Lateral-Directional stability and control derivatives

Next are presented the stability and control derivatives that are employed in the building of the state matrix C.

Yaw y-force derivatives

$$Cy_{p_{CG}} = CL \cdot \frac{AR_{W\_B}+\cos(\Lambda_{W\_B})}{AR_{W\_B}+4\cdot\cos(\Lambda_{W\_B})} \cdot \tan(\Lambda_{W\_B}) \quad (2.265)$$

$$Y_v = \frac{q\cdot S_{aero_{W\_BIP}}\cdot Cy_{\beta_{CG}}}{m} \cdot U_0 \quad (2.266)$$

$$Y_p = \frac{q\cdot S_{aero_{W\_BIP}}\cdot b_{W\_B}\cdot Cy_{p_{CG}}}{2\cdot m\cdot U_0} \quad (2.267)$$

$$Y_r = \frac{q\cdot S_{aero_{W\_BIP}}\cdot b_{W\_B}\cdot Cy_{r_{CG}}}{2\cdot m\cdot U_0} \quad (2.268)$$

Yaw moment derivatives

$$N_p = \frac{q\cdot S_{aero_{W\_BIP}}\cdot {b_{W\_B}}^2\cdot Cn_{p_{CG}}}{2\cdot I_{zz_{cg}}\cdot U_0} \quad (2.269)$$

$$N_r = \frac{q\cdot S_{aero_{W\_BIP}}\cdot {b_{W\_B}}^2\cdot Cn_{r_{CG}}}{2\cdot I_{zz_{cg}}\cdot U_0} \quad (2.270)$$

$$N_v = \frac{q\cdot S_{aero_{W\_BIP}}\cdot b_{W\_B}\cdot Cn_{\beta_{CG}}}{I_{zz_{cg}}} \cdot U_0 \quad (2.271)$$

Roll moment derivatives

$$L_p = \frac{q\cdot S_{aero_{W\_BIP}}\cdot {b_{W\_B}}^2\cdot Cl_{p_{CG}}}{2\cdot I_{xx_{cg}}\cdot U_0} \quad (2.272)$$

$$L_r = \frac{q \cdot S_{aero_{W\_BIP}} \cdot {b_{W\_B}}^2 \cdot Cl_{r_{CG}}}{2 \cdot I_{xx_{cg}} \cdot U_0} \quad (2.273)$$

$$L_v = \frac{q \cdot S_{aero_{W\_BIP}} \cdot b_{W\_B} \cdot Cl_{\beta_{CG}}}{I_{xx_{cg}}} \cdot U_0 \quad (2.274)$$

2.5.9.4. Lateral-Directional flying qualities considerations

For assessing the lateral-directional behavior of an aircraft, the classification of the aircraft category and in flight phase are done the same way as was proceed for the longitudinal motion, by applying the Table 2.28, Table 2.29 and the Table 2.30.

The assessing of the three lateral-directional modes is performed by comparing its results to the values obtained from the Table 2.33, to the Table 2.36.

Table 2.33 - Roll control requirements (Sadraey, 2013).

(a) Time to achieve a specified bank angle change for Class I			
Level	Flight phase category		
	A	B	C
	Time to achieve a bank angle of 60° (s)	Time to achieve a bank angle of 45° (s)	Time to achieve a bank angle of 30° (s)
1	1.3	1.7	1.3
2	1.7	2.5	1.8
3	2.6	3.4	2.6

Table 2.34 - Roll mode specification maximum value (Sadraey, 2013).

Flight phase	Aircraft class	T_R (s)		
		Level 1	Level 2	Level 3
A	I, IV	1.0	1.4	10
	II, III	1.4	3.0	10
B	All	1.4	3.0	10
C	I, IV	1.0	1.4	10
	II, III	1.4	3.0	10

The table above indicates the maximum time in seconds for an aircraft to return to its initial bank angle, when laterally disturbed.

Table 2.35 - Time to double amplitude in spiral mode (Sadraey, 2013).

Aircraft class	Flight phase	Minimum time to double amplitude in spiral mode		
		Level 1 (s)	Level 2 (s)	Level 3 (s)
I and IV	A	12	8	4
	B and C	20	8	4
II and III	A, B, and C	20	8	4

Table 2.36 - Dutch-roll mode handling qualities (Sadraey, 2013).

Level	Flight phase	Aircraft class	Minimum ζ_d	Minimum $\zeta_d\omega_{nd}$ (rad/s)	Minimum ω_{nd} (rad/s)
1	A	I, IV	0.19	0.35	1.0
1		II, III	0.19	0.35	0.4
1	B	All	0.08	0.15	0.4
1	C	I, II, and IV	0.08	0.15	1.0
1		III	0.08	0.15	0.4
2	All	All	0.02	0.05	0.4
3	All	All	0.02	No limit	0.4

2.6. PERFORMANCE

This chapter present the theory related to the performance characteristics of an aircraft based on the flight phases showed on the Figure 2.6. It is also presented, how to obtain the estimative of excess of power and thrust of an aircraft.

There are many ways to estimate the performance of an aircraft at each flight phase, this work is based mainly on that presented on the bibliography (Roskam, 1991 and 1997).

2.6.1. Excess of power and thrust

When analyzing the performance of an aircraft it is necessary to know if there is enough thrust or power for perform the flight phase that this airplane will face, this impact specifically the climb and cruise phases. Assuming that the aircraft is in a steady flight condition, the sum of forces and moment acting must to be null.

Considering the thrust or power available for maintain the flight at certain speed or change it within the climb or cruise, this is directly related to the drag generated by the aircraft, leading to the analysis of the excess of power or thrust, which is evaluated at the longitudinal axis of the aircraft, and is defined by the Equation 2.275 which gives the excess of power relation and the Equation 2.276 which gives the excess of thrust relation.

Obviously the two first equations must to assume values bigger than zero for the aircraft be able to change its speed and at the limit, this equations must to assume values equal to zero for maintain the steady flight condition, other way, the drag or equivalent power would be greater than the thrust or power generated by the propulsive system, what necessarily cause the reduction of the flight speed reaching again the equilibrium of forces at the longitudinal axis.

$$P_{EX} = E_{T_P} - E_{D_P} \tag{2.275}$$

$$T_{EX} = T - D \tag{2.276}$$

$$E_{T_P} = T \cdot V_T \tag{2.277}$$

$$E_{D_P} = D \cdot V_T \tag{2.278}$$

2.6.2. Take-off performance

Here is presented how to estimate the take-off distances given by the Equation 2.279 and the Equation 2.280, which are based in the Figure 2.64 and the Table 2.37. The fuel consumption during this phase is given by the Equation 2.284. The Equation 2.282 is solved with the help of the Table 2.38. Note that the subscript TO and LOF mean take-off and Lift-off respectively.

$$S_{TO} = S_{TO_G} + S_{TO_A} = f_{TO} \cdot h_{TO} \cdot \left\{ \frac{1}{\gamma_{LOF}} + \frac{\left(\frac{V_3}{V_{S_{TO}}}\right)^2 \cdot \left(\frac{W}{S_{aero} W_{BIP}}\right)_{TO} \cdot \left[\left(\frac{\bar{T}}{W}\right)_{TO} - \mu'\right]^{-1} + 1.414}{\left(h_{TO} \cdot \rho_{FL} \cdot g \cdot CL_{max_{TO}}\right) \cdot (1 + 1.414 \cdot \gamma_{LOF})} \right\} \quad (2.279)$$

$$S_{TO_G} = \frac{S_{TO}}{1.66} \quad (2.280)$$

$$\bar{T} = 4.60 \cdot P_{TO} \cdot \left(\frac{\sigma \cdot N_{eng} \cdot D_P^2}{P_{TO}}\right)^{1/3} \quad (2.281)$$

$$\mu' = \mu_g + 0.72 \cdot \frac{CD_0}{CL_{max_{TO}}} \quad (2.282)$$

$$\gamma_{LOF} = \left(\frac{T-D}{W}\right)_{LOF} \quad (2.283)$$

$$GAS_{TOF} = N_{eng} \cdot SFC_{TO} \cdot t_{TO} \cdot P_{S_{TO}} \quad (2.284)$$

Table 2.37 - Take-off parameters.

Regulation	V_3/V_{S_TO}	f_{TO}	h_{TO} (ft)
FAR 23	1.3	1.0	50
FAR 25	1.25 - 1.3	1.15	35
AS-5263	1.2	1.0	50
MIL-C-005011B	1.15	1.0	50

Table 2.38 - Wheel-ground rolling friction coefficient.

Runway Surface	Friction Coefficient - μ_g
Concrete	0.02
Asphalt	0.02
Hard turf	0.04
Short grass	0.05
Long grass	0.10
Soft ground	0.10 - 0.30

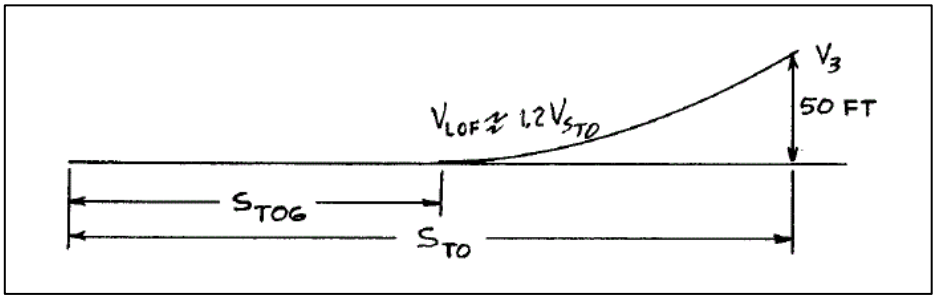


Figure 2.64 - Definition of FAR 23 take-off distance (After Roskam, 1991).

2.6.3. Climb performance

The climb performance is characterized by three main parameters which are the rate of climb, the climb gradient and the flight ceiling.

2.6.3.1. Rate of climb

The rate of climb of an aircraft is estimated by applying the Equation 2.285, inspecting this equation is noted that the result obtained is for a given aerodynamic configuration at a given flight altitude and at a defined engine power. This equation provides the rate of climb in feet per minute, and its dimensional parameters must be in the English system.

The maximum rate of climb is reached when the relation between the lift coefficient and the drag coefficient presented in the Equation 2.286 is satisfied.

$$RC = 33{,}000 \cdot \left[\frac{\eta_P}{(W/P_{climb})} - \frac{\left(W/S_{aero_{W_{BIP}}}\right)^{0.5}}{19 \cdot \left(\frac{CL^{1.5}}{CD}\right) \cdot \sigma^{0.5}} \right] \tag{2.285}$$

$$\left(\frac{CL^{1.5}}{CD}\right)_{max} = 1.345 \cdot \frac{\left(AR_{W\_B} \cdot e_{W\_B}\right)^{0.75}}{{CD_0}^{0.25}} \tag{2.286}$$

2.6.3.2. Climb gradient

The estimative of the climb gradient of an aircraft is done applying the Equation 2.287 and its result is in rad. All the considerations done for the equation of the rate of climb are valid here.

$$CGR = -\left(\frac{L}{D}\right)^{-1} + \left[\frac{CL^{0.5} \cdot 18.97 \cdot \eta_P \cdot \sigma^{0.5}}{(W/P_{climb}) \cdot \left(W/S_{aero_{W_{BIP}}}\right)^{0.5}} \right] \tag{2.287}$$

2.6.3.3. Flight ceiling

The flight ceiling is a concept that is applied to define the altitude limit for the climb capability of an aircraft. This performance parameter is strongly affected by the propulsive system installed in the aircraft, the aerodynamic characteristics are relevant too as can be noted by inspecting the Equation 2.285.

It is interesting to say that the ceiling of an aircraft may be limited by other considerations as for example structural limits or environmental limitations related to the pilots and passengers cabin.

The Table 2.39 presents the definitions of ceiling based on the airplane type and the magnitude of the rate of climb of the aircraft.

Table 2.39 - Aircrafts flight ceilings.

Ceiling Type	Airplane Type	Minimum Required Rate of Climb [ft/min]
Absolute ceiling	All	0
Service ceiling	Commercial - Piston-prop	100
	Commercial - Jet	500
	Military at maximum power	100

2.6.4. Cruise performance

Now it is presented how to estimate the range of an aircraft, it is done by applying the Equation 2.288. This equation is based in English units and its result is in nautical miles.

$$R = 326 \cdot \frac{\eta_P}{SFC_{CRU}} \cdot \left(\frac{L}{D}\right)_{CRU} \cdot \ln\left(\frac{W_i}{W_e}\right) \tag{2.288}$$

2.6.5. Descent performance

Assuming that the engine is at idle setting, the descent path angle and the range may be estimated by applying the Equation 2.289 and Equation 2.290 respectively. This equation is given in ft/s.

$$\gamma_{DES} = \tan^{-1}\left(\frac{CD}{CL}\right)_{DES} \tag{2.289}$$

$$RD = \left[\left(\frac{W}{S_{aero_{W_{BIP}}}}\right) \cdot \left(\frac{2}{\rho_{FL}}\right) \cdot \left(\frac{CD^2}{CL^{1.5}}\right) \cdot (\cos\gamma_{DES})^3\right]^{0.5} \quad (2.290)$$

2.6.6. Landing performance

The landing performance may be obtained by considering the FAR 23 specification as showed on the Figure 2.65.

$$S_{LG} = 0.265 \cdot V_{SL}^2 \quad (2.291)$$

$$S_L = 1.938 \cdot S_{LG} \quad (2.292)$$

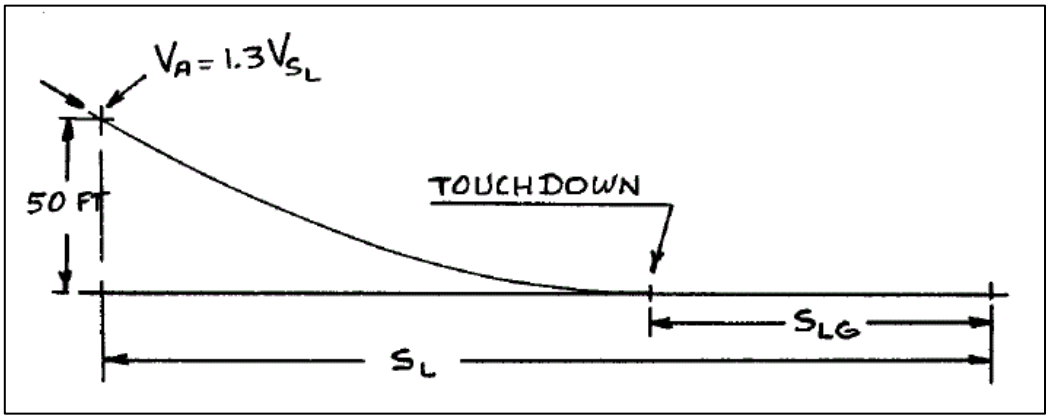


Figure 2.65 - Definition of FAR 23 landing distance (Roskam, 1997).

2.7. LOADS

For dimensioning the structure of an aircraft it is necessary to know the loads that it must support, these loads have aerodynamic origin due the several flight conditions and have ground origin due the taxi and running for take-off and landing.

Specifically related to the aerodynamic loads it is convenient to define it graphically at the V-n diagram, which relate the structural speeds to the limit load factors. There are two V-n diagrams one that consider the maneuver loads and other that consider the gust loads due the atmosphere conditions. The final V-n diagram is the composition of both as showed on the Figure 2.66, this work will consider just the maneuver one.

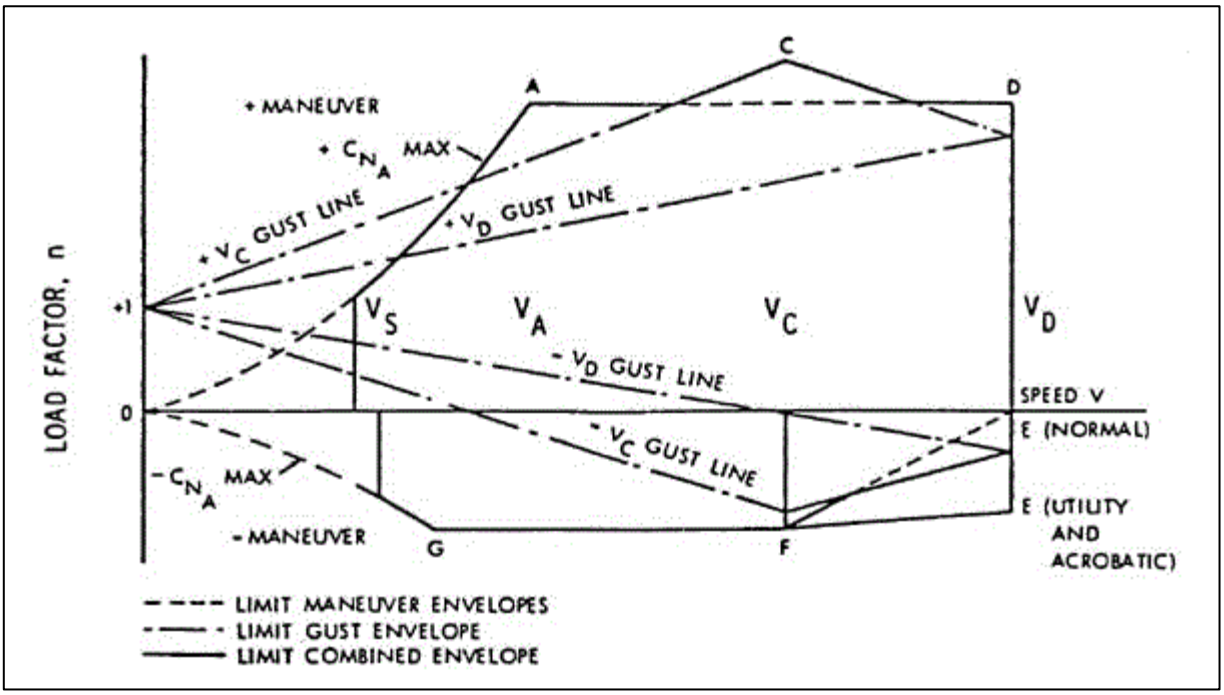


Figure 2.66 - FAR 23.333 combined V-n diagram.

2.7.1. Maneuver V-n diagram

For each atmosphere condition as flight altitude and its correspondent air density, and aircraft aerodynamic and weight configuration, it is defined one V-n diagram. The design airspeeds are provided by the FAR 23.335 and the limit maneuvering load factors are provided by the FAR 23.337.

2.7.1.1. Design airspeeds

<u>Stall speed - V_S</u>

This speed is dependent of the aerodynamic configuration of the aircraft, as for example the flaps are deflected or not. This speed determines the left limit of the V-n diagram.

$$V_S = \sqrt{\frac{2 \cdot W_0}{\rho_{FL} \cdot S_{aero_{W_{BIP}}} \cdot CL_{max}}} \tag{2.293}$$

Design cruising speed - V_C

This is the limit speed for which the aircraft structure must support the loads due the maximum positive and negative load factors.

$$V_C \geq 33 \cdot \sqrt{\frac{W_0}{S_{aero_{W_{BIP}}}}} \tag{2.294}$$

Design dive speed - V_D

This speed is that for maneuvering at a descendent flight condition, with the maximum positive load factor.

$$V_D \geq 1.25 \cdot V_C \tag{2.295}$$

Design maneuvering speed - V_A

This is the lowest speed for what the structure of the aircraft must support the maximum positive and negative load factors.

$$V_A \geq V_S \cdot \sqrt{n^+_{max}} \tag{2.296}$$

2.7.1.2. Limit maneuvering load factors

As defined into the FAR 23.337 these load factors are obtained considering the aircraft design maximum take-off weight in pounds.

$$n^+_{max} \geq 2.1 + \frac{24000}{W_0 + 10000} \tag{2.297}$$

$$n^-_{max} \leq -0.4 \cdot n^+_{max} \tag{2.298}$$

2.8. STRUCTURAL LAYOUT

The structure of an aircraft must to support the static and dynamics loads generated during its operation as mentioned above.

For the structure to resist such loads it must be strong and rigid enough, these characteristic are obtained by the combination between the mechanical characteristics of the material employed on its manufacturing with the structural layout of the main parts as the wing, tails and fuselage, for example. Once the aspects related to the materials had already been treated, this chapter is dedicated to expose some possibilities of structural layout.

2.8.1. Wing structural layout

The four main structural elements of a wing are the spar, the rib, the stringer and the skin, the first three have exclusively structural function, but the skin has the aerodynamic function too, once it must guaranty the aerodynamic loft of the wing.

During the definition of the structural layout of a wing there must be considered the location of the landing gear legs, engine mounts, fuel tank and control devices for the ailerons, flaps and spoilers, between other components, once the wing many times accommodate all these components, therefore space for them must be guaranteed.

Normally the structure of a wing may be classified as multi-rib or multi-spar. Considering a structure of the kind multi-rib, the wing is conceived with two spars, the front one is located normally around 15% of the chord of the profile and the rear one is normally located around 60% of the chord of the profile. The two kinds of wing structures are presented on the Figure 2.67 and on the Figure 2.68.

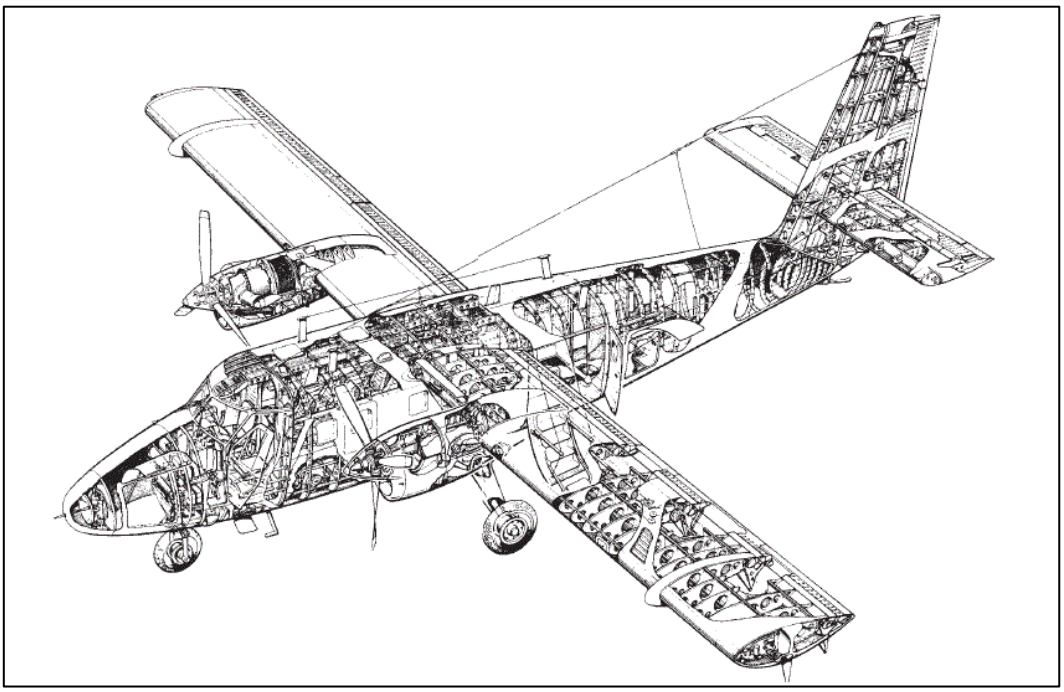


Figure 2.67 - Multi-rib wing structure example (Megson, 2010).

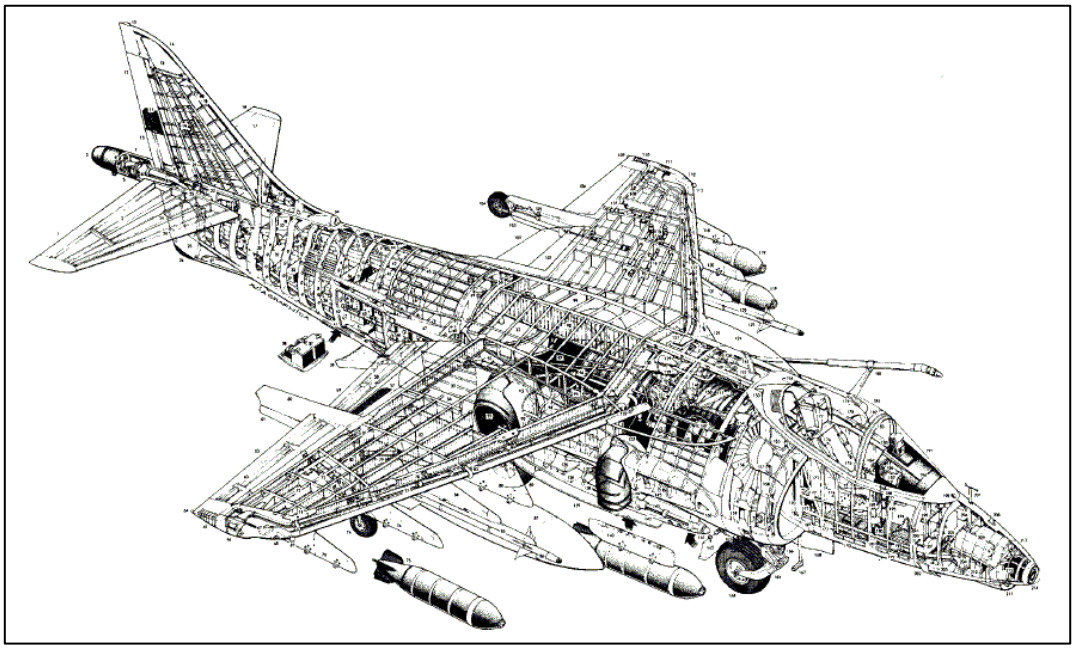


Figure 2.68 - Multi-spar wing structure example (Megson, 2010).

2.8.2. Horizontal & Vertical tail structural layout

All the considerations done for the wing structure are valid for both horizontal and vertical tail. For airplanes of the general aviation category it is common a light layout composed by a single spar combined with ribs. The Figure 2.67 and the Figure 2.68 provide examples of tail structure layout.

2.8.3. Fuselage structural layout

The four main structural elements of a fuselage are the bulkhead, the stringer, the central beam in certain cases and the skin, as for the wings, the first three components have exclusively structural function, but the skin has the aerodynamic function too, once it must guaranty the aerodynamic loft of the fuselage. The Figure 2.69 and the Figure 2.70 provides examples of fuselage structure layout.

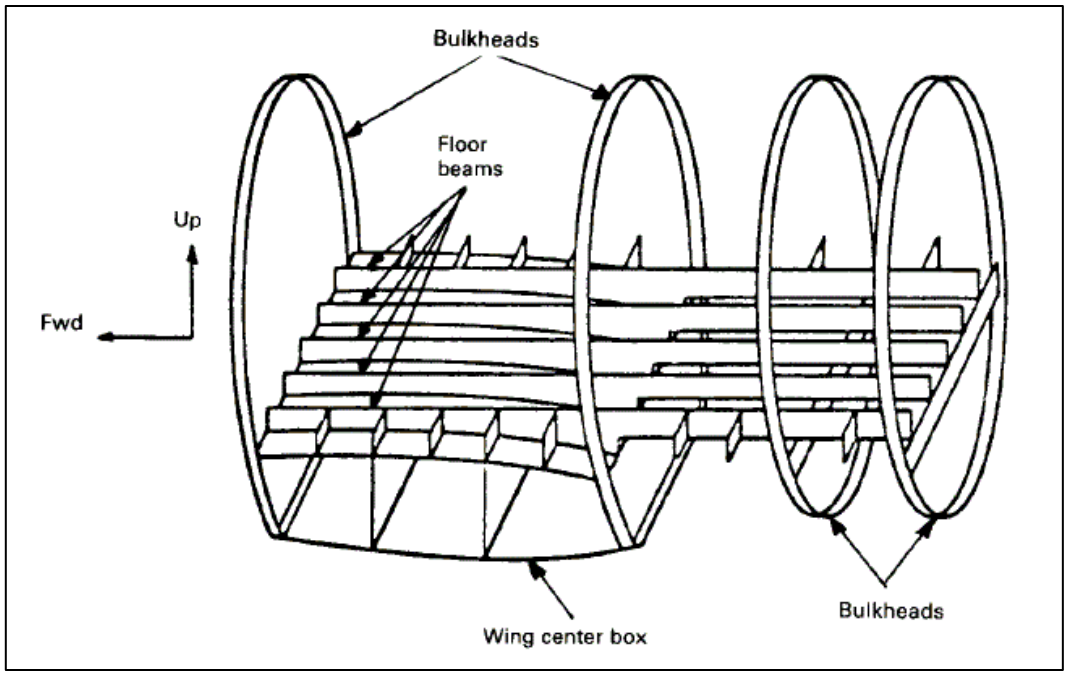


Figure 2.69 - Fuselage structural layout (Niu, 1995).

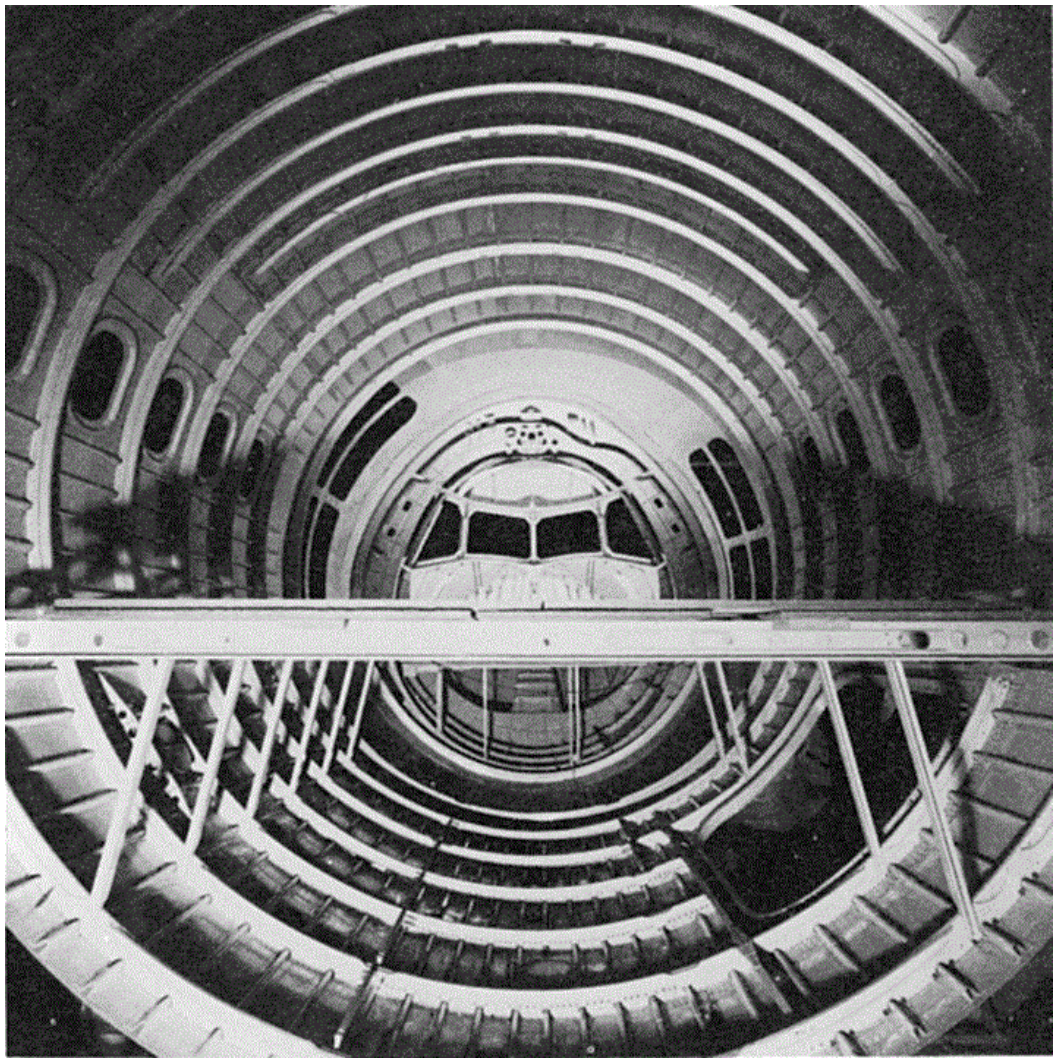


Figure 2.70 - Fuselage structural layout (Megson, 2010).

2.9. LANDING GEAR SYSTEM

There are many landing gear configurations, this work present a summary about the tricycle one, based on the bibliography (Raymer, 2006). This configuration is characterized by having the main landing gear legs behind the location of the CG, and the nose gear leg located forward the CG location. The tricycle configuration make the aircraft stable at the ground and make the unaligned landings relative to the runway axis more safe, other advantage of this configuration is the good view of the runway when on the ground.

2.9.1. Main landing gear leg considerations

The length of the main legs should be enough for to avoid the contact of the tail with the ground during the take-off rolling and during the landing touch-down, it is common that the pitch angle during these flight phases be between $10°$ and $15°$. The minimum distance between the ground and the tip of the blade of the propeller should be at least $18\ [cm]$.

2.9.2. Nose landing gear leg considerations

The nose gear leg must to support at least 5% of the aircraft weight, if the nose gear is loaded with less than this minimum value the maneuvering during the taxi and take-off and landing running may be impaired due the low friction with the ground, what could induce the shimmy.

The nose gear must to support no more than 20% of the aircraft weight, if the nose gear is loaded above this maximum limit the pitch generated by the elevator will be impacted. Ideally these loading values must vary between 8% for the forward CG and 15% for the rear CG.

Considering the landing, the nose gear leg should be inclined forward around $7°$ it can turn the touch-down more smooth, however values up to $10°$ back are acceptable.

2.9.2.1. Castoring wheel geometry

During the landing and take-off rolling the nose wheel can suffer a phenomenon known as shimmy, which is a directional instability of the wheel, when it starts to present an oscillatory motion, what even can to collapse the leg assembly.

For a configuration in which the nose wheel is free the shimmy can be avoided by introducing a rake angle and a stem called trail as showed on the Figure 2.71. Negative values for the rake varying between $4°$ and $6°$ and for the trail varying between 0.2 to 1.2 times the tire radius normally avoid this phenomenon.

For a configuration in which the nose wheel is steerable, the rake should be positive and the trail should be minimized intending to alleviate the pilot effort during curves at the ground.

For small airplanes positive values around $15°$ for the rake and trail around 20% are commonly employed.

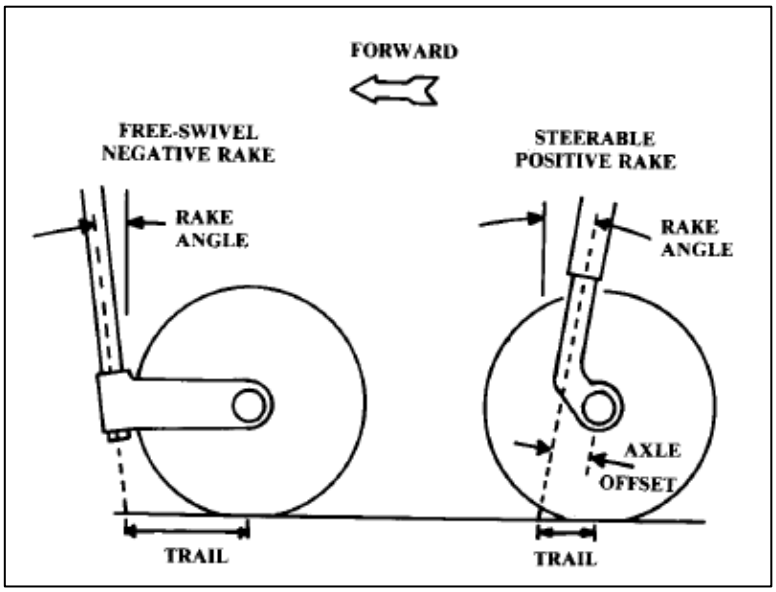


Figure 2.71 - Castoring wheel geometry (Raymer, 2006).

2.9.3. Tire sizing

The initial sizing of the tires for the main landing gear leg may be done by applying the statistical Equation 2.299 and the Equation 2.300 which provide the results in centimeter. If the aircraft is planned to operate on a non-prepared runway these results must be increased around 30%. The nose tire may be assumed as having between 60% and 100% of the dimensions of the tire of the main leg.

$$d = 5.1 \cdot W_{tire}^{0.349} \tag{2.299}$$

$$w = 2.3 \cdot W_{tire}^{0.312} \tag{2.300}$$

The minimum and maximum static loads supported by each landing gear leg tire may be estimated by applying the Equation 2.301 to the Equation 2.304, with the help of the Figure 2.72.

$$W_{main\_max} = W_0 \cdot \frac{N_a}{B} \tag{2.301}$$

$$W_{main\_min} = W_0 \cdot \frac{N_f}{B} \tag{2.302}$$

$$W_{nose\_max} = W_0 \cdot \frac{M_f}{B} \tag{2.303}$$

$$W_{nose\_min} = W_0 \cdot \frac{M_a}{B} \tag{2.304}$$

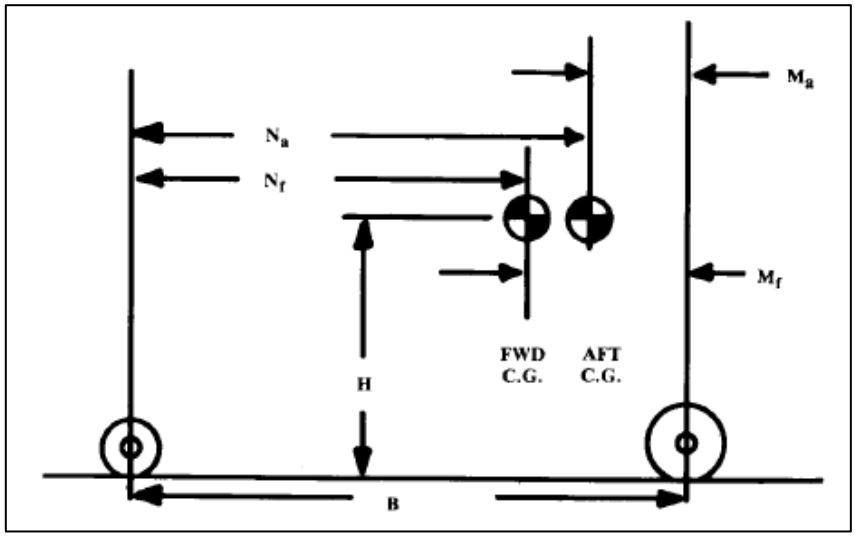


Figure 2.72 - Wheel load geometry (Raymer, 2006).

Despite the nose landing gear carry the lowest parcel of the aircraft weight, the dynamic loads applied on it are normally big and must be considered. The dynamic load at a standard deceleration $a = 3.048\ [m/s^2]$ due the break application and for a standard breaking friction coefficient $\mu = 0.3$, may be estimated by applying the Equation 2.305, with the help of the Figure 2.72.

$$W_{nose\_dyn} = \frac{10 \cdot H.W_0}{g \cdot B} \tag{2.305}$$

The tires must be defined as that with the smallest dimensions able to support the loads obtained by the equations showed above. The nose tire may be defined considering the biggest load between the static and dynamic one.

As the tire get old its diameter can increase around 2% or 3%, and its width around 4%, so these dimensions must be considered during the dimensioning of the fairings and tires compartment, etc.

Finally after done this dimensioning, the tires should be selected based on the catalogs provided by the manufacturers.

DESIGN, DIMENSIONING & SPECIFICATION

CHAPTER III

This chapter is dedicated to present the design and dimensioning of the airplane UFU-1, including the results of the conceptual design phase, and the results of the preliminary design phase, that were both based on the previously presented theory.

All the results presented on the topics relative to aerodynamics, dynamics of flight and performance were based on the airplane mass properties obtained during the conceptual design phase.

3.1. CONCEPTUAL DESIGN

Considering that the mission of the airplane was treated on the introduction of this text, here will be defined the technical specification of the airplane, what is result of the mission to which the airplane was conceived.

$$N_{crew} = 2$$

$$W_{pilot} = 86.0\ [kgf]$$

$$W_{payload} = 20.0\ [kgf]$$

$$V_{cruise} = 170\ [k\,m/h]$$

$$FL_{cruise} = 8000\ [ft]$$

$$R = 600.0\ [km]$$

Due the peculiar aerodynamics and dynamics of flight of the airplane, and changes on the configuration as mentioned above at introduction, the conceptual design had to be reassessed during the preliminary design, so, the values of the parameters presented below are that obtained during these activities. The algorithm presented at APPENDIX B, was implemented considering these three aspects, and at this moment were defined the positioning

of the wings, avionics and propulsive system, in order to turn acceptable the behavior of the airplane regarding “in flight” stability and control.

As described on the chapter II, the conceptual design of an airplane is commonly based on historical trend, and these data are organized in airplane categories. The airplane here developed was classified as *“General aviation and utility single-engine piston/propeller”*.

3.1.1. General configuration

As indicated at the introduction of this work, the intention is to conceive an airplane cheap and easy to build. Based on it and considering the configuration adopted, the two wings will be the same having the same movable panels, being that of the lower wing the flaps and on the upper wing the ailerons; the same design philosophy was adopted for both canard and for both vertical tails. The upper wing was positioned on a way that the second occupant is free from its structure.

The general aerodynamic configuration of the airplane is presented next, for the wings, canards and vertical tail.

$$AR_{W\_low} = 8.0$$

$$AR_{W\_up} = 8.0$$

$$\lambda_{W\_low} = 1.00$$

$$\lambda_{W\_up} = 1.00$$

$$\Gamma_{W\_low} = 0.0\ [°]$$

$$\Gamma_{W\_up} = 0.0\ [°]$$

$$\Lambda_{W\_low} = 0.00\ [°]$$

$$\Lambda_{W\_up} = 0.00\ [°]$$

$$AR_{CAN\_low} = 8.1$$

$$AR_{CAN\_up} = 8.1$$

$$\lambda_{CAN\_low} = 1.00$$

$$\lambda_{CAN\_up} = 1.00$$

$$\Gamma_{CAN\_low} = 0.0\ [°]$$

$$\Gamma_{CAN\_up} = 0.0\ [°]$$

$$\Lambda_{CAN\_low} = 0.00\ [°]$$

$$\Lambda_{CAN\_up} = 0.00\ [°]$$

$$AR_{VT\_lef} = 1.636$$

$$AR_{VT\_rig} = 1.636$$

$$\lambda_{VT\_lef} = 0.688$$

$$\lambda_{VT\_rig} = 0.688$$

$$\Lambda_{VT\_lef} = 9.532\ [°]$$

$$\Lambda_{VT\_rig} = 9.532\ [°]$$

The values for aspect ratio defined above were based on historical tendencies, and considered too, geometric constraints as avoid a too small wing and canard chords, once the airplane has a biplane configuration for both wings and canards; other important constraint considered was the aeroelastic characteristic, since wings or canards which the aspect ratio are bigger than 9.0 may present low rigidity, even that in this case in particular, the structure is built in composite material, what provide great rigidity. The taper ratio, dihedral and sweep angles was defined respecting the philosophy adopted initially of to develop an airplane simple, easy and cheap to be built.

3.1.2. Drag polar estimate

The initial values obtained from the historical data to determine the approximated parasite drag coefficient of the airplane are:

$$C_{fe} = 0.0080$$

$$\frac{S_{wet_{ap}}}{S_W} = 4.5$$

Despite the span efficiency factor for biplane given by the Equation 2.65, considering that at the moment of the conceptual design the parameters available were not enough, were applied the methods given by the Figure 2.5 and that given by the Equation 2.8, due two reasons, first was to compare the results obtained, the other was based on the fact that each method consider distinct geometric parameters.

As presented next, there is a big difference between the two values, and once the two methods are based in different parameters, both may be considered as complementary. Therefore was decided consider the mean value from the two as the final result for the estimative of the Oswald factor.

$$e_{wing} = 0.9174$$

$$e_o = 0.6569$$

$$e_{mean} = 0.7872$$

The method for estimates the drag polar of the airplane was implemented on the algorithm presented on the APPENDIX A and the results are showed next.

$$CD_0 = 0.0273$$

$$K_2 = 0.0505$$

$$CD = 0.0273 + 0.0505 \cdot CL^2$$

3.1.3. Weight estimate

For the weight estimative, the initial guess for the gross take-off weight and the weight fraction values obtained from the Table 2.8 are showed below. The specific fuel consumption is obtained from the engine technical specification given on APPENDIX H.

$$g = 9.81\ [m/s^2]$$

$$W_0 = 500.0\ [kgf]$$

$$W_1/W_0 = 0.990$$

$$W_2/W_1 = 0.992$$

$$W_4/W_3 = 0.993$$

$$W_6/W_5 = 0.993$$

$$\eta_H = 0.8\ (initial\ guess)$$

$$SFC_{cruise} = 3.8663 \times 10^{-8}\ [kg/W \cdot s]$$

$$SFC_{loiter} = 3.3451 \times 10^{-8}\ [kg/W \cdot s]$$

The method for estimates the results for the weight fractions and weights provide too, corrected estimates for wing loading, wing reference area and airplane wetted area. This method was implemented on the algorithm presented on the APPENDIX A, providing the following results.

$$\left(\frac{L}{D}\right)_{cruise} = 10.87$$

$$\left(\frac{L}{D}\right)_{loiter} = 10.15$$

$$W_3/W_2 = 0.9742$$

$$W_5/W_4 = 0.9986$$

$$TOW = 560.8\ [kgf]$$

$$OEW = 423.5\ [kgf]$$

$$BEW = 337.5\ [kgf]$$

$$TFW = 33.1\ [kgf]$$

$$\frac{W_0}{S} = 42.13\ [kgf/m^2]$$

$$S_W = 13.25\ [m^2]$$

$$S_{wet_{ap}} = 45.28\ [m^2]$$

After the estimative of the weights of parts and components of the airplane, a new value for de basic empty weight (BEW) is obtained, different of the preview one, therefore the others main weights have its values modified.

$$BEW = 367.9\ [kgf]$$

3.1.4. Performance estimate

One of the parameters involved on the performance estimative is the wing loading. The historical data for this parameter indicates values around $78\ [Kg/m^2]$ if considered the category "General aviation and utility single-engine piston" or $43\ [Kg/m^2]$ if the category is "LSA or Homebuilt" as presented on the Table 2.9.

The result obtained in the topic above is considerably lower, and that was the intention, forcing lower stall speeds and a lighter structure, at first. The stall speed at this phase was obtained for the sea level at ISA.

$$\rho_{SL} = 1.225\ [kg/m^3]$$

$$CL_{max} = 1.8$$

$$\frac{W}{S_W} = 42.13\ [kgf/m^2]$$

$$V_S = \sqrt{\frac{2}{\rho_{FL} \cdot CL_{max}} \cdot \left(\frac{W}{S_W}\right)} = 19.36\ [m/s] = 69.7\ [km/h]$$

Despite the power-to-weight ratio could be estimated by historical tendencies data, it was done based on the value of SEP of the engine defined for the airplane, as will be described on the topic that describes the propulsive system.

$$SEP = 80.0\ [hp]$$

$$\frac{SEP}{W_0} = 0.143\ [hp/kg]$$

Applying the historical tendencies data, it is possible estimate the thrust-to-power ratio and the correspondent thrust, once the SEP is known.

$$\frac{T}{SEP} = 19.45\ [N/shp]$$

$$T = 1555.7\ [N]$$

The distances of take-off and landing are estimated based on the historical tendencies, for the sea level at ISA.

$$\left(\frac{W}{S_W}\right)_{take-off} = 42.13\ [kgf/m^2]$$

$$\left(\frac{W}{S_W}\right)_{landing} = 42.13\ [kgf/m^2]$$

$$\sigma = \frac{\rho_{SL}}{\rho_0} = 1$$

$$CL_{take-off} = 1.25\ (initial\ guess)$$

$$\left(\frac{SEP}{W}\right)_{take-off} = 0.143\ [hp/kg]$$

$$TOP = \frac{\left(\frac{W}{S_W}\right)_{take-off}}{\sigma \cdot CL_{take-off} \cdot \left(\frac{SEP}{W}\right)_{take-off}} = 30.49$$

$$R_T = 8.23 \cdot TOP = 250.9\ [m]$$

$$R_{T\_obst} = 9.30 \cdot TOP = 283.6\ [m]$$

$$R_L = 1.136 \cdot \frac{1}{\rho_{SL} \cdot CL_{max}} \cdot \left(\frac{W}{S_W}\right)_{landing} = 212.9\ [m]$$

$$R_{L\_obst} = 1.524 \cdot \frac{1}{\rho_{SL} \cdot CL_{max}} \cdot \left(\frac{W}{S_W}\right)_{landing} = 285.7\ [m]$$

The estimative for the total range of the airplane is done for four distinct conditions as defined below on Table 3.1. As for the preview performance results, the total range was based on the ISA. The Payload-range Diagram for these four points is showed on Figure 3.1.

Table 3.1 - Total range estimated for the airplane UFU-1.

Point	***Condition***	***R_T [km]***	***$W_{Payload}$ [kgf]***
1	Zero fuel; total payload	0	106.0
2	Total fuel; total payload	668.43	106.0
3	Total fuel; zero cargo	709.09	86.0
4	Total fuel; zero payload	894.87	0.0

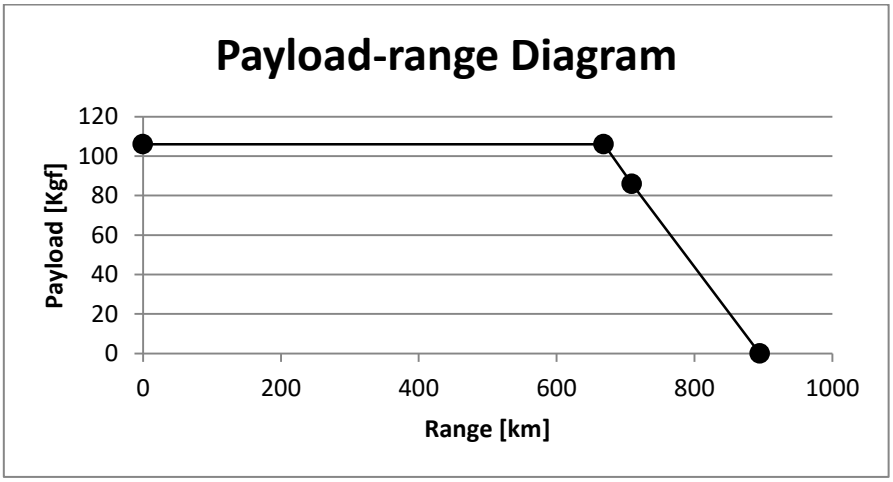


Figure 3.1 - Payload-range Diagram for the airplane UFU-1.

3.1.5. Sizing estimate

The sizing estimative of the airplane was implemented on the algorithm of the APPENDIX B. It is important to note that, the values of tail arm, tail volume coefficient and

moments of inertia, varies as the values of the pilots, cargo and fuel weights changes. The results presented next are based on the following weights as standard.

$$W_{pilot\_1} = 86.0\ [kgf]$$

$$W_{pilot\_2} = 86.0\ [kgf]$$

$$W_{payload} = 20.0\ [kgf]$$

$$W_{fuel} = 33.0\ [kgf]$$

$$X_{fus} = 6.13\ [m]$$

$$X_N = 1.48\ [m]$$

$$X_C = 2.90\ [m]$$

$$Y_C = 1.00\ [m]$$

At this moment some geometrical parameters as wings chord and span, canards areas and vertical tail areas are estimated, with these values the tail volume coefficients are estimated and compared to the historical tendencies data.

$$b_{W\_B} = 7.28\ [m]$$

$$\bar{C}_{W\_B} = 1.83\ [m]$$

$$S_{CAN\_low} = 1.30\ [m^2]$$

$$l_{CAN\_low} = 2.33\ [m]$$

$$S_{CAN\_up} = 1.30\ [m^2]$$

$$l_{CAN\_up} = 2.23\ [m]$$

$$S_{VT\_lef} = 0.76\ [m^2]$$

$$l_{VT\_lef} = 1.48\ [m]$$

$$S_{VT\_rig} = 0.76\ [m^2]$$

$$l_{VT\_rig} = 1.48\ [m]$$

$$V_{CAN\_low} = -0.124$$

$$V_{CAN\_up} = -0.119$$

$$V_{CAN} = -0.243$$

$$V_{VT\_lef} = 0.012$$

$$V_{VT_{rig}} = 0.012$$

$$V_{VT} = 0.024$$

Next are presented the parameters for the sizing estimative for the primary flight control surfaces.

$$Ail_{rate} = 0.07$$

$$S_{ail} = 0.46\ [m^2]$$

$$Elev_{rate} = 0.41$$

$$S_{elev\_low} = 0.53\ [m^2]$$

$$S_{elev\_up} = 0.53\ [m^2]$$

$$Rud_{rate} = 0.36$$

$$S_{rud\_lef} = 0.27\ [m^2]$$

$$S_{rud\_rig} = 0.27\ [m^2]$$

Finally the moment of inertia on the three axis based on the historical tendencies data may be estimated.

$$R_X = 0.25$$

$$R_Y = 0.38$$

$$R_Z = 0.39$$

$$I_{XX} = 495.35\ [kg \cdot m^2]$$

$$I_{YY} = 811.40\ [kg \cdot m^2]$$

$$I_{ZZ} = 1022.55\ [kg \cdot m^2]$$

3.1.6. Parts weights estimate

The main airplane parts weights are defined based on the historical trend method, however, some components or systems as the equipped engine, engine suspension frame, propeller, avionic system and battery have its weights defined by the suppliers. The estimative of these parts weights was implemented on the algorithm presented on the APPENDIX B.

$$W_{W\_low} = 50.45\ [kgf]$$

$$W_{W\_up} = 50.45\ [kgf]$$

$$W_{CAN\_low} = 4.50\ [kgf]$$

$$W_{CAN\_up} = 4.50\ [kgf]$$

$$W_{VT\_lef} = 3.11\ [kgf]$$

$$W_{VT\_rig} = 3.11\ [kgf]$$

$$W_{fus} = 63.31\ [kgf]$$

$$W_{MLG} = 28.57\ [kgf]$$

$$W_{NLG} = 9.60\ [kgf]$$

$$W_{Control.Surf} = 8.46\ [kgf]$$

$$W_{Engine\_equ} = 66.20\ [kgf]$$

$$W_{Engine\_susp} = 2.00\ [kgf]$$

$$W_{Prop} = 4.10\ [kgf]$$

$$W_{oil.syst} = 0.66\ [kgf]$$

$$W_{fuel.syst} = 5.84\ [kgf]$$

$$W_{Flig.cont.syst} = 10.70\ [kgf]$$

$$W_{Flap.cont.syst} = 1.45\ [kgf]$$

$$W_{Avionic} = 3.30\ [kgf]$$

$$W_{Elect\_mod} = 4.77\ [kgf]$$

$$W_{Bat} = 19.10\ [kgf]$$

$$W_{Seat\_pil} = 10.60\ [kgf]$$

3.1.7. CG-Weight envelope diagram estimate

Running the algorithm of the APPENDIX B, the Table 3.2 was built and the CG-Weight envelope presented on the Figure 3.2 could be generated.

Table 3.2 - CG positioning for some weights configurations.

Point	***Condition***	***CG [mm]***	***W [kgf]***
1	OEW	3794	453.9
2	No Pilot 2; total fuel; zero cargo	3875	486.9
3	No Pilot 2; zero fuel; total cargo	3684	473.9
4	No Pilot 2; total fuel; total cargo	3770	506.9
5	Pilot 2; total fuel; zero cargo	3894	572.9
6	Pilot 2; zero fuel; total cargo	3733	559.9
7	Pilot 2; total fuel; total cargo (MTOW)	3803	592.9
8	Pilot 1 (90 kg); No Pilot 2; zero fuel; total cargo	3678	477.9
9	Pilot 1 (50 kg); Pilot 2 (90 kg); total fuel; zero cargo	3954	540.9

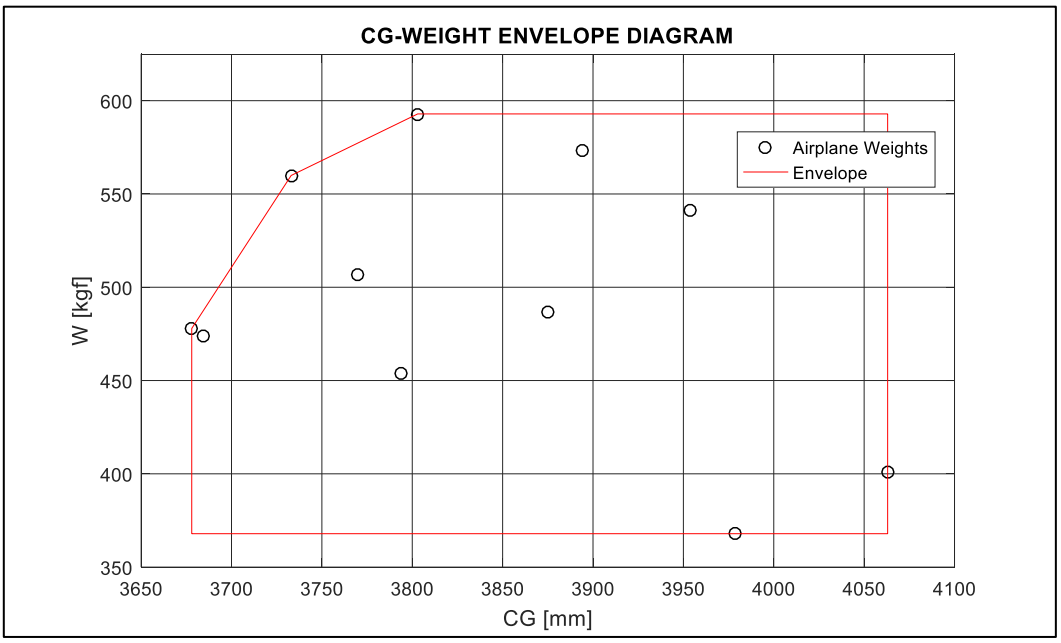


Figure 3.2 - Estimated CG-Weight envelope for the airplane UFU-1.

3.2. SELECTION OF MATERIALS

This topic presents the materials selected for each part or component of the airplane and its mechanical properties.

3.2.1. Selected material

Wings

The lower surface, the upper surface, the ribs and spars will be manufactured in carbon fiber composite.

Canards

The lower surface, the upper surface, the ribs and spars will be manufactured in carbon fiber composite. The fairing and booms will be manufactured in fiberglass composite.

Vertical tails

The lower surface, the upper surface, the ribs, the spars and the booms will be manufactured in carbon fiber composite.

Fuselage

The main body surface, the bulkheads and spars of the main body will be manufactured in carbon fiber composite. The forward section composed by the radome and nose will be entirely manufactured in fiberglass composite.

Canopy

The canopy will be manufactured in acrylic.

Engine suspension frame

The engine suspension frame will be manufactured in aluminum alloy *2024-T3 (Alclad)* tubes, or will be installed the one supplied for the engine manufacturer.

Fuel tank

The fuel tank will be manufactured in aluminum alloy *5052H-32*.

Firewall

The firewall that will isolate the engine from the cockpit, will be manufactured in stainless steel alloy *17-4PH* plates.

Landing gear

The landing gear legs will be manufactured in carbon fiber composite. The fairings will be manufactured in fiberglass composite.

Pilot's seats

The structure will be manufactured in carbon fiber composite. The padded will be manufactured in foam.

Instruments panel

The instruments panel will be manufactured in fiberglass composite.

Side consoles

The side consoles where will be installed some of the flight control levers, will be manufactured in fiberglass composite.

Flight control system

The ailerons mechanism will be manufactured in aluminum alloy *2024-T3 (Alclad)* and *6061-T6 (Alclad)*. The elevator mechanism will be manufactured in aluminum alloy *2024-T3 (Alclad)* and *6061-T6 (Alclad)*. The rudder mechanism will be manufactured in aluminum alloy *6061-T6 (Alclad)*.

3.2.2. Material properties

All the material properties presented below were obtained from the bibliography (*ASM HANDBOOK Vol 2, 1995; Carraher, 2003*).

Acrylic:

- $\rho = 1185{,}37\ [kg/m^3]$
- $S_{ut} = 68{,}95\ [MPA]$
- $S_{uc} = 103{,}42\ [MPA]$
- $E = 2{,}757\ [GPA]$

Epoxy resin: (for ambient temperature cure)

- $\rho = 1300\ [kg/m^3]$
- $S_{yt} = 60\ [MPA]$
- $S_{yc} = 250\ [MPA]$
- $E_t = 3400\ [MPA]$

Carbon fiber composite:

- $\rho = 1550{,}1\ [kg/m^3]$
- $S_{ut} = 1172\ [MPA]$
- $S_{uc} = 965\ [MPA]$
- $E = 0{,}1516847\ [MPA]$

Fiberglass composite:

- $\rho = 1799{,}2\ [kg/m^3]$
- $S_{ut} = 551{,}58\ [MPA]$
- $S_{uc} = 413{,}68\ [MPA]$
- $E = 0{,}03447379\ [MPA]$

Aluminum alloy 2024-T3 (Alclad):

- $\rho = 2770\ [kg/m^3]$
- $S_{yt} = 310\ [MPA]$
- $S_{ut} = 450\ [MPA]$
- $S_{yc} = 310\ [MPA]$
- $S_{su} = 275\ [MPA]$
- $E_t = 72{,}4\ [GPA]$
- $E_c = 73{,}8\ [GPA]$
- $E_s = 28\ [GPA]$
- $\mu = 0{,}33$

Aluminum alloy 5052H-32:

- $\rho = 2680\ [kg/m^3]$
- $S_{yt} = 195\ [MPA]$
- $S_{ut} = 230\ [MPA]$
- $S_{yc} = 195\ [MPA]$
- $S_{su} = 140\ [MPA]$
- $E_t = 69{,}3\ [GPA]$
- $E_c = 70{,}7\ [GPA]$
- $E_s = 25{,}9\ [GPA]$
- $\mu = 0{,}33$

Aluminum alloy 6061-T6 (Alclad):

- $\rho = 2700\ [kg/m^3]$
- $S_{yt} = 276\ [MPA]$
- $S_{ut} = 310\ [MPA]$
- $S_{su} = 207\ [MPA]$
- $E_t = 68{,}9\ [GPA]$
- $E_c = 69{,}7\ [GPA]$

Stainless steel alloy 17-4PH:

- $\rho = 7861{,}12\ [kg/m^3]$
- $S_{yt} = 724\ [MPA]$
- $S_{ut} = 930{,}8\ [MPA]$
- $E_t = 196{,}5\ [GPA]$

3.3. ERGONOMICS

After the work done under the conceptual design phase, the activities of the preliminary design phase began by the definition of the ergonomics dimensions that affects the final dimensions of the fuselage.

3.3.1. Human body

Initially were defined four sizes for the human body dimensions based on the references presented on the theory chapter. The parameters for each mannequin are showed next, and the Figure 3.3 and Figure 3.4 presents the standard mannequin.

Standard pilot:

- Gender: male
- Weight: 80 [Kg]
- Stature: 1.75 [m]
- Crotch height, standing: 0.832 [m]
- Sitting height: 0.912 [m]
- Hip breadth, sitting: 0.370 [m]
- Thigh, flexion (front seat): 75 [°]
- Thigh, flexion (back seat): 75 [°]
- Thigh, abduction (front seat) : 9 [°]
- Thigh, abduction (back seat) : 16 [°]
- Leg, flexion: 45 [°]

Me pilot:

- Gender: male
- Weight: 60 [Kg]
- Stature: 1.70 [m]
- Crotch height, standing: 0.816 [m]
- Sitting height: 0.888 [m]
- Hip breadth, sitting: 0.322 [m]
- Thigh, flexion (front seat): 75 [°]
- Thigh, flexion (back seat): 75 [°]
- Thigh, abduction (front seat) : 9 [°]
- Thigh, abduction (back seat) : 16 [°]
- Leg, flexion: 45 [°]

Big pilot:

- Gender: male
- Weight: 90 [Kg]
- Stature: 1.85 [m]
- Crotch height, standing: 0.891 [m]
- Sitting height: 0.952 [m]
- Hip breadth, sitting: 0.388 [m]
- Thigh, flexion (front seat): 75 [°]
- Thigh, flexion (back seat): 75 [°]
- Thigh, abduction (front seat) : 9 [°]
- Thigh, abduction (back seat) : 16 [°]
- Leg, flexion: 45 [°]

Small pilot:

- Gender: female
- Weight: 50 [Kg]
- Stature: 1.55 [m]
- Crotch height, standing: 0.729 [m]
- Sitting height: 0.818 [m]
- Hip breadth, sitting: 0.355 [m]
- Thigh, flexion (front seat): 75 [°]
- Thigh, flexion (back seat): 75 [°]
- Thigh, abduction (front seat) : 9 [°]
- Thigh, abduction (back seat) : 16 [°]
- Leg, flexion: 45 [°]

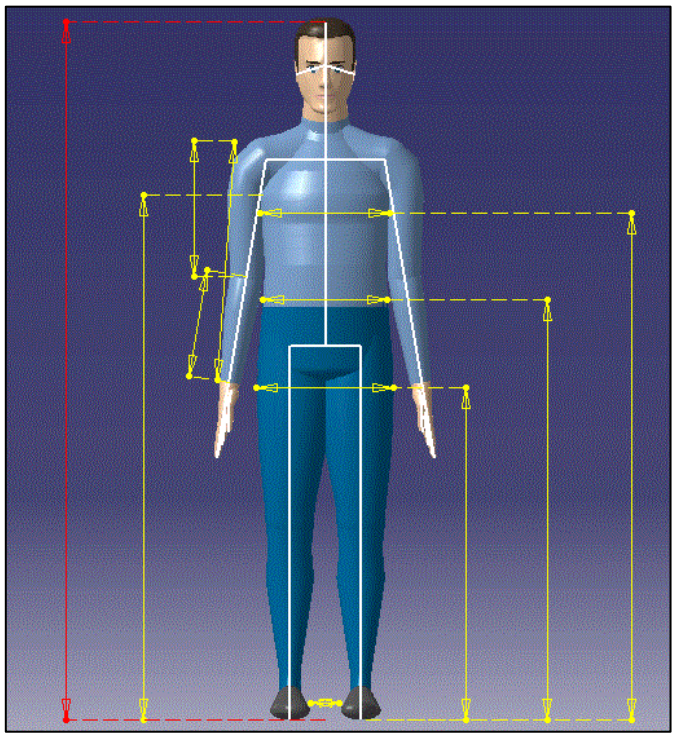


Figure 3.3 - Standard pilot standing dimensioning.

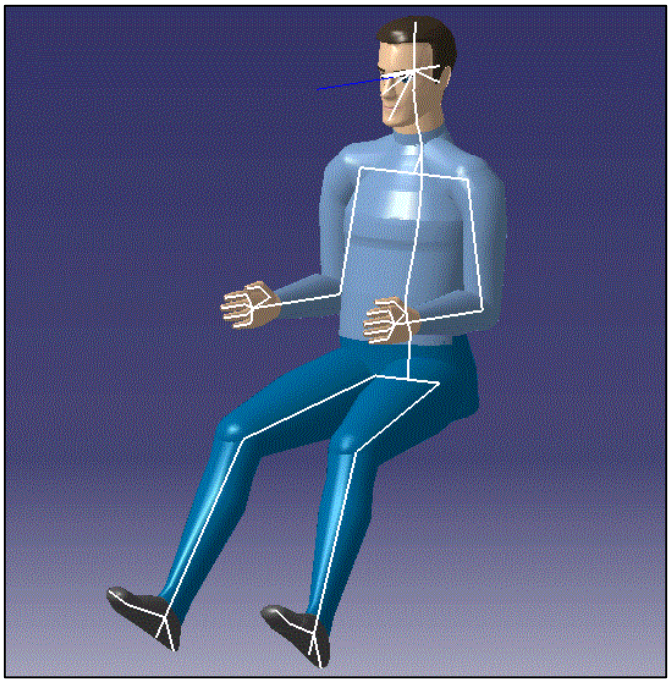


Figure 3.4 - Standard pilot sitting position.

3.3.2. Cockpit design

The next step was design the seats of the airplane, based on the results obtained by the definition of the mannequins. The structure of the seat has the function of to protect the pilot in the event of to pyloning. Both front and back seats are the same. The Figure 3.5 shows the final seat draw.

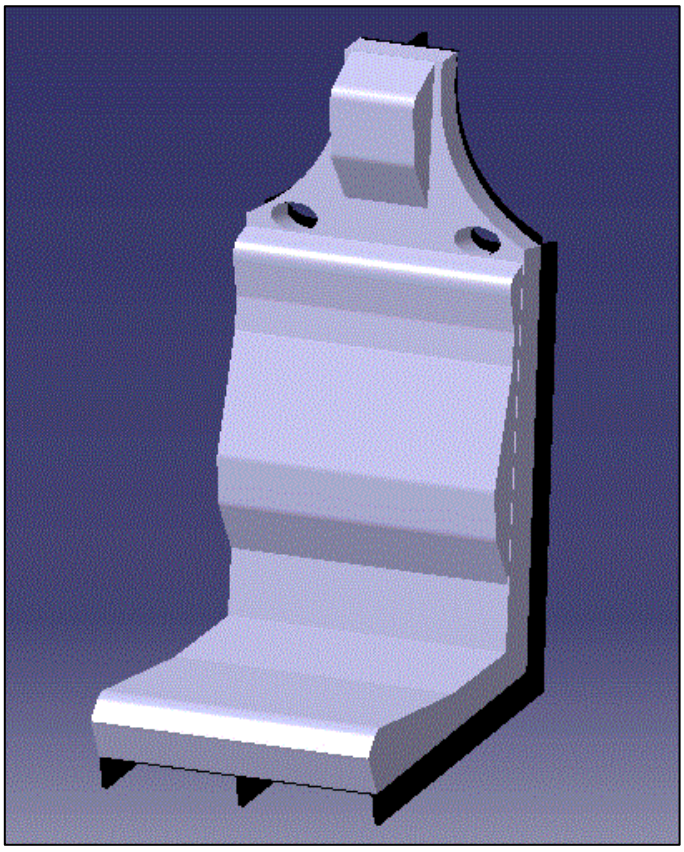


Figure 3.5 - Airplane seat.

With the mannequins and seats defined, the two seats were positioned properly for the dimensioning of the cockpit. The Figure 3.6 presents the result.

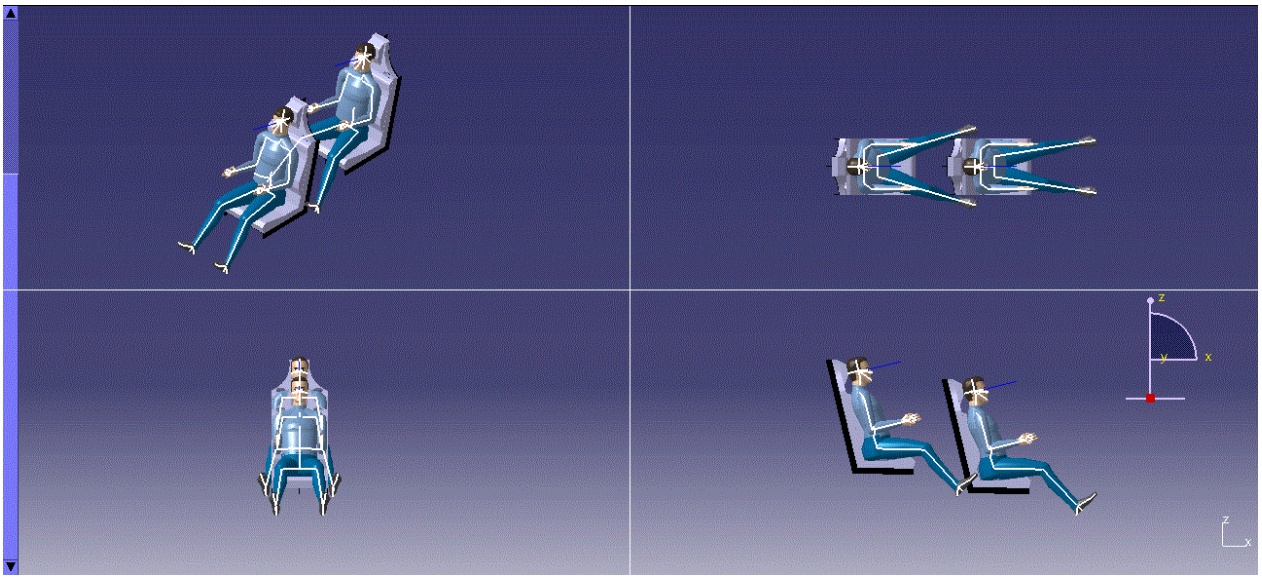


Figure 3.6 - Pilots seats positioning inside the cockpit.

Continuing the activities, the next steps done were the definition of the external loft of the entire fuselage and the geometry of the avionics panel based on the pilots seats positioning, here will be showed the segment of the cockpit on the Figure 3.7 and avionics panel on the Figure 3.8. The final result regarding the ergonomics and designing of the cockpit is presented on the Figure 3.9.

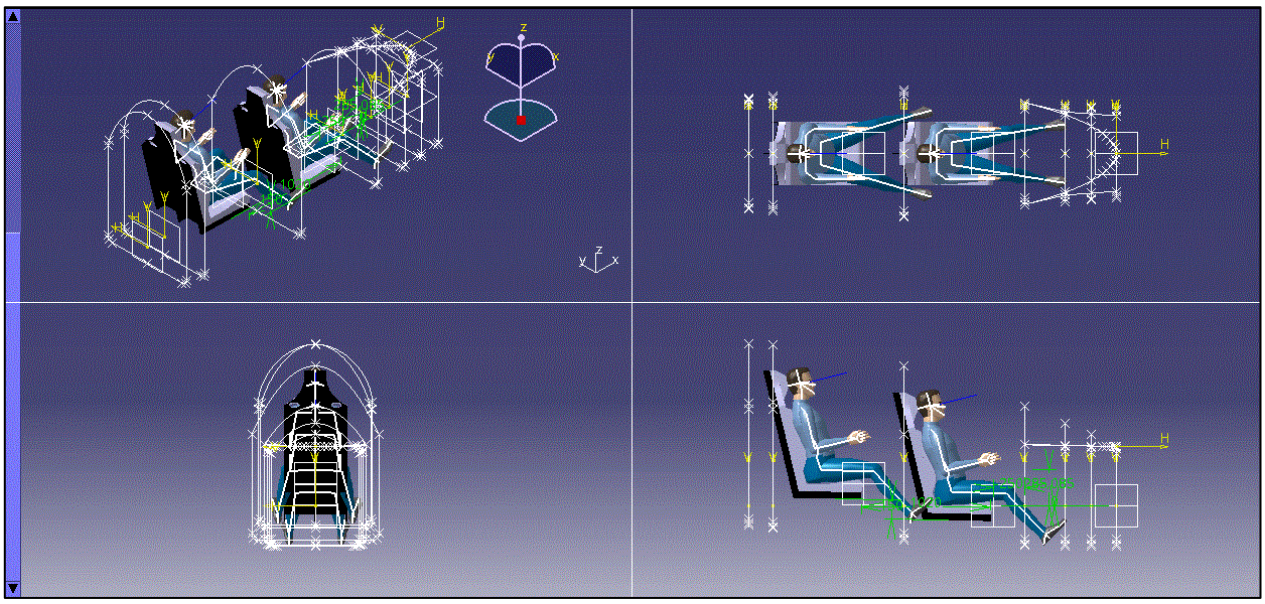


Figure 3.7 - Cockpit frames drawings.

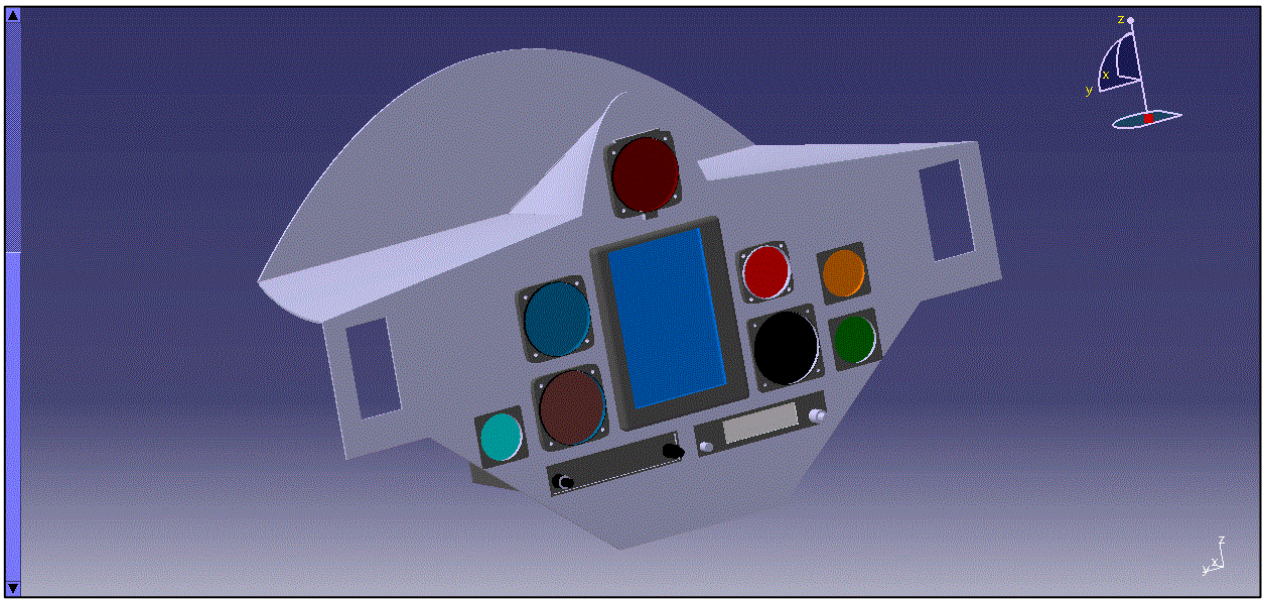


Figure 3.8 - Equipped avionics panel.

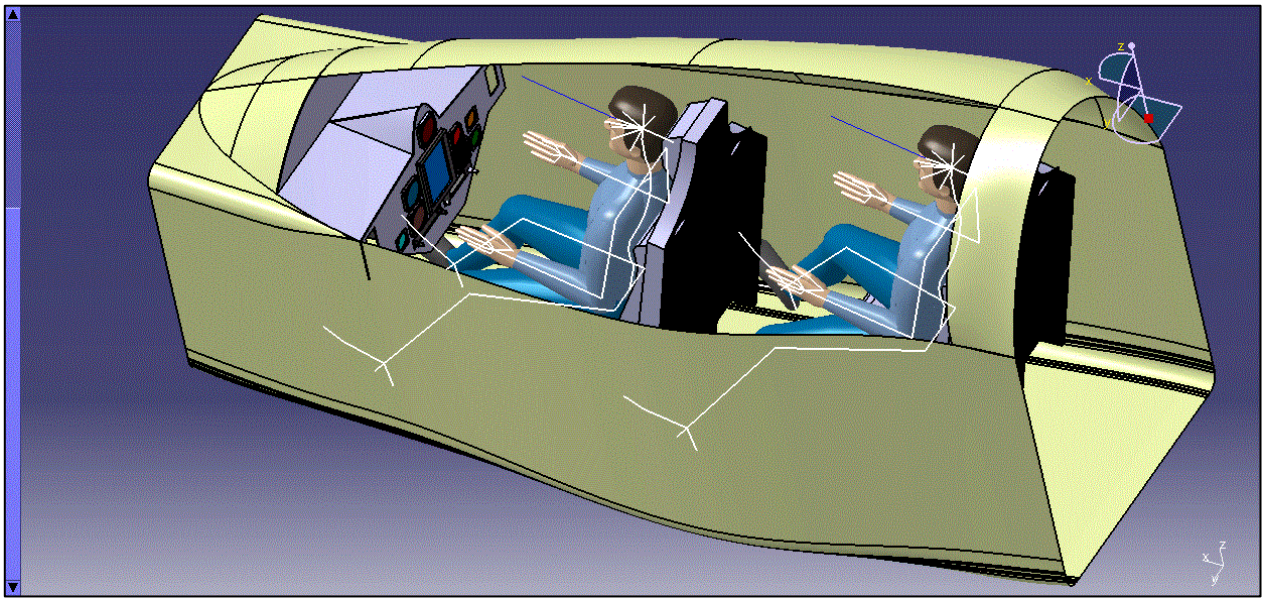


Figure 3.9 - Cockpit assembly.

The Figure 2.13 suggests a minimum inclination angle for the canopy of $25°$, but the canopy was drawing with an inclination slightly lower with value of $23.758°$.

3.4. AERODYNAMICS

The aerodynamic design was developed initially considering the 2D characteristics, essentially the aerodynamic of the airfoils used on the airplane. After the phase of choice of the aerodynamic profiles the development was basically dedicated to the estimation of the 3D aerodynamic parameter which are basically the lift, drag and moment and its aerodynamic coefficients, CL, CD and CM.

3.4.1. 2D – Aerodynamics

There are two path to following when the airfoils of an airplane must be defined, the first is the selection of the airfoils from the huge variety already developed, the second is to develop a new one that meets for the characteristics desired for the airplane. On this work it was decided for the first way, once there was not the intent of to develop new airfoils at this work.

Generally speaking, the airfoil must preferably present a pitch moment at most moderate, with the purpose of avoiding high trimming drag and torsional loads on the structure. The aerodynamic characteristics must not be too sensitive to the manufacturing deviations on its shape nor dirt, what could degrade its characteristics and induce the stall during flight conditions in which the stall is not desired.

3.4.1.1. Airfoils preselection

Considering the characteristics of the configuration of the airplane UFU-1, the most important choice is related to the airfoils to be employed on the wings and on the canards, due flight safety issues. On the development of airplanes with canard configuration it is mandatory that the profiles of both, wing and canard, be selected together with the objective to guarantee the safety aspect, as was explained earlier on the theory development in this text, which predict that the canard must stall first the wing.

Initially, it was done a pre-selection of asymmetrical and symmetrical airfoils that are presented on the Table 3.3 and the Table 3.4, that shows the main aerodynamic characteristics of these profiles.

As can be observed, only airfoils from the NACA family were preselected, it is due these profiles be well known and studied, once more, this decision was taken having the flight safety in mind. All the data considered on these two tables except for one airfoil, were obtained from the report from NACA that performed a large research about the aerodynamic characteristics of these airfoils.

Table 3.3 - Airfoils stall characteristics.

Airfoil	***Chord (m)***	***Re***	***α (°)***	***Cl_max***	***Stall***	***Bibliography***
NACA0009	0.61	3.00E+06	13	1.25	Abrupt	NACA, Report 824
NACA63-009	0.61	3.00E+06	11	0.9	Moderate	NACA, Report 824
NACA64-009	0.61	3.00E+06	10.5	1.1	Abrupt	NACA, Report 824
NACA65-009	0.61	3.00E+06	10	1.08	Abrupt	NACA, Report 824
NACA66-009	0.61	3.00E+06	10	0.85	Moderate	NACA, Report 824
NACA0012	Not defined	3.00E+06	16	1.5	Abrupt	Brandt
NACA63-012	0.61	3.00E+06	10	1	Moderate	NACA, Report 824
NACA64-012	0.61	3.00E+06	14	1.4	Abrupt	NACA, Report 824
NACA65-012	0.61	3.00E+06	12	1.15	Abrupt	NACA, Report 824
NACA66-012	0.61	3.00E+06	13	1.25	Abrupt	NACA, Report 824
NACA63-015	0.61	3.00E+06	14	1.4	Moderate	NACA, Report 824
NACA64-015	0.61	3.00E+06	15	1.3	Moderate	NACA, Report 824
NACA65-015	0.61	3.00E+06	15	1.35	Moderate	NACA, Report 824
NACA66-015	0.61	3.00E+06	16	1.3	Abrupt	NACA, Report 824
NACA2415	0.61	3.00E+06	14	1.4	Moderate	NACA, Report 824
NACA2418	0.61	2.90E+06	14	1.35	Smooth	NACA, Report 824
NACA4415	0.61	3.00E+06	12	1.4	Smooth	NACA, Report 824
NACA4418	0.61	3.00E+06	14	1.42	Smooth	NACA, Report 824
NACA23015	0.61	2.60E+06	15	1.5	Moderate	NACA, Report 824
NACA63-215	0.61	3.00E+06	14	1.42	Moderate	NACA, Report 824
NACA63-415	0.61	3.00E+06	14	1.5	Moderate	NACA, Report 824
NACA63-615	0.61	3.00E+06	13	1.45	Moderate	NACA, Report 824
NACA64-215	0.61	3.00E+06	15	1.4	Moderate	NACA, Report 824
NACA64-415	0.61	3.00E+06	15	1.5	Smooth	NACA, Report 824
NACA65-215	0.61	3.00E+06	16	1.4	Moderate	NACA, Report 824
NACA65-415	0.61	3.00E+06	16	1.45	Smooth	NACA, Report 824
NACA66-215	0.61	3.00E+06	16	1.4	Abrupt	NACA, Report 824
NACA66-415	0.61	3.00E+06	18	1.5	Abrupt	NACA, Report 824

Continues on the next page

NACA23018	0.61	3.00E+06	15	1.4	Moderate	NACA, Report 824
NACA63-218	0.61	2.90E+06	12	1.3	Smooth	NACA, Report 824
NACA63-418	0.61	3.00E+06	13	1.4	Smooth	NACA, Report 824
NACA63-618	0.61	3.00E+06	12	1.4	Smooth	NACA, Report 824
NACA64-218	0.61	3.00E+06	14	1.3	Smooth	NACA, Report 824
NACA64-418	0.61	3.00E+06	14	1.35	Smooth	NACA, Report 824
NACA64-618	0.61	3.00E+06	16	1.4	Smooth	NACA, Report 824
NACA65-218	0.61	3.00E+06	15	1.3	Moderate	NACA, Report 824
NACA65-418	0.61	3.00E+06	16	1.35	Smooth	NACA, Report 824
NACA65-618	0.61	3.00E+06	16	1.4	Smooth	NACA, Report 824
NACA66-218	0.61	3.00E+06	17	1.35	Moderate	NACA, Report 824
NACA66-418	0.61	3.00E+06	18	1.4	Moderate	NACA, Report 824

Table 3.4 - Airfoils drag polar bottom and pitch moment.

Airfoil	***Cl_init***	***Cl_final***	***Cd***	***Cm***	***Bibliography***
NACA0009	-0.1	0.1	0.00525	0	NACA, Report 824
NACA63-009	-0.1	0.1	0.004	0	NACA, Report 824
NACA64-009	-0.2	0.2	0.0045	0	NACA, Report 824
NACA65-009	-0.15	0.2	0.0043	0	NACA, Report 824
NACA66-009	-0.1	0.1	0.0035	0	NACA, Report 824
NACA0012	-0.25	0.1	0.0055	0	Brandt
NACA63-012	-0.1	0.1	0.005	0	NACA, Report 824
NACA64-012	-0.25	0.3	0.005	0	NACA, Report 824
NACA65-012	-0.2	0.25	0.004	0	NACA, Report 824
NACA66-012	-0.1	0.2	0.004	0	NACA, Report 824
NACA63-015	-0.1	0.25	0.0055	0	NACA, Report 824
NACA64-015	-0.3	0.2	0.0055	0	NACA, Report 824
NACA65-015	-0.35	0.35	0.005	0	NACA, Report 824
NACA66-015	-0.25	0.3	0.0045	0	NACA, Report 824
NACA2415	0.3	0.5	0.0065	-0.05	NACA, Report 824
NACA2418	0.1	0.3	0.00725	-0.05	NACA, Report 824
NACA4415	0.4	0.8	0.00725	-0.1	NACA, Report 824
NACA4418	0.4	0.6	0.00775	-0.19	NACA, Report 824
NACA23015	0.1	0.3	0.007	-0.005	NACA, Report 824
NACA63-215	0	0.3	0.00575	-0.025	NACA, Report 824
NACA63-415	0.3	0.5	0.00575	-0.075	NACA, Report 824
NACA63-615	0.2	0.4	0.00575	-0.1	NACA, Report 824
NACA64-215	-0.1	0.5	0.0053	-0.025	NACA, Report 824

Continues on the next page

NACA64-415	0.1	0.4	0.0055	-0.06	NACA, Report 824
NACA65-215	-0.15	0.5	0.005	-0.035	NACA, Report 824
NACA65-415	0.1	0.6	0.005	-0.06	NACA, Report 824
NACA66-215	0	0.5	0.0045	-0.025	NACA, Report 824
NACA66-415	0.2	0.6	0.0045	-0.075	NACA, Report 824
NACA23018	-0.1	0.2	0.0073	-0.005	NACA, Report 824
NACA63-218	-0.2	0.6	0.006	-0.025	NACA, Report 824
NACA63-418	0.1	0.5	0.006	-0.07	NACA, Report 824
NACA63-618	0.2	0.5	0.006	-0.1	NACA, Report 824
NACA64-218	-0.2	0.6	0.0059	-0.025	NACA, Report 824
NACA64-418	0	0.6	0.006	-0.062	NACA, Report 824
NACA64-618	0.2	0.9	0.006	-0.087	NACA, Report 824
NACA65-218	-0.2	0.4	0.0055	-0.025	NACA, Report 824
NACA65-418	0.05	0.5	0.005	-0.06	NACA, Report 824
NACA65-618	0.2	0.6	0.0055	-0.1	NACA, Report 824
NACA66-218	-0.2	0.5	0.0047	-0.05	NACA, Report 824
NACA66-418	0	0.7	0.005	-0.075	NACA, Report 824

Among all these airfoils, those that were considered having the properties more adequate for being employed on the airplane UFU-1 were assessed considering the flight conditions, mainly the Reynolds number as near as possible of that expected for the airplane operation, these parameters are presented into the next subsections.

Next are presented the studies done for the selection of the airfoils to be used on the wings, canards and vertical tails. All data were obtained considering the mean aerodynamic chord of each aerodynamic surface.

3.4.1.2. Wings airfoil

To specify the airfoil to be employed on the wing, first it is necessary to estimate the lift coefficient of the wing for the cruise flight condition. Applying on the Equation 2.68 the parameters obtained on the conceptual design phase, the lift coefficient obtained for the wings is $CL = 0.4484$. As the airplane is a canard, the real lift coefficient will be a few lower than it. However, this value is valid for the selection of the airfoil, which is done in a way that, this lift coefficient of the wing be near the value of the bottom of the drag polar of the

profile to be selected, this is necessary to ensure that the drag generated by the airplane in the cruise condition will remain small.

On the aerodynamic specification of the wings was defined that only one airfoil will be used, with the objective to simplify the calculus and the manufacturing of the wings. It was defined too that the thickness of the airfoil should be between 15% and 18%, for the purpose to turn the structure light and facilitate the installation of the control mechanical system and flight instrumentation sensors.

Initially were assessed the lift curve $Cl \times \alpha$ for various profiles as presented on the NACA report 824 and summarized on the Table 3.3 and the Table 3.4, from these results were selected 4 airfoils that presented characteristics coherent to the airplane mission.

To generate the geometry of the airfoils was used the software GNacaLt, which permit to generate variations on an airfoil, modifying the mean line of this original airfoil. During the activities related to selection of the airfoil it was defined to assess the 4 preselected profiles considering two distinct mean camber lines for each one, the first called “a-0” and the second called “a-1”.

On the aerodynamic assessing it was used the software XFLR5 (V6), the airfoils were simulated for a range of angle of attack between -8° and $+24^{\circ}$, and two values for Reynolds number, $Re = 1.06E6$ expected for the stall condition and $Re = 3.00E6$ that was considered on the tests presented on the report of the NACA. The Reynolds number of interest is that for the stall, once this is the critical condition for the canard configuration, the other Reynolds number was simulated as reference to validate the simulations performed on the software XFLR5, once this value was considered on the tests presented on the NACA report 824. The results of these simulations are presented on the Figure 3.10 to Figure 3.15.

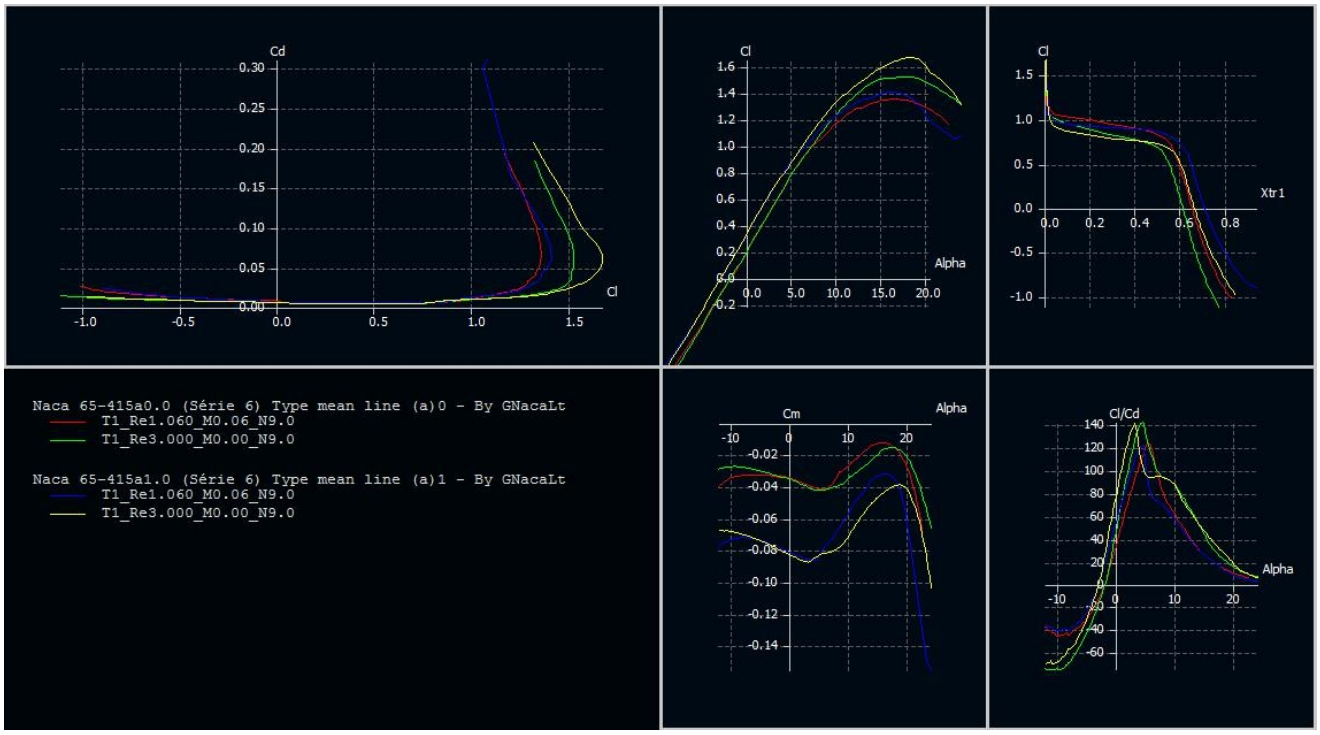


Figure 3.10 - Aerodynamic data for the airfoils NACA 65-415.

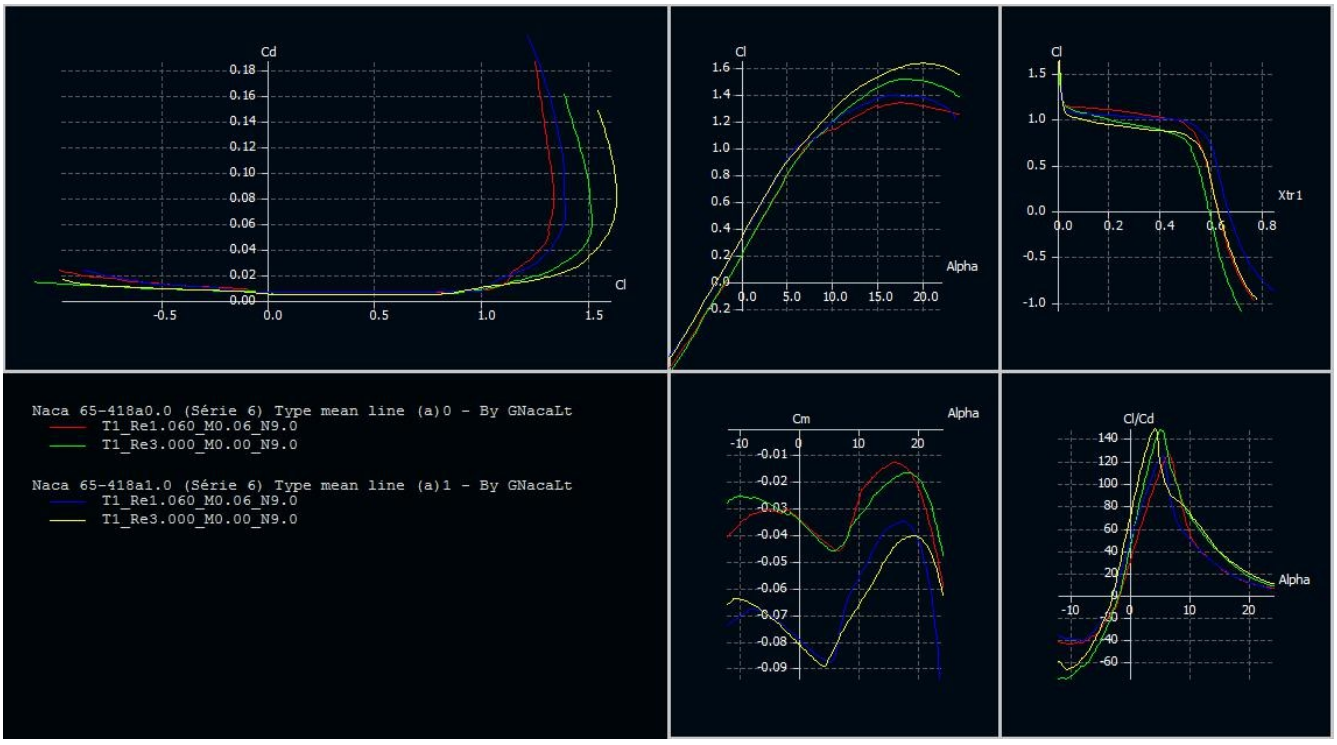


Figure 3.11 - Aerodynamic data for the airfoils NACA 65-418.

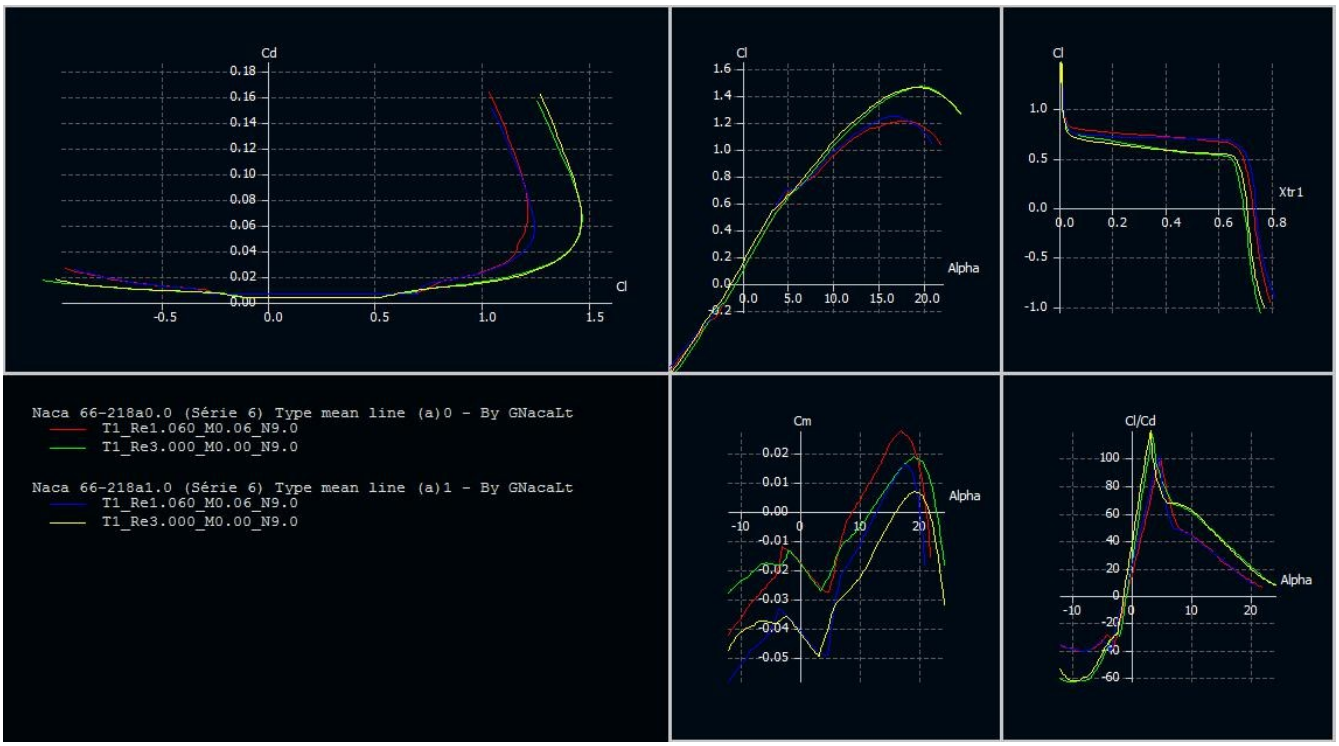


Figure 3.12 - Aerodynamic data for the airfoils NACA 66-218.

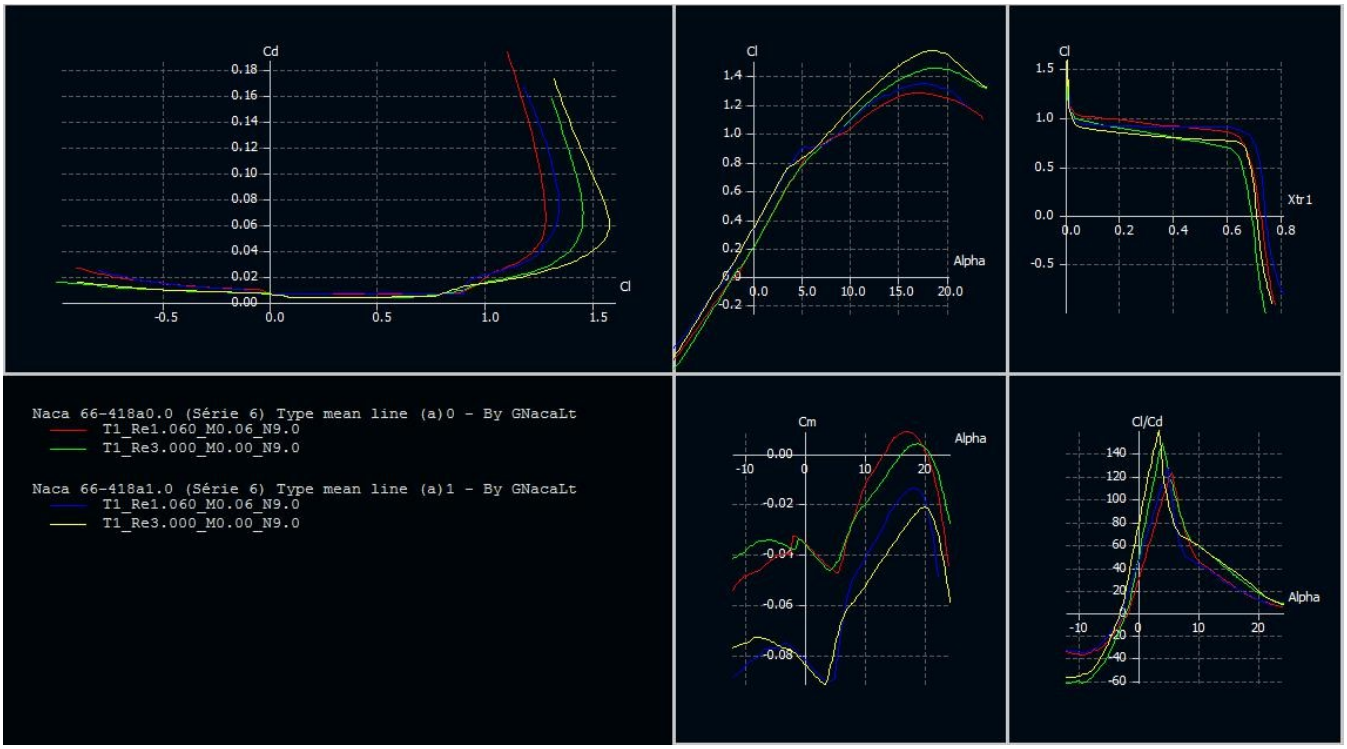


Figure 3.13 - *Aerodynamic data for the airfoils NACA 66-418.*

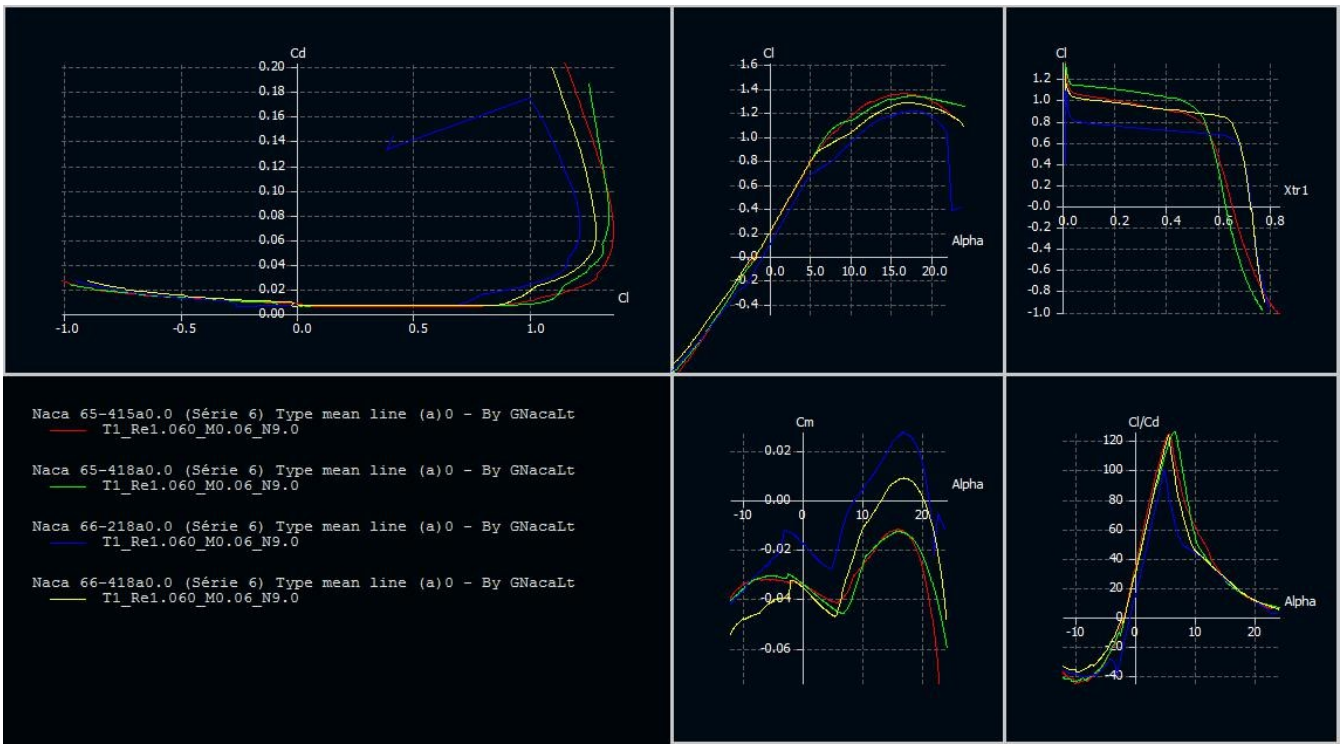


Figure 3.14 - Aerodynamic data for the airfoils with mean camber line "a-0".

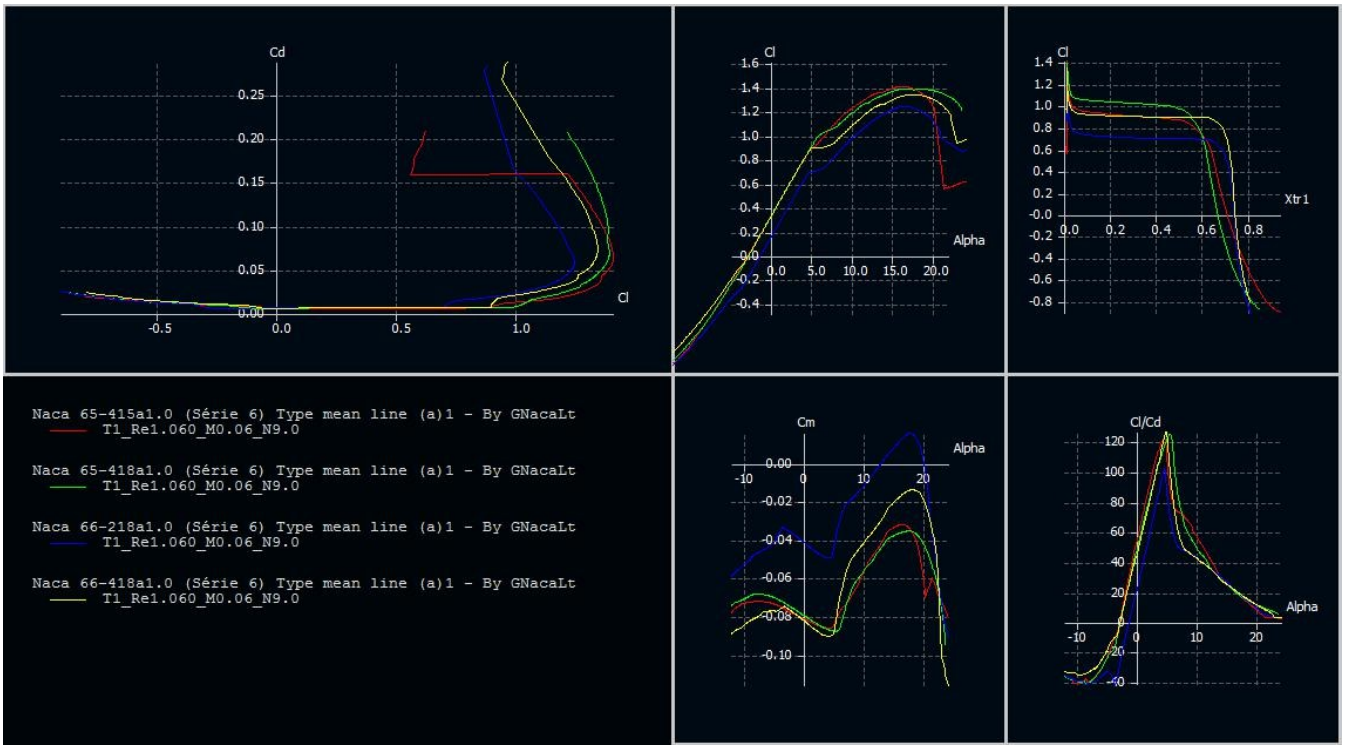


Figure 3.15 - Aerodynamic data for the airfoils with mean camber line "a-1".

Based on the results above, it is observed that the airfoils with mean camber line “a-0” are that which the aerodynamic characteristics are more similar to those presented on the NACA report 824. Therefore, the airfoil to be employed on the wing must be one of the 4 that are based on the mean camber line of the kind “a-0”.

Considering the characteristics for the 4 final airfoils obtained from the NACA report 824 and obtained from the results of the simulations and considering yet, the properties for the airfoil to be used on the canards that will be detailed next, it was selected the laminar airfoil ***NACA 65-418*** with mean camber line “a-0”. The results of the simulation indicate that this profile has stall for $\alpha = 15^{\circ}$ and correspondent lift coefficient $cl = 1.31$. As presented on the report and as can be observed on the lift curve slope generated on the simulation, this airfoil presents a smooth stall, what is a very important characteristic, considering the mission of the airplane, once it tends to generate enough buffet, indicating the imminence of the stall. Finally, as the bottom of the drag polar of this airfoil is between $cl = 0$ and $cl = 0.5$, considering the lift coefficient for the wing specified earlier $CL = 0.4484$, this profile is adequate for the cruise flight condition of the airplane. The Figure 3.16 present the geometry of the airfoil specified.

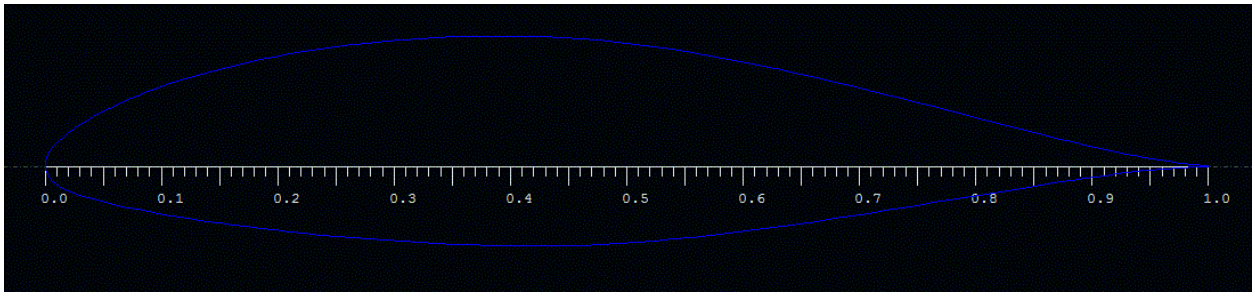


Figure 3.16 - Airfoil NACA 65-418 “a0”.

Geometric characteristics of the airfoil

- Thickness: 18%
- Thickness location in % of the chord: 39.8%
- Maximum camber: 2.1247%
- Maximum camber location in % of the chord: 35.1%

Aerodynamic characteristics of the airfoil

The aerodynamic characteristics of the airfoil NACA 65-418 “a-0” were obtained for the stall flight condition and for the cruise flight condition, they are presented on the APPENDIX D. Below is presented an approximation for the lift curve slope for the airfoil.

$$a_{0_w} = 0.1186\ [1/°]$$

$$\alpha_{cl=0_w} = -1.78\ [°]$$

3.4.1.3. Canards airfoil

On the aerodynamic specification of the canards it was defined that only one airfoil will be used, with the objective to simplify the calculus and the manufacturing of the canards.

For the choice of the profile it was considered essentially its stall and drag characteristics. One concern that was considered on the canards development since the specification of the airfoil is its aerodynamic wake influence on the lower wing, in this sense, was tried to develop canards that generates weak induced drag and in consequence weak downwash, what help reduces the drag of the airplane as a whole.

Specifically about the airfoil selection, preference was given for the airfoils from the NACA families as was mentioned earlier, due the fact that its profiles to be much studied and have its characteristics well known. The selection was done using the software XFLR5 (V6), simulating the aerodynamic coefficients for the 5 airfoils preselected, these simulations were performed for a range of angle of attack between -11° and $+20^{\circ}$ considering the stall condition.

Initially the chord for the canards was defined having the dimension $C_{CAN} = 0.61\ (m)$, simulations for the 5 airfoils were performed and are presented on the Figure 3.17, and the airfoil selected was the NACA 63-009, a laminar profile. However, due the preliminary calculus done for the dynamics of flight, the chord had to be reduced for $C_{CAN} = 0.40\ (m)$ and the results of the simulation are presented on the Figure 3.18.

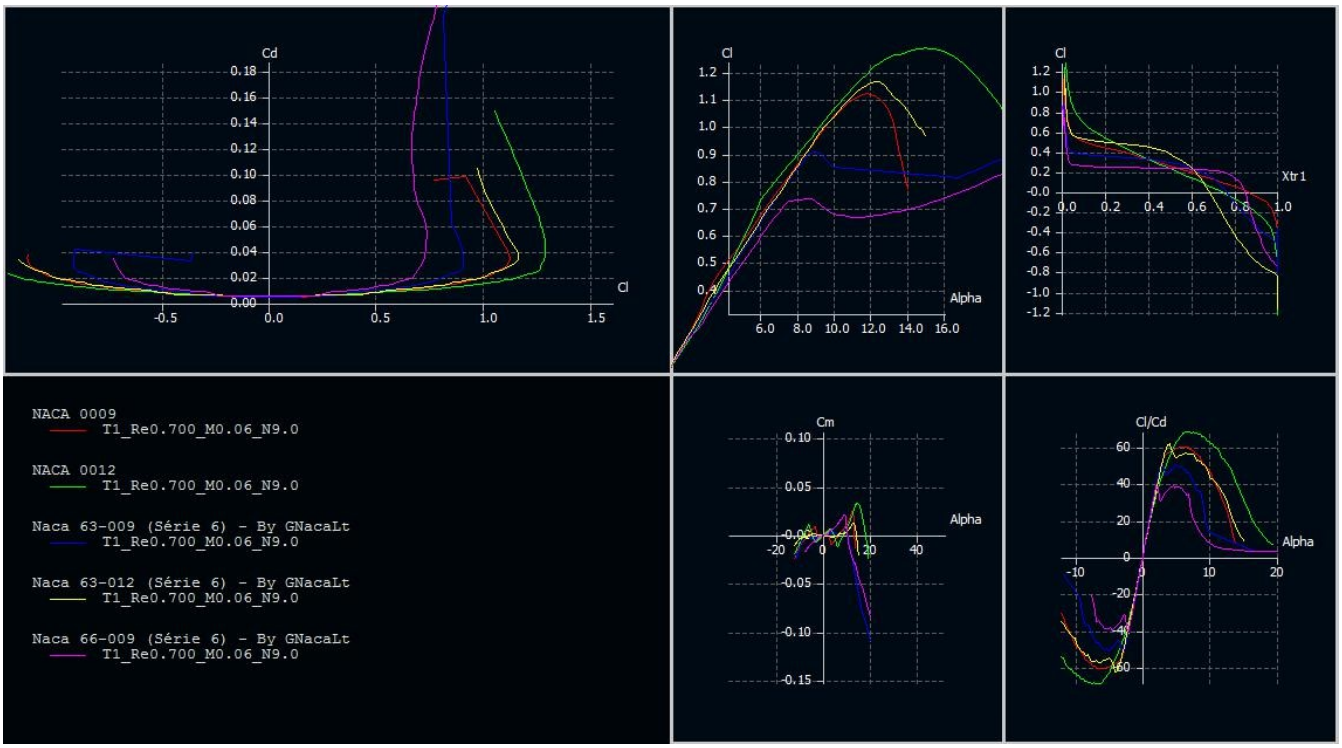


Figure 3.17 - Aerodynamic data for the airfoils with chord equal to 0.61m.

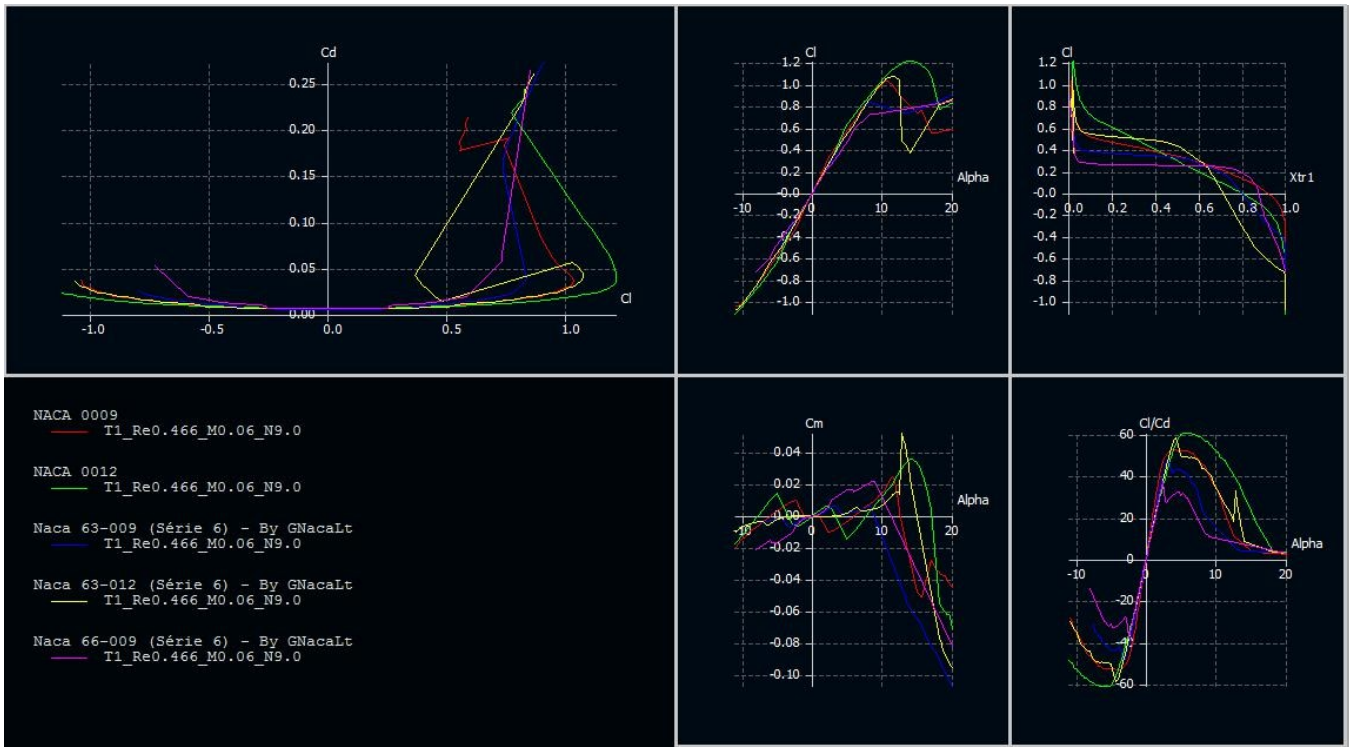


Figure 3.18 - Aerodynamic data for the airfoils with chord equal to 0.40m.

Based on these new results, it was noted that the angle of stall for the NACA 63-009 was significantly reduced, which would reduce the operational envelope of the airplane. This forced the substitution for the airfoil ***NACA 0009***, that has an angle of stall bigger than that of the preview airfoil, but around 4° below than that observed for the airfoil selected for the wings, what ensure a safety condition for the stall of the airplane.

The results of the simulation indicate that this profile has stall for $\alpha = 10.75^{\circ}$ and correspondent lift coefficient $cl = 1.03$. Finally as can be observed on the results showed on the NACA report 824 its stall is abrupt, what helps to avoid the wings stalls first the canards. The Figure 3.19 present the geometry of the airfoil selected.

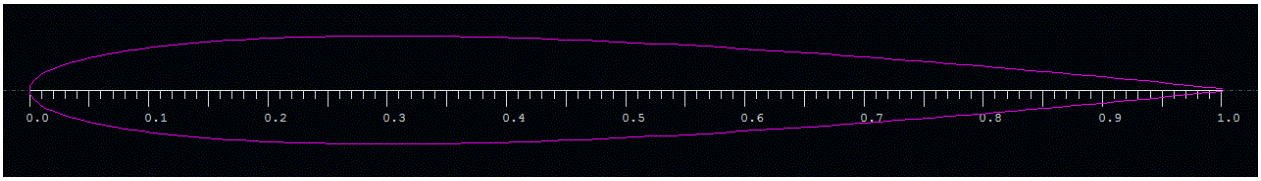


Figure 3.19 - Airfoil NACA 0009.

Geometric characteristics of the airfoil

- Thickness: 9%
- Thickness location in % of the chord: 30%

Aerodynamic characteristics of the airfoil

The aerodynamic characteristics of the airfoil NACA 0009 for the stall flight condition are presented on the APPENDIX E. Below it is presented an approximation for the lift curve slope for the airfoil.

$$a_{0_{can}} = 0.1112\ [1/^{\circ}]$$

$$\alpha_{cl=0_{can}} = 0.0\ [^{\circ}]$$

3.4.1.4. Vertical tails airfoil

For the aerodynamic specification of the vertical tails was defined that only one airfoil will be used, with the objective to simplify the calculus and the manufacturing of the vertical tails.

The airfoil selected is the very studied ***NACA 0012***, that present good characteristics for be employed on the vertical tail, once its drag generated is not too high, and it is effective for a considerably range of angle of attack. The results of the simulation performed on the software XFLR5 (V6) are presented on the Figure 3.20, and the geometry of the airfoil is presented on the Figure 3.21.

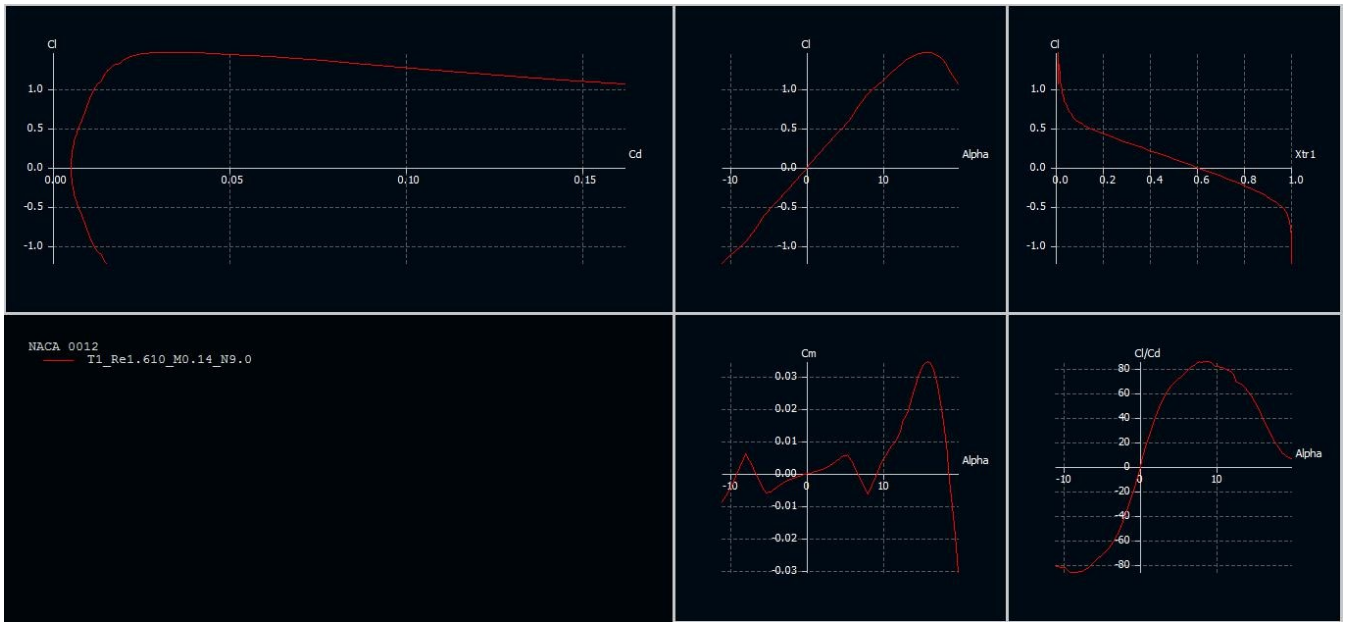


Figure 3.20 - Aerodynamic data for the airfoil NACA 0012.

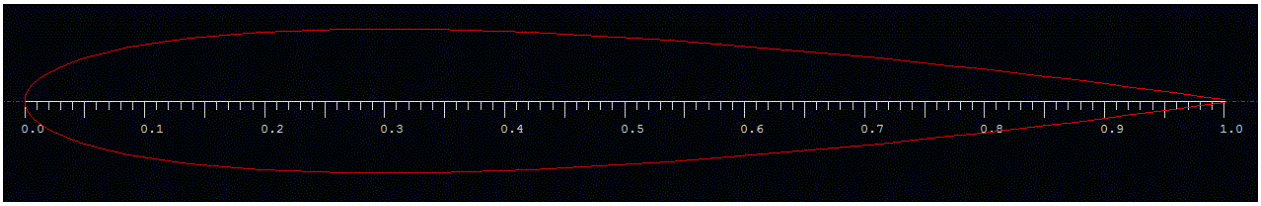


Figure 3.21 - Airfoil NACA 0012.

Geometric characteristics of the airfoil

- Thickness: 12%
- Thickness location in % of the chord: 30%

Aerodynamic characteristics of the airfoil

The aerodynamic characteristics of the airfoil NACA 0009 for the cruise flight condition are presented on the APPENDIX F. Below is presented an approximation for the lift curve slope for the airfoil.

$$cl_{vt_{max}} = 1.46$$

$$a_{0_{vt}} = 0.1119\ [1/°]$$

$$\alpha_{cl=0_{vt}} = 0.0\ [°]$$

3.4.2. 3D – Aerodynamics

This topic presents just the aerodynamic parameters necessary for the aerodynamic dimensioning of the airplane; the geometric parameters used for the aerodynamic development are presented on the chapter 4 that is dedicated to the technical description of the airplane.

Based on these parameters the results obtained are presented. As there are several flight conditions that can be considered, resulting in a large volume of data for each aerodynamic component and for the complete airplane, the results of lift, drag and moments for these components will not be presented here.

The complete aerodynamic dimensioning of the airplane UFU-1 was implemented on the algorithm presented on the APPENDIX C, all the parameters and results presented in this topic were obtained by this algorithm.

3.4.2.1. Biplane wing

Initially there are presented below the aerodynamic parameters defined or estimated, which were applied on the aerodynamic dimensioning of the biplane wing.

The span efficiency factor for the biplane wing is obtained as defined on the theory chapter, this value is considered the same for the lower wing and for the upper wing.

$$\bar{C}_{W\_B} = 1.83\ [m]$$

$$S_{aero_{W\_B}} = 12.21\ [m^2]$$

$$CL_{\alpha_{W\_B}} = 0.0835\ [1/°]$$

$$AC_{W\_B} = 4.23\ [m]$$

$$AR_{W\_B} = 4.03$$

$$\lambda_{W\_B} = 1$$

$$\mu_W = 1$$

$$r_W = 0.9116$$

$$GAP_{W\_B}/b_{W\_B} = 0.153$$

$$\sigma_W = 0.56$$

$$e_{W\_B} = 0.642$$

3.4.2.2. Lower Wing

There are presented below the aerodynamic parameters defined or estimated, which were applied on the aerodynamic dimensioning of the lower wing.

$$\bar{C}_{W\_LOW} = 0.91\ [m]$$

$$S_{aero_{W\_LOW}} = 5.82\ [m^2]$$

$$AR_{W\_LOW} = 8.02$$

$$\lambda_{W\_LOW} = 1$$

Aerodynamic center

Despite of the location of the aerodynamic center of the wings indicated on the theory of biplanes, the initial position of the aerodynamic center of the lower wing will be considered at 25% of the $\bar{C}_{W_LOW}$, due the relative positioning between both wings, specifically due first to the GAP that is bigger than the length of the chord of the wings, and second, related to the $Stagger$ that is very large, these two parameters are presented on the chapter 4, that present the technical description of the airplane.

As explained on the theory, the aerodynamic center of the lower wing suffers a shift along the x axis due the interference of the fuselage. Below are presented on the Figure 3.22 and on the Figure 3.23 the divisions done on the fuselage that were used to estimate the shift on aerodynamic center of the lower wing employing the Equation 2.131 to the Equation 2.133.

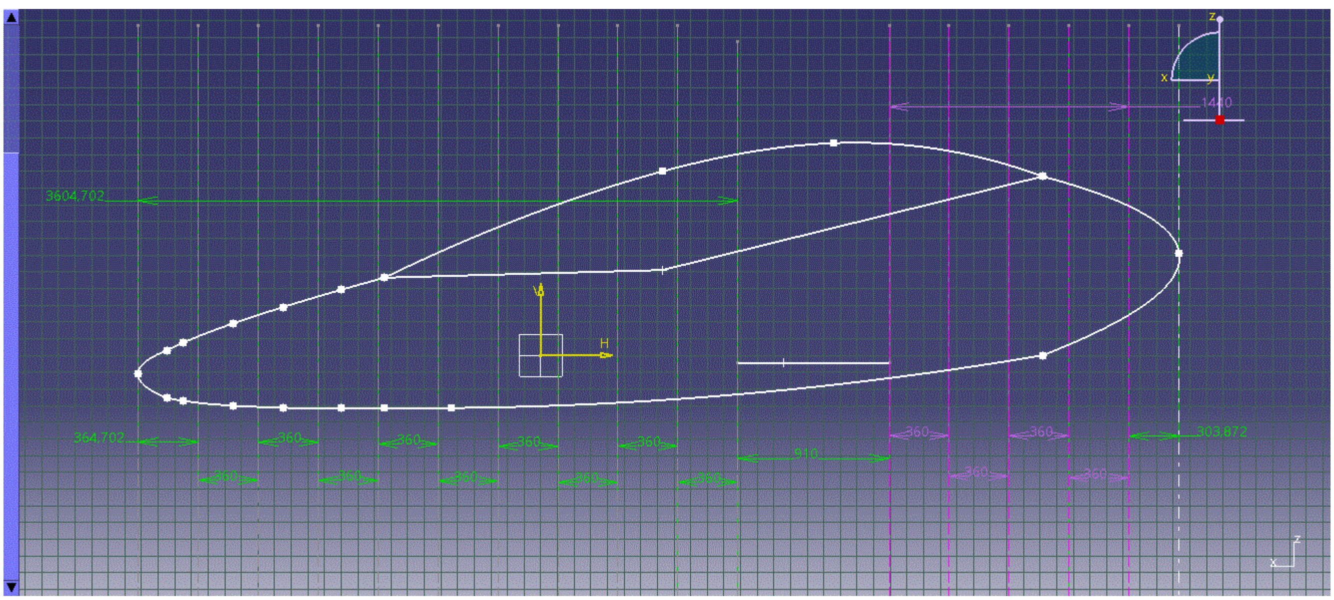


Figure 3.22 - Fuselage division for the lower wing.

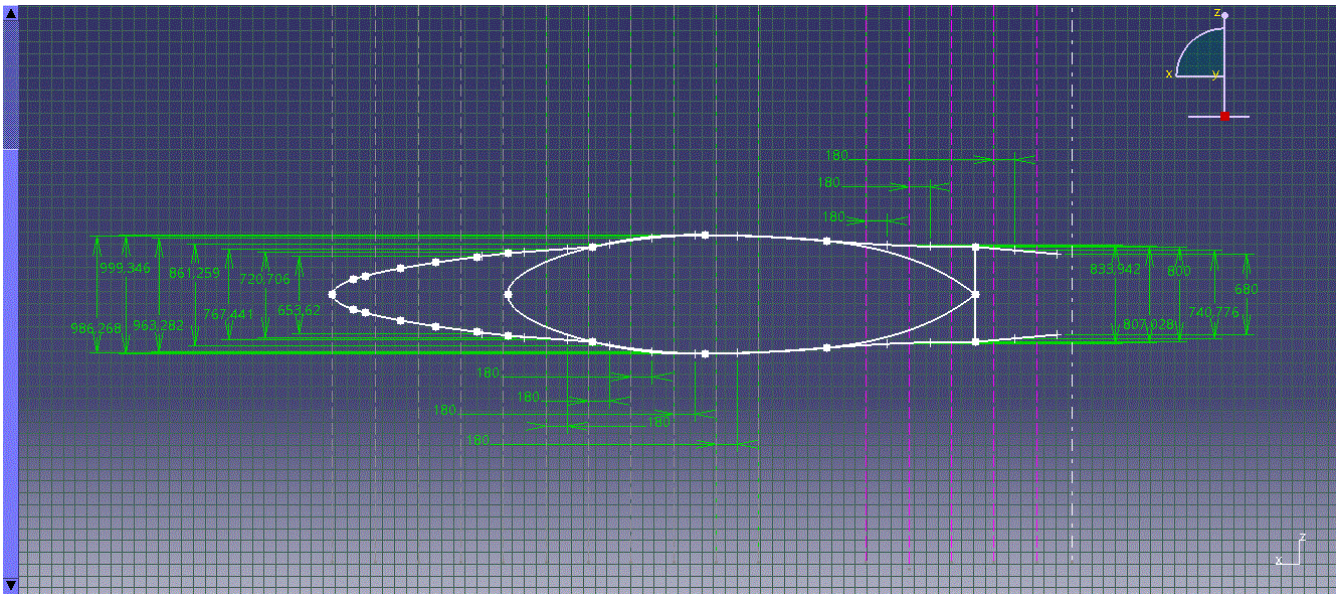


Figure 3.23 - Fuselage division for the lower wing.

The geometric parameters showed on the figures above were applied on the formulation described on the theory, for estimate the position of the aerodynamic center of the lower wing and its shift, the results are presented next.

$$AC_{W\_LOW} = 3.77\ [m]$$

$$\Delta AC_{W\_LOW} = -0.064\ [m]$$

Lift

The lift generated by the lower wing is incremented by the flaps that equip it. Despite to be not necessary equip the wing with flaps, respecting the philosophy adopted on the conception of the airplane, both wings must be equal and, once the upper wing is equipped with ailerons, these surfaces on the lower wing were converted for flaps. Therefore, due the academical purpose of this airplane, the flaps has merely theoretical purpose, as for example, permit future studies and research on disciplines like aerodynamics, dynamics of flight and structures, considering the influence of the flaps.

The parameters defined or calculated for the aerodynamic characterization related to the lift generated by the lower wing are presented next. Note that it is used the equation for the lift increment due the global wash field.

$$CL_{\alpha_{W\_LOW}} = 0.0835\ [1/°]$$

$$CL_{\alpha=0_{W\_LOW}} = 0.1483$$

$$\Delta CL_{\alpha_{W\_LOW}} = 0.1376\ [1/°]$$

$$\delta_f = 0; 10; 20\ [°]$$

$$\frac{cl_\alpha}{(cl_\alpha)_{theory}} = 1.0815$$

$$\left\{\frac{cl_\delta}{(cl_\delta)_{theory}}\right\} = 1.0$$

$$(cl_\delta)_{theory} = 0.4$$

$$k' = 1.0; 1.0;\ 0.85 \rightarrow (0^\circ;\ 10^\circ;\ 20^\circ)$$

$$k_1 = 0.95$$

$$k_2 = 0;\ 0.33;\ 0.58 \rightarrow (0^\circ;\ 10^\circ;\ 20^\circ)$$

$$k_3 = 1.0$$

$$\left(\Delta_{cl_{max}}\right)_{base} = 1.52$$

$$k_b = 0.563$$

$$\frac{(\alpha_\delta)_{CL}}{(\alpha_\delta)_{cl}} = 1.043$$

$$k_\Lambda = 0.923$$

Drag

As it was employed the laminar airfoil NACA 65-418 on the lower wing, for which the aerodynamic data are known by numerical simulation, the formulation for the drag generated by this wing is that which consider the Equation 2.93. The aerodynamic parameters defined for the drag formulation are presented below.

$$R_{wf} = 1.065$$

$$R_{LS} = 1.07$$

3.4.2.3. Upper Wing

There are presented below the aerodynamic parameters defined or estimated, which were applied on the aerodynamic dimensioning of the upper wing.

$$\bar{C}_{W\_UP} = 0.91\ [m]$$

$$S_{aero_{W\_UP}} = 6.39\ [m^2]$$

$$AR_{W\_UP} = 8.02$$

$$\lambda_{W\_UP} = 1$$

Aerodynamic center

As it was done for the lower wing, the initial positioning of the aerodynamic center of the upper wing will be considered at 25% of the $\bar{C}_{W\_UP}$, due the relative positioning between both wings. Next are presented on the Figure 3.24 and on the Figure 3.25 the divisions done on the fuselage that were used to estimate the shift on aerodynamic center of the upper wing.

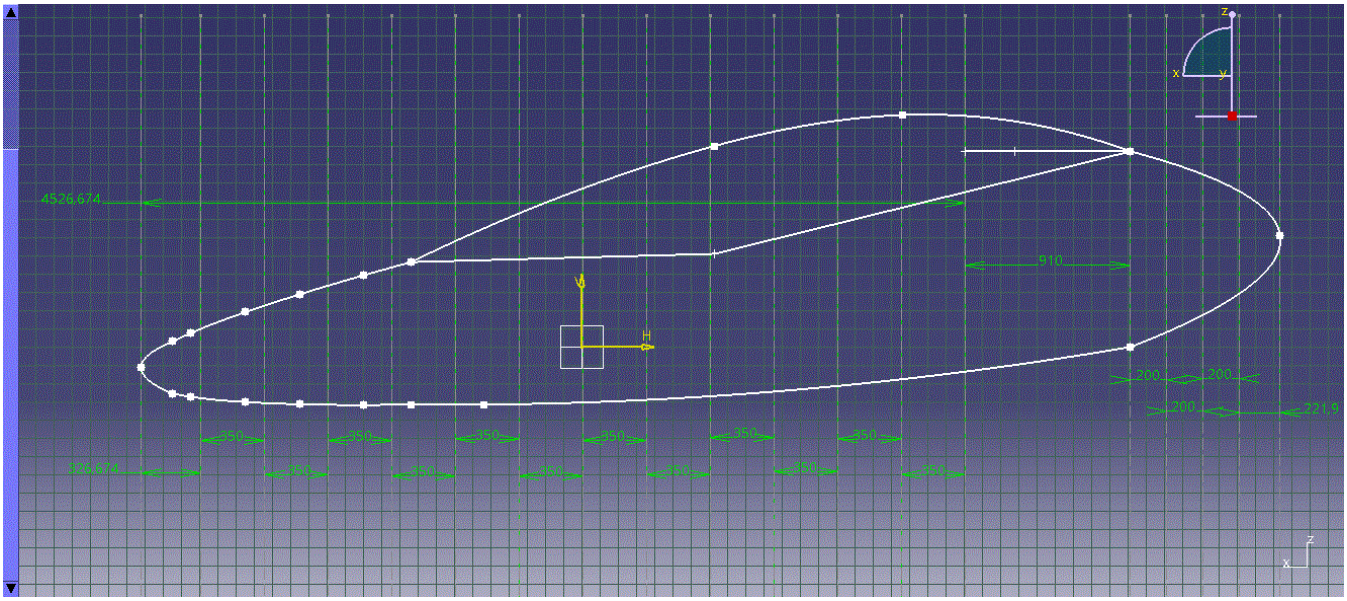


Figure 3.24 - Fuselage division for the upper wing.

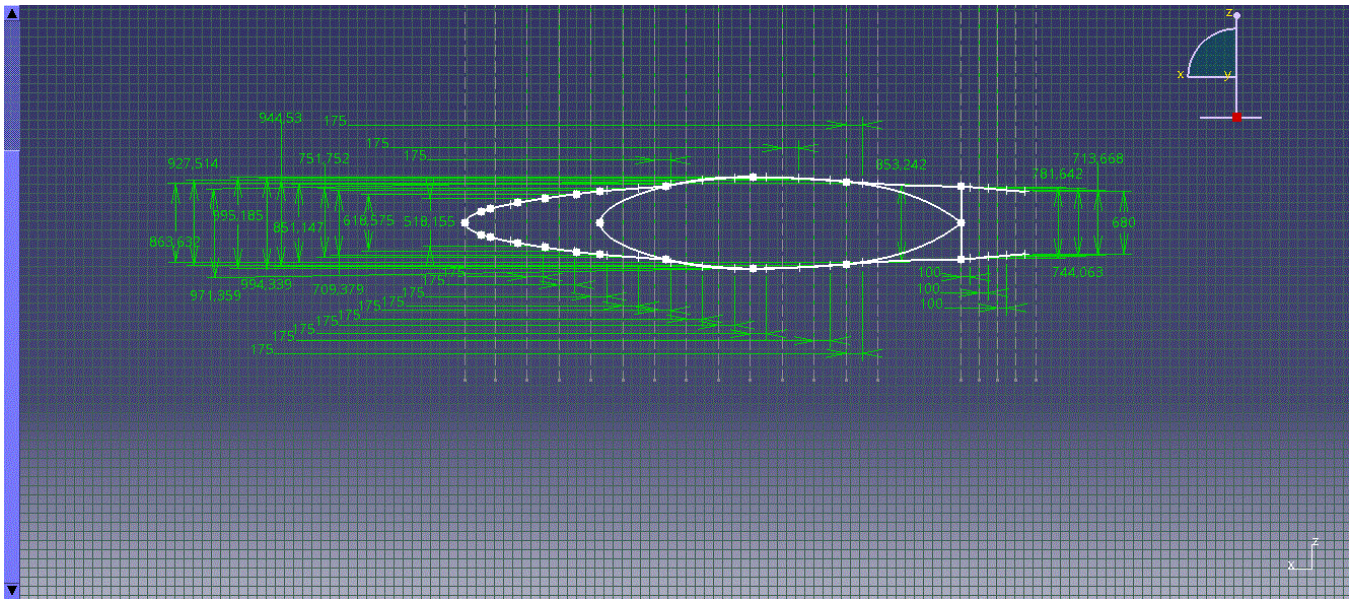


Figure 3.25 - Fuselage division for the upper wing.

The results for the shift on the aerodynamic center of the upper wing and its position are presented next.

$$AC_{W\_UP} = 4.69\ [m]$$

$$\Delta AC_{W\_UP} = -0.067\ [m]$$

Lift

The upper wing is equipped with the ailerons panel, so the lift generated by the upper wing is incremented or decremented by the deflection of these panels.

As the aileron is a primary control surface it was dimensioned considering the lateral stability and control characteristics desired for the airplane, its development is presented on the topic related to it.

The parameters obtained for the aerodynamic characterization related to the lift generated by the upper wing are presented next. Note that it is used the equation for the lift increment due the global wash field.

$$CL_{\alpha_{W\_UP}} = 0.0835\ [1/°]$$

$$CL_{\alpha=0_{W\_UP}} = 0.1483$$

$$\Delta CL_{\alpha_{W\_UP}} = 0.0564\ [1/°]$$

$$C_{L_{W_{\delta A}}} = 0.0234\ [1/°]$$

Drag

All the consideration done for the lower wing is valid for the upper wing. The aerodynamic parameters defined for the drag formulation are the same of the lower wing.

3.4.2.4. Biplane canard

Initially there are presented below the aerodynamic parameters defined or estimated, which were applied on the aerodynamic dimensioning of the biplane canard. The span efficiency factor for the biplane canard is obtained as defined on the theory chapter, this value is considered the same for the lower canard and for the upper canard.

The upper canard was positioned intending to diminish its vortex wake interference on the lower wing, and in consequence reduce the interference of the lower canard vortex wake on the lower wing too.

$$S_{aero_{CAN\_BIP}} = 2.01\ [m^2]$$

$$\mu_{CAN} = 1$$

$$r_{CAN} = 1$$

$$GAP_{CAN\_B}/b_{CAN\_B} = 0.093$$

$$\sigma_{CAN} = 0.68$$

$$e_{CAN\_B} = 0.595$$

$$AR_{CAN\_B} = 4.05$$

$$\lambda_{CAN\_B} = 1$$

3.4.2.5. Lower canard

There are presented below the aerodynamic parameters that were defined or estimated, which were applied on the aerodynamic dimensioning of the lower canard.

As the stall is related to the aspect ratio and the Reynolds number for a given aerodynamic surface, the aspect ratio of the lower canard was defined just a bit bigger than that for the lower and upper wings with the objective to contribute to the canard reach the stall first the wings, and as the Reynolds number for the lower canard is considerably lower than that for the both wings, it contributes for the canard to stall first too.

$$\bar{C}_{CAN\_LOW} = 0.40\ [m]$$

$$S_{aero_{CAN\_LOW}} = 1.01\ [m^2]$$

$$AR_{CAN\_LOW} = 8.1$$

$$\lambda_{CAN\_LOW} = 1$$

Aerodynamic center

Respecting the theory of biplanes, the initial position of the aerodynamic center of the lower canard will be considered at 23% of the $\bar{C}_{CAN\_LOW}$.

As well as for the wings, the aerodynamic center of the lower canard suffers a shift along the x axis due the interference of the fuselage. Next are presented on the Figure 3.26 and on the Figure 3.27 the divisions done on the fuselage that were used to estimate the shift on aerodynamic center of the lower canard employing the Equation 2.131 to the Equation 2.133.

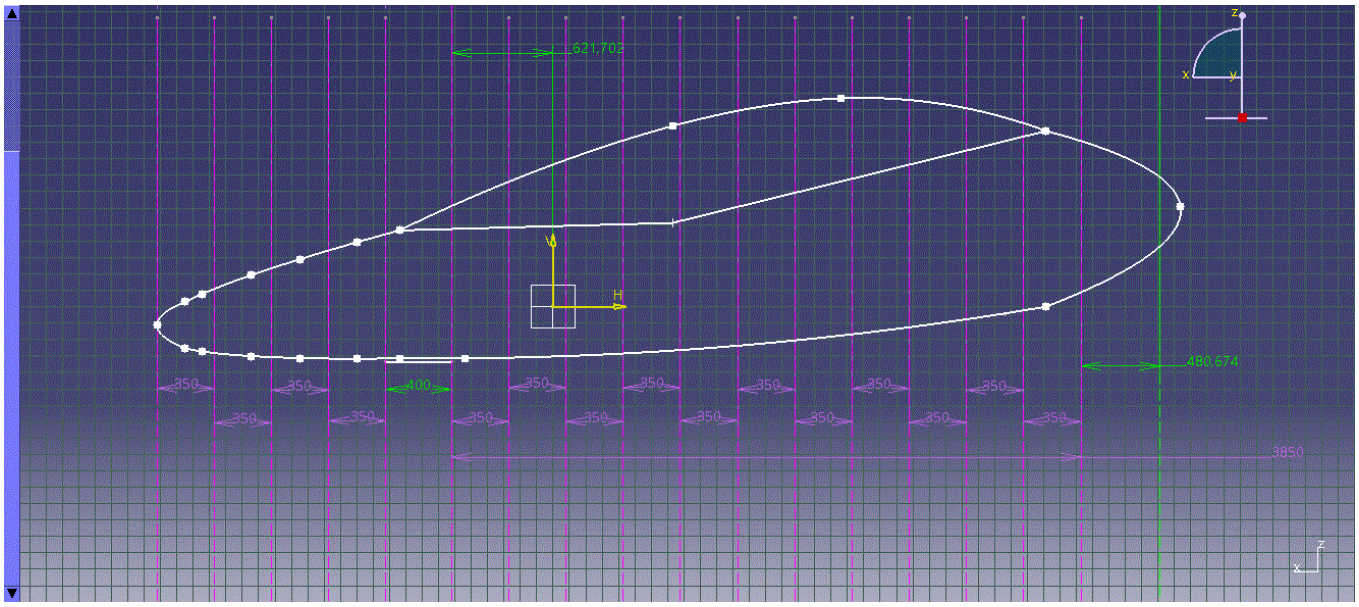


Figure 3.26 - Fuselage division for the lower canard.

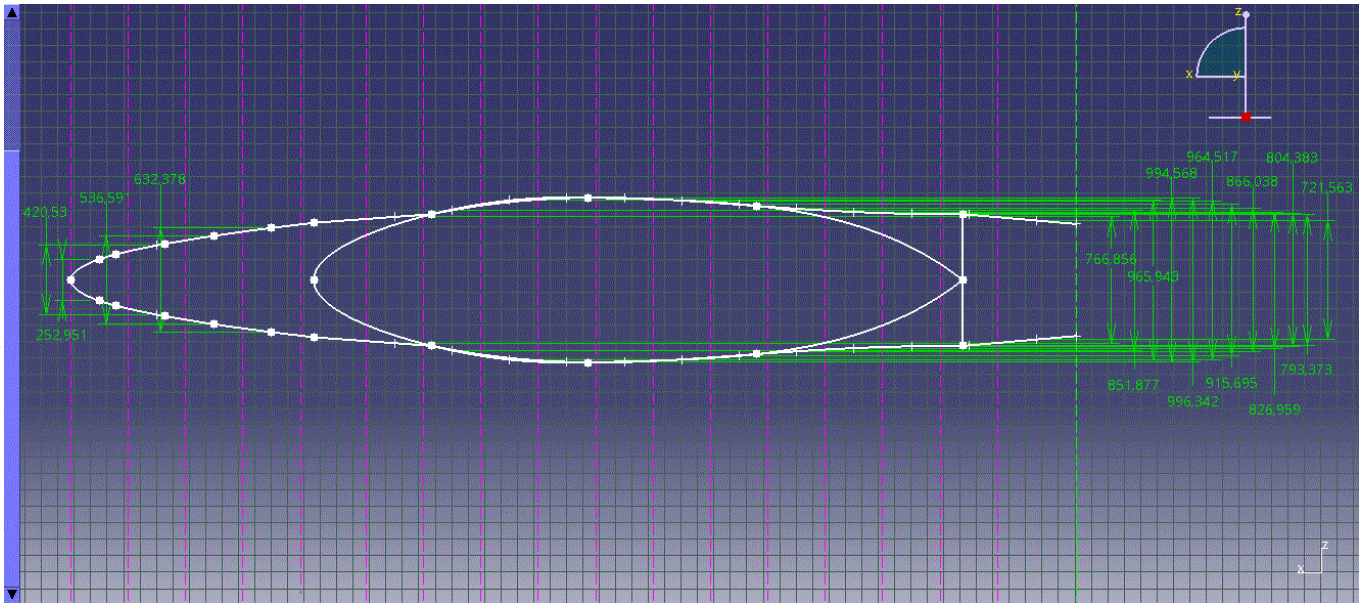


Figure 3.27 - Fuselage division for the lower canard.

The results for the shift on the aerodynamic center of the lower canard and its position are presented below.

$$AC_{CAN\_LOW} = 1.09\ [m]$$

$$\Delta AC_{CAN\_LOW} = -0.402\ [m]$$

Analyzing the results above, it's clear the huge shift on the aerodynamic center, positioning it out of the lower canard when compared to the shift on the wings aerodynamic centers. Assessing the formulation, is noted that this result is due the relation between the geometric parameters of the fuselage, of the lower canard and of the wings, as the canard is smaller than each wing, the canard naturally suffers an interference due the fuselage bigger than that suffered by the wings.

Lift

The lift generated by the lower canard is incremented or decremented by the deflection of the elevators that equip it.

As the elevator is a primary control surface it was dimensioned considering the longitudinal stability and control characteristics desired for the airplane, its development is presented on the topic related to it.

The parameters obtained for the aerodynamic characterization related to the lift generated by the lower canard are presented next. Note that is used the equation for the lift increment due the global wash field.

$$CL_{\alpha_{CAN\_LOW}} = 0.0783\ [1/°]$$

$$CL_{\alpha=0_{CAN\_LOW}} = 0.0$$

$$\Delta CL_{\alpha_{CAN\_LOW}} = 0.2587\ [1/°]$$

$$C_{L_{CAN\_LOW_{\delta E}}} = 0.0524\ [1/°]$$

Drag

The aerodynamic parameters defined for the drag formulation of the lower canard are presented below.

$$R_{cf} = 1.065$$

$$R_{LS} = 1.07$$

3.4.2.6. Upper canard

All the considerations done for the lower canard are valid for the upper canard. The aerodynamic parameters that were defined or estimated, which were applied on the aerodynamic dimensioning of the upper canard are presented next.

$$\bar{C}_{CAN\_UP} = 0.40\ [m]$$

$$S_{aero_{CAN\_UP}} = 1.01\ [m^2]$$

$$AR_{CAN\_UP} = 8.1$$

$$\lambda_{CAN\_UP} = 1$$

Aerodynamic center

As well as was done for the lower canard, the initial position of the aerodynamic center of the upper canard will be considered at 23% of the $\bar{C}_{CAN\_UP}$.

Once the positioning of the upper canard on the fuselage is just a bit behind of the lower canard, the divisions of the fuselage were considered the same, resulting in exactly the same huge value of shift for the aerodynamic center.

The results for the shift on the aerodynamic center of the upper canard and its position are presented next.

$$AC_{CAN\_UP} = 1.19\ [m]$$

$$\Delta AC_{CAN\_UP} = -0.402\ [m]$$

Lift

All considerations done for the lower canard are valid for the upper canard. The parameters obtained for the aerodynamic characterization related to the lift generated by the upper canard are presented next.

$$CL_{\alpha_{CAN\_UP}} = 0.0783\ [1/°]$$

$$CL_{\alpha=0_{CAN\_UP}} = 0.0$$

$$\Delta CL_{\alpha_{CAN\_UP}} = 0.0592\ [1/°]$$

$$C_{L_{CAN\_UP_{\delta E}}} = 0.0524\ [1/°]$$

Drag

The same parameters applied for the lower canard are valid for the upper canard.

3.4.2.7. Vertical tails

The aerodynamic parameters that were defined or estimated for the aerodynamic dimensioning of both vertical tails are presented below.

$$\bar{C}_{VT\_LEF} = 0.68\ [m]$$

$$S_{aero_{VT\_LEF}} = 0.76\ [m^2]$$

$$AR_{VT\_LEF} = 1.64$$

$$\lambda_{VT\_LEF} = 0.69$$

$$\bar{C}_{VT\_RIG} = 0.68\ [m]$$

$$S_{aero_{VT\_RIG}} = 0.76\ [m^2]$$

$$AR_{VT\_RIG} = 1.64$$

$$\lambda_{VT\_RIG} = 0.69$$

Despite the airplane UFU-1 to be equipped with two vertical tails, it does not characterize a biplane configuration, therefore, the span efficiency factor for each surface was estimated applying the conventional equation presented on the theory, and its results are showed below.

$$e_{VT\_LEF} = 0.68$$

$$e_{VT\_RIG} = 0.68$$

Aerodynamic center

As the vertical tails do not suffer the interference of the fuselage, there is no shift on its respective aerodynamic centers, which are located at 25% of each mean aerodynamic chord. The values are presented next.

$$AC_{VT\_LEF} = 5.47\ [m]$$

$$AC_{VT\_RIG} = 5.47\ [m]$$

Lift

With respect to the lift generated by the vertical tail surfaces, some commentaries must be done. First, on the calculus to estimate the sidewash, as the vertical tails are positioned between both wings, which are at distances equivalents from the fuselage centerline, its position is assumed $Z_w = 0$. Second, the aspect ratio considered on the estimative for the sidewash is that of the biplane wing.

The parameters obtained for the aerodynamic characterization related to the lift generated by the two vertical tails are presented below.

$$CL_{\alpha_{VT\_LEF}} = 0.0393\ [1/°]$$

$$C_{L_{VT\_LEF_{\delta R}}} = 0.0226\ [1/°]$$

$$CL_{\alpha_{VT\_RIG}} = 0.0393\ [1/°]$$

$$C_{L_{VT\_RIG_{\delta R}}} = 0.0226\ [1/°]$$

Drag

The aerodynamic parameters defined for the drag formulation of the vertical tail surfaces are presented below.

$$R_{vtf} = 1; \quad there\ is\ no\ interference\ between\ vertical\ tail\ and\ booms$$

$$R_{LS} = 1.07$$

3.4.2.8. Fuselage

Lift

The parameters defined or calculated for the aerodynamic characterization related to the lift generated by the fuselage are presented next.

$$k_{wf} = 0.997$$

$$C_{L_{\alpha_{W-F}}} = 0.0833\ [1/°]$$

$$C_{L_{\alpha_F}} = -0.00025\ [1/°]$$

Drag

The parameters defined or calculated for the aerodynamic characterization related to the drag generated by the fuselage are presented next.

$$R_{wf} = 1.065$$

$$\frac{l_f}{d_f} = 4.959$$

$$\eta_{fus} = 0.62$$

$$c_{d_c} = 1.2$$

3.4.2.9. Complete airplane

Next are presented the main aerodynamic results for the airplane as a whole, as parameters for the lift and the drag, and the estimative for the position of the lateral airplane aerodynamic center.

$$S_{wet_{ap}} = 72.4\ [m^2]$$

Lateral aerodynamic center

The location of the aerodynamic center of the side area of the complete airplane was estimated based on the area segments presented on the Figure 3.28 .

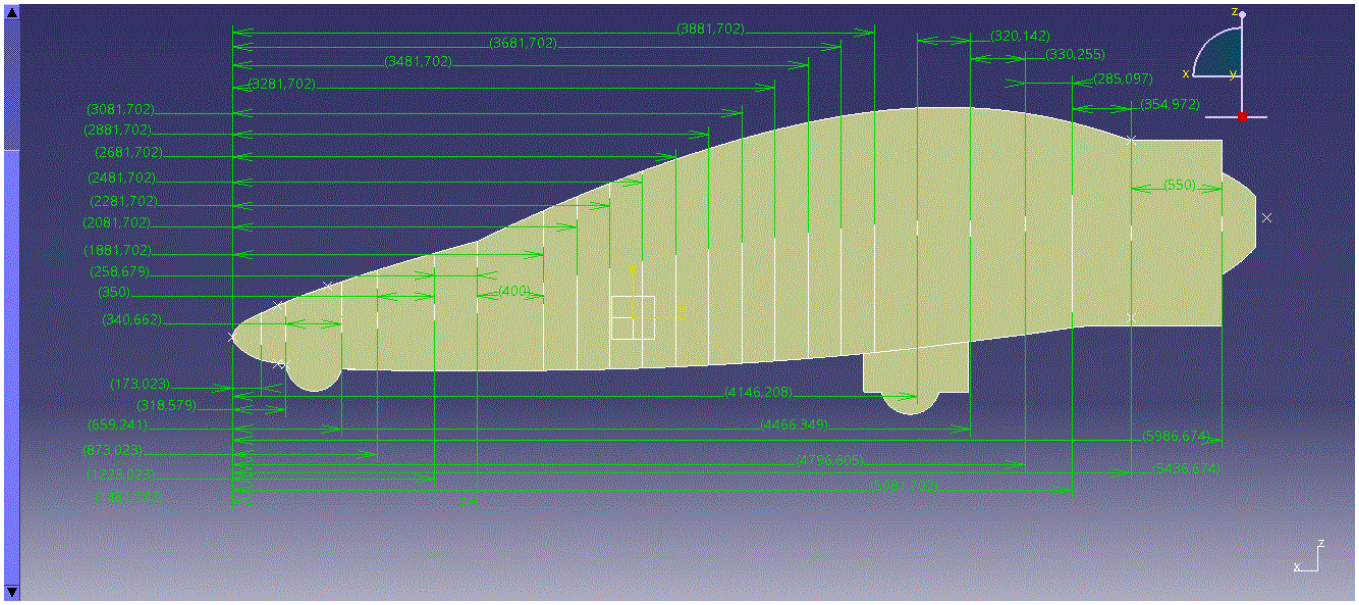


Figure 3.28. Complete airplane side segmentation.

The geometric parameters obtained from the figure above, as the area of each segment and its location along the x axis, were applied on the Equation 2.134, the result is presented below.

$$AC_{AP\_SIDE} = 3.48\ [m]$$

Lift

Related to the lift generated by the complete airplane some results obtained must be commented here, as that obtained for the canards. During the lift simulations done for the canards, it was observed that the lifts generated by each surface are completely different between them, assessing these results was observed that this occur due the parcels $\Delta CL_{\alpha_{CAN\_LOW}}$ and $\Delta CL_{\alpha_{CAN\_UP}}$, which presented very different values as can be observed above on the results for the canard surfaces. The values for these parcels are coherent to its formulation, once they are function of the global wash field in which, each canard is immersed. The same

phenomenon occurs to the wings. The Table 3.5 resumes these values to facilitate the comparison.

Table 3.5 - Lift increment due the global wash fields, comparison.

ΔCL_α	$[1/°]$
Lower wing	0.1376
Upper wing	0.0564
Lower canard	0.2587
Upper canard	0.0592

One important aerodynamic parameter is the airplane lift curve slope that is presented on the Figure 3.29 for the cruise flight configuration.

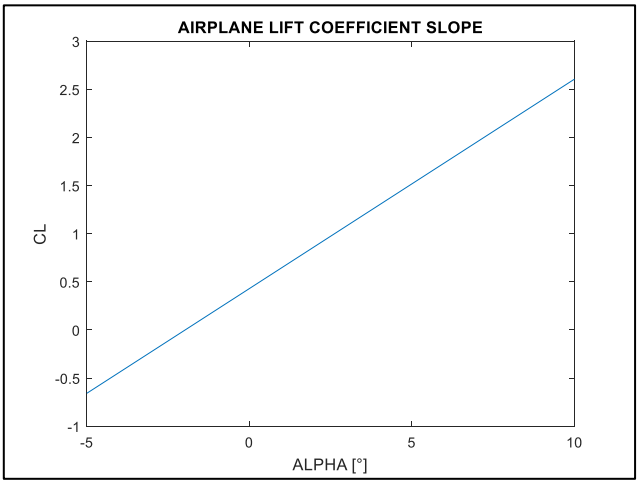


Figure 3.29 - Airplane UFU-1 lift curve slope.

Running the algorithm of the APPENDIX C for many airplane and flight parameters settings, it was observed that the lift curve slope for the airplane remains the same, its numerical result is given next.

$$CL_{\alpha_{AP}} = 0.2176\ [1/°]$$

Below there are presented some relative lift results related to the total lift generated by the airplane, for the flight configurations 12 and 27 showed on the Table 3.6 to the Table 3.9.

$$L_{FUS_{12}} = 0.052\ [\%]$$

$$L_{W\_LOW_{12}} = 36.15\ [\%]$$

$$L_{W\_UP_{12}} = 25.09\ [\%]$$

$$L_{W\_B_{12}} = 61.24\ [\%]$$

$$L_{CAN\_LOW_{12}} = 27.63\ [\%]$$

$$L_{CAN\_UP_{12}} = 11.27\ [\%]$$

$$L_{CAN\_B_{12}} = 38.90\ [\%]$$

$$L_{FUS_{27}} = 0.05\ [\%]$$

$$L_{W\_LOW_{27}} = 37.97\ [\%]$$

$$L_{W\_UP_{27}} = 26.35\ [\%]$$

$$L_{W\_B_{27}} = 64.32\ [\%]$$

$$L_{CAN\_LOW_{27}} = 25.44\ [\%]$$

$$L_{CAN\_UP_{27}} = 10.37\ [\%]$$

$$L_{CAN\_B_{27}} = 35.81\ [\%]$$

Drag

Regarding the drag formulation of the complete airplane, it is interesting to note that the factor of interference between the fuselage and each wing and for the interference between the fuselage and each canard assume the same value, once it is function of the Reynolds number of the fuselage.

For simplification of the calculus, it was fixed in $R_{wf} = 1.065$, once the flight condition of interest is the cruise, and its change with the Reynolds variation is not broad.

Next there are presented the drag results for the flight configurations 12 and 27 showed on the Table 3.6 to the Table 3.9.

$$D_{12} = 467.142\ [N]$$

$$Di_{12} = 86.987\ [N]$$

$$\frac{Di_{12}}{D_{12}} = 18.62\ [\%]$$

$$D_{27} = 460.395\ [N]$$

$$Di_{27} = 80.758\ [N]$$

$$\frac{Di_{27}}{D_{27}} = 17.54\ [\%]$$

Drag polar

The Figure 3.30 presents the drag polar of the airplane for the trimmed cruise flight configuration 12 presented on the Table 3.6 to the Table 3.9. Note that this flight condition is located on the bottom region of the curve, near its lowest point, what indicates that the airplane in the cruise flight presents a very good aerodynamic efficiency. The lift and drag coefficients for the airplane trimmed on this flight point are presented next.

$$CL_{12} = 0.1974$$

$$CD_{12} = 0.0199$$

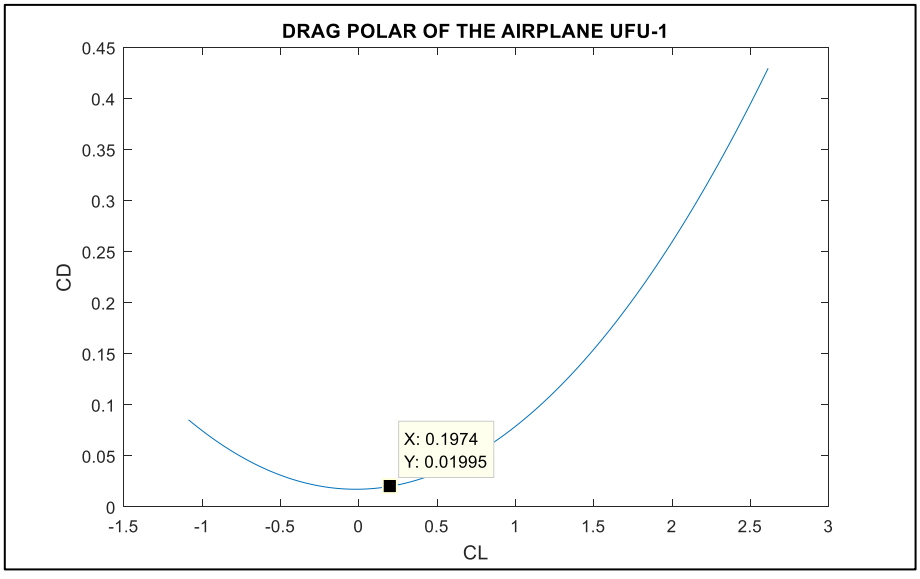


Figure 3.30 - Drag polar for W=473.9 Kgf, FL080 and V = 235 [km/h].

The Figure 3.31 presents the drag polar for the flight configuration 27 presented on the Table 3.6 to the Table 3.9. The comments done above are valid for this flight configuration. The lift and drag coefficients for the airplane trimmed on this flight point are presented next.

$$CL_{27} = 0.1991$$

$$CD_{27} = 0.0197$$

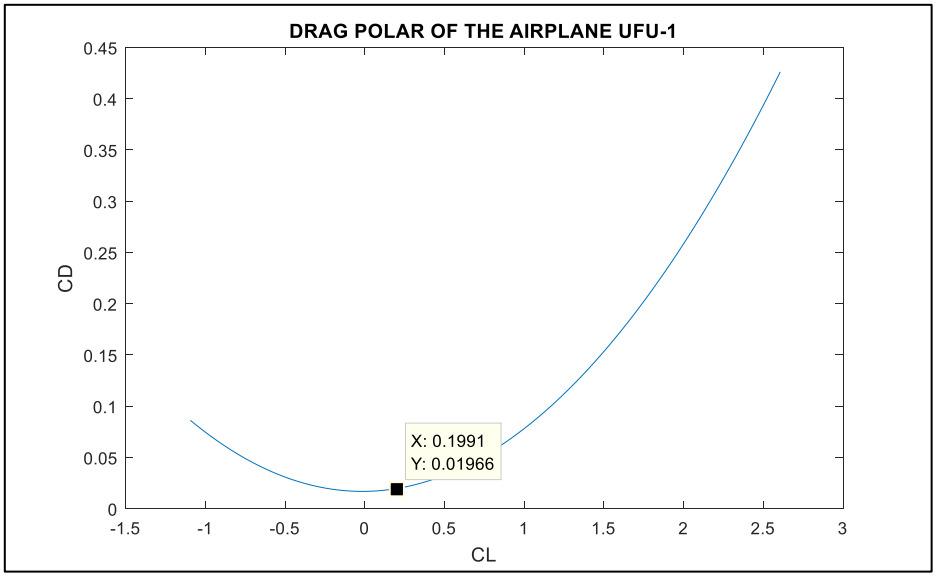


Figure 3.31 - Drag polar for W=478.9 Kgf, FL080 and V = 235 [km/h].

3.5. DYNAMICS OF FLIGHT

Initially the development of the calculus of the dynamics of flight were based on the CG-Weight envelope presented on the Figure 3.2, but, the results for the longitudinal dynamic stability and even for the longitudinal static stability demonstrated that the airplane for most of the CG-Weight configurations is divergent.

Based on these first results was decided to dislocate forward the location of the fuel tank with the intention to turn the airplane more stable longitudinally. The first change, positioned the fuel tank well behind the position of the second pilot, but even in this position the airplane presented to be still unstable, then was decided to locate the fuel tank the most forward as possible, between the two spars of the lower wing, but, even at this location the envelope of the airplane resultant is too limited.

The Table 3.6 and the Table 3.7 provides the mass configurations considered for the dynamics of flight of the airplane UFU-1, the Table 3.8 and the Table 3.9 provides the trimmed cruise flight configurations for each of these mass configurations. Based on the Table 3.6 a new CG-Weight envelope was defined and presented on the Figure 3.32.

As will be explained into the next topics, considering the Table 3.7, the last column indicate the algorithm used for the initial assessing of the longitudinal response of the airplane, if there is a letter ***A*** it means that this mass and flight configuration presented to be statically and dynamically stable when evaluated at the algorithm that uses the aerodynamic areas of the wings and tails, and if there is a letter ***R*** it means that was employed the algorithm that uses the reference areas of the wings and tails. This algorithm is presented on the APPENDIX C and was used for to obtain all the results related to the dynamics of flight presented into this chapter.

Table 3.6 - Mass configurations for dynamics of flight assessing.

Configuration	***W_P1 [kgf]***	***W_P2 [kgf]***	***W_f [kgf]***	***W_Pay_L [kgf]***	***CG [mm]***	***W [kgf]***
1	0	0	0	0	3963	367.9
2	0	0	33	0	3967	400.9
3	50	0	0	0	3848	417.9
4	50	0	0	20	3727	437.9
5	50	0	33	0	3859	450.9
6	50	0	33	20	3746	470.9
7	50	90	0	0	3875	507.9
8	50	90	0	20	3774	527.9
Continues on the next page						

9	50	90	33	0	3883	540.9
10	50	90	33	20	3787	560.9
11	86	0	0	0	3781	453.9
12	86	0	0	20	3672	473.9
13	86	0	33	0	3796	486.9
14	86	0	33	20	3693	506.9
15	86	86	0	0	3816	539.9
16	86	86	0	20	3722	559.9
17	86	86	33	0	3827	572.9
18	86	86	33	20	3738	592.9
19	90	0	0	0	3774	457.9
20	90	0	0	20	3666	477.9
21	90	0	33	0	3789	490.9
22	90	0	33	20	3688	510.9
23	90	50	0	0	3796	507.9
24	90	50	0	20	3698	527.9
25	90	50	33	0	3809	540.9
26	90	50	33	20	3716	560.9
27	60	0	33	18	3741	478.9
28	60	0	33	30	3679	490.9
29	60	50	33	23	3742	533.9
30	60	50	33	37	3677	547.9

Table 3.7 - Mass configurations for dynamics of flight assessing continuation.

Configuration	***I_xx [kg*m^2]***	***I_yy [kg*m^2]***	***I_zz [kg*m^2]***	***I_xz [kg*m^2]***	***MATLAB - Code***
1	304.686	499.081	628.961	189.689	-----
2	332.015	543.846	685.376	206.703	-----
3	346.093	566.907	714.439	215.468	-----
4	362.656	594.038	748.63	225.779	-----
5	373.422	611.673	770.854	232.482	-----
6	389.985	638.803	805.045	242.794	-----
7	420.627	688.995	868.298	261.87	-----
8	437.19	716.125	902.489	272.182	-----
9	447.956	733.76	924.713	278.884	-----
10	464.519	760.891	958.904	289.196	-----
11	375.907	615.742	775.982	234.029	-----
12	392.47	642.873	810.173	244.34	R
13	403.235	660.508	832.397	251.043	-----
14	419.798	687.638	866.588	261.355	A
15	447.127	732.404	923.003	278.369	-----
Continues on the next page					

16	463.69	759.534	957.194	288.681	-----
17	474.456	777.169	979.419	295.383	-----
18	491.019	804.299	1013.61	305.695	-----
19	379.219	621.168	782.821	236.091	-----
20	395.782	648.299	817.012	246.403	R
21	406.548	665.934	839.236	253.105	-----
22	423.111	693.064	873.427	263.417	A
23	420.627	688.995	868.298	261.87	-----
24	437.19	716.125	902.489	272.182	-----
25	447.956	733.76	924.713	278.884	-----
26	464.519	760.891	958.904	289.196	-----
27	396.61	649.655	818.721	246.918	A
28	406.548	665.934	839.236	253.105	R
29	442.159	724.264	912.746	275.275	A
30	453.753	743.256	936.68	282.494	R

Table 3.8 - Trimmed cruise flight configuration for dynamics of flight assessing.

Configuration	***V [km/h]***	***FL [ft]***	***ρ [kg/m^3]***	***α (°)***
12	235	8000	0.9	-1.1
14	-----	8000	0.9	----
20	235	8000	0.9	-1.1
22	-----	8000	0.9	----
27	235	8000	0.9	-1.06
28	-----	8000	0.9	----
29	-----	8000	0.9	----
30	-----	8000	0.9	----

Table 3.9 - Trimmed cruise flight configuration for dynamics of flight assessing continuation.

Configuration	***Flap [°]***	***CAN_i [°]***	***ELEV [°]***	***ENG [%]***	***cd_W***	***cd_Can***	***cd_Vt***	***cf_fus***
12	0	3.06	0	70	0.00494	0.00509	0.00514	0.0026
14	0	-----	0	70	-----	-----	0.00514	-----
20	0	-----	0	70	-----	-----	0.00514	0.0026
22	0	-----	0	70	-----	-----	0.00514	-----
27	0	2.88	0	70	0.00494	0.00498	0.00514	0.0026
28	0	-----	0	70	-----	-----	0.00514	-----
29	0	-----	0	70	-----	-----	0.00514	-----
30	0	-----	0	70	-----	-----	0.00514	-----

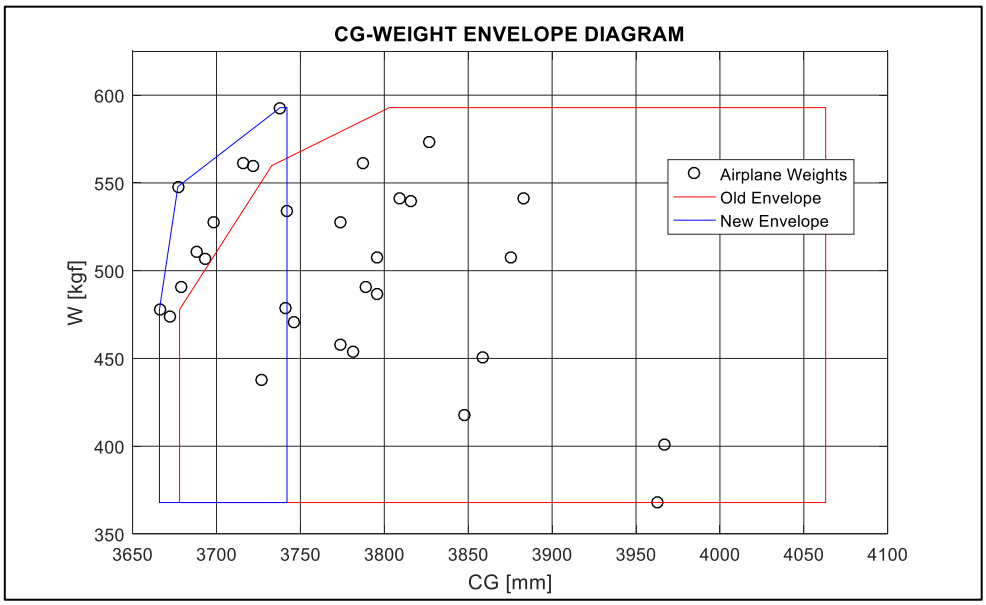


Figure 3.32 - CG-Weight envelopes comparison.

As mentioned at the beginning of the chapter of the theory of dynamics of flight, this work adopted the aerodynamic areas as parameter for the estimates of the in-flight airplane behavior.

But, it was decided to realize these calculi based on the reference areas too, and compare the results obtained by the two methods. The results based on the reference areas showed to be more conservative relative to that obtained based on the aerodynamic areas.

3.5.1. Longitudinal static stability

As numerical simulations or wind tunnel tests were not performed in order to define more accurate values, the tail efficiency for both canards were assumed as showed next.

$$\eta_{CAN\_LOW} = 0.9$$

$$\eta_{CAN\_UP} = 0.8$$

By analyzing the equations related to the longitudinal static stability some observations may be done.

Considering the horizontal tail volume coefficient Equation 2.32, for an airplane with conventional configuration in which the horizontal tail is located behind the wing; by fixing the

value of the area of the wing (aerodynamic or reference), and remembering that the reference area will always to be bigger or equal the aerodynamic one, as much as greater to be the difference between the aerodynamic area and the reference area of the horizontal tail, it is valid to affirm that less conservative will be the result of static longitudinal stability generated by this surface, once the stability will increase; the opposite is valid for an airplane with canard configuration. For the airplane UFU-1 particularly, the difference between the reference area and the aerodynamic area of the biplane wing is relatively smaller than that observed for the canards, therefore the calculus based on the reference areas are more conservative compared to that based on the aerodynamic ones.

Considering the Equation 2.157 and the Equation 2.158, as much as greater to be the difference between the aerodynamic and reference areas of the wing, less conservative will be the result of static longitudinal stability generated by the fuselage, once the stability will increase.

The Table 3.10 to the Table 3.12 and the Figure 3.33 and the Figure 3.34 present the results for the longitudinal static stability of the airplane UFU-1 based on the theory proposed on this work, which consider the aerodynamic areas of the aerodynamic surfaces. These results were based on the trimmed cruise flight configurations given on the Table 3.6 to the Table 3.9.

Table 3.10 - Longitudinal static stability results.

Config	***α (°)***	**β (°)**	***Cm_0_C_Low***	***Cm_α_C_Low [1/rad]***	***Cm_0_C_Up***	***Cm_α_C_Up [1/rad]***
12	-10 to 10	0	0.1315	4.653	0.0083	-0.172
27	-10 to 10	0	0.1285	4.777	0.0085	-0.177

Table 3.11 - Longitudinal static stability results continuation.

Config	***Cm_0_W_Low***	***Cm_α_W_Low [1/rad]***	***Cm_0_W_Up***	***Cm_α_W_Up [1/rad]***	***Cm_0_f***	***Cm_α_f [1/rad]***
12	-0.0531	-0.505	-0.2029	-5.338	-0.0244	0.229
27	-0.0419	-0.142	-0.1917	-4.975	-0.0244	0.229

Table 3.12 - Longitudinal static stability results continuation.

Config	***Cm_0***	***Cm_α [1/rad]***	***X_NP [%]***	***Stat.Margin***
12	-0.1406	-1.133	8.68	0.05003
27	-0.1209	-0.288	8.13	0.00690

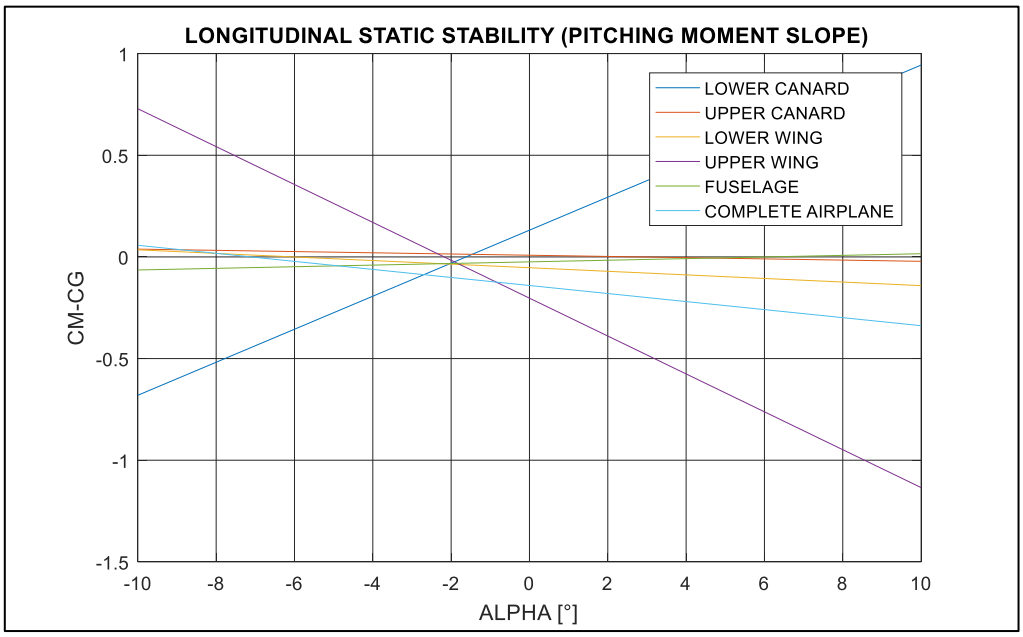


Figure 3.33 - Longitudinal static stability for the configuration 12.

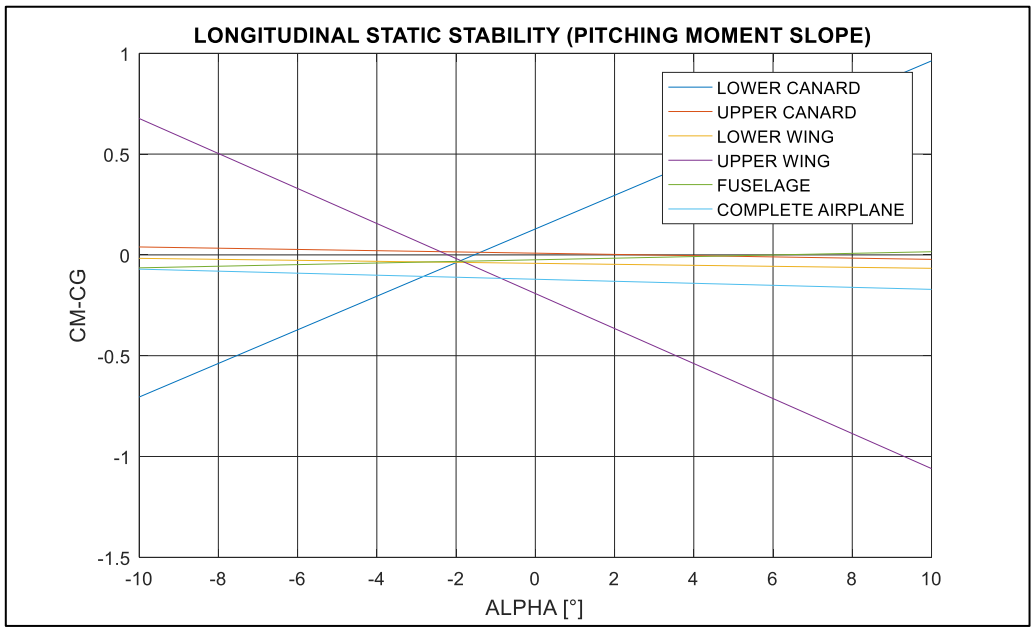


Figure 3.34 - Longitudinal static stability for the configuration 27.

The results indicate that the airplane is stable even for the most rear CG position, but in this condition the longitudinal static stability is very marginal as compared to the limits showed on the Table 2.23.

3.5.2. Longitudinal control

The theory predicts that the longitudinal control of an airplane must have power enough for lift up the nose during the take-off phase for the most forward CG position and heaviest weight as possible.

The longitudinal control dimensioning is directly dependent of the pitch moment generated by the airplane at the lift-off, and as predicted by the theory, the pitch moment of an airplane is the sum of the moments generated by its components.

For the pitch moment generated by the fuselage its length was assumed as been its main aerodynamic chord, and its aerodynamic area was assumed as been the projected area at the plane xy. The drag generated by the fuselage was assumed having its application point at a location $z = 1\ [m]$ from the runway.

The flaps were considered on its maximum deflection $\delta_f = 20\ [°]$, once it increases the pitch down moment.

Initially the dimensioning of the longitudinal control of the airplane assumed fixed canards and was based on the earliest mass properties obtained during the conceptual design phase and some operational parameters considered at the sea level (ISA) which are presented below.

$$W = 655\ [Kgf]$$

$$CG = 3.64\ [m]$$

$$I_{yy} = 888\ [Kg \cdot m^2]$$

$$\alpha = 0\ [°]$$

$$V_{MC} = 0{,}8 \cdot V_{STALL} = 19.32 \times 0.8 = 15{,}46\ [m/s] = 55.66\ [km/h]$$

$$Eng.Pow = 100\ [\%]$$

$$\eta_P = 49\ [\%]$$

The elevators dimensions and its deflections were defined as the maximum as possible, however, the results indicated that the elevators had not enough power to rotate the airplane at the lift-off, and at cruise flight its deflection should be the kept near the maximum positive limit, what led to a configuration with an entire movable canards and no elevators, but this configuration also shown to be insufficient. The final solution was to assume a configuration with

movable canards equipped with elevators and a higher lift-off speed as indicated on the Table 3.13.

Once it was decided that the longitudinal control will be performed by movable canards equipped with elevators, some calculus were done for to define the take-off behavior of the airplane related to the dynamics of flight, the performance results are presented into the pertinent chapter. The Table 3.13 to the Table 3.14, the Figure 3.35 and the Figure 3.36 provides the parameters used and the results for these analysis. Note that the angle of attack considered in the tables is that obtained for the airplane with all the tires in contact with the runway as presented on the Figure 3.67.

Table 3.13 - Longitudinal control dimensioning parameters and results.

Configuration	V_lof [km/h]	FL [ft]	ρ [kg/m^3]	α (°)	cd_W	cd_Can	cd_Vt	cf_fus
20	105	3100	1.047	-1.429	0.00660	0.0071	0.00520	0.00295
30	105	3100	1.047	-1.429	0.00660	0.00752	0.00520	0.00295

Table 3.14 - Longitudinal control dimensioning parameters and results continuation.

Configuration	Flap [°]	CAN_i [°]	ELEV [°]	ENG [%]	η_P	θ_2_dot [°/s^2]
20	20	3.9	20	100	0.73	10.05
30	20	4.3	20	100	0.73	9.88

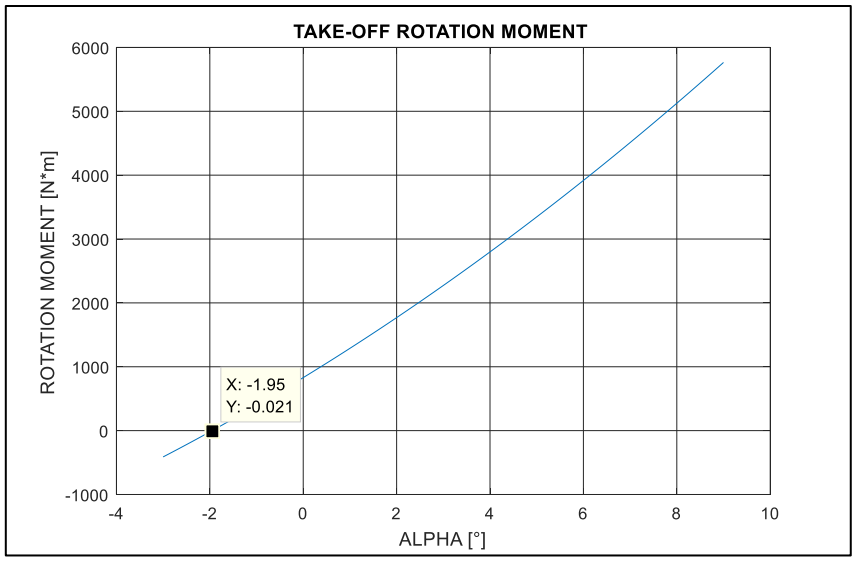


Figure 3.35 - Take-off rotation moment for the configuration 20.

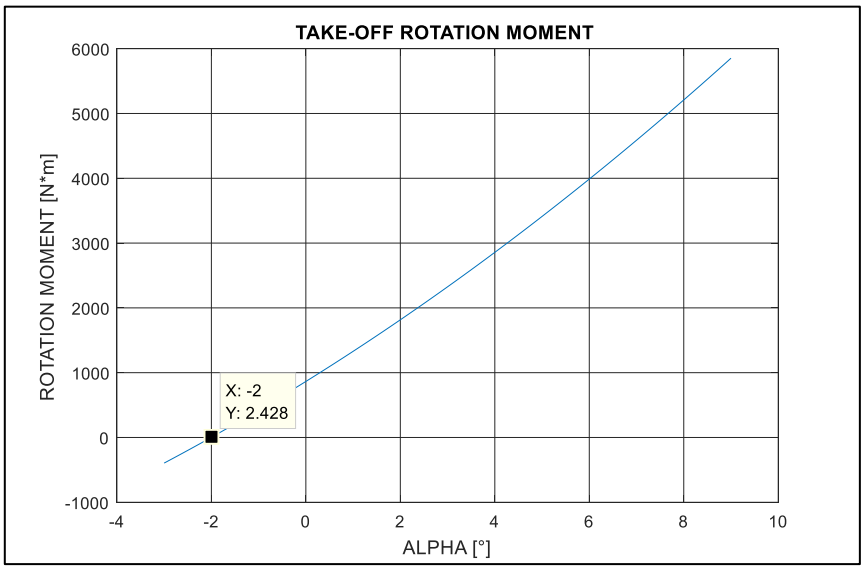


Figure 3.36 - Take-off rotation moment for the configuration 30.

For both configurations the lift-off angular acceleration is in accordance with the predicted by the bibliography as given on the Table 2.25.

3.5.2.1. Elevators parameters

The elevators dimensioning was done for the maximum geometrical limits as was mentioned before. Its maximum deflections were assumed conservatively, once there were not performed CFD simulations nor wind tunnel tests, which could indicate the maximum deflections for which do not occurs the flow separation. Next there are presented the geometrical parameters which are valid for both panels.

$$C_{root_E} = 0.20\ [m]$$

$$C_{tip_E} = 0.20\ [m]$$

$$b_E = 2.1\ [m]$$

$$b_{E_i} = 0.4\ [m]$$

$$S_E = 0.420\ [m^2]$$

$$\delta_{E\_up.max} = -20\ [°]$$

$$\delta_{E\_down.max} = +20\ [°]$$

$$\tau_E = 0.67$$

$$C_E/\bar{C}_{CAN} = 0.5$$

$$b_E/b_{CAN} = 0.65$$

$$S_E/S_{CAN} = 0.32$$

3.5.3. Lateral static stability

The parameters that were obtained for the estimative of the lateral static stability are given next.

$$\frac{C_{l_\beta}}{\Gamma} = -0.00026$$

$$\Delta C_{l_\beta} = 0$$

As can be observed on the theory, the estimative of the lateral static stability is obtained by applying a simple equation, and based on the values of the parameters for this equation the airplane has a neutral lateral behavior.

$$Cl_{\beta_{CG}} = 0$$

3.5.4. Lateral control

As it was considered for the elevators, the most critical flight conditions are that in low speeds, once the rolling speeds tend to be lower, this way, its dimensioning of the ailerons was done for the stall speed.

Stall speed

The stall speed was estimated based on the angle of stall of the canard airfoil $\alpha = 10.75\ [°]$ and on the airplane and flight configurations that lead to the lowest as possible speed

as presented on the Table 3.15 and on the Table 3.16, one considering the airplane at the airport level and the other for the airplane at the cruise flight level.

Rolling estimative

For the rolling estimative the airplane drag parameter was assumed conservatively as being $C_{D_R} = 1{,}2$. The results for the airplane lateral control are presented on the Table 3.15 and on the Table 3.16.

Table 3.15 - Lateral control dimensioning parameters and results.

Configuration	V_S [km/h]	FL [ft]	ρ [kg/m^3]	α (°)	CL	cd_W	cd_Can	cd_Vt	cf_fus
12	63.85	3100	1.047	7.7	2.31	0.01025	0.03740	0.00554	0.0032
12	69.17	8000	0.9	7.7	2.29	0.01025	0.03740	0.00554	0.0032

Table 3.16 - Lateral control dimensioning parameters and results continuation.

Configuration	Flap [°]	CAN_i [°]	ELEV [°]	Ail_lef [°]	Ail_rig [°]	ENG [%]	P_ss [°/s]
12	20	3.06	20	20	-25	0	167.4
12	0	3.06	20	20	-25	0	181.4

As the results indicate despite the low air dynamic pressure, for the maximum specified deflections of the ailerons the roll angular speeds are high, what mean a high command authority.

3.5.4.1. Ailerons parameters

Considering that the ailerons panels and the flaps panels are the same, and are installed at the same position, and due the fact that the lower wing and the upper wing to be the same structure, the dimensioning of the ailerons had as constraint the location of the main landing gear legs, with the intention of avoiding the interference between both. Next are presented the geometrical parameters which are valid for both panels.

$$C_{root_A} = 0.2\ [m]$$

$$C_{tip_A} = 0.2\ [m]$$

$$b_A = 1.5\ [m]$$

$$b_{A_i} = 1.9\ [m]$$

$$S_A = 0.300\ [m^2]$$

$$\delta_{A\_up.max} = -25\ [°]$$

$$\delta_{A\_down.max} = +20\ [°]$$

$$\tau_A = 0.28$$

$$C_A/\bar{C}_{W\_UP} = 0.22$$

$$b_A/b_{W\_UP} = 0.41$$

$$S_A/S_{W\_BIP} = 0.045$$

3.5.5. Directional static stability

The parameters used for to estimate the directional static stability contribution of the wing-body and vertical tails are showed below.

$$h_1 = 0.804\ [m]$$

$$h_2 = 1.380\ [m]$$

$$h = 1.450\ [m]$$

$$\frac{{l_f}^2}{S_{F\_s}} = 5.965$$

$$\sqrt{\frac{h_1}{h_1}} = 0.763$$

$$\frac{h}{w_f} = 1.450$$

$$k_{n\_12} = 0.00169$$

$$k_{n\_27} = 0.00185$$

$$\eta_V = 1$$

For the estimative of the directional static stability were considered the same configurations that were considered for the longitudinal static stability, and were obtained at the same way, based on the theory proposed on this work, that consider the aerodynamic areas of the aerodynamic surfaces. The results are presented on the Table 3.17, on the Figure 3.37 and on the Figure 3.38.

Table 3.17 - Directional static stability results.

Config	α (°)	β (°)	Cn_β_W_f [1/rad]	Cn_β_VT_L [1/rad]	Cn_β_VT_R [1/rad]	Cn_0	Cn_β [1/rad]
12	0	-10 to 10	-0.0671	0.0294	0.0294	0	-0.0082
27	0	-10 to 10	-0.0733	0.0283	0.0283	0	-0.0167

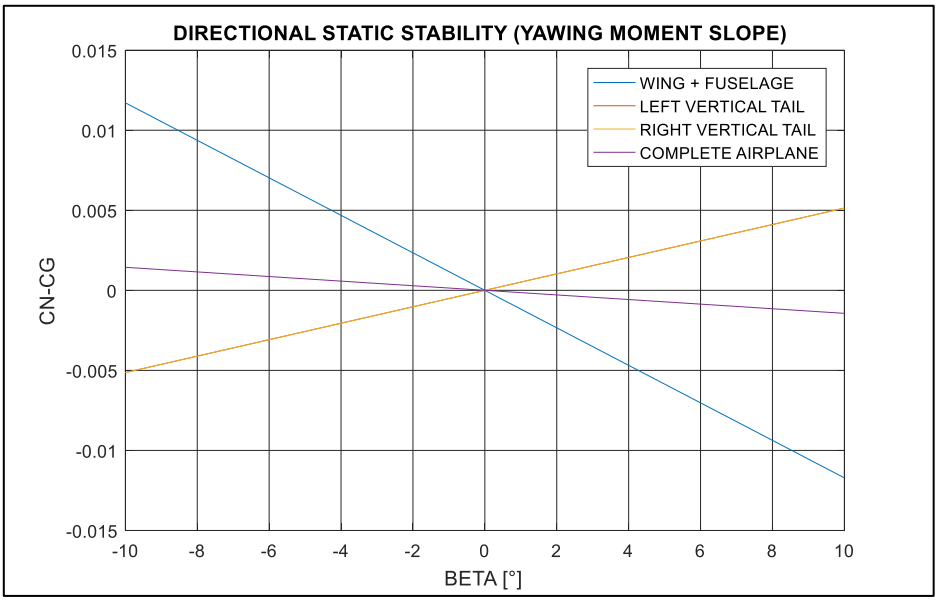


Figure 3.37 - Directional static stability for the configuration 12.

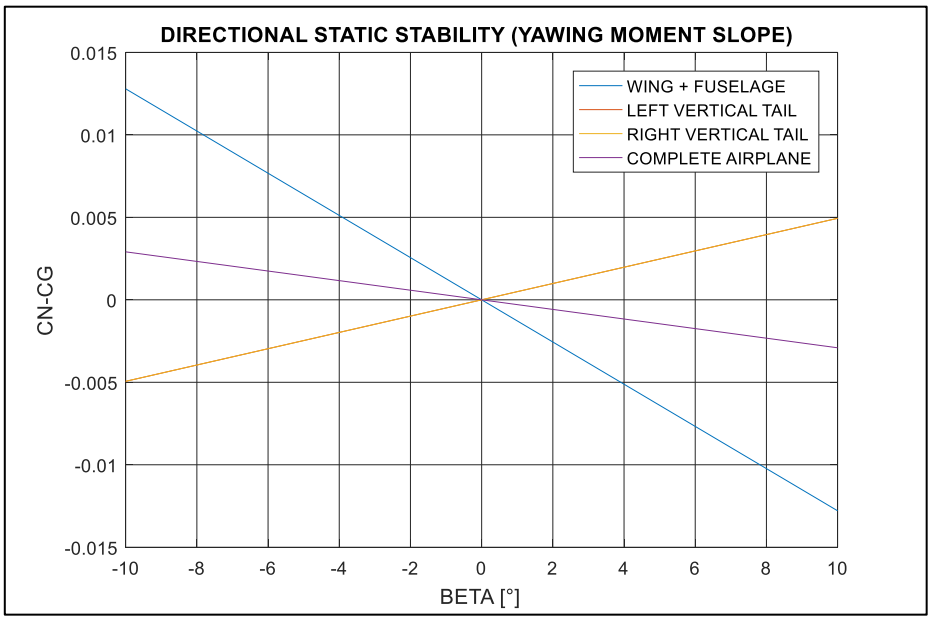


Figure 3.38 - Directional static stability for the configuration 27.

The results show that the airplane is marginally instable for the directional static stability as compared to the limits showed on the Table 2.23. By running some simulations, it was obtained that the airplane becomes directionally static stable for $CG = 3.6\ [m]$.

3.5.6. Directional control

For the parameters used to estimate the directional control of the airplane were assumed the conservative values showed next.

$$C_{D_y} = 0{,}8$$

$$k_{f2} = 1{,}3$$

For dimensioning the rudders were considered what predict both the FAR 23 and CS-VLA, that consider a cross wind bigger than $0{,}2 \cdot V_{SO}$ and at least $10\ [\text{knots}] = 5.14\ [\text{m/s}]$ respectively. The estimates were performed for the CG located at the most behind position as possible, once this condition is the most critical for the directional control, due the smaller vertical tail volume coefficient. The parameters used and the results are presented on the Table 3.18 and on the Table 3.19.

Table 3.18 - Directional control dimensioning parameters.

Config	V_so [km/h]	Cross-Wind [m/s]	FL [ft]	ρ [kg/m^3]	α (°)	CL	cd_W	cd_Can	cd_Vt	cf_fus
27	63.64	3.54	3100	1.047	7.9	2.35	0.01088	0.03740	0.00554	0.0032
27	63.64	5.14	3100	1.047	7.9	2.35	0.01088	0.03740	0.00554	0.0032

Table 3.19 - Directional control dimensioning parameters and results.

Config	Flap [°]	CAN_i [°]	ELEV [°]	Rud_lef [°]	Rud_rig [°]	ENG [%]	σ [°]
27	20	2.88	20	-17.60	-17.60	0	31.45
27	20	2.88	20	-25.72	-25.72	0	50.80

The deflections of the rudders are coherent to the limits indicated by the bibliography, which are ± 30 [°]. The results indicate also the non-linearity between the rudder deflection and the crab angle.

3.5.6.1. Rudders parameters

Next are presented the geometrical parameters which are valid for both rudders. The parameter b_{R_i} is defined relative to the chord line of the root profile of the vertical tail.

$$C_{root_R} = 0.25\ [m]$$

$$C_{tip_R} = 0.25\ [m]$$

$$b_R = 0.9\ [m]$$

$$b_{R_i} = 0.1\ [m]$$

$$S_R = 0.225\ [m^2]$$

$$\delta_{R\_rig.max} = -30\ [°]$$

$$\delta_{R\_lef.max} = +30\ [°]$$

$$\tau_R = 0.575$$

$$C_R/\bar{C}_{VT} = 0.37$$

$$b_R/b_{VT} = 0.81$$

$$S_R/S_{VT} = 0.295$$

3.5.7. Lateral-Directional static stability & control coupling

Despite the lateral-directional coupling to be relevant and considered during the dimensioning of the airplane, there are no physical results of interest to present here. Next is presented just one parameter that is necessary to obtain the control derivative $Cn_{\delta A}$.

$$K = 0.232$$

3.5.8. Longitudinal dynamic stability

The longitudinal dynamic stability assess was done for the same configurations assessed at the longitudinal static stability, considering at the same way, the aerodynamic areas of the aerodynamic surfaces.

As the airplane UFU-1 has low speeds and accelerations, two derivatives related to the forward speed was assumed as showed next. The results are presented on the Table 3.20, Table 3.21, and on the Figure 3.39 to the Figure 3.42.

$$CD_u = 0$$

$$CM_u = 0$$

Table 3.20 - Longitudinal dynamic stability results.

Config	***α (°)***	***Cm_q [1/rad]***	***θ_disturb [°]***	***(ω_n)s_P [rad/s]***	***(ω_d)s_P [rad/s]***	***ξ_s_P***
12	-1.1	-2.406	10	10.030	7.699	0.641
27	-1.06	-2.539	10	6.617	1.731	0.965

Table 3.21 - Longitudinal dynamic stability results continuation.

Config	Vert.Disturb [m]	$(\omega_n)_{Phu}$ [rad/s]	$(\omega_d)_{Phu}$ [rad/s]	ξ_{Phu}
12	10	0.185	0.179	0.258
27	10	0.141	0.112	0.604

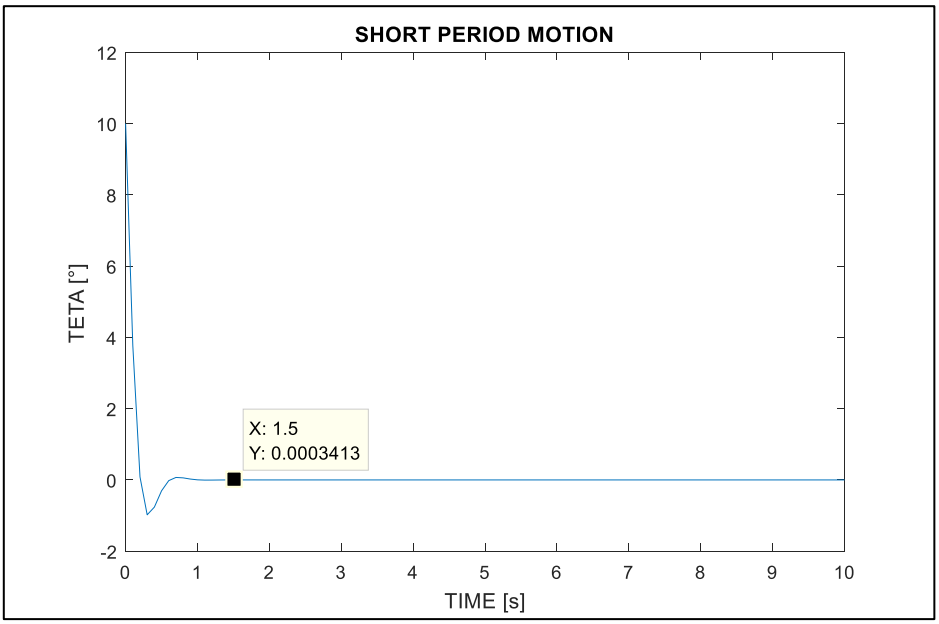


Figure 3.39 - Short period response for the configuration 12.

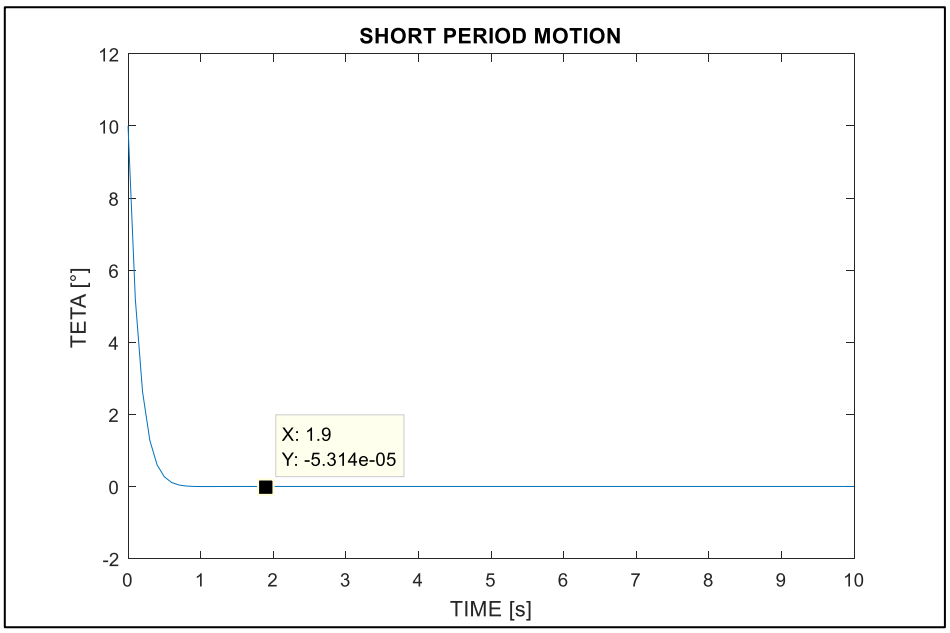


Figure 3.40 - Short period response for the configuration 27.

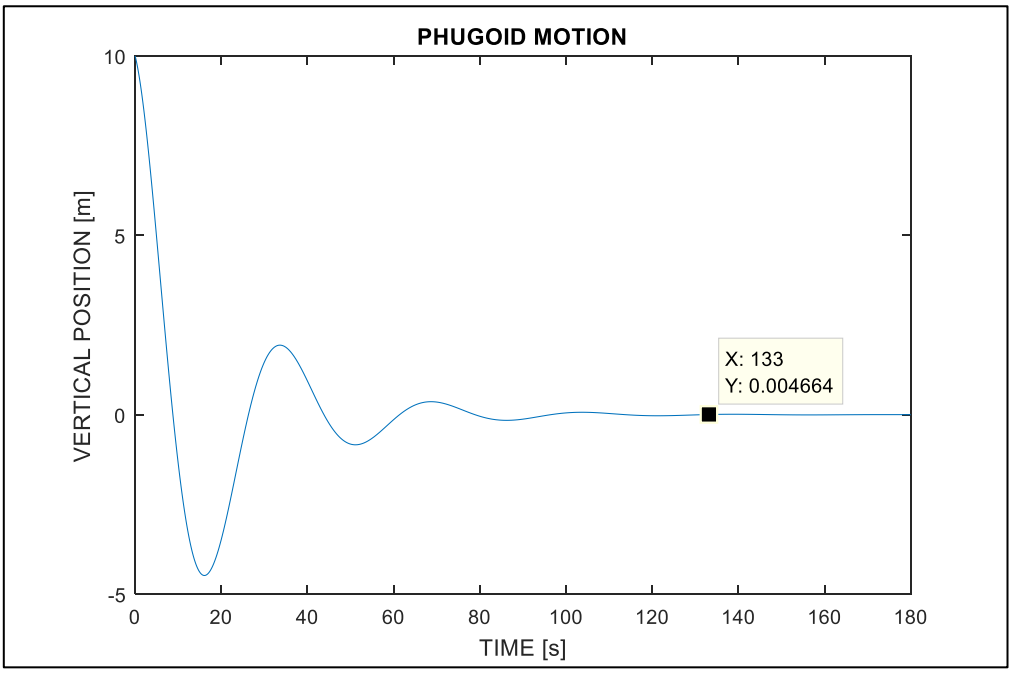


Figure 3.41 - Phugoid response for the configuration 12.

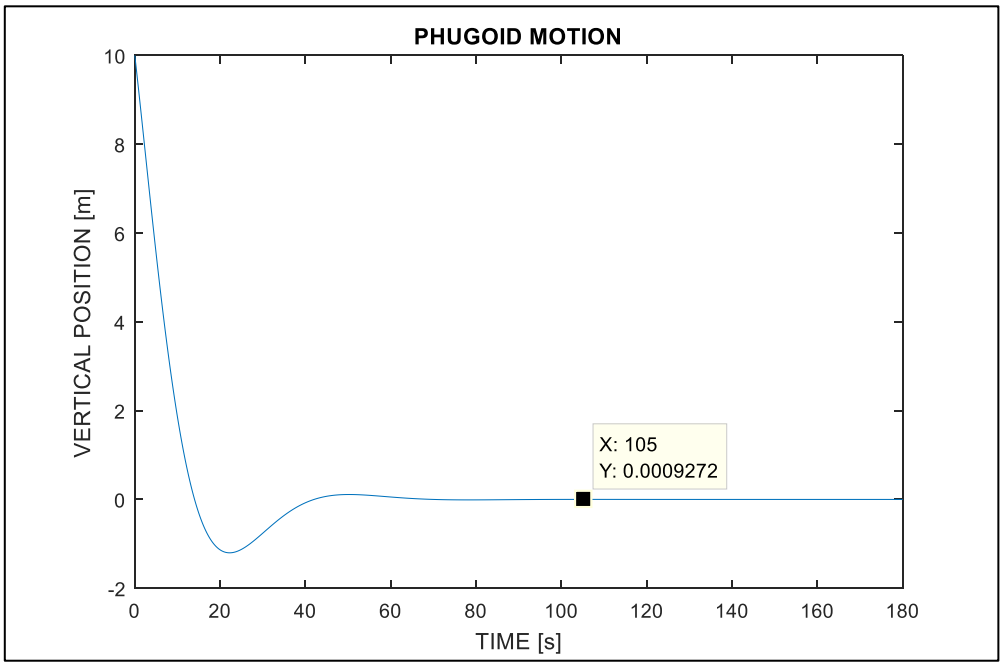


Figure 3.42 - Phugoid response for the configuration 27.

The two configurations simulated were that with the most rear CG and lowest weight possible, once this is the critical condition for the longitudinal dynamic stability of an airplane.

As the results indicate, the airplane is convergent for both modes at this rear CG limit, and both modes are inside the limits of the level 1 of flying qualities specified by the *MIL-F-8785C*.

3.5.9. Lateral-Directional dynamic stability

The directional dynamics stability was simulated for the same configurations that were considered for all the other static and dynamic stability, and the considerations done before are valid here. The results are presented on the Table 3.22, Table 3.23, and on the Figure 3.43 to the Figure 3.48.

Table 3.22 - Lateral-directional dynamic stability results.

Config	**β *(°)***	**θ_*0* *[°]***	***Cn_r [s/rad]***	***Rol_disturb [°]***	***(ω_n)Roll [rad/s]***	***(ω_d)Roll [rad/s]***	***ξ_Roll***
12	0	0	-0.0343	10	1363.68	0	1
27	0	0	-0.0317	10	1356.23	0	1

Table 3.23 - Lateral-directional dynamic stability results continuation.

Config	***Spi_disturb [°]***	***(ω_n)Spi [rad/s]***	***(ω_d)Spi [rad/s]***	***ξ_Spi***	***Dut_disturb [°]***	***(ω_n)Dut [rad/s]***	***(ω_d)Dut [rad/s]***	***ξ_Dut***
12	10	0.063	0	1	10	33.185	25.184	0.651
27	10	0.186	0	1	10	27.370	20.738	0.653

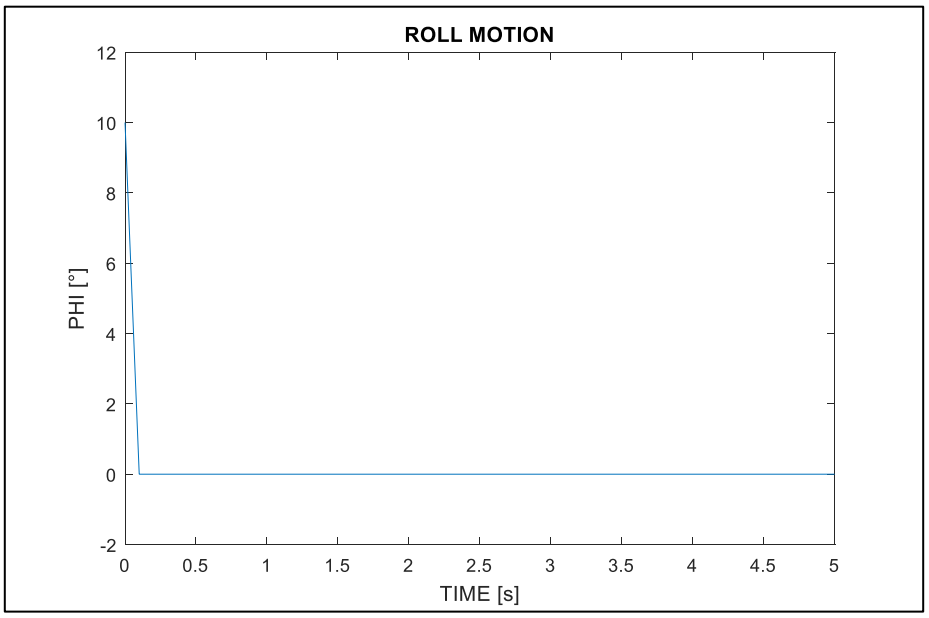


Figure 3.43 - Roll response for the configuration 12.

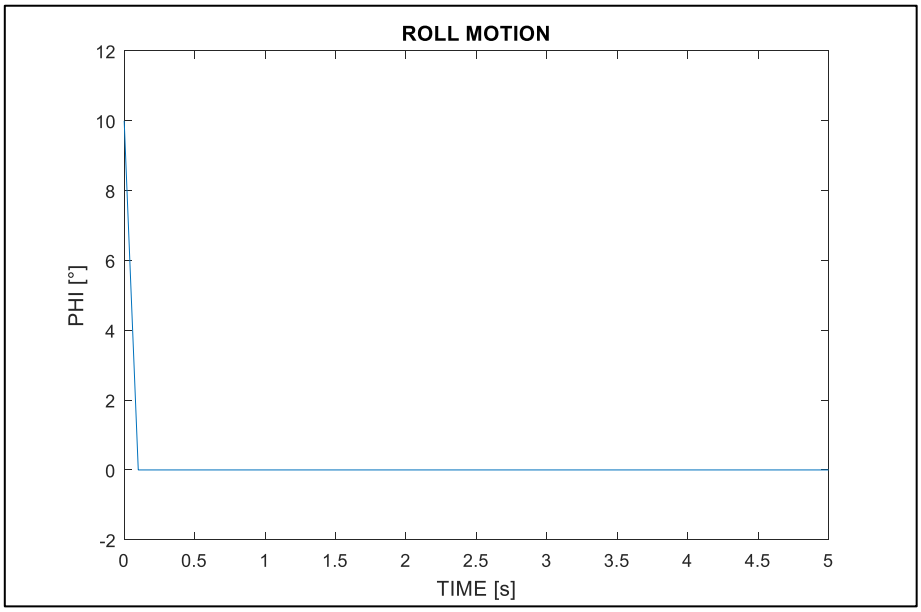


Figure 3.44 - Roll response for the configuration 27.

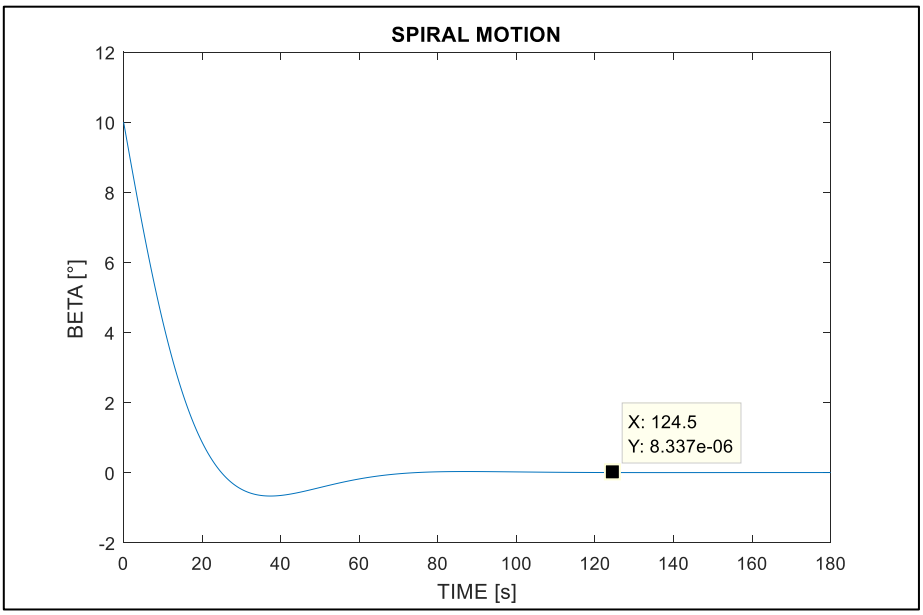


Figure 3.45 - Spiral response for the configuration 12.

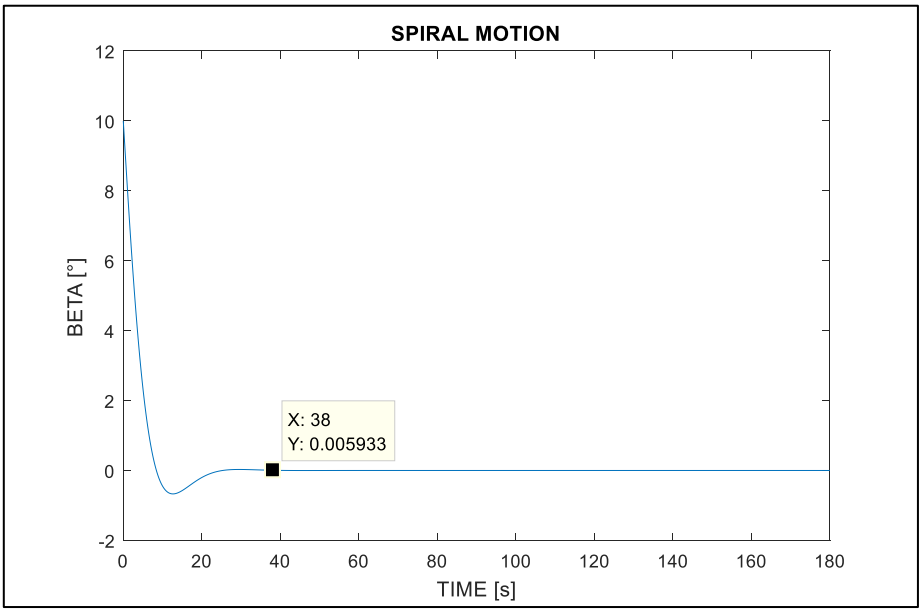


Figure 3.46 - Spiral response for the configuration 27.

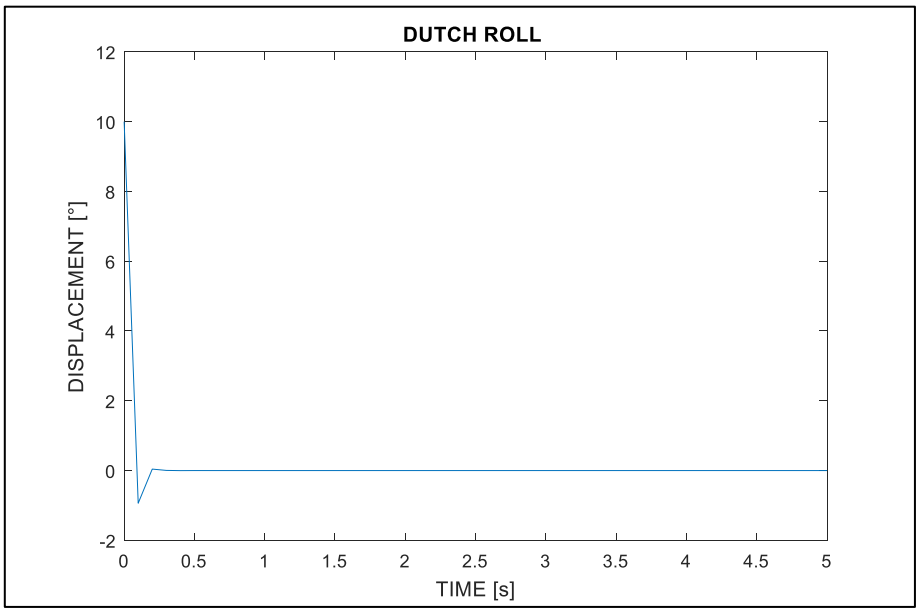


Figure 3.47 - Dutch-roll response for the configuration 12.

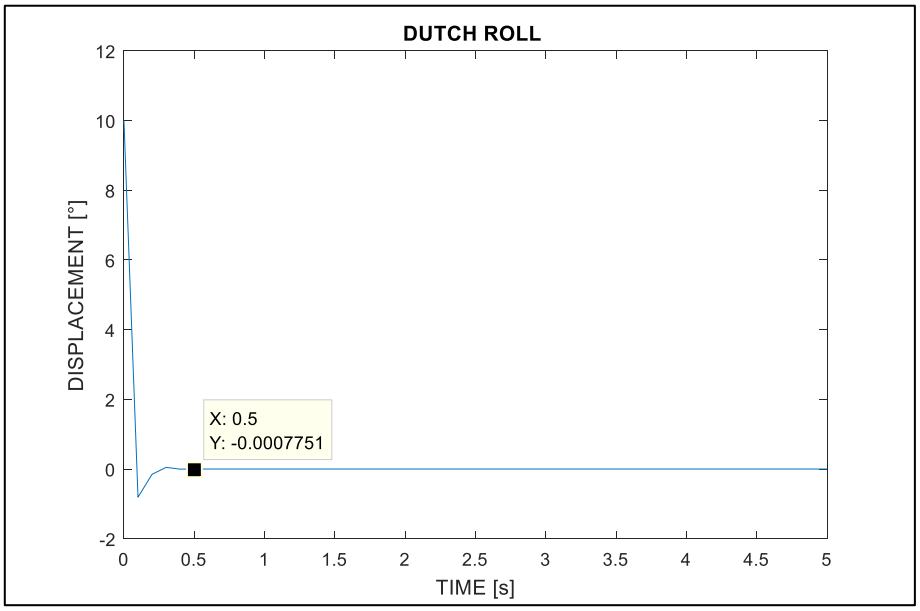


Figure 3.48 - Dutch-roll response for the configuration 27.

These results indicate that the airplane is inside the limits of the level 1 of flying qualities specified by the *MIL-F-8785C*.

Next there are presented the results of the dynamic derivative which are used for indicate if the airplane is resistant to enter into a spiral departure.

$$Cn_{\beta_{dyn\_12}} = -2.51 \times e^{-6}\ [1/°]$$

$$Cn_{\beta_{dyn\_27}} = -5.08 \times e^{-6}\ [1/°]$$

It is necessary make some comments related to the lateral-directional dynamic stability. As presented earlier, the directional static stability $Cn_{\beta_{CG}}$ of the airplane is marginally divergent. When a system presents a divergent static behavior, it is expected that the dynamic response be divergent too. But as presented above, the lateral-directional dynamic behavior of the airplane is convergent.

By inspecting the derivative $Cn_{\beta_{CG}}$ is verified that its most divergent result is 33.4% of the minimum value indicated on the Table 2.23, and the derivative $Cl_{\beta_{CG}}$ is neutral. As the lateral-directional dynamic stability is dependent of the marginal results of these two derivatives and several other parameters, the dynamic response resulted positive.

Finally the dynamic derivative $Cn_{\beta_{dyn}}$ presented results very marginal, what is one more indicative that, despite the airplane to be directional statically divergent, its dynamic response is convergent.

3.6. PERFORMANCE

For the estimates of the performance of the airplane UFU-1 it was defined to do some simple estimates relative to the main aspects which are important for the operation of the airplane.

Regarding the stall speed, this parameter is dependent of the airplane weight and aerodynamic configuration, so, some of the stall speeds necessary to estimate the characteristics of flight of the airplane were obtained into the chapter dedicated to the dynamics of flight and are available at the Table 3.15 and on the Table 3.18.

3.6.1. Excess of power and thrust

For the estimates of excess of power and thrust were considered the airplane and the trimmed cruise flight configurations 12 and 27 provided on the Table 3.6 to the Table 3.9. The results are presented on the Figure 3.49 to the Figure 3.56.

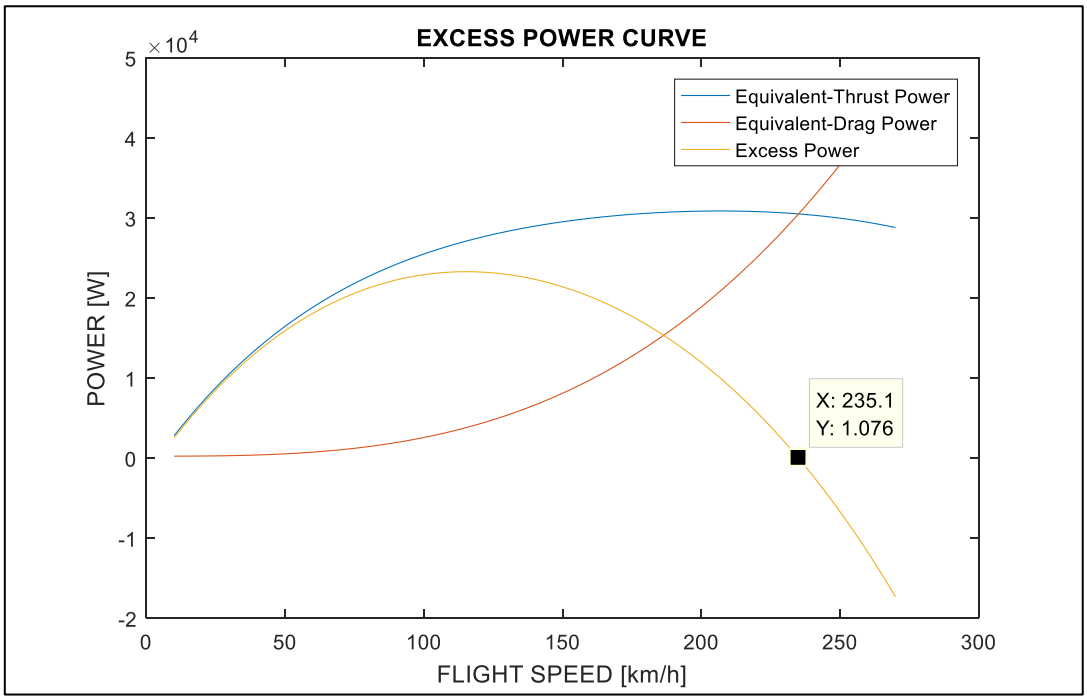


Figure 3.49 - Excess of power for the configuration 12 and engine power at 70%.

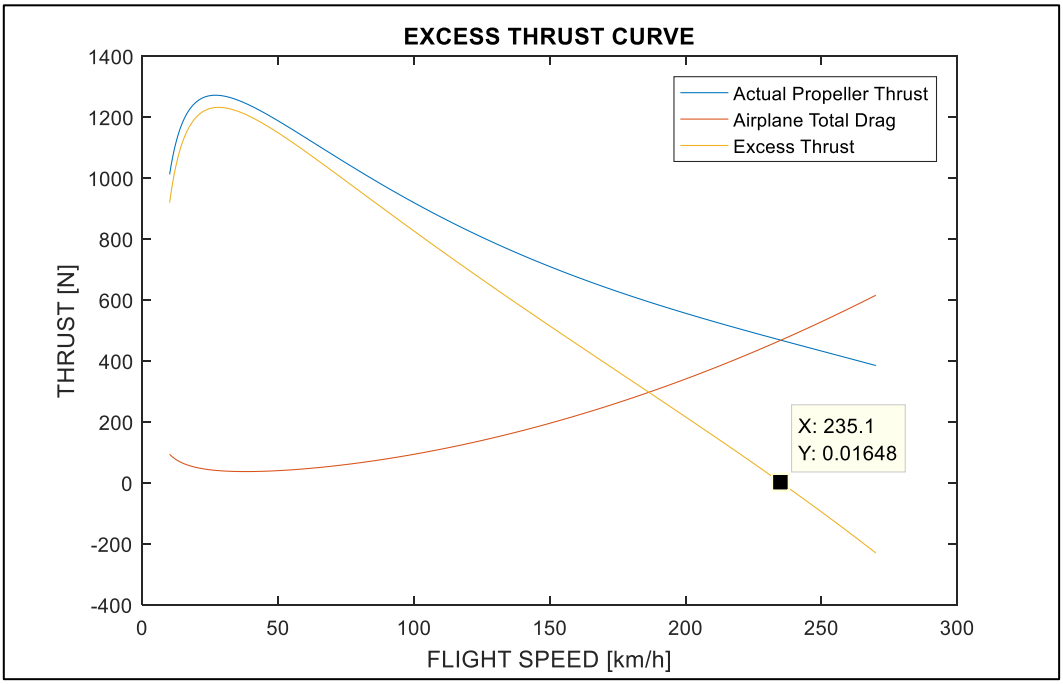


Figure 3.50 - Excess of thrust for the configuration 12 and engine power at 70%.

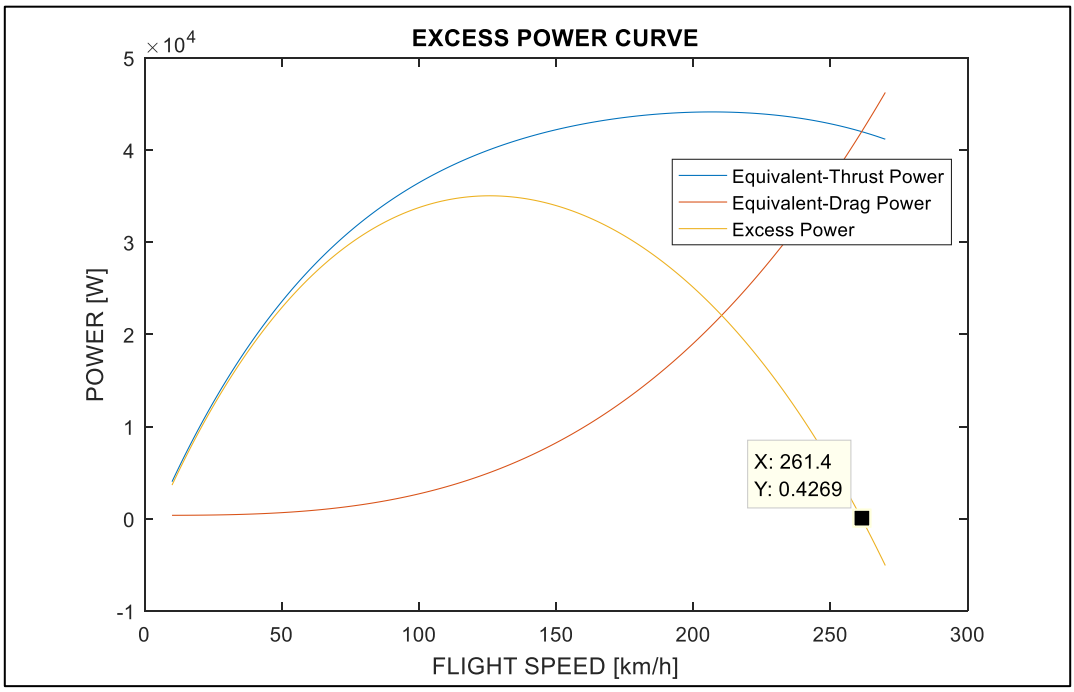


Figure 3.51 - Excess of power for the configuration 12 and engine power at 100%.

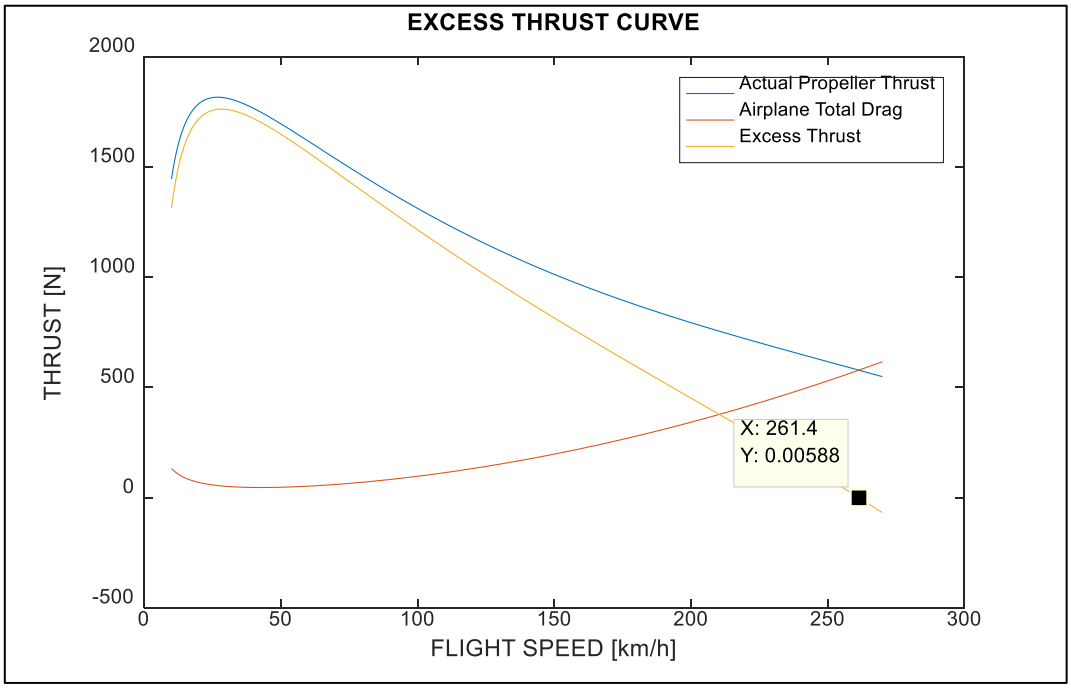


Figure 3.52 - Excess of thrust for the configuration 12 and engine power at 100%.

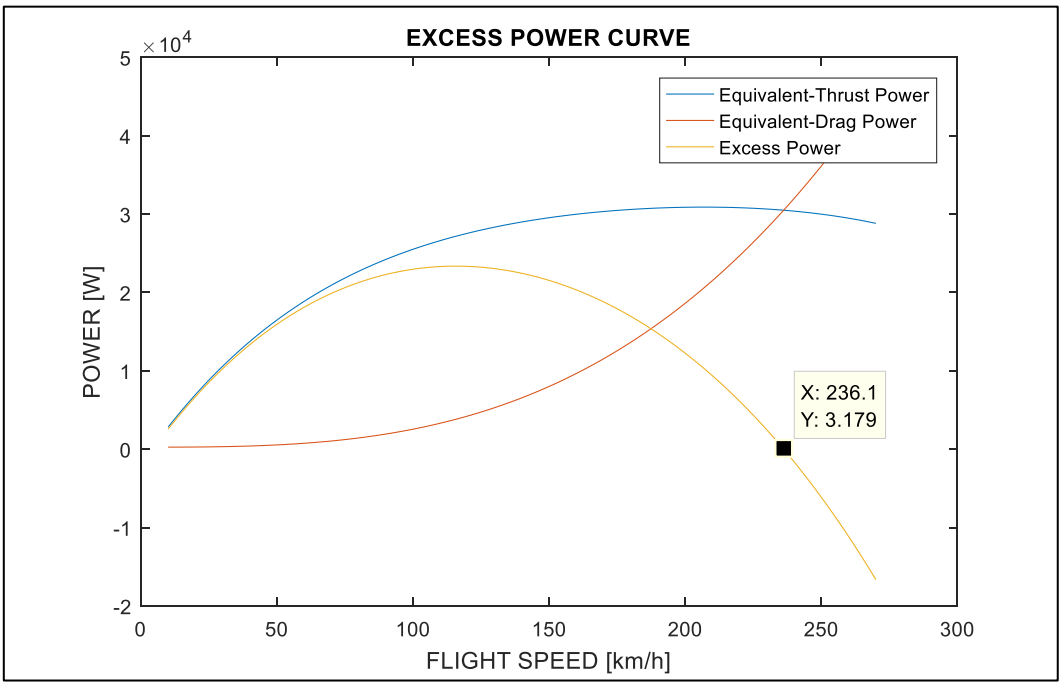


Figure 3.53 - Excess of power for the configuration 27 and engine power at 70%.

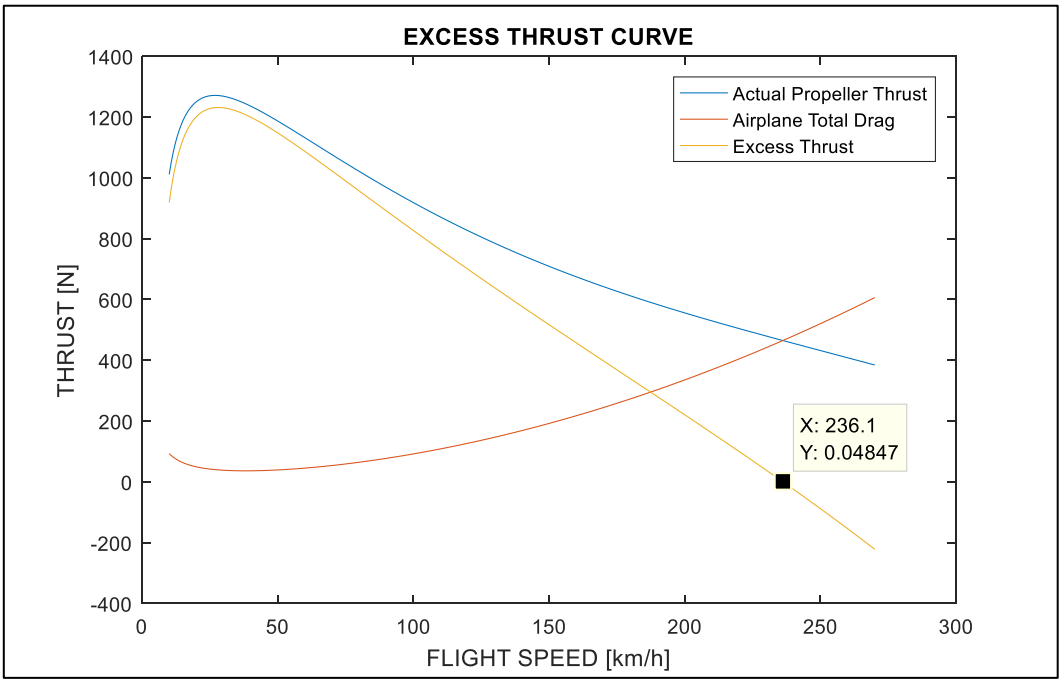


Figure 3.54 - Excess of thrust for the configuration 27 and engine power at 70%.

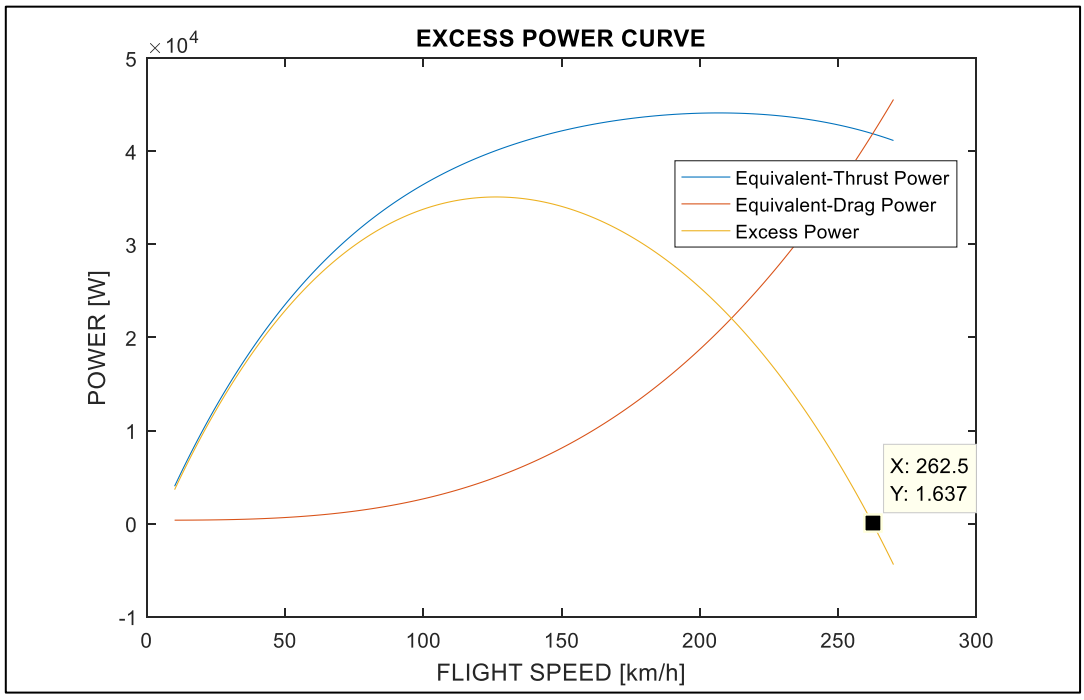


Figure 3.55 - Excess of power for the configuration 27 and engine power at 100%.

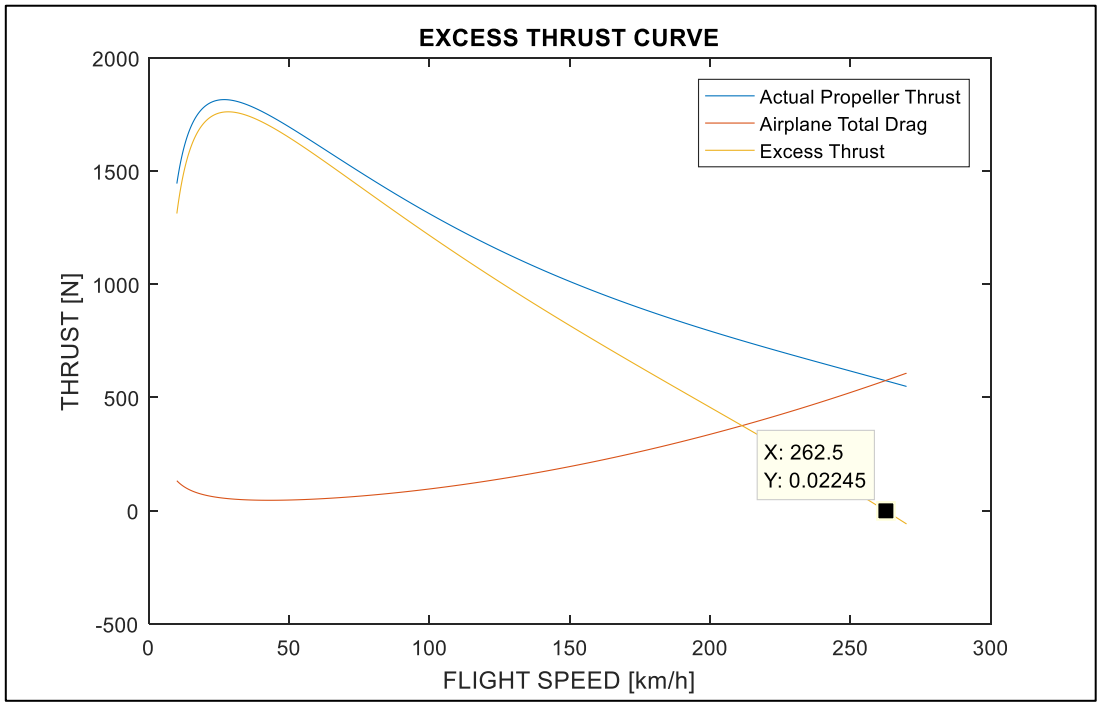


Figure 3.56 - Excess of thrust for the configuration 27 and engine power at 100%.

The results for the engine power adjusted for 70% indicate that the cruise speed of the airplane will be around $235\ [km/h]$. For the engine power adjusted for 100% the results indicate that the maximum cruise speed of the airplane will be around $260\ [km/h]$, within the limits of the propeller as indicated on the manufacturer technical data available on the APPENDIX I.

3.6.2. Take-off performance

For the take-off estimate were considered the airplane rolling on an asphalt runway, for the take-off configurations 20 and 30 provided on the Table 3.6, Table 3.24 and Table 3.25. The results are presented on the Table 3.26.

Table 3.24 - Take-off estimative airplane setting.

Configuration	***V_TO [km/h]***	***FL [ft]***	***α_ground (°)***	***cd_W***	***cd_Can***	***cd_Vt***	***cf_fus***
20	105	3100	-1.429	0.00660	0.0071	0.00520	0.00295
20	105	3100	-1.429	0.00660	0.0071	0.00520	0.00295
20	105	3100	-1.429	0.00660	0.0071	0.00520	0.00295
30	105	3100	-1.429	0.00660	0.00752	0.00520	0.00295
30	105	3100	-1.429	0.00660	0.00752	0.00520	0.00295
30	105	3100	-1.429	0.00660	0.00752	0.00520	0.00295

Table 3.25 - Take-off estimative setting and runway parameters.

Configuration	***Flap [°]***	***CAN_i [°]***	***ELEV [°]***	***ENG [%]***	***η_P***	***Obstacle [ft]***	***μg***
20	0	3.9	0	100	0.73	50	0.02
20	10	3.9	0	100	0.73	50	0.02
20	20	3.9	0	100	0.73	50	0.02
30	0	4.3	0	100	0.73	50	0.02
30	10	4.3	0	100	0.73	50	0.02
30	20	4.3	0	100	0.73	50	0.02

Table 3.26 - Take-off estimative results.

Configuration	Ground Distance [m]	Airborne Distance [m]	Total Take-off Distance [m]	Total Take-off Time [s]
20	256.6	169.3	425.9	16.3
20	256.6	169.3	425.9	16.3
20	256.6	169.3	425.9	16.3
30	313.1	206.7	519.8	18.7
30	313.0	206.6	519.6	18.7
30	313.0	206.6	519.6	18.7

Comparing these results to those obtained during the conceptual design, it is noted a big difference between them, this is due the lift-off speed that during the preliminary design had to be increased as explained at the chapter relative to the dynamics of flight results, these results were obtained at ISA.

3.6.3. Climb performance

The climb performance estimative was done considering the ISA, for the configurations 12 and 27, which are provided on the Table 3.27 and on the Table 3.28. The results are presented on the Table 3.29, and were based on the mean altitude-density between the runway level and the cruise flight level.

Table 3.27 - Climb estimative airplane setting.

Configuration	Runw.Level [ft]	Cruise FL [ft]	V_{climb} [km/h]	ENG [%]
12	3100	8000	200	75
27	3100	8000	200	75

Table 3.28 - Climb estimative airplane setting continuation.

Configuration	α_{climb} (°)	cd_W	cd_Can	cd_Vt	cf_fus	Flap [°]	CAN_i [°]	ELEV [°]
12	0	0.00530	0.00619	0.00520	0.0027	0	3.2	0
27	0	0.00530	0.00582	0.00520	0.0027	0	2.9	0

Table 3.29 - Climb estimative results.

Configuration	***Climb Rate [ft/min]***	***Climb Gradient [°]***	***Climb Time [s]***	***Service Ceiling [ft]***	***Absolute Ceiling [ft]***
12	1074	7.25	274	**27378**	**30581**
27	1058	7.00	278	**27075**	**30303**

It is import to observe that, the ceiling values above were obtained based on an theoretical estimative which consider the engine power decreasing proportionally to the square root of the ratio between the air density at actual flight level and the air density at the sea level. However, for engines that are not equipped with turbocharger as is the engine selected for this airplane, this approach does not represent the reality, so once the real data of the engine selected were not available at the moment of this estimative, the ceiling values above are overestimated.

3.6.4. Cruise performance

Initially, on the conception phase was defined that the airplane should have a cruise speed $V_0 = 170\ [km/h]$, but during the development of the aerodynamic calculus for dynamics of flight concerning the longitudinal trimming of the airplane, and for performance concerning the equilibrium between the thrust and drag generated by the airplane, it was obtained a new cruise speed around $V_0 = 235\ [km/h]$, and was obtained too the maximum cruise speed around $V_0 = 260\ [km/h]$ as presented on the results of excess of power and thrust.

The estimative for the trimmed cruise flight performance range was done based on the ISA, for the configurations 12 and 27 provided on the Table 3.6 to the Table 3.9. The results are indicted next and were obtained considering no loiter.

$$R_{12} = 1165.62\ [km]$$

$$t_{12} = 4.96\ [hour]$$

$$R_{27} = 1179.17\ [km]$$

$$t_{27} = 5.02\ [hour]$$

3.6.5. Descent performance

The descent estimative was performed considering the ISA condition and engine at idle setting for the configurations 12 and 27 provided on the Table 3.30. The results are presented on the Table 3.31.

Table 3.30 - Descent estimative airplane setting.

Config	***Runw.Level [ft]***	***Cruise FL [ft]***	***α_desc (°)***	***cd_W***	***cd_Can***	***cd_Vt***	***cf_fus***	***Flap [°]***	***CAN_i [°]***	***ELEV [°]***
12	3100	8000	-2.2	0.00751	0.00450	0.00520	0.0027	0	2.9	0
27	3100	8000	-2.2	0.00751	0.00446	0.00520	0.0027	0	2.8	0

Table 3.31 - Descent estimative results.

Configuration	***Descent Rate [ft/min]***	***Descent Gradient [°]***	***Descent Time [s]***
12	915	-22.31	321
27	878	-20.71	335

3.6.6. Landing performance

As was done for all the flight phases, the landing performance was performed considering the ISA condition. The estimates were done as the adjustments provided on the Table 3.32 and on the Table 3.33, the results are presented on the Table 3.34.

Table 3.32 - Landing estimative airplane setting.

Configuration	***V_TD [km/h]***	***FL [ft]***	***α_ground (°)***	***cd_W***	***cd_Can***	***cd_Vt***	***cf_fus***
20	105	3100	-1.429	0.00660	0.0071	0.00520	0.00295
30	105	3100	-1.429	0.00660	0.00752	0.00520	0.00295

Table 3.33 - Landing estimative airplane setting continuation.

Configuration	Flap [°]	CAN_i [°]	ELEV [°]	Obstacle [ft]	μg
20	20	3.9	0	50	0.02
30	20	4.3	0	50	0.02

Table 3.34 - Landing estimative results.

Configuration	Ground Distance [m]	Airborne Distance [m]	Total Landing Distance [m]	Total Landing Time [s]
20	73.9	69.3	143.2	22.6
30	84.2	79.0	163.2	25.0

3.7. LOADS

The parameters used to determine the maneuver V-n diagram are provided next and were considered at the ISA. The flap was set for no deflection, the maximum lift coefficient is that for the complete airplane.

$$W_0 = 592.9\ [kgf]$$

$$\rho_{0\_ft} = 1.225\ [kg/m^3]$$

$$\rho_{8000\_ft} = 0.963\ [kg/m^3]$$

$$CL_{max} = 2.29$$

The results of the load factors and speeds that are necessary to build the V-n diagram are presented next, ant the maneuver diagram is presented on the Figure 3.57.

$$n^{+}_{max} \geq 4.22$$

$$n^{-}_{max} \leq -1.70$$

$$V_S = 66.3\ [km/h]$$

$$V_C \geq 192.7\ [km/h]$$

$$V_D \geq 240.9\ [km/h]$$

$$V_A \geq 136.3\ [km/h]$$

As the cruise speed was considered that defined earlier at the trimmed cruise configurations, the dive speed had to be re-defined, these new speeds are indicated on the V-n diagram below.

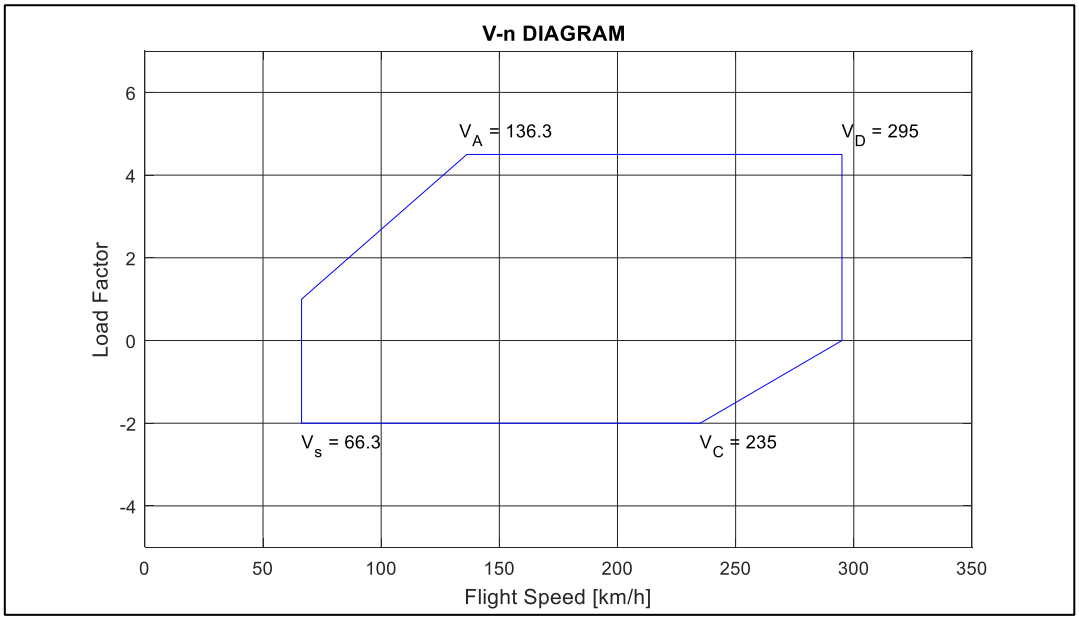


Figure 3.57 - Airplane UFU-1 maneuvering V-n diagram.

3.8. STRUCTURAL LAYOUT

Next are presented the proposed layout for structure of the wings, the canards, the vertical tails and the fuselage, indicating its respective main structural elements.

3.8.1. Wing structural layout

The structural layout for both wings with the main elements are presented on the Figure 3.58 and on the Figure 3.59.

Lower & Upper wings

As both wings have the same structure, the structural layout of each wing is constituted by two spars, the front one is located at 30% of the $\bar{C}_W$, the rear one is located at 67% of the $\bar{C}_W$; each semi-wing is constituted by three ribs, the rib 1 is located at $500\ [mm]$, the rib 2 is located at $1900\ [mm]$ and the rib 3 is located at $3400\ [mm]$ relative to the wing root.

Ailerons & Flaps

The ailerons and the flaps are the same structure as was explained before. Each panel is constituted by one spar at the leading edge closing its structure; each panel is constituted by two ribs which are the trailing edge of the ribs 2 and 3 of the respective semi-wing.

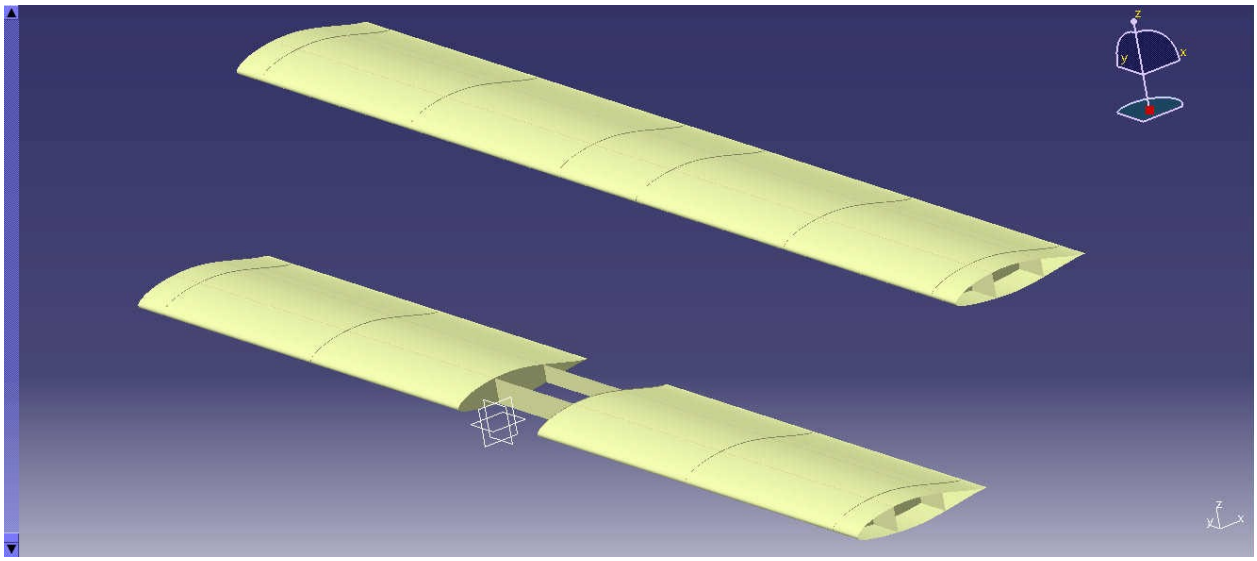


Figure 3.58 - Wings structural layout with skin.

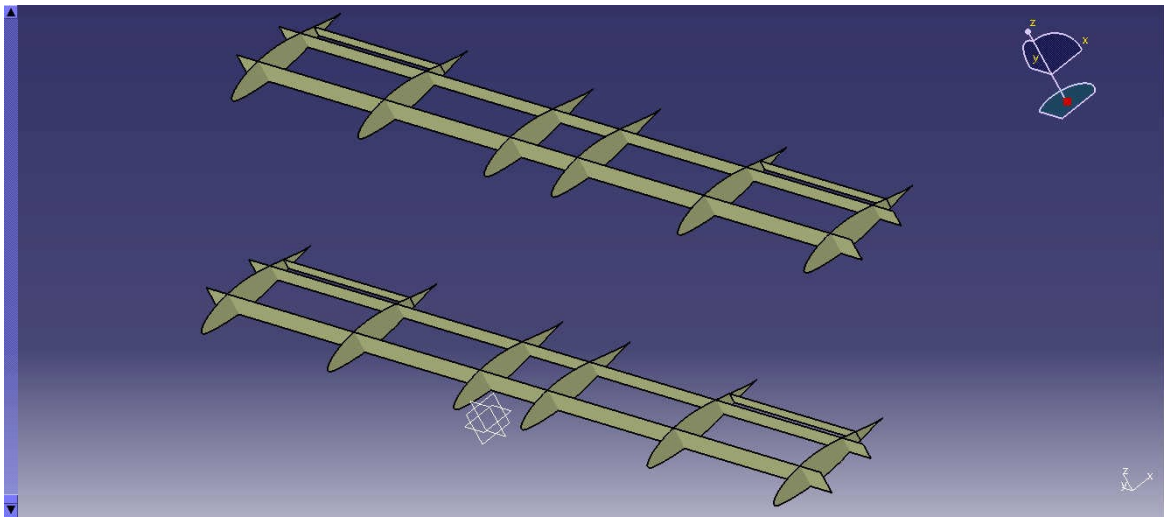


Figure 3.59 - Wings structural layout.

3.8.2. Canards & Vertical tail structural layout

3.8.2.1. Canards structural layout

The structural layout both canards with the main elements are presented on the Figure 3.60 and on the Figure 3.61.

Lower & Upper canards

Once both canards have the same structure, the structural layout of each semi-canard is constituted by two ribs, the rib 1 is located at $400\ [mm]$, and the rib 2 is located at $1450\ [mm]$ relative to the canard root; each canard is constituted by two spars, the front one is located at 30% of the $\bar{C}_W$ between the rib 2L and the rib 2R, the rear one is located at 60% of the $\bar{C}_W$ between the rib 1L and the rib 1R.

Elevators

Each elevator is constituted by one spar at the leading edge closing its structure; each panel is constituted by two ribs which are the trailing edge of the ribs 1 and 2 of each semi-canard.

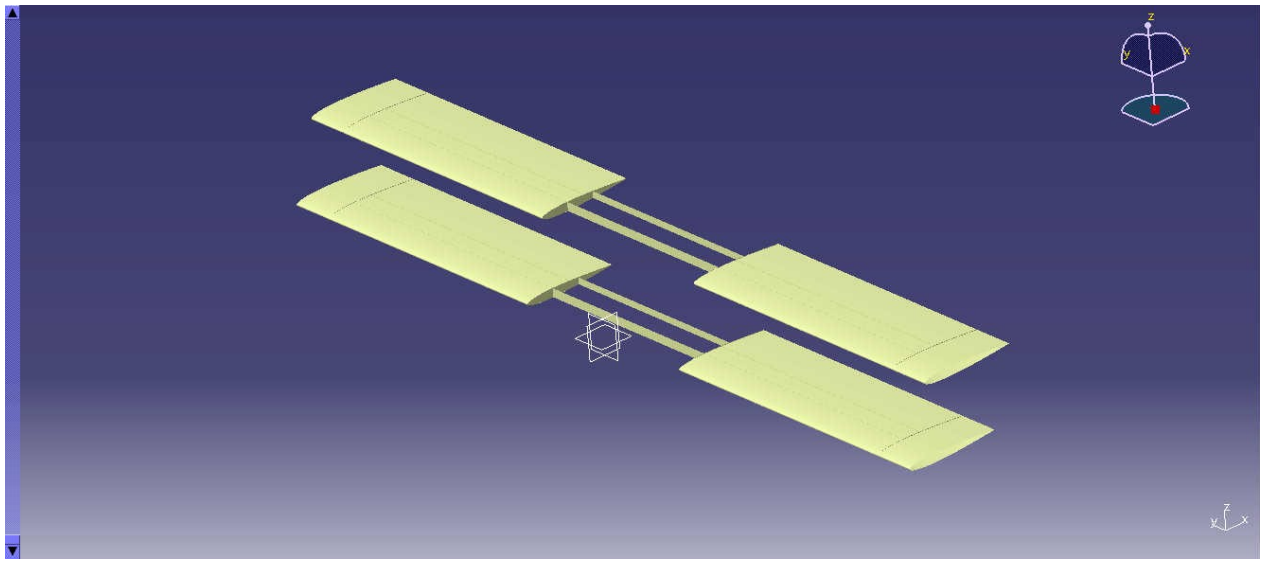


Figure 3.60 - Canards structural layout with skin.

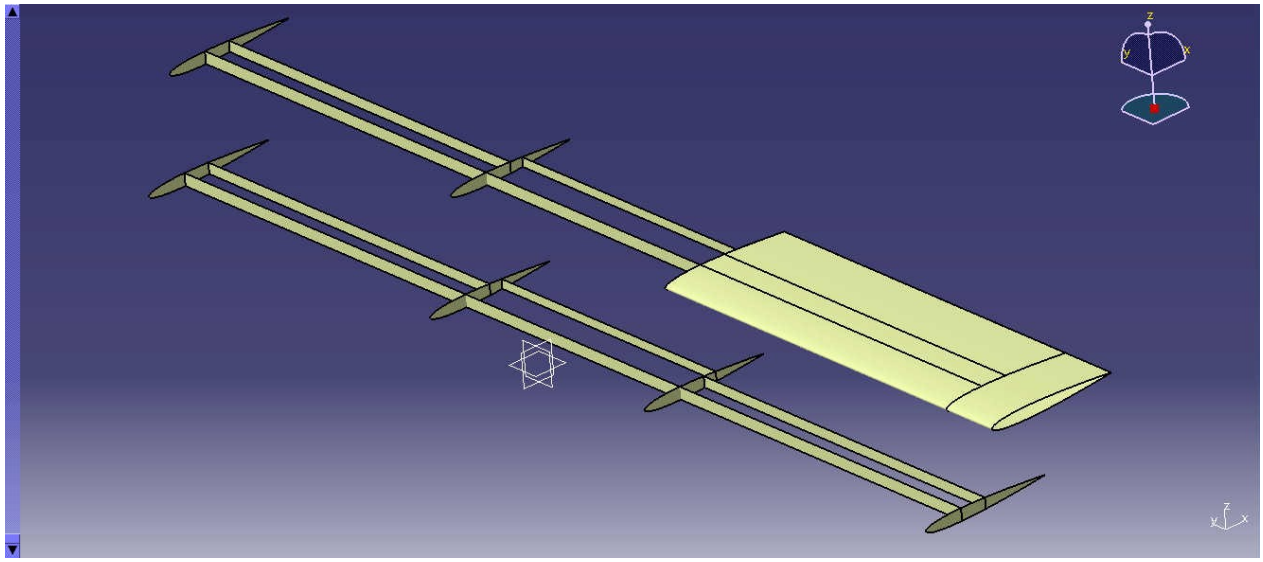


Figure 3.61 - Canards structural layout.

3.8.2.2. Vertical tails structural layout

The structural layout for both vertical tails with the main elements is presented on the Figure 3.62 and on the Figure 3.63.

Left & Right vertical tails

The structural layout of each vertical tail is constituted by two ribs, the rib 1 is located at $100\ [mm]$ and the rib 2 is located at $1000\ [mm]$ relative to the vertical tail root; each vertical tail is constituted by one spar located at $250\ [mm]$ from its trailing edge; each vertical tail is constituted by two booms fixed on its lower and upper edge.

Rudders

Each rudder is constituted by one spar at the leading edge closing its structure; each panel is constituted by two ribs which are the trailing edge of the ribs 1 and 2 of each vertical tail.

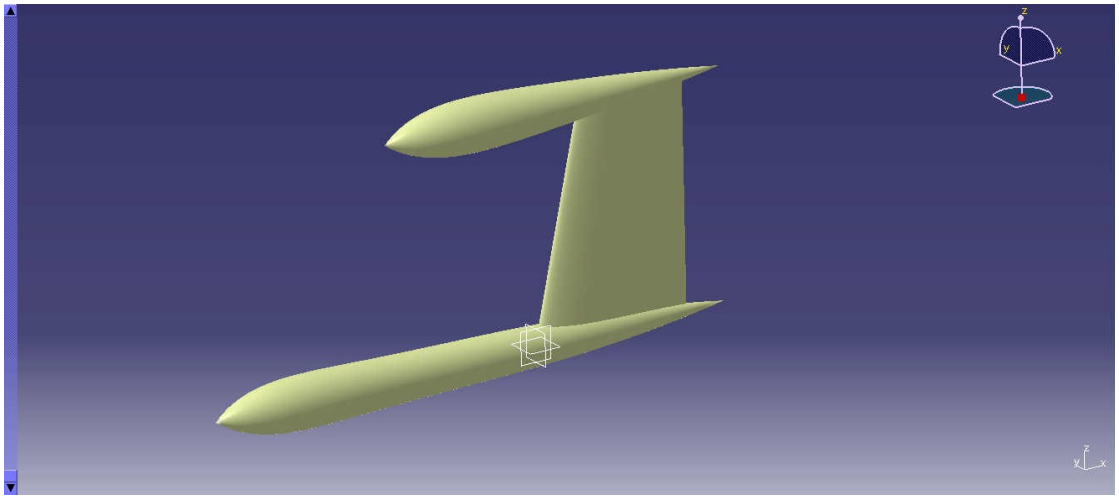


Figure 3.62 - Vertical tail structural layout with skin.

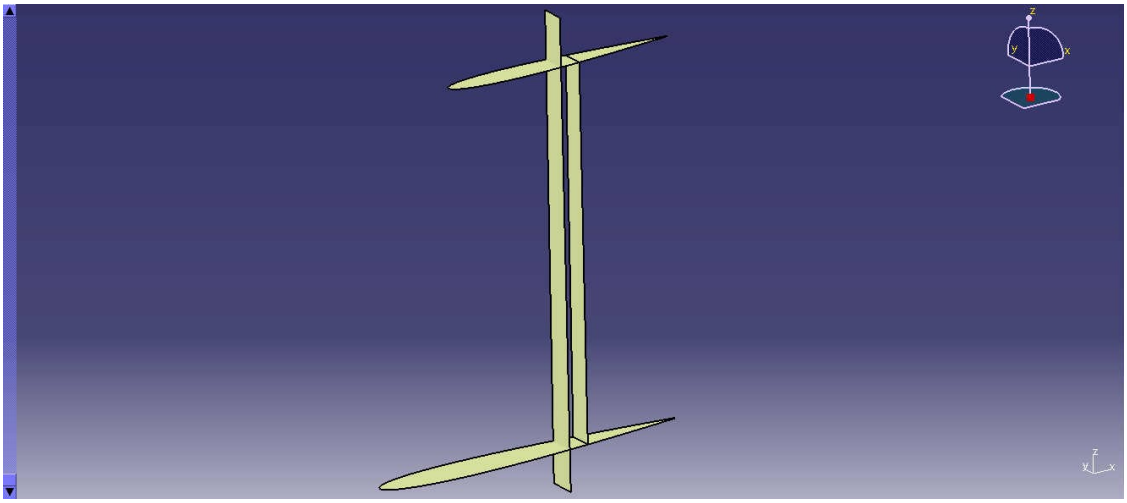


Figure 3.63 - Vertical tail structural layout.

3.8.3. Fuselage structural layout

The fuselage structural layout was segmented in four sections, the radome section; forward section which is located between the radome and the cockpit; cockpit section which is located between the forward section and the rear section; and the rear section which is located after the cockpit section. All the bulkheads except the firewall have primary structural function.

The forward section is constituted by three bulkheads completely closed to isolate the nose gear compartment, the cargo compartment and the electronic compartment. The first bulkhead $F-1$ is located at $273\ [mm]$ from the tip of the radome, with the function to isolate the ELT compartment and working as support to it; the second bulkhead $F-2$ is located at $573\ [mm]$ from the tip of the radome defining the nose gear compartment and working as support for to fixate the gear structure; the third bulkhead $F-3$ is located at $1023\ [mm]$ from the tip of the radome defining the cargo compartment of the airplane.

The cockpit section is constituted by four bulkheads, the first bulkhead $C-1$ is completely closed to isolate the electronic compartment from the cockpit and is located at $1473\ [mm]$ from the tip of the radome; the second bulkhead $C-2$ is located at $400\ [mm]$ from the bulkhead $C-1$ and has the function to fixate the avionic panel; the third bulkhead $C-3$ is located at $1270\ [mm]$ from the bulkhead $C-2$; the fourth bulkhead $C-4$ is located at $1030\ [mm]$ from the bulkhead $C-3$ and. The bulkheads $C-3$ and $C-4$ are reinforce with a central beam that has the function to protect the head of the pilots in the event of to pylon.

The rear section is constituted by two bulkhead, the first bulkhead $R-1$ is located at $1255\ [mm]$ from the bulkhead $C-4$ and has the function to support the engine suspension frame; the second bulkhead $R-2$ is located at the same location of the bulkhead $R-1$ and has the function of firewall between the engine and the cockpit.

The fuselage is constituted by two beams, the first at the bottom of the left side and the second on the bottom of the right side; both has primary structural function. The Figure 3.64 to the Figure 3.66 presents the fuselage structural layout details.

One note is convenient, the bulkhead $C-4$ was conceived considering the technical data provided by the installation manual of the selected engine.

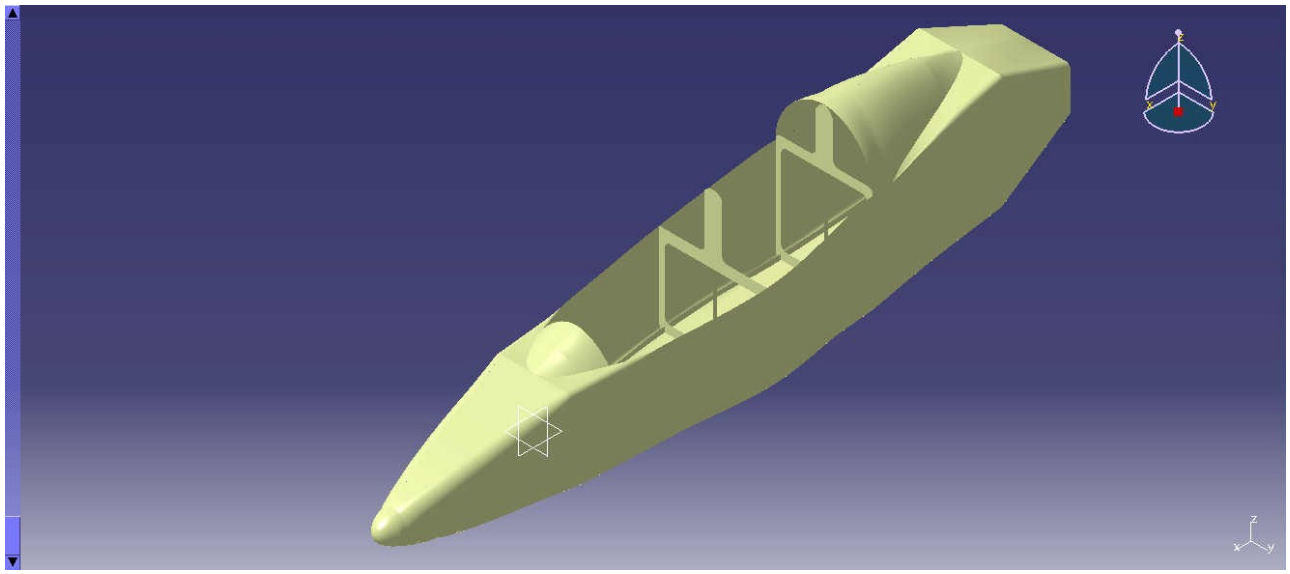


Figure 3.64 - Fuselage structural layout with skin.

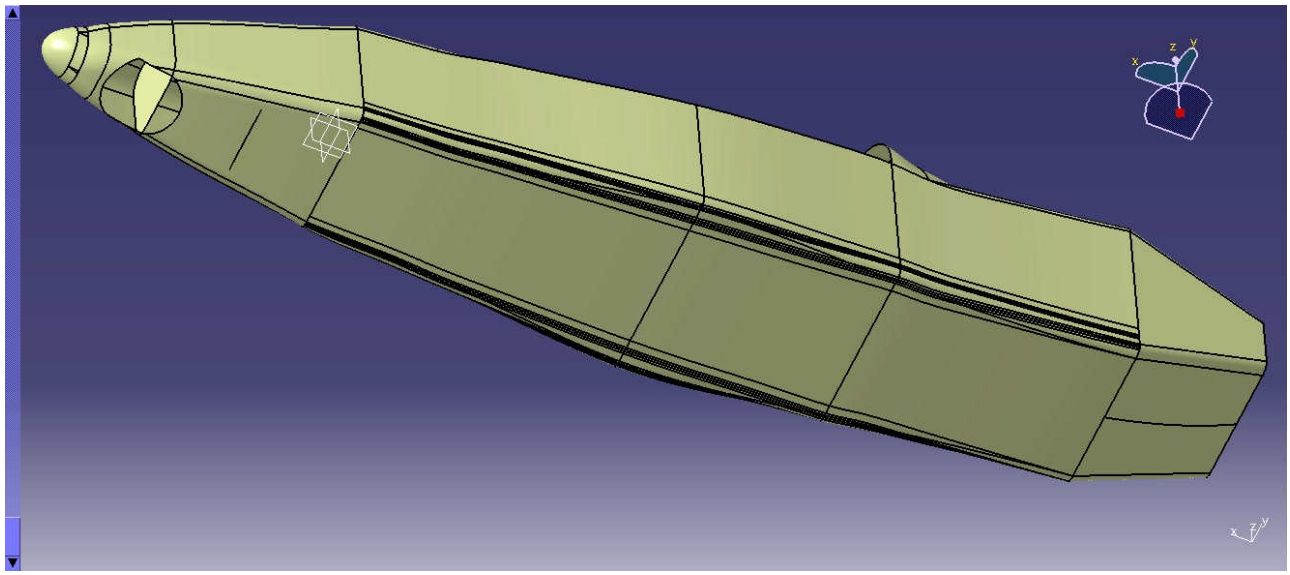


Figure 3.65 - Fuselage structural layout, nose gear compartment detail.

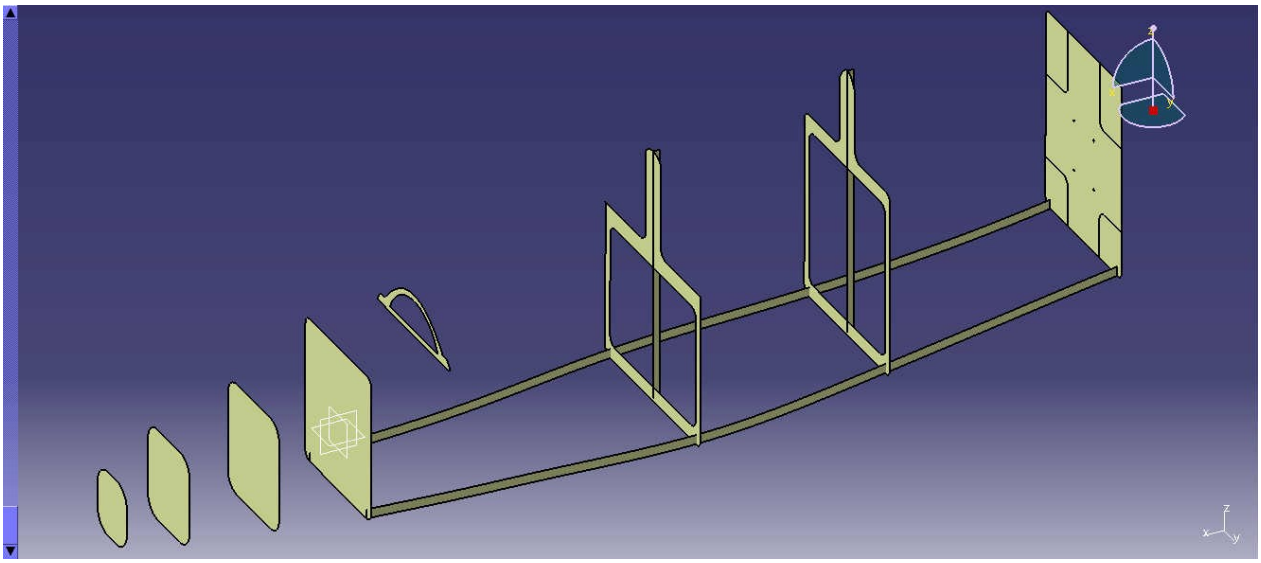


Figure 3.66 - Fuselage structural layout.

It is necessary to make an observation, note that were not conceived the structural elements that will fasten the wings on the fuselage. To define it, there are necessary some more studies.

Probably will be created two ventral transversal beams at the location of the two spars of the lower wing for fasten it on the fuselage, and for the upper wing probably will be created two dorsal transversal beams at the location of the two spars for the same purpose.

3.9. LANDING GEAR SYSTEM

Next are presented the defined solutions and results obtained for the landing gear system of the airplane UFU-1. The results were obtained by running the algorithm presented on the APPENDIX G.

3.9.1. Landing gear legs locations & considerations

The location of each landing gear leg and in consequence the location of the contact point with the ground of each tire took into account three variables, the first was the percent loading at each leg, the second was the geometric constraint imposed by airplane shape, the third variable was the effectivity of the elevators during the lift-off rotation.

The location of each landing gear leg and the track of the main landing gear are presented next and on the Figure 3.67.

$$X_{nose} = 0.493\ [m]$$

$$X_{main} = 4.100\ [m]$$

$$track_{main} = 3.200\ [m]$$

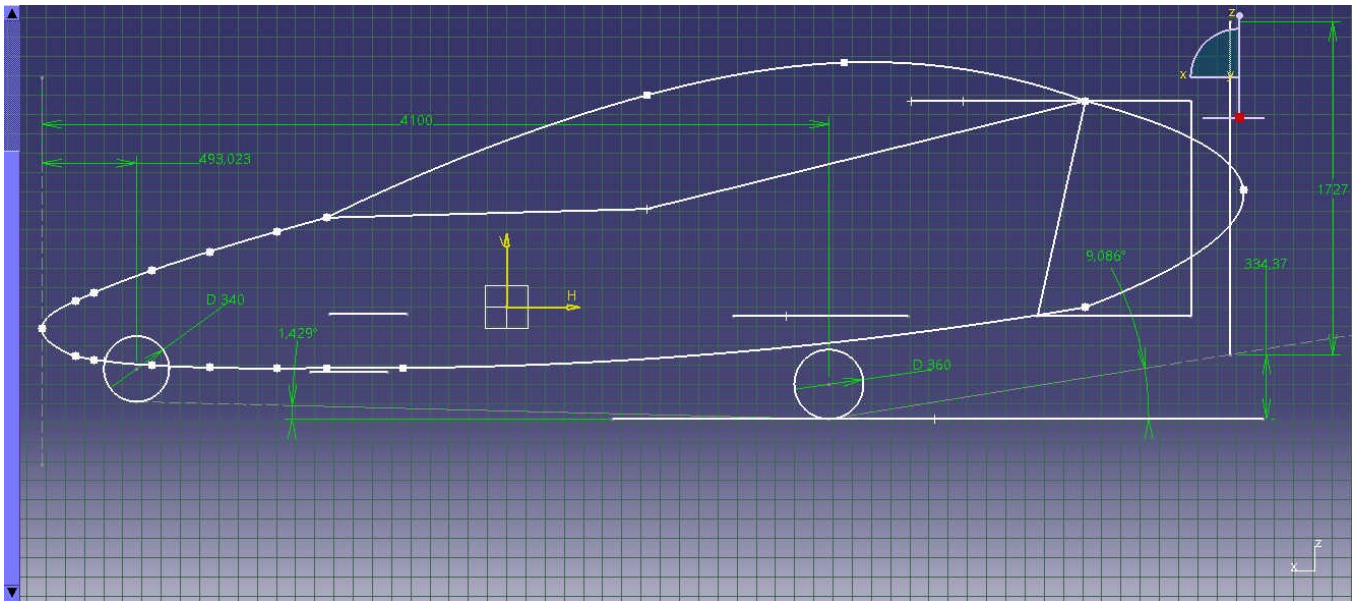


Figure 3.67 - Landing gear geometric parameters.

The location of the legs as defined on the figure above indicate that the tip of the blade of the propeller will not strike the ground for a pitch angle of at maximum $9°$, and remembering that the angle of stall of the canard is around $10.75°$, the pitch angle become an operational constraint of the airplane.

The landing gear legs located at this form will contribute for the elevators effectivity at the take-off rotation. The main legs will be fixed on the lower wing structure between the two spars, and will be faired for to contribute to the aerodynamic properties of the airplane.

The minimum and maximum percent loading at each leg of the landing gear is dependent of the CG location and is presented next.

$$L_{MG\_MIN} = 87.25\ [\%]$$

$$L_{MG\_MAX} = 95.00\ [\%]$$

$$L_{NG\_MIN} = 4.99\ [\%]$$

$$L_{NG\_MAX} = 12.75\ [\%]$$

3.9.2. Tires dimensioning

For the tires dimensioning, were defined the following parameters.

$$W_0 = 600\ [kgf]$$

$$B = 3.607\ [m]$$

$$H = 1\ [m]$$

The results for the tires dimensioning are presented next.

$$d = 48.53\ [cm]$$

$$w = 17.72\ [cm]$$

$$W_{main\_max} = 285.0\ [kgf]$$

$$W_{main\_min} = 261.7\ [kgf]$$

$$W_{nose\_max} = 38.3\ [kgf]$$

$$W_{nose\_min} = 15.0\ [kgf]$$

$$W_{nose\_dyn} = 3.3\ [kgf]$$

Based on the results showed above the tires were specified consulting the manufacturer catalog (Goodyear, 2016), the specifications are presented next.

Nose tire

$$Size: 5.00 - 4$$

$$d_{max} = 337\ [mm]$$

$$w_{max} = 128\ [mm]$$

Main tire

$$Size: 5.00 - 5$$

$$d_{max} = 361\ [mm]$$

$$w_{max} = 126\ [mm]$$

3.9.3. Shock absorber considerations

As the design philosophy employed on the conception of this airplane was to make an airplane the most simple as possible related to its manufacturing and the cheapest as possible, and considering the low weight of the airplane, was decided that the shock damping during the landings will be done by the own tires of the landing gear, so obviously the structural dimensioning must consider for these loads.

3.9.4. Steering considerations

For the maneuvering of the airplane on ground was defined that it should provide the bigger steering angle of the nose wheel as possible, the study showed on the Figure 3.68 indicated initially an maximum angle of $73°$, but due the geometric limitation of the nose gear compartment this angle had to be reduced to $50°$.

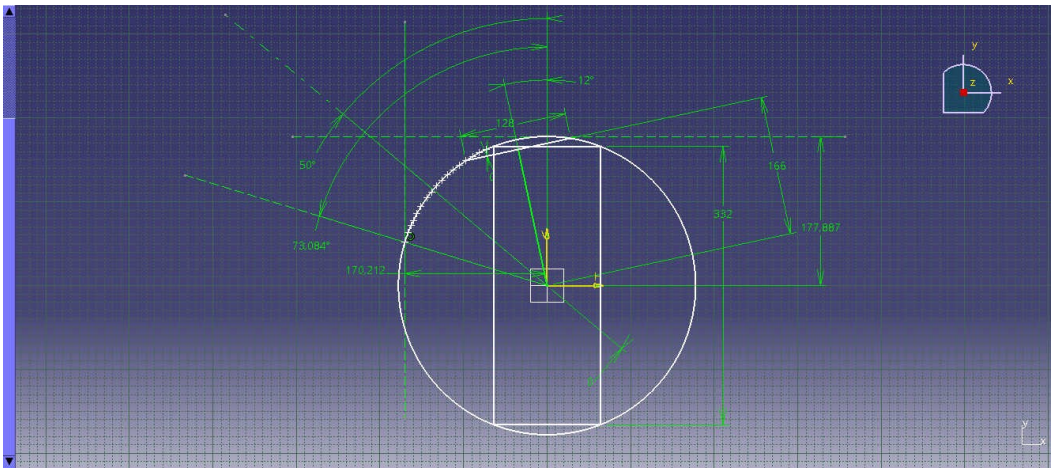


Figure 3.68 - Nose wheel steering study.

3.9.5. Breaking system

The break system to be employed on the airplane UFUF-1 will use two conventional disc brakes one on each main wheel.

3.10. FUEL SYSTEM

Initially the intention was to employ a fuel feeding by gravity, as the fuel tank initially had been positioned at the rear fuselage section, but as the final position the fuel tank is between both spars of the lower wing, will be necessary the installation of a fuel pump.

At this phase of the development of the airplane the specification of the fuel system components is not done, just the main dimensions of the fuel tank were defined as indicated next and are enough for carry the $33\ [kgf]$ of gas obtained during the conception of the airplane.

$$l = 0.25\ [m]$$

$$w = 1.60\ [m]$$

$$h = 0.12\ [m]$$

$$V_{tank} = l \times w \times h = 0.048\ [m^3]$$

3.11. PROPULSIVE SYSTEM

The propulsive system employed on the airplane UFU-1 is constituted by one alternative engine equipped with one propeller, these two main elements are detailed next.

3.11.1. Engine

The engine was selected earlier during the development of the airplane, at the conceptual phase. The engine selected is the *ROTAX 912* from the family *UL/A/F*, this engine was selected for being well known and tested, and to provide a cheap operation and maintenance, its technical specifications are presented on the APPENDIX H. The positioning of the engine on the airplane is shown on the Figure 3.69. The engine suspension frame is supplied by the manufacturer.

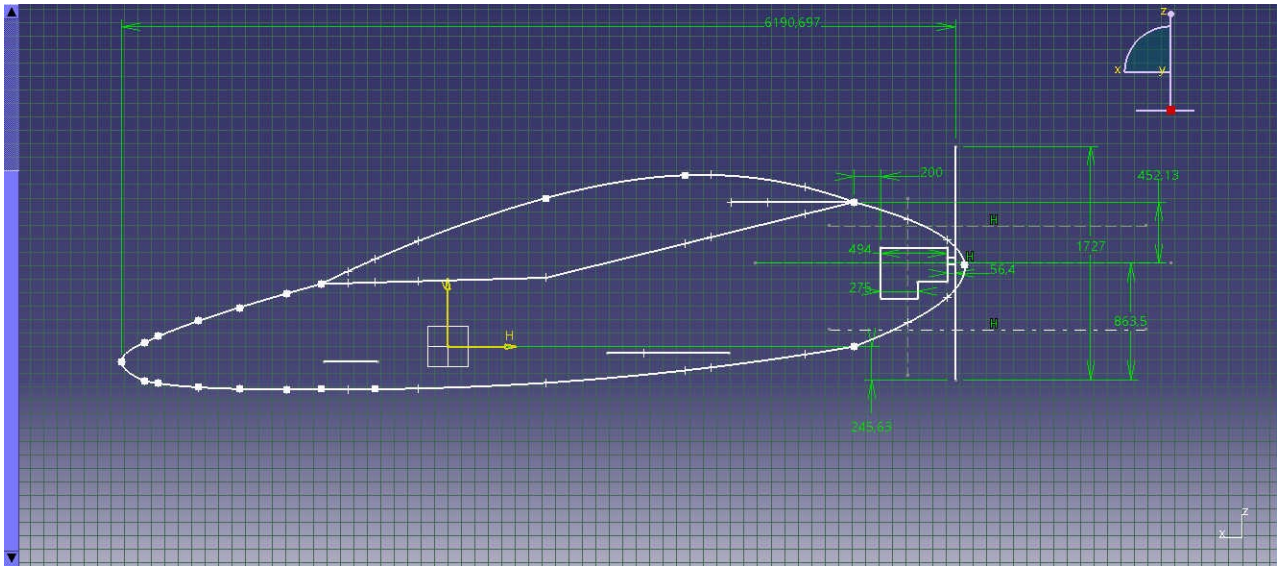


Figure 3.69 - Engine pusher positioning on the airplane.

3.11.2. Propeller

The propeller selection was done together the engine, the selected one is the Sensenich three blades model *3B0R5 L68C*. The physic characteristics of this propeller are presented next, and the performance curves are presented on the APPENDIX I.

$$W_{prop} = 4.1\ [Kgf]$$

$$\emptyset_{prop} = 1.73\ [m]$$

All the results of aerodynamic, dynamic of flight and performance were based on the 5th degree polynomial fitting curve obtained from the Figure 3.70, which is based on the technical data of the APPENDIX I, this equation is written into the algorithm of the APPENDIX C.

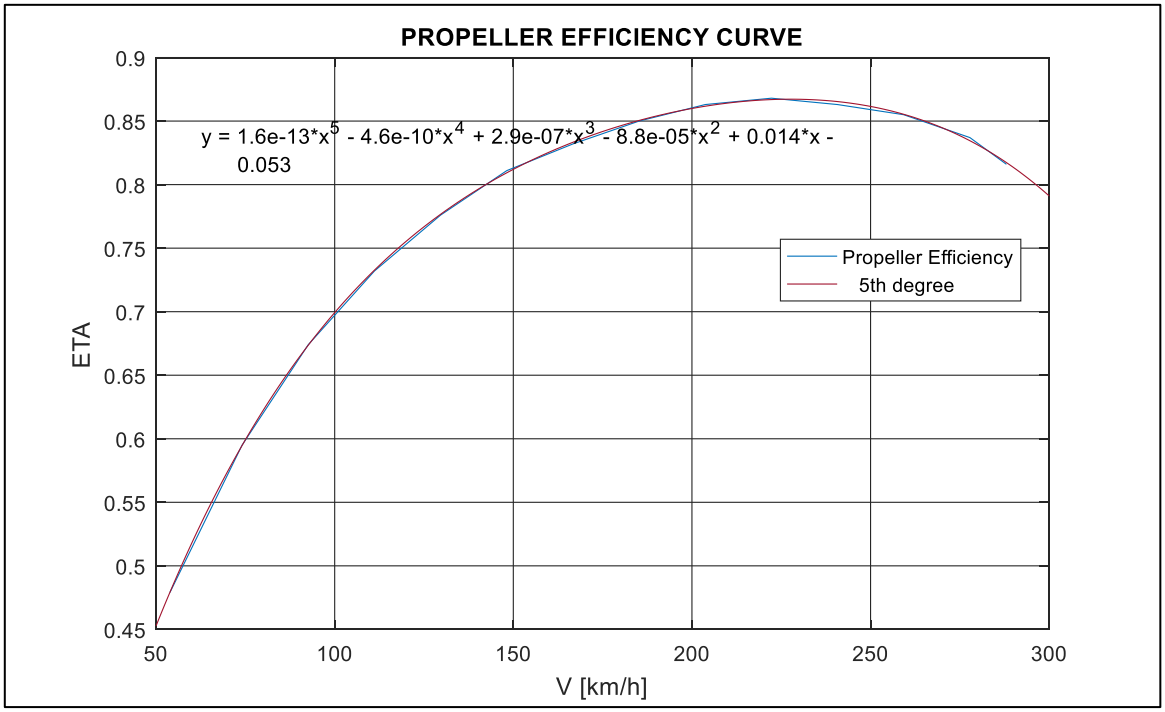


Figure 3.70 - Approximate propeller efficiency curve.

3.12. AVIONIC SYSTEM

The avionic suite is constituted by a MFD system as the main component and by redundant analogical gauges which provide the primary information related to the flight and the engine operation, if occur some electrical or electronic fail. The communication system is constituted by radio and transponder. The necessary antennas for the navigation and communication systems were not specified.

3.12.1. Main suite

The main avionic suite is based on the Garmin G3X system that is an electronic system that provides navigation, engine, airframe and location data for the flight.

Basically the system is constituted by one MFD that can be expanded for a maximum of three, and electronic modules that generate these flight data and transmit it to the MFD. All the electric power data related to this system will be described into the electrical system chapter.

For the airplane UFU-1 was selected the suite constitute by only one MFD, this system is described next, and presented on the Figure 3.71.

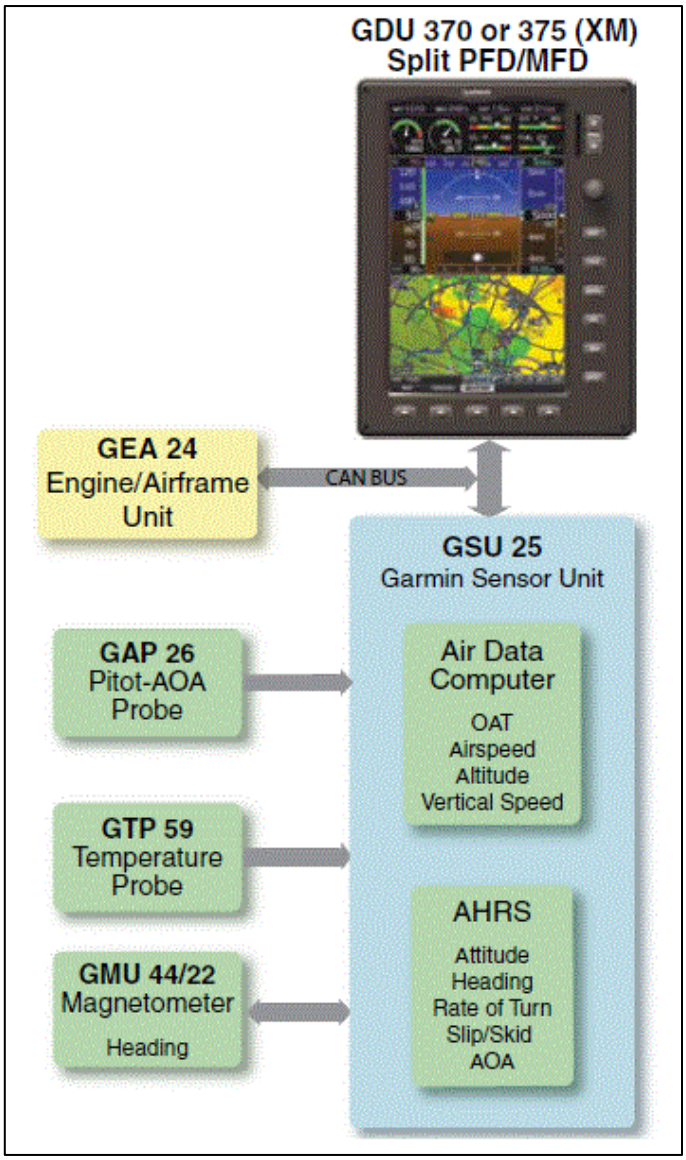


Figure 3.71 - Garmin suite architecture (Garmin G3X pilot's guide).

GDU 370

This component of the suite display the navigation data as the airplane speeds and attitude, maps and GPS information; communication data as transponder and radio; engine operation data and airframe data.

GEA 24

This electronic module receives and process the data generated by the engine and airframe sensors. This module is compatible to the ROTAX 912/914 engine family.

GSU 25

This is the electronic module that is responsible for to process the air data provided by the pitot and the out air temperature sensor; generate and provide the airplane attitude and heading data.

GAP 26

This component is the pitot probe that provides the static and the total air pressure data, if working paired with GSU 25 provide the angle of attack. The airplane UFU-1 is equipped with two pitot, one at each side of the airplane nose.

GTP 59

This is the out air temperature probe that provide the raw air temperature data.

GMU 22

This component is the magnetometer, which measure the local magnetic field and send the obtained data for the module GSU 25 to determine the magnetic heading of the airplane.

GPS 20A

This electronic module generates and provides the GPS data for the display GDU 370.

3.12.2. Redundancy suite

The redundancy suite has the objective to provide the essential flight data if some electrical or electronic fail occur. It is constituted by one unit of each gauge described next.

- Compass
- Altimeter
- Airspeed indicator
- Fuel level indicator
- Tachometer
- Engine oil temperature indicator
- Battery voltmeter
- Battery ammeter

3.12.3. Communication suite

The communication suite is constituted by devices that provide communication between the airplane and the traffic control and between the crew, these devices are supplied by the Garmin, and an emergency locator supplied by the Ameri-King.

GTR-200

This is the radio selected for the airplane, it operate at VHF in a band between $118.000\ MHz$ and $136.9750\ MHz$ and an step of $25\ KHz$.

GTX 23

This is the transponder electronic module, which operates at the S mode and is able to operate with TCAS systems.

GMA-240

This is the audio panel that manages the inputs and outputs of audio from the external and internal communication and music devices.

AK-450

This is the emergency locator transmitter module, and operate at the frequencies $121.5\ MHz$ and $243.0\ MHz$.

3.12.4. Avionic panel layout

The Figure 3.72 shows the proposed layout for the avionic panel of the airplane UFU-1.

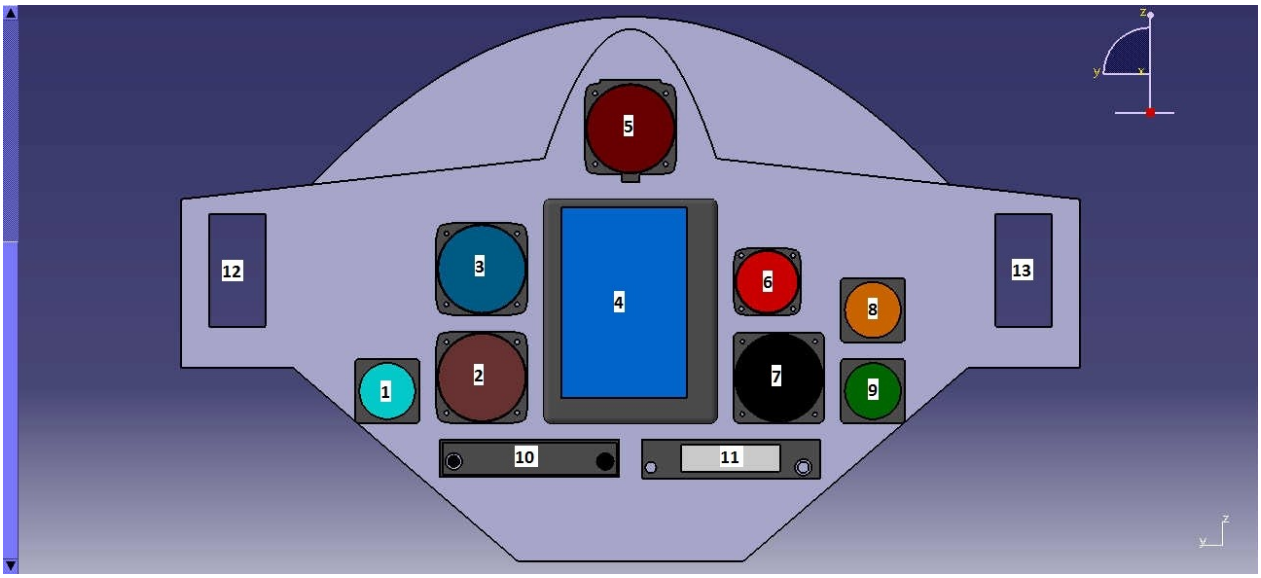


Figure 3.72 - Avionic panel layout.

1. Fuel level indicator
2. Airspeed indicator
3. Altimeter
4. MFD display
5. Compass
6. Engine oil temperature indicator
7. Tachometer
8. Ammeter
9. Voltmeter
10. Audio panel
11. Radio VHF

12. Cockpit air inlet
13. Cockpit air inlet

3.13. ELECTRICAL SYSTEM

The electrical system is constituted by only one battery that provides electrical power for the electric and electronic devices necessary for to operate the airplane. At this design phase the electrical system is incomplete once some components were not specified.

Next it is presented the Table 3.35 which indicates the electrical consumption of the components already specified, such electrical power demand must be considered for to specify the battery.

Table 3.35 - Electrical & Electronic devices electrical characteristics.

Device	Model	Tension (V)	Nominal Current (A)	Nominal Power (W)	Quantity
Intercom	GMA-240	11 to 33	0.31 to 0.54	4.3 to 7.5	1
Radio	GTR-200	14 or 28	0.3 to 7.5	10	1
Voltmeter	VM30-2Q	6 to 16	----	----	1
Ammeter	A30-001	6 to 16	----	----	1
PFD	GDU 370	14 or 28	0.54 to 1.1	----	1
Transponder	GTX 23 ES	11 to 33	----	250	1
EIS	GEA 24	14 to 28	0.43	----	1
GPS	GPS 20A	14 to 28	0.1 to 0.2	----	1
ADAHRS	GSU 25	14 to 28	0.11 to 0.2	----	1
Tachometer	IM533	10 to 30	----	----	1
Compass	----	12	----	----	1
Airspeed indicator	----	14	----	----	1

Battery

As it was not the intent of this work to develop the electrical system, just some of the electrical data were defined, therefore the battery could not be specified, remembering that it is

necessary first to know the electrical demand from all the avionics, lights and other electrical devices installed on the airplane.

Considering the engine specifications, the engine starter input is of $12\ [VDC]$, requiring a battery that provide at least an current of $16\ [Ah]$, the rectifier regulator out-put is of $14.2\ [VDC]$ providing a maximum current of $22\ [A]$, as provided by the manufacturer installation manual.

Finally, by assessing the electrical data from the devices to be installed on the airplane and the batteries capacities available, probably the electrical circuit will be supplied by the engine rectifier out-put, instead to be directly supplied by the battery to be defined for the airplane.

TECHNICAL DESCRIPTION

CHAPTER IV

This chapter is dedicated to present the geometric parameters of the aircraft, its three view and some other descriptions.

4.1. External dimensions

The first parameters obtained during the conceptual design phase were preliminary, now are presented the geometrical parameter for the final configuration of the airplane UFU-1.

4.1.1. Wings

4.1.1.1. Biplane wing

Biplane main parameters

- $GAP = 1116{,}6\ [mm]$
- $Span\ Ratio = 1$
- $Stagger = -39.546\ [°]$
- $Decalage = 0\ [°]$

Geometric parameters

- $b_{W\_B} = 7.30\ [m]$
- $S_{W\_BIP} = 13.23\ [m^2]$
- $\Gamma_{W\_B} = 0.0\ [°]$

4.1.1.2. Lower wing

Lower wing geometric parameters

- $C_{root_{W\_LOW}} = 0.91\ [m]$
- $C_{tip_{W\_LOW}} = 0.91\ [m]$
- $b_{W\_LOW} = 7.30\ [m]$
- $S_{W\_LOW} = 6.64\ [m^2]$
- $\Lambda_{W\_LOW} = 0\ [°]$
- $\Gamma_{W\_LOW} = 0\ [°]$
- $i_{W\_LOW} = 0\ [°]$

Flaps geometric parameters

Below there are presented the geometric parameters for each flap panel.

- $C_{root_F} = 0.2\ [m]$
- $C_{tip_F} = 0.2\ [m]$
- $b_F = 1.5\ [m]$
- $b_{F_i} = 1.9\ [m]$
- $S_{Flap} = 0.30\ [m^2]$
- $C_F/\bar{C}_{W\_LOW} = 0.22$
- $b_F/b_{W\_LOW} = 0.41$

4.1.1.3. Upper wing

Upper wing geometric parameters

- $C_{root_{W\_UP}} = 0.91\ [m]$
- $C_{tip_{W\_UP}} = 0.91\ [m]$
- $b_{W\_UP} = 7.30\ [m]$
- $S_{W\_UP} = 6.64\ [m^2]$
- $\Lambda_{W\_UP} = 0\ [°]$

- $\Gamma_{W\_UP} = 0$ [°]
- $i_{W\_UP} = 0$ [°]

Ailerons geometric parameters

All the geometric parameters related to the ailerons were specified into the lateral control results chapter.

4.1.2. Canards

4.1.2.1. Biplane canard

Biplane main parameters

- $GAP = 300$ $[mm]$
- $Span\ Ratio = 1$
- $Stagger = -18.435$ [°]
- $Decalage = 0$ [°]

Geometric parameters

- $b_{CAN\_B} = 3.24$ $[m]$
- $S_{CAN\_BIP} = 2.59$ $[m^2]$
- $\Gamma_{CAN\_B} = 0.0$ [°]

4.1.2.2. Lower canard

Lower canard geometric parameters

- $C_{root_{CAN\_LOW}} = 0.40$ $[m]$
- $C_{tip_{CAN\_LOW}} = 0.40$ $[m]$
- $b_{CAN\_LOW} = 3.24$ $[m]$
- $S_{CAN\_LOW} = 1.30$ $[m^2]$
- $\Lambda_{CAN\_LOW} = 0$ [°]

- $\Gamma_{CAN\_LOW} = 0$ [°]
- $i_{CAN\_LOW} = variable$ [°]

Elevators geometric parameters

All the geometric parameters related to the elevators were specified into the longitudinal control results chapter.

4.1.2.3. Upper canard

Upper canard geometric parameters

- $C_{root_{CAN\_UP}} = 0.40$ $[m]$
- $C_{tip_{CAN\_UP}} = 0.40$ $[m]$
- $b_{CAN\_UP} = 3.24$ $[m]$
- $S_{CAN\_UP} = 1.30$ $[m^2]$
- $\Lambda_{CAN\_UP} = 0$ [°]
- $\Gamma_{CAN\_UP} = 0$ [°]
- $i_{CAN\_UP} = variable$ [°]

Elevators geometric parameters

All the geometric parameters related to the elevators were specified into the longitudinal control results chapter.

4.1.3. Vertical tails

4.1.3.1. Left vertical tail

Left vertical tail geometric parameters

- $C_{root_{VT\_LEF}} = 0.80$ $[m]$
- $C_{tip_{VT\_LEF}} = 0.55$ $[m]$
- $b_{VT\_LEF} = 1.17$ $[m]$

- $S_{VT\_LEF} = 0.76\ [m^2]$
- $\Lambda_{VT\_LEF} = 9.53\ [°]$
- $\Gamma_{VT\_LEF} = 0\ [°]$
- $i_{VT\_LEF} = 0\ [°]$

Rudder geometric parameters

All the geometric parameters related to the rudder were specified into the directional control results chapter.

4.1.3.2. Right vertical tail

Right vertical tail geometric parameters

- $C_{root_{VT\_RIG}} = 0.80\ [m]$
- $C_{tip_{VT\_RIG}} = 0.55\ [m]$
- $b_{VT\_RIG} = 1.17\ [m]$
- $S_{VT\_RIG} = 0.76\ [m^2]$
- $\Lambda_{VT\_RIG} = 9.53\ [°]$
- $\Gamma_{VT\_RIG} = 0\ [°]$
- $i_{VT\_RIG} = 0\ [°]$

Rudder geometric parameters

All the geometric parameters related to the rudder were specified into the directional control results chapter.

4.1.4. Fuselage

- $l_f = 6.13\ [m]$
- $Y_C = 1.00\ [m]$
- $\emptyset_{fus} = 1.24\ [m]$

4.2. Airplane views

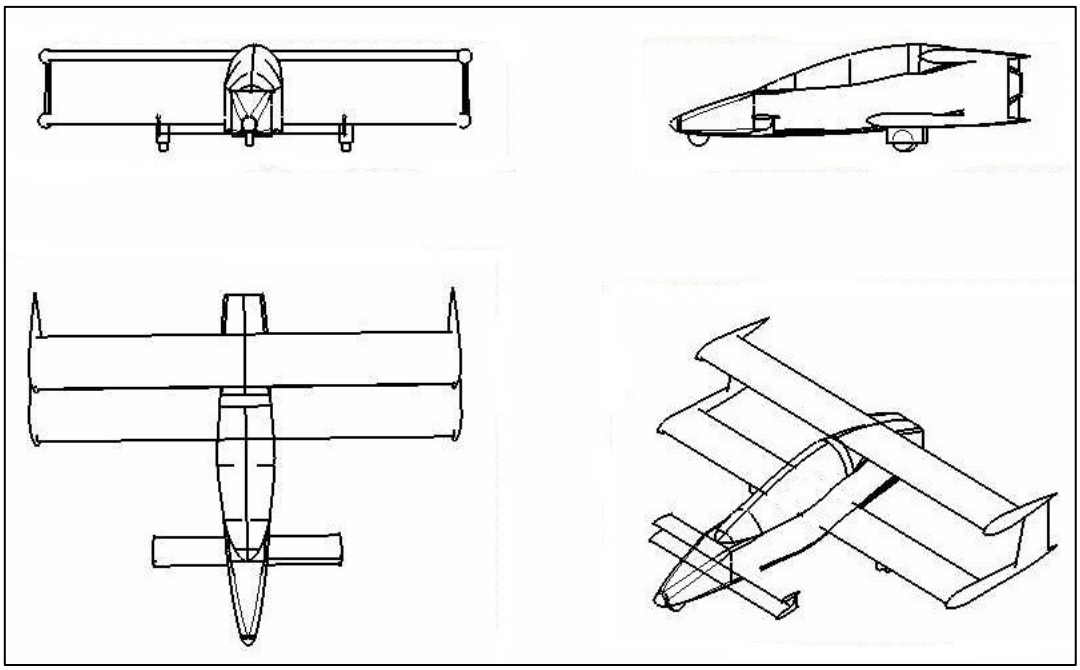


Figure 4.1 - Airplane UFU-1 views.

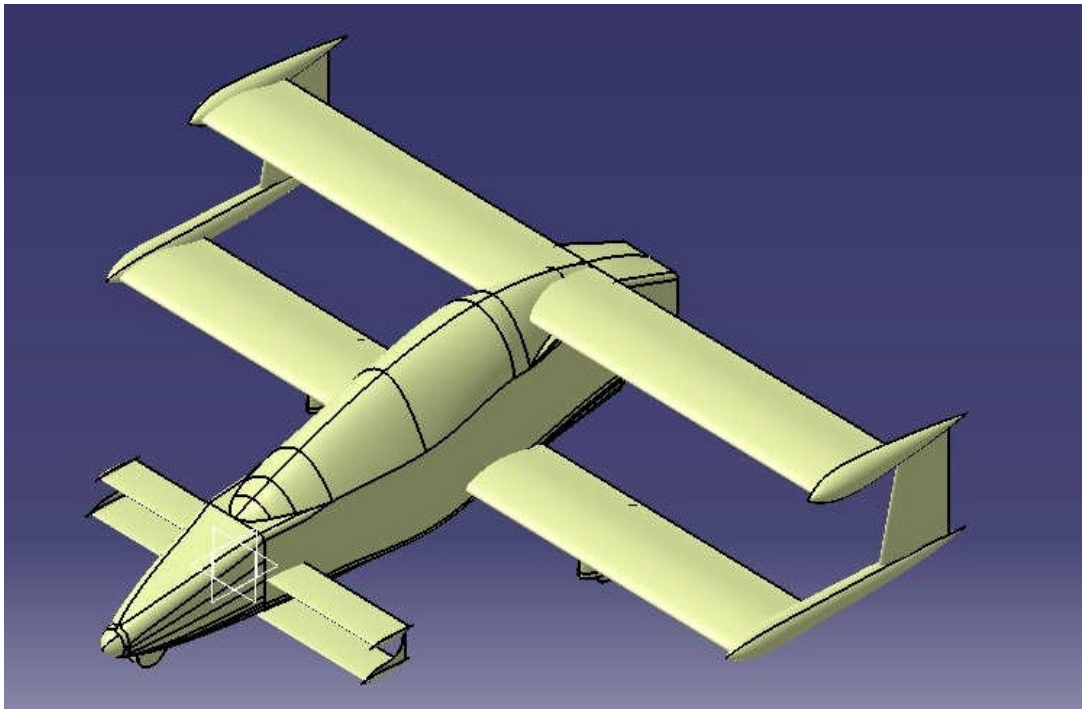


Figure 4.2 - Airplane isometric view.

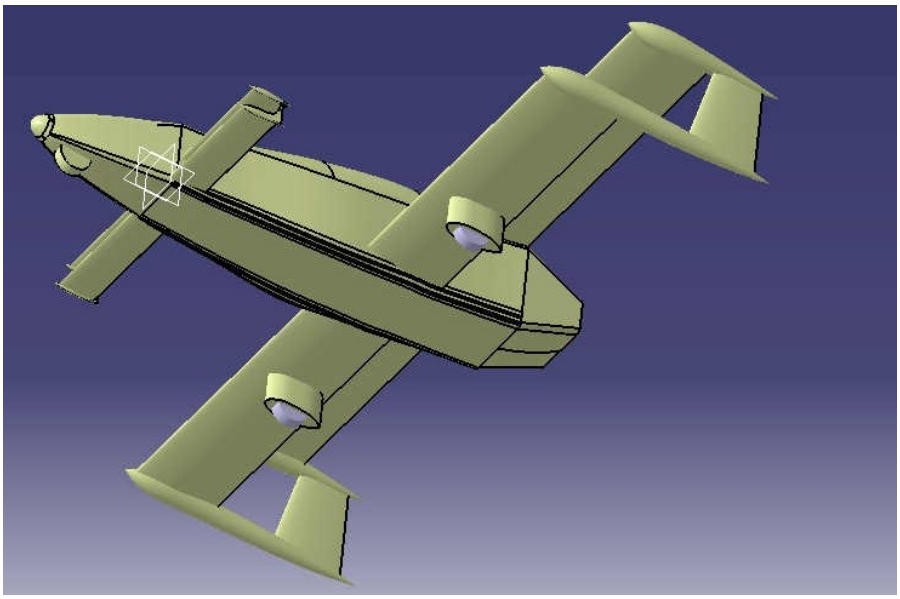


Figure 4.3 - Airplane bottom view.

4.3. Airplane internal compartments

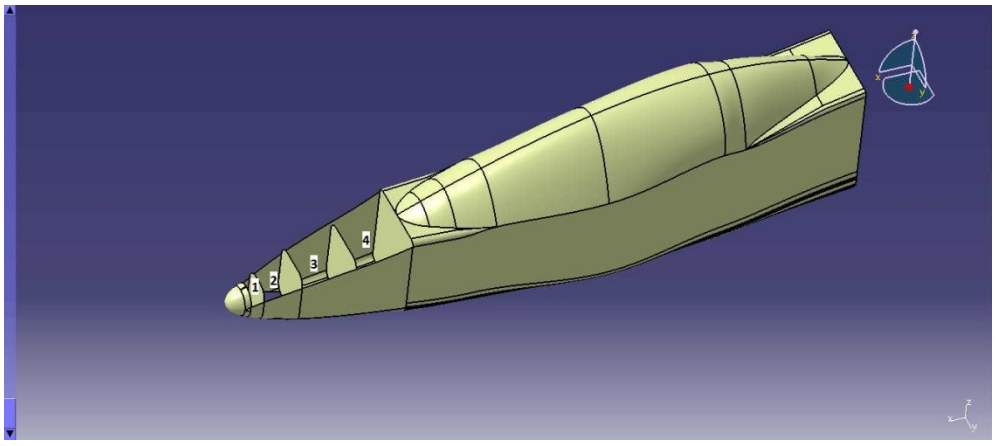


Figure 4.4 - Airplane internal compartments.

1. ELT compartment
2. Nose landing gear compartment
3. Cargo compartment
4. Electronic compartment

CONCLUSION

CHAPTER V

As described into the introduction of this work, the intent was to conceive an airplane that could be a platform for teaching and research for both the undergraduate and postgraduate levels, being therefore a practical and theoretical tool, however, along its development the technical results far exceeded the expectations, what is in accordance to the initial propose of this work of serving as research source on the aeronautical area.

The conception activities of the airplane UFU-1 had to be revaluated due its uncommon characteristics, once such activities were based on the available historical data, unfortunately poor for airplanes of similar configuration, or even nonexistent by considering the exact configuration adopted for the airplane UFU-1.

With respect to the systems aspects that were poorly developed in this work, there is no one relevant aspect that should be commented.

Along the development of this work, a set of twelve theoretical changes or suggestion were proposed relative to the aerodynamics and dynamics of flight. The intention here was not to create any new theory but only applying some corrections and/or adjustment for the current theory. Next there are discussed in topics, these suggestions.

1. For the lift increment due the primary control surfaces deflection, the theory presents a given method, and separately it is presented a method to obtain the lift increment of a wing due the flaps deflection. What this work proposed is to assume that the primary control surfaces may be considered as “flaps” installed in its respectively aerodynamic surfaces, which are the horizontal and vertical tail. The limitation on this approach is that the graphical developed for the flap method do not consider negative deflections see Figure 2.17 and Figure 2.21, what could be bypassed, considering the fact that normally the airfoils employed on these tails are symmetrical, therefore, the deflections at both directions could be considered as being positive.
2. The theory available normally consider the lift generate by the set wing-fuselage and never the fuselage alone, therefore, this work proposed to estimate lift generated by the

fuselage alone by working the lift generate by the wing and the one generated by the set wing-fuselage, what resulted on the Equation 2.85 and on the Equation 2.86.

3. As the theory normally do not present a method to estimate the lift of the entire airplane in terms of aerodynamic coefficient, nor its curve slope, this work proposed a method to estimate it, by parametrizing the lift coefficient parcels due each aerodynamic surface as wing for example, by the biplane aerodynamic area, and in sequence, by obtaining the lift coefficient for two angle of attack for the complete airplane it is obtained the lift curve slope for the complete airplane. The development of this method was needs that arise to solve the formulation of the dynamics of flight, which employs these parameters.
4. The theory presents an approach to estimate the profile drag of a wing when there is no airfoil data available yet, such theory consider corrections for the interference drag and for the three dimensional effects. Once the airfoil to be employed on the wings and tails were defined and considering that its aerodynamic data were known, and by inspecting the formulation given in this method, this work proposed a modified formulation provided by the Equation 2.93, which consider the known aerodynamic drag coefficient for the airfoil.
5. During the development activities of the airplane UFU-1 there were faced challenges related to the airflow around the aerodynamic surfaces as the wing and canards, specifically relative to the downwash and upwash fields in which these surfaces are immersed during the airplane flight, these challenges are basically due the uncommon aerodynamic configuration of the aircraft. Researches in the bibliography available were performed, but were not found a theory or method that addressed the aerodynamic configuration peculiarities of this airplane, practically obligating the proposition of a different approach what was called by the author as *“Global Wash Field”*. In this case, it was formulated a method to account for all the wash fields in which a given aerodynamic surface may be immersed, the mathematical description of this approach is given in the Equation 2.124 to the Equation 2.128 and in the Equation 2.130.
6. This work assumes that, once the canards can be aerodynamically considered as wings installed on the fuselage of the airplane, it is reasonable to consider that these surfaces will suffer a shift on its aerodynamic center as occur for the wings. Therefore, this work proposed to apply for the canards, the method used to estimate the aerodynamic center shift of the wings.

7. During the development of this work was noted that the bibliography normally uses the reference areas of the wings and tails to define the dynamics of flight derivatives, which are essentially aerodynamic parameters, but, considering that these reference areas do not generate aerodynamic force nor moment, this work proposed that it is coherent to substitute these reference areas by its respective aerodynamic areas.
8. This proposition is a consequence of the proposition 5, by substituting the downwash and the upwash approaches by the global wash field one into the formulation of the longitudinal static stability due the canards.
9. This proposition is also a consequence of the proposition 5, by substituting the downwash and the upwash approaches by the global wash field one into the formulation of the static longitudinal neutral point and static margin of the airplane. Was also proposed to consider in this formulation the aerodynamic mean chord of the equivalent biplane wing.
10. Once the available theory broadly considers only the conventional configuration aircrafts, there were experienced some difficulties on modeling the dynamics of flight of the airplane UFU-1, being necessary do some adaptations in the available formulation, this way, all the stability and control derivatives that employ the wings parameters were on this work, changed by the biplane wing parameters.
11. By inspecting the theory of the contribution of the set wing-fuselage to the directional static stability, this work proposes to change the signal of the Equation 2.188 in accordance to the location of the lateral aerodynamic center of the fuselage relative to the position of the center of gravity of the airplane, turning this signal positive if the aerodynamic center is located behind the center of gravity.
12. As the activities of development of the airplane did not considered the structural design nor the mechanical system design, was not possible to estimate the airplane inertia products necessary for the dynamics of flight formulation, such inertia products could be found by implementing a digital mockup. Therefore, was necessary to develop a method of estimating these parameters based on the available theory, assuming that the mass of the airplane is concentrated on a single point.

Concluding, it is considered that this work reached its finality of proposing and designing (even in a preliminary phase) an unconventional airplane at Federal University of Uberlândia.

The activities to come, there are related to that which were not developed during this preliminary design phase as the structural development and the aeroelastic ones, which normally are developed into the preliminary phase but that were not the purpose of this work. In the sequence there must be developed the detailed design activities involving mainly the development of the systems of the airplane. After concluded all the design activities it is necessary to perform the activities related to the manufacturing and conception and development of the flying campaign.

It is important to say that some mathematical and numerical propositions were considered in this work. However, the intention was not to create any new theory or model, but only to apply some corrections and/or adjustment in the design calculation procedure. All corrections applied must be confirmed by the author or even in further studies at Federal University of Uberlândia.

REFERENCES

[1] Raymer, D. P., Aircraft Design: A Conceptual Approach, AIAA, 4th Ed., 2006.

[2] Torenbeek, E., Synthesis of subsonic airplane design, Delf University Press, 1976.

[3] Roskam, J., Airplane Design Part I: Preliminary Sizing of Airplanes, DARcorporation, 1997.

[4] Roskam, J., Airplane Design Part II: Preliminary Configuration Design and Integration of the Propulsive System, DARcorporation, 1997.

[5] Roskam, J., Airplane Design Part III: Layout Design of Cockpit, Fuselage, Wing and Empennage: Cutaways and Inboard Profiles, DARcorporation, 1997.

[6] Roskam, J., Airplane Design Part IV: Layout of Landing Gear and Systems, DARcorporation, 2000.

[7] Roskam, J., Airplane Design Part V: Component Weight Estimation, DARcorporation, 1999.

[8] Roskam, J., Airplane Design Part VI: Preliminary Calculation of Aerodynamic, Thrust and Power Characteristics, DARcorporation, 2000.

[9] Roskam, J., Airplane Design Part VII: Determination of Stability, Control and Performance Characteristics: FAR and Military Requirements, DARcorporation, 1991.

[10] Sadraey, M. H., Aircraft Design A Systems Engineering Approach, John Wiley & Sons, First Ed., 2013.

[11] Brandt, S. A., Stiles, R. J., Bertin, J. J., Whitford, R., Introduction to Aeronautics: A Design Perspective, United States Air Force Academy.

[12] Pazmany, L., LIGHT AIRPLANE DESIGN, THIRD EDITION, 1965.

[13] Kroo, I., Aircraft Design: Synthesis and Analysis, Desktop Aeronautics Inc, 2001.

[14] Jenkinson, L. R., Marchman, J. F., Aircraft Design Projects for engineering students, Butterworth Heinemann, First Ed., 2003.

[15] Matthews, C., Aeronautical Engineer's Data Book, Butterworth Heinemann, First Ed., 2002.

[16] Rodrigues, L. E. M. J., Fundamentos da Engenharia Aeronáutica Aplicações ao Projeto SAE-AERODESIGN Volume Único, 1ª edição., 2011.

[17] Gudmundsson, S., GENERAL AVIATION AIRCRAFT DESIGN: APPLIED METHODS AND PROCEDURES, Elsevier Inc, First Ed., 2014.

[18] FAR Federal Aviation Regulations Part 23 Airworthiness Standards: Normal, Utility, Acrobat and Commuter Category Airplanes, Federal Aviation Administration.

[19] Anderson, J. D., Fundamentals of Aerodynamics, McGraw-Hill, 3th Ed., 2001.

[20] Bertin, J. J., Cummings, R. M., AERODYNAMICS FOR ENGINEERS, PEARSON Prentice Hall, Fifth Edition, 2009.

[21] Smith, H. C. “Skip”., THE ILLUSTRATED GUIDE TO AERODYNAMICS, TAB Books, 2ND EDITION, 1992.

[22] Roskam, J., Lan, C. T. E., Airplane Aerodynamics and Performance, DARcorporation, First Ed., 1997.

[23] Houghton. E. L., Carpenter. P. W., Aerodynamics for Engineering Students, Butterworth Heinemann, Fifth Edition, 2003.

[24] Talay. T. A., INTRODUCTION TO THE AERODYNAMICS OF FLIGHT, NATIONAL AERONAUTICS AND SPACE ADMINISTRATION, 1975.

[25] Thomson. L. M. M., THEORETICAL AERODYNAMICS, DOVER PUBLICATIONS INC, FOURTH EDITION, 1973.

[26] White. F. M., Fluid Mechanics, McGrall-Hill, Fourth Edition, 2001.

[27] Etkin, B., Dynamics of Atmospheric Flight, DOVER, First Ed., 2005.

[28] Nelson, R. C., Flight Stability and Automatic Control, McGraw-Hill, 2th Ed., 1998.

[29] Eshelby, E. M., Aircraft Performance Theory and practice, Elsevier, 2000.

[30] Anderson, J. D., Aircraft Performance and Design, McGraw-Hill, 1999.

[31] Niu, M. C. Y., AIRFRAME STRUCTURAL DESIGN Practical Design Information and Data on Aircraft Structures, Conmilit Press LTD, Eighth printing., 1995.

[32] Niu, M. C. Y., AIRFRAME STRESS ANALYSIS AND SIZING, Conmilit Press LTD, Second Ed., 1999.

[33] Megson, T. H. G., Aircraft Structures for Engineering Students, Elsevier, Fourth Edition, 2010.

[34] ASM HANDBOOK Vol 02 Properties and Selection: Nonferrous Alloys and Special-Purpose Materials, ASM International, Fourth Printing, 1995.

[35] Carraher, C. E. Jr., GIANT MOLECULES Essential Materials for Everyday Living and Problem solving, John Wiley & Sons Inc, SECOND EDITION., 2003.

[36] Jane’s ALL THE WORLD’S AIRCRAFT 2004-2005, Jane’s Information Group Limited, 2004.

[37] Endress. G., Gething. M. J., Jane's Aircraft Recognition Guide, HarperCollins Publishers, 2007.

[38] Schick, W., Meyer, I., LUFTWAFFE SECRET PROJECTS FIGHTERS 1939 - 1945, Midland Publishing Limited, 1997.

[39] Herwig, D., Rode, H., LUFTWAFFE SECRET PROJECTS STRATEGIC BOMBERS 1935 - 1945, Midland Publishing Limited, 2000.

[40] Pimlott, J. Dr., Luftwaffe The illustrated history of the German Air Force in WWII, Motorbooks International Publishers & Wholesalers, 1998.

[41] Grant. R. G., FLIGHT THE COMPLETE HISTORY, DK Publishing, 2007.

[42] Caoimh. F. O., THE AVIATION BOOK A SURVEY OF THE WORLD'S AIRCRAFT, Chronicle Books LLC, 2006.

[43] Heppenheimer. T. A., Flight A History of Aviation in Photographs, Firefly Books Ltd, 2004.

[44] Hibbeler, R. C., DINÂMICA MECÂNICA PARA ENGENHARIA, PEARSON Prentice Hall, 10ª EDIÇÃO., 2005.

[45] Ira, H., Abbott., Albert, E., Doenhoff, V., Stivers, L. S., "SUMMARY OF AIRFOIL DATA", REPORT Nº 824, NACA.

[46] "NACA-INDUSTRY CONFERENCE ON PERSONAL AIRCRAFT RESEARCH", NACA, 1946.

[47] Loftin, L. K., "THEORETICAL AND EXPERIMENTAL DATA FOR A NUMBER OF NACA 6A-SERIES AIRFOIL SECTIONS", REPORT 903, NACA, 1947.

[48] Loftin, L. K., Smith, H. A., "AERODYNAMIC CHARACTERISTICS OF 15 NACA AIRFOIL SECTIONS AT SEVEN REYNOLDS NUMBERS", TN-1945, NACA, 1949.

[49] Goranson, F., "A METHOD FOR PREDITING THE ELEVATOR DEFLECTION REQUIRED TO LAND", WR L-95, NACA, 1944.

[50] McLean, D., "Wingtip Devices: What They Do and How They Do it", Article 4, Boeing Aerodynamics, Performance and Flight Operations Engineering Conference, 2005.

[51] Chappell, "AN INTRODUCTION TO AIRCRAFT EXCRESCENCE DRAG", ESDU-90029.

[52] Mitchell, D. J., "ESTIMATION OF AIRFRAME DRAG BY SUMMATION OF COMPONENTS: PRINCIPLES AND EXAMPLES", ESDU-97016.

[53] VENSON, Giuliano Gardolinski. Layout geral de aeronaves: Configurações de Aeronaves, Geometria das Superfícies Aerodinâmicas, Alongamento, Afilamento e Enflechamento. 01-31 oct 2013. 79 p. Class Notes.

[54] VENSON, Giuliano Gardolinski. Estimativa de polar de arrasto de aeronaves: Tipos de Arrasto Aerodinâmico em Aeronaves, Método Simplificado para Determinação da Polar de Arrasto de Aeronaves. 01-30 apr 2015. 37 p. Class Notes.

[55] VENSON, Giuliano Gardolinski. Pesos de aeronaves e estimativa de pesos: Pesos Característicos de Aeronaves, Estimativa das Frações de Peso da Aeronave, Estimativa do Peso de Decolagem. 01-30 apr 2015. 95 p. Class Notes.

[56] VENSON, Giuliano Gardolinski. Relações de desempenho de aeronaves: Carga Alar de Aeronaves Razão Empuxo-Peso de Aeronaves a Jato Razão Potência-Peso de Aeronaves à Hélice Estimativa de Desempenho de Aeronaves. 01-30 apr 2015. 156 p. Class Notes.

[57] VENSON, Giuliano Gardolinski. Dimensionamento inicial de aeronaves: Estimativa do Comprimento de Aeronaves, Empenagens e Superfícies de Controle, Posicionamento de Trem de Pouso e Motores, Estimativa do Momento de Inércia. 01-30 sep 2015. 61 p. Class Notes.

[58] VENSON, Giuliano Gardolinski. Layout de cabine de passageiros e carga: Configurações de Cabine de Aeronaves, Proporções Geométricas em Fuselagens, Compartimento e Dispositivos de Carga. 01-31 may 2014. 47 p. Class Notes.

[53] INSTALATION MANUAL FOR ROTAX ENGINE TYPE 912 SERIES, BRP-Powertrain GmbH & Co KG, 2015.

[54] Manual do Operador para todas as versões do ROTAX 912, 1998.

[55] G3X/G3T Touch Installation Manual, Garmin Ltd, Revision Z, 2016.

[56] G3X Pilot’s Guide, Garmin Ltd, 2016.

[57] GTR 200 Pilot’s Guide, Garmin Ltd, 2013.

[58] Aircraft Spruce & Specialty Catalog, 2016-2017.

[59] http://www.sciencedirect.com/

[60] https://www.aiaa.org/Publications/

[61] http://www.fisica.ufmg.br/~lab1/roteiros/Exp10_MovimentoHarmonicoAmortecido.pdf

[62] http://www.ifsc.usp.br/~strontium/Teaching/Material2013-2%20FCM0102%20Fisica%20II-EESC/Exercicio%20T14.77.pdf

APPENDIX A

```
%-------------------------------------------------------------------------
                % UNIVERSIDADE FEDERAL DE UBERLÂNDIA - UFU
                    % FACULDADE DE ENGENHARIA MECÂNICA
              % CURSO DE GRADUAÇÃO EM ENGENHARIA AERONÁUTICA

             % DISCIPLINE: PROJETO DE AERONAVES I - FEMEC43085

% Author: Frederico Carnevalli De Miranda
%-------------------------------------------------------------------------
% Commencement Date: 02/10/2015 (OCTOBER)
% Conclusion Date: 02/10/2015
%-------------------------------------------------------------------------
% Revision Date: 11/05/2017

    % THIS REVISION WAS FULFILLED FOR TRANSLATE THE TEXT OF THE PROGRAM

%-------------------------------------------------------------------------

% This program estimates the preliminar drag polar of the airplane
% This program makes the initial estimation of weights of the airplane

%-------------------------------------------------------------------------
clc;
clear all;

%-------------------------------------------------------------------------

%*************************************************************************
%*********************************ENTRY DATA******************************

%---GEOMETRICS PARAMETERS OF THE AIRPLANE---
Swet_Sref = 4.5; % Ratio between the total wet area and the reference area
                 % of the equivalent wing (From Slide 23/37 of the class
                 % material "polar drag estimation").

AR_w = 8; % Equivalent wing Aspect Ratio

Gam_W = 0; % [°] Wing SweepBack
Cos_Gam_W = cos((Gam_W*pi)/180);

REL_e = 0.09; % (1-e/e). (From slide 28/37 of the class material "polar drag
estimation")

Cfe = 0.0080; % From slide 14/37 of the class material "polar drag estimation"
%---------------------------

%---OPERATIONAL WEIGHTS-------
g = 9.81; % [m/s^2] Gravity acceleration
PASS = 1; % Number of passengers
```

```
PESOPASSNORM = 86*g; % [N] Weight per passengers
TRIPTEC = 1; % Number of pilots
TRIPCAB = 0; % Number of cabin crew
PESOTRIPNORM = 86*g; % [N] Weight per crew
CARG = 20*g; % [N] Cargo weight
%-----------------------------

%---PARAMETERS-ADJUSTMENT-CURVE-WEIGHT-FRACTION---
A = 0.925; % Coefficient of the adjustment curve
C = -0.047; % Coefficient of the adjustment curve
KVS = 1; % Sweep correction (1-> fixed / 1.04 -> variable)
CCM = 0.97; % Material correction (<1 for composite material; conventional ~
0.95)
%-----------------------------

%---PERFORMANCE PARAMETERS---
VEL = 47.222; % [m/s] Cruise Speed.
RHO_cruz = 0.96281;% [kg/m^3] Air density on cruise altitude (8000ft).
ALCAN = 600000; %  [m] Range.
TEMPESP = 12*60;% [s] Loiter time.
SFCCRUZ = 3.8663*10^-8; % [kg/W.s] Cruise Specific fuel consumption.
SFCESP = 3.3451*10^-8; % [kg/W.s] Loiter Specific fuel consumption.
EFICIEN = 0.8; % Propeller Efficiency.

%---PARAMETERS-ADJUSTMENT-CURVE-WING-LOADING--
A1 = 0.408; % Coefficient of the adjustment curve
C1 = 0.804; % Coefficient of the adjustment curve

%---PARAMETERS-ADJUSTMENT-CURVE-WETTED-AREA--
A2 = 0.6762; % Coefficient of the adjustment curve
C2 = 0.4884; % Coefficient of the adjustment curve

%---FUEL FRACTION---
PERCENTCOMBNAUTIL = 2; % Percentage of Fuel not Used.
PES_IN_EST = 500*9.81; % [N] Initial Estimated Airplane Gross Weight.
NUMITER = 1139; % Iteration Number.
INCREM = 0.5; % [N] Weight increment per iteration.
NUMITER_corr = 1193; % Second estimative iteration.
W1_0 = 0.990; % Taxi and takeoff Fuel fraction.
W2_1 = 0.992; % Climb Fuel fraction.
W4_3 = 0.993; % Descent Fuel fraction.
W6_5 = 0.993; % Landing and Taxi Fuel fraction.
%*************************************************************************
%*************************************************************************



%_________________________________________________________________________
%_____________________________________CALCULUS____________________________

fprintf('********************RESULTS FOR THE 1ª WEIGHT
ESTIMATIVE*********************');

%--------------------PRELIMINARY DRAG POLAR ESTIMATIVE---------------------
CD0 = Cfe*(Swet_Sref)
```

```
e_w_0_1 = (1/(1+REL_e)) % Oswald Factor
e_w_0_2 = 4.61*(1-0.045*(AR_w^0.68))*(Cos_Gam_W^0.15) - 3.1  % Oswald Factor
(Brandt, S. A., Stiles; "Introduction to Aeronautics: A Design Perspective")
e_w_0 = (e_w_0_1 + e_w_0_2)/2

k2 = (1/(pi*AR_w*e_w_0))
%-------------------------------------------------------------------------


%------------------INITIAL AIRPLANE WEIGHT ESTIMATIVE----------------------
PESOPASS = PESOPASSNORM*PASS; % Total Passenger Weight.
PESOTRIPTEC = PESOTRIPNORM*TRIPTEC; % Total Technical Crew Weight.
PESOTRIPCAB = PESOTRIPNORM*TRIPCAB; % Total Cabin Crew Weight.
CARGPAG = PESOPASS+CARG; % Total Payload.
PESOTRIP = PESOTRIPTEC+PESOTRIPCAB; % Total Crew Weight.

%---PARAMETERS - ADJUSTMENT-CURVE---
RAZLDC = 1/(2*sqrt(k2*CD0)) % Cruise L/D
RAZLDE = 3/(4*sqrt(3*k2*CD0)) % Loiter L/D

%---FUEL FRACTION & BASIC WEIGHTS----

%---W3/W2-(CRUISE)
W3_2 = exp((-g*ALCAN*SFCCRUZ)/(EFICIEN*RAZLDC))

%---W5/W4-(LOITER)
W5_4 = exp((-g*TEMPESP*VEL*SFCESP)/(EFICIEN*RAZLDE))

%---W6/W0-(TOTAL FRACTION)---
W6_0 = W1_0*W2_1*W3_2*W4_3*W5_4*W6_5;

%---Wf/W0---
PERCCOMB=PERCENTCOMBNAUTIL/100;

WFW0=(1+PERCCOMB)*(1-W6_0)

%---We/W0---
WEW0=(A*(PES_IN_EST^C)*KVS)*CCM;

%---BASIC WEIGHTS CALCULUS---

    PESOITER = PES_IN_EST;
    WEW01 = WEW0;

    for iter = 0:1:NUMITER

        W0 = (PESOTRIP + CARGPAG)/(1 - WFW0 - WEW0); % TOW.
        WEW0=(A*(PESOITER^C)*KVS)*CCM;

        PESOITER = PESOITER+INCREM;
        RESIDUO = PESOITER-W0;
```

```
        %-----------------
        WF = W0*WFW0; % TOTAL FUEL WEIGHT.

        %-----------------
        WE = W0*WEW01; % BASIC EMPTY WEIGHT.

        %-----------------
        OEW = WE+PESOTRIP;

    end

W0_kgf = W0/9.81;
OEW_kgf = OEW/9.81;
WE_kgf = WE/9.81;
WF_kgf = WF/9.81;

fprintf('TOW [kgf]:%f',W0_kgf);
fprintf('\n\n');
fprintf('OEW [kgf]:%f',OEW_kgf);
fprintf('\n\n');
fprintf('BEW [kgf]:%f',WE_kgf);
fprintf('\n\n');
fprintf('TFW [kgf]:%f',WF_kgf);
fprintf('\n\n');
fprintf('RESIDUE [kgf]:%f',RESIDUO);
fprintf('\n\n');
fprintf('**********************************************************************
***********');
%--------------------------------------------------------------------------


%------------------FINAL AIRPLANE WEIGHT ESTIMATIVE-----------------------

fprintf('\n\n');
fprintf('******************RESULTS FOR THE FINAL WEIGHT
ESTIMATIVE*********************');
fprintf('\n');



%---BASIC WEIGHT CALCULUS---

    PESOITER_corr = PES_IN_EST;

    for iter = 0:1:NUMITER_corr

        W_S = A1*(W0^C1); % Wing Loading Iterative Calculus.
        Sref_corr = W0/W_S; % Corrected Reference Area.

        W_cruz = (2*W0 - WF)/2; % Airplane Mean Weight during the cruise.
```

```
        CL_cruz_corr = (2*W_cruz)/(RHO_cruz*Sref_corr*(VEL^2));

        Swet_corr = A2*(W0^C2);
        CD0_corr = Cfe*(Swet_corr/Sref_corr);
        RAZLD_cruz = 1/((CD0_corr/CL_cruz_corr)+(k2*CL_cruz_corr)); % L/D_cruz
corrected.
        %---------------------------------

        %---W3/W2-(CRUISE)
        W3_2_corr = exp((-g*ALCAN*SFCCRUZ)/(EFICIEN*RAZLD_cruz));

        %---W6/W0-(TOTAL FRACTION)---
        W6_0_corr = W1_0*W2_1*W3_2_corr*W4_3*W5_4*W6_5;

        %---Wf/W0---
        WFW0_corr=(1+PERCCOMB)*(1-W6_0_corr);

        %-----------------
        W0_corr = (PESOTRIP + CARGPAG)/(1 - WFW0_corr - WEW0); % TOW.
        WEW0=(A*(PESOITER_corr^C)*KVS)*CCM;

        PESOITER_corr = PESOITER_corr + INCREM;
        RESIDUO_corr = PESOITER_corr - W0_corr;

        %-----------------
        WF_corr = W0_corr*WFW0_corr;

        %-----------------
        WE_corr = W0_corr*WEW01;

        %-----------------
        OEW_corr = WE_corr+PESOTRIP;

    end

W0_kgf_corr = W0_corr/9.81;
OEW_kgf_corr = OEW_corr/9.81;
WE_kgf_corr = WE_corr/9.81;
WF_kgf_corr = WF_corr/9.81;
W_S_kgf = W_S/9.81;

fprintf('TOW_corr [kgf] :%f',W0_kgf_corr);
fprintf('\n\n');
fprintf('OEW_corr [kgf] :%f',OEW_kgf_corr);
fprintf('\n\n');
fprintf('BEW_corr [kgf] :%f',WE_kgf_corr);
fprintf('\n\n');
fprintf('TFW_corr [kgf] :%f',WF_kgf_corr);
fprintf('\n\n');
fprintf('WING LOADING [kgf/m^2] :%f',W_S_kgf);
fprintf('\n\n');
fprintf('Sref_corr [m^2] :%f',Sref_corr);
fprintf('\n\n');
```

```
fprintf('Swet_corr [m^2] :%f',Swet_corr);
fprintf('\n\n');
fprintf('CD0_corr :%f',CD0_corr);
fprintf('\n\n');
fprintf('RESIDUE_corr [kgf] :%f',RESIDUO_corr);
fprintf('\n\n');
fprintf('**********************************************************************
***********');
fprintf('\n');
%-------------------------------------------------------------------------
```

APPENDIX B

```
%--------------------------------------------------------------------------
                % UNIVERSIDADE FEDERAL DE UBERLÂNDIA - UFU
                    % FACULDADE DE ENGENHARIA MECÂNICA
              % CURSO DE GRADUAÇÃO EM ENGENHARIA AERONÁUTICA

            % DISCIPLINE: PROJETO DE CONCLUSÃO DE CURSO - FEMEC43100

% Author: Frederico Carnevalli De Miranda
%--------------------------------------------------------------------------
% Commencement Date: 03/11/2016 (NOVEMBER)
% Conclusion Date: 07/11/2016

    %***Changes done (23/08/2017)***
    % 1 - Changed the position of the fuel system x_cg_fuel_Sys from the
    %     initial guess (5 [m]) for the defined final position (4.3 [m]).
    %***

    %***Changes done (26/08/2017)***
    % 1 - Changed the position of the fuel system x_cg_fuel_Sys from the
    %     position (5 [m]) for the defined final position (4.0 [m]).
    % 2 - Included the calculus of the product of inertia I_xz.
    %***

%--------------------------------------------------------------------------

%******************INITIAL SIZING OF THE AIRPLANE UFU-1******************

% This program makes the initial geometric dimensioning of the aircraft;
% estimate the main weights of cell and systems and estimate the CG of the
% aircraft; alter the results obtained in studies 3 and 5 from
% Discipline "Projeto de Aeronaves I - FEMEC43085".

clear all;
close all;
clc;

%_____________________________________HEADING_____________________________________
fprintf ('########################PROGRAM FOR INICIAL SIZING OF THE AIRPLANE
UFU-1#########################');
fprintf ('\n\n\n');
%_____________________________________________________________________________


%____________________GEOMETRICS PARAMETERS OF THE AIRPLANE____________________
fprintf ('_________________________________GEOMETRIC PARAMETERS OF THE
AIRPLANE_________________________________\n\n');

%***GENERAL PARAMETERS***
fprintf ('***GENERAL PARAMETERS***\n\n');
```

```
MTOW = 560.8*9.81; % [N] obtido do trabalho 2 da disciplina FEMEC43085

%*BiPlane Parameters*
S_W = 13.25; % [m^2] Total Wing Reference Area (obtido do trabalho 2 da
disciplina FEMEC43085)

GAP = 1.116604; % [m]

fprintf ('MTOW [N]: %g', MTOW);
fprintf ('\n\n');

fprintf ('--Bi Plane Parameters--\n\n');
fprintf ('Total Wing Area [m^2]: %g', S_W);
fprintf ('\n');
fprintf ('GAP [m]: %g', GAP);
fprintf ('\n\n');

%*Lower Wing*
C_r_W_low = 0.91; % [m] Lower Wing Root Cord
C_t_W_low = 0.91; % [m] Lower Wing Tip Cord
Thick_W_low = 0.18; % Cord Thickness
Lamb_W_low = C_t_W_low/C_r_W_low; % Lower Wing Taper Ratio
mac_W_low = (2/3)*C_r_W_low*((1+Lamb_W_low+(Lamb_W_low^2))/(1+Lamb_W_low)); %
[m] mac Lower Wing
S_W_low = S_W/2; % [m^2] Lower Wing Area
b_W_low = S_W_low/mac_W_low; % [m] Lower WingSpan
AR_W_low = (b_W_low^2)/S_W_low; % Lower Wing Aspect Ratio
Gam_W_low = 0; % [°] Lower Wing SweepBack

fprintf ('--Lower Wing Parameters--\n\n');
fprintf ('Lower Wing Root Cord [m]: %g', C_r_W_low);
fprintf ('\n')
fprintf ('Lower Wing Tip Cord [m]: %g', C_t_W_low);
fprintf ('\n');
fprintf ('Lower Wing Cord Thickness: %g', Thick_W_low);
fprintf ('\n');
fprintf ('Lower Wing Taper Ratio: %g', Lamb_W_low);
fprintf ('\n');
fprintf ('Lower Wing MAC [m]: %g', mac_W_low);
fprintf ('\n')
fprintf ('Lower Wing Reference Area [m^2]: %g', S_W_low);
fprintf ('\n');
fprintf ('Lower WingSpan [m]: %g', b_W_low);
fprintf ('\n');
fprintf ('Lower Wing Aspect Ratio: %g', AR_W_low);
fprintf ('\n');
fprintf ('Lower Wing SweepBack: %g', Gam_W_low);
fprintf ('\n\n')

%*Upper Wing*
C_r_W_up = 0.91; % [m] Upper Wing Root Cord
C_t_W_up = 0.91; % [m] Upper Wing Tip Cord
Thick_W_up = 0.18; % Cord Thickness
```

```
Lamb_W_up = C_t_W_up/C_r_W_up; % Upper Wing Taper Ratio
mac_W_up = (2/3)*C_r_W_up*((1+Lamb_W_up+(Lamb_W_up^2))/(1+Lamb_W_up)); % [m]
mac Upper Wing
S_W_up = (S_W - S_W_low); % [m^2] Upper Wing Area
b_W_up = S_W_up/mac_W_up; % [m] Upper WingSpan
AR_W_up = (b_W_up^2)/S_W_up; % Upper Wing Aspect Ratio
Gam_W_up = 0; % [°] Upper Wing SweepBack

fprintf ('--Upper Wing Parameters--\n\n');
fprintf ('Upper Wing Root Cord [m]: %g', C_r_W_up);
fprintf ('\n')
fprintf ('Upper Wing Tip Cord [m]: %g', C_t_W_up);
fprintf ('\n');
fprintf ('Upper Wing Cord Thickness: %g', Thick_W_up);
fprintf ('\n');
fprintf ('Upper Wing Taper Ratio: %g', Lamb_W_up);
fprintf ('\n');
fprintf ('Upper Wing MAC [m]: %g', mac_W_up);
fprintf ('\n')
fprintf ('Upper Wing Reference Area [m^2]: %g', S_W_up);
fprintf ('\n');
fprintf ('Upper WingSpan [m]: %g', b_W_up);
fprintf ('\n');
fprintf ('Upper Wing Aspect Ratio: %g', AR_W_up);
fprintf ('\n')
fprintf ('Upper Wing SweepBack: %g', Gam_W_up);
fprintf ('\n\n')

%*Average Wing
mac_W = 1.832; % [m] mac Equivalent Wing, Between low wing mac Leading Edge
and up wing mac T Edge.
b_W = (b_W_low + b_W_up)/2; % [m] Span Average Wing

fprintf ('--Average Wing Parameters--\n\n');
fprintf ('Average Wing MAC [m]: %g', mac_W);
fprintf ('\n');
fprintf ('Average Wing Span [m]: %g', b_W);
fprintf ('\n');
fprintf ('***************');
fprintf ('\n\n')
%**********************

%**Fuselage Sizing**
fprintf ('***FUSELAGE SIZING***\n\n');

    % Parameters obtained from CAD Design
x_L = 6.13; % [m] Fuselage lenght
y_C = 1.00; % [m] Fuselage Max Widht
x_N = 1.48; % [m] Fuselage Nose Lenght
x_C = 2.90; % [m] Cockpit Lenght
x_T = 1.75; % [m] Fuselage Tail Lenght

S_F_wet = 20.156; % [m^2] Obtained from Final Drawn of CAD Design
```

```
fprintf ('Fuselage Lenght [m]: %g', x_L);
fprintf ('\n')
fprintf ('Fuselage Max Widht [m]: %g', y_C);
fprintf ('\n')
fprintf ('Fuselage Nose Lenght [m]: %g', x_N);
fprintf ('\n')
fprintf ('Cockpit Lenght [m]: %g', x_C);
fprintf ('\n')
fprintf ('Fuselage Tail Lenght [m]: %g', x_T);
fprintf ('\n');
fprintf ('***************');
fprintf ('\n\n')
%**********************

%**Canards Sizing**
fprintf ('***CANARDS SIZING***\n\n');

%*Lower Canard*
C_r_can_low = 0.4; % [m] Lower Canard Root Cord
C_t_can_low = C_r_can_low; % [m] Lower Canard Tip Cord
Thick_can_low = 0.09; % Cord Thickness
Lamb_can_low = C_t_can_low/C_r_can_low; % Lower Canard Taper Ratio
mac_can_low =
(2/3)*C_r_can_low*((1+Lamb_can_low+(Lamb_can_low^2))/(1+Lamb_can_low)); % [m]
mac Lower Canard
AR_can_low = 8.1; % Lower Canard Aspect Ratio
b_can_low = AR_can_low*mac_can_low; % [m] Lower CanardSpan
S_can_low = mac_can_low*b_can_low; % [m^2] Lower Canard Reference Area
Gam_can_low = 0; % [°] Lower Canard SweepBack

fprintf ('--Lower Canard Parameters--\n\n');
fprintf ('Lower Canard Root Cord [m]: %g', C_r_can_low);
fprintf ('\n')
fprintf ('Lower Canard Tip Cord [m]: %g', C_t_can_low);
fprintf ('\n')
fprintf ('Lower Canard Cord Thickness: %g', Thick_can_low);
fprintf ('\n');
fprintf ('Lower Canard Taper Ratio: %g', Lamb_can_low);
fprintf ('\n')
fprintf ('Lower Canard MAC [m]: %g', mac_can_low);
fprintf ('\n')
fprintf ('Lower CanardSpan [m]: %g', b_can_low);
fprintf ('\n')
fprintf ('Lower Canard Reference Area [m^2]: %g', S_can_low);
fprintf ('\n')
fprintf ('Lower Canard Aspect Ratio: %g', AR_can_low);
fprintf ('\n')
fprintf ('Lower Canard SweepBack: %g', Gam_can_low);
fprintf ('\n\n')

%*Upper Canard*
C_r_can_up = C_r_can_low; % [m] Upper Canard Root Cord
C_t_can_up = C_r_can_up; % [m] Upper Canard Tip Cord
Thick_can_up = 0.09; % Cord Thickness
Lamb_can_up = C_t_can_up/C_r_can_up; % Upper Canard Taper Ratio
```

```
mac_can_up =
(2/3)*C_r_can_up*((1+Lamb_can_up+(Lamb_can_up^2))/(1+Lamb_can_up)); % [m] mac
Upper Canard
AR_can_up = 8.1; % Upper Canard Aspect Ratio
b_can_up = AR_can_up*mac_can_up; % [m] Upper CanardSpan
S_can_up = mac_can_up*b_can_up; % [m^2] Upper Canard Reference Area
Gam_can_up = 0; % [°] Upper Canard SweepBack

fprintf ('--Upper Canard Parameters--\n\n');
fprintf ('Upper Canard Root Cord [m]: %g', C_r_can_up);
fprintf ('\n')
fprintf ('Upper Canard Tip Cord [m]: %g', C_t_can_up);
fprintf ('\n')
fprintf ('Upper Canard Cord Thickness: %g', Thick_can_up);
fprintf ('\n');
fprintf ('Upper Canard Taper Ratio: %g', Lamb_can_up);
fprintf ('\n')
fprintf ('Upper Canard MAC [m]: %g', mac_can_up);
fprintf ('\n')
fprintf ('Upper CanardSpan [m]: %g', b_can_up);
fprintf ('\n')
fprintf ('Upper Canard Reference Area [m^2]: %g', S_can_up);
fprintf ('\n')
fprintf ('Upper Canard Aspect Ratio: %g', AR_can_up);
fprintf ('\n')
fprintf ('Upper Canard SweepBack: %g', Gam_can_up);
fprintf ('\n');
fprintf ('****************');
fprintf ('\n\n\n')
%**********************

%**Vertical Tail Sizing**
fprintf ('***VERTICAL TAIL SIZING***\n\n');

%*Left Vertical Tail*
C_r_vt_lef = 0.8; % [m] Left Vertical Tail Root Cord
C_t_vt_lef = 0.55; % [m] Left Vertical Tail Tip Cord
Thick_vt_lef = 0.12; % Cord Thickness
Lamb_vt_lef = C_t_vt_lef/C_r_vt_lef; % Left Vertical Tail Taper Ratio
mac_vt_lef =
(2/3)*C_r_vt_lef*((1+Lamb_vt_lef+(Lamb_vt_lef^2))/(1+Lamb_vt_lef)); % [m] mac
Left Vertical Tail
b_vt_lef = GAP; % [m] Left Vertical Tail Span
S_vt_lef = mac_vt_lef*b_vt_lef; % [m^2] Left Vertical Tail Reference Area
AR_vt_lef = (b_vt_lef^2)/S_vt_lef; % Left Vertical Tail Aspect Ratio
Gam_vt_lef = 9.532; % [°] Left Vertical Tail SweepBack

fprintf ('--Left Vertical Tail Parameters--\n\n');
fprintf ('Left Vertical Tail Root Cord [m]: %g', C_r_vt_lef);
fprintf ('\n')
fprintf ('Left Vertical Tail Tip Cord [m]: %g', C_t_vt_lef);
fprintf ('\n')
fprintf ('Left Vertical Tail Cord Thickness: %g', Thick_vt_lef);
fprintf ('\n');
fprintf ('Left Vertical Tail Taper Ratio: %g', Lamb_vt_lef);
```

```
fprintf ('\n')
fprintf ('Left Vertical Tail MAC [m]: %g', mac_vt_lef);
fprintf ('\n')
fprintf ('Left Vertical Tail Span [m]: %g', b_vt_lef);
fprintf ('\n')
fprintf ('Left Vertical Tail Reference Area [m^2]: %g', S_vt_lef);
fprintf ('\n')
fprintf ('Left Vertical Tail Aspect Ratio: %g', AR_vt_lef);
fprintf ('\n')
fprintf ('Left Vertical Tail SweepBack: %g', Gam_vt_lef);
fprintf ('\n\n')

%*Right Vertical Tail*
C_r_vt_rig = C_r_vt_lef; % [m] Right Vertical Tail Root Cord
C_t_vt_rig = C_t_vt_lef; % [m] Right Vertical Tail Tip Cord
Thick_vt_rig = Thick_vt_lef; % Cord Thickness
Lamb_vt_rig = C_t_vt_rig/C_r_vt_rig; % Right Vertical Tail Taper Ratio
mac_vt_rig =
(2/3)*C_r_vt_rig*((1+Lamb_vt_rig+(Lamb_vt_rig^2))/(1+Lamb_vt_rig)); % [m] mac
Right Vertical Tail
b_vt_rig = GAP; % [m] Right Vertical Tail Span
S_vt_rig = mac_vt_rig*b_vt_rig; % [m^2] Right Vertical Tail Reference Area
AR_vt_rig = (b_vt_rig^2)/S_vt_rig; % Right Vertical Tail Aspect Ratio
Gam_vt_rig = Gam_vt_lef; % [°] Right Vertical Tail SweepBack

fprintf ('--Right Vertical Tail Parameters--\n\n');
fprintf ('Right Vertical Tail Root Cord [m]: %g', C_r_vt_rig);
fprintf ('\n');
fprintf ('Right Vertical Tail Tip Cord [m]: %g', C_t_vt_rig);
fprintf ('\n');
fprintf ('Right Vertical Tail Cord Thickness: %g', Thick_vt_rig);
fprintf ('\n');
fprintf ('Right Vertical Tail Taper Ratio: %g', Lamb_vt_rig);
fprintf ('\n');
fprintf ('Right Vertical Tail MAC [m]: %g', mac_vt_rig);
fprintf ('\n');
fprintf ('Right Vertical Tail Span [m]: %g', b_vt_rig);
fprintf ('\n');
fprintf ('Right Vertical Tail Reference Area [m^2]: %g', S_vt_rig);
fprintf ('\n');
fprintf ('Right Vertical Tail Aspect Ratio: %g', AR_vt_rig);
fprintf ('\n');
fprintf ('Right Vertical Tail SweepBack: %g', Gam_vt_rig);
fprintf ('\n\n');

%*Primary Flight Control Surfaces*
S_ail_S_w = 0.07; % Area Ratio (S_ail/S_W) Obtained from classes material
(FEMEC43085)
S_ail = S_ail_S_w*S_W_up; % [m^2] Total Aileron Area

S_elev_S_Can = 0.41; % Area Ratio (S_elev/S_Can) Obtained from classes
material (FEMEC43085)
S_elev_low = S_elev_S_Can*S_can_low; % [m^2] Elevator Area
S_elev_up = S_elev_S_Can*S_can_up; % [m^2] Elevator Area
```

```
S_rud_S_vt = 0.36; % Area Ratio (S_rud/S_vt) Obtained from classes material
(FEMEC43085)
S_rud_lef = S_rud_S_vt*S_vt_lef; % [m^2] Rudder Area
S_rud_rig = S_rud_S_vt*S_vt_rig; % [m^2] Rudder Area

fprintf ('--Primary Flight Control Surfaces--\n\n');
fprintf ('Total Ailerons Area [m^2]: %g', S_ail);
fprintf ('\n');
fprintf ('Lower Elevator Area [m^2]: %g', S_elev_low);
fprintf ('\n');
fprintf ('Upper Elevator Area [m^2]: %g', S_elev_up);
fprintf ('\n');
fprintf ('Left Rudder Area [m^2]: %g', S_rud_lef);
fprintf ('\n');
fprintf ('Right Rudder Area [m^2]: %g', S_rud_rig);
fprintf ('\n\n');

fprintf
('_____
_____\n\n');
%_____


%_____POSITIONING THE MAIN COMPONENTS OF THE AIRPLANE_____
%fprintf ('_____POSITIONING THE MAIN COMPONENTS OF THE
AIRPLANE_____\n\n');

        % PS: ALL THE POSITIONING ARE OBTAINED FROM THE CAD DESEIGN DRAW

%*Lower Wing*
X_LE_Cr_W_low = 3.604702; % [m] Lower Wing Root cord Leading Edge positioning
along "X" axix
X_TE_Cr_W_low = X_LE_Cr_W_low + C_r_W_low; % [m] Lower Wing Root cord Trailing
Edge positioning along "X" axix
X_LE_mac_W_low = X_LE_Cr_W_low; % [m] Lower Wing MAC Leading Edge positioning
along "X" axix
X_TE_mac_W_low = X_TE_Cr_W_low; % [m] Lower Wing MAC Trailing Edge positioning
along "X" axix
X_ac_mac_W_low = X_LE_mac_W_low + 0.23*mac_W_low; % [m] Lower Wing MAC
Aerodynamic Center positioning along "X" axix

%*Upper Wing*
X_LE_Cr_W_up = 4.526674; % [m] Upper Wing Root cord Leading Edge positioning
along "X" axix
X_TE_Cr_W_up = X_LE_Cr_W_up + C_r_W_up; % [m] Upper Wing Root cord Trailing
Edge positioning along "X" axix
X_LE_mac_W_up = X_LE_Cr_W_up; % [m] Upper Wing MAC Leading Edge positioning
along "X" axix
X_TE_mac_W_up = X_TE_Cr_W_up; % [m] Upper Wing MAC Trailing Edge positioning
along "X" axix
X_ac_mac_W_up = X_LE_mac_W_up + 0.23*mac_W_up; % [m] Upper Wing MAC
Aerodynamic Center positioning along "X" axix

%*Average Wing*
```

```
X_ac_mac_W = (X_ac_mac_W_low + X_ac_mac_W_up)/2; % [m]

%*Lower Canard*
X_LE_Cr_can_low = 1.4; % [m] Lower Canard Root cord Leading Edge positioning
along "X" axix
X_TE_Cr_can_low = X_LE_Cr_can_low + C_r_can_low; % [m] Lower Canard Root cord
Trailing Edge positioning along "X" axix
X_LE_mac_can_low = X_LE_Cr_can_low; % [m] Lower Canard MAC Leading Edge
positioning along "X" axix
X_TE_mac_can_low = X_TE_Cr_can_low; % [m] Lower Canard MAC Trailing Edge
positioning along "X" axix
X_ac_mac_can_low = X_LE_mac_can_low + 0.23*mac_can_low; % [m] Lower Canard MAC
Aerodynamic Center positioning along "X" axix

%*Upper Canard*
X_LE_Cr_can_up = 1.5; % [m] Upper Canard Root cord Leading Edge positioning
along "X" axix
X_TE_Cr_can_up = X_LE_Cr_can_up + C_r_can_up; % [m] Upper Canard Root cord
Trailing Edge positioning along "X" axix
X_LE_mac_can_up = X_LE_Cr_can_up; % [m] Upper Canard MAC Leading Edge
positioning along "X" axix
X_TE_mac_can_up = X_TE_Cr_can_up; % [m] Upper Canard MAC Trailing Edge
positioning along "X" axix
X_ac_mac_can_up = X_LE_mac_can_up + 0.23*mac_can_up; % [m] Upper Canard MAC
Aerodynamic Center positioning along "X" axix

%*Left Vertical Tail*
X_LE_Cr_vt_lef = 5.187; % [m] Left Vertical Tail Root cord Leading Edge
positioning along "X" axix
X_TE_Cr_vt_lef = X_LE_Cr_vt_lef + C_r_vt_lef; % [m] Left Vertical Tail Root
cord Trailing Edge positioning along "X" axix
Z_mac_vt_lef = ((GAP/6)*((1+2*Lamb_vt_lef)/(1+Lamb_vt_lef))); % [m] MAC
position from VT Root
Teta_vt_lef = 12.62; % [°] Angle between "Z" axix and Vertical Tail Leading
Edge
X_LE_mac_vt_lef = X_LE_Cr_vt_lef - (Z_mac_vt_lef*tan(Teta_vt_lef*pi/180)); %
[m] Left Vertical Tail MAC Leading Edge positioning along "X" axix
X_TE_mac_vt_lef = X_LE_mac_vt_lef + mac_vt_lef; % [m] Left Vertical Tail MAC
Trailing Edge positioning along "X" axix
X_ac_mac_vt_lef = X_LE_mac_vt_lef + 0.25*mac_vt_lef; % [m] Left Vertical Tail
MAC Aerodynamic Center positioning along "X" axix

%*Right Vertical Tail*
X_LE_Cr_vt_rig = X_LE_Cr_vt_lef; % [m] Right Vertical Tail Root cord Leading
Edge positioning along "X" axix
X_TE_Cr_vt_rig = X_LE_Cr_vt_rig + C_r_vt_rig; % [m] Right Vertical Tail Root
cord Trailing Edge positioning along "X" axix
Z_mac_vt_rig = ((GAP/6)*((1+2*Lamb_vt_rig)/(1+Lamb_vt_rig))); % [m] MAC
position from VT Root
Teta_vt_rig = Teta_vt_lef; % [°] Angle beteen "Z" axix and Vertical Tail
Leading Edge
X_LE_mac_vt_rig = X_LE_Cr_vt_rig - (Z_mac_vt_rig*tan(Teta_vt_rig*pi/180)); %
[m] Right Vertical Tail MAC Leading Edge positioning along "X" axix
X_TE_mac_vt_rig = X_LE_mac_vt_rig + mac_vt_rig; % [m] Right Vertical Tail MAC
Trailing Edge positioning along "X" axix
```

```
X_ac_mac_vt_rig = X_LE_mac_vt_rig + 0.25*mac_vt_rig; % [m] Right Vertical Tail
MAC Aerodynamic Center positioning along "X" axix

%*Lending Gear*
X_gear_nose = 0.540; % [m]
X_gear_main = 4.1; % [m]

%*Engine*
X_engine = 5.836674; % [m]

%fprintf
('_____________________________________________________________________________
_____________________\n\n');
%_____________________________________________________________________________


%_________________WEIGHT & BALANCE PROPERTIES OF THE AIRPLANE_________________
fprintf ('_______________________________WEIGHT & BALANCE PROPRERTIES OF THE
AIRPLANE_______________________________\n\n');

%***GENERAL PARAMETERS***

%**Unit Conversion Parameters**
ft2_m2 = 0.09290304; % ft^2 --> m^2
lbs_kgf = 0.4535929; % lbs --> kgf
lb_ft3__kg_m3 = (lbs_kgf)/(0.3048^3); % lb/ft^3 --> kg/m^3
%lb_ft2__N_m2 = (lbs_kgf*9.81)/(0.3048^2); % lb/ft^2 --> N/m^2
N_m2__lb_ft2 = 0.02088543; % N/m^2 --> lb/ft^2
%***********************

%**Miscelaneous Parameters**
rho = 0.96281; % [kg/m^3] Density at flight level (8000ft)
V = 47.222; % [m/s] Cruise speed
q = (0.5*rho*(V^2))*N_m2__lb_ft2; % [lb/ft^2] Dynamic pressure
L_D_crus = 11.23; % L/D_cruise (studies 4 from Discipline "Projeto de
Aeronaves I - FEMEC43085")
R = 600; % [Km] Airplane Maximum Range

N_lim = 4.3; % Limit Load Factor
N_U = N_lim*1.5; % Ultimate Load Factor
N_gear = 1.7; % Preliminary estiamtion
N_l = N_gear*1.5; % Landing Ultimate Load Factor
W_0 = MTOW/9.81; % [KG]
W_l = W_0; % [KG]

Ht_Hv = 0; % From  bibliography [1]
l_t = (X_ac_mac_W - X_ac_mac_can_low)/0.3048; % [ft]
%l_t = (X_ac_mac_vt_lef - X_ac_mac_W)/0.3048; % [ft]
L_m = 25.59; % [in] Preliminary estiamtion
L_n = 23.62; % [in] Preliminary estiamtion
B_W = b_W_low + b_W_up; % [m]
V_i = (36.857/0.72)*0.2641721; % [gal] Fuel tank volume
V_t = V_i + 0.05; % [gal] Fuel tank volume plus piping volume
S_flap = S_ail_S_w*S_W_low; % [m^2] Flaps Area
```

```
Delt = (30*pi)/180; % [rad] Max Flap Deflection (Preliminary estimation)

N_t = 1; % Number of Tanks
N_en = 1; % Number of Engines

K_door = 1.0;
K_ldg = 1.12;
K_ws = 1;
%**********************

%***COMPONENTS WEIGHT & CG POSITION***
fprintf ('***COMPONENTS WEIGHT***\n\n');

%*Wings*
W_1_1_1 =
(0.036*((S_W_low/ft2_m2)^0.758)*((AR_W_low/(cos(Gam_W_low*pi/180)*cos(Gam_W_lo
w*pi/180)))^0.6)*(q^0.006)*(Lamb_W_low^0.04)*(((100*Thick_W_low)/cos(Gam_W_low
*pi/180))^-0.3)*(N_U*(W_0/lbs_kgf))^0.49)*lbs_kgf; % [Kgf]
x_cg_W_low = X_LE_mac_W_low + (0.398*mac_W_low); % [m] where '0.398' is the
position os max profile thickness
m_1_1_1 = W_1_1_1*x_cg_W_low; % [Kgf*m]

W_1_1_2 =
(0.036*((S_W_up/ft2_m2)^0.758)*((AR_W_up/(cos(Gam_W_up*pi/180)*cos(Gam_W_up*pi
/180)))^0.6)*(q^0.006)*(Lamb_W_up^0.04)*(((100*Thick_W_up)/cos(Gam_W_up*pi/180
))^-0.3)*(N_U*(W_0/lbs_kgf))^0.49)*lbs_kgf; % [Kgf]
x_cg_W_up = X_LE_mac_W_up + (0.398*mac_W_up); % [m] where '0.398' is the
position os max profile thickness
m_1_1_2 = W_1_1_2*x_cg_W_low; % [Kgf*m]

fprintf ('Lower Wing Estimated Weight [Kgf]: %g', W_1_1_1);
fprintf ('\n');
fprintf ('Upper Wing Estimated Weight [Kgf]: %g', W_1_1_2);
fprintf ('\n');

%*Canards*
W_1_2_1 =
(0.016*((N_U*(W_0/lbs_kgf))^0.414)*(q^0.168)*((S_can_low/ft2_m2)^0.896)*(((100
*Thick_can_low)/cos(Gam_can_low*pi/180))^-
0.12)*((AR_can_low/(cos(Gam_can_low*pi/180)*cos(Gam_can_low*pi/180)))^0.043)*(
Lamb_can_low^-0.02))*lbs_kgf; % [Kgf]
x_cg_Can_low = X_LE_mac_can_low + (0.352*mac_can_low); % [m] where '0.352' is
the position os max profile thickness
m_1_2_1 = W_1_2_1*x_cg_Can_low; % [Kgf*m]

W_1_2_2 =
(0.016*((N_U*(W_0/lbs_kgf))^0.414)*(q^0.168)*((S_can_up/ft2_m2)^0.896)*(((100*
Thick_can_up)/cos(Gam_can_up*pi/180))^-
0.12)*((AR_can_up/(cos(Gam_can_up*pi/180)*cos(Gam_can_up*pi/180)))^0.043)*(Lam
b_can_up^-0.02))*lbs_kgf; % [Kgf]
x_cg_Can_up = X_LE_mac_can_up + (0.352*mac_can_up); % [m] where '0.352' is the
position os max profile thickness
m_1_2_2 = W_1_2_2*x_cg_Can_up; % [Kgf*m]
```

```
fprintf ('Lower Canard Estimated Weight [Kgf]: %g', W_1_2_1);
fprintf ('\n');
fprintf ('Upper Canard Estimated Weight [Kgf]: %g', W_1_2_2);
fprintf ('\n');

%*Vertical Tails*
W_1_3_1 =
(0.073*(1+0.2*Ht_Hv)*((N_U*(W_0/lbs_kgf))^0.376)*(q^0.122)*((S_vt_lef/ft2_m2)^
0.873)*(((100*Thick_vt_lef)/cos(Gam_vt_lef*pi/180))^-
0.49)*((AR_vt_lef/(cos(Gam_vt_lef*pi/180)*cos(Gam_vt_lef*pi/180)))^0.357)*(Lam
b_vt_lef^0.039))*lbs_kgf; % [Kgf]
x_cg_VT_lef = X_LE_mac_vt_lef + (0.3*mac_vt_lef); % [m] where '0.3' is the
position os max profile thickness
m_1_3_1 = W_1_3_1*x_cg_VT_lef; % [Kgf*m]

W_1_3_2 =
(0.073*(1+0.2*Ht_Hv)*((N_U*(W_0/lbs_kgf))^0.376)*(q^0.122)*((S_vt_rig/ft2_m2)^
0.873)*(((100*Thick_vt_rig)/cos(Gam_vt_rig*pi/180))^-
0.49)*((AR_vt_rig/(cos(Gam_vt_rig*pi/180)*cos(Gam_vt_rig*pi/180)))^0.357)*(Lam
b_vt_rig^0.039))*lbs_kgf; % [Kgf]
x_cg_VT_rig = X_LE_mac_vt_rig + (0.3*mac_vt_rig); % [m] where '0.3' is the
position os max profile thickness
m_1_3_2 = W_1_3_2*x_cg_VT_rig; % [Kgf*m]

fprintf ('Left Vertical Tail Estimated Weight [Kgf]: %g', W_1_3_1);
fprintf ('\n');
fprintf ('Right Vertical Tail Estimated Weight [Kgf]: %g', W_1_3_2);
fprintf ('\n');

%*Fuselage*
%W_F = input ('Which Fuselage Weight Formula?: ');
%if (W_F == 1)
 %   W_1_4 =
0.6083*K_door*K_ldg*((W_0*N_U)^0.5)*(x_L^0.25)*(S_F_wet^0.302)*((1+K_ws)^0.04)
*((x_L/y_C)^0.1); % [Kgf]
%end

%if (W_F == 2)
    W_1_4 =
(0.052*((S_F_wet/ft2_m2)^1.086)*((N_U*(W_0/lbs_kgf))^0.177)*((l_t)^-
0.051)*(L_D_crus^-0.072)*(q^0.241))*lbs_kgf; % [Kgf]
%end

x_cg_Fus = 0.6*6.11; % [m] Initial guess
m_1_4 = W_1_4*x_cg_Fus; % [Kgf*m]

fprintf ('Fuselage Estimated Weight [Kgf]: %g', W_1_4);
fprintf ('\n');

%*Landing Gear*
W_1_5 = (0.095*((N_l*(W_l/lbs_kgf))^0.768)*((L_m/12)^0.409))*lbs_kgf; % [Kgf]
x_cg_gear_main = X_gear_main; % [m]
m_1_5 = W_1_5*x_cg_gear_main; % [Kgf*m]
```

```
W_1_6 = (0.125*((N_l*(W_l/lbs_kgf))^0.566)*((L_n/12)^0.845))*lbs_kgf; % [Kgf]
x_cg_gear_nose = X_gear_nose; % [m]
m_1_6 = W_1_6*x_cg_gear_nose; % [Kgf*m]

fprintf ('Main Landing Gear Estimated Weight [Kgf]: %g', W_1_5);
fprintf ('\n');
fprintf ('Nose Landing Gear Estimated Weight [Kgf]: %g', W_1_6);
fprintf ('\n');

%*Surface Controls*
W_1_7 = (0.053*((x_L*3.28083)^1.536)*(((b_W_low
+b_W_up)*3.28083)^0.371)*((N_U*(W_0/lbs_kgf)*(10^-4))^0.8))*lbs_kgf; % [Kgf]
x_cg_Sur_cont = (X_TE_mac_W_low + X_TE_mac_W_up)/2; % [m]
m_1_7 = W_1_7*x_cg_Sur_cont; % [Kgf*m]

fprintf ('Surface Controls Estimated Weight [Kgf]: %g', W_1_7);
fprintf ('\n');

%*Engine Equiped*
W_2_1 = 55.4+1.7+4+3+0.8+1.3; % [Kgf] (From ROTAX)
x_cg_Engine = 5.836674; % [m]
m_2_1 = W_2_1*x_cg_Engine; % [Kgf*m]

W_2_8 = 2.0; % [Kgf] Engine suspension frame (From ROTAX)
x_cg_en_moun = 5.836674; % [m]
m_2_8 = W_2_8*x_cg_en_moun; % [Kgf*m]

fprintf ('Engine Equiped Estimated Weight [Kgf]: %g', W_2_1);
fprintf ('\n');
fprintf ('Engine Mounting Estimated Weight [Kgf]: %g', W_2_8);
fprintf ('\n');

%*Oil System*
W_2_3 = 0.01*N_en*W_2_1; % [Kgf]
x_cg_Oil_sys = 5.5; % [m] Initial guess
m_2_3 = W_2_3*x_cg_Oil_sys; % [Kgf*m]

fprintf ('Oil System Estimated Weight [Kgf]: %g', W_2_3);
fprintf ('\n');

%*Fuel System*
W_2_4 = (2.49*(V_t^0.726)*((1/(1+(V_i/V_t)))^0.363)*(N_t^0.242)*(N_en^-
0.157))*lbs_kgf; % [Kgf]
x_cg_fuel_Sys = 4.003; % [m] (Old guess position 5.0m) (2nd guess position
4.3m)
m_2_4 = W_2_4*x_cg_fuel_Sys; % [Kgf*m]

fprintf ('Fuel System Estimated Weight [Kgf]: %g', W_2_4);
fprintf ('\n');

%*Propeller Instalation*
W_2_6 = 4.1; % [Kgf] Sensenich Propeller assembly
x_cg_prop = 6.190697; % [m]
```

```
m_2_6 = W_2_6*x_cg_prop; % [Kgf*m]

fprintf ('Propeller Instalation Estimated Weight [Kgf]: %g', W_2_6);
fprintf ('\n');

%*Flight Control System*
W_3_1_1 = 0.154*(W_0)^0.67; % [Kgf]
x_cg_fli_cont = x_cg_Sur_cont; % [m]
m_3_1_1 = W_3_1_1*x_cg_fli_cont; % [Kgf*m]

W_3_1_2 = 5.569*((S_flap*sin(Delt))^0.92); % [Kgf]
x_cg_flap = x_cg_fli_cont; % [m]
m_3_1_2 = W_3_1_2*x_cg_flap; % [Kgf*m]

fprintf ('Flight Control System Estimated Weight [Kgf]: %g', W_3_1_1);
fprintf ('\n');
fprintf ('Flaps System Estimated Weight [Kgf]: %g', W_3_1_2);
fprintf ('\n');

%*Avionics System*
W_3_2_1 = 0.44+0.608+0.124+0.124+0.725+0.124+0.133+0.22+0.303+0.246+0.244; %
[Kgf]
x_cg_avionic = 2.201702; % [m]
m_3_2_1 = W_3_2_1*x_cg_avionic; % [Kgf*m]

W_3_2_2 = 2.0+1.2+0.725+0.226+0.304+0.310; % [Kgf]
x_cg_eletronic_modul = 1.4; % [m] Initial Guess
m_3_2_2 = W_3_2_2*x_cg_eletronic_modul; % [Kgf*m]

fprintf ('Avionics Estimated Weight [Kgf]: %g', W_3_2_1);
fprintf ('\n');
fprintf ('Avionics Eletronic Modulus Estiamted Weight [Kgf]: %g', W_3_2_2);
fprintf ('\n');

%*Eletrical System*
W_3_4 = 19.1; % [Kgf] Estimated  10.5KGF
x_cg_batterie = 0.5; % [m]
m_3_4 = W_3_4*x_cg_batterie; % [Kgf*m]

fprintf ('Battery Estiamted Weight [Kgf]: %g', W_3_4);
fprintf ('\n');

%*Other Components*
W_Seat_1 = 9.298 + (1.3); % [Kgf] (1.5 seat belt estimated)
x_cg_seat_1 = 3.0; % [m]
m_seat_1 = W_Seat_1*x_cg_seat_1; % [Kgf*m]

W_Seat_2 = 9.298 + (1.3); % [Kgf] (1.5 seat belt estimated)
x_cg_seat_2 = 4.0; % [m]
m_seat_2 = W_Seat_2*x_cg_seat_2; % [Kgf*m]

W_av_pan = 2.558; % [Kgf] Avionics Panel
x_cg_av_pan = 2.1; % [m]
```

```
m_av_pan = W_av_pan*x_cg_av_pan; % [Kgf*m]

fprintf ('Seat Pilot 1 + Seat Belt Estimated Weight [Kgf]: %g', W_Seat_1);
fprintf ('\n');
fprintf ('Seat Pilot 2 + Seat Belt Estiamted Weight [Kgf]: %g', W_Seat_2);
fprintf ('\n');
fprintf ('Avionics Panel Estiamted Weight [Kgf]: %g', W_av_pan);
fprintf ('\n');
fprintf ('****************');
fprintf ('\n\n');
%***********************

%***EMPTY AIRPLANE WEIGHT & BALANCE***
fprintf ('***EMPTY AIRPLANE WEIGHT & BALANCE***\n\n');

W_AIRPLANE_TOTAL =
W_1_1_1+W_1_1_2+W_1_2_1+W_1_2_2+W_1_3_1+W_1_3_2+W_1_4+W_1_5+W_1_6+W_1_7+W_2_1+
W_2_8+W_2_3+W_2_4+W_2_6+W_3_1_1+W_3_1_2+W_3_2_1+W_3_2_2+W_3_4+W_Seat_1+W_Seat_
2+W_av_pan; % [Kgf]
M_AIRPLANE_TOTAL =
m_1_1_1+m_1_1_2+m_1_2_1+m_1_2_2+m_1_3_1+m_1_3_2+m_1_4+m_1_5+m_1_6+m_1_7+m_2_1+
m_2_8+m_2_3+m_2_4+m_2_6+m_3_1_1+m_3_1_2+m_3_2_1+m_3_2_2+m_3_4+m_seat_1+m_seat_
2+m_av_pan; % [Kgf*m]
CG_EMPTY_AIRPLANE = M_AIRPLANE_TOTAL/W_AIRPLANE_TOTAL; % [m]

fprintf ('Empty Airplane Weight [Kgf]: %g', W_AIRPLANE_TOTAL);
fprintf ('\n');
fprintf ('Empty Airplane CG [m]: %g', CG_EMPTY_AIRPLANE);
fprintf ('\n');
fprintf ('****************');
fprintf ('\n\n');
%***********************

%***AIRPLANE OEW & BALANCE***
fprintf ('***AIRPLANE OEW & BALANCE***\n\n');

W_Pilot_1 = input ('Pilot 1 Weight (50 - 90) [Kgf]: ' ); % [kgf]
m_Pil_1 = W_Pilot_1*x_cg_seat_1; % [Kgf*m]

OEW = W_AIRPLANE_TOTAL + W_Pilot_1; % [kgf]
M_OEW = M_AIRPLANE_TOTAL + m_Pil_1; % [Kgf*m]
CG_OEW = M_OEW/OEW; % [m]

fprintf ('OEW [Kgf]: %g', OEW);
fprintf ('\n');
fprintf ('OEW CG [m]: %g', CG_OEW);
fprintf ('\n');
fprintf ('****************');
fprintf ('\n\n');
%***********************

%***AIRPLANE WEIGHT & BALANCE VARIATION***
fprintf ('***AIRPLANE WEIGHT & BALANCE VARIATION***\n\n');
```

```
W_Pilot_2 = input ('Pilot 2 Weight (0 - 90) [Kgf]: ' ); % [kgf]
m_Pil_2 = W_Pilot_2*x_cg_seat_2; % [Kgf*m]

W_Pay_Load = input ('Pay Load (0 - 20) [Kgf]: ' ); % [kgf]
x_Pay_Load = 1.2; % [m]
m_Pay_Load = W_Pay_Load*x_Pay_Load; % [Kgf*m]

W_Fuel = input ('Fuel Weight (0 - 33) [Kgf]: ' ); % [kgf]
m_Fuel = W_Fuel*x_cg_fuel_Sys; % [Kgf*m]

W = OEW + W_Pilot_2 + W_Pay_Load + W_Fuel; % [kgf] AIRPLANE ATUAL WEIGHT
M_W = M_OEW + m_Pil_2 + m_Pay_Load + m_Fuel; % [Kgf*m]
CG_W = M_W/W; % [m] WEIGHT CG

fprintf ('\n\n');
fprintf ('AIRPLANE ATUAL WEIGHT [Kgf]: %g', W);
fprintf ('\n');
fprintf ('AIRPLANE ATUAL CG [m]: %g', CG_W);
fprintf ('\n');
fprintf ('***************');
fprintf ('\n\n');

%***ESTIMATED MEAN WING CG - AC***
fprintf ('***ESTIMATED MEAN WING CG - AC***\n\n');

%x_AC =
(((X_LE_mac_W_low+(mac_can_low*0.23))+(X_LE_mac_W_up+(mac_can_up*0.23)))/2)*1;
% [m] Estimated position of Mean Wing AC for Fuselage interference
x_AC = 4.215; % [m] Estimated position of Mean Wing AC for Fuselage
interference
CG_AC = CG_W - x_AC; % [m]

fprintf ('ESTIMATED MEAN WING AC [m]: %g', x_AC);
fprintf ('\n\n');
fprintf ('ESTIMATED CG - AC [m]: %g', CG_AC);
fprintf ('\n\n');

fprintf
('_____________________________________________________________________________
_____________________\n\n');
%_____________________________________________________________________________


%_____________________________MASS PROPERTIES_____________________________
fprintf ('_____________________________________________MASS
PROPERTIES_____________________________________________\n\n');
g = 9.801; % [m/s^2)

m = W; % Mass [Kg]
W_N = m*g; % [N]

R_x = 0.25; % from SLIDE 60/61 (Classroom materials "FEMEC43085"
R_y = 0.38;
```

```
R_z = 0.39;

I_xx = ((b_W^2)*W_N*(R_x^2))/(4*g);
I_yy = ((x_L^2)*W_N*(R_y^2))/(4*g);
I_zz = (((b_W + x_L)/2)^2)*(W_N*(R_z^2))/(4*g);

r_xx = sqrt(I_xx/W);
r_yy = sqrt(I_yy/W);
r_zz = sqrt(I_zz/W);
z_m = sqrt((r_xx^2 + r_yy^2 - r_zz^2)/2);
x_m = sqrt(r_yy^2 - z_m^2);
y_m = sqrt(r_xx^2 - z_m^2);
I_xy = x_m*y_m*W;
I_xz = x_m*z_m*W;
I_yz = y_m*z_m*W;

fprintf ('Mass Moment of Inertia - I_xx [Kg*m^2]: %g', I_xx);
fprintf ('\n');
fprintf ('Mass Moment of Inertia - I_yy [Kg*m^2]: %g', I_yy);
fprintf ('\n');
fprintf ('Mass Moment of Inertia - I_zz [Kg*m^2]: %g', I_zz);
fprintf ('\n');
fprintf ('Mass Product of Inertia - I_xz [Kg*m^2]: %g', I_xz);
fprintf ('\n');
fprintf ('Mass Product of Inertia - I_xy [Kg*m^2]: %g', I_xy);
fprintf ('\n');
fprintf ('Mass Product of Inertia - I_yz [Kg*m^2]: %g', I_yz);
fprintf ('\n\n');

fprintf
('_____________________________________________________________________________
_____________________\n\n');
%_____________________________________________________________________________


%_____________________FLIGHT MECHANICAL OF THE AIRPLANE_____________________
fprintf ('_____________________________________FLIGHT MECHANICAL OF THE
AIRPLANE_____________________________________\n\n');

%**Canards**
l_can_low = CG_W - X_ac_mac_can_low; % [m] Lower Canard Arm
V_can_low = -(l_can_low*S_can_low)/(mac_W*S_W); % Tail Volume Coeficient Lower
Canard (Negative)

l_can_up = CG_W - X_ac_mac_can_up; % [m] Upper Canard Arm
V_can_up = -(l_can_up*S_can_up)/(mac_W*S_W); % Tail Volume Coeficient Upper
Canard (Negative)

V_can = V_can_low + V_can_up; % Tail Volume Coeficient Canard

fprintf ('--Canards Parameters--\n\n');

fprintf ('Lower Canard Arm: %g', l_can_low);
```

```
fprintf ('\n')
fprintf ('Lower Canard Tail Volume Coeficient: %g', V_can_low);
fprintf ('\n\n')

fprintf ('Upper Canard Arm: %g', l_can_up);
fprintf ('\n')
fprintf ('Upper Canard Tail Volume Coeficient: %g', V_can_up);
fprintf ('\n\n')

fprintf ('Total Canard Tail Volume Coeficient: %g', V_can);
fprintf ('\n');
fprintf ('***************');
fprintf ('\n\n\n')
%**********************

%**Vertical Tails**
l_vt_lef = X_ac_mac_vt_lef - CG_W; % [m] Left Vertical Tail Arm
V_vt_lef = (l_vt_lef*S_vt_lef)/(b_W*S_W); % Tail Volume Coeficient Left
Vertical Tail

l_vt_rig = X_ac_mac_vt_rig - CG_W; % [m] Right Vertical Tail Arm
V_vt_rig = (l_vt_rig*S_vt_rig)/(b_W*S_W); % Tail Volume Coeficient Right
Vertical Tail

V_vt = V_vt_lef + V_vt_rig; % Tail Volume Coeficient Vertical Tail

fprintf ('--Vertical Tail Parameters--\n\n');

fprintf ('Left Vertical Tail Arm: %g', l_vt_lef);
fprintf ('\n')
fprintf ('Left Vertical Tail Tail Volume Coeficient: %g', V_vt_lef);
fprintf ('\n\n')

fprintf ('Right Vertical Tail Arm: %g', l_vt_rig);
fprintf ('\n')
fprintf ('Right Vertical Tail Tail Volume Coeficient: %g', V_vt_rig);
fprintf ('\n\n')

fprintf ('Total Vertical Tail Volume Coeficient: %g', V_vt);
fprintf ('\n\n');

fprintf
('_____________________________________________________________________
_____________________\n\n');
%_____________________________________________________________________
```

APPENDIX C

OBS: this algorithm uses the aerodynamic areas of the wings and tails.

```
%-------------------------------------------------------------------------
                % UNIVERSIDADE FEDERAL DE UBERLÂNDIA - UFU
                    % FACULDADE DE ENGENHARIA MECÂNICA
              % CURSO DE GRADUAÇÃO EM ENGENHARIA AERONÁUTICA

            % DISCIPLINE: PROJETO DE CONCLUSÃO DE CURSO - FEMEC43100

% Author: Frederico Carnevalli De Miranda
%-------------------------------------------------------------------------
% Commencement Date: 15/11/2016
% Conclusion Date: 07/09/2017

%-------------------------------------------------------------------------

%***************AERONAUTIC CALCULUS FOR THE AIRPLANE UFU-1*****************

% This program estimate the aerodynamic, flight mechanics and performance
% characteristics for the complete airplane.

clear all;
close all;
clc;
%*************************************************************************
%****************************SOFTWARE MANNUAL*****************************
%     GENERAL:
%     #FLAPS: If is desired just one position simulation type the same
%     value for "First Flaps Deflection" and "Last Flaps Deflection".
%
%     #CANARD INCIDENCE: If is desired just one position for simulation,
%     type the value desired for "First Canard Incidence"; type "1" for the
%     "Canard Incidence Increment"; type the value desired for
%     "Last Canard Incidence".
%
%     #ELEVATOR DEFLECTION: If is desired just one position for simulation,
%     type the value desired for "First Elevator Deflection"; type "1" for
%     the "Elevator Deflection Increment"; type the value desired for
%     "Last Elevator Deflection".
%
% 1 - COMPLETE ANALYSIS:
%
% 2 - AERODYNAMICS ANALYSIS:
%     # Alpha definition: if it is a vector, type -> Alp_i:Alp_inc:Alp_f
%
%     # Beta definition: if it is a vector, type -> Bet_i:Bet_inc:Bet_f
%
%     # OBS: if Alpha is a vector, Beta should not be a vector at the same
%     time for a same simulation, and vice versa.
```

```
%
% 3 - STATIC STABILITY & CONTROL ANALYSIS:
%     # Alpha definition: if it is a vector, type -> Alp_i:Alp_inc:Alp_f
%
%     # Beta definition: if it is a vector, type -> Bet_i:Bet_inc:Bet_f
%
%     # OBS: if Alpha is a vector, Beta should not be a vector at the same
%     time for a same simulation, and vice versa.
%
% 4 - DYNAMIC STABILITY ANALYSIS:
%     # Alpha and Beta must be a scalar number.
%
% 5 - PERFORMANCE ANALYSIS:
%     # For estimate the Power and Thrus curves, it is necessary enter the
%     'Airplane Cruise Flight Speed' as a vector of the kind: v_i:0.1:v_f;
%     it is necessary that v_i > 10.
%
%     # For estimate the Power and Thrus curves, it is necessary enter the
%     'Alpha as a scalar number.
%
%     # Alpha definition: if it is a VECTOR Type: [Alp-ground Alp-liftoff
%     Alp-Stall Alp-Climb Alp-Cru Alp-Descent].
%
% 6 - SHOW GEOMETRIC PROPERTIES OF THE AIRPLANE:
%     # It is necessary for Alpha: type '0' for "First Angle...", type '1'
%     for "Angle...increment..." and type '0' for "Last Angle...". For
%     Flap: type '0' for "First Flap Deflecion" and type '0' for
%     "Last Flap...". For Canard Incidence: type '0' for "First Canard...",
%     type '1' for "Canard...increment" and type '0' for "Last Canard...".
%     For Elevator Deflection: type '0' for "First Elevator...", type '1'
%     for "Elevator...increment" and type '0' for "Last Elevator...".
%
%     # ALL THE OTHER PARAMETERS MAY BE LEFT BLANK.
%**************************************************************************

%_____________________________________HEADING_____________________________________
fprintf ('###PROGRAM FOR ESTIMATE THE AERODYNAMIC, FLIGHT MECHANIC AND
PERFORMANCE CHARACTERISTICS OF THE AIRPLANE UFU-1###');

fprintf ('\n\n\n');
%_____________________________________________________________________________

%_____________________________________MAIN MENU_____________________________________
fprintf ('_____________________________________________MAIN
MENU_____________________________________________\n\n');

fprintf ('1 - COMPLETE ANALYSIS');
fprintf ('\n');
fprintf ('2 - AERODYNAMICS ANALYSIS');
fprintf ('\n');
fprintf ('3 - STATIC STABILITY & CONTROL ANALYSIS');
fprintf ('\n');
fprintf ('4 - DYNAMIC STABILITY ANALYSIS');
fprintf ('\n');
fprintf ('5 - PERFORMANCE ANALYSIS');
```

```
fprintf ('\n');
fprintf ('6 - SHOW GEOMETRIC PROPERTIES OF THE AIRPLANE');
fprintf ('\n\n');

main_menu = input ('Enter the Analysis Option: ' );
fprintf ('\n\n\n');
%_____________________________________________________________________________

%____________________________AIRPLANE FLIGHT PARAMETERS_____________________________
fprintf ('_____________________________________AIRPLANE FLIGHT
PARAMETERS_____________________________________\n\n');

V_wind = input ('Cross Wind Speed [m/s]: ' );

if (main_menu == 1 | main_menu == 2 | main_menu == 3 | main_menu == 4 |
main_menu == 6)

     VEL = input ('Airplane Cruise Flight Speed [km/h]: ' );
        VEL_m_s = VEL/3.6;
        V_T = sqrt((VEL_m_s.^2) + (V_wind.^2)); % [m/s] Airplane Total Speed
due the Cross Wind
            V_T_km = V_T*3.6; % [km/h]
end

if (main_menu == 5)

    V_LOF_const = input ('V_LOF (Lift-off Speed) [km/h]: ' );
        V_LOF_const_ft_s = V_LOF_const*0.9113444; % [ft/s]

    VEL_Climb = input ('Airplane Climb Speed [km/h]: ' );
        VEL_Climb_m_s = VEL_Climb/3.6;
        V_T_Climb = sqrt((VEL_Climb_m_s.^2) + (V_wind.^2));

    VEL = input ('Airplane Cruise Flight Speed [km/h]: ' );
        VEL_m_s = VEL/3.6;
        V_T = sqrt((VEL_m_s.^2) + (V_wind.^2)); % [m/s] Airplane Total Speed
due the Cross Wind
            V_T_km = V_T*3.6; % [km/h]
end

fprintf ('\n');

if (main_menu == 1 | main_menu == 2 | main_menu == 3 | main_menu == 4 |
main_menu == 6)

    H = input ('Flight Altitude [ft] (May be a vector): ' );
end

if (main_menu == 5)

    H_run = input ('Runway Altitude [ft]: ' );
    H = input ('Flight Altitude [ft] (May be a vector): ' );
end
```

```
%-ISA ATMOSPHERE-
RHO_SEAL = 1.225; % [kg/m^3]
MI_ZERO = 1.79*(10^-5); % [Kg/(m*s)] Reference Air Absolute Viscosity
R = 287.05287; % Gas Universal Constant [N m/kg K]
T_SEA = 15+273.15; % Sea Level Temperature [K]
TEMP = T_SEA - (0.0019812.*H); % Flight Level ISA Temperature [K]
TETA = TEMP./T_SEA; % Temperature Ratio
DELTA = (TETA.^(5.2561)); % Pressure Ratio
SIGMA = DELTA./TETA; % Density Ratio
RHO = RHO_SEAL.*SIGMA; % Air Density [Kg/m^3]
MI = MI_ZERO*((TEMP/T_SEA).^(3/4)); % [Kg/(m*s)] Air Absolute Viscosity
NI = MI/RHO; % [m^2/s] Air Kinematic Viscosity
fprintf ('Flight Level ISA Temperature [°C]: %g', TEMP);
fprintf ('\n');
fprintf ('Air Density [Kg/m^3]: %g', RHO);
fprintf ('\n');
fprintf ('Air Absolute Viscosity [Kg/(m*s)]: %g', MI);
fprintf ('\n');
fprintf ('Air Kinematic Viscosity [m^2/s]: %g', NI);
fprintf ('\n');

gam = 1.4;
a = sqrt(gam*R*TEMP);
Mach = V_T./a;

if (length(Mach) == 1)
    fprintf ('Flight Mach Number - M: %g', Mach);
    fprintf ('\n\n');
end

fprintf ('\n');
Dens = input ('Want to change the Air density Press -> 1): ' );
fprintf ('\n\n');
if (Dens == 1)
    RHO = input ('New Air density [Kg/m^3]: ' );
    fprintf ('\n\n');
end

q = (0.5*RHO*(V_T.^2)); % [Kg/(m^2 * s^2] Dynamic Pressure
q_I = q*(0.06242796)*(3.28083); % [Lb/(ft^2 * s^2] Dynamic Pressure
%---

if (main_menu == 1)

    Alpha_f = input ('First Angle of Attack [°]: ');
    Alpha_i = input ('Angle of Attack Increment (Must be different from Zero)
[°]: ');
    Alpha_l = input ('Last Angle of Attack [°]: ');

end

if (main_menu == 2 | main_menu == 3 | main_menu == 4 | main_menu == 5 |
main_menu == 6)
```

```
    Alpha_f = 0;
    Alpha_i = 1;
    Alpha_l = 0;
end

for Alpha = Alpha_f:Alpha_i:Alpha_l;
    Alpha_rad = Alpha*pi/180; % [rad]

    if (main_menu == 2)
        Alpha = input ('Angle of Attck [°] (Max - 15°; May be a vector): ' );
            Alpha_rad = Alpha*pi/180; % [rad]
    end

    if (main_menu == 3)
        Alpha = input ('Angle of Attack. If is a Vector Type (Alp_i:inc:Alp_f)
[°]: ');
            Alpha_rad = Alpha*pi/180; % [rad]
    end

    if (main_menu == 4)
        Alpha = input ('Angle of Attack [°]: ');
            Alpha_rad = Alpha*pi/180; % [rad]
    end

    if (main_menu == 5)
        Alpha = input ('Angle of Attack. If a VECTOR -> [Alp-ground | Alp-
liftoff | Alp-Stall | Alp-Climb | Alp-Cru | Alp-Descent] [°]: ');
            Alpha_rad = Alpha*pi/180; % [rad]
    end

fprintf ('\n\n');
Delt_Fa_f = input ('First Flaps Deflection (0; 10; 20) [°]: ' ); % [°]
Delt_Fa_l = input ('Last Flaps Deflection (0; 10; 20) [°]: ' ); % [°]
for Delt_F = Delt_Fa_f:10:Delt_Fa_l;
    Delt_f_rad = (2*pi*Delt_F)/360; % [rad]
    fprintf ('Flap Deflection [°]: %g', Delt_F);
    fprintf ('\n\n');

i_can_low_f = input ('First Canard Incidence [°]: '); % [°] Lower Canard
Incidence
i_can_low_i = input ('Canard Incidence Increment (Must be different from Zero)
[°]: ');
i_can_low_l = input ('Last Canard Incidence [°]: '); % [°] Lower Canard
Incidence
for i_can_low = i_can_low_f:i_can_low_i:i_can_low_l;
    i_can_low_rad = (2*pi*i_can_low)/360; % [rad]
    fprintf ('Canards Incicende [°]: %g', i_can_low);
    fprintf ('\n\n');

Delt_elev_f = input ('First Elevator Deflection (min: -20; max: +20) [°]: ' );
% [°]
Delt_elev_i = input ('Elevator Deflection Increment (Must be different from
Zero) [°]: ' ); % [°]
```

```
Delt_elev_l = input ('Last Elevator Deflection (min: -20; max: +20) [°]: ' );
% [°]
for Delt_elev = Delt_elev_f:Delt_elev_i:Delt_elev_l;
    fprintf ('Elevators Deflection [°]: %g', Delt_elev);
    fprintf ('\n\n');

if (V_wind ~= 0)
    Beta_rad = atan(V_wind/VEL_m_s);
    Beta = Beta_rad*180/pi;
    fprintf ('Yaw Angle (Sideslip) [°]: %g', Beta);
    fprintf ('\n');
end
if (V_wind == 0)
    Beta = input ('Yaw Angle (Sideslip). If is a Vector Type (Bet_i:inc:Bet_f)
[°]: ' );
    Beta_rad = Beta*pi/180; % [rad]
end
Phi = input ('Roll Angle [°]: ' );
    Phi_rad = Phi*pi/180; % [rad]

fprintf ('\n');
fprintf ('---Control Surfaces & Lift---');
fprintf ('\n\n');
Delt_rud = input ('Rudder Deflection (min: -30; max: +30) [°] : ' ); % [°]
    Delt_rud_rad = Delt_rud*pi/180; % [rad]
Delt_ail_lef = input ('Left Aileron Deflection (min: -25; max: +20) [°]: ' );
% [°]
Delt_ail_rig = input ('Right Aileron Deflection (min: -25; max: +20) [°]: ' );
% [°]

fprintf
('_____________________________________________________________________________
_____________________\n\n');

%_______________________________AIRPLANE PARAMETERS_______________________________

if (main_menu == 1 | main_menu == 2 | main_menu == 3 | main_menu == 4 |
main_menu == 5)
fprintf ('_____________________________________________AIRPLANE
PARAMETERS_____________________________________________\n\n');

%-----------------------------MASS PROPERTIES-----------------------------
fprintf ('-----------------------------------------MASS PROPERTIES------------
---------------------------\n\n');
g = 9.801; % [m/s^2)
    g_ft =g*3.280853; % [ft/s^2]

m_Pil_1 = input ('Pilot 1 Mass (50 - 90) [Kg]: ' );
W_Pil_1 = m_Pil_1*g; % [N]
W_Pil_1_lb = W_Pil_1*0.2248089; % [lbs]

m_Pil_2 = input ('Pilot 2 Mass (0 - 90) [Kg]: ' );
W_Pil_2 = m_Pil_2*g; % [N]
W_Pil_2_lb = W_Pil_2*0.2248089; % [lbs]
```

```
m_gas = input ('Fuel Mass (0 - 33) [Kg]: ' );
W_gas = m_gas*g; % [N]
W_gas_lb = W_gas*0.2248089; % [lbs]

m_Pay_Load = input ('Pay Load (0 - 20) [Kg]: ' );
W_Pay_Load = m_Pay_Load*g; % [N]
W_Pay_Load_lb = W_Pay_Load*0.2248089; % [lbs]

m_ap = 367.911; % [Kg]
W_ap = m_ap*g; % [N]
W_ap_lb = W_ap*0.2248089; % [lbs]

m = m_ap + m_Pil_1 + m_Pil_2 + m_gas + m_Pay_Load; % [Kg] Airplane Total Mass
W = m*g; % [N]
W_lb = W*0.2248089; % [lbs]
fprintf ('Airplane Total Mass [Kg]: %g', m);
fprintf ('\n\n');

    if (main_menu == 1 | main_menu == 3 | main_menu == 4)

        X_CG = input ('Airplane CG Position on X axix [m]: ' );
        Y_CG = input ('Airplane CG Position on Y axix [m]: ' );
        Z_CG = input ('Airplane CG Position on Z axix (relative to runway)
[m]: ' );

        I_xx = input ('Mass Moment of Inertia at CG - I_xx [Kg*m^2]: ' );
        I_yy = input ('Mass Moment of Inertia at CG - I_yy [Kg*m^2]: ' );
        I_zz = input ('Mass Moment of Inertia at CG - I_zz [Kg*m^2]: ' );
        I_xz = input ('Mass Product of Inertia at CG - I_xz [Kg*m^2]: ' );
    end

fprintf ('-------------------------------------------------------------------------
--------------------------\n\n');

%-------------------------------------------------------------------------

%-------------------PROPULSION PROPERTIES OF THE AIRPLANE------------------
fprintf ('----------------------------PROPULSION PROPERTIES OF THE AIRPLANE--
--------------------------\n\n');

N_eng = 1; % Number of Engines
Z_Thrust = 1.187; % [m] Thrust Line position in "z" axis (from CAD drawing)

%*Engine Properties*
POW_max = 59655.99; % [Watt] Power maximum at Sea Level ISA

if (main_menu == 2 | main_menu == 3 | main_menu == 4)

    Pow_perc = input ('Cruise Flight Engine Power Percentage [%]: ' );
    POWER = (Pow_perc/100)*POW_max; % [Watt]
    POWER_hp = POWER*0.001341022; % [hp]
```

```
end

if (main_menu == 1 | main_menu == 5)

Pow_perc_Tof = input ('Take-off Engine Power Percentage [%]: ' );
POWER_Tof = (Pow_perc_Tof/100)*POW_max; % [Watt]
    POWER_Tof_hp = POWER_Tof*0.001341022; % [hp]

Pow_perc_Climb = input ('Climb Engine Power Percentage [%]: ' );
POWER_Climb = (Pow_perc_Climb/100)*POW_max; % [Watt]
    POWER_Climb_hp = POWER_Climb*0.001341022; % [hp]

Pow_perc = input ('Cruise Flight Engine Power Percentage [%]: ' );
POWER = (Pow_perc/100)*POW_max; % [Watt]
    POWER_hp = POWER*0.001341022; % [hp]

POWER_Loit = (58.5/100)*POW_max; % [Watt]
    POWER_Loit_hp = POWER_Loit*0.001341022; % [hp]

Pow_perc_Desc = input ('Descent Flight Engine Power Percentage [%]: ' );
POWER_Desc = (Pow_perc_Desc/100)*POW_max; % [Watt]
    POWER_Desc_hp = POWER_Desc*0.001341022; % [hp]
end

    %¨¨SFC¨¨
    RHO_GAS = 0.713; % [kg/l]
    SFC_TOF = 7.42708*10^-8; % [kg/W.s] Take-off Specific fuel consumption @
100%.
        SFC_TOF_lb_h = 0.442095; % [lb/hp/hr]
    SFC_CRUZ = 3.8663*10^-8; % [kg/W.s] Cruise Specific fuel consumption @
70%.
        SFC_CRUZ_lb_h = 0.304509; % [lb/hp/hr]
    SFC_LOIT = 3.3451*10^-8; % [kg/W.s] Loiter Specific fuel consumption. @
58.5%
    SFC_LAND = 3.0946*10^-8; % [kg/W.s] Landing Specific fuel consumption @
53%.
        SFC_LAND_lb_h = 0.245608; % [lb/hp/hr]


%*Propeller Properties
n_prop = 3; % Number of blades
Prop_Diam = 1.7272; % [m] Diameter of the Propeller
    Prop_Diam_ft = Prop_Diam*3.28083; % [ft]

    %*Eta_prop obtention
    V_FLI = 1.852*[29.091 40 50 60 70 80 90 100 110 120 130 140 150 155.522];
    ETA_PROP = [0.479 0.595 0.674 0.732 0.776 0.811 0.832 0.85 0.863 0.868
0.863 0.855 0.837 0.816];

        %*Plot*
        figure (1)
        plot (V_FLI,ETA_PROP)
        grid on;
```

```
        title ('PROPELLER EFFICIENCY CURVE');
        xlabel ('V [km/h]');
        ylabel ('ETA');
        legend ('Propeller Efficiency');
        hold on

    if (main_menu == 5)
    if (length(VEL_Climb) == 1)
        if (VEL_Climb < 53.87)
            Eta_prop_climb = 0.479;
        end
        if (VEL_Climb >= 53.87)
            Eta_prop_climb = ((1.6*10^-13)*VEL_Climb^5)-((4.6*10^-
10)*VEL_Climb^4)+((2.9*10^-7)*VEL_Climb^3)-((8.8*10^-
5)*VEL_Climb^2)+(0.014*VEL_Climb)-0.053; %ADJUST MORE OR LESS
        end

        %*Power & Thrust
        TEP_Climb = POWER_Climb*Eta_prop_climb*sqrt(RHO/RHO_SEAL); % [W] Power
Available at Flight Level (Thurst Equivalebt Power)

    end
    end

    if (length(VEL) == 1)
        if (VEL < 53.87)
            Eta_prop = 0.479;
        end
        if (VEL >= 53.87)
            Eta_prop = ((1.6*10^-13)*VEL^5)-((4.6*10^-10)*VEL^4)+((2.9*10^-
7)*VEL^3)-((8.8*10^-5)*VEL^2)+(0.014*VEL)-0.053; %ADJUST MORE OR LESS
        end

        %*Power & Thrust
        TEP = POWER*Eta_prop*sqrt(RHO/RHO_SEAL); % [W] Power Available at
Flight Level (Thurst Equivalebt Power)
        T_Fli_lev = (TEP./V_T)*cos(Alpha_rad); % [N]
    end

    if (length(VEL) > 1) % Valid for the Performance Power and Thurst curves
        fprintf ('\n');
        aux_1 = input ('Enter the first value of the Flight Speed [km/h]: ');
        aux_2 = input ('Enter the the value of the Flight Speed increment
[km/h]: ');
        aux_3 = input ('Enter the last value of the Flight Speed [km/h]: ');

        V = aux_1:aux_2:aux_3
            Eta_prop = ((1.6*10^-13)*V.^5)-((4.6*10^-10)*V.^4)+((2.9*10^-
7)*V.^3)-((8.8*10^-5)*V.^2)+(0.014*V)-0.053;

            %*Power & Thrust
            TEP = POWER*Eta_prop*sqrt(RHO/RHO_SEAL); % [W] Power Available at
Flight Level (Thurst Equivalebt Power)
            T_Fli_lev = (TEP./V_T)*cos(Alpha_rad); % [N]
```

```
    end

    fprintf ('Propeller Eta: %g', Eta_prop);
    fprintf ('\n');
    fprintf ('Thrust at Flight Level [N]: %g', T_Fli_lev);
    fprintf ('\n\n');

fprintf ('------------------------------------------------------------------------
--------------------------\n\n');
end
%-------------------------------------------------------------------------

%-------------------GEOMETRIC PROPERTIES OF THE AIRPLANE-------------------
fprintf ('------------------------------GEOMETRIC PROPERTIES OF THE AIRPLANE--
--------------------------\n\n');

%……….……….……….……….……….……FUSELAGE……….……….……….……….……….……
fprintf ('***FUSELAGE***\n\n');

x_L = 6.13; % [m] Fuselage lenght
y_C = 1.00; % [m] Fuselage Max Widht
z_C = 1.37; % [m] Fuselage Height for y_C
h = 1.45; % [m] Fuselage Max Height (depth)
F_c_l = h/2; % [m] Fuselage center Line
S_cross_fus_max = 1.2; % [m^2] from CAD drawings (Area of the maximum cross
section)
S_b_fus = 0.286; % [m^2] from CAD drawings (Area of the cross section of the
end of the fuselage)

d_f = sqrt((4/pi)*S_cross_fus_max); % [m] from theory [Roskam VI; pg45]
d_b = sqrt((4/pi)*S_b_fus); % [m] from theory [Roskam VI; pg45]

S_xy_fus = 4.67; % [m^2] from CAD drawings
S_wet_fus = 20.155 - (1.818 - 1.704); % [m^2] from CAD drawings
Z_fus = 1; % [m] fuselage ac position in "z" axis (assumed)

if (main_menu == 1 | main_menu == 6)
fprintf ('Fuselage Lenght [m]: %g', x_L);
fprintf ('\n');
fprintf ('Maximum Fuselage Widht [m]: %g', y_C);
fprintf ('\n');
fprintf ('Fuselage Equivalent Diameter [m]: %g', d_f);
fprintf ('\n');
fprintf ('Fuselage Wetted Area [m^2]: %g', S_wet_fus);
fprintf ('\n\n\n');
end
%……….……….……….……….……….……….……….……….……….……….……….……….……

%……….……….……….……….……….……WING……….……….……….……….……….……
fprintf ('***WINGS***\n\n');

%*BiPlane Parameters*
S_W = 13.23; % [m^2] Total Wing Reference Area (from CONCEPTUAL DESIGN)
```

```
GAP = 1.116604; % [m]
Span_Ratio_W = 1;
Stagger_W = -39.546; % [°]
Decal_W = 0; % [°] Angle of Decalage

if (main_menu == 1 | main_menu == 6)
fprintf ('***Wings Biplane Parameters***\n\n');
fprintf ('Total Reference Area [m^2]: %g', S_W);
fprintf ('\n');
fprintf ('GAP [m]: %g', GAP);
fprintf ('\n');
fprintf ('Span Ratio: %g', Span_Ratio_W);
fprintf ('\n');
fprintf ('Angle of Stagger [°]: %g', Stagger_W);
fprintf ('\n');
fprintf ('Angle of Decalage [°]: %g', Decal_W);
fprintf ('\n\n\n');
end

%*Upper Wing*
C_r_W_up = 0.91; % [m] Upper Wing Root Chord
C_t_W_up = 0.91; % [m] Upper Wing Tip Chord
Thick_W_up = 0.18; % Chord Thickness
Lamb_W_up = C_t_W_up/C_r_W_up; % Upper Wing Taper Ratio
mac_W_up = (2/3)*C_r_W_up*((1+Lamb_W_up+(Lamb_W_up^2))/(1+Lamb_W_up)); % [m]
mac Upper Wing
b_W_up = 7.30; % [m] Upper WingSpan
S_W_up = b_W_up*mac_W_up; % [m^2] Upper Wing Reference Are
S_aero_W_up = S_W_up - (0.559*mac_W_up/2); % [m^2] Upper Wing Aerodynamic Area
(b*h/2-> local triangle área of fuselage)
AR_W_up = (b_W_up^2)/S_W_up; % Upper Wing Aspect Ratio
Gam_W_up = 0; % [°] Upper Wing SweepBack
    Gam_W_up_rad = (2*pi*Gam_W_up)/360; % [rad]
Tao_W_up = 0; % [°] Upper Wing Dihedral
    Tao_W_up_rad = (2*pi*Tao_W_up)/360; % [rad]
i_W_up = 0; % [°] Upper Wing Incidence

X_LE_mac_W_up = 4.526674; % [m] Upper Wing MAC Leading Edge positioning along
"X" axix
Z_W_up = 1.65; % [m] MAC Line position in "z" axis (from CAD drawing)

if (main_menu == 1 | main_menu == 6)
fprintf ('***Upper Wing***\n\n');
fprintf ('Upper Wing Root Chord [m]: %g', C_r_W_up);
fprintf ('\n');
fprintf ('Upper Wing Tip Chord [m]: %g', C_t_W_up);
fprintf ('\n');
fprintf ('Chord Thickness: %g', Thick_W_up);
fprintf ('\n');
fprintf ('Upper Wing Taper Ratio: %g', Lamb_W_up);
fprintf ('\n');
fprintf ('Upper Wing MAC [m]: %g', mac_W_up);
fprintf ('\n');
fprintf ('Upper Wing Span [m]: %g', b_W_up);
```

```
fprintf ('\n');
fprintf ('Upper Wing Reference Area [m^2]: %g', S_W_up);
fprintf ('\n');
fprintf ('Upper Wing Aerodynamic Area [m^2]: %g', S_aero_W_up);
fprintf ('\n');
fprintf ('Upper Wing Aspect Ratio: %g', AR_W_up);
fprintf ('\n');
fprintf ('Upper Wing Angle of SweepBack [°]: %g', Gam_W_up);
fprintf ('\n');
fprintf ('Upper Wing Angle of Dihedral [°]: %g', Tao_W_up);
fprintf ('\n');
fprintf ('Upper Wing Angle of Incidence [°]: %g', i_W_up);
fprintf ('\n\n');
fprintf ('Upper Wing MAC Leading Edge positioning along "X" axix [m]: %g',
X_LE_mac_W_up);
fprintf ('\n\n\n');
end

    %*Aileron Geometric Parameters*
    fprintf ('***Ailerons***\n\n');

    C_ail = 0.2;
    b_ail = 3.0;
    b_ail_i = 1.9;

    S_a = C_ail*b_ail; % [m^2] Total Ailerons Area

    C_a_b_a = C_ail/b_ail;
    S_a_S = S_a/S_W; % (between 0.05 and 0.1)
    eta_ail = b_ail/b_W_up; % (between 0.2 and 0.3)
    C_a_C = C_ail/mac_W_up; % (between 0.15 and 0.25)
    b_a_i_b = (2*b_ail_i)/b_W_up; % (between 0.6 and 0.8)

    if (main_menu == 1 | main_menu == 6)
    fprintf ('Aileron Chord [m]: %g', C_ail);
    fprintf ('\n');
    fprintf ('Aileron Total Span (2 surfaces) [m]: %g', b_ail);
    fprintf ('\n');
    fprintf ('Aileron Inner Chord Position along Semi-Span [m]: %g', b_ail_i);
    fprintf ('\n');
    fprintf ('Aileron Total Area [m^2]: %g', S_a);
    fprintf ('\n');
    fprintf ('Aileron Chord / Aileron Span: %g', C_a_b_a);
    fprintf ('\n');
    fprintf ('Total Aileron Area / Total Wing Reference Area: %g', S_a_S);
    fprintf ('\n');
    fprintf ('Aileron Span / Upper Wing Span: %g', eta_ail);
    fprintf ('\n');
    fprintf ('Aileron Chord / Upper Wing Chord Ratio: %g', C_a_C);
    fprintf ('\n');
    fprintf ('Aileron Inner Position / Upper Wing Span: %g', b_a_i_b);
    fprintf ('\n\n\n');
    end
```

```
%*Lower Wing*
C_r_W_low = 0.91; % [m] Lower Wing Root Chord
C_t_W_low = 0.91; % [m] Lower Wing Tip Chord
Thick_W_low = 0.18; % Chord Thickness
Lamb_W_low = C_t_W_low/C_r_W_low; % Lower Wing Taper Ratio
mac_W_low = (2/3)*C_r_W_low*((1+Lamb_W_low+(Lamb_W_low^2))/(1+Lamb_W_low)); %
[m] mac Lower Wing
b_W_low = b_W_up; % [m] Lower WingSpan
S_W_low = b_W_low*mac_W_low; % [m^2] Lower Wing Reference Area
S_aero_W_low = S_W_low - (mac_W_low*0.900); % [m^2] Lower Wing Aerodynamic
Area (0.900-> local fuselage widht)
AR_W_low = (b_W_low^2)/S_W_low; % Lower Wing Aspect Ratio
Gam_W_low = 0; % [°] Lower Wing SweepBack
    Gam_W_low_rad = (2*pi*Gam_W_low)/360; % [rad]
Tao_W_low = 0; % [°] Lower Wing Dihedral
    Tao_W_low_rad = (2*pi*Tao_W_low)/360; % [rad]
i_W_low = 0; % [°] Lower Wing Incidence
    i_W_low_rad = (2*pi*i_W_low)/360; % [rad]

X_LE_mac_W_low = 3.604702; % [m] Lower Wing MAC Leading Edge positioning along
"X" axix
Z_W_low = 0.533; % [m] MAC Line position in "z" axis (from CAD drawing)

if (main_menu == 1 | main_menu == 6)
fprintf ('***Lower Wing***\n\n');
fprintf ('Lower Wing Root Chord [m]: %g', C_r_W_low);
fprintf ('\n');
fprintf ('Lower Wing Tip Chord [m]: %g', C_t_W_low);
fprintf ('\n');
fprintf ('Chord Thickness: %g', Thick_W_low);
fprintf ('\n');
fprintf ('Lower Wing Taper Ratio: %g', Lamb_W_low);
fprintf ('\n');
fprintf ('Lower Wing MAC [m]: %g', mac_W_low);
fprintf ('\n');
fprintf ('Lower Wing Span [m]: %g', b_W_low);
fprintf ('\n');
fprintf ('Lower Wing Reference Area [m^2]: %g', S_W_low);
fprintf ('\n');
fprintf ('Lower Wing Aerodynamic Area [m^2]: %g', S_aero_W_low);
fprintf ('\n');
fprintf ('Lower Wing Aspect Ratio: %g', AR_W_low);
fprintf ('\n');
fprintf ('Lower Wing Angle of SweepBack [°]: %g', Gam_W_low);
fprintf ('\n');
fprintf ('Lower Wing Angle of Dihedral [°]: %g', Tao_W_low);
fprintf ('\n');
fprintf ('Lower Wing Angle of Incidence [°]: %g', i_W_low);
fprintf ('\n\n');
fprintf ('Lower Wing MAC Leading Edge positioning along "X" axix [m]: %g',
X_LE_mac_W_low);
fprintf ('\n\n\n');
end

    %*Flaps Geometric Parameters*
```

```
    fprintf ('***Flaps***\n\n');

    C_flap = C_ail; % [m] Flap Chord
    b_flap = b_ail; % [m] Flaps Total Span (2 surfaces)
    b_flap_i = b_ail_i; % [m] Flap Inner Chord Position along Semi-Span

    S_flap = C_flap*b_flap; % [m^2] Total Flaps Area
    C_f_C_W_low = C_flap/mac_W_low;
    eta_flap = b_flap/(b_W_low - 0.900); % (0.900-> local fuselage widht)

    if (main_menu == 1 | main_menu == 6)
    fprintf ('Flap Chord [m]: %g', C_flap);
    fprintf ('\n');
    fprintf ('Flaps Total Span [m]: %g', b_flap);
    fprintf ('\n');
    fprintf ('Flap Inner Chord Position along Semi-Span [m]: %g', b_flap_i);
    fprintf ('\n');
    fprintf ('Total Flaps Area [m^2]: %g', S_flap);
    fprintf ('\n');
    fprintf ('Flap_Chord/Wing_Chord: %g',C_f_C_W_low);
    fprintf ('\n');
    fprintf ('Flaps Span / Lower Wing Span: %g', eta_flap);
    fprintf ('\n\n\n');
    end

%*Equivalent Wing (For Longitudinal & Directional Stability)
mac_W = 1.832; % [m] mac Equivalent Wing, Between low wing mac Leading Edge
and up wing mac T Edge.
C_r = mac_W; % [m] Root chord of the Equivalent Wing,
C_t = C_r; % [m] Tip chord of the Equivalent Wing
b_W = (b_W_low + b_W_up)/2; % [m] Span Equivalent Wing
Lamb_W = C_t/C_r; % Equivalent Wing Taper Ratio
Gam_W = (Gam_W_low + Gam_W_up)/2; % [°] Equivalent Wing SweepBack
    Gam_W_rad = (2*pi*Gam_W)/360; % [rad]
Tao_W = (Tao_W_up + Tao_W_up)/2; % [°] Equivalent Wing Angle of Dihedral
AR_W = (b_W^2)/S_W; % Equivalent Wing Aspect Ratio
S_aero_W = S_aero_W_low + S_aero_W_up; % [m^2] Total Wing Aerodynamic Area
    S_W_ft = S_aero_W*10.76391; % [ft^2] Total Wing Aerodynamic Area

X_LE_mac_W = X_LE_mac_W_low; % [m] Equivalent Wing MAC Leading Edge
positioning along "X" axix
X_TE_mac_W = X_LE_mac_W + mac_W; % [m] Equivalent Wing MAC Trailing Edge
positioning along "X" axix

if (main_menu == 1 | main_menu == 6)
fprintf ('***Equivalent Wing***\n\n');
fprintf ('Equivalent Wing MAC [m]: %g', mac_W);
fprintf ('\n');
fprintf ('Equivalent Wing Root Chord [m]: %g', C_r);
fprintf ('\n');
fprintf ('Equivalent Wing Tip Chord [m]: %g', C_t);
fprintf ('\n');
fprintf ('Span of the Equivalent Wing [m^2]: %g', b_W);
fprintf ('\n');
```

```
fprintf ('Equivalent Wing Taper Ratio [m]: %g', Lamb_W);
fprintf ('\n');
fprintf ('Equivalent Wing Angle of SweepBack [°]: %g', Gam_W);
fprintf ('\n');
fprintf ('Equivalent Wing Angle of Dihedral [°]: %g', Tao_W);
fprintf ('\n');
fprintf ('Biplane Wing Aspect Ratio [m]: %g', AR_W);
fprintf ('\n');
fprintf ('Total Wing Aerodynamic Area [m^2]: %g', S_aero_W);
fprintf ('\n\n\n');
end
%……….

%……….CANARDS……….
fprintf ('***CANARDS***\n\n');

%*BiPlane Parameters*
S_CAN = 1.296 + 1.296; % [m^2] Total Canard Reference Area

GAP_can = 0.3; % [m]
Span_Ratio_can = 1;
Stagger_can = -18.435; % [°]
Decal_can = 0; % [°] Angle of Decalage

if (main_menu == 1 | main_menu == 6)
fprintf ('***Canards Biplane Parameters***\n\n');
fprintf ('Total Reference Area [m^2]: %g', S_CAN);
fprintf ('\n');
fprintf ('GAP [m]: %g', GAP_can);
fprintf ('\n');
fprintf ('Span Ratio: %g', Span_Ratio_can);
fprintf ('\n');
fprintf ('Angle of Stagger [°]: %g', Stagger_can);
fprintf ('\n');
fprintf ('Angle of Decalage [°]: %g', Decal_can);
fprintf ('\n\n\n');
end

%*Lower Canard*
C_r_can_low = 0.4; % [m] Lower Canard Root Chord
C_t_can_low = C_r_can_low; % [m] Lower Canard Tip Chord
Thick_can_low = 0.09; % Chord Thickness
Lamb_can_low = C_t_can_low/C_r_can_low; % Lower Canard Taper Ratio
mac_can_low =
(2/3)*C_r_can_low*((1+Lamb_can_low+(Lamb_can_low^2))/(1+Lamb_can_low)); % [m]
mac Lower Canard
AR_can_low = 8.1; % Lower Canard Aspect Ratio
b_can_low = AR_can_low*mac_can_low; % [m] Lower CanardSpan
S_can_low = mac_can_low*b_can_low; % [m^2] Lower Canard Reference Area
S_aero_can_low = S_can_low - (mac_can_low*0.724); % [m^2] Lower Canard
Aerodynamic Area (0.724-> local fuselage widht)
Gam_can_low = 0; % [°] Lower Canard SweepBack
Tao_can_low = 0; % [°] Lower Canard Dihedral
    Tao_can_low_rad = (2*pi*Tao_can_low)/360; % [rad]
```

```
X_LE_mac_can_low = 1.4; % [m] Lower Canard MAC Leading Edge positioning along
"X" axix
Z_can_low = 0.265; % [m] MAC Line position in "z" axis (from CAD drawing)

if (main_menu == 1 | main_menu == 6)
fprintf ('***Lower Canard***\n\n');
fprintf ('Lower Canard Root Chord [m]: %g', C_r_can_low);
fprintf ('\n');
fprintf ('Lower Canard Tip Chord [m]: %g', C_t_can_low);
fprintf ('\n');
fprintf ('Lower Canard Chord Thickness: %g', Thick_can_low);
fprintf ('\n');
fprintf ('Lower Canard Taper Ratio: %g', Lamb_can_low);
fprintf ('\n');
fprintf ('Lower Canard MAC [m]: %g', mac_can_low);
fprintf ('\n');
fprintf ('Lower Canard Aspect Ratio: %g', AR_can_low);
fprintf ('\n');
fprintf ('Lower Canard Span [m]: %g', b_can_low);
fprintf ('\n');
fprintf ('Lower Canard Reference Area [m^2]: %g', S_can_low);
fprintf ('\n');
fprintf ('Lower Canard Aerodynamic Area [m^2]: %g', S_aero_can_low);
fprintf ('\n');
fprintf ('Lower Canard Angle of SweepBack [°]: %g', Gam_can_low);
fprintf ('\n');
fprintf ('Lower Canard Angle of Dihedral [°]: %g', Tao_can_low);
fprintf ('\n\n');
fprintf ('Lower Canard MAC Leading Edge positioning along "X" axix [m]: %g',
X_LE_mac_can_low);
fprintf ('\n\n\n');
end

    %*Elevator Geometric Parameters*
    fprintf ('***Lower Elevator***\n\n');

    C_elv_low = 0.2;
    b_elv_low = 2.1;
    b_elv_low_i = 0.4;

    S_elev_low = C_elv_low*b_elv_low; % [m^2] Total Elevator Area

    S_ellow_S_canlow = S_elev_low/S_can_low; % (between 0.15 and 0.4)
    b_ellow_b_canlow = b_elv_low/b_can_low; % (between 0.8 and 1.0)
    C_ellow_C_canlow = C_elv_low/mac_can_low; % (between 0.2 and 0.4)

    if (main_menu == 1 | main_menu == 6)
    fprintf ('Lower Elevator Chord [m]: %g', C_elv_low);
    fprintf ('\n');
    fprintf ('Lower Elevator Total Span (2 surfaces) [m]: %g', b_elv_low);
    fprintf ('\n');
    fprintf ('Lower Elevator Inner Chord Position along Semi-Span [m]: %g',
b_elv_low_i);
```

```
    fprintf ('\n');
    fprintf ('Lower Elevator Total Area [m^2]: %g', S_elev_low);
    fprintf ('\n');
    fprintf ('Lower Elevator Area / Lower Canard Area: %g', S_ellow_S_canlow);
    fprintf ('\n');
    fprintf ('Lower Elevator Span / Lower Canard Span: %g', b_ellow_b_canlow);
    fprintf ('\n');
    fprintf ('Lower Elevator Chord / Lower Canard Chord: %g',
C_ellow_C_canlow);
    fprintf ('\n\n\n');
    end

%*Upper Canard*
C_r_can_up = C_r_can_low; % [m] Upper Canard Root Chord
C_t_can_up = C_r_can_up; % [m] Upper Canard Tip Chord
Thick_can_up = 0.09; % Chord Thickness
Lamb_can_up = C_t_can_up/C_r_can_up; % Upper Canard Taper Ratio
mac_can_up =
(2/3)*C_r_can_up*((1+Lamb_can_up+(Lamb_can_up^2))/(1+Lamb_can_up)); % [m] mac
Upper Canard
AR_can_up = 8.1; % Upper Canard Aspect Ratio
b_can_up = AR_can_up*mac_can_up; % [m] Upper CanardSpan
S_can_up = mac_can_up*b_can_up; % [m^2] Upper Canard Reference Area
S_aero_can_up = S_can_up - (mac_can_up*0.724); % [m^2] Upper Canard
Aerodynamic Area (0.724-> local fuselage widht)
Gam_can_up = 0; % [°] Upper Canard SweepBack
Tao_can_up = 0; % [°] Upper Canard Dihedral
    Tao_can_up_rad = (2*pi*Tao_can_up)/360; % [rad]
i_can_up = i_can_low; % [°] Upper Canard Incidence
    i_can_up_rad = (2*pi*i_can_up)/360; % [rad]

X_LE_mac_can_up = 1.5; % [m] Upper Canard MAC Leading Edge positioning along
"X" axix
Z_can_up = 0.565; % [m] MAC Line position in "z" axis (from CAD drawing)

if (main_menu == 1 | main_menu == 6)
fprintf ('***Upper Canard***\n\n');
fprintf ('Upper Canard Root Chord [m]: %g', C_r_can_up);
fprintf ('\n');
fprintf ('Upper Canard Tip Chord [m]: %g', C_t_can_up);
fprintf ('\n');
fprintf ('Upper Canard Chord Thickness: %g', Thick_can_up);
fprintf ('\n');
fprintf ('Upper Canard Taper Ratio: %g', Lamb_can_up);
fprintf ('\n');
fprintf ('Upper Canard MAC [m]: %g', mac_can_up);
fprintf ('\n');
fprintf ('Upper Canard Aspect Ratio: %g', AR_can_up);
fprintf ('\n');
fprintf ('Upper Canard Span [m]: %g', b_can_up);
fprintf ('\n');
fprintf ('Upper Canard Reference Area [m^2]: %g', S_can_up);
fprintf ('\n');
fprintf ('Upper Canard Aerodynamic Area [m^2]: %g', S_aero_can_up);
fprintf ('\n');
```

```
fprintf ('Upper Canard Angle of SweepBack [°]: %g', Gam_can_up);
fprintf ('\n');
fprintf ('Upper Canard Angle of Dihedral [°]: %g', Tao_can_up);
fprintf ('\n');
fprintf ('Upper Canard Angle of Incidence [°]: %g', i_can_up);
fprintf ('\n\n');
fprintf ('Upper Canard MAC Leading Edge positioning along "X" axix [m]: %g',
X_LE_mac_can_up);
fprintf ('\n\n\n');
end

    %*Elevator Geometric Parameters*
    fprintf ('***Upper Elevator***\n\n');

    C_elv_up = C_elv_low; %[m]
    b_elv_up = b_elv_low; %[m]
    b_elv_up_i = b_elv_low_i; %[m]

    S_elev_up = C_elv_up*b_elv_up; % [m^2] Total Elevator Area

    S_elup_S_canup = S_elev_up/S_can_up; % (between 0.15 and 0.4)
    b_elup_b_canup = b_elv_up/b_can_up; % (between 0.8 and 1.0)
    C_elup_C_canup = C_elv_up/mac_can_up; % (between 0.2 and 0.4)

    if (main_menu == 1 | main_menu == 6)
    fprintf ('Upper Elevator Chord [m]: %g', C_elv_up);
    fprintf ('\n');
    fprintf ('Upper Elevator Total Span (2 surfaces) [m]: %g', b_elv_up);
    fprintf ('\n');
    fprintf ('Upper Elevator Inner Chord Position along Semi-Span [m]: %g',
b_elv_up_i);
    fprintf ('\n');
    fprintf ('Upper Elevator Total Area [m^2]: %g', S_elev_up);
    fprintf ('\n');
    fprintf ('Upper Elevator Area / Lower Canard Area: %g', S_elup_S_canup);
    fprintf ('\n');
    fprintf ('Upper Elevator Span / Lower Canard Span: %g', b_elup_b_canup);
    fprintf ('\n');
    fprintf ('Upper Elevator Chord / Lower Canard Chord: %g', C_elup_C_canup);
    fprintf ('\n\n\n');
    end

%*Equivalent Canard
mac_CAN = 0.4 + 0.4 + 0.1; % [m] mac Equivalent Canard, Between low canard mac
Leading Edge and up canard mac T Edge.
C_r_C = mac_CAN; % [m] Root chord fo the Equivalent Canard,
C_t_C = C_r_C; % [m] Tip chord fo the Equivalent Canard
b_CAN = (b_can_low + b_can_up)/2; % [m] Span Equivalent Canard
Lamb_C = C_t_C/C_r_C; % Equivalent Canard Taper Ratio
Gam_C = (Gam_can_low + Gam_can_up)/2; % [°] Equivalent Canard SweepBack
    Gam_C_rad = (2*pi*Gam_C)/360; % [rad]
Tao_C = (Tao_can_up + Tao_can_up)/2; % [°] Equivalent Canard Angle of Dihedral
AR_CAN = (b_CAN^2)/S_CAN; % Biplane Canard Aspect Ratio
```

```
S_aero_CAN = S_aero_can_low + S_aero_can_up; % [m^2] Total Canard Aerodynamic
Area

X_LE_mac_C = X_LE_mac_can_low; % [m] Equivalent Canard MAC Leading Edge
positioning along "X" axix
X_TE_mac_C = X_LE_mac_C + mac_CAN; % [m] Equivalent Canard MAC Trailing Edge
positioning along "X" axix

if (main_menu == 1 | main_menu == 6)
fprintf ('***Equivalent Canard***\n\n');
fprintf ('Equivalent Canard MAC [m]: %g', mac_CAN);
fprintf ('\n');
fprintf ('Equivalent Canard Root Chord [m]: %g', C_r_C);
fprintf ('\n');
fprintf ('Equivalent Canard Tip Chord [m]: %g', C_t_C);
fprintf ('\n');
fprintf ('Span of the Biplane Canard [m^2]: %g', b_CAN);
fprintf ('\n');
fprintf ('Equivalent Canard Taper Ratio [m]: %g', Lamb_C);
fprintf ('\n');
fprintf ('Equivalent Canard Angle of SweepBack [°]: %g', Gam_C);
fprintf ('\n');
fprintf ('Equivalent Canard Angle of Dihedral [°]: %g', Tao_C);
fprintf ('\n');
fprintf ('Biplane Canard Aspect Ratio [m]: %g', AR_CAN);
fprintf ('\n');
fprintf ('Total Biplane Canard Aerodynamic Area [m^2]: %g', S_aero_CAN);
fprintf ('\n\n\n');
end

%*Fairings + Booms*
S_lef_fairing = 0.21; % [m^2] Wetted Area from CAD drawing
S_rig_fairing = 0.21; % [m^2] Wetted Area from CAD drawing

if (main_menu == 1 | main_menu == 6)
fprintf ('***Canards Fairings + Booms***\n\n');
fprintf ('Left Fairing + Boom Wetted Area [m^2]: %g', S_lef_fairing);
fprintf ('\n');
fprintf ('Right Fairing + Boom Wetted Area [m^2]: %g', S_rig_fairing);
fprintf ('\n\n\n');
end
%……….……….……….……….……….……….……….……….……….……….……….……….……….……….……

%……….……….……….……….……VERTICAL TAIL……….……….……….……….……….……….……
fprintf ('***VERTICAL TAIL***\n\n');

%*Left Vertical Tail*
C_r_vt_lef = 0.8; % [m] Left Vertical Tail Root Cord
C_t_vt_lef = 0.55; % [m] Left Vertical Tail Tip Cord
Thick_vt_lef = 0.12; % Cord Thickness
Lamb_vt_lef = C_t_vt_lef/C_r_vt_lef; % Left Vertical Tail Taper Ratio
b_vt_lef = GAP; % [m] Left Vertical Tail Span
```

```
mac_vt_lef =
(2/3)*C_r_vt_lef*((1+Lamb_vt_lef+(Lamb_vt_lef^2))/(1+Lamb_vt_lef)); % [m] mac
Left Vertical Tail
z_vt_lef = (b_vt_lef/6)*((1 + 2*Lamb_vt_lef)/(1 + Lamb_vt_lef)); % [m] AC
position from VT root on z axis
S_vt_lef = mac_vt_lef*b_vt_lef; % [m^2] Left Vertical Tail Reference Area
(Equal aerodynamic area)
AR_vt_lef = (b_vt_lef^2)/S_vt_lef; % Left Vertical Tail Aspect Ratio
Gam_vt_lef = 9.532; % [°] Left Vertical Tail SweepBack (at 25%)
Tao_vt_lef = 0; % [°] Left Vertical Tail Dihedral
    Tao_vt_lef_rad = (2*pi*Tao_vt_lef)/360; % [rad]
i_vt_lef = 0; % [°] Left Vertical Tail Incidence

X_LE_C_r_vt_lef = 5.186674; % [m] Left Vertical Tail Root Chord Leading Edge
positioning along "X" axix
X_LE_mac_vt_lef = X_LE_C_r_vt_lef + 0.117284; % [m] Left Vertical Tail MAC
Leading Edge positioning along "X" axix
Z_mac_vt_lef = z_vt_lef + 0.533 % [m] MAC Line position in "z" axis (from CAD
drawing)

if (main_menu == 1 | main_menu == 6)
fprintf ('***Left Vertical Tail***\n\n');
fprintf ('Left Vertical Tail Root Chord [m]: %g', C_r_vt_lef);
fprintf ('\n');
fprintf ('Left Vertical Tail Tip Chord [m]: %g', C_t_vt_lef);
fprintf ('\n');
fprintf ('Left Vertical Tail Chord Thickness: %g', Thick_vt_lef);
fprintf ('\n');
fprintf ('Left Vertical Tail Taper Ratio: %g', Lamb_vt_lef);
fprintf ('\n');
fprintf ('Left Vertical Tail MAC [m]: %g', mac_vt_lef);
fprintf ('\n');
fprintf ('MAC Position on Left Vertical Tail Span [m]: %g', z_vt_lef);
fprintf ('\n');
fprintf ('Left Vertical Tail Span [m]: %g', b_vt_lef);
fprintf ('\n');
fprintf ('Left Vertical Tail Reference Area [m^2]: %g', S_vt_lef);
fprintf ('\n');
fprintf ('Left Vertical Tail Aerodynamic Area [m^2]: %g', S_vt_lef);
fprintf ('\n');
fprintf ('Left Vertical Tail Aspect Ratio: %g', AR_vt_lef);
fprintf ('\n');
fprintf ('Left Vertical Tail Angle of SweepBack [°]: %g', Gam_vt_lef);
fprintf ('\n');
fprintf ('Left Vertical Tail Angle of Dihedral [°]: %g', Tao_vt_lef);
fprintf ('\n');
fprintf ('Left Vertical Tail Angle of Incidence [°]: %g', i_vt_lef);
fprintf ('\n\n');
fprintf ('Left Vertical Tail Root Chord Leading Edge positioning along "X"
axix [m]: %g', X_LE_C_r_vt_lef);
fprintf ('\n');
fprintf ('Left Vertical Tail MAC Leading Edge positioning along "X" axix [m]:
%g', X_LE_mac_vt_lef);
fprintf ('\n\n\n');
end
```

```
    %*Rudder Geometric Parameters*
    fprintf ('***Left Rudder***\n\n');

    C_rud_lef = 0.25; % [m]
    b_rud_lef = 0.9; % [m]
    b_rud_lef_i = 0.1; % [m]

    S_rud_lef = C_rud_lef*b_rud_lef; % [m^2] Total Left Rudder Area

    S_rudlef_S_vtlef = S_rud_lef/S_vt_lef; % (between 0.15 and 0.35)
    b_rudlef_b_vtlef = b_rud_lef/b_vt_lef; % (between 0.7 and 1.0)
    C_rudlef_C_vtlef = C_rud_lef/mac_vt_lef; % (between 0.15 and 0.4)

    if (main_menu == 1 | main_menu == 6)
    fprintf ('Left Rudder Chord [m]: %g', C_rud_lef);
    fprintf ('\n');
    fprintf ('Left Rudder Span [m]: %g', b_rud_lef);
    fprintf ('\n');
    fprintf ('Left Rudder Inner Chord Position along Span [m]: %g',
b_rud_lef_i);
    fprintf ('\n');
    fprintf ('Left Rudder Total Area [m^2]: %g', S_rud_lef);
    fprintf ('\n');
    fprintf ('Left Rudder Area / Left Vertical Tail Area: %g',
S_rudlef_S_vtlef);
    fprintf ('\n');
    fprintf ('Left Rudder Span / Left Vertical Tail Span: %g',
b_rudlef_b_vtlef);
    fprintf ('\n');
    fprintf ('Left Rudder Chord / Left Vertical Tail Chord: %g',
C_rudlef_C_vtlef);
    fprintf ('\n\n\n');
    end

    %*Booms*
    S_low_boom_lef = 1.481; % [m^2] from CAD drawing
    S_up_boom_lef = 0.892; % [m^2] from CAD drawing

    if (main_menu == 1 | main_menu == 6)
    fprintf ('***Left Booms***\n\n');
    fprintf ('Left Lower Boom Area [m^2]: %g', S_low_boom_lef);
    fprintf ('\n');
    fprintf ('Left Upper Boom Area [m^2]: %g', S_up_boom_lef);
    fprintf ('\n\n\n');
    end

%*Right Vertical Tail*
C_r_vt_rig = C_r_vt_lef; % [m] Right Vertical Tail Root Cord
C_t_vt_rig = C_t_vt_lef; % [m] Right Vertical Tail Tip Cord
Thick_vt_rig = Thick_vt_lef; % Cord Thickness
Lamb_vt_rig = C_t_vt_rig/C_r_vt_rig; % Right Vertical Tail Taper Ratio
b_vt_rig = GAP; % [m] Right Vertical Tail Span
```

```
mac_vt_rig =
(2/3)*C_r_vt_rig*((1+Lamb_vt_rig+(Lamb_vt_rig^2))/(1+Lamb_vt_rig)); % [m] mac
Right Vertical Tail
z_vt_rig = z_vt_lef; % [m] AC position from VT root on z axis
S_vt_rig = mac_vt_rig*b_vt_rig; % [m^2] Right Vertical Tail Reference Area
(Equal aerodynamic area)
AR_vt_rig = (b_vt_rig^2)/S_vt_rig; % Right Vertical Tail Aspect Ratio
Gam_vt_rig = Gam_vt_lef; % [°] Right Vertical Tail SweepBack
Tao_vt_rig = 0; % [°] Right Vertical Tail Dihedral
    Tao_vt_rig_rad = (2*pi*Tao_vt_rig)/360; % [rad]
i_vt_rig = 0; % [°] Right Vertical Tail Incidence

X_LE_mac_vt_rig = X_LE_mac_vt_lef; % [m] Right Vertical Tail MAC Leading Edge
positioning along "X" axix
Z_mac_vt_rig = Z_mac_vt_lef; % [m] MAC Line position in "z" axis (from CAD
drawing)

if (main_menu == 1 | main_menu == 6)
fprintf ('***Right Vertical Tail***\n\n');
fprintf ('Right Vertical Tail Root Chord [m]: %g', C_r_vt_rig);
fprintf ('\n');
fprintf ('Right Vertical Tail Tip Chord [m]: %g', C_t_vt_rig);
fprintf ('\n');
fprintf ('Right Vertical Tail Chord Thickness: %g', Thick_vt_rig);
fprintf ('\n');
fprintf ('Right Vertical Tail Taper Ratio: %g', Lamb_vt_rig);
fprintf ('\n');
fprintf ('Right Vertical Tail MAC [m]: %g', mac_vt_rig);
fprintf ('\n');
fprintf ('MAC Position on Left Vertical Tail Span [m]: %g', z_vt_rig);
fprintf ('\n');
fprintf ('Right Vertical Tail Span [m]: %g', b_vt_rig);
fprintf ('\n');
fprintf ('Right Vertical Tail Reference Area [m^2]: %g', S_vt_rig);
fprintf ('\n');
fprintf ('Right Vertical Tail Aerodynamic Area [m^2]: %g', S_vt_rig);
fprintf ('\n');
fprintf ('Right Vertical Tail Aspect Ratio: %g', AR_vt_rig);
fprintf ('\n');
fprintf ('Right Vertical Tail Angle of SweepBack [°]: %g', Gam_vt_rig);
fprintf ('\n');
fprintf ('Right Vertical Tail Angle of Dihedral [°]: %g', Tao_vt_rig);
fprintf ('\n');
fprintf ('Right Vertical Tail Angle of Incidence [°]: %g', i_vt_rig);
fprintf ('\n\n');
fprintf ('Right Vertical Tail MAC Leading Edge positioning along "X" axix [m]:
%g', X_LE_mac_vt_rig);
fprintf ('\n\n\n');
end

    %*Rudder Geometric Parameters*
    fprintf ('**Right Rudder***\n\n');

    C_rud_rig = C_rud_lef; % [m]
    b_rud_rig = b_rud_lef; % [m]
```

```
    b_rud_rig_i = b_rud_lef_i; % [m]

    S_rud_rig = C_rud_rig*b_rud_rig; % [m^2] Total Left Rudder Area

    S_rudrig_S_vtrig = S_rud_rig/S_vt_rig; % (between 0.15 and 0.35)
    b_rudrig_b_vtrig = b_rud_rig/b_vt_rig; % (between 0.7 and 1.0)
    C_rudrig_C_vtrig = C_rud_rig/mac_vt_rig; % (between 0.15 and 0.4)

    if (main_menu == 1 | main_menu == 6)
    fprintf ('Right Rudder Chord [m]: %g', C_rud_rig);
    fprintf ('\n');
    fprintf ('Right Rudder Span [m]: %g', b_rud_rig);
    fprintf ('\n');
    fprintf ('Right Rudder Inner Chord Position along Span [m]: %g',
b_rud_rig_i);
    fprintf ('\n');
    fprintf ('Right Rudder Total Area [m^2]: %g', S_rud_rig);
    fprintf ('\n');
    fprintf ('Right Rudder Area / Right Vertical Tail Area: %g',
S_rudrig_S_vtrig);
    fprintf ('\n');
    fprintf ('Right Rudder Span / Right Vertical Tail Span: %g',
b_rudrig_b_vtrig);
    fprintf ('\n');
    fprintf ('Right Rudder Chord / Right Vertical Tail Chord: %g',
C_rudrig_C_vtrig);
    fprintf ('\n\n\n');
    end

    %*Booms*
    S_low_boom_rig = 1.481; % [m^2] from CAD drawing
    S_up_boom_rig = 0.892; % [m^2] from CAD drawing

    if (main_menu == 1 | main_menu == 6)
    fprintf ('***Right Booms***\n\n');
    fprintf ('Right Lower Boom Area [m^2]: %g', S_low_boom_rig);
    fprintf ('\n');
    fprintf ('Right Upper Boom Area [m^2]: %g', S_up_boom_rig);
    fprintf ('\n\n\n');
    end
%¨¨¨¨¨¨¨¨¨¨¨¨¨¨¨¨¨¨¨¨¨¨¨¨¨¨¨¨¨¨¨¨¨¨¨¨¨¨¨¨¨¨¨¨¨¨¨¨¨¨¨¨¨¨¨¨¨¨¨¨¨¨¨¨¨¨¨¨¨¨¨¨¨¨¨¨¨¨¨¨¨¨¨¨¨¨¨¨¨¨

%¨¨¨¨¨¨¨¨¨¨¨¨¨¨¨¨¨¨¨¨¨¨¨¨¨¨¨¨¨¨LANDING GEAR¨¨¨¨¨¨¨¨¨¨¨¨¨¨¨¨¨¨¨¨¨¨¨¨¨¨¨¨¨¨
%¨¨¨¨Landing Gear Geometric Parameters¨¨¨
fprintf ('***LANDING GEAR***\n\n');

S_lef_main_gear = 1.287; % [m^2] Total Wetted Area (with fairings) from CAD
drawings
S_rig_main_gear = 1.287; % [m^2] Total Wetted Area (with fairings) from CAD
drawings
S_nose_gear = 0.155; % [m^2] Wetted Area from CAD drawings

X_lef_main_gear = 4.1; % [m] Left Landig Gear touch point along "X" axix
```

```
X_rig_main_gear = X_lef_main_gear; % [m] Right Landig Gear touch point along
"X" axix
X_nose_gear = 0.493; % [m] Nose Landig Gear touch point along "X" axix

if (main_menu == 1 | main_menu == 6)
fprintf ('Left Landing Gear Total Wetted Area [m^2]: %g', S_lef_main_gear);
fprintf ('\n');
fprintf ('Right Landing Gear Total Wetted Area [m^2]: %g', S_rig_main_gear);
fprintf ('\n');
fprintf ('Nose Landing Gear Total Wetted Area [m^2]: %g', S_nose_gear);
fprintf ('\n');
fprintf ('Main Landing Gear touch point along "X" axix [m]: %g',
X_lef_main_gear);
fprintf ('\n');
fprintf ('Nose Landing Gear touch point along "X" axix [m]: %g', X_nose_gear);
fprintf ('\n\n')
end
%¨¨¨¨¨¨¨¨¨¨¨¨¨¨¨¨¨¨¨¨¨¨¨¨¨¨¨¨¨¨¨¨¨¨¨¨¨¨¨¨¨¨¨¨¨¨¨¨¨¨¨¨¨¨¨¨¨¨¨¨¨¨¨¨¨¨¨¨¨¨¨¨¨¨¨¨

%¨¨¨¨¨¨¨¨¨¨¨¨¨¨¨¨¨¨¨¨¨¨¨¨¨¨¨¨¨¨COMPLETE AIRPLANE¨¨¨¨¨¨¨¨¨¨¨¨¨¨¨¨¨¨¨¨¨¨¨¨¨¨¨¨¨
fprintf ('***COMPLETE AIRPLANE***\n\n');

S_wet = 72.391; % [m^2] Total Wetted Area of the Airplane (Estimated from CAD
drawings)

if (main_menu == 1 | main_menu == 6)
fprintf ('Total Wetted Area of the Airplane [m^2]: %g', S_wet);
fprintf ('\n\n')
end
%¨¨¨¨¨¨¨¨¨¨¨¨¨¨¨¨¨¨¨¨¨¨¨¨¨¨¨¨¨¨¨¨¨¨¨¨¨¨¨¨¨¨¨¨¨¨¨¨¨¨¨¨¨¨¨¨¨¨¨¨¨¨¨¨¨¨¨¨¨¨¨¨¨¨¨¨
fprintf
('_____________________________________________________________________________
____________________\n\n');
%___________________________________________________________________________

if (main_menu == 1 | main_menu == 2 | main_menu == 3 | main_menu == 4 |
main_menu == 5)
%_______________AERODYNAMIC CHARACTERIZATION OF THE AIRPLANE_______________
fprintf ('__________________________AERODYNAMIC CHARACTERIZATION OF THE
AIRPLANE__________________________\n\n');

%¨¨¨¨¨¨¨¨¨¨¨¨¨¨¨¨¨¨¨¨¨¨¨¨¨¨¨¨¨¨¨¨¨¨¨PERFILAGE¨¨¨¨¨¨¨¨¨¨¨¨¨¨¨¨¨¨¨¨¨¨¨¨¨¨¨¨¨¨¨
fprintf ('-----------------------------------------PERFILAGE------------------
----------------------------\n\n');

%¨¨Wings Perfilage¨¨
fprintf ('***Wings Perfilage***\n\n');

    %¨¨Lower Wing¨¨
    %¨¨NACA 65-418¨¨
    cl_max_W_low = 1.31; % for Alpha = 15°
    Alf_Cl_zer_W_low = -1.7755; % [°]
    if (Alpha < 15 | length(Alpha) > 1)
```

```
        Cl_alf_W_low = (0.9222 - 0)/(6 - Alf_Cl_zer_W_low); % [1/°] Profile
Lift Slope
        Cl_alf_W_low_rad = Cl_alf_W_low*57.29579; % [1/rad] Profile Lift Slope
    end
    if (Alpha == 15) % JUST A ESTIMATIVE NOT EXACT (From XFLR5)
        Cl_alf_W_low = (cl_max_W_low - 0)/(15 - Alf_Cl_zer_W_low); % [1/°]
Profile Lift Slope
        Cl_alf_W_low_rad = Cl_alf_W_low*57.29579; % [1/rad] Profile Lift Slope
    end

    fprintf ('Cl_alf_W_low [1/°]: %g', Cl_alf_W_low);
    fprintf ('\n\n');
    Cd_0_W_low = input ('Cd - Lower Wing (Profile Drag): ' ); % Friction Drag
+ Pressure Drag
    Cm_W_low = -0.0375; % Mean value, based on results of XFLR5

    %¨¨Upper Wing¨¨
    %¨¨NACA 65-418¨¨
    cl_max_W_up = 1.31; % for Alpha = 15°
    Alf_Cl_zer_W_up = Alf_Cl_zer_W_low; % [°]
    if (Alpha < 15 | length(Alpha) > 1)
        Cl_alf_W_up = (0.9222 - 0)/(6 - Alf_Cl_zer_W_up); % [1/°] Profile Lift
Slope
        Cl_alf_W_up_rad = Cl_alf_W_up*57.29579; % [1/rad] Profile Lift Slope
    end
    if (Alpha == 15) % JUST A ESTIMATIVE NOT EXACT
        Cl_alf_W_up = (cl_max_W_up - 0)/(15 - Alf_Cl_zer_W_up); % [1/°]
Profile Lift Slope
        Cl_alf_W_up_rad = Cl_alf_W_up*57.29579; % [1/rad] Profile Lift Slope
    end
    fprintf ('Cl_alf_W_up [1/°]: %g', Cl_alf_W_up);
    fprintf ('\n\n');
    Cd_0_W_up = Cd_0_W_low;
    Cm_W_up = Cm_W_low;


%¨¨Canards Perfilage¨¨
fprintf ('***Canards Perfilage***\n\n');

    %¨¨Lower Canard¨¨
    %¨¨NACA 0009¨¨ Data from XFLR5 simulation
    cl_max_can_low = 1.03; % for Alpha = 10.75°
    Alph_Cl_zer_can_low = 0.0; % [°]
    if (Alpha < 10.75 | length(Alpha) > 1)
        Cl_alph_can_low = (0.6672 - 0)/(6 - Alph_Cl_zer_can_low); % [1/°]
Profile Lift Slope
        Cl_alph_can_low_rad = Cl_alph_can_low*57.29579; % [1/rad] Profile Lift
Slope
    end
    if (Alpha == 10.75) % JUST A ESTIMATIVE NOT EXACT (From XFLR5)
        Cl_alph_can_low = (cl_max_can_low - 0)/(10.75 - Alph_Cl_zer_can_low);
% [1/°] Profile Lift Slope
        Cl_alph_can_low_rad = Cl_alph_can_low*57.29579; % [1/rad] Profile Lift
Slope
    end
```

```
    fprintf ('Cl_alph_can_low [1/°]: %g', Cl_alph_can_low);
    fprintf ('\n\n');
    Cd_0_can_low = input ('Cd - Lower Canard (Profile Drag): ' ); % Friction
Drag + Pressure Drag
    Cm_can_low = 0.0;

    %¨¨Upper Canard¨¨
    %¨¨NACA 0009¨¨
    cl_max_can_up = cl_max_can_low; % for Alpha = 10.75°
    Alph_Cl_zer_can_up = Alph_Cl_zer_can_low; % [°]
    if (Alpha < 10.75 | length(Alpha) > 1)
        Cl_alph_can_up = (0.6672 - 0)/(6 - Alph_Cl_zer_can_up); % [1/°]
Profile Lift Slope
        Cl_alph_can_up_rad = Cl_alph_can_up*57.29579; % [1/rad] Profile Lift
Slope
    end
    if (Alpha == 10.75) % JUST A ESTIMATIVE NOT EXACT (From XFLR5)
        Cl_alph_can_up = (cl_max_can_up - 0)/(10.75 - Alph_Cl_zer_can_up); %
[1/°] Profile Lift Slope
        Cl_alph_can_up_rad = Cl_alph_can_up*57.29579; % [1/rad] Profile Lift
Slope
    end

    fprintf ('Cl_alph_can_up [1/°]: %g', Cl_alph_can_up);
    fprintf ('\n\n');
    Cd_0_can_up = Cd_0_can_low; % Friction Drag + Pressure Drag
    Cm_can_up = Cm_can_low;


%¨¨Vertical Tails Perfilage¨¨
fprintf ('***Vertical Tails Perfilage***\n\n');

    %¨¨Left Vertical Tail¨¨
    %¨¨NACA 0012¨¨ Data from XFLR5 simulation
    cl_max_vt_lef = 1.4556; % for Alpha = 15.75°
    Alph_Cl_zer_vt_lef = 0.0; % [°]
    Cl_alph_vt_lef = (0.6715 - 0)/(6 - Alph_Cl_zer_vt_lef); % [1/°] Profile
Lift Slope
    Cl_alph_vt_lef_rad = Cl_alph_vt_lef*57.29579; % [1/rad] Profile Lift Slope

    fprintf ('Cl_alph_vt_lef [1/°]: %g', Cl_alph_vt_lef);
    fprintf ('\n\n');
    Cd_0_vt_lef = input ('Cd - Left Vertical Tail (Profile Drag): ' ); %
Friction Drag + Pressure Drag
    Cm_vt_lef = 0.0;

    %¨¨Right Vertical Tail¨¨
    %¨¨¨¨Perfilage¨¨¨¨
    %¨¨NACA 0012¨¨ Data from XFLR5 simulation
    cl_max_vt_rig = 1.4556; % for Alpha = 15.75°
    Alph_Cl_zer_vt_rig = 0.0; % [°]
    Cl_alph_vt_rig = (0.6715 - 0)/(6 - Alph_Cl_zer_vt_rig); % [1/°] Profile
Lift Slope
```

```
    Cl_alph_vt_rig_rad = Cl_alph_vt_rig*57.29579; % [1/rad] Profile Lift Slope

    fprintf ('Cl_alph_vt_rig [1/°]: %g', Cl_alph_vt_rig);
    fprintf ('\n\n');
    Cd_0_vt_rig = Cd_0_vt_lef; % Friction Drag + Pressure Drag
    Cm_vt_rig = 0.0;

fprintf ('---------------------------------------------------------------------
----------------------------\n\n');
%¨¨¨¨¨¨¨¨¨¨¨¨¨¨¨¨¨¨¨¨¨¨¨¨¨¨¨¨¨¨¨¨¨¨¨¨¨¨¨¨¨¨¨¨¨¨¨¨¨¨¨¨¨¨¨¨¨¨¨¨¨¨¨¨¨¨¨¨¨¨¨¨¨¨¨¨¨¨¨¨¨¨¨¨¨¨

%¨¨¨¨¨¨¨¨¨¨¨¨¨¨¨¨¨¨¨¨¨¨¨¨¨¨¨¨¨¨¨¨¨SURFACES AERODYNAMIC CENTER¨¨¨¨¨¨¨¨¨¨¨¨¨¨¨¨¨¨¨¨¨¨¨¨¨¨¨¨¨¨¨¨
fprintf ('-----------------------------------------SURFACES AERODYNAMIC
CENTER----------------------------------------------\n\n');

%¨¨Wings Aerodynamic Center¨¨
fprintf ('***Wings Aerodynamic Center***\n\n');

    %¨¨Biplane Wing Span Efficiency Factor¨¨
    mi_W = b_W_up/b_W_low; % (From Raymer, 2006)
    r_W = S_aero_W_low/S_aero_W_up; % (From Raymer, 2006)
    ratio_W = GAP/b_W; % (From Raymer, 2006)
    sig_W = 0.56; % Obtained from graph (From Raymer, 2006)
    e_W = ((mi_W^2)*(1 + r_W^2))/((mi_W^2) + 2*sig_W*mi_W*r_W + (r_W^2)); %
Biplane Span efficiency Factor

    if (main_menu == 1 | main_menu == 2)
    fprintf ('mi_W:  %g', mi_W);
    fprintf ('\n');
    fprintf ('r_W:  %g', r_W);
    fprintf ('\n');
    fprintf ('sig_W:  %g', sig_W);
    fprintf ('\n');
    fprintf ('ratio_W:  %g', ratio_W);
    fprintf ('\n\n');
    fprintf ('BIPLANE WING SPAN EFFICIENCY FACTOR "e":  %g', e_W);
    fprintf ('\n\n\n');
    end

    %¨¨¨¨¨Lower Wing¨¨¨¨¨
    fprintf ('***Lower Wing***\n\n');

    e_W_low = e_W;

    CL_alf_W_low_rad = Cl_alf_W_low_rad/(1 +
(Cl_alf_W_low_rad/(pi*e_W_low*AR_W_low))); % [1/rad]
    CL_alf_W_low = CL_alf_W_low_rad/57.29579; % [1/°]

    C_f_W = C_r_W_low*3.28083; % [ft] Lower Wing Root Cord
    x_h_W_low = 1.592*3.28083; % [ft] Distance between centroid of last
fuselage segment and Trailing Edge of the Lower wing Root Chord
    dEps_dAlp_W_low = (2*CL_alf_W_low_rad)/(pi*AR_W_low); % Downwash gradient
(from Nelson page 51)
```

```
        %*Fuselage Parameters*
        x_low_W_1 = 3.422*3.28083; % [ft] Distance between centroid of
fuselage segment and Leading Edge of the Lower wing Root Chord
        Delt_x_W_low_1 = 0.365*3.28083; % [ft] Lenght of the fuselage segment
        W_f_W_low_1 = 0.253*3.28083; % [ft] Average width of the fuselage
segment
        x_low_W_1_Cf = x_low_W_1/C_f_W; % Curve (1) from Roskam part 6 page
327
        dEps_dAlp_W_low_1 = 1.05; % Change in local flow angle with angle of
attack (Roskam part 6; pg 327)
        Sum_W_low_1 = (W_f_W_low_1^2)*dEps_dAlp_W_low_1*Delt_x_W_low_1;

        x_low_W_2 = 3.060*3.28083;
        Delt_x_W_low_2 = 0.360*3.28083;
        W_f_W_low_2 = 0.438*3.28083;
        x_low_W_2_Cf = x_low_W_2/C_f_W;
        dEps_dAlp_W_low_2 = 1.05;
        Sum_W_low_2 = (W_f_W_low_2^2)*dEps_dAlp_W_low_2*Delt_x_W_low_2;

        x_low_W_3 = 2.700*3.28083;
        Delt_x_W_low_3 = 0.360*3.28083;
        W_f_W_low_3 = 0.635*3.28083;
        x_low_W_3_Cf = x_low_W_3/C_f_W;
        dEps_dAlp_W_low_3 = 1.05;
        Sum_W_low_3 = (W_f_W_low_3^2)*dEps_dAlp_W_low_3*Delt_x_W_low_3;

        x_low_W_4 = 2.340*3.28083;
        Delt_x_W_low_4 = 0.360*3.28083;
        W_f_W_low_4 = 0.654*3.28083;
        x_low_W_4_Cf = x_low_W_4/C_f_W;
        dEps_dAlp_W_low_4 = 1.05;
        Sum_W_low_4 = (W_f_W_low_4^2)*dEps_dAlp_W_low_4*Delt_x_W_low_4;

        x_low_W_5 = 1.980*3.28083;
        Delt_x_W_low_5 = 0.360*3.28083;
        W_f_W_low_5 = 0.721*3.28083;
        x_low_W_5_Cf = x_low_W_5/C_f_W;
        dEps_dAlp_W_low_5 = 1.05;
        Sum_W_low_5 = (W_f_W_low_5^2)*dEps_dAlp_W_low_5*Delt_x_W_low_5;

        x_low_W_6 = 1.620*3.28083;
        Delt_x_W_low_6 = 0.360*3.28083;
        W_f_W_low_6 = 0.767*3.28083;
        x_low_W_6_Cf = x_low_W_6/C_f_W;
        dEps_dAlp_W_low_6 = 1.05;
        Sum_W_low_6 = (W_f_W_low_6^2)*dEps_dAlp_W_low_6*Delt_x_W_low_6;

        x_low_W_7 = 1.260*3.28083;
        Delt_x_W_low_7 = 0.360*3.28083;
        W_f_W_low_7 = 0.861*3.28083;
        x_low_W_7_Cf = x_low_W_7/C_f_W;
        dEps_dAlp_W_low_7 = 1.1;
        Sum_W_low_7 = (W_f_W_low_7^2)*dEps_dAlp_W_low_7*Delt_x_W_low_7;
```

```
        x_low_W_8 = 0.900*3.28083;
        Delt_x_W_low_8 = 0.360*3.28083;
        W_f_W_low_8 = 0.963*3.28083;
        x_low_W_8_Cf = x_low_W_8/C_f_W;
        dEps_dAlp_W_low_8 = 1.18;
        Sum_W_low_8 = (W_f_W_low_8^2)*dEps_dAlp_W_low_8*Delt_x_W_low_8;

        x_low_W_9 = 0.540*3.28083;
        Delt_x_W_low_9 = 0.360*3.28083;
        W_f_W_low_9 = 0.999*3.28083;
        x_low_W_9_Cf = x_low_W_9/C_f_W;
        dEps_dAlp_W_low_9 = 1.35;
        Sum_W_low_9 = (W_f_W_low_9^2)*dEps_dAlp_W_low_9*Delt_x_W_low_9;

        Delt_x_W_low_10 = 0.360*3.28083;
        W_f_W_low_10 = 0.986*3.28083;
        Delt_x_low_W_10_Cf = Delt_x_W_low_10/C_f_W; % Curve (2) from Roskam
part 6 page 327
        dEps_dAlp_W_low_10 = 2.65;
        Sum_W_low_10 = (W_f_W_low_10^2)*dEps_dAlp_W_low_10*Delt_x_W_low_10;

        dEps_dAlp_W_low_11 = 0;
        Sum_W_low_11 = 0;

        x_low_W_12 = 0.180*3.28083; % [ft] Distance between centroid of
fuselage segment and Trailing Edge of the Lower wing Root Chord
        Delt_x_W_low_12 = 0.360*3.28083;
        W_f_W_low_12 = 0.834*3.28083;
        dEps_dAlp_W_low_12 = (x_low_W_12/x_h_W_low)*(1 - dEps_dAlp_W_low);
        Sum_W_low_12 = (W_f_W_low_12^2)*dEps_dAlp_W_low_12*Delt_x_W_low_12;

        x_low_W_13 = 0.540*3.28083;
        Delt_x_W_low_13 = 0.360*3.28083;
        W_f_W_low_13 = 0.807*3.28083;
        dEps_dAlp_W_low_13 = (x_low_W_13/x_h_W_low)*(1 - dEps_dAlp_W_low);
        Sum_W_low_13 = (W_f_W_low_13^2)*dEps_dAlp_W_low_13*Delt_x_W_low_13;

        x_low_W_14 = 0.900*3.28083;
        Delt_x_W_low_14 = 0.360*3.28083;
        W_f_W_low_14 = 0.800*3.28083;
        dEps_dAlp_W_low_14 = (x_low_W_14/x_h_W_low)*(1 - dEps_dAlp_W_low);
        Sum_W_low_14 = (W_f_W_low_14^2)*dEps_dAlp_W_low_14*Delt_x_W_low_14;

        x_low_W_15 = 1.260*3.28083;
        Delt_x_W_low_15 = 0.360*3.28083;
        W_f_W_low_15 = 0.741*3.28083;
        dEps_dAlp_W_low_15 = (x_low_W_15/x_h_W_low)*(1 - dEps_dAlp_W_low);
        Sum_W_low_15 = (W_f_W_low_15^2)*dEps_dAlp_W_low_15*Delt_x_W_low_15;

        x_low_W_16 = 1.592*3.28083;
        Delt_x_W_low_16 = 0.304*3.28083;
        W_f_W_low_16 = 0.680*3.28083;
        dEps_dAlp_W_low_16 = (x_low_W_16/x_h_W_low)*(1 - dEps_dAlp_W_low);
```

```
        Sum_W_low_16 = (W_f_W_low_16^2)*dEps_dAlp_W_low_16*Delt_x_W_low_16;

    Sum_W_low =
Sum_W_low_1+Sum_W_low_2+Sum_W_low_3+Sum_W_low_4+Sum_W_low_5+Sum_W_low_6+Sum_W_
low_7+Sum_W_low_8+Sum_W_low_9+Sum_W_low_10+Sum_W_low_11+Sum_W_low_12+Sum_W_low
_13+Sum_W_low_14+Sum_W_low_15+Sum_W_low_16;
    dM_dAlp_W_low_rad = (q_I/36.5)*(CL_alf_W_low_rad/0.08)*Sum_W_low; %
[1/rad]
    dM_dAlp_W_low = dM_dAlp_W_low_rad/57.29579; % [1/°]

    delt_x_ac_w_low = -
(dM_dAlp_W_low)/(q_I*(S_aero_W_low*10.76391)*(mac_W_low*3.28083)*CL_alf_W_low)
; % [ft] Lower Wing AC shift due to the fuselage
    DELT_X_AC_W_LOW = delt_x_ac_w_low*0.3048; % [m] Lower Wing AC shift due to
the fuselage

    X_AC_W_LOW = X_LE_mac_W_low + (0.25*mac_W_low) + DELT_X_AC_W_LOW; % [m]
Position of the AC for the Lower Wing

    if (main_menu == 1 | main_menu == 2 | main_menu == 3 | main_menu == 4)
    fprintf ('CL_alf_W_low [1/°]:  %g', CL_alf_W_low);
    fprintf ('\n\n');
    fprintf ('AC SHIFT FOR LOW WING + FUSELAGE [m]: %g', DELT_X_AC_W_LOW);
    fprintf ('\n');
    fprintf ('AC POSITION FOR LOW WING + FUSELAGE [m]: %g', X_AC_W_LOW);
    fprintf ('\n\n\n');
    end

    %¨¨¨¨¨Upper Wing¨¨¨¨¨
    fprintf ('***Upper Wing***\n\n');

    e_W_up = e_W;

    CL_alf_W_up_rad = Cl_alf_W_up_rad/(1 +
(Cl_alf_W_up_rad/(pi*e_W_up*AR_W_up))); % [1/rad]
    CL_alf_W_up = CL_alf_W_up_rad/57.29579 % [1/°]

    x_h_W_up = 0.711*3.28083; % [ft] Distance between centroid of last
fuselage segment and Trailing Edge of the Upper wing Root Chord
    dEps_dAlp_W_up = (2*CL_alf_W_up_rad)/(pi*AR_W_up); % Downwash gradient
(from Nelson page 51)

        %*Fuselage Parameters*
        x_up_W_1 = 4.363*3.28083; % [ft] Distance between centroid of fuselage
segment and Leading Edge of the Upper wing Root Chord
        Delt_x_W_up_1 = 0.327*3.28083; % [ft] Lenght of the fuselage segment
        W_f_W_up_1 = 0.253*3.28083; % [ft] Average width of the fuselage
segment
        x_up_W_1_Cf = x_up_W_1/C_f_W; % Curve (1) from Roskam part 6 page 327
        dEps_dAlp_W_up_1 = 1.05; % Change in local flow angle with angle of
attack (Roskam part 6; pg 327)
        Sum_W_up_1 = (W_f_W_up_1^2)*dEps_dAlp_W_up_1*Delt_x_W_up_1;

        x_up_W_2 = 4.025*3.28083; % [ft]
```

```
Delt_x_W_up_2 = 0.350*3.28083; % [ft]
W_f_W_up_2 = 0.406*3.28083; % [ft]
x_up_W_2_Cf = x_up_W_2/C_f_W;
dEps_dAlp_W_up_2 = 1.05;
Sum_W_up_2 = (W_f_W_up_2^2)*dEps_dAlp_W_up_2*Delt_x_W_up_2;

x_up_W_3 = 3.675*3.28083; % [ft]
Delt_x_W_up_3 = 0.350*3.28083; % [ft]
W_f_W_up_3 = 0.518*3.28083; % [ft]
x_up_W_3_Cf = x_up_W_3/C_f_W;
dEps_dAlp_W_up_3 = 1.05;
Sum_W_up_3 = (W_f_W_up_3^2)*dEps_dAlp_W_up_3*Delt_x_W_up_3;

x_up_W_4 = 3.325*3.28083; % [ft]
Delt_x_W_up_4 = 0.350*3.28083; % [ft]
W_f_W_up_4 = 0.619*3.28083; % [ft]
x_up_W_4_Cf = x_up_W_4/C_f_W;
dEps_dAlp_W_up_4 = 1.05;
Sum_W_up_4 = (W_f_W_up_4^2)*dEps_dAlp_W_up_4*Delt_x_W_up_4;

x_up_W_5 = 2.975*3.28083; % [ft]
Delt_x_W_up_5 = 0.350*3.28083; % [ft]
W_f_W_up_5 = 0.709*3.28083; % [ft]
x_up_W_5_Cf = x_up_W_5/C_f_W;
dEps_dAlp_W_up_5 = 1.05;
Sum_W_up_5 = (W_f_W_up_5^2)*dEps_dAlp_W_up_5*Delt_x_W_up_5;

x_up_W_6 = 2.625*3.28083; % [ft]
Delt_x_W_up_6 = 0.350*3.28083; % [ft]
W_f_W_up_6 = 0.752*3.28083; % [ft]
x_up_W_6_Cf = x_up_W_6/C_f_W;
dEps_dAlp_W_up_6 = 1.05;
Sum_W_up_6 = (W_f_W_up_6^2)*dEps_dAlp_W_up_6*Delt_x_W_up_6;

x_up_W_7 = 2.275*3.28083; % [ft]
Delt_x_W_up_7 = 0.350*3.28083; % [ft]
W_f_W_up_7 = 0.851*3.28083; % [ft]
x_up_W_7_Cf = x_up_W_7/C_f_W;
dEps_dAlp_W_up_7 = 1.05;
Sum_W_up_7 = (W_f_W_up_7^2)*dEps_dAlp_W_up_7*Delt_x_W_up_7;

x_up_W_8 = 1.925*3.28083; % [ft]
Delt_x_W_up_8 = 0.350*3.28083; % [ft]
W_f_W_up_8 = 0.945*3.28083; % [ft]
x_up_W_8_Cf = x_up_W_8/C_f_W;
dEps_dAlp_W_up_8 = 1.05;
Sum_W_up_8 = (W_f_W_up_8^2)*dEps_dAlp_W_up_8*Delt_x_W_up_8;

x_up_W_9 = 1.575*3.28083; % [ft]
Delt_x_W_up_9 = 0.350*3.28083; % [ft]
W_f_W_up_9 = 0.994*3.28083; % [ft]
x_up_W_9_Cf = x_up_W_9/C_f_W;
dEps_dAlp_W_up_9 = 1.1;
Sum_W_up_9 = (W_f_W_up_9^2)*dEps_dAlp_W_up_9*Delt_x_W_up_9;
```

```
        x_up_W_10 = 1.225*3.28083; % [ft]
        Delt_x_W_up_10 = 0.350*3.28083; % [ft]
        W_f_W_up_10 = 0.995*3.28083; % [ft]
        x_up_W_10_Cf = x_up_W_10/C_f_W;
        dEps_dAlp_W_up_10 = 1.15;
        Sum_W_up_10 = (W_f_W_up_10^2)*dEps_dAlp_W_up_10*Delt_x_W_up_10;

        x_up_W_11 = 0.875*3.28083; % [ft]
        Delt_x_W_up_11 = 0.350*3.28083; % [ft]
        W_f_W_up_11 = 0.971*3.28083; % [ft]
        x_up_W_11_Cf = x_up_W_11/C_f_W;
        dEps_dAlp_W_up_11 = 1.225;
        Sum_W_up_11 = (W_f_W_up_11^2)*dEps_dAlp_W_up_11*Delt_x_W_up_11;

        x_up_W_12 = 0.525*3.28083; % [ft]
        Delt_x_W_up_12 = 0.350*3.28083; % [ft]
        W_f_W_up_12 = 0.928*3.28083; % [ft]
        x_up_W_12_Cf = x_up_W_12/C_f_W;
        dEps_dAlp_W_up_12 = 1.35;
        Sum_W_up_12 = (W_f_W_up_12^2)*dEps_dAlp_W_up_12*Delt_x_W_up_12;

        Delt_x_W_up_13 = 0.350*3.28083;
        W_f_W_up_13 = 0.864*3.28083;
        Delt_x_up_W_13_Cf = Delt_x_W_up_13/C_f_W; % Curve (2) from Roskam part
6 page 327
        dEps_dAlp_W_up_13 = 2.65;
        Sum_W_up_13 = (W_f_W_up_13^2)*dEps_dAlp_W_up_13*Delt_x_W_up_13;

        Sum_W_up_14 = 0;

        x_up_W_15 = 0.100*3.28083; % [ft] Distance between centroid of
fuselage segment and Trailing Edge of the Upper wing Root Chord
        Delt_x_W_up_15 = 0.200*3.28083;
        W_f_W_up_15 = 0.782*3.28083;
        dEps_dAlp_W_up_15 = (x_up_W_15/x_h_W_up)*(1 - dEps_dAlp_W_up);
        Sum_W_up_15 = (W_f_W_up_15^2)*dEps_dAlp_W_up_15*Delt_x_W_up_15;

        x_up_W_16 = 0.300*3.28083; % [ft]
        Delt_x_W_up_16 = 0.200*3.28083;
        W_f_W_up_16 = 0.744*3.28083;
        dEps_dAlp_W_up_16 = (x_up_W_16/x_h_W_up)*(1 - dEps_dAlp_W_up);
        Sum_W_up_16 = (W_f_W_up_16^2)*dEps_dAlp_W_up_16*Delt_x_W_up_16;

        x_up_W_17 = 0.500*3.28083; % [ft]
        Delt_x_W_up_17 = 0.200*3.28083;
        W_f_W_up_17 = 0.714*3.28083;
        dEps_dAlp_W_up_17 = (x_up_W_17/x_h_W_up)*(1 - dEps_dAlp_W_up);
        Sum_W_up_17 = (W_f_W_up_17^2)*dEps_dAlp_W_up_17*Delt_x_W_up_17;

        x_up_W_18 = 0.711*3.28083; % [ft]
        Delt_x_W_up_18 = 0.222*3.28083;
        W_f_W_up_18 = 0.680*3.28083;
        dEps_dAlp_W_up_18 = (x_up_W_18/x_h_W_up)*(1 - dEps_dAlp_W_up);
```

```
        Sum_W_up_18 = (W_f_W_up_18^2)*dEps_dAlp_W_up_18*Delt_x_W_up_18;

    Sum_W_up =
Sum_W_up_1+Sum_W_up_2+Sum_W_up_3+Sum_W_up_4+Sum_W_up_5+Sum_W_up_6+Sum_W_up_7+S
um_W_up_8+Sum_W_up_9+Sum_W_up_10+Sum_W_up_11+Sum_W_up_12+Sum_W_up_13+Sum_W_up_
14+Sum_W_up_15+Sum_W_up_16+Sum_W_up_17+Sum_W_up_18;
    dM_dAlp_W_up_rad = (q_I/36.5)*(CL_alf_W_up_rad/0.08)*Sum_W_up; % [1/rad]
    dM_dAlp_W_up = dM_dAlp_W_up_rad/57.29579; % [1/°]

    delt_x_ac_w_up = -
(dM_dAlp_W_up)/(q_I*(S_aero_W_up*10.76391)*(mac_W_up*3.28083)*CL_alf_W_up); %
[ft] Upper Wing AC shift due to the fuselage
    DELT_X_AC_W_UP = delt_x_ac_w_up*0.3048; % [m] Upper Wing AC shift due to
the fuselage

    X_AC_W_UP = X_LE_mac_W_up + (0.25*mac_W_up) + DELT_X_AC_W_UP; % [m]
Position of the AC for the Upper Wing

    if (main_menu == 1 | main_menu == 2 | main_menu == 3 | main_menu == 4)
    fprintf ('AC SHIFT FOR UPPER WING + FUSELAGE [m]: %g', DELT_X_AC_W_UP);
    fprintf ('\n');
    fprintf ('AC POSITION FOR UPPER WING + FUSELAGE [m]: %g', X_AC_W_UP);
    fprintf ('\n\n\n');
    end

    %¨¨¨¨¨Equivalent Wing¨¨¨¨¨
    CL_alph_W = (CL_alf_W_low*(S_aero_W_low/S_aero_W)) +
(CL_alf_W_up*(S_aero_W_up/S_aero_W)); % [1/°]

    X_AC_AP = (X_AC_W_LOW + X_AC_W_UP)/2; % [m]

    if (main_menu == 1 | main_menu == 2 | main_menu == 3 | main_menu == 4)
    fprintf ('AC POSITION FOR THE EQUIVALENT WING + FUSELAGE [m]: %g',
X_AC_AP);
    fprintf ('\n\n');
    end


%¨¨Canards Aerodynamic Center¨¨
fprintf ('***Canards Aerodynamic Center***\n\n');

    %¨¨Biplane Canard Span Efficiency Factor¨¨
    mi_Can = b_can_up/b_can_low; % (From Raymer, 2006)
    r_Can = S_aero_can_low/S_aero_can_up; % (From Raymer, 2006)
    ratio_Can = GAP_can/b_CAN; % (From Raymer, 2006)
    sig_Can = 0.68; % Obtained from graph (From Raymer, 2006)
    e_CAN = ((mi_Can^2)*(1 + r_Can^2))/((mi_Can^2) + 2*sig_Can*mi_Can*r_Can +
(r_Can^2)); % Biplane Span efficiency Factor

    if (main_menu == 1 | main_menu == 2)
    fprintf ('mi_Can:  %g', mi_Can);
    fprintf ('\n');
    fprintf ('r_Can:  %g', r_Can);
```

```
    fprintf ('\n');
    fprintf ('ratio_Can:  %g', ratio_Can);
    fprintf ('\n\n');
    fprintf ('BIPLANE CANARD SPAN EFFICIENCY FACTOR "e": %g', e_CAN);
    fprintf ('\n\n\n');
    end

    %¨¨¨¨¨Lower Canard¨¨¨¨¨
    fprintf ('***Lower Canard***\n\n');

    e_can_low = e_CAN;

    CL_alph_can_low_rad = Cl_alph_can_low_rad/(1 +
(Cl_alph_can_low_rad/(pi*e_can_low*AR_can_low)))
    CL_alph_can_low = CL_alph_can_low_rad/57.29579 % [1/°]

    C_f_can_low = C_r_can_low*3.28083; % [ft] Lower Canard Root Cord
    x_h_can_low = 4.0903*3.28083; % [ft] Distance between centroid of last
fuselage segment and Trailing Edge of the Lower canard Root Chord
    dEps_dAlp_CAN_low = (2*CL_alph_can_low_rad)/(pi*AR_can_low); % Downwash
gradient (from Nelson page 51)

        %*Fuselage Parameters*
        x_low_can_1 = 1.225*3.28083; % [ft] Distance between centroid of
fuselage segment and Leading Edge of the Lower canard Root Chord
        Delt_x_can_low_1 = 0.350*3.28083; % [ft] Lenght of the fuselage
segment
        W_f_can_low_1 = 0.253*3.28083; % [ft] Average width of the fuselage
segment
        x_low_can_1_Cf = x_low_can_1/C_f_can_low; % Curve (1) from Roskam part
6 page 327
        dEps_dAlp_CAN_low_1 = 1.05; % Change in local flow angle with angle of
attack (Roskam part 6; pg 327)
        Sum_CAN_low_1 =
(W_f_can_low_1^2)*dEps_dAlp_CAN_low_1*Delt_x_can_low_1;

        x_low_can_2 = 0.875*3.28083; % [ft]
        Delt_x_can_low_2 = 0.350*3.28083; % [ft]
        W_f_can_low_2 = 0.421*3.28083; % [ft]
        x_low_can_2_Cf = x_low_can_2/C_f_can_low;
        dEps_dAlp_CAN_low_2 = 1.05;
        Sum_CAN_low_2 =
(W_f_can_low_2^2)*dEps_dAlp_CAN_low_2*Delt_x_can_low_2;

        x_low_can_3 = 0.525*3.28083; % [ft]
        Delt_x_can_low_3 = 0.350*3.28083; % [ft]
        W_f_can_low_3 = 0.537*3.28083; % [ft]
        x_low_can_3_Cf = x_low_can_3/C_f_can_low;
        dEps_dAlp_CAN_low_3 = 1.15;
        Sum_CAN_low_3 =
(W_f_can_low_3^2)*dEps_dAlp_CAN_low_3*Delt_x_can_low_3;

        x_low_can_4 = 0.175*3.28083; % [ft]
        Delt_x_can_low_4 = 0.350*3.28083; % [ft]
```

```
        W_f_can_low_4 = 0.632*3.28083; % [ft]
        x_low_can_4_Cf = x_low_can_4/C_f_can_low;
        dEps_dAlp_CAN_low_4 = 1.4;
        Sum_CAN_low_4 =
(W_f_can_low_4^2)*dEps_dAlp_CAN_low_4*Delt_x_can_low_4;

        dEps_dAlp_CAN_low_5 = 0;
        Sum_CAN_low_5 = 0;

        x_low_can_6 = 0.175*3.28083; % [ft] Distance between centroid of
fuselage segment and Trailing Edge of the Lower canard Root Chord
        Delt_x_can_low_6 = 0.350*3.28083;
        W_f_can_low_6 = 0.767*3.28083;
        dEps_dAlp_CAN_low_6 = (x_low_can_6/x_h_can_low)*(1 -
dEps_dAlp_CAN_low);
        Sum_CAN_low_6 =
(W_f_can_low_6^2)*dEps_dAlp_CAN_low_6*Delt_x_can_low_6;

        x_low_can_7 = 0.525*3.28083; % [ft]
        Delt_x_can_low_7 = 0.350*3.28083; % [ft]
        W_f_can_low_7 = 0.852*3.28083; % [ft]
        dEps_dAlp_CAN_low_7 = (x_low_can_7/x_h_can_low)*(1 -
dEps_dAlp_CAN_low);
        Sum_CAN_low_7 =
(W_f_can_low_7^2)*dEps_dAlp_CAN_low_7*Delt_x_can_low_7;

        x_low_can_8 = 0.875*3.28083; % [ft]
        Delt_x_can_low_8 = 0.350*3.28083; % [ft]
        W_f_can_low_8 = 0.966*3.28083; % [ft]
        dEps_dAlp_CAN_low_8 = (x_low_can_8/x_h_can_low)*(1 -
dEps_dAlp_CAN_low);
        Sum_CAN_low_8 =
(W_f_can_low_8^2)*dEps_dAlp_CAN_low_8*Delt_x_can_low_8;

        x_low_can_9 = 1.225*3.28083; % [ft]
        Delt_x_can_low_9 = 0.350*3.28083; % [ft]
        W_f_can_low_9 = 0.995*3.28083; % [ft]
        dEps_dAlp_CAN_low_9 = (x_low_can_9/x_h_can_low)*(1 -
dEps_dAlp_CAN_low);
        Sum_CAN_low_9 =
(W_f_can_low_9^2)*dEps_dAlp_CAN_low_9*Delt_x_can_low_9;

        x_low_can_10 = 1.575*3.28083; % [ft]
        Delt_x_can_low_10 = 0.350*3.28083; % [ft]
        W_f_can_low_10 = 0.996*3.28083; % [ft]
        dEps_dAlp_CAN_low_10 = (x_low_can_10/x_h_can_low)*(1 -
dEps_dAlp_CAN_low);
        Sum_CAN_low_10 =
(W_f_can_low_10^2)*dEps_dAlp_CAN_low_10*Delt_x_can_low_10;

        x_low_can_11 = 1.925*3.28083; % [ft]
        Delt_x_can_low_11 = 0.350*3.28083; % [ft]
        W_f_can_low_11 = 0.965*3.28083; % [ft]
```

```
        dEps_dAlp_CAN_low_11 = (x_low_can_11/x_h_can_low)*(1 -
dEps_dAlp_CAN_low);
        Sum_CAN_low_11 =
(W_f_can_low_11^2)*dEps_dAlp_CAN_low_11*Delt_x_can_low_11;

        x_low_can_12 = 2.275*3.28083; % [ft]
        Delt_x_can_low_12 = 0.350*3.28083; % [ft]
        W_f_can_low_12 = 0.916*3.28083; % [ft]
        dEps_dAlp_CAN_low_12 = (x_low_can_12/x_h_can_low)*(1 -
dEps_dAlp_CAN_low);
        Sum_CAN_low_12 =
(W_f_can_low_12^2)*dEps_dAlp_CAN_low_12*Delt_x_can_low_12;

        x_low_can_13 = 2.625*3.28083; % [ft]
        Delt_x_can_low_13 = 0.350*3.28083; % [ft]
        W_f_can_low_13 = 0.866*3.28083; % [ft]
        dEps_dAlp_CAN_low_13 = (x_low_can_13/x_h_can_low)*(1 -
dEps_dAlp_CAN_low);
        Sum_CAN_low_13 =
(W_f_can_low_13^2)*dEps_dAlp_CAN_low_13*Delt_x_can_low_13;

        x_low_can_14 = 2.975*3.28083; % [ft]
        Delt_x_can_low_14 = 0.350*3.28083; % [ft]
        W_f_can_low_14 = 0.827*3.28083; % [ft]
        dEps_dAlp_CAN_low_14 = (x_low_can_14/x_h_can_low)*(1 -
dEps_dAlp_CAN_low);
        Sum_CAN_low_14 =
(W_f_can_low_14^2)*dEps_dAlp_CAN_low_14*Delt_x_can_low_14;

        x_low_can_15 = 3.325*3.28083; % [ft]
        Delt_x_can_low_15 = 0.350*3.28083; % [ft]
        W_f_can_low_15 = 0.804*3.28083; % [ft]
        dEps_dAlp_CAN_low_15 = (x_low_can_15/x_h_can_low)*(1 -
dEps_dAlp_CAN_low);
        Sum_CAN_low_15 =
(W_f_can_low_15^2)*dEps_dAlp_CAN_low_15*Delt_x_can_low_15;

        x_low_can_16 = 3.675*3.28083; % [ft]
        Delt_x_can_low_16 = 0.350*3.28083; % [ft]
        W_f_can_low_16 = 0.793*3.28083; % [ft]
        dEps_dAlp_CAN_low_16 = (x_low_can_16/x_h_can_low)*(1 -
dEps_dAlp_CAN_low);
        Sum_CAN_low_16 =
(W_f_can_low_16^2)*dEps_dAlp_CAN_low_16*Delt_x_can_low_16;

        x_low_can_17 = x_h_can_low; % [ft]
        Delt_x_can_low_17 = 0.481*3.28083; % [ft]
        W_f_can_low_17 = 0.722*3.28083; % [ft]
        dEps_dAlp_CAN_low_17 = (x_low_can_17/x_h_can_low)*(1 -
dEps_dAlp_CAN_low);
        Sum_CAN_low_17 =
(W_f_can_low_17^2)*dEps_dAlp_CAN_low_17*Delt_x_can_low_17;
```

```
    Sum_CAN_low =
Sum_CAN_low_1+Sum_CAN_low_2+Sum_CAN_low_3+Sum_CAN_low_4+Sum_CAN_low_5+Sum_CAN_
low_6+Sum_CAN_low_7+Sum_CAN_low_8+Sum_CAN_low_9+Sum_CAN_low_10+Sum_CAN_low_10+
Sum_CAN_low_11+Sum_CAN_low_12+Sum_CAN_low_13+Sum_CAN_low_14+Sum_CAN_low_15+Sum
_CAN_low_16+Sum_CAN_low_17;
    dM_dAlp_CAN_low_rad = (q_I/36.5)*(CL_alph_can_low_rad/0.08)*Sum_CAN_low; %
[1/rad]
    dM_dAlp_CAN_low = dM_dAlp_CAN_low_rad/57.29579; % [1/°]

    delt_x_ac_can_low = -
(dM_dAlp_CAN_low)/(q_I*(S_aero_can_low*10.76391)*(mac_can_low*3.28083)*CL_alph
_can_low); % [ft] Lower Canard AC shift due to the fuselage
    DELT_X_AC_CAN_LOW = delt_x_ac_can_low*0.3048; % [m] Lower Canard AC shift
due to the fuselage

    X_AC_CAN_LOW = X_LE_mac_can_low + (0.23*mac_can_low) + DELT_X_AC_CAN_LOW;
% [m] Position of the AC for the Lower Canard

    if (main_menu == 1 | main_menu == 2 | main_menu == 3 | main_menu == 4)
    fprintf ('AC SHIFT FOR LOWER CANARD + FUSELAGE [m]: %g',
DELT_X_AC_CAN_LOW);
    fprintf ('\n');
    fprintf ('AC POSITION FOR LOWER CANARD + FUSELAGE [m]: %g', X_AC_CAN_LOW);
    fprintf ('\n\n');
    end

    %¨¨¨¨¨Upper Canard¨¨¨¨¨
    fprintf ('***Upper Canard***\n\n');

    e_can_up = e_CAN;

    CL_alph_can_up_rad = Cl_alph_can_up_rad/(1 +
(Cl_alph_can_up_rad/(pi*e_can_up*AR_can_up)));
    CL_alph_can_up = CL_alph_can_up_rad/57.29579 % [1/°]

    DELT_X_AC_CAN_UP = DELT_X_AC_CAN_LOW;
    X_AC_CAN_UP = X_LE_mac_can_up + (0.23*mac_can_up) + DELT_X_AC_CAN_UP; %
[m] Position of the AC for the Upper Canard

    if (main_menu == 1 | main_menu == 2 | main_menu == 3 | main_menu == 4)
    fprintf ('AC SHIFT FOR UPPER CANARD + FUSELAGE [m]: %g',
DELT_X_AC_CAN_UP);
    fprintf ('\n');
    fprintf ('AC POSITION FOR UPPER CANARD + FUSELAGE [m]: %g', X_AC_CAN_UP);
    fprintf ('\n\n');
    end


%¨¨Vertical Tails Aerodynamic Center¨¨
fprintf ('***Vertical Tails Aerodynamic Center***\n\n');

    %¨¨¨¨¨Left Vertical Tail¨¨¨¨¨
    fprintf ('***Left Vertical Tail***\n\n');
```

```
    X_AC_VT_LEF = X_LE_mac_vt_lef + (0.25*mac_vt_lef); % [m] Position of the
AC for the Left Vertical Tail

    if (main_menu == 1 | main_menu == 2 | main_menu == 3 | main_menu == 4)
    fprintf ('LEFT VERTICAL TAIL AC POSITION [m]: %g', X_AC_VT_LEF);
    fprintf ('\n\n\n');
    end

    %¨¨¨¨¨Right Vertical Tail¨¨¨¨¨
    fprintf ('***Right Vertical Tail***\n\n');

    X_AC_VT_RIG = X_LE_mac_vt_rig + (0.25*mac_vt_rig); % [m] Position of the
AC for the Right Vertical Tail

    if (main_menu == 1 | main_menu == 2 | main_menu == 3 | main_menu == 4)
    fprintf ('RIGHT VERTICAL TAIL AC POSITION [m]: %g', X_AC_VT_RIG);
    fprintf ('\n\n\n');
    end


%¨¨Aerodynamic Center of the Total Airplane Side Area¨¨
fprintf ('***Aerodynamic Center of the Total Airplane Side Area***\n\n');

    A_acft_1 = 0.033; % [m^2] Segment of the airplane projected side area
(Estimated from CAD drawing)
    x_acft_1 = 0.173/2; % [m] position of center of the projected side area
(Estimated from CAD drawing)
    sum_acft_1 = A_acft_1*x_acft_1;

    A_acft_2 = 0.048; % [m^2]
    x_acft_2 = 0.173 + (0.15/2); % [m]
    sum_acft_2 = A_acft_2*x_acft_2;

    A_acft_3 = 0.192; % [m^2]
    x_acft_3 = 0.319 + (0.341/2); % [m]
    sum_acft_3 = A_acft_3*x_acft_3;

    A_acft_4 = 0.121; % [m^2]
    x_acft_4 = 0.659 + (0.214/2); % [m]
    sum_acft_4 = A_acft_4*x_acft_4;

    A_acft_5 = 0.230; % [m^2]
    x_acft_5 = 0.873 + (0.350/2); % [m]
    sum_acft_5 = A_acft_5*x_acft_5;

    A_acft_6 = 0.193; % [m^2]
    x_acft_6 = 1.223 + (0.259/2); % [m]
    sum_acft_6 = A_acft_6*x_acft_6;

    A_acft_7 = 0.349; % [m^2]
    x_acft_7 = 1.482 + 0.200; % [m]
    sum_acft_7 = A_acft_7*x_acft_7;
```

```
A_acft_8 = 0.201; % [m^2]
x_acft_8 = 1.882 + 0.100; % [m]
sum_acft_8 = A_acft_8*x_acft_8;

A_acft_9 = 0.217; % [m^2]
x_acft_9 = 2.082 + 0.100; % [m]
sum_acft_9 = A_acft_9*x_acft_9;

A_acft_10 = 0.231; % [m^2]
x_acft_10 = 2.282 + 0.100; % [m]
sum_acft_10 = A_acft_10*x_acft_10;

A_acft_11 = 0.244; % [m^2]
x_acft_11 = 2.482 + 0.100; % [m]
sum_acft_11 = A_acft_11*x_acft_11;

A_acft_12 = 0.256; % [m^2]
x_acft_12 = 2.682 + 0.100; % [m]
sum_acft_12 = A_acft_12*x_acft_12;

A_acft_13 = 0.266; % [m^2]
x_acft_13 = 2.882 + 0.100; % [m]
sum_acft_13 = A_acft_13*x_acft_13;

A_acft_14 = 0.275; % [m^2]
x_acft_14 = 3.082 + 0.100; % [m]
sum_acft_14 = A_acft_14*x_acft_14;

A_acft_15 = 0.282; % [m^2]
x_acft_15 = 3.282 + 0.100; % [m]
sum_acft_15 = A_acft_15*x_acft_15;

A_acft_16 = 0.287; % [m^2]
x_acft_16 = 3.482 + 0.100; % [m]
sum_acft_16 = A_acft_16*x_acft_16;

A_acft_17 = 0.290; % [m^2]
x_acft_17 = 3.682 + 0.100; % [m]
sum_acft_17 = A_acft_17*x_acft_17;

A_acft_18 = 0.384; % [m^2]
x_acft_18 = 3.882 + (0.265/2); % [m]
sum_acft_18 = A_acft_18*x_acft_18;

A_acft_19 = 0.458; % [m^2]
x_acft_19 = 4.146 + 0.160; % [m]
sum_acft_19 = A_acft_19*x_acft_19;

A_acft_20 = 0.454; % [m^2]
x_acft_20 = 4.466 + (0.331/2); % [m]
sum_acft_20 = A_acft_20*x_acft_20;
```

```
    A_acft_21 = 0.367; % [m^2]
    x_acft_21 = 4.797 + (0.285/2); % [m]
    sum_acft_21 = A_acft_21*x_acft_21;

    A_acft_22 = 0.417; % [m^2]
    x_acft_22 = 5.082 + (0.355/2); % [m]
    sum_acft_22 = A_acft_22*x_acft_22;

    A_acft_23 = 0.614; % [m^2]
    x_acft_23 = 5.437 + 0.275; % [m]
    sum_acft_23 = A_acft_23*x_acft_23;

    A_acft_24 = 0.098; % [m^2]
    x_acft_24 = 5.987 + (0.204/2); % [m]
    sum_acft_24 = A_acft_24*x_acft_24;

    A_acft_25 = 0.202; % [m^2] MAIN LANDING GEAR AREA
    x_acft_25 = 3.820 + (0.630/2); % [m]
    sum_acft_25 = A_acft_25*x_acft_25;

    Sum_acft =
sum_acft_1+sum_acft_2+sum_acft_3+sum_acft_4+sum_acft_5+sum_acft_6+sum_acft_7+s
um_acft_8+sum_acft_9+sum_acft_10+sum_acft_11+sum_acft_12+sum_acft_13+sum_acft_
14+sum_acft_15+sum_acft_16+sum_acft_17+sum_acft_18+sum_acft_19+sum_acft_20+sum
_acft_21+sum_acft_22+sum_acft_23+sum_acft_24+sum_acft_25;
    Sum_A_acft =
A_acft_1+A_acft_2+A_acft_3+A_acft_4+A_acft_5+A_acft_6+A_acft_7+A_acft_8+A_acft
_9+A_acft_10+A_acft_11+A_acft_12+A_acft_13+A_acft_14+A_acft_15+A_acft_16+A_acf
t_17+A_acft_18+A_acft_19+A_acft_20+A_acft_21+A_acft_22+A_acft_23+A_acft_24+A_a
cft_25;
    X_AC_ACFT = Sum_acft/Sum_A_acft; % [m] Position of the Aerodynamic Center
of the Airplane Projected side area

    if (main_menu == 1 | main_menu == 2 | main_menu == 3 | main_menu == 4)
    fprintf ('Position of the Aerodynamic Center of the Airplane Projected
side area [m]: %g', X_AC_ACFT);
    fprintf ('\n\n');
    end

fprintf ('-------------------------------------------------------------------
---------------------------\n\n');
%……….……….……….……….……….……….……….……….……….……….……….……….……….……….……

%……….……….……….……….……FUSELAGE……….……….……….……….……….……….……….……
fprintf ('-----------------------------------------FUSELAGE-----------------
---------------------------\n\n');

%¨¨Lift¨¨
K_w_f = 1 + 0.025*(d_f/b_W) - 0.25*(d_f/b_W)^2;

CL_alph_W_f = K_w_f*((CL_alf_W_low + CL_alf_W_up)/2);
CL_alph_f = CL_alph_W_f - (CL_alf_W_low + CL_alf_W_up)/2;
```

```
CL_FUS = CL_alph_f*Alpha;
L_FUS = 0.5*RHO.*CL_FUS*S_xy_fus.*(V_T.^2);

if (main_menu == 1 | main_menu == 2)
fprintf ('K_w_f: %g', K_w_f);
fprintf ('\n');
fprintf ('CL_alph_W_f [1/°]: %g', CL_alph_W_f);
fprintf ('\n');
fprintf ('CL_alph_f [1/°]: %g', CL_alph_f);
fprintf ('\n\n');
fprintf ('Lift due the Fuselage [N]: %g', L_FUS);
fprintf ('\n');
end

%¨¨Drag¨¨
C_fe = 0.0030;

R_lf = (V_T*x_L)/NI;

if (length(R_lf) == 1)
    fprintf ('Fuselage Reynolds R_N_fus on Graph: %g', R_lf);
    fprintf ('\n');
end

R_wf = 1.065; % Wing/Fuselage Interference Factor from graph 4.1 [Roskam VI;
pg24]
C_f_fus = input ('Sikin-friction coefficient of the Fuselage (C_f_fus) from
graph 4.3 [Roskam VI; pg25]: ' ); % from graph 4.3 [Roskam VI; pg25]
L_d = x_L/d_f;
eta_fus = 0.62; % from graph 4.19 [Roskam VI; pg47]
c_d_c = 1.2; % from graph 4.20 [Roskam VI; pg47]

if (main_menu == 1 | main_menu == 2)
fprintf ('R_wf: %g', R_wf);
fprintf ('\n');
fprintf ('Fuselage Fineness Ratio L_f/d_f: %g', L_d);
fprintf ('\n');
fprintf ('eta_fus: %g', eta_fus);
fprintf ('\n');
fprintf ('c_d_c: %g', c_d_c);
fprintf ('\n\n');
end

Aux_fus_1 = 60/((x_L/d_f)^3);
Aux_fus_2 = 0.0025*(x_L/d_f);
CD_0_FUS = R_wf*C_f_fus*(1 + Aux_fus_1 + Aux_fus_2)*(S_wet_fus/S_aero_W); %+
CD_b_fus;

CD_L_FUS = ((2*(Alpha_rad.^2)*S_b_fus)/S_aero_W) +
((eta_fus*c_d_c*(abs(Alpha_rad).^3)*S_xy_fus)/S_aero_W);

CD_FUS = CD_0_FUS + CD_L_FUS;

D_FUS = 0.5*RHO*CD_FUS*S_aero_W*(V_T.^2);
```

```
if (main_menu == 1 | main_menu == 2)
fprintf ('CD_0_FUS: %g', CD_0_FUS);
fprintf ('\n');
fprintf ('CD_L_FUS: %g', CD_L_FUS);
fprintf ('\n');
fprintf ('CD_FUS: %g', CD_FUS);
fprintf ('\n');
fprintf ('Drag due to Fuselage [N]: %g', D_FUS);
fprintf ('\n\n\n');
end

fprintf ('-------------------------------------------------------------------
----------------------------\n\n');
%……….……….……….……….……….……….……….……….……….……….……….……….……….……….……….……….……….……….……

%……….……….……….……….……….……….……WINGS……….……….……….……….……….……….……….……….……….……….……
fprintf ('-----------------------------------------WINGS--------------------
----------------------------\n\n');

%¨¨¨¨¨Lower Wing Aerodynamic Forces¨¨¨¨¨
fprintf ('***Lower Wing Aerodynamic Forces***\n\n');

Re_W_low = (RHO*V_T*mac_W_low)/MI;
fprintf ('Lower Wing Reynolds Number (Re): %g', Re_W_low);
fprintf ('\n\n');


S_lam_W_low = (2*S_aero_W_low)*0.398; % [m^2] Lower Wing Wetted Area for
Laminar flow
S_turb_W_low = (2*S_aero_W_low)*(1 - 0.398); % [m^2] Lower Wing Wetted Area
for Turbulent flow

%¨¨Lift¨¨
CL_alph_zer_W_low = CL_alf_W_low*(0 - Alf_Cl_zer_W_low); % CL for Alpha == 0

    %*Flaps Contribution
    %2D
    if (Delt_F == 0 | Delt_F == 10)
        k_apst_low = 1.0; % k' for Flaps (from graph)
    end
    if (Delt_F == 20)
        k_apst_low = 0.85; % k' for Flaps (from graph)
    end
    if (length(Delt_F) == 3)
        k_apst_low = [1.0 1.0 0.85];
    end
    cl_delt_theor_low = 0.4; % 'cl_delta_theory' [1/rad] (from graph)
    cl_alph_theor = 2*pi;
    cl_alph_cl_alph_theor_low = Cl_alf_W_low_rad/cl_alph_theor; % Obtained on
Graph
    cl_delt_cl_delt_theor_low = 1; % Obtained from graph
```

```
    Delt_cl_flap =
Delt_f_rad*cl_delt_cl_delt_theor_low*cl_delt_theor_low.*k_apst_low; % Profiel
cl Increment due to Flap Deflection

    k_1 = 0.95; % Obtained from graph
    if (Delt_F == 0)
        k_2 = 0; % Obtained from graph
    end
    if (Delt_F == 10)
        k_2 = 0.33; % Obtained from graph
    end
    if (Delt_F == 20)
        k_2 = 0.58; % Obtained from graph
    end
    if (length(Delt_F) == 3)
        k_2 = [0 0.33 0.58];
    end
    k_3 = 1.0;
    Delt_cl_max_base = 1.52; % Obtained on Graph

    Delt_cl_max_flap = k_1.*k_2*k_3*Delt_cl_max_base; % Increment on Profiel
cl_max due to Flap Deflection

    %3D
    k_b = 0.56; % Obtained from graph
    alph_delt_CL_alph_delt_cl = 1.043; % Obtained from graph

    Delt_CL_flap =
k_b*Delt_cl_flap*(CL_alf_W_low/Cl_alf_W_low)*alph_delt_CL_alph_delt_cl; % Wing
CL Increment due to Flap Deflection

    S_W_f = b_flap*mac_W_low; % [m^2] Wing Flapped Area
    k_Gam = 0.923;

    Delt_CL_max_flap = Delt_cl_max_flap*(S_W_f/S_aero_W_low)*k_Gam; %
Increment on Wing CL_max due to Flap Deflection

    %*Downwash & Upwash Influence*
    l_can_up_W_low = X_AC_W_LOW - X_AC_CAN_UP;
    z_can_W = 0.057; % [m] obtained from CAD Draw
    DEps_DAlp_W_low_1 =
(21*CL_alph_can_up/(AR_can_up^0.725))*(mac_can_up/l_can_up_W_low)*((10 -
3*Lamb_can_up)/7)*(1 - (z_can_W/b_can_up)); % Downwash rate due to Upper
Canard
    Delt_CL_alp_W_low_1_rad = CL_alf_W_low_rad*(1 -
DEps_DAlp_W_low_1)*(b_can_up/b_W_low);
    Delt_CL_alp_W_low_1 = Delt_CL_alp_W_low_1_rad/57.29579;

    l_W_W = X_AC_W_UP - X_AC_W_LOW;
    DEps_DAlp_W_low_2 = (0.3*(AR_W_up^0.3) - 0.33)*((l_W_W/mac_W_up)^-(1.04 +
6*(AR_W_up^-1.7))); % Upwash rate due to Upper Wing
    Delt_CL_alp_W_low_2_rad = CL_alf_W_low_rad*(1 +
DEps_DAlp_W_low_2)*(b_W_up/b_W_low);
    Delt_CL_alp_W_low_2 = Delt_CL_alp_W_low_2_rad/57.29579;
```

```
    Delt_CL_alp_W_low = Delt_CL_alp_W_low_1 + Delt_CL_alp_W_low_2; % [1/°]
    Delt_CL_alp_W_low_rad = Delt_CL_alp_W_low*57.29579; % [1/rad]

    %*Gorund Effect*
    Delt_CL_ground_low = 0; % CL Increment on Lower Wing due the Ground Effect

CL_W_low = (((CL_alf_W_low + Delt_CL_alp_W_low).*((Alpha - Alf_Cl_zer_W_low) +
i_W_low)).*cos(Tao_W_low_rad)) + Delt_CL_flap + Delt_CL_ground_low; % Total
Lower Wing CL

CL_max_W_low = (((CL_alf_W_low + Delt_CL_alp_W_low)*((Alpha -
Alf_Cl_zer_W_low) + i_W_low))*cos(Tao_W_low_rad)) + Delt_CL_max_flap +
Delt_CL_ground_low; % Total Lower Wing CL_max

L_W_low = 0.5*RHO*CL_W_low*S_aero_W_low*(V_T.^2); % Lift Generated by the
Lower Wing
L_max_W_low = 0.5*RHO*CL_max_W_low*S_aero_W_low*(V_T.^2); % Maximum Lift
(Stall condition) Generated by the Lower Wing

if (main_menu == 1 | main_menu == 2)
fprintf ('Airfoil cl Increment due to Flap Deflection: %g', Delt_cl_flap);
fprintf ('\n');
fprintf ('Wing CL Increment due to Flap Deflection: %g', Delt_CL_flap);
fprintf ('\n');
if (length(CL_W_low) == 1)
    fprintf ('Lower Wing CL: %g', CL_W_low);
    fprintf ('\n');
    fprintf ('Lower Wing CL_max: %g', CL_max_W_low);
    fprintf ('\n');
end
fprintf ('Lift Generated by the Lower Wing [N]: %g', L_W_low);
fprintf ('\n\n');
fprintf ('Airfoil cl_max Increment due to Flap Deflection: %g',
Delt_cl_max_flap);
fprintf ('\n');
fprintf ('Wing CL_max Increment due to Flap Deflection: %g',
Delt_CL_max_flap);
fprintf ('\n');
fprintf ('Maximum Lift (Stall condition) Generated by the Lower Wing [N]: %g',
L_max_W_low);
fprintf ('\n\n');
end

%¨¨Drag¨¨
R_L_S = 1.07; % from graph 4.2 [Roskam VI; pg24]

CD_0_W_LOW_MY = R_wf*R_L_S*Cd_0_W_low; % Wing Profile Drag

CD_I_W_low = CL_W_low.^2/(pi*e_W_low*AR_W_low); % Induced Drag Coefficient
CD_I_max_W_low = CL_max_W_low.^2/(pi*e_W_low*AR_W_low); % Induced Drag
Coefficient for CL_max

CD_W_low = CD_0_W_LOW_MY + CD_I_W_low; % Total Drag Coefficient
```

```
CD_max_W_low = CD_0_W_LOW_MY + CD_I_max_W_low; % Total Max Drag Coefficient

D_W_low = 0.5*RHO*CD_W_low*S_aero_W_low*(V_T.^2);
D_max_W_low = 0.5*RHO*CD_max_W_low*S_aero_W_low*(V_T.^2);
D_I_W_low = 0.5*RHO*CD_I_W_low*S_aero_W_low*(V_T.^2);
D_I_max_W_low = 0.5*RHO*CD_I_max_W_low*S_aero_W_low*(V_T.^2);

if (main_menu == 1 | main_menu == 2)
fprintf ('R_L_S: %g', R_L_S);
fprintf ('\n\n');
fprintf ('CD_0_W_LOW: %g', CD_0_W_LOW_MY);
fprintf ('\n');
fprintf ('CD_I_W_LOW: %g', CD_I_W_low);
fprintf ('\n');
fprintf ('CD_I_MAX_W_LOW: %g', CD_I_max_W_low);
fprintf ('\n');
fprintf ('CD_W_LOW: %g', CD_W_low);
fprintf ('\n\n');
fprintf ('CD_MAX_W_LOW: %g', CD_max_W_low);
fprintf ('\n\n');
fprintf ('Drag Generated by the Lower Wing [N]: %g', D_W_low);
fprintf ('\n');
fprintf ('Maximum Drag (Stall condition) Generated by the Lower Wing [N]: %g',
D_max_W_low);
fprintf ('\n\n');
fprintf ('Induced Drag Generated by the Lower Wing [N]: %g', D_I_W_low);
fprintf ('\n');
fprintf ('Maximum Induced Drag (Stall condition) Generated by the Lower Wing
[N]: %g', D_I_max_W_low);
fprintf ('\n\n');
end

%¨¨Pitch Moment¨¨
Delt_Cm_W_low = 0; % Delta CM of Lower Wing due Flaps Deflection

CM_W_low = Cm_W_low + Delt_Cm_W_low % Total Pitch Moment Coefficient

    % Developed under Longitudinal Static Stability section


%¨¨¨¨¨Upper Wing Aerodynamic Forces¨¨¨¨¨
fprintf ('***Upper Wing Aerodynamic Forces***\n\n');

Re_W_up = (RHO*V_T*mac_W_up)/MI;
fprintf ('Upper Wing Reynolds Number (Re): %g', Re_W_up);
fprintf ('\n\n');

S_lam_W_up = (2*S_aero_W_up)*0.398; % [m^2] Upper Wing Wetted Area for Laminar
flow
S_turb_W_up = (2*S_aero_W_up)*(1 - 0.398); % [m^2] Upper Wing Wetted Area for
Turbulent flow

%¨¨Lift¨¨
CL_alph_zer_W_up = CL_alf_W_up*(0 - Alf_Cl_zer_W_up); % CL for Alpha == 0
```

```
    %*Ailerons Contribution [18; pag 673-674]
    tao_aileron = 0.28; % Aileron effectiveness; from graphic
    CL_W_up_delt_ail_lef = CL_alf_W_up*tao_aileron; % [1/°] Upper Wing CL
Increment rate due to Left Aileron Deflection
    CL_W_up_delt_ail_lef_rad = CL_W_up_delt_ail_lef*57.29579 % [1/rad]
    CL_W_up_delt_ail_rig = CL_W_up_delt_ail_lef; % [1/°] Upper Wing CL
Increment rate due to Right Aileron Deflection
    CL_W_up_delt_ail_rig_rad = CL_W_up_delt_ail_lef_rad; % [1/rad]

    Delt_CL_ail_lef = CL_W_up_delt_ail_lef*Delt_ail_lef; % Upper Wing CL
Increment rate due to Left Aileron Deflection
    Delt_CL_ail_rig = CL_W_up_delt_ail_rig*Delt_ail_rig; % Upper Wing CL
Increment rate due to Right Aileron Deflection

    %*Downwash & Upwash Influence*
    DEps_DAlp_W_up = (21*CL_alf_W_low/(AR_W_low^0.725))*(mac_W_low/l_W_W)*((10
- 3*Lamb_W_low)/7)*(1 - (GAP/b_W_low)); % Downwash rate due to Lower Wing
    Delt_CL_alp_W_up_rad = CL_alf_W_up_rad*(1 -
DEps_DAlp_W_up)*(b_W_low/b_W_up);
    Delt_CL_alp_W_up = Delt_CL_alp_W_up_rad/57.29579; % [1/°]

    %*Ground Effect*
    Delt_CL_ground_up = 0; % CL Increment on Upper Wing due the Ground Effect

CL_W_up = (((CL_alf_W_up + Delt_CL_alp_W_up)*((Alpha - Alf_Cl_zer_W_up) +
i_W_up))*cos(Tao_W_up_rad)) + Delt_CL_ail_lef + Delt_CL_ail_rig +
Delt_CL_ground_up; % Total Upper Wing CL

CL_max_W_up = CL_W_up; % Total Upper Wing CL_max

L_W_up = 0.5*RHO*CL_W_up*S_aero_W_up*(V_T.^2); % Total Lift Generated by the
Upper Wing
L_max_W_up = 0.5*RHO*CL_max_W_up*S_aero_W_up*(V_T.^2); % Total Maximum Lift
(Stall condition) Generated by the Upper Wing

if (main_menu == 1 | main_menu == 2)
fprintf ('Wing CL Increment due to Left Aileron Deflection: %g',
Delt_CL_ail_lef);
fprintf ('\n');
fprintf ('Wing CL Increment due to Right Aileron Deflection: %g',
Delt_CL_ail_rig);
fprintf ('\n');
if (length(CL_W_up) == 1)
    fprintf ('Upper Wing CL: %g', CL_W_up);
    fprintf ('\n');
    fprintf ('Upper Wing CL_max: %g', CL_max_W_up);
    fprintf ('\n');
end
fprintf ('Lift Generated by the Upper Wing [N]: %g', L_W_up);
fprintf ('\n\n');
fprintf ('Maximum Lift (Stall condition) Generated by the Upper Wing [N]: %g',
L_max_W_up);
fprintf ('\n\n');
```

```
end

%¨¨Drag¨¨
CD_0_W_UP_MY = R_wf*R_L_S*Cd_0_W_up; % Wing Profile Drag

CD_I_W_up = CL_W_up.^2/(pi*e_W_up*AR_W_up); % Induced Drag Coefficient
CD_I_max_W_up = CL_max_W_up.^2/(pi*e_W_up*AR_W_up); % Induced Drag Coefficient
for CL_max

CD_W_up = CD_0_W_UP_MY + CD_I_W_up; % Total Drag Coefficient
CD_max_W_up = CD_0_W_UP_MY + CD_I_max_W_up; % Total Max Drag Coefficient

D_W_up = 0.5*RHO*CD_W_up*S_aero_W_up*(V_T.^2);
D_max_W_up = 0.5*RHO*CD_max_W_up*S_aero_W_up*(V_T.^2);
D_I_W_up = 0.5*RHO*CD_I_W_up*S_aero_W_up*(V_T.^2);
D_I_max_W_up = 0.5*RHO*CD_I_max_W_up*S_aero_W_up*(V_T.^2);

if (main_menu == 1 | main_menu == 2)
fprintf ('CD_0_W_UP: %g', CD_0_W_UP_MY);
fprintf ('\n');
fprintf ('CD_I_W_UP: %g', CD_I_W_up);
fprintf ('\n');
fprintf ('CD_I_MAX_W_UP: %g', CD_I_max_W_up);
fprintf ('\n');
fprintf ('CD_W_UP: %g', CD_W_up);
fprintf ('\n');
fprintf ('CD_MAX_W_UP: %g', CD_max_W_up);
fprintf ('\n\n');
fprintf ('Drag Generated by the Upper Wing [N]: %g', D_W_up);
fprintf ('\n');
fprintf ('Maximum Drag (Stall condition) Generated by the Upper Wing [N]: %g',
D_max_W_up);
fprintf ('\n\n');
fprintf ('Induced Drag Generated by the Upper Wing [N]: %g', D_I_W_up);
fprintf ('\n');
fprintf ('Maximum Induced Drag (Stall condition) Generated by the Upper Wing
[N]: %g', D_I_max_W_up);
fprintf ('\n\n');
end

%¨¨Pitch Moment¨¨
Delt_Cm_W_up = 0; % Delta CM of Upper Wing due Ailerons Deflection

CM_W_up = Cm_W_up + Delt_Cm_W_up % Total Pitch Moment Coefficient

    % Developed under Longitudinal Static Stability section

fprintf ('-----------------------------------------------------------------
----------------------------\n\n');
%¨¨¨¨¨¨¨¨¨¨¨¨¨¨¨¨¨¨¨¨¨¨¨¨¨¨¨¨¨¨¨¨¨¨¨¨¨¨¨¨¨¨¨¨¨¨¨¨¨¨¨¨¨¨¨¨¨¨¨¨¨¨¨¨¨¨¨¨¨¨¨¨¨¨¨¨¨¨¨¨¨¨¨¨¨¨

%¨¨¨¨¨¨¨¨¨¨¨¨¨¨¨¨¨¨¨¨¨¨¨¨¨¨¨¨¨¨¨¨¨¨¨¨¨¨¨¨¨¨CANARDS¨¨¨¨¨¨¨¨¨¨¨¨¨¨¨¨¨¨¨¨¨¨¨¨¨¨¨¨¨¨¨¨¨¨¨¨¨¨
fprintf ('---------------------------------------------CANARDS----------------
----------------------------\n\n');
```

```
%¨¨¨¨¨Lower Canard Aerodynamic Forces¨¨¨¨¨
fprintf ('***Lower Canard Aerodynamic Forces***\n\n');

%¨¨Lift¨¨
CL_alph_zer_can_low = CL_alph_can_low*(0 - Alph_Cl_zer_can_low); % CL for
Alpha == 0

    %*Downwash & Upwash Influence*
    l_can_low_1 = X_AC_CAN_UP - X_AC_CAN_LOW;
    dEps_dAlp_can_low_1 = (0.3*(AR_can_up^0.3) -
0.33)*((l_can_low_1/mac_can_up)^-(1.04 + 6*(AR_can_up^-1.7))); % Upwash rate
due to Upper Canard
    Delt_CL_alp_can_low_1_rad = CL_alph_can_low_rad*(1 +
dEps_dAlp_can_low_1)*(b_can_up/b_can_low);
    Delt_CL_alp_can_low_1 = Delt_CL_alp_can_low_1_rad/57.29579;

    l_can_low_2 = X_AC_W_LOW - X_AC_CAN_LOW;
    dEps_dAlp_can_low_2 = (0.3*(AR_W_low^0.3) -
0.33)*((l_can_low_2/mac_W_low)^-(1.04 + 6*(AR_W_low^-1.7))); % Upwash rate due
to Lower Wing
    Delt_CL_alp_can_low_2_rad = CL_alph_can_low_rad*(1 +
dEps_dAlp_can_low_2)*(1); % --> (1) due the wing span be bigger than canard
span
    Delt_CL_alp_can_low_2 = Delt_CL_alp_can_low_2_rad/57.29579;

    Delt_CL_alp_can_low = Delt_CL_alp_can_low_1 + Delt_CL_alp_can_low_2; %
[1/°]
    Delt_CL_alp_can_low_rad = Delt_CL_alp_can_low*57.29579; % [1/rad]

    %*Ground Effect*
    Delt_CL_can_low_grou = 0; % Increment on CL due to Ground Effect

    %*Elevator contribution
    tao_elev_can_low = 0.67; % Elevator effectiveness from graphic
    CL_can_low_delt_elev = CL_alph_can_low*tao_elev_can_low; % [1/°] Canard
Lift Coefficient increment due to elevator deflection
    CL_can_low_delt_elev_rad = CL_can_low_delt_elev*57.29579; % [1/rad]

CL_can_low = (((CL_alph_can_low + Delt_CL_alp_can_low)*((Alpha -
Alph_Cl_zer_can_low) + i_can_low))*cos(Tao_can_low_rad)) +
(CL_can_low_delt_elev*Delt_elev) + Delt_CL_can_low_grou;

L_can_low = 0.5*RHO*CL_can_low*S_aero_can_low*(V_T.^2);

if (main_menu == 1 | main_menu == 2)
fprintf ('tao_elev_can_low: %g', tao_elev_can_low);
fprintf ('\n\n');
if (length(CL_can_low) == 1)
    fprintf ('Lower Canard CL: %g', CL_can_low);
    fprintf ('\n');
end
fprintf ('Lift Generated by the Lower Canard [N]: %g', L_can_low);
fprintf ('\n\n');
```

```
end

%¨¨Drag¨¨
R_cf = R_wf; % Canard/Fuselage Interference Factor (R_wf) from graph 4.1
[Roskam VI; pg24]
R_L_S_can = 1.07; % from graph 4.2 [Roskam VI; pg24]

CD_0_CAN_LOW_MY = R_cf*R_L_S_can*Cd_0_can_low; % Canard Profile Drag

CD_I_can_low = CL_can_low.^2/(pi*e_can_low*AR_can_low); % Induced Drag
Coefficient
CD_can_low = CD_0_CAN_LOW_MY + CD_I_can_low; % Total Drag Coefficient

D_can_low = 0.5*RHO*CD_can_low*S_aero_can_low*(V_T.^2);
D_I_can_low = 0.5*RHO*CD_I_can_low*S_aero_can_low*(V_T.^2);

if (main_menu == 1 | main_menu == 2)
fprintf ('R_cf: %g', R_cf);
fprintf ('\n');
fprintf ('R_L_S_can: %g', R_L_S_can);
fprintf ('\n\n');
fprintf ('CD_0_CAN_LOW: %g', CD_0_CAN_LOW_MY);
fprintf ('\n');
fprintf ('CD_I_CAN_LOW: %g', CD_I_can_low);
fprintf ('\n');
fprintf ('CD_CAN_LOW: %g', CD_can_low);
fprintf ('\n');
fprintf ('Drag Generated by the Lower Canard [N]: %g', D_can_low);
fprintf ('\n');
fprintf ('Induced Drag Generated by the Lower Canard [N]: %g', D_I_can_low);
fprintf ('\n\n');
end

%¨¨Pitch Moment¨¨
Delt_Cm_can_low = 0; % Delta CM of Lower Canard due Elevator Deflection

CM_can_low = Cm_can_low + Delt_Cm_can_low % Total Pitch Moment Coefficient

    % Developed under Longitudinal Static Stability section

%¨¨¨¨Upper Canard Aerodynamic Forces¨¨¨¨
fprintf ('***Upper Canard Aerodynamic Forces***\n\n');

%¨¨Lift¨¨
CL_alph_zer_can_up = CL_alph_can_up*(0 - Alph_Cl_zer_can_up); % CL for Alpha
== 0

    %*Downwash & Upwash Influence*
    l_can_up_1 = X_AC_CAN_UP - X_AC_CAN_LOW;
    dEps_dAlp_can_up_1 =
(21*CL_alph_can_low/(AR_can_low^0.725))*(mac_can_low/l_can_up_1)*((10 -
3*Lamb_can_low)/7)*(1 - (GAP_can/b_can_low)) % Downwash rate due to Lower
Canard
```

```
    Delt_CL_alp_can_up_1_rad = CL_alph_can_up_rad*(1 -
dEps_dAlp_can_up_1)*(b_can_low/b_can_up)
    Delt_CL_alp_can_up_1 = Delt_CL_alp_can_up_1_rad/57.29579;

    l_can_up_2 = X_AC_W_LOW - X_AC_CAN_UP;
    dEps_dAlp_can_up_2 = (0.3*(AR_W_low^0.3) - 0.33)*((l_can_up_2/mac_W_low)^-
(1.04 + 6*(AR_W_low^-1.7))) % Upwash rate due to Lower Wing
    Delt_CL_alp_can_up_2_rad = CL_alph_can_up_rad*(1 + dEps_dAlp_can_up_2)*(1)
% --> (1) due the wing span be bigger than canard span
    Delt_CL_alp_can_up_2 = Delt_CL_alp_can_up_2_rad/57.29579;

    Delt_CL_alp_can_up = Delt_CL_alp_can_up_1 + Delt_CL_alp_can_up_2 % [1/°]
    Delt_CL_alp_can_up_rad = Delt_CL_alp_can_up*57.29579 % [1/rad]

    %*Ground Effect*
    Delt_CL_can_up_grou = 0; % Increment on CL due to Ground Effect

    %*Elevator contribution
    tao_elev_can_up = tao_elev_can_low; % from graphic
    CL_can_up_delt_elev = CL_alph_can_up*tao_elev_can_up % [1/°] Canard Lift
Coefficient increment due to elevator deflection
    CL_can_up_delt_elev_rad = CL_can_up_delt_elev*57.29579 % [1/rad]

CL_can_up = (((CL_alph_can_up + Delt_CL_alp_can_up)*((Alpha -
Alph_Cl_zer_can_up) + i_can_up))*cos(Tao_can_up_rad)) +
(CL_can_up_delt_elev*Delt_elev) + Delt_CL_can_up_grou;

L_can_up = 0.5*RHO*CL_can_up*S_aero_can_up*(V_T.^2);

if (main_menu == 1 | main_menu == 2)
if (length(CL_can_up) == 1)
    fprintf ('Upper Canard CL: %g', CL_can_up);
    fprintf ('\n');
end
fprintf ('Lift Generated by the Upper Canard [N]: %g', L_can_up);
fprintf ('\n\n');
end

%¨¨Drag¨¨
CD_0_CAN_UP_MY = R_cf*R_L_S_can*Cd_0_can_low; % Canard Profile Drag

CD_I_can_up = CL_can_up.^2/(pi*e_can_up*AR_can_up); % Induced Drag Coefficient
CD_can_up = CD_0_CAN_UP_MY + CD_I_can_up; % Total Drag Coefficient

D_can_up = 0.5*RHO*CD_can_up*S_aero_can_up*(V_T.^2);
D_I_can_up = 0.5*RHO*CD_I_can_up*S_aero_can_up*(V_T.^2);

if (main_menu == 1 | main_menu == 2)
fprintf ('CD_0_CAN_UP: %g', CD_0_CAN_UP_MY);
fprintf ('\n');
fprintf ('CD_I_CAN_UP: %g', CD_I_can_up);
fprintf ('\n');
fprintf ('CD_CAN_UP: %g', CD_can_up);
```

```
fprintf ('\n\n');
fprintf ('Drag Generated by the Upper Canard [N]: %g', D_can_up);
fprintf ('\n');
fprintf ('Induced Drag Generated by the Upper Canard [N]: %g', D_I_can_up);
fprintf ('\n\n');
end

%¨¨Pitch Moment¨¨
Delt_Cm_can_up = 0; % Delta CM of Upper Canard due Elevator Deflection

CM_can_up = Cm_can_up + Delt_Cm_can_up % Total Pitch Moment Coefficient

    % Developed under Longitudinal Static Stability section

%¨¨¨¨Fairings + Booms Aerodynamic Forces¨¨¨
fprintf ('***Fairings + Booms Aerodynamic Forces***\n\n');

CD_FairBoo = C_fe;
D_FairBoo_can_lef = 0.5*RHO*CD_FairBoo*S_lef_fairing*(V_T.^2);
D_FairBoo_can_rig = 0.5*RHO*CD_FairBoo*S_rig_fairing*(V_T.^2);

if (main_menu == 1 | main_menu == 2)
fprintf ('Drag Generated by the Left Fairing + Booms [N]: %g',
D_FairBoo_can_lef);
fprintf ('\n');
fprintf ('Drag Generated by the Right Fairing + Booms [N]: %g',
D_FairBoo_can_rig);
fprintf ('\n\n');
end

fprintf ('----------------------------------------------------------------------
----------------------------\n\n');
%¨¨¨¨¨¨¨¨¨¨¨¨¨¨¨¨¨¨¨¨¨¨¨¨¨¨¨¨¨¨¨¨¨¨¨¨¨¨¨¨¨¨¨¨¨¨¨¨¨¨¨¨¨¨¨¨¨¨¨¨¨¨¨¨¨¨¨¨¨¨¨¨¨¨¨¨¨¨¨¨¨

%¨¨¨¨¨¨¨¨¨¨¨¨¨¨¨¨¨¨¨¨¨¨¨¨¨¨¨¨¨¨VERTICAL TAIL¨¨¨¨¨¨¨¨¨¨¨¨¨¨¨¨¨¨¨¨¨¨¨¨¨¨¨¨¨¨¨¨¨
fprintf ('------------------------------------------VERTICAL TAIL-------------
----------------------------\n\n');

%¨¨¨¨Left Vertical Tail Aerodynamic Forces¨¨¨
fprintf ('***Left Vertical Tail Aerodynamic Forces***\n\n');

Tg_Gam_vt_lef = tan((Gam_vt_lef*pi)/180);
e_vt_lef = 2/(2 - AR_vt_lef + sqrt(4 + (AR_vt_lef^2)*(1 + (Tg_Gam_vt_lef^2))))
% Span Efficiency Factor

%¨¨Lift¨¨
CL_alph_vt_lef_rad = Cl_alph_vt_lef_rad/(1 +
(Cl_alph_vt_lef_rad/(pi*e_vt_lef*AR_vt_lef))); % [1/rad]
CL_alph_vt_lef = CL_alph_vt_lef_rad/57.29579; % [1/°]
CL_alph_zer_vt_lef = CL_alph_vt_lef*(0 - Alph_Cl_zer_vt_lef); % CL for Alpha
== 0
```

```
Z_w = 0; % [m] assumed due the position of the two wing regarding the fuselage
center line
Aux_sig_1 = (S_vt_lef/S_W)/(1 + cos(Gam_W_rad));
dSig_dBet_vt_lef = 0.724 + 3.06*Aux_sig_1 + 0.4*(Z_w/h) + 0.009*AR_W - 1; %
Sidewash gradient
Sigma_lef = dSig_dBet_vt_lef*Beta; % [°] Left Vertical Tail Sidewash Angle

    %*Rudder contribution
    tao_rud_vt_lef = 0.575; % Rudder effectiveness from graphic
    CL_vt_lef_delt_rud = CL_alph_vt_lef*tao_rud_vt_lef % Left Vertical Tail
Lift Coefficient increment due to Rudder deflection

CL_vt_lef = ((CL_alph_vt_lef*(Beta + i_vt_lef +
Sigma_lef))*cos(Tao_vt_lef_rad)) + (CL_vt_lef_delt_rud*Delt_rud)

L_vt_lef = 0.5*RHO*CL_vt_lef*S_vt_lef*(V_T.^2);

if (main_menu == 1 | main_menu == 2)
fprintf ('Span Efficiency factor "e": %g', e_vt_lef);
fprintf ('\n');
fprintf ('Z_w: %g', Z_w);
fprintf ('\n');
fprintf ('tao_rud_vt_lef: %g', tao_rud_vt_lef);
fprintf ('\n\n');
fprintf ('Lift Generated by the Left Vertical Tail [N]: %g', L_vt_lef);
fprintf ('\n\n');
end

%¨¨Drag¨¨
R_vtf = 1;
R_L_S_vt = 1.07; % from graph 4.2 [Roskam VI; pg24]

CD_0_VT_LEF_MY = R_vtf*R_L_S_vt*Cd_0_vt_lef; % Vertical Tail Profile Drag

CD_I_vt_lef = CL_vt_lef.^2/(pi*e_vt_lef*AR_vt_lef); % Induced Drag Coefficient
CD_vt_lef = CD_0_VT_LEF_MY + CD_I_vt_lef; % Total Drag Coefficient

D_vt_lef = 0.5*RHO*CD_vt_lef*S_vt_lef*(V_T.^2);
D_I_vt_lef = 0.5*RHO*CD_I_vt_lef*S_vt_lef*(V_T.^2);

if (main_menu == 1 | main_menu == 2)
fprintf ('R_vtf: %g', R_vtf);
fprintf ('\n');
fprintf ('R_L_S_vt: %g', R_L_S_vt);
fprintf ('\n\n');
fprintf ('CD_0_VT_LEF: %g', CD_0_VT_LEF_MY);
fprintf ('\n');
fprintf ('CD_I_VT_LEF: %g', CD_I_vt_lef);
fprintf ('\n');
fprintf ('CD_VT_LEF: %g', CD_vt_lef);
fprintf ('\n\n');
fprintf ('Drag Generated by the Left Vertical Tail [N]: %g', D_vt_lef);
fprintf ('\n');
```

```
fprintf ('Induced Drag Generated by the Left Vertical Tail [N]: %g',
D_I_vt_lef);
fprintf ('\n\n');
end

%¨¨Yaw Moment¨¨
Delt_Cm_vt_lef = 0; % Delta CM of Left Vertical Tail due Rudder Deflection

CM_vt_lef = Cm_vt_lef + Delt_Cm_vt_lef % Total Yaw Moment Coefficient

M_vt_lef = 0.5*RHO*CM_vt_lef*S_vt_lef*(V_T.^2)*mac_vt_lef;

if (main_menu == 1 | main_menu == 2)
fprintf ('Yaw Moment Generated by the Left Vertical Tail [N*m]: %g',
M_vt_lef);
fprintf ('\n\n');
end


%¨¨¨¨¨Right Vertical Tail Aerodynamic Forces¨¨¨¨
fprintf ('***Right Vertical Tail Aerodynamic Forces***\n\n');

Tg_Gam_vt_rig = tan((Gam_vt_rig*pi)/180);
e_vt_rig = 2/(2 - AR_vt_rig + sqrt(4 + (AR_vt_rig^2)*(1 + (Tg_Gam_vt_rig^2))))
% Span Efficiency Factor

%¨¨Lift¨¨
CL_alph_vt_rig_rad = Cl_alph_vt_rig_rad/(1 +
(Cl_alph_vt_rig_rad/(pi*e_vt_rig*AR_vt_rig))); % [1/rad]
CL_alph_vt_rig = CL_alph_vt_rig_rad/57.29579; % [1/°]
CL_alph_zer_vt_rig = CL_alph_vt_rig*(0 - Alph_Cl_zer_vt_rig); % CL for Alpha
== 0

dSig_dBet_vt_rig = dSig_dBet_vt_lef; % Sidewash gradient
Sigma_rig = dSig_dBet_vt_rig*Beta; % [°] Right Vertical Tail Sidewash Angle

    %*Rudder contribution
    tao_rud_vt_rig = tao_rud_vt_lef; % from graphic
    CL_vt_rig_delt_rud = CL_alph_vt_rig*tao_rud_vt_rig % Right Vertical Tail
Lift Coefficient increment due to Rudder deflection

CL_vt_rig = ((CL_alph_vt_rig*(Beta + i_vt_rig +
Sigma_rig))*cos(Tao_vt_rig_rad)) + (CL_vt_rig_delt_rud*Delt_rud)

L_vt_rig = 0.5*RHO*CL_vt_rig*S_vt_rig*(V_T.^2);

if (main_menu == 1 | main_menu == 2)
fprintf ('Span Efficiency factor "e": %g', e_vt_rig);
fprintf ('\n\n');
fprintf ('Lift Generated by the Right Vertical Tail [N]: %g', L_vt_rig);
fprintf ('\n\n');
end
```

```
%¨¨Drag¨¨
CD_0_VT_RIG_MY = R_vtf*R_L_S_vt*Cd_0_vt_rig; % Vertical Tail Profile Drag

CD_I_vt_rig = CL_vt_rig.^2/(pi*e_vt_rig*AR_vt_rig); % Induced Drag Coefficient
CD_vt_rig = CD_0_VT_RIG_MY + CD_I_vt_rig; % Total Drag Coefficient

D_vt_rig = 0.5*RHO*CD_vt_rig*S_vt_rig*(V_T.^2);
D_I_vt_rig = 0.5*RHO*CD_I_vt_rig*S_vt_rig*(V_T.^2);

if (main_menu == 1 | main_menu == 2)
fprintf ('CD_0_VT_RIG: %g', CD_0_VT_RIG_MY);
fprintf ('\n');
fprintf ('CD_I_VT_RIG: %g', CD_I_vt_rig);
fprintf ('\n');
fprintf ('CD_VT_RIG: %g', CD_vt_rig);
fprintf ('\n\n');
fprintf ('Drag Generated by the Right Vertical Tail [N]: %g', D_vt_rig);
fprintf ('\n');
fprintf ('Induced Drag Generated by the Right Vertical Tail [N]: %g',
D_I_vt_rig);
fprintf ('\n\n');
end

%¨¨Yaw Moment¨¨
Delt_Cm_vt_rig = 0; % Delta CM of Right Vertical Tail due Rudder Deflection

CM_vt_rig = Cm_vt_rig + Delt_Cm_vt_rig % Total Yaw Moment Coefficient

M_vt_rig = 0.5*RHO*CM_vt_rig*S_vt_rig*(V_T.^2)*mac_vt_rig;

if (main_menu == 1 | main_menu == 2)
fprintf ('Yaw Moment Generated by the Right Vertical Tail [N*m]: %g',
M_vt_rig);
fprintf ('\n\n');
end

%¨¨¨¨Booms Aerodynamic Forces¨¨¨
fprintf ('***Booms Aerodynamic Forces***\n\n');

CD_Boo = C_fe;
D_Boom_vt_lef = 0.5*RHO*CD_Boo*(S_low_boom_lef + S_up_boom_lef)*(V_T.^2);
D_Boom_vt_rig = 0.5*RHO*CD_Boo*(S_low_boom_rig + S_up_boom_rig)*(V_T.^2);

if (main_menu == 1 | main_menu == 2)
fprintf ('Drag Generated by the Left Booms [N]: %g', D_Boom_vt_lef);
fprintf ('\n');
fprintf ('Drag Generated by the Right Booms [N]: %g', D_Boom_vt_rig);
fprintf ('\n\n');
end

fprintf ('---------------------------------------------------------------------
----------------------------\n\n');
%¨¨¨¨¨¨¨¨¨¨¨¨¨¨¨¨¨¨¨¨¨¨¨¨¨¨¨¨¨¨¨¨¨¨¨¨¨¨¨¨¨¨¨¨¨¨¨¨¨¨¨¨¨¨¨¨¨¨¨¨¨¨¨¨¨¨¨¨¨¨¨¨¨¨¨¨¨¨
```

```
%¨¨¨¨¨¨¨¨¨¨¨¨¨¨¨¨¨¨¨¨¨¨¨¨¨¨¨¨¨¨¨¨¨¨¨¨¨¨¨¨¨¨¨LANDING GEAR¨¨¨¨¨¨¨¨¨¨¨¨¨¨¨¨¨¨¨¨¨¨¨¨¨¨¨¨¨¨¨¨¨¨¨¨¨¨¨¨¨
fprintf ('-------------------------------------------LANDING GEAR--------------
----------------------------\n\n');

%¨¨Lift¨¨
CL_LDG = 0;
L_LDG_lef = 0;
L_LDG_rig = 0;
L_LDG_nose = 0;

if (main_menu == 1 | main_menu == 2)
fprintf ('Lift Generated by the Left Landing Gear [N]: %g', L_LDG_lef);
fprintf ('\n');
fprintf ('Lift Generated by the Right Landing Gear [N]: %g', L_LDG_rig);
fprintf ('\n');
fprintf ('Lift Generated by the Right Landing Gear [N]: %g', L_LDG_nose);
fprintf ('\n\n');
end

%¨¨Drag¨¨
CD_0_LDG = C_fe;
CD_i_LDG = 0;
CD_LDG = CD_0_LDG + CD_i_LDG;

D_LDG_lef = 0.5*RHO*CD_LDG*S_lef_main_gear*(V_T.^2);
D_LDG_rig = 0.5*RHO*CD_LDG*S_rig_main_gear*(V_T.^2);
D_LDG_nose = 0.5*RHO*CD_LDG*S_nose_gear*(V_T.^2);

if (main_menu == 1 | main_menu == 2)
fprintf ('Drag Generated by the Left Landing Gear [N]: %g', D_LDG_lef);
fprintf ('\n');
fprintf ('Drag Generated by the Right Landing Gear [N]: %g', D_LDG_rig);
fprintf ('\n');
fprintf ('Drag Generated by the Right Landing Gear [N]: %g', D_LDG_nose);
fprintf ('\n\n');
end

%¨¨Pitch Moment¨¨
M_LDG_lef = 0;
M_LDG_rig = 0;
M_LDG_nose = 0;

fprintf ('------------------------------------------------------------------------
----------------------------\n\n');
%¨¨¨¨¨¨¨¨¨¨¨¨¨¨¨¨¨¨¨¨¨¨¨¨¨¨¨¨¨¨¨¨¨¨¨¨¨¨¨¨¨¨¨¨¨¨¨¨¨¨¨¨¨¨¨¨¨¨¨¨¨¨¨¨¨¨¨¨¨¨¨¨¨¨¨¨¨¨¨¨¨¨¨¨¨¨¨¨¨¨¨¨¨¨

%¨¨¨¨¨¨¨¨¨¨¨¨¨¨¨¨¨¨¨¨¨¨¨¨¨¨¨¨¨¨¨¨¨¨¨¨¨¨¨¨¨¨¨¨PROPELLER¨¨¨¨¨¨¨¨¨¨¨¨¨¨¨¨¨¨¨¨¨¨¨¨¨¨¨¨¨¨¨¨¨¨¨¨¨¨¨¨¨¨¨
fprintf ('---------------------------------------------PROPELLER---------------
----------------------------\n\n');

%¨¨Lift¨¨
L_PROP = T_Fli_lev.*sin(Alpha_rad); % [N]
CL_PROP = L_PROP./(0.5*RHO.*S_aero_W*(V_T.^2));
```

```
%¨¨Drag¨¨
U_1 = V_T*3.28084; % [ft/s] Flight speed

if (POWER == 0)
    CD_prop = 0.00125*n_prop*(Prop_Diam^2)/S_aero_W;
end

if (POWER > 0)
    CD_prop = 33*(1./(q_I*S_W_ft)).*(POWER_hp./U_1);
end

D_PROP = 0.5*RHO.*CD_prop*(S_aero_W).*(V_T.^2);

if (main_menu == 1 | main_menu == 2)
fprintf ('Propeller Drag Coefficient: %g', CD_prop);
fprintf ('\n');
fprintf ('Drag Generated by Propeller [N]: %g', D_PROP);
fprintf ('\n\n');
end

%¨¨¨¨¨¨¨¨¨¨¨¨¨¨¨¨¨¨¨¨¨¨¨¨¨¨¨¨¨¨¨¨¨¨¨¨¨¨¨¨¨¨¨¨¨¨¨¨¨¨¨¨¨¨¨¨¨¨¨¨¨¨¨¨¨¨¨¨¨¨¨¨¨¨¨¨¨¨¨¨¨¨¨¨¨¨¨¨¨¨¨¨¨¨¨¨¨

%¨¨¨¨¨¨¨¨¨¨¨¨¨¨¨¨¨¨¨¨¨¨¨¨¨¨¨¨¨¨¨¨¨¨¨¨¨¨¨¨¨¨¨¨¨¨¨¨¨¨¨¨¨¨¨COMPLETE AIRPLANE¨¨¨¨¨¨¨¨¨¨¨¨¨¨¨¨¨¨¨¨¨¨¨¨¨¨¨¨¨¨¨¨¨¨¨¨¨¨¨¨¨¨¨¨¨¨¨¨¨¨¨¨¨¨¨¨
fprintf ('----------------------------------------COMPLETE AIRPLANE-----------
----------------------------\n\n');

%¨¨Lift¨¨
L_AIRPLANE = L_FUS + L_W_low + L_W_up + L_can_low + L_can_up + L_LDG_lef +
L_LDG_rig + L_LDG_nose + L_PROP;
L_AIRPLANE_MAX = L_FUS + L_max_W_low + L_max_W_up + L_can_low + L_can_up +
L_LDG_lef + L_LDG_rig + L_LDG_nose + L_PROP;

if (length(L_AIRPLANE) == 1 & main_menu == 1 | main_menu == 2 | main_menu ==
3)

    Load_factor = L_AIRPLANE/W;
    Load_factor_max = L_AIRPLANE_MAX/W;

end

if (main_menu == 1 | main_menu == 2)
fprintf ('Lift Generated by the Complete Airplane [N]: %g', L_AIRPLANE);
fprintf ('\n');
end
if (length(L_AIRPLANE) == 1 & main_menu == 1 | main_menu == 2 | main_menu ==
3)
    fprintf ('Flight Load Factor: %g', Load_factor);
    fprintf ('\n\n');
end
if (main_menu == 1 | main_menu == 2)
fprintf ('Maximum Lift (Stall condition) Generated by the Complete Airplane
[N]: %g', L_AIRPLANE_MAX);
```

```
fprintf ('\n');
end
if (length(L_AIRPLANE) == 1 & main_menu == 1 | main_menu == 2 | main_menu ==
3)
    fprintf ('Flight Maximum Load Factor: %g', Load_factor_max);
end
fprintf ('\n\n');


%¨¨Drag¨¨
D_AIRPLANE = D_FUS + D_W_low + D_W_up + D_can_low + D_can_up +
D_FairBoo_can_lef + D_FairBoo_can_rig + D_vt_lef + D_vt_rig + D_Boom_vt_lef +
D_Boom_vt_rig + D_LDG_lef + D_LDG_rig + D_LDG_nose + D_PROP;
D_AIRPLANE_MAX = D_FUS + D_max_W_low + D_max_W_up + D_can_low + D_can_up +
D_FairBoo_can_lef + D_FairBoo_can_rig + D_vt_lef + D_vt_rig + D_Boom_vt_lef +
D_Boom_vt_rig + D_LDG_lef + D_LDG_rig + D_LDG_nose + D_PROP;

D_I_AIRPLANE = D_I_W_low + D_I_W_up + D_I_can_low + D_I_can_up + D_I_vt_lef +
D_I_vt_rig;
D_I_AIRPLANE_MAX = D_I_max_W_low + D_I_max_W_up + D_I_can_low + D_I_can_up +
D_I_vt_lef + D_I_vt_rig;

EXC_T = T_Fli_lev - D_AIRPLANE;
EXC_T_max = T_Fli_lev - D_AIRPLANE_MAX;

if (main_menu == 1 | main_menu == 2)
fprintf ('Drag Generated by the Complete Airplane [N]: %g', D_AIRPLANE);
fprintf ('\n');
fprintf ('Induced Drag Generated by the Complete Airplane [N]: %g',
D_I_AIRPLANE);
fprintf ('\n');
end
if (length(L_AIRPLANE) == 1 & main_menu == 1 | main_menu == 2 | main_menu ==
3)
    fprintf ('Flight Excess of Thrust [N]: %g', EXC_T);
    fprintf ('\n\n');
end
if (main_menu == 1 | main_menu == 2)
fprintf ('Maximum Drag (Stall condition) Generated by the Complete Airplane
[N]: %g', D_AIRPLANE_MAX);
fprintf ('\n\n');
fprintf ('Maximum Induced Drag (Stall condition) Generated by the Complete
Airplane [N]: %g', D_I_AIRPLANE_MAX);
fprintf ('\n');
end
if (length(L_AIRPLANE) == 1 & main_menu == 1 | main_menu == 2 | main_menu ==
3)
    fprintf ('Flight Maximum Excess of Thrust [N]: %g', EXC_T_max);
end
fprintf ('\n\n');
%end

%¨¨Pitch Moment¨¨
```

```
    % Developed under Longitudinal Static Stability section

%¨¨AIRPLANE DRAG POLAR¨¨
CL_W = CL_W_low*(S_aero_W_low/S_aero_W) + CL_W_up*(S_aero_W_up/S_aero_W);
CL_CAN = CL_can_low*(S_aero_can_low/S_aero_W) +
CL_can_up*(S_aero_can_up/S_aero_W);
CL_VT = CL_vt_lef*(S_vt_lef/S_aero_W) + CL_vt_rig*(S_vt_rig/S_aero_W);
CL_FUSEL = CL_FUS*(S_xy_fus/S_aero_W);

CL_AIRPLANE = CL_FUSEL + CL_W + CL_CAN + CL_VT + CL_PROP;

CD_W = CD_W_low*(S_aero_W_low/S_aero_W) + CD_W_up*(S_aero_W_up/S_aero_W);
CD_CAN = CD_can_low*(S_aero_can_low/S_aero_W) +
CD_can_up*(S_aero_can_up/S_aero_W);
CD_FAIR_CAN = CD_FairBoo*(S_lef_fairing/S_aero_W) +
CD_FairBoo*(S_rig_fairing/S_aero_W);
CD_VT = CD_vt_lef*(S_vt_lef/S_aero_W) + CD_vt_rig*(S_vt_rig/S_aero_W);
CD_VT_BOOM = CD_Boo*((S_low_boom_lef + S_up_boom_lef)/S_aero_W) +
CD_Boo*((S_low_boom_rig + S_up_boom_rig)/S_aero_W);
CD_LGEAR = CD_LDG*(S_lef_main_gear/S_aero_W) +
CD_LDG*(S_rig_main_gear/S_aero_W) + CD_LDG*(S_nose_gear/S_aero_W);

CD_AIRPLANE = CD_FUS + CD_W + CD_CAN + CD_FAIR_CAN + CD_VT + CD_VT_BOOM +
CD_LGEAR + CD_prop; % Airplane Drag Polar

if (main_menu == 1 | main_menu == 2 & length(Alpha) == 1)
fprintf ('Airplane Lift Coefficient: %g', CL_AIRPLANE);
fprintf ('\n');
fprintf ('Airplane Drag Coefficient: %g', CD_AIRPLANE);
fprintf ('\n\n');
end

    %*Airplane Lift Coefficient Solpe - CL_alpha*
    if (length(Alpha) > 1)
        N = length(Alpha);
        CL_2 = CL_AIRPLANE(N);
        CL_1 = CL_AIRPLANE(1);
        alpha_2 = Alpha(N);
        alpha_1 = Alpha(1);
        CL_ALPH_AIRPLANE = (CL_2 - CL_1)/(alpha_2 - alpha_1)
    end

    if (length(Alpha) == 1)

        if (main_menu == 1 | main_menu == 3 | main_menu == 4)

            CL_ALPH_AIRPLANE = input ('Estimated CL_ALPH_AIRPLANE: ' );

        end
    end

    %*Plots*
    if (main_menu == 1 | main_menu == 2)
```

```
    figure (2)
    plot (CL_AIRPLANE,CD_AIRPLANE)
    title ('DRAG POLAR OF THE AIRPLANE UFU-1');
    xlabel ('CL');
    ylabel ('CD');
    hold on

    figure (3)
    plot (Alpha,CL_AIRPLANE)
    title ('AIRPLANE LIFT COEFFICIENT SLOPE');
    xlabel ('ALPHA [°]');
    ylabel ('CL');
    hold on

    figure (4)
    plot (Alpha,CD_AIRPLANE)
    title ('AIRPLANE DRAG COEFFICIENT SLOPE');
    xlabel ('ALPHA [°]');
    ylabel ('CD');
    hold on
    end
%¨¨¨¨¨¨¨¨¨¨¨¨¨¨¨¨¨¨¨¨¨¨¨¨¨¨¨¨¨¨¨¨¨¨¨¨¨¨¨¨¨¨¨¨¨¨¨¨¨¨¨¨¨¨¨¨¨¨¨¨¨¨¨¨¨¨¨¨¨¨¨¨¨¨¨
fprintf ('---------------------------------------------------------------
----------------------------\n\n');
%___________________________________________________________________________

if (main_menu == 1 | main_menu == 3 | main_menu == 4)
%___________________________DYNAMICS OF FLIGHT ____________________________
fprintf ('_______________________________________DYNAMICS OF
FLIGHT_______________________________________\n\n');

%¨¨¨¨¨¨¨¨¨¨¨¨¨¨¨¨LONGITUDINAL STATIC STABILITY & CONTROL¨¨¨¨¨¨¨¨¨¨¨¨¨¨¨¨¨¨¨
fprintf ('--------------------------------LONGITUDINAL STATIC STABILITY &
CONTROL-------------------------\n\n');

fprintf ('Longitudinal Static Stability');
fprintf ('\n\n');

%¨¨CANARD CONTRIBUTION¨¨

    %*Lower Canard*
    l_can_low = X_AC_CAN_LOW - X_CG; % [m] Lower Canard Arm
    V_can_low = (l_can_low*S_aero_can_low)/(mac_W*S_aero_W); % Lower Canard
Volume Coefficient (Negative) (RAYMER Chapter 6)

    if (main_menu == 1 | main_menu == 3)
    fprintf ('Lower Canard Volume Coefficient: %g', V_can_low);
    fprintf ('\n\n');
    end

    Eta_can_low = 0.9; % Efficiency factor (Nelson; page:47 - 48)
    Epslon_zer_can_up = (2*CL_alph_zer_can_up)/(pi*AR_can_up); % [rad] Upwash
angle for Upper canard alpha zero
```

```
    Epslon_zer_W_low = (2*CL_alph_zer_W_low)/(pi*AR_W_low); % [rad] Upwash
angle for Lower wing alpha zero
    dEps_dAlp_can_low = dEps_dAlp_can_low_1 + dEps_dAlp_can_low_2;

    CM_zer_can_low = CM_can_low - Eta_can_low*V_can_low*(CL_alph_can_low_rad +
Delt_CL_alp_can_low_rad)*(Epslon_zer_W_low + Epslon_zer_can_up +
i_can_low_rad);
    CM_alph_can_low_rad = -Eta_can_low*V_can_low*(CL_alph_can_low_rad +
Delt_CL_alp_can_low_rad)*(1 + dEps_dAlp_can_low); % [1/rad]
    CM_alph_can_low = CM_alph_can_low_rad/57.29579; % [1/°]

    CM_CAN_LOW = CM_alph_can_low*Alpha;
    CM_CG_CAN_LOW = CM_zer_can_low + CM_CAN_LOW;

    if (main_menu == 1 | main_menu == 3)
    fprintf ('CM_zer_can_low: %g', CM_zer_can_low);
    fprintf ('\n');
    fprintf ('CM_alph_can_low [1/°]: %g', CM_alph_can_low);
    fprintf ('\n\n');
    fprintf ('CM_alph_can_low [1/rad]: %g', CM_alph_can_low_rad);
    fprintf ('\n\n');
    end

    %*Upper Canard*
    l_can_up = X_AC_CAN_UP - X_CG; % [m] Upper Canard Arm
    V_can_up = (l_can_up*S_aero_can_up)/(mac_W*S_aero_W); % Upper Canard
Volume Coefficient (Negative)

    if (main_menu == 1 | main_menu == 3)
    fprintf ('Upper Canard Volume Coefficient: %g', V_can_up);
    fprintf ('\n\n');
    end

    Eta_can_up = 0.8; % Efficiency factor (Nelson; page:47 - 48)
    Epslon_zer_can_low = (2*CL_alph_zer_can_low)/(pi*AR_can_low); % [rad]
Downwash angle for Lower canard alpha zero
    dEps_dAlp_can_up = dEps_dAlp_can_up_2 - dEps_dAlp_can_up_1; % (Lower Wing
Upwash - Lower Canard Downwash)

    CM_zer_can_up = CM_can_up - Eta_can_up*V_can_up*(CL_alph_can_up_rad +
Delt_CL_alp_can_up_rad)*(Epslon_zer_W_low - i_can_low_rad - Epslon_zer_can_low
+ i_can_up_rad);
    CM_alph_can_up_rad = -Eta_can_up*V_can_up*(CL_alph_can_up_rad +
Delt_CL_alp_can_up_rad)*(1 + dEps_dAlp_can_up); % [1/rad]
    CM_alph_can_up = CM_alph_can_up_rad/57.29579; % [1/°]

    CM_CAN_UP = CM_alph_can_up*Alpha;
    CM_CG_CAN_UP = CM_zer_can_up + CM_CAN_UP;

    if (main_menu == 1 | main_menu == 3)
    fprintf ('CM_zer_can_up: %g', CM_zer_can_up);
    fprintf ('\n');
    fprintf ('CM_alph_can_up [1/°]: %g', CM_alph_can_up);
    fprintf ('\n\n');
```

```
    fprintf ('CM_alph_can_up [1/rad]: %g', CM_alph_can_up_rad);
    fprintf ('\n\n');
    end

    %Total Canard*
    V_can = V_can_low + V_can_up;

    if (main_menu == 1 | main_menu == 3)
    fprintf ('Total Canard Volume Coefficient: %g', V_can);
    fprintf ('\n\n');
    end

%¨¨WING CONTRIBUTION¨¨

    %*Lower Wing*
    h_ac_W_low = 0.25 + (DELT_X_AC_W_LOW/mac_W_low); % Lower wing AC position
relative to the leading edge of it's own mac
    h_W_low = (X_CG - X_LE_mac_W_low)/mac_W_low; % CG position regarding Lower
wing LE in % of mac

    CM_zer_W_low = CM_W_low + CL_alph_zer_W_low*(h_W_low - h_ac_W_low);
    CM_alph_W_low = (h_W_low - h_ac_W_low)*CL_alf_W_low; % [1/°]
    CM_alph_W_low_rad = CM_alph_W_low*57.29579; % [1/rad]

    Epslon_zer_W_up = (2*CL_alph_zer_W_up)/(pi*AR_W_up); % [rad] Upwash angle
for Upper wing alpha zero
    CM_W_LOW = CM_alph_W_low*Alpha;
    CM_CG_W_LOW = CM_zer_W_low + CM_W_LOW;

    if (main_menu == 1 | main_menu == 3)
    fprintf ('CM_zer_W_low: %g', CM_zer_W_low);
    fprintf ('\n');
    fprintf ('CM_alph_W_low [1/°]: %g', CM_alph_W_low);
    fprintf ('\n\n');
    fprintf ('CM_alph_W_low [1/rad]: %g', CM_alph_W_low_rad);
    fprintf ('\n\n');
    end

    %*Upper Wing*
    h_ac_W_up = 0.25 + (DELT_X_AC_W_UP/mac_W_up); % Upper wing AC position
regarding itself
    h_W_up = (X_CG - X_LE_mac_W_up)/mac_W_up; % CG position regarding Upper
wing LE in % of mac

    CM_zer_W_up = CM_W_up + CL_alph_zer_W_up*(h_W_up - h_ac_W_up);
    CM_alph_W_up = (h_W_up - h_ac_W_up)*CL_alf_W_up; % [1/°]
    CM_alph_W_up_rad = CM_alph_W_up*57.29579; % [1/rad]

    CM_W_UP = CM_alph_W_up*Alpha;
    CM_CG_W_UP = CM_zer_W_up + CM_W_UP;

    if (main_menu == 1 | main_menu == 3)
    fprintf ('CM_zer_W_up: %g', CM_zer_W_up);
```

```
    fprintf ('\n');
    fprintf ('CM_alph_W_up [1/°]: %g', CM_alph_W_up);
    fprintf ('\n\n');
    fprintf ('CM_alph_W_up [1/rad]: %g', CM_alph_W_up_rad);
    fprintf ('\n\n');
    end

%¨¨FUSELAGE CONTRIBUTION¨¨
%L_d = x_L/d_fus;
K2_K1 = 0.825; % from Nelson page 53 - 54
Alph_W_zer = Alf_Cl_zer_W_low; % [°]

    %*CM_zero*
    i_fus_1 = -9.476; % [°] from CAD drawing
    Sum_fus_zer_1 = (W_f_W_low_1^2)*(Alph_W_zer + i_fus_1)*Delt_x_W_low_1; %
From Nelsom page 60

    i_fus_2 = -9.629; % [°] from CAD drawing
    Sum_fus_zer_2 = (W_f_W_low_2^2)*(Alph_W_zer + i_fus_2)*Delt_x_W_low_2;

    i_fus_3 = -9.77; % [°] from CAD drawing
    Sum_fus_zer_3 = (W_f_W_low_3^2)*(Alph_W_zer + i_fus_3)*Delt_x_W_low_3;

    i_fus_4 = -9.971; % [°] from CAD drawing
    Sum_fus_zer_4 = (W_f_W_low_4^2)*(Alph_W_zer + i_fus_4)*Delt_x_W_low_4;

    i_fus_5 = -9.971; % [°] from CAD drawing
    Sum_fus_zer_5 = (W_f_W_low_5^2)*(Alph_W_zer + i_fus_5)*Delt_x_W_low_5;

    i_fus_6 = -9.496; % [°] from CAD drawing
    Sum_fus_zer_6 = (W_f_W_low_6^2)*(Alph_W_zer + i_fus_6)*Delt_x_W_low_6;

    i_fus_7 = -9.079; % [°] from CAD drawing
    Sum_fus_zer_7 = (W_f_W_low_7^2)*(Alph_W_zer + i_fus_7)*Delt_x_W_low_7;

    i_fus_8 = -8.403; % [°] from CAD drawing
    Sum_fus_zer_8 = (W_f_W_low_8^2)*(Alph_W_zer + i_fus_8)*Delt_x_W_low_8;

    i_fus_9 = -7.724; % [°] from CAD drawing
    Sum_fus_zer_9 = (W_f_W_low_9^2)*(Alph_W_zer + i_fus_9)*Delt_x_W_low_9;

    i_fus_10 = -7.421; % [°] from CAD drawing
    Sum_fus_zer_10 = (W_f_W_low_10^2)*(Alph_W_zer + i_fus_10)*Delt_x_W_low_10;

    i_fus_11 = 0; % [°] from CAD drawing
    Delt_x_W_low_11 = 0.91*3.28083; % [ft]
    W_f_W_low_11 = 0.918*3.28083; % [ft]
    Sum_fus_zer_11 = (W_f_W_low_11^2)*(Alph_W_zer + i_fus_11)*Delt_x_W_low_11;

    i_fus_12 = 2.863; % [°] from CAD drawing
    Sum_fus_zer_12 = (W_f_W_low_12^2)*(Alph_W_zer + i_fus_12)*Delt_x_W_low_12;

    i_fus_13 = 0.944; % [°] from CAD drawing
```

```
    Sum_fus_zer_13 = (W_f_W_low_13^2)*(Alph_W_zer + i_fus_13)*Delt_x_W_low_13;

    i_fus_14 = 0; % [°] from CAD drawing
    Sum_fus_zer_14 = (W_f_W_low_14^2)*(Alph_W_zer + i_fus_14)*Delt_x_W_low_14;

    i_fus_15 = 0.346; % [°] from CAD drawing
    Sum_fus_zer_15 = (W_f_W_low_15^2)*(Alph_W_zer + i_fus_15)*Delt_x_W_low_15;

    i_fus_16 = 1.15; % [°] from CAD drawing
    Sum_fus_zer_16 = (W_f_W_low_16^2)*(Alph_W_zer + i_fus_16)*Delt_x_W_low_16;

    Sum_fus_zero =
Sum_fus_zer_1+Sum_fus_zer_2+Sum_fus_zer_3+Sum_fus_zer_4+Sum_fus_zer_5+Sum_fus_
zer_6+Sum_fus_zer_7+Sum_fus_zer_8+Sum_fus_zer_9+Sum_fus_zer_10+Sum_fus_zer_11+
Sum_fus_zer_12+Sum_fus_zer_13+Sum_fus_zer_14+Sum_fus_zer_15+Sum_fus_zer_16;

    %*CM_alpha*
    Sum_fus_alph_1 = (W_f_W_low_1^2)*dEps_dAlp_W_low_1*Delt_x_W_low_1;
    Sum_fus_alph_2 = (W_f_W_low_2^2)*dEps_dAlp_W_low_2*Delt_x_W_low_2;
    Sum_fus_alph_3 = (W_f_W_low_3^2)*dEps_dAlp_W_low_3*Delt_x_W_low_3;
    Sum_fus_alph_4 = (W_f_W_low_4^2)*dEps_dAlp_W_low_4*Delt_x_W_low_4;
    Sum_fus_alph_5 = (W_f_W_low_5^2)*dEps_dAlp_W_low_5*Delt_x_W_low_5;
    Sum_fus_alph_6 = (W_f_W_low_6^2)*dEps_dAlp_W_low_6*Delt_x_W_low_6;
    Sum_fus_alph_7 = (W_f_W_low_7^2)*dEps_dAlp_W_low_7*Delt_x_W_low_7;
    Sum_fus_alph_8 = (W_f_W_low_8^2)*dEps_dAlp_W_low_8*Delt_x_W_low_8;
    Sum_fus_alph_9 = (W_f_W_low_9^2)*dEps_dAlp_W_low_9*Delt_x_W_low_9;
    Sum_fus_alph_10 = (W_f_W_low_10^2)*dEps_dAlp_W_low_10*Delt_x_W_low_10;
    Sum_fus_alph_11 = (W_f_W_low_11^2)*dEps_dAlp_W_low_11*Delt_x_W_low_11;
    Sum_fus_alph_12 = (W_f_W_low_12^2)*dEps_dAlp_W_low_12*Delt_x_W_low_12;
    Sum_fus_alph_13 = (W_f_W_low_13^2)*dEps_dAlp_W_low_13*Delt_x_W_low_13;
    Sum_fus_alph_14 = (W_f_W_low_14^2)*dEps_dAlp_W_low_14*Delt_x_W_low_14;
    Sum_fus_alph_15 = (W_f_W_low_15^2)*dEps_dAlp_W_low_15*Delt_x_W_low_15;
    Sum_fus_alph_16 = (W_f_W_low_16^2)*dEps_dAlp_W_low_16*Delt_x_W_low_16;

    Sum_fus_alph =
Sum_fus_alph_1+Sum_fus_alph_2+Sum_fus_alph_3+Sum_fus_alph_4+Sum_fus_alph_5+Sum
_fus_alph_6+Sum_fus_alph_7+Sum_fus_alph_8+Sum_fus_alph_9+Sum_fus_alph_10+Sum_f
us_alph_11+Sum_fus_alph_12+Sum_fus_alph_13+Sum_fus_alph_14+Sum_fus_alph_15+Sum
_fus_alph_16;

CM_zer_fus = (K2_K1/(36.5*(S_aero_W*10.76391)*(mac_W*3.28083)))*Sum_fus_zero;
CM_alph_fus = (1/(36.5*(S_aero_W*10.76391)*(mac_W*3.28083)))*Sum_fus_alph; %
[1/°]
CM_alph_fus_rad = CM_alph_fus*57.29579; % [1/rad]

CM_CG_FUS = CM_zer_fus + CM_alph_fus*Alpha;

if (main_menu == 1 | main_menu == 3)
fprintf ('CM_zer_fus: %g', CM_zer_fus);
fprintf ('\n');
fprintf ('CM_alph_fus [1/°]: %g', CM_alph_fus);
fprintf ('\n\n');
fprintf ('CM_alph_fus [1/rad]: %g', CM_alph_fus_rad);
fprintf ('\n\n');
```

```
end

%¨¨COMPLETE AIRPLANE¨¨
CM_ZER = CM_zer_can_low + CM_zer_can_up + CM_zer_W_low + CM_zer_W_up +
CM_zer_fus;
CM_ALPHA_RAD = (CM_alph_can_low + CM_alph_can_up + CM_alph_W_low +
CM_alph_W_up + CM_alph_fus)*57.29579; % [1/rad]
CM_ALPHA = CM_ALPHA_RAD/57.29579; % [1/°]
CM_CG_AIRPLANE = CM_ZER + CM_ALPHA*Alpha;

if (main_menu == 1 | main_menu == 3)
fprintf ('CM_ZER_AIRPLANE: %g', CM_ZER);
fprintf ('\n');
fprintf ('CM_ALPHA_AIRPLANE [1/°]: %g', CM_ALPHA);
fprintf ('\n\n');
fprintf ('CM_ALPHA_AIRPLANE [1/rad]: %g', CM_ALPHA_RAD);
fprintf ('\n\n');

    %*Plots*
    figure (5)
    plot
(Alpha,CM_CG_CAN_LOW,Alpha,CM_CG_CAN_UP,Alpha,CM_CG_W_LOW,Alpha,CM_CG_W_UP,Alp
ha,CM_CG_FUS,Alpha,CM_CG_AIRPLANE)
    grid on;
    title ('LONGITUDINAL STATIC STABILITY (PITCHING MOMENT SLOPE)');
    xlabel ('ALPHA [°]');
    ylabel ('CM-CG');
    legend ('LOWER CANARD','UPPER CANARD','LOWER WING','UPPER
WING','FUSELAGE','COMPLETE AIRPLANE');
    hold on
end

%¨¨STICK FIXED NEUTRAL POINT & STATIC MARGIN¨¨
x_n_W = (X_AC_AP - X_LE_mac_W)/mac_W; % Equivalent Wing Contribution for the
Neutral point
x_n_fus = -CM_alph_fus/CL_alph_W; % Fuselage Contribution for the Neutral
point

x_n_can_low = Eta_can_low*V_can_low*(CL_alph_can_low/CL_alph_W)*(1 +
dEps_dAlp_can_low); % Lower Canard Contribution
x_n_can_up = Eta_can_up*V_can_up*(CL_alph_can_up/CL_alph_W)*(1 +
dEps_dAlp_can_up); % Lower Canard Contribution

X_NP = (x_n_W + x_n_fus + x_n_can_low + x_n_can_up);
X_NP_perc = (x_n_W + x_n_fus + x_n_can_low + x_n_can_up)*100;

K_STAT = X_NP - ((X_CG - X_LE_mac_W)/mac_W);

if (main_menu == 1 | main_menu == 3)
fprintf ('Position of the Neutral Point (X_NP) for the Equivalent Wing MAC
[Percent]: %g', X_NP_perc);
fprintf ('\n');
fprintf ('Static Margin for the Airplane: %g', K_STAT);
fprintf ('\n\n');
```

```
fprintf ('¨¨¨¨¨¨¨¨¨¨¨¨¨\n\n');
end

%¨¨LONGITUDINAL CONTROL¨¨
fprintf ('Longitudinal Control');
fprintf ('\n\n');

    %*Control Derivatives*
    fprintf ('Pitching Derivative');
    fprintf ('\n\n');

    tao_elevator = tao_elev_can_low; % from graphic

    Cm_delt_E_rad = -
CL_alph_can_low_rad*Eta_can_low*V_can_low*(b_elv_low/b_can_low)*tao_elevator;
% [1/rad] aircraft pitching moment rate coefficient due to lower canard
elevator deflection derivative
    Cm_delt_E = Cm_delt_E_rad/57.29579; % [1/°]

    CL_delt_E_rad =
CL_alph_can_low_rad*Eta_can_low*(S_aero_can_low/S_aero_W)*(b_elv_low/b_can_low
)*tao_elevator; % [1/rad] aircraft Lift rate coefficient due to lower canard
elevator deflection derivative
    CL_delt_E = CL_delt_E_rad/57.29579; % [1/°]

    if (main_menu == 1 | main_menu == 3)
    fprintf ('Cm_delt_Elev [1/°]: %g', Cm_delt_E);
    fprintf ('\n');
    fprintf ('CL_delt_Elev [1/°]: %g', CL_delt_E);
    fprintf ('\n\n');
    fprintf ('¨¨¨¨¨¨¨¨¨¨¨¨¨\n\n');
    end

    %*Longitudinal Trim*
    fprintf ('Longitudinal Trim');
    fprintf ('\n\n');

    Z_T = Z_CG - Z_Thrust;
    Aux_elev_1 = (T_Fli_lev*Z_T/(q*S_aero_W*mac_W)) + CM_ZER;
    Aux_elev_2 = (CL_alf_W_low + CL_alf_W_up)/2; % CL_alph for Equivalent Wing
    Aux_elev_3 = Aux_elev_1*Aux_elev_2 + (Aux_elev_2*Alpha +
CL_delt_E*Delt_elev)*CM_ALPHA;
    Aux_elev_4 = Aux_elev_2*Cm_delt_E - CM_ALPHA*CL_delt_E;
    Aux_elev_5 = Aux_elev_1*CL_delt_E + (Aux_elev_2*Alpha +
CL_delt_E*Delt_elev)*Cm_delt_E;

    Delt_elev_trim = Aux_elev_3/Aux_elev_4; % [°] for Equivalent Elevator
    Delt_elev_low_trim = Delt_elev_trim/2; % [°]
    Delt_elev_up_trim = Delt_elev_trim/2; % [°]

    Alph_trim = Aux_elev_5/Aux_elev_4;

    if (main_menu == 1 | main_menu == 3)
```

```
        if (length(Alpha) == 1)
            fprintf ('Lower Elevator Trim Deflection [°]: %g',
Delt_elev_low_trim);
            fprintf ('\n');
            fprintf ('Upper Elevator Trim Deflection [°]: %g',
Delt_elev_up_trim);
            fprintf ('\n');
            fprintf ('Airplane Alpha Trim [°]: %g', Alph_trim);
            fprintf ('\n\n');
        end
    end

    %*TakeOff Rotation Moment*
    M_FUS = 0.5*RHO*CM_CG_FUS*S_xy_fus*(V_T.^2)*x_L;
    M_W_low = 0.5*RHO*CM_CG_W_LOW*S_aero_W_low*(V_T.^2)*mac_W_low;
    M_W_up = 0.5*RHO*CM_CG_W_UP*S_aero_W_up*(V_T.^2)*mac_W_up;
    M_can_low = 0.5*RHO*CM_CG_CAN_LOW*S_aero_can_low*(V_T.^2)*mac_can_low;
    M_can_up = 0.5*RHO*CM_CG_CAN_UP*S_aero_can_up*(V_T.^2)*mac_can_up;
    M_AIRPLANE = M_FUS + M_W_low + M_W_up + M_can_low + M_can_up + M_LDG_lef +
M_LDG_rig + M_LDG_nose;

    M_Rot_can_low = L_can_low*(X_lef_main_gear - X_AC_CAN_LOW) +
D_can_low*Z_can_low; % [N*m] Lower Canard moment on Main gear
    M_Rot_can_up = L_can_up*(X_lef_main_gear - X_AC_CAN_UP) +
D_can_up*Z_can_up; % [N*m] Upper Canard moment on Main gear
    M_Rot_W_low = L_W_low*(X_lef_main_gear - X_AC_W_LOW) + D_W_low*Z_W_low; %
[N*m] Lower Wing moment on Main gear
    M_Rot_W_up = L_W_up*(X_lef_main_gear - X_AC_W_UP) + D_W_up*Z_W_up; % [N*m]
Upper Wing moment on Main gear
    M_Rot_vt_lef = D_vt_lef*Z_mac_vt_lef; % [N*m] Left Vertical Tail moment on
Main gear
    M_Rot_vt_rig = D_vt_rig*Z_mac_vt_rig; % [N*m] Right Vertical Tail moment
on Main gear
    M_Rot_Fus = D_FUS*Z_fus; % [N*m]
    M_rot_T = -T_Fli_lev*Z_Thrust; % [N*m] Thrust moment on Main gear
    M_WEIG = W*(X_CG - X_lef_main_gear); % [N*m] Weight moment on Main gear

    M_rot_airp = M_Rot_can_low + M_Rot_can_up + M_Rot_W_low + M_Rot_W_up +
M_Rot_vt_lef + M_Rot_vt_rig + M_Rot_Fus + M_rot_T; % [N*m]
    M_Rot = M_AIRPLANE + M_rot_airp + M_WEIG;

    d_cg_mg = sqrt((X_lef_main_gear - X_CG)^2 + Z_CG^2); % [m] distance
between aircraft cg and main gear contact point
    I_yy_mg = I_yy + m*(d_cg_mg^2);
    Teta_dot_dot_Rot_rad = M_Rot/I_yy_mg; % [rad/s^2]
    Teta_dot_dot_Rot = Teta_dot_dot_Rot_rad*(180/pi); % [°/s^2]

    if (main_menu == 1 | main_menu == 3)
    fprintf ('Airplane Takeoff Rotation Moment [N*m]: %g', M_Rot);
    fprintf ('\n');
    fprintf ('Airplane Takeoff Angular Aceleration [°/s^2]: %g',
Teta_dot_dot_Rot);
    fprintf ('\n\n');
```

```
    figure (6)
    plot (Alpha,M_Rot)
    grid on;
    title ('TAKE-OFF ROTATION MOMENT');
    xlabel ('ALPHA [°]');
    ylabel ('ROTATION MOMENT [N*m]');
    hold on
    end

    %*In Flight Pitch Moment*
    M_CG_can_low = L_can_low*(X_CG - X_AC_CAN_LOW) + D_can_low*(Z_can_low -
Z_CG) + M_can_low; % [N*m] Lower Canard moment on CG
    M_CG_can_up = L_can_up*(X_CG - X_AC_CAN_UP) + D_can_up*(Z_can_up - Z_CG) +
M_can_up; % [N*m] Upper Canard moment on CG
    M_CG_vt_lef = D_vt_lef*(Z_mac_vt_lef - Z_CG); % [N*m] Left Vertical Tail
moment on CG
    M_CG_vt_rig = D_vt_rig*(Z_mac_vt_rig - Z_CG); % [N*m] Right Vertical Tail
moment on CG
    M_CG_W_low = L_W_low*(X_CG - X_AC_W_LOW) + D_W_low*(Z_W_low - Z_CG) +
M_W_low; % [N*m] Lower Wing moment on CG
    M_CG_W_up = L_W_up*(X_CG - X_AC_W_UP) + D_W_up*(Z_W_up - Z_CG) + M_W_up; %
[N*m] Upper Wing moment on CG
    M_CG_Fus = D_FUS*(Z_fus - Z_CG) + M_FUS; % [N*m] Fuselage moment on CG
    M_T = T_Fli_lev*Z_T; % [N*m] Thrust moment on CG

    M_PIT = M_CG_can_low + M_CG_can_up + M_CG_vt_lef + M_CG_vt_rig +
M_CG_W_low + M_CG_W_up + M_CG_Fus + M_T;

    Teta_dot_dot_rad = M_PIT/I_yy; % [rad/s^2]
    Teta_dot_dot = Teta_dot_dot_rad*(180/pi); % [°/s^2]

    if (main_menu == 1 | main_menu == 3)
    fprintf ('Airplane In Flight Pitch Rotation Moment [N*m]: %g', M_PIT);
    fprintf ('\n');
    fprintf ('Airplane In Flight Pitch Angular Aceleration [°/s^2]: %g',
Teta_dot_dot);
    fprintf ('\n\n');
    end

fprintf ('-------------------------------------------------------------------
--------------------------\n\n');
%.....................................................................................

%.....................LATERAL STATIC STABILITY & CONTROL.....................
fprintf ('----------------------------------LATERAL STATIC STABILITY &
CONTROL--------------------------\n\n');

fprintf ('Lateral Static Stability');
fprintf ('\n\n');

Cl_beta_Tao = -0.00026; % Estimated from graph 3.11 [Nelson; pg122]
Delt_Cl_beta = 0; % Estimated from [Nelson; pg122]

Cl_beta = Cl_beta_Tao*Tao_W + Delt_Cl_beta; % [1/°]
```

```
Cl_beta_rad = Cl_beta*57.29579; % [1/rad]
Cl_stab = Cl_beta*Beta;

if (main_menu == 1 | main_menu == 3)
fprintf ('Cl_beta [1/°]: %g', Cl_beta);
fprintf ('\n');
fprintf ('Cl: %g', Cl_stab);
fprintf ('\n\n');
end

%¨¨LATERAL CONTROL¨¨
fprintf ('Lateral Control');
fprintf ('\n\n');

y_A = b_ail_i; % [m] Location of the aileron AC on y axis
y_A_o = y_A + (b_ail/2); % [m] Location of the aileron out chord on y axis
y_D = 0.4*b_W; % [m] Assumed as on the theory
CD_R = 1.2; % Assumed

Delt_L_ail_lef = 0.5*RHO*Delt_CL_ail_lef*S_aero_W_up*(V_T.^2); % [N] Increment
of lift on Upper Wing due the left aileron deflection
Delt_L_max_ail_lef = Delt_L_ail_lef; % [N] Maximum Increment of lift (stall
condition) on Upper Wing due the left aileron deflection

Delt_L_ail_rig = 0.5*RHO*Delt_CL_ail_rig*S_aero_W_up*(V_T.^2); % [N] Increment
of lift on Upper Wing due the right aileron deflection
Delt_L_max_ail_rig = Delt_L_ail_rig; % [N] Maximum Increment of lift (stall
condition) on Upper Wing due the right aileron deflection

L_A = y_A*(abs(Delt_L_ail_lef) + abs(Delt_L_ail_rig)); % [N*m] Rolling moment
due the ailerons deflection
L_A_max = y_A*(abs(Delt_L_max_ail_lef) + abs(Delt_L_max_ail_rig)); % [N*m]
Stall condition Rolling moment due the ailerons deflection

P_dot = L_A/I_xx; % [rad/s^2] Temporal Rate of rolling rate
P_ss_rad = sqrt((2*L_A)/(RHO*(S_aero_W + S_aero_CAN + S_vt_lef +
S_vt_rig)*CD_R*(y_D^3))); % [rad/s] Constant roll rate
P_ss = P_ss_rad*(180/pi); % [°/s]
P_rad = sqrt(2*P_dot*(Phi_rad)); % [rad/s] Instantaneous roll rate
P = P_rad*(180/pi); % [°/s]

P_dot_rad_max = L_A_max/I_xx; % [rad/s^2]
P_ss_rad_max = sqrt((2*L_A_max)/(RHO*(S_aero_W + S_aero_CAN + S_vt_lef +
S_vt_rig)*CD_R*(y_D^3))); % [rad/s]
P_ss_max = P_ss_rad_max*(180/pi); % [°/s]
P_rad_max = sqrt(2*P_dot_rad_max*(Phi_rad)); % [rad/s]
P_max = P_rad_max*(180/pi); % [°/s]

if (main_menu == 1 | main_menu == 3)
fprintf ('Constant Roll Rate - P_ss [°/s]: %g', P_ss);
fprintf ('\n');
fprintf ('Instantaneous Roll Rate - P [°/s]: %g', P);
fprintf ('\n\n');
fprintf ('Constant Max Roll Rate - P_ss [°/s]: %g', P_ss_max);
```

```
fprintf ('\n');
fprintf ('Instantaneous Max Roll Rate - P [°/s]: %g', P_max);
fprintf ('\n\n');
end

    %*Rolling Moment Derivative*
    fprintf ('Rolling Moment Derivative');
    fprintf ('\n\n');

    Delt_ail = (abs(Delt_ail_lef) + abs(Delt_ail_rig))/2;
    Delt_ail_rad = Delt_ail*(pi/180); % [rad]
    C_A_C_r = C_ail/C_r
    CL_alph_W_rad = CL_alph_W*57.29579; % [1/rad] for Equivalent Wing

    Cl_delt_A_rad =
((2*CL_alph_W_rad*tao_aileron*C_r)/(S_aero_W*b_W))*(((y_A_o/2) + 2/3*((Lamb_W-
1)/b_W)*y_A_o^3) - ((y_A/2) + 2/3*((Lamb_W-1)/2)*y_A^3)); % [1/rad] aircraft
rolling moment rate coefficient due to aileron deflection derivative
    Cl_delt_A = Cl_delt_A_rad/57.29579; % [1/°]

    Cl_p = -(CL_ALPH_AIRPLANE/12)*((1 + 3*Lamb_W)/(1 + Lamb_W)); % [1/°]
    Cl_p_rad = Cl_p*57.29579; % [1/rad]

    if (main_menu == 1 | main_menu == 3)
    fprintf ('Cl_delt_Ail [1/°]: %g', Cl_delt_A);
    fprintf ('\n');
    fprintf ('Cl_p [1/°]: %g', Cl_p);
    fprintf ('\n\n');
    end

fprintf ('-------------------------------------------------------------------
--------------------------\n\n');
%……….……….……….……….……….……….……….……….……….……….……….……….……….……….……….……

%¨¨¨¨¨¨¨¨¨¨¨¨¨¨¨¨¨¨¨¨DIRECTIONAL STATIC STABILITY & CONTROL¨¨¨¨¨¨¨¨¨¨¨¨¨¨¨¨¨¨¨¨¨¨¨¨
fprintf ('---------------------------------DIRECTIONAL STATIC STABILITY &
CONTROL-------------------------\n\n');

fprintf ('Directional Static Stability');
fprintf ('\n\n');

%¨¨WING + FUSELAGE CONTRIBUTION¨¨
S_fs = 6.3; % [m^2] Projected Side Area of the Fuselage (Estimated from CAD
drawing)
h_1 = 0.804; % [m] Fuselage height for l_f/4 (Estimated from CAD drawing)
h_2 = 1.38; % [m] Fuselage height for l_f*(3/4) (Estimated from CAD drawing)

xm_lf = X_CG/x_L;
lf2_Sfs = (x_L^2)/S_fs;
sq_h1_h2 = sqrt(h_1/h_2);
h_wf = h/y_C;
```

```
K_n = ((0.00169 - 0.00185)*((X_CG - 3.743)/(3.672 - 3.743))) + 0.00185; %
Empirical Wing-Body Interference Factor; from graphic [Nelson; pg74-75]

if (main_menu == 1 | main_menu == 3)
fprintf ('Xm/lf on Grafh: %g', xm_lf);
fprintf ('\n');
fprintf ('lf^2/S_fs on Grafh: %g', lf2_Sfs);
fprintf ('\n');
fprintf ('Square Root of h1/h2 on Grafh: %g', sq_h1_h2);
fprintf ('\n');
fprintf ('h/wf on Grafh: %g', h_wf);
fprintf ('\n');
fprintf ('Empirical Wing-Body Interference Factor - K_n: %g', K_n);
fprintf ('\n\n');
end

fprintf ('Fuselage Reynolds R_lf on Graph: %g', R_lf);
fprintf ('\n\n');
K_Rl = input ('Empirical Correction Factor (K_Rl): ' ); % from graphic
[Nelson; pg74-75];

Cn_bet_w_f = -K_n*K_Rl*((S_fs*x_L)/(S_aero_W*b_W)); % [1/°] (Nelson; pg74)
Cn_bet_w_f_rad = Cn_bet_w_f*57.29579; % [1/rad]
CN_W_F = Cn_bet_w_f*Beta;

if (main_menu == 1 | main_menu == 3)
fprintf ('Cn_bet_w_f [1/°]: %g', Cn_bet_w_f);
fprintf ('\n');
fprintf ('Cn_bet_w_f [1/rad]: %g', Cn_bet_w_f_rad);
fprintf ('\n\n');
end

%¨¨VERTICAL TAIL CONTRIBUTION¨¨
Eta_vt = 1.0; % Assumed

    %*Left Vertical Tail*
    l_vt_lef = X_AC_VT_LEF - X_CG; % [m] Yaw Moment Left Vertical tail arm
    V_vt_lef = (l_vt_lef*S_vt_lef)/(b_W*S_aero_W); % Left Vertical Tail Volume
Coefficient (RAYMER Chapter 6)

    if (main_menu == 1 | main_menu == 3)
    fprintf ('Left Vertical Tail Volume Coefficient: %g', V_vt_lef);
    fprintf ('\n\n');
    end

    %*Right Vertical Tail*
    l_vt_rig = X_AC_VT_RIG - X_CG; % [m] Yaw Moment Right Vertical tail arm
    V_vt_rig = (l_vt_rig*S_vt_rig)/(b_W*S_aero_W); % Right Vertical Tail
Volume Coefficient (RAYMER Chapter 6)

    if (main_menu == 1 | main_menu == 3)
    fprintf ('Right Vertical Tail Volume Coefficient: %g', V_vt_rig);
    fprintf ('\n\n');
    end
```

```
    %Total Vertical Tail*
    V_vt_tot = V_vt_lef + V_vt_rig;

    if (main_menu == 1 | main_menu == 3)
    fprintf ('Total Vertical Tail Volume Coefficient: %g', V_vt_tot);
    fprintf ('\n\n');
    end

Cn_bet_v_lef = V_vt_lef*Eta_vt*CL_alph_vt_lef*(1 + dSig_dBet_vt_lef); % [1/°]
(Nelson; pg76)
Cn_bet_v_lef_rad = Cn_bet_v_lef*57.29579; % [1/rad]
CN_V_LEF = Cn_bet_v_lef*Beta;

Cn_bet_v_rig = V_vt_rig*Eta_vt*CL_alph_vt_rig*(1 + dSig_dBet_vt_rig); % [1/°]
Cn_bet_v_rig_rad = Cn_bet_v_rig*57.29579; % [1/rad]
CN_V_RIG = Cn_bet_v_rig*Beta;

if (main_menu == 1 | main_menu == 3)
fprintf ('Cn_bet_vt_lef [1/°]: %g', Cn_bet_v_lef);
fprintf ('\n');
fprintf ('Cn_bet_vt_lef [1/rad]: %g', Cn_bet_v_lef_rad);
fprintf ('\n\n');
fprintf ('Cn_bet_vt_rig [1/°]: %g', Cn_bet_v_rig);
fprintf ('\n');
fprintf ('Cn_bet_vt_rig [1/rad]: %g', Cn_bet_v_rig_rad);
fprintf ('\n\n');
end

%¨¨COMPLETE AIRPLANE¨¨
Cn_zero = 0; % airplane symmetric at xz plane

Cn_beta = Cn_bet_w_f + Cn_bet_v_lef + Cn_bet_v_rig;
Cn_beta_rad = Cn_beta*57.29579; % [1/rad]
CN_CG_AIRPLANE = Cn_zero + Cn_beta*Beta;

if (main_menu == 1 | main_menu == 3)
fprintf ('CN_BETA_AIRPLANE [1/°]: %g', Cn_beta);
fprintf ('\n\n');
fprintf ('CN_BETA_AIRPLANE [1/rad]: %g', Cn_beta_rad);
fprintf ('\n\n');

    %*Plots*
    figure (7)
    plot (Beta,CN_W_F,Beta,CN_V_LEF,Beta,CN_V_RIG,Beta,CN_CG_AIRPLANE)
    grid on;
    title ('DIRECTIONAL STATIC STABILITY (YAWING MOMENT SLOPE)');
    xlabel ('BETA [°]');
    ylabel ('CN-CG');
    legend ('WING + FUSELAGE','LEFT VERTICAL TAIL','RIGHT VERTICAL
TAIL','COMPLETE AIRPLANE');
    hold on
    fprintf ('¨¨¨¨¨¨¨¨¨¨¨¨\n\n');
```

```
%¨¨DIRECTIONAL CONTROL¨¨
fprintf ('Directional Control');
fprintf ('\n\n');

%*Yaw Moment due the Vertical Tail Lift*
N_A = l_vt_lef*L_vt_lef + l_vt_rig*L_vt_rig; % [N*m]
Cn_vt = N_A/(q*S_aero_W*b_W);

%*Cross Wind Force & Moment*
CD_y = 0.8; % Conservative value assumed
S_S = Sum_A_acft; % [m^2] Total Airplane Projected Side Area
d_c = X_AC_ACFT - X_CG; % [m] distance between aircraf CG and it's projected
side área CA

F_W = 0.5*RHO*CD_y*S_S*(V_wind.^2); % [N]

if (V_wind >= 0)
    N_F_W = -(F_W*d_c); % [N*m]
end

if (V_wind < 0)
    N_F_W = F_W*d_c; % [N*m]
end

N_GLOB = N_A + N_F_W; % [N*m]

if (length(Beta) == 1)
    fprintf ('Yawing Moment due the Vertical Tail and Rudder Deflection [N*m]:
%g', N_A);
    fprintf ('\n');
    fprintf ('Yawing Coefficient due the Vertical Tail and Rudder Deflection:
%g', Cn_vt);
    fprintf ('\n\n');
    fprintf ('Aerodynamic Force Generated by the Cross Wind [N]: %g', F_W);
    fprintf ('\n');
    fprintf ('Yawing Moment due the Cross Wind [N*m]: %g', N_F_W);
    fprintf ('\n\n');
    fprintf ('Global Yawing Moment (Must to be ZERO) [N*m]: %g', N_GLOB);
    fprintf ('\n\n');
end

%*Yawing Derivative*
fprintf ('Yawing Derivative');
fprintf ('\n\n');
end

    %*Yawing Y-Force Derivatives*
    K_f2 = 1.3; % Conservative value assumed

    Cy_zero = 0;

    Cy_bet_vt_lef = -K_f2*CL_alph_vt_lef*(1 -
dSig_dBet_vt_lef)*Eta_vt*(S_vt_lef/S_aero_W); % [1/°]
```

```
    Cy_bet_vt_lef_rad = Cy_bet_vt_lef*57.29579; % [1/rad]
    Cy_bet_vt_rig = -K_f2*CL_alph_vt_rig*(1 -
dSig_dBet_vt_rig)*Eta_vt*(S_vt_rig/S_aero_W); % [1/°]
    Cy_bet_vt_rig_rad = Cy_bet_vt_rig*57.29579; % [1/rad]

    Cy_delt_R_lef =
CL_alph_vt_lef*Eta_vt*tao_rud_vt_lef*(b_rud_lef/b_vt_lef)*(S_vt_lef/S_aero_W);
% [1/°]
    Cy_delt_R_lef_rad = Cy_delt_R_lef*57.29579; % [1/rad]
    Cy_delt_R_rig =
CL_alph_vt_rig*Eta_vt*tao_rud_vt_rig*(b_rud_rig/b_vt_rig)*(S_vt_rig/S_aero_W);
% [1/°]
    Cy_delt_R_rig_rad = Cy_delt_R_rig*57.29579; % [1/rad]

    Cy_r_lef = -2*(l_vt_lef/b_W)*Cy_bet_vt_lef; % [1/°]
    Cy_r_lef_rad = Cy_r_lef*57.29579; % [1/rad]
    Cy_r_rig = -2*(l_vt_rig/b_W)*Cy_bet_vt_rig; % [1/°]
    Cy_r_rig_rad = Cy_r_rig*57.29579; % [1/rad]

    if (main_menu == 1 | main_menu == 3)
    fprintf ('Cy_zero: %g', Cy_zero);
    fprintf ('\n');
    fprintf ('Cy_bet_vt_lef [1/°]: %g', Cy_bet_vt_lef);
    fprintf ('\n');
    fprintf ('Cy_bet_vt_rig [1/°]: %g', Cy_bet_vt_rig);
    fprintf ('\n');
    fprintf ('Cy_delt_Rud_lef [1/°]: %g', Cy_delt_R_lef);
    fprintf ('\n');
    fprintf ('Cy_delt_Rud_rig [1/°]: %g', Cy_delt_R_rig);
    fprintf ('\n');
    fprintf ('Cy_r_lef [1/°]: %g', Cy_r_lef);
    fprintf ('\n');
    fprintf ('Cy_r_rig [1/°]: %g', Cy_r_rig);
    fprintf ('\n\n');
    end

    %*Yawing Moment Derivatives*
    Cn_delt_R_lef_rad = -
CL_alph_vt_lef_rad*V_vt_lef*Eta_vt*tao_rud_vt_lef*(b_rud_lef/b_vt_lef); %
[1/rad]
    Cn_delt_R_lef = Cn_delt_R_lef_rad/57.29579; % [1/°]
    Cn_delt_R_rig_rad = -
CL_alph_vt_rig_rad*V_vt_rig*Eta_vt*tao_rud_vt_rig*(b_rud_rig/b_vt_rig); %
[1/rad]
    Cn_delt_R_rig = Cn_delt_R_rig_rad/57.29579; % [1/°]

    Cn_r_lef = -2*Eta_vt*V_vt_lef*(l_vt_lef/b_W)*CL_alph_vt_lef; % [1/°]
    Cn_r_lef_rad = Cn_r_lef*57.29579; % [1/rad]
    Cn_r_rig = -2*Eta_vt*V_vt_rig*(l_vt_rig/b_W)*CL_alph_vt_rig; % [1/°]
    Cn_r_rig_rad = Cn_r_rig*57.29579; % [1/rad]
    Cn_r = Cn_r_lef + Cn_r_rig; % [1/°]
    Cn_r_rad = Cn_r*57.29579; % [1/rad]

    if (main_menu == 1 | main_menu == 3)
```

```
        fprintf ('Cn_delt_Rud_lef [1/°]: %g', Cn_delt_R_lef);
        fprintf ('\n');
        fprintf ('Cn_delt_Rud_rig [1/°]: %g', Cn_delt_R_rig);
        fprintf ('\n');
        fprintf ('Cn_r_lef [1/°]: %g', Cn_r_lef);
        fprintf ('\n');
        fprintf ('Cn_r_rig [1/°]: %g', Cn_r_rig);
        fprintf ('\n\n');
        fprintf ('Cn_r [1/°]: %g', Cn_r);
        fprintf ('\n');
        fprintf ('Cn_r [1/rad]: %g', Cn_r_rad);
        fprintf ('\n\n');

Aux_rud_1 = ((V_wind.^2)*S_S*CD_y)/((V_T.^2)*S_aero_W);
SIGMA_lef_rad = -((Aux_rud_1 - Cy_delt_R_lef_rad*Delt_rud_rad -
Cy_zero)/Cy_bet_vt_lef_rad) + (Beta_rad/2); % [rad] Crab Angle due the Left
Rudder
SIGMA_rig_rad = -((Aux_rud_1 - Cy_delt_R_rig_rad*Delt_rud_rad -
Cy_zero)/Cy_bet_vt_rig_rad) + (Beta_rad/2); % [rad] Crab Angle due the Right
Rudder
SIGMA_rad = SIGMA_lef_rad + SIGMA_rig_rad; % [rad] Airplane Crab Angle due the
Rudder deflection
SIGMA = SIGMA_rad*57.2958; % [rad]

Aux_rud_2 = Cn_delt_R_lef_rad*Delt_rud_rad + Cn_delt_R_rig_rad*Delt_rud_rad;
Aux_rud_3 = Cn_zero + Cn_beta_rad*(Beta_rad - SIGMA_rad) + Aux_rud_2;
Eq_vert_1 = q*S_aero_W*b_W*Aux_rud_3 + F_W*d_c*cos(SIGMA_rad); % Equation (1)
of the system of two equations. Used for verification of Crab Angle

N_W = (F_W*sin(SIGMA_rad))*d_c; % [N*m]

    if (length(Beta) == 1)
        fprintf ('Airplane Crab Angle [°]: %g', SIGMA);
        fprintf ('\n\n');
        fprintf ('Equation of verification of the Crab Angle (Must be equal
Zero): %g', Eq_vert_1);
        fprintf ('\n\n');
        fprintf ('Yawing Moment due the Lateral Aerodynamic Force [N*m]: %g',
N_W);
        fprintf ('\n\n');
    end

    end

fprintf ('-----------------------------------------------------------------
----------------------------\n\n');
%¨¨¨¨¨¨¨¨¨¨¨¨¨¨¨¨¨¨¨¨¨¨¨¨¨¨¨¨¨¨¨¨¨¨¨¨¨¨¨¨¨¨¨¨¨¨¨¨¨¨¨¨¨¨¨¨¨¨¨¨¨¨¨¨¨¨¨¨¨¨¨¨¨¨¨¨¨¨¨

%¨¨¨¨¨¨¨¨¨¨¨¨¨¨¨LATERAL-DIRECTIONAL STATIC STABILITY COUPLING¨¨¨¨¨¨¨¨¨¨¨¨¨¨¨¨
fprintf ('-------------------------------LATERAL-DIRECTIONAL STATIC STABILITY
COUPLING--------------------\n\n');

%¨¨Lateral Coupling¨¨
fprintf ('Lateral Coupling');
```

```
fprintf ('\n\n');

    z_v = abs(F_c_l - z_vt_lef); % [m]
    Cl_delt_R_lef = (S_vt_lef/S_aero_W)*(z_v/b_W)*tao_rud_vt_lef*CL_alph_W; %
[1/°]
    Cl_delt_R_rig = (S_vt_rig/S_aero_W)*(z_v/b_W)*tao_rud_vt_rig*CL_alph_W; %
[1/°]
    Cl_delt_R = Cl_delt_R_lef + Cl_delt_R_rig; % [1/°]
    Cl_delt_R_rad = Cl_delt_R*57.29579; % [1/rad]

    Cl_r_lef = 0.5*(CL_AIRPLANE/4) - 2*(l_vt_lef/b_W)*(z_v/b_W)*Cy_bet_vt_lef;
% [1/°]
    Cl_r_rig = 0.5*(CL_AIRPLANE/4) - 2*(l_vt_rig/b_W)*(z_v/b_W)*Cy_bet_vt_rig;
% [1/°]
    Cl_r = Cl_r_lef + Cl_r_rig; % [1/°]
    Cl_r_rad = Cl_r*57.29579; % [1/rad]

    if (main_menu == 1 | main_menu == 3)
        if (length(Beta) == 1)
            fprintf ('Cl_delt_Rud_lef [1/°]: %g', Cl_delt_R_lef);
            fprintf ('\n');
            fprintf ('Cl_delt_Rud_rig [1/°]: %g', Cl_delt_R_rig);
            fprintf ('\n');
            fprintf ('Cl_delt_Rud [1/°]: %g', Cl_delt_R);
            fprintf ('\n\n');
            fprintf ('Cl_r_lef [1/°]: %g', Cl_r_lef);
            fprintf ('\n');
            fprintf ('Cl_r_rig [1/°]: %g', Cl_r_rig);
            fprintf ('\n');
            fprintf ('Cl_r [1/°]: %g', Cl_r);
            fprintf ('\n\n');
        end

Cl = Cl_beta*Beta + Cl_delt_A*Delt_ail + Cl_delt_R*Delt_rud; % Airplane
rolling derivative

    if (length(Beta) == 1)
        fprintf ('Airplane Rolling Derivative - Cl: %g', Cl);
        fprintf ('\n\n');
    end

    end

%¨¨Directional Couling¨¨
fprintf ('Directional Coupling');
fprintf ('\n\n');

    Y_1 = (b_ail_i + 0.45); % [m]
    eta_ail_stab = Y_1/(b_W/2);
    K = 0.232; % Estimated from graph 3.12 [Nelson; pg122]

    if (main_menu == 1 | main_menu == 3)
    fprintf ('Eta_A: %g', eta_ail_stab);
    fprintf ('\n');
```

```
    fprintf ('Empirical Factor for Cn_delt_A (K): %g', K);
    fprintf ('\n\n');
    end

    Cn_delt_A = 2*K*CL_AIRPLANE*Cl_delt_A; % [1/°]
    Cn_delt_A_rad = Cn_delt_A*57.29579; % [1/rad]

    Cn_p = -CL_AIRPLANE/8; % [1/°]
    Cn_p_rad = Cn_p*57.29579; % [1/rad]


Cn_lef = Cn_bet_v_lef*(Beta - Sigma_lef) + Cn_delt_R_lef*Delt_rud;
Cn_rig = Cn_bet_v_rig*(Beta - Sigma_rig) + Cn_delt_R_rig*Delt_rud;
Cn = Cn_zero + Cn_lef + Cn_rig + Cn_delt_A*Delt_ail;

if (main_menu == 1 | main_menu == 3)
    if (length(Beta) == 1)
        fprintf ('Cn_delt_Ail [1/°]: %g', Cn_delt_A);
        fprintf ('\n');
        fprintf ('Cn_p [1/°]: %g', Cn_p);
        fprintf ('\n');
        fprintf ('Cn_lef: %g', Cn_lef);
        fprintf ('\n');
        fprintf ('Cn_rig: %g', Cn_rig);
        fprintf ('\n');
        fprintf ('Cn_AIRPLANE: %g', Cn);
        fprintf ('\n\n');
    end
end

fprintf ('--------------------------------------------------------------------
----------------------------\n\n');
%¨¨¨¨¨¨¨¨¨¨¨¨¨¨¨¨¨¨¨¨¨¨¨¨¨¨¨¨¨¨¨¨¨¨¨¨¨¨¨¨¨¨¨¨¨¨¨¨¨¨¨¨¨¨¨¨¨¨¨¨¨¨¨¨¨¨¨¨¨¨¨¨¨¨¨¨
if (main_menu == 1 | main_menu == 4)
%¨¨¨¨¨¨¨¨¨¨¨¨¨¨¨¨¨¨¨¨¨LONGITUDINAL DYNAMIC STABILITY¨¨¨¨¨¨¨¨¨¨¨¨¨¨¨¨¨¨¨¨¨¨
fprintf ('--------------------------------LONGITUDINAL DYNAMIC STABILITY------
----------------------------\n\n');

%¨¨X-Force Derivatives¨¨
fprintf ('X-Force Derivatives');
fprintf ('\n\n');

CD_u = 0;
CT_u = -CD_AIRPLANE;
CX_u = -(CD_u + 2*CD_AIRPLANE) + CT_u;
CX_alph = CL_AIRPLANE*(1 - (2*CL_ALPH_AIRPLANE/(pi*e_W*AR_W))); % [1/°]
CX_alph_rad = CX_alph*57.29579; % [1/rad]
CX_alph_dot = 0;
CX_q = 0;
CX_alph_e = 0; % due the elevator

XU = CX_u*((q*S_aero_W)/(m*V_T)); % [1/s]
XW = CX_alph_rad*((q*S_aero_W)/(m*V_T)); % [1/s]
```

```
fprintf ('CD_u: %g', CD_u);
fprintf ('\n');
fprintf ('CT_u: %g', CT_u);
fprintf ('\n');
fprintf ('CX_u [1/°]: %g', CX_u);
fprintf ('\n');
fprintf ('CX_alph [1/°]: %g', CX_alph);
fprintf ('\n\n');
fprintf ('X_U [1/s]: %g', XU);
fprintf ('\n');
fprintf ('X_W [1/s]: %g', XW);
fprintf ('\n\n');
fprintf ('¨¨¨¨¨¨¨¨¨¨¨¨¨¨\n\n');

%¨¨Z-Force Derivatives¨¨
fprintf ('Z-Force Derivatives');
fprintf ('\n\n');

CZ_u = -(Mach^2/(1 - Mach^2))*CL_AIRPLANE - 2*CL_AIRPLANE;
CZ_alph = -(CL_ALPH_AIRPLANE + CD_AIRPLANE); % [1/°]
CZ_alph_rad = CZ_alph*57.29579; % [1/rad]
CZ_alph_dot_low_rad = -
2*Eta_can_low*CL_alph_can_low_rad*V_can_low*dEps_dAlp_can_low;
CZ_alph_dot_up_rad = -
2*Eta_can_up*CL_alph_can_up_rad*V_can_up*dEps_dAlp_can_up;
CZ_alph_dot_rad = CZ_alph_dot_low_rad + CZ_alph_dot_up_rad;
CZ_q_low_rad = -2*Eta_can_low*CL_alph_can_low_rad*V_can_low;
CZ_q_up_rad = -2*Eta_can_up*CL_alph_can_up_rad*V_can_up;
CZ_q_rad = CZ_q_low_rad + CZ_q_up_rad;
CZ_delt_e_low_rad = -
(S_can_low/S_aero_W)*Eta_can_low*CL_can_low_delt_elev_rad;  % [1/rad]
CZ_delt_e_up_rad = -(S_can_up/S_aero_W)*Eta_can_up*CL_can_up_delt_elev_rad; %
[1/rad]
CZ_delt_e_rad = CZ_delt_e_low_rad + CZ_delt_e_up_rad; % [1/rad]

ZU = CZ_u*((q*S_aero_W)/(m*V_T)); % [1/s]
ZW = CZ_alph_rad*((q*S_aero_W)/(m*V_T)); % [1/s]
ZW_dot = CZ_alph_dot_rad*((q*S_aero_W)/m)*(mac_W/(2*V_T));
Zalph = V_T*ZW; % [m/s^2]
Zalph_dot = V_T*ZW_dot; % [m/s]
Zq = CZ_q_rad*((q*S_aero_W)/m)*(mac_W/(2*V_T)); % [m/s]
Z_delt_e = CZ_delt_e_rad*((q*S_aero_W)/m); % [m/s^2]

fprintf ('CZ_u: %g', CZ_u);
fprintf ('\n\n');
fprintf ('CZ_alph [1/rad]: %g', CZ_alph_rad);
fprintf ('\n');
fprintf ('CZ_alph_dot_low_rad: %g', CZ_alph_dot_low_rad);
fprintf ('\n');
fprintf ('CZ_alph_dot_up_rad: %g', CZ_alph_dot_up_rad);
fprintf ('\n');
fprintf ('CZ_alph_dot_rad: %g', CZ_alph_dot_rad);
fprintf ('\n\n');
fprintf ('CZ_q_low_rad: %g', CZ_q_low_rad);
fprintf ('\n');
```

```
fprintf ('CZ_q_up_rad: %g', CZ_q_up_rad);
fprintf ('\n');
fprintf ('CZ_q_rad: %g', CZ_q_rad);
fprintf ('\n\n');
fprintf ('CZ_delt_e_low_rad: %g', CZ_delt_e_low_rad);
fprintf ('\n');
fprintf ('CZ_delt_e_up_rad: %g', CZ_delt_e_up_rad);
fprintf ('\n');
fprintf ('CZ_delt_e_rad: %g', CZ_delt_e_rad);
fprintf ('\n\n');
fprintf ('ZU [1/s]: %g', ZU);
fprintf ('\n');
fprintf ('ZW [1/s]: %g', ZW);
fprintf ('\n');
fprintf ('ZW_dot: %g', ZW_dot);
fprintf ('\n');
fprintf ('Zalph [m/s^2]: %g', Zalph);
fprintf ('\n');
fprintf ('Zalph_dot [m/s]: %g', Zalph_dot);
fprintf ('\n');
fprintf ('Zq [m/s]: %g', Zq);
fprintf ('\n');
fprintf ('Z_delt_e [m/s^2]: %g', Z_delt_e);
fprintf ('\n\n');
fprintf ('¨¨¨¨¨¨¨¨¨¨¨¨¨\n\n');

%¨¨Pitching Moment Derivatives¨¨
fprintf ('Pitching Moment Derivatives');
fprintf ('\n\n');

CM_u = 0;
% CM_ALPHA: Developed under Longitudinal Static Stability section
CM_ALPHA_dot_low_rad = CZ_alph_dot_low_rad*(l_can_low/mac_W);
CM_ALPHA_dot_up_rad = CZ_alph_dot_up_rad*(l_can_up/mac_W);
CM_ALPHA_dot_rad = CM_ALPHA_dot_low_rad + CM_ALPHA_dot_up_rad;
CM_q_low_rad = CZ_q_low_rad*(l_can_low/mac_W);
CM_q_up_rad = CZ_q_up_rad*(l_can_up/mac_W);
CM_q_rad = CM_q_low_rad + CM_q_up_rad;
CM_delt_e_low_rad = -Eta_can_low*V_can_low*CL_can_low_delt_elev_rad;
CM_delt_e_up_rad = -Eta_can_up*V_can_up*CL_can_up_delt_elev_rad;
CM_delt_e_rad = CM_delt_e_low_rad + CM_delt_e_up_rad;

MU = CM_u*((q*S_aero_W*mac_W)/(V_T*I_yy)); % [1/m.s]
MW = CM_ALPHA_RAD*((q*S_aero_W*mac_W)/(V_T*I_yy)); % [1/m.s]
MW_dot_low =
CM_ALPHA_dot_low_rad*((q*S_aero_W*mac_W)/(V_T*I_yy))*(mac_W/(2*V_T)); % [1/m]
MW_dot_up =
CM_ALPHA_dot_up_rad*((q*S_aero_W*mac_W)/(V_T*I_yy))*(mac_W/(2*V_T)); % [1/m]
MW_dot = MW_dot_low + MW_dot_up; % [1/m]
MALPHA = V_T*MW; % [1/s^2]
MALPHA_dot = V_T*MW_dot; % [1/s]
Mq = CM_q_rad*(mac_W/(2*V_T))*((q*S_aero_W*mac_W)/I_yy); % [1/s]
M_delt_e_low = CM_delt_e_low_rad*((q*S_aero_W*mac_W)/I_yy); % [1/s^2]
M_delt_e_up = CM_delt_e_up_rad*((q*S_aero_W*mac_W)/I_yy); % [1/s^2]
M_delt_e = M_delt_e_low + M_delt_e_up; % [1/s^2]
```

```
fprintf ('CM_u: %g', CM_u);
fprintf ('\n\n');
fprintf ('CM_ALPHA_dot_low_rad: %g', CM_ALPHA_dot_low_rad);
fprintf ('\n');
fprintf ('CM_ALPHA_dot_up_rad: %g', CM_ALPHA_dot_up_rad);
fprintf ('\n');
fprintf ('CM_ALPHA_dot_rad: %g', CM_ALPHA_dot_rad);
fprintf ('\n\n');
fprintf ('CM_q_low_rad: %g', CM_q_low_rad);
fprintf ('\n');
fprintf ('CM_q_up_rad: %g', CM_q_up_rad);
fprintf ('\n');
fprintf ('CM_q_rad: %g', CM_q_rad);
fprintf ('\n\n');
fprintf ('CM_delt_e_low_rad: %g', CM_delt_e_low_rad);
fprintf ('\n');
fprintf ('CM_delt_e_up_rad: %g', CM_delt_e_up_rad);
fprintf ('\n');
fprintf ('CM_delt_e_rad: %g', CM_delt_e_rad);
fprintf ('\n\n');
fprintf ('MU [1/m.s]: %g', MU);
fprintf ('\n\n');
fprintf ('MW [1/m.s]: %g', MW);
fprintf ('\n');
fprintf ('MW_dot_low [1/m]: %g', MW_dot_low);
fprintf ('\n');
fprintf ('MW_dot_up [1/m]: %g', MW_dot_up);
fprintf ('\n');
fprintf ('MW_dot [1/m]: %g', MW_dot);
fprintf ('\n\n');
fprintf ('M_ALPHA [1/s^2]: %g', MALPHA);
fprintf ('\n');
fprintf ('M_ALPHA_dot [1/s]: %g', MALPHA_dot);
fprintf ('\n\n');
fprintf ('Mq [1/s]: %g', Mq);
fprintf ('\n\n');
fprintf ('M_delt_e_low [1/s^2]: %g', M_delt_e_low);
fprintf ('\n');
fprintf ('M_delt_e_up [1/s^2]: %g', M_delt_e_up);
fprintf ('\n');
fprintf ('M_delt_e [1/s^2]: %g', M_delt_e);
fprintf ('\n\n');
fprintf ('¨¨¨¨¨¨¨¨¨¨¨¨¨\n\n');

%¨¨MATRIX OF STABILITY DERIVATIVES & VECTOR OF EIGENVALUES¨¨
A_3_1 = MU + MW_dot*ZU;
A_3_2 = MW + MW_dot*ZW;
A_3_3 = Mq + MW_dot*V_T;

fprintf ('MATRIX OF STABILITY DERIVATIVES:');
fprintf ('\n');

A = [XU,XW,0,-g; ZU,ZW,V_T,0; A_3_1,A_3_2,A_3_3,0; 0,0,1,0]
```

```
fprintf ('VECTOR OF EIGENVALUES:');
fprintf ('\n');

EIG_A = eig(A)
fprintf ('¨¨¨¨¨¨¨¨¨¨¨¨\n\n');

if (abs(imag(EIG_A(1))) > abs(imag(EIG_A(3))))
    lamb_sp = EIG_A(1);
    lamb_ph = EIG_A(3);
end

if (abs(imag(EIG_A(3))) > abs(imag(EIG_A(1))))
    lamb_sp = EIG_A(3);
    lamb_ph = EIG_A(1);
end

%¨¨SHORT PERIOD¨¨
fprintf ('SHORT PERIOD PROPERTIES');
fprintf ('\n\n');

fprintf ('Short Period Eigenvalues:');
fprintf ('\n');
lamb_sp = lamb_sp

eta_sp = real(lamb_sp);
omeg_sp = imag(lamb_sp); % [rad/s] Damped Natural FrequEncy

ksi_sp = sqrt(eta_sp^2/(eta_sp^2 + omeg_sp^2)); % Damping Ratio
omeg_n_sp = -eta_sp/ksi_sp; % [rad/s] Undamped Natural Frequency
k_sp = (omeg_n_sp^2)*m; % Spring constant
C_cr_sp = 2*sqrt(k_sp*m); % Critical Damping constant
C_sp = ksi_sp*C_cr_sp; % Damping constant
period_sp = 2*pi/omeg_sp; % [s] Period of oscilatory movement
t_halve_sp = 0.693/abs(eta_sp); % [s] Time for halving amplitude
N_halve_sp = (1/period_sp)*t_halve_sp; % Cilce Number for halving amplitude

fprintf ('Short Period Undamped Natural Frequency [rad/s]: %g', omeg_n_sp);
fprintf ('\n');
fprintf ('Short Period Damping Ratio: %g', ksi_sp);
fprintf ('\n');
fprintf ('Short Period Spring constant: %g', k_sp);
fprintf ('\n');
fprintf ('Short Period Critical Damping constant: %g', C_cr_sp);
fprintf ('\n');
fprintf ('Short Period Damping constant: %g', C_sp);
fprintf ('\n');
fprintf ('Short Period Damped Natural Frequency [rad/s]: %g', omeg_sp);
fprintf ('\n');
fprintf ('Period of Oscillation of the Short Period Motion [s]: %g',
period_sp);
fprintf ('\n');
fprintf ('Short Period Time for halving amplitude [s]: %g', t_halve_sp);
fprintf ('\n');
fprintf ('Short Period Cicle Number for halving amplitude: %g', N_halve_sp);
```

```
fprintf ('\n');
fprintf ('¨¨¨¨¨¨¨¨¨¨¨¨¨\n\n');

%¨¨PHUGOID¨¨
fprintf ('PHUGOID PROPERTIES');
fprintf ('\n\n');

fprintf ('Phugoid Eigenvalues:');
fprintf ('\n');
lamb_ph = lamb_ph

eta_ph = real(lamb_ph);
omeg_ph = imag(lamb_ph); % [rad/s] Damped Natural FrequEncy

ksi_ph = sqrt(eta_ph^2/(eta_ph^2 + omeg_ph^2)); % Damping Ratio
omeg_n_ph = -eta_ph/ksi_ph; % [rad/s] Undamped Natural Frequency
k_ph = (omeg_n_ph^2)*m; % Spring constant
C_cr_ph = 2*sqrt(k_ph*m); % Critical Damping constant
C_ph = ksi_ph*C_cr_ph; % Damping constant
period_ph = 2*pi/omeg_ph; % [s] Period of oscilatory movement
t_halve_ph = 0.693/abs(eta_ph); % [s] Time for halving amplitude
N_halve_ph = (1/period_ph)*t_halve_ph; % Cilce Number for halving amplitude

fprintf ('Phugoid Undamped Natural Frequency [rad/s]: %g', omeg_n_ph);
fprintf ('\n');
fprintf ('Phugoid Damping Ratio: %g', ksi_ph);
fprintf ('\n');
fprintf ('Phugoid Spring constant: %g', k_ph);
fprintf ('\n');
fprintf ('Phugoid Critical Damping constant: %g', C_cr_ph);
fprintf ('\n');
fprintf ('Phugoid Damping constant: %g', C_ph);
fprintf ('\n');
fprintf ('Phugoid Damped Natural Frequency [rad/s]: %g', omeg_ph);
fprintf ('\n');
fprintf ('Period of Oscillation of the Phugoid Motion [s]: %g', period_ph);
fprintf ('\n');
fprintf ('Phugoid Time for halving amplitude [s]: %g', t_halve_ph);
fprintf ('\n');
fprintf ('Phugoid Cicle Number for halving amplitude: %g', N_halve_ph);
fprintf ('\n\n');

%*Plots*
disp_sp = input ('Inicial displacement (perturbation) for the Short Period
Motion [°]: ' );
    disp_sp_rad = disp_sp*0.01745329; % [rad] Inicial displacement
(perturbation) regarding neutral position
duration_sp = input ('Duration of the Short Period Motion Analysis [s]: ' );

disp_ph = input ('Inicial displacement (perturbation) for the Phugoid Motion
[m]: ' );
duration_ph = input ('Duration of the Phugoid Motion Analysis [s]: ' );

time_sp = 0:0.1:duration_sp;
```

```
time_ph = 0:0.1:duration_ph;

teta_sp_rad = disp_sp_rad*exp(-time_sp./(2*(m/C_sp))).*cos(omeg_sp*time_sp); %
[rad] Instantaneous Position
    teta_sp = teta_sp_rad*57.2958; % [°]
osci_ph = disp_ph*exp(-time_ph./(2*(m/C_ph))).*cos(omeg_ph*time_ph); % [m]
Instantaneous Position

figure (8);
plot (time_sp,teta_sp);
title ('SHORT PERIOD MOTION');
xlabel ('TIME [s]');
ylabel ('TETA [°]');
hold on;

figure (9);
plot (time_ph,osci_ph);
title ('PHUGOID MOTION');
xlabel ('TIME [s]');
ylabel ('VERTICAL POSITION [m]');
hold on;

fprintf ('-------------------------------------------------------------------
----------------------------\n\n');
%¨¨¨¨¨¨¨¨¨¨¨¨¨¨¨¨¨¨¨¨¨¨¨¨¨¨¨¨¨¨¨¨¨¨¨¨¨¨¨¨¨¨¨¨¨¨¨¨¨¨¨¨¨¨¨¨¨¨¨¨¨¨¨¨¨¨¨¨¨¨¨¨¨¨¨¨¨¨

%¨¨¨¨¨¨¨¨¨¨¨¨¨¨¨¨¨¨¨¨¨¨¨¨LATERAL-DIRECTIONAL DYNAMIC STABILITY¨¨¨¨¨¨¨¨¨¨¨¨¨¨¨¨¨¨¨¨¨¨¨¨
fprintf ('-----------------------------LATERAL-DIRECTIONAL DYNAMIC STABILITY--
----------------------------\n\n');

AUX_latdir_dyn = 1 - (I_xz^2/(I_xx*I_zz));

%¨¨Y-Force Derivatives¨¨
fprintf ('Y-Force Derivatives');
fprintf ('\n\n');

Cy_bet_rad = Cy_bet_vt_lef_rad + Cy_bet_vt_rig_rad; % [1/rad]
Cy_p_rad = CL_AIRPLANE*((AR_W + cos(Gam_W_rad))/(AR_W +
4*cos(Gam_W_rad)))*tan(Gam_W_rad);
Cy_r_rad = Cy_r_lef_rad + Cy_r_rig_rad; % [1/rad]
Cy_delt_A_rad = 0; % {1/rad]
Cy_delt_R_rad = Cy_delt_R_lef_rad + Cy_delt_R_rig_rad; % [1/rad]

YBETA = (q*S_aero_W*Cy_bet_rad)/m; % [m/s^2]
Yv = YBETA*V_T;
Yp = (q*S_aero_W*b_W*Cy_p_rad)/(2*m*V_T); % [m/s]
Yr = (q*S_aero_W*b_W*Cy_r_rad)/(2*m*V_T); % [m/s]
Ydelt_A = (q*S_aero_W*Cy_delt_A_rad)/m; % [m/s^2]
Ydelt_R = (q*S_aero_W*Cy_delt_R_rad)/m; % [m/s^2]

fprintf ('Cy_bet_rad [1/rad]: %g', Cy_bet_rad);
fprintf ('\n');
fprintf ('Cy_p_rad: %g', Cy_p_rad);
fprintf ('\n');
```

```
fprintf ('Cy_r [1/rad]: %g', Cy_r_rad);
fprintf ('\n');
fprintf ('Cy_delt_A [1/rad]: %g', Cy_delt_A_rad);
fprintf ('\n');
fprintf ('Cy_delt_R [1/rad]: %g', Cy_delt_R_rad);
fprintf ('\n\n');
fprintf ('Y_BETA [m/s^2]: %g', YBETA);
fprintf ('\n');
fprintf ('Y_v: %g', Yv);
fprintf ('\n');
fprintf ('Y_p [m/s]: %g', Yp);
fprintf ('\n');
fprintf ('Y_r [m/s]: %g', Yr);
fprintf ('\n');
fprintf ('Y_delt_A [m/s^2]: %g', Ydelt_A);
fprintf ('\n');
fprintf ('Y_delt_R [m/s^2]: %g', Ydelt_R);
fprintf ('\n\n');
fprintf ('¨¨¨¨¨¨¨¨¨¨¨¨¨\n\n');

%¨¨Yawing Moment Derivatives¨¨
fprintf ('Yawing Moment Derivatives');
fprintf ('\n\n');

%Cn_beta: Developed under Directional Static Stability section
%Cn_p: Developed under Lateral-Directional Static Stability Coupling section
%Cn_r:  Developed under Directional Static Stability section
%Cn_delt_A: Developed under Lateral-Directional Static Stability Coupling
section
Cn_delt_R_rad = Cn_delt_R_lef_rad + Cn_delt_R_rig_rad; % [1/rad]

NBETA = (q*S_aero_W*b_W*Cn_beta_rad)/I_zz; % [1/s^2]
Np = (q*S_aero_W*(b_W^2)*Cn_p_rad)/(2*I_zz*V_T); % [1/s]
Nr = (q*S_aero_W*(b_W^2)*Cn_r_rad)/(2*I_zz*V_T); % [1/s]
Ndelt_A = (q*S_aero_W*b_W*Cn_delt_A_rad)/I_zz; % [1/s^2]
Ndelt_R = (q*S_aero_W*b_W*Cn_delt_R_rad)/I_zz; % [1/s^2]
Nv = NBETA*V_T;
Nv_aster = Nv/AUX_latdir_dyn;
Np_aster = Np/AUX_latdir_dyn;
Nr_aster = Nr/AUX_latdir_dyn;

fprintf ('Cn_delt_R_rad [1/rad]: %g', Cn_delt_R_rad);
fprintf ('\n\n');
fprintf ('N_BETA [1/s^2]: %g', NBETA);
fprintf ('\n');
fprintf ('N_p [1/s]: %g', Np);
fprintf ('\n');
fprintf ('N_r [1/s]: %g', Nr);
fprintf ('\n');
fprintf ('N_delt_A [1/s^2]: %g', Ndelt_A);
fprintf ('\n');
fprintf ('N_delt_R [1/s^2]: %g', Ndelt_R);
fprintf ('\n\n');
fprintf ('N_v: %g', Nv);
fprintf ('\n');
```

```
fprintf ('Nv_aster: %g', Nv_aster);
fprintf ('\n');
fprintf ('Np_aster: %g', Np_aster);
fprintf ('\n');
fprintf ('Nr_aster: %g', Nr_aster);
fprintf ('\n\n');
fprintf ('¨¨¨¨¨¨¨¨¨¨¨¨\n\n');

%¨¨Rolling Moment Derivatives¨¨
fprintf ('Rolling Moment Derivatives');
fprintf ('\n\n');

%Cl_beta: Developed under Lateral Static Stability section
%Cl_p: Developed under Lateral Static Stability section
%Cl_r: Developed under Lateral-Directional Static Stability Coupling section
%Cl_delt_A: Developed under Lateral Static Stability section
%Cl_delt_R: Developed under Lateral-Directional Static Stability Coupling
section

LBETA = (q*S_aero_W*b_W*Cl_beta_rad)/I_xx; % [1/s^2]
Lp = (q*S_aero_W*(b_W^2)*Cl_p_rad)/(2*I_xx*V_T); % [1/s]
Lr = (q*S_aero_W*(b_W^2)*Cl_r_rad)/(2*I_xx*V_T); % [1/s]
Ldelt_A = (q*S_aero_W*b_W*Cl_delt_A_rad)/I_xx; % [1/s^2]
Ldelt_R = (q*S_aero_W*b_W*Cl_delt_R_rad)/I_xx; % [1/s^2]
Lv = LBETA*V_T;
Lv_aster = Lv/AUX_latdir_dyn;
Lp_aster = Lp/AUX_latdir_dyn;
Lr_aster = Lr/AUX_latdir_dyn;

fprintf ('LBETA [1/s^2]: %g', LBETA);
fprintf ('\n');
fprintf ('L_p [1/s]: %g', Lp);
fprintf ('\n');
fprintf ('L_r [1/s]: %g', Lr);
fprintf ('\n');
fprintf ('L_delt_A [1/s^2]: %g', Ldelt_A);
fprintf ('\n\n');
fprintf ('L_delt_R [1/s^2]: %g', Ldelt_R);
fprintf ('\n\n');
fprintf ('L_v: %g', Lv);
fprintf ('\n');
fprintf ('Lv_aster: %g', Lv_aster);
fprintf ('\n');
fprintf ('Lp_aster: %g', Lp_aster);
fprintf ('\n');
fprintf ('Lr_aster: %g', Lr_aster);
fprintf ('\n\n');
fprintf ('¨¨¨¨¨¨¨¨¨¨¨¨\n\n');

%¨¨MATRIX OF STABILITY DERIVATIVES & VECTOR OF EIGENVALUES¨¨
C_1_3 = -(V_T - Yr);
Theta_0 = input ('Inicial Pitch Angle [°]: ' );
Theta_0_rad = Theta_0*0.01745329; % [rad]
C_1_4 = g*cos(Theta_0_rad);
C_2_1 = Lv_aster + (I_xz/I_xx)*Nv_aster;
```

```
C_2_2 = Lp_aster + (I_xz/I_xx)*Np_aster;
C_2_3 = Lr_aster + (I_xz/I_xx)*Nr_aster;
C_3_1 = Nv_aster + (I_xz/I_zz)*Lv_aster;
C_3_2 = Np_aster + (I_xz/I_zz)*Lp_aster;
C_3_3 = Nr_aster + (I_xz/I_zz)*Lr_aster;

fprintf ('MATRIX OF STABILITY DERIVATIVES:');
fprintf ('\n');

C = [Yv,Yp,C_1_3,C_1_4; C_2_1,C_2_2,C_2_3,0; C_3_1,C_3_2,C_3_3,0; 0,1,0,0]

fprintf ('VECTOR OF EIGENVALUES:');
fprintf ('\n');

EIG_C = eig(C)
fprintf ('¨¨¨¨¨¨¨¨¨¨¨¨¨\n\n');

if (abs(imag(EIG_C(1))) == 0 & abs(imag(EIG_C(2))) == 0)
    if (abs(real(EIG_C(1))) > abs(real(EIG_C(2))))
        lamb_roll = EIG_C(1);
        lamb_spir = EIG_C(2);
    end

    if (abs(real(EIG_C(2))) > abs(real(EIG_C(1))))
        lamb_roll = EIG_C(2);
        lamb_spir = EIG_C(1);
    end
end

if (abs(imag(EIG_C(1))) == 0 & abs(imag(EIG_C(3))) == 0)
    if (abs(real(EIG_C(1))) > abs(real(EIG_C(3))))
        lamb_roll = EIG_C(1);
        lamb_spir = EIG_C(3);
    end

    if (abs(real(EIG_C(3))) > abs(real(EIG_C(1))))
        lamb_roll = EIG_C(3);
        lamb_spir = EIG_C(1);
    end
end

if (abs(imag(EIG_C(1))) == 0 & abs(imag(EIG_C(4))) == 0)
    if (abs(real(EIG_C(1))) > abs(real(EIG_C(4))))
        lamb_roll = EIG_C(1);
        lamb_spir = EIG_C(4);
    end

    if (abs(real(EIG_C(4))) > abs(real(EIG_C(1))))
        lamb_roll = EIG_C(4);
        lamb_spir = EIG_C(1);
    end
end
```

```
if (abs(imag(EIG_C(2))) == 0 & abs(imag(EIG_C(3))) == 0)
    if (abs(real(EIG_C(2))) > abs(real(EIG_C(3))))
        lamb_roll = EIG_C(2);
        lamb_spir = EIG_C(3);
    end

    if (abs(real(EIG_C(3))) > abs(real(EIG_C(2))))
        lamb_roll = EIG_C(3);
        lamb_spir = EIG_C(2);
    end
end

if (abs(imag(EIG_C(2))) == 0 & abs(imag(EIG_C(4))) == 0)
    if (abs(real(EIG_C(2))) > abs(real(EIG_C(4))))
        lamb_roll = EIG_C(2);
        lamb_spir = EIG_C(4);
    end

    if (abs(real(EIG_C(4))) > abs(real(EIG_C(2))))
        lamb_roll = EIG_C(4);
        lamb_spir = EIG_C(2);
    end
end

if (abs(imag(EIG_C(3))) == 0 & abs(imag(EIG_C(4))) == 0)
    if (abs(real(EIG_C(3))) > abs(real(EIG_C(4))))
        lamb_roll = EIG_C(3);
        lamb_spir = EIG_C(4);
    end

    if (abs(real(EIG_C(4))) > abs(real(EIG_C(3))))
        lamb_roll = EIG_C(4);
        lamb_spir = EIG_C(3);
    end
end

if (abs(imag(EIG_C(1))) ~= 0 & abs(imag(EIG_C(2))) ~= 0)
    if (imag(EIG_C(1)) > imag(EIG_C(2)))
        lamb_dut = EIG_C(1);
    end

    if (imag(EIG_C(2)) > imag(EIG_C(1)))
        lamb_dut = EIG_C(2);
    end
end

if (abs(imag(EIG_C(1))) ~= 0 & abs(imag(EIG_C(3))) ~= 0)
    if (imag(EIG_C(1)) > imag(EIG_C(3)))
        lamb_dut = EIG_C(1);
    end

    if (imag(EIG_C(3)) > imag(EIG_C(1)))
        lamb_dut = EIG_C(3);
    end
```

```
end

if (abs(imag(EIG_C(1))) ~= 0 & abs(imag(EIG_C(4))) ~= 0)
    if (imag(EIG_C(1)) > imag(EIG_C(4)))
        lamb_dut = EIG_C(1);
    end

    if (imag(EIG_C(4)) > imag(EIG_C(1)))
        lamb_dut = EIG_C(4);
    end
end

if (abs(imag(EIG_C(2))) ~= 0 & abs(imag(EIG_C(3))) ~= 0)
    if (imag(EIG_C(2)) > imag(EIG_C(3)))
        lamb_dut = EIG_C(2);
    end

    if (imag(EIG_C(3)) > imag(EIG_C(2)))
        lamb_dut = EIG_C(3);
    end
end

if (abs(imag(EIG_C(2))) ~= 0 & abs(imag(EIG_C(4))) ~= 0)
    if (imag(EIG_C(2)) > imag(EIG_C(4)))
        lamb_dut = EIG_C(2);
    end

    if (imag(EIG_C(4)) > imag(EIG_C(2)))
        lamb_dut = EIG_C(4);
    end
end

if (abs(imag(EIG_C(3))) ~= 0 & abs(imag(EIG_C(4))) ~= 0)
    if (imag(EIG_C(3)) > imag(EIG_C(4)))
        lamb_dut = EIG_C(3);
    end

    if (imag(EIG_C(4)) > imag(EIG_C(3)))
        lamb_dut = EIG_C(4);
    end
end

%¨¨ROLL¨¨
fprintf ('ROLL PROPERTIES');
fprintf ('\n\n');

fprintf ('Roll Eigenvalues:');
fprintf ('\n');
lamb_roll = lamb_roll

eta_roll = real(lamb_roll);
omeg_roll = imag(lamb_roll); % [rad/s] Damped Natural FrequEncy
```

```
ksi_roll = sqrt(eta_roll^2/(eta_roll^2 + omeg_roll^2)); % Damping Ratio
omeg_n_roll = -eta_roll/ksi_roll; % [rad/s] Undamped Natural Frequency
k_roll = (omeg_n_roll^2)*m; % Spring constant
C_cr_roll = 2*sqrt(k_roll*m); % Critical Damping constant
C_roll = ksi_roll*C_cr_roll; % Damping constant
period_roll = 2*pi/omeg_roll; % [s] Period of oscilatory movement
t_halve_roll = 0.693/abs(eta_roll); % [s] Time for halving amplitude

fprintf ('Roll Undamped Natural Frequency [rad/s]: %g', omeg_n_roll);
fprintf ('\n');
fprintf ('Roll Damping Ratio: %g', ksi_roll);
fprintf ('\n');
fprintf ('Roll Spring constant: %g', k_roll);
fprintf ('\n');
fprintf ('Roll Critical Damping constant: %g', C_cr_roll);
fprintf ('\n');
fprintf ('Roll Damping constant: %g', C_roll);
fprintf ('\n');
fprintf ('Roll Damped Natural Frequency [rad/s]: %g', omeg_roll);
fprintf ('\n');
fprintf ('Period of Oscillation of the Roll Motion [s]: %g', period_roll);
fprintf ('\n');
fprintf ('Roll Time for halving amplitude [s]: %g', t_halve_roll);
fprintf ('\n');
fprintf ('¨¨¨¨¨¨¨¨¨¨¨¨\n\n');

%¨¨SPIRAL¨¨
fprintf ('SPIRAL PROPERTIES');
fprintf ('\n\n');

fprintf ('Spiral Eigenvalues:');
fprintf ('\n');
lamb_spir = lamb_spir

eta_spir = real(lamb_spir);
omeg_spir = imag(lamb_spir); % [rad/s] Damped Natural FrequEncy

ksi_spir = sqrt(eta_spir^2/(eta_spir^2 + omeg_spir^2)); % Damping Ratio
omeg_n_spir = -eta_spir/ksi_spir; % [rad/s] Undamped Natural Frequency
k_spir = (omeg_n_spir^2)*m; % Spring constant
C_cr_spir = 2*sqrt(k_spir*m); % Critical Damping constant
C_spir = ksi_spir*C_cr_spir; % Damping constant
period_spir = 2*pi/omeg_spir; % [s] Period of oscilatory movement
t_halve_spir = 0.693/abs(eta_spir); % [s] Time for halving amplitude

    %*Spiral Avoidance
    Cn_beta_dyn_rad = (Cn_beta -
(I_zz/I_xx)*Cl_beta*tan(Alpha_rad))*cos(Alpha_rad); % [1/rad]
    Cn_beta_dyn = Cn_beta_dyn_rad/57.29579; % [1/°]


fprintf ('Spiral Undamped Natural Frequency [rad/s]: %g', omeg_n_spir);
fprintf ('\n');
fprintf ('Spiral Damping Ratio: %g', ksi_spir);
```

```
fprintf ('\n');
fprintf ('Spiral Spring constant: %g', k_spir);
fprintf ('\n');
fprintf ('Spiral Critical Damping constant: %g', C_cr_spir);
fprintf ('\n');
fprintf ('Spiral Damping constant: %g', C_spir);
fprintf ('\n');
fprintf ('Spiral Damped Natural Frequency [rad/s]: %g', omeg_spir);
fprintf ('\n');
fprintf ('Period of Oscillation of the Spiral Motion [s]: %g', period_spir);
fprintf ('\n');
fprintf ('Spiral Time for halving amplitude [s]: %g', t_halve_spir);
fprintf ('\n\n');
fprintf ('Cn_beta_dyn: for avoid the Spiral mode this parameter must be > 0
[1/°]: %g', Cn_beta_dyn);
fprintf ('\n');
fprintf ('¨¨¨¨¨¨¨¨¨¨¨¨\n\n');

%¨¨DUTCH ROLL¨¨
fprintf ('DUTCH ROLL PROPERTIES');
fprintf ('\n\n');

fprintf ('Dutch Roll Eigenvalues:');
fprintf ('\n');
lamb_dut = lamb_dut

eta_dut = real(lamb_dut);
omeg_dut = imag(lamb_dut); % [rad/s] Damped Natural FrequEncy

ksi_dut = sqrt(eta_dut^2/(eta_dut^2 + omeg_dut^2)); % Damping Ratio
omeg_n_dut = -eta_dut/ksi_dut; % [rad/s] Undamped Natural Frequency
k_dut = (omeg_n_dut^2)*m; % Spring constant
C_cr_dut = 2*sqrt(k_dut*m); % Critical Damping constant
C_dut = ksi_dut*C_cr_dut; % Damping constant
period_dut = 2*pi/omeg_dut; % [s] Period of oscilatory movement
t_halve_dut = 0.693/abs(eta_dut); % [s] Time for halving amplitude
N_halve_dut = (1/period_dut)*t_halve_dut; % Cilce Number for halving amplitude

fprintf ('Dutch Roll Undamped Natural Frequency [rad/s]: %g', omeg_n_dut);
fprintf ('\n');
fprintf ('Dutch Roll Damping Ratio: %g', ksi_dut);
fprintf ('\n');
fprintf ('Dutch Roll Spring constant: %g', k_dut);
fprintf ('\n');
fprintf ('Dutch Roll Critical Damping constant: %g', C_cr_dut);
fprintf ('\n');
fprintf ('Dutch Roll Damping constant: %g', C_dut);
fprintf ('\n');
fprintf ('Dutch Roll Damped Natural Frequency [rad/s]: %g', omeg_dut);
fprintf ('\n');
fprintf ('Period of Oscillation of the Dutch Roll Motion [s]: %g',
period_dut);
fprintf ('\n');
fprintf ('Dutch Roll Time for halving amplitude [s]: %g', t_halve_dut);
fprintf ('\n');
```

```
fprintf ('Dutch Roll Cicle Number for halving amplitude: %g', N_halve_dut);
fprintf ('\n');
fprintf ('¨¨¨¨¨¨¨¨¨¨¨¨\n\n');

%*Plots*
disp_roll = input ('Inicial displacement (perturbation) for Roll motion [°]: '
);
duration_rol = input ('Duration of the Roll Motion Analysis [s]: ' );

disp_spir = input ('Inicial displacement (perturbation) for Spiral motion [°]:
' );
duration_spi = input ('Duration of Spiral Motion Analysis [s]: ' );

disp_dut = input ('Inicial displacement (perturbation) for Dutch Roll motion
[°]: ' );
duration_dut = input ('Duration of the Dutch-Roll Motion Analysis [s]: ' );

disp_roll_rad = disp_roll*0.01745329; % [rad] Inicial displacement
(perturbation) regarding neutral position
disp_spir_rad = disp_spir*0.01745329; % [rad] Inicial displacement
(perturbation) regarding neutral position
disp_dut_rad = disp_dut*0.01745329; % [rad]

time_rol = 0:0.1:duration_rol;
time_spi = 0:0.1:duration_spi;
time_dut = 0:0.1:duration_dut;

phi_roll_rad = disp_roll_rad*exp(-
time_rol./(2*(m/C_roll))).*cos(omeg_n_roll*time_rol); % [rad] Instantaneous
Position
    phi_roll = phi_roll_rad*57.2958; % [°]
psi_spir_rad = disp_spir_rad*exp(-
time_spi./(2*(m/C_spir))).*cos(omeg_n_spir*time_spi); % [rad] Instantaneous
Position
    psi_spir = psi_spir_rad*57.2958; % [°]
betphi_dut_rad = disp_dut_rad*exp(-
time_dut./(2*(m/C_dut))).*cos(omeg_dut*time_dut); % [rad] Instantaneous
Position = betphi_dut_rad
    betphi_dut = betphi_dut_rad*57.2958; % [°]

figure (10);
plot (time_rol,phi_roll);
title ('ROLL MOTION');
xlabel ('TIME [s]');
ylabel ('PHI [°]');
hold on;

figure (11);
plot (time_spi,psi_spir);
title ('SPIRAL MOTION');
xlabel ('TIME [s]');
ylabel ('BETA [°]');
hold on;
```

```
figure (12);
plot (time_dut,betphi_dut);
title ('DUTCH ROLL ');
xlabel ('TIME [s]');
ylabel ('DISPLACEMENT [°]');
hold on;

fprintf ('-----------------------------------------------------------------------------------------------------------\n');
%¨¨¨¨¨¨¨¨¨¨¨¨¨¨¨¨¨¨¨¨¨¨¨¨¨¨¨¨¨¨¨¨¨¨¨¨¨¨¨¨¨¨¨¨¨¨¨¨¨¨¨¨¨¨¨¨¨¨¨¨¨¨¨¨¨¨¨¨¨¨¨¨¨¨¨¨¨¨
fprintf
('_____________________________________________________________________________________________\n\n\n');
%__________________________________________________________________________
end
end
%______________________________PERFORMANCE ________________________________
if (main_menu == 1 | main_menu == 5)
fprintf
('__________________________________________PERFORMANCE________________________________________________\n\n');

%¨¨¨¨¨¨¨¨¨¨¨¨¨¨¨¨¨¨¨¨¨¨¨¨¨¨¨¨¨¨EXCESS POWER CURVE¨¨¨¨¨¨¨¨¨¨¨¨¨¨¨¨¨¨¨¨¨¨¨¨¨¨¨¨
fprintf ('-------------------------------------EXCESS POWER CURVE-----------------------------------------\n\n');

%¨¨Equivalent-Thrust Power¨¨
EQ_T_POW = T_Fli_lev.*V_T;

%¨¨Equivalent-Drag Power¨¨
EQ_D_POW = D_AIRPLANE.*V_T;

%¨¨Excess Power¨¨
EXC_POW = EQ_T_POW - EQ_D_POW;
EXC_T = T_Fli_lev - D_AIRPLANE;

%*Plots*
figure (13)
plot (VEL,EQ_T_POW,VEL,EQ_D_POW,VEL,EXC_POW)
title ('EXCESS POWER CURVE');
xlabel ('FLIGHT SPEED [km/h]');
ylabel ('POWER [W]');
legend ('Equivalent-Thrust Power','Equivalent-Drag Power','Excess Power');
hold on

figure (14)
plot (VEL,T_Fli_lev,VEL,D_AIRPLANE,VEL,EXC_T)
title ('EXCESS THRUST CURVE');
xlabel ('FLIGHT SPEED [km/h]');
ylabel ('THRUST [N]');
legend ('Actual Propeller Thrust','Airplane Total Drag','Excess Thrust');
hold on
```

```
fprintf ('-------------------------------------------------------------------
--------------------------\n\n');
%……….……….……….……….……….……….……….……….……….……….……….……….……….……….……….……….……

%……….……….……….……….……TAKE-OFF DISTANCE……….……….……….……….……….……
fprintf ('-----------------------------------TAKE-OFF DISTANCE-------------
--------------------------\n\n');

CD_0 = CD_0_FUS + CD_0_W_LOW_MY + CD_0_W_UP_MY + CD_0_CAN_LOW_MY +
CD_0_CAN_UP_MY + CD_FAIR_CAN + CD_0_VT_LEF_MY + CD_0_VT_RIG_MY + CD_VT_BOOM +
CD_LGEAR + CD_prop;

    slugFt3_kgm3 = 515.3788; % Slug/ft3 -> kg/m^3
    kgm3_slugFt3 = 0.00194032; % kg/m^3 -> Slug/ft3

    %-ISA ATMOSPHERE-
    TEMP_TOF = T_SEA - (0.0019812.*H_run); % Flight Level ISA Temperature [K]
    TETA_TOF = TEMP_TOF./T_SEA; % Temperature Ratio
    DELTA_TOF = (TETA_TOF.^(5.2561)); % Pressure Ratio
    SIGMA_TOF = DELTA_TOF./TETA_TOF; % Density Ratio
    RHO_TOF = RHO_SEAL.*SIGMA_TOF; % Air Density [Kg/m^3]

f_TO = 1; % Table 5.1 Roskam Part VII
Obst_tof = input ('Take-off Obstacle Height [ft] (Standard = 50ft): ' );
Mi_g = input ('Runway Coefficient of Rolling Friction: ' );

CL_max = CL_AIRPLANE(3); % Airplane Stall Lift Coefficient
V_S_TOF = sqrt((2*W)/(RHO_TOF*S_aero_W*CL_max)); % [m/s] Airplane Stall Speed
    V_S_TOF_ft_s = V_S_TOF*3.28084; % [ft/s]
V_3_ft_s = V_LOF_const_ft_s; % [ft/s]
    V_3_m_s = V_3_ft_s*0.3048; % [m/s]
V_T_Tof = sqrt((V_3_m_s.^2) + (V_wind.^2)); % [m/s] Total Take-off Speed

ETA_prop_Tof = 0;
cont_tof = 0;
for (V = 0:0.1:V_LOF_const)

        Eta_prop_Tof = ((1.6*10^-13)*V^5)-((4.6*10^-10)*V^4)+((2.9*10^-
7)*V^3)-((8.8*10^-5)*V^2)+(0.014*V)-0.053;

        ETA_prop_Tof = ETA_prop_Tof + Eta_prop_Tof;
        cont_tof = cont_tof +1;

end

Eta_prop_TOF = ETA_prop_Tof/cont_tof;

POWER_Tof_run = POWER_Tof_hp*Eta_prop_TOF*sqrt(RHO_TOF/RHO_SEAL); % [hp]
Available Power at the Runway level during take-off
    POWER_Tof_run_Wat = POWER_Tof_run*745.6999; % [Watt]
T_barr =
4.6*POWER_Tof_run*(((SIGMA_TOF*N_eng*(Prop_Diam_ft^2))/POWER_Tof_run)^(1/3));
```

```
F_N_grou_i = (POWER_Tof_run_Wat/V_3_m_s)*1.2; % Static Thrust Guess
F_N_grou_f = POWER_Tof_run_Wat/V_3_m_s;
F_N_TOF = (F_N_grou_i + F_N_grou_f)/2;

    CD_ground = CD_AIRPLANE(1); % CD for the Airplane running
    D_ground = 0.5*RHO_TOF.*CD_ground*(S_aero_W).*(V_T_Tof.^2);

Gam_LOF = (F_N_TOF - D_ground)/W;
Mi_g_corr = Mi_g + 0.72*(CD_0/CL_max);

%¨¨Total Take-off Distance¨¨
Num_TOF = ((V_3_ft_s/V_S_TOF_ft_s)^2)*(W_lb/S_W_ft)*(((T_barr/W_lb) -
Mi_g_corr)^-1) + 1.414;
Denom_TOF = (Obst_tof*(RHO_TOF*kgm3_slugFt3)*g_ft*CL_max)*(1 + 1.414*Gam_LOF);

S_TOF_ft = f_TO*Obst_tof*((1/Gam_LOF) + Num_TOF/Denom_TOF); % [ft]
S_TOF = S_TOF_ft*0.3048; % [m]

    %¨¨Ground Take-off Distance¨¨
    S_T_G = S_TOF/1.66; % [m]

    %¨¨Airborne Take-off Distance¨¨
    S_T_A = S_TOF - S_T_G; % [m]

    %¨¨Take-off Time¨¨
    a_i = F_N_grou_i/(W/g); % [m/s^2] Airplane initial aceleration on ground
    a_f = (F_N_grou_f - D_ground)/(W/g); % [m/s^2] Airplane final aceleration
on ground
    a = (a_i + a_f)/2;

    t_S_TOF = (V_3_m_s - 0)/a; % [s] Time to take-off running ground

    %¨¨Take-off Gas comsumption¨¨
    SFC_TOF_rated = ((SFC_CRUZ - SFC_TOF)*((Pow_perc_Tof - 100)/(70 - 100))) +
SFC_TOF;
    GAS_TOF = SFC_TOF_rated*t_S_TOF*POWER_Tof;

fprintf ('Airplane Ground running Distance [m]: %g', S_T_G);
fprintf ('\n');
fprintf ('Airplane Airborne Distance [m]: %g', S_T_A);
fprintf ('\n');
fprintf ('Airplane Total Take-off Distance [m]: %g', S_TOF);
fprintf ('\n');
fprintf ('Airplane Total Take-off Distance Time [s]: %g', t_S_TOF);
fprintf ('\n');
fprintf ('Airplane Gas comsumption durng the Take-off Phase [kg]: %g',
GAS_TOF);
fprintf ('\n\n');

fprintf ('-----------------------------------------------------------------
----------------------------\n\n');
%¨¨¨¨¨¨¨¨¨¨¨¨¨¨¨¨¨¨¨¨¨¨¨¨¨¨¨¨¨¨¨¨¨¨¨¨¨¨¨¨¨¨¨¨¨¨¨¨¨¨¨¨¨¨¨¨¨¨¨¨¨¨¨¨¨¨¨¨¨¨¨¨¨¨¨¨¨¨¨¨¨¨
```

```
%¨¨¨¨¨¨¨¨¨¨¨¨¨¨¨¨¨¨¨¨¨¨¨¨¨¨¨¨¨¨¨¨¨¨¨¨¨¨¨¨¨¨¨¨¨¨¨¨¨¨¨¨¨CLIMB¨¨¨¨¨¨¨¨¨¨¨¨¨¨¨¨¨¨¨¨¨¨¨¨¨¨¨¨¨¨¨¨¨¨¨¨¨¨¨¨¨¨¨¨¨¨¨¨
fprintf ('--------------------------------------------CLIMB--------------------
----------------------------\n\n');

%¨¨Rate of Climb¨¨
Cont = 0;
SIG_Climb = 0;
for H_Climb = H_run:0.1:H;

    %-ISA ATMOSPHERE-
    T_SEA_CILMB = 15+273.15; % Sea Level Temperature [K]
    TEMP_CLIMB = T_SEA_CILMB - (0.0019812.*H_Climb); % Flight Level ISA
Temperature [K]
    TETA_CLIMB = TEMP_CLIMB./T_SEA_CILMB; % Temperature Ratio
    DELTA_CLIMB = (TETA_CLIMB.^(5.2561)); % Pressure Ratio
    SIGMA_Climb = DELTA_CLIMB./TETA_CLIMB; % Density Ratio
    RHO_CLIMB = RHO_SEAL.*SIGMA_Climb; % Air Density [Kg/m^3]

    Cont = Cont + 1;
    SIG_Climb = SIG_Climb + SIGMA_Climb;

end

SIGMA_CLIMB = SIG_Climb/Cont;

RC = 33000*((Eta_prop_climb/(W_lb/POWER_Climb_hp)) -
(((W_lb/S_W_ft)^0.5)/(19*((CL_AIRPLANE(4)^(3/2))/CD_AIRPLANE(4))*SIGMA_CLIMB^0
.5)));

t_Climb_Rate = (H - H_run)/RC; % [min]
    t_Climb_Rate_s = t_Climb_Rate*60; % [s]
SFC_CLIMB = ((SFC_CRUZ - SFC_TOF)*((Pow_perc_Climb - 100)/(70 - 100))) +
SFC_TOF;
GAS_Climb_Rate = SFC_CLIMB*t_Climb_Rate_s*POWER_Climb;

fprintf ('Airplane Rate of Climb [ft/min]: %g', RC);
fprintf ('\n');
fprintf ('Airplane Climb Time for Reach the Cruising Flight Level [s]: %g',
t_Climb_Rate_s);
fprintf ('\n');
fprintf ('Airplane Gas comsumption durng the Climb Phase [kg]: %g',
GAS_Climb_Rate);
fprintf ('\n\n');

    %¨¨Maximum Rate of Climb¨¨
    fprintf ('          ---Maximum Rate of Climb---\n\n');

    CL_3_2_CD_max = (1.345*((AR_W*e_W)^(3/4)))/(CD_0^0.25);
    CL_3_2_CD = (CL_AIRPLANE(4)^(3/2))/CD_AIRPLANE(4);

    fprintf ('          Airplane Required {(CL^3/2)/CD}_max: %g',
CL_3_2_CD_max);
    fprintf ('\n');
```

```
    fprintf ('          Airplane Actual {(CL^3/2)/CD}: %g', CL_3_2_CD);
    fprintf ('\n\n');

%¨¨Climb Gradient¨¨
CGR_rad = (-((L_AIRPLANE(4)/D_AIRPLANE(4))^-1)) +
(((CL_AIRPLANE(4)^0.5)*18.97*Eta_prop_climb*SIGMA^0.5)/((W_lb/POWER_Climb_hp)*
((W_lb/S_W_ft)^0.5)));
CGR = CGR_rad*(180/pi()); % [°]

fprintf ('Airplane Climb Gradient [°]: %g', CGR);
fprintf ('\n\n');

%¨¨Flight Ceiling¨¨

    %¨¨Service Ceiling¨¨
    RC_SERV = 3000; % [ft/min] Initial Rate of Climb for the iteration
    H_SERV = 0; % [ft] Initial Altitude for the iteration
    RHO_SERV = RHO_SEAL; % [Kg/m^3] Initial Air Density for the iteration

    while RC_SERV > 100 % (ft/min)

        %-ISA ATMOSPHERE-
        T_SEA_SERV = 15+273.15; % Sea Level Temperature [K]
        TEMP_SERV = T_SEA_SERV - (0.0019812.*H_SERV); % Flight Level ISA
Temperature [K]
        TETA_SERV = TEMP_SERV./T_SEA_SERV; % Temperature Ratio
        DELTA_SERV = (TETA_SERV.^(5.2561)); % Pressure Ratio
        SIGMA_SERV = DELTA_SERV./TETA_SERV; % Density Ratio
        RHO_SERV = RHO_SEAL.*SIGMA_SERV; % Air Density [Kg/m^3]

        POWER_hp_SERV =
POWER_Climb*Eta_prop_climb*sqrt(RHO_SERV/RHO_SEAL)*0.001341022;
        RC_SERV = 33000*((Eta_prop_climb/(W_lb/POWER_hp_SERV)) -
(((W_lb/S_W_ft)^0.5)/(19*((CL_AIRPLANE(4)^(3/2))/CD_AIRPLANE(4))*SIGMA_SERV^0.
5)));
        H_SERV = H_SERV + 0.1;

    end

    fprintf ('Airplane Service Ceiling [ft]: %g', H_SERV);
    fprintf ('\n');
    fprintf ('Airplane Rate of Climb at the Service Ceiling [ft/min]: %g',
RC_SERV);
    fprintf ('\n\n');

    %¨¨Absolute Ceiling¨¨
    RC_ABS = 3000; % [ft/min] Initial Rate of Climb for the iteration
    H_ABS = 0; % [ft] Initial Altitude for the iteration
    RHO_ABS = RHO_SEAL; % [Kg/m^3] Initial Air Density for the iteration

    while RC_ABS > 0.1 % (ft/min)

        %-ISA ATMOSPHERE-
```

```
        T_SEA_ABS = 15+273.15; % Sea Level Temperature [K]
        TEMP_ABS = T_SEA_ABS - (0.0019812.*H_ABS); % Flight Level ISA
Temperature [K]
        TETA_ABS = TEMP_ABS./T_SEA_ABS; % Temperature Ratio
        DELTA_ABS = (TETA_ABS.^(5.2561)); % Pressure Ratio
        SIGMA_ABS = DELTA_ABS./TETA_ABS; % Density Ratio
        RHO_ABS = RHO_SEAL.*SIGMA_ABS; % Air Density [Kg/m^3]

        POWER_hp_ABS =
POWER_Climb*Eta_prop_climb*sqrt(RHO_ABS/RHO_SEAL)*0.001341022;
        RC_ABS = 33000*((Eta_prop_climb/(W_lb/POWER_hp_ABS)) -
(((W_lb/S_W_ft)^0.5)/(19*((CL_AIRPLANE(4)^(3/2))/CD_AIRPLANE(4))*SIGMA_ABS^0.5
)));
        H_ABS = H_ABS + 0.1;

    end

    fprintf ('Airplane Absolute Ceiling [ft]: %g', H_ABS);
    fprintf ('\n');
    fprintf ('Airplane Rate of Climb at the Absolute Ceiling [ft/min]: %g',
RC_ABS);
    fprintf ('\n\n');

fprintf ('------------------------------------------------------------------
-----------------------------\n\n');
%..........................................................................

%.....................................LOITER.....................................
fprintf ('-----------------------------------------LOITER--------------------
-----------------------------\n\n');

t_Loiter = input ('Loiter Time (12 minutes assumed at Conceptual Design)
[minute]: ' );
    t_Loiter_s = t_Loiter*60;

GAS_Loiter = SFC_LOIT*t_Loiter_s*POWER_Loit;

fprintf ('\n');
fprintf ('Airplane Gas comsumption durng the Loiter Phase [kg]: %g',
GAS_Loiter);
fprintf ('\n\n');

fprintf ('------------------------------------------------------------------
-----------------------------\n\n');
%..........................................................................

%.....................................DESCENT....................................
fprintf ('-----------------------------------------DESCENT-------------------
-----------------------------\n\n');

RHO_DESC = RHO_SEAL.*SIGMA_CLIMB; % [Kg/m^3] Mean air density at descent phase

CL_desc = CL_AIRPLANE(6); % Airplane CL at descent phase
```

```
    CL_desc_abs = abs(CL_desc);
CD_desc = CD_AIRPLANE(6); % Airplane CD at descent phase

Gam_desc = atan(CD_desc/CL_desc);
    Gam_desc_deg = Gam_desc*57.2958; % [°] Airplane Descent Path Angle

RD =
((W_lb/S_W_ft)*(2/(RHO_DESC*kgm3_slugFt3))*((CD_desc^2)/(CL_desc_abs^(3/2)))*(
cos(Gam_desc)^3))^0.5; % [ft/s]
    RD_min = RD*60; % [ft/min]

t_Desc = (H - H_run)/RD; % [s]

SFC_DESC = SFC_LAND;
GAS_Desc = SFC_DESC*t_Desc*POWER_Desc;

fprintf ('Airplane Rate of Descent [ft/min]: %g', RD_min);
fprintf ('\n');
fprintf ('Airplane Descent Path Angle [°]: %g', Gam_desc_deg);
fprintf ('\n');
fprintf ('Airplane Descent Time from the Flight Level for the Runway Level
[s]: %g', t_Desc);
fprintf ('\n');
fprintf ('Airplane Gas comsumption durng the Descent Phase [kg]: %g',
GAS_Desc);
fprintf ('\n\n');

fprintf ('-------------------------------------------------------------------
---------------------------\n\n');
%……….……….……….……….……….……….……….……….……….……….……….……….……….……….……….……….……

%……….……….……….……….……..LANDING DISTANCE……..……….……….……….……….……….……….……
fprintf ('-------------------------------------LANDING DISTANCE--------------
---------------------------\n\n');

%¨¨Ground Distance¨¨
V_TD = V_3_m_s; % [m/s] Touchdown Speed
V_S_LAD = V_S_TOF; % [m/s] Landing Stall Speed
S_G_land_ft = 0.265*((V_S_LAD*1.943844)^2); % [ft]
S_G_land = S_G_land_ft*0.3048; % [m]

D_ground_land = D_AIRPLANE(1);

F_B_grou_i = -(POWER_Tof_run_Wat/V_TD); % Brake force guess
F_B_grou_f = 0;

a_i = (F_B_grou_i - D_ground_land)/(W/g); % [m/s^2] Airplane final aceleration
on ground
a_f = F_B_grou_f/(W/g); % [m/s^2] Airplane initial aceleration on ground
a = (a_i + a_f)/2; % [m/s^2]

t_S_G_land = (0 - V_TD)/a; % [s] Time to take-off running ground
```

```
fprintf ('Airplane Ground running Distance [m]: %g', S_G_land);
fprintf ('\n');
fprintf ('Airplane Ground running Time [s]: %g', t_S_G_land);
fprintf ('\n\n');

%¨¨Airborne Distance & Total Landing Distance¨¨
S_LAND_TOT_FT = 1.938*S_G_land_ft; % [ft]
S_LAND_TOT = S_LAND_TOT_FT*0.3048; % [m]

S_A_land = S_LAND_TOT - S_G_land; % [m]

V_A = 1.3*V_S_LAD; % [m/s] Approach Speed
t_S_A_land = S_A_land/V_A; % [s]

t_Tot_land = t_S_G_land + t_S_A_land; % [s]
GAS_land = SFC_LAND*t_Tot_land*(53.3/100)*POW_max;

fprintf ('Airplane Air Distance [m]: %g', S_A_land);
fprintf ('\n');
fprintf ('Airplane Air Distance Time [s]: %g', t_S_A_land);
fprintf ('\n\n');
fprintf ('Airplane Total Landing Distance [m]: %g', S_LAND_TOT);
fprintf ('\n');
fprintf ('Airplane Total Landing Distance Time [s]: %g', t_Tot_land);
fprintf ('\n');
fprintf ('Airplane Gas comsumption durng the Landing Phase [kg]: %g',
GAS_land);
fprintf ('\n\n');

fprintf ('---------------------------------------------------------------------
----------------------------\n\n');
%¨¨¨¨¨¨¨¨¨¨¨¨¨¨¨¨¨¨¨¨¨¨¨¨¨¨¨¨¨¨¨¨¨¨¨¨¨¨¨¨¨¨¨¨¨¨¨¨¨¨¨¨¨¨¨¨¨¨¨¨¨¨¨¨¨¨¨¨¨¨¨¨¨¨¨¨

%¨¨¨¨¨¨¨¨¨¨¨¨¨¨¨¨¨¨¨¨¨¨¨¨¨¨¨¨¨¨¨¨¨¨CRUISING¨¨¨¨¨¨¨¨¨¨¨¨¨¨¨¨¨¨¨¨¨¨¨¨¨¨¨¨¨¨¨¨
fprintf ('------------------------------------------CRUISING------------------
----------------------------\n\n');

f_mp = 326; % For nautical miles

if (Pow_perc < 70)
    SFC_CRUS_rated = ((SFC_LAND_lb_h - SFC_CRUZ_lb_h)*((Pow_perc - 70)/(53 -
70))) + SFC_CRUZ_lb_h;
end

if (Pow_perc >= 70)
    SFC_CRUS_rated = ((SFC_CRUZ_lb_h - SFC_TOF_lb_h)*((Pow_perc - 100)/(70 -
100))) + SFC_TOF_lb_h;
end

W_in = W - (GAS_TOF + GAS_Climb_Rate + GAS_Loiter + GAS_Desc+GAS_land)*g; %
[N]
W_gas_in = W_gas - (GAS_TOF + GAS_Climb_Rate + GAS_Loiter + GAS_Desc +
GAS_land)*g; % [N]
```

```
W_end = W_in - W_gas_in; % [N]

R_NM =
f_mp*(Eta_prop/SFC_CRUS_rated)*(L_AIRPLANE(5)/D_AIRPLANE(5))*log(W_in/W_end);
% [Nautical Mile]
    R = R_NM*1.852;

t_R = R/V_T_km;

fprintf ('Airplane Range [km]: %g', R);
fprintf ('\n');
fprintf ('Airplane Cruise Flight Time [Hour]: %g', t_R);
fprintf ('\n\n');

fprintf ('-------------------------------------------------------------------
----------------------------\n\n');
%……….……….……….……….……….……….……….……….……….……….……….……….……….……….……….……….……….……….……
fprintf
('_____________________________________________________________________________
_____________________\n\n');
end
end
%_____________________________________________________________________________
end % Elevators deflection "FOR LOOP"
end % Canards Incidence "FOR LOOP"
end % Flap deflection "FOR LOOP"
end % Angle of Attack (Alpha) "FOR LOOP"
```

APPENDIX D

All the wings airfoil aerodynamic coefficients data were obtained by simulating the flight conditions at the software XFLR5 V6, these flight conditions are provided next. Will be indicated too, some results for some angles of attack for the stall condition as example, for the other flight conditions and airfoils these data will not be provided.

Stall data for the airfoil NACA 65-418 "a-0"

XFLR5 v6.09.01 beta

Calculated polar for: Naca 65-418a0.0 (Série 6) Type mean line (a)0 - By GNacaLt

1 1 Reynolds number fixed Mach number fixed

xtrf = 1.000 (top) 1.000 (bottom)
Mach = 0.056 Re = 1.060 e 6 Ncrit = 9.000

alpha	CL	CD	CDp	Cm	Top Xtr	Bot Xtr	Cpmin	Chinge	XCp
-12.000	-0.9726	0.02383	0.01835	-0.0405	0.7697	0.0185	-7.3375	0.0000	0.1919
-11.900	-0.9655	0.02357	0.01806	-0.0402	0.7675	0.0187	-7.2508	0.0000	0.1920
-11.800	-0.9584	0.02331	0.01776	-0.0400	0.7654	0.0188	-7.1645	0.0000	0.1921
-11.700	-0.9512	0.02306	0.01747	-0.0398	0.7634	0.0190	-7.0786	0.0000	0.1921
-11.600	-0.9438	0.02279	0.01719	-0.0395	0.7615	0.0192	-6.9925	0.0000	0.1922
-11.500	-0.9364	0.02254	0.01691	-0.0393	0.7594	0.0194	-6.9061	0.0000	0.1922
-11.400	-0.9288	0.02231	0.01665	-0.0391	0.7573	0.0195	-6.8194	0.0000	0.1922
-11.300	-0.9211	0.02208	0.01640	-0.0389	0.7553	0.0197	-6.7321	0.0000	0.1922
-11.200	-0.9133	0.02189	0.01617	-0.0387	0.7533	0.0198	-6.6437	0.0000	0.1922
-11.100	-0.9053	0.02172	0.01596	-0.0385	0.7515	0.0200	-6.5540	0.0000	0.1922
-11.000	-0.8972	0.02157	0.01578	-0.0383	0.7496	0.0201	-6.4634	0.0000	0.1921
-10.900	-0.8890	0.02143	0.01562	-0.0381	0.7478	0.0202	-6.3719	0.0000	0.1921
-10.800	-0.8806	0.02131	0.01548	-0.0380	0.7459	0.0203	-6.2801	0.0000	0.1920
-10.700	-0.8764	0.02039	0.01450	-0.0373	0.7441	0.0208	-6.2371	0.0000	0.1926
-10.600	-0.8694	0.02004	0.01413	-0.0370	0.7422	0.0211	-6.1582	0.0000	0.1927
-10.500	-0.8616	0.01981	0.01389	-0.0368	0.7404	0.0214	-6.0714	0.0000	0.1927
-10.400	-0.8534	0.01963	0.01369	-0.0366	0.7386	0.0216	-5.9823	0.0000	0.1927
-10.300	-0.8450	0.01947	0.01351	-0.0364	0.7368	0.0217	-5.8927	0.0000	0.1926
-10.200	-0.8365	0.01930	0.01334	-0.0362	0.7351	0.0219	-5.8033	0.0000	0.1924

-10.100	-0.8280	0.01913	0.01317	-0.0361	0.7333	0.0221	-5.7147	0.0000	0.1923
-10.000	-0.8194	0.01897	0.01299	-0.0359	0.7314	0.0223	-5.6270	0.0000	0.1922
-1.000	0.0877	0.00663	0.00183	-0.0317	0.6206	0.6401	-0.6933	0.0000	0.6175
-0.900	0.0995	0.00665	0.00184	-0.0319	0.6194	0.6434	-0.6995	0.0000	0.5749
-0.800	0.1113	0.00669	0.00185	-0.0321	0.6183	0.6465	-0.7057	0.0000	0.5413
-0.700	0.1232	0.00671	0.00186	-0.0323	0.6174	0.6491	-0.7119	0.0000	0.5141
-0.600	0.1349	0.00668	0.00186	-0.0325	0.6167	0.6517	-0.7181	0.0000	0.4918
-0.500	0.1467	0.00668	0.00187	-0.0326	0.6160	0.6540	-0.7243	0.0000	0.4730
-0.400	0.1586	0.00668	0.00187	-0.0328	0.6152	0.6565	-0.7308	0.0000	0.4570
-0.300	0.1705	0.00668	0.00188	-0.0330	0.6143	0.6588	-0.7373	0.0000	0.4432
-0.200	0.1824	0.00669	0.00188	-0.0332	0.6134	0.6610	-0.7439	0.0000	0.4312
-0.100	0.1943	0.00670	0.00188	-0.0335	0.6125	0.6628	-0.7504	0.0000	0.4207
0.000	0.2062	0.00670	0.00188	-0.0337	0.6115	0.6646	-0.7570	0.0000	0.4115
0.100	0.2179	0.00669	0.00188	-0.0338	0.6105	0.6667	-0.7635	0.0000	0.4032
0.200	0.2297	0.00669	0.00189	-0.0340	0.6096	0.6685	-0.7700	0.0000	0.3957
0.300	0.2416	0.00669	0.00189	-0.0342	0.6087	0.6699	-0.7765	0.0000	0.3890
0.400	0.2534	0.00669	0.00189	-0.0344	0.6078	0.6712	-0.7831	0.0000	0.3830
0.500	0.2653	0.00670	0.00189	-0.0346	0.6068	0.6724	-0.7896	0.0000	0.3774
0.600	0.2771	0.00672	0.00190	-0.0348	0.6059	0.6737	-0.7962	0.0000	0.3724
0.700	0.2890	0.00674	0.00190	-0.0350	0.6048	0.6749	-0.8027	0.0000	0.3678
0.800	0.3008	0.00677	0.00191	-0.0352	0.6036	0.6762	-0.8094	0.0000	0.3635
0.900	0.3126	0.00680	0.00193	-0.0355	0.6023	0.6774	-0.8161	0.0000	0.3596
1.000	0.3246	0.00681	0.00193	-0.0357	0.6015	0.6785	-0.8230	0.0000	0.3559
1.100	0.3364	0.00679	0.00193	-0.0359	0.6007	0.6799	-0.8298	0.0000	0.3525
1.200	0.3482	0.00677	0.00194	-0.0361	0.5996	0.6813	-0.8366	0.0000	0.3493
1.300	0.3600	0.00677	0.00194	-0.0363	0.5985	0.6826	-0.8434	0.0000	0.3464
1.400	0.3719	0.00676	0.00195	-0.0365	0.5974	0.6840	-0.8503	0.0000	0.3436
1.500	0.3837	0.00676	0.00196	-0.0367	0.5962	0.6855	-0.8572	0.0000	0.3409
1.600	0.3956	0.00677	0.00197	-0.0369	0.5950	0.6870	-0.8643	0.0000	0.3385
1.700	0.4074	0.00677	0.00197	-0.0371	0.5939	0.6885	-0.8715	0.0000	0.3361
1.800	0.4193	0.00678	0.00198	-0.0373	0.5927	0.6900	-0.8788	0.0000	0.3340
1.900	0.4311	0.00680	0.00199	-0.0375	0.5916	0.6915	-0.8867	0.0000	0.3319
2.000	0.4429	0.00682	0.00199	-0.0378	0.5904	0.6928	-0.8947	0.0000	0.3299
23.000	1.2679	0.16636	0.16332	-0.0470	0.0097	1.0000	-8.6311	0.0000	0.2413
23.100	1.2663	0.16818	0.16517	-0.0481	0.0097	1.0000	-8.6398	0.0000	0.2419
23.200	1.2650	0.16996	0.16698	-0.0492	0.0097	1.0000	-8.6499	0.0000	0.2425
23.300	1.2631	0.17187	0.16893	-0.0504	0.0097	1.0000	-8.6535	0.0000	0.2432
23.400	1.2612	0.17380	0.17089	-0.0515	0.0096	1.0000	-8.6558	0.0000	0.2439

23.500	1.2596	0.17566	0.17278	-0.0527	0.0096	1.0000	-8.6610	0.0000	0.2446
23.600	1.2579	0.17755	0.17471	-0.0539	0.0096	1.0000	-8.6641	0.0000	0.2453
23.700	1.2557	0.17958	0.17677	-0.0552	0.0096	1.0000	-8.6601	0.0000	0.2461
23.800	1.2538	0.18155	0.17877	-0.0564	0.0096	1.0000	-8.6587	0.0000	0.2469
23.900	1.2520	0.18349	0.18075	-0.0577	0.0096	1.0000	-8.6581	0.0000	0.2477
24.000	1.2496	0.18559	0.18289	-0.0591	0.0096	1.0000	-8.6490	0.0000	0.2486

Cruise data for the airfoil NACA 65-418 “a-0”

XFLR5 v6.09.01 beta

Calculated polar for: Naca 65-418a0.0 (Série 6) Type mean line (a)0 - By GNacaLt

1 1 Reynolds number fixed Mach number fixed

xtrf = 1.000 (top) 1.000 (bottom)
Mach = 0.191 Re = 2.966 e 6 Ncrit = 9.000

alpha	CL	CD	CDp	Cm	Top Xtr	Bot Xtr	Cpmin	Chinge	XCp
-10.000	-0.9136	0.01311	0.00777	-0.0293	0.6835	0.0175	-6.5701	0.0000	0.2041

APPENDIX E

All the canards airfoil aerodynamic coefficients data were obtained by simulating the flight conditions at the software XFLR5 V6, these flight conditions are provided next.

Stall data for the airfoil NACA 0009

XFLR5 v6.09.01 beta

Calculated polar for: NACA 0009

1 1 Reynolds number fixed Mach number fixed

xtrf = 1.000 (top) 1.000 (bottom)
Mach = 0.056 Re = 0.466 e 6 Ncrit = 9.000

alpha	CL	CD	CDp	Cm	Top Xtr	Bot Xtr	Cpmin	Chinge	XCp
-10.750	-1.0309	0.03739	0.03314	-0.0193	1.0000	0.0150	-7.3500	0.0000	0.2215

Cruise data for the airfoil NACA 0009

XFLR5 v6.09.01 beta

Calculated polar for: NACA 0009

1 1 Reynolds number fixed Mach number fixed

xtrf = 1.000 (top) 1.000 (bottom)
Mach = 0.191 Re = 1.304 e 6 Ncrit = 9.000

alpha	CL	CD	CDp	Cm	Top Xtr	Bot Xtr	Cpmin	Chinge	XCp
-10.000	-1.0847	0.01875	0.01422	-0.0114	1.0000	0.0090	-8.7942	0.0000	0.2300

APPENDIX F

All the vertical tails airfoil aerodynamic coefficients data were obtained by simulating the flight conditions at the software XFLR5 V6, these flight conditions are provided next.

Stall data for the airfoil NACA 0012

XFLR5 v6.09.01 beta

Calculated polar for: NACA 0012

1 1 Reynolds number fixed Mach number fixed

xtrf = 1.000 (top) 1.000 (bottom)
Mach = 0.057 Re = 0.791 e 6 Ncrit = 9.000

alpha	CL	CD	CDp	Cm	Top Xtr	Bot Xtr	Cpmin	Chinge	XCp
-10.000	-1.0704	0.01641	0.01047	-0.0075	1.0000	0.0253	-5.4770	0.0000	0.2320

Cruise data for the airfoil NACA 0012

XFLR5 v6.09.01 beta

Calculated polar for: NACA 0012

1 1 Reynolds number fixed Mach number fixed

xtrf = 1.000 (top) 1.000 (bottom)
Mach = 0.191 Re = 2.216 e 6 Ncrit = 9.000

alpha	CL	CD	CDp	Cm	Top Xtr	Bot Xtr	Cpmin	Chinge	XCp
-10.000	-1.1351	0.01259	0.00755	-0.0042	1.0000	0.0172	-6.1255	0.0000	0.2350

APPENDIX G

```
%--------------------------------------------------------------------------
                % UNIVERSIDADE FEDERAL DE UBERLÂNDIA - UFU
                    % FACULDADE DE ENGENHARIA MECÂNICA
              % CURSO DE GRADUAÇÃO EM ENGENHARIA AERONÁUTICA

            % DISCIPLINE: PROJETO DE CONCLUSÃO DE CURSO - FEMEC43100

% Author: Frederico Carnevalli De Miranda
%--------------------------------------------------------------------------
% Commencement Date: 10/12/2016
% Conclusion Date: 16/12/2016
%--------------------------------------------------------------------------

%************LANDING GEAR DIMENSIONING FOR THE AIRPLANE UFU-1**************

% This program estimate the Landing Gear system calculus for the airplane.

clear all;
close all;
clc;

%_____________________________________HEADING_____________________________________
fprintf ('##########PROGRAM FOR ESTIMATE THE LANDING GEAR SYSTEM DIMENSIONING
OF THE AIRPLANE UFU-1###########');
fprintf ('\n\n\n');
%_____________________________________________________________________________


%------------------------------MASS PROPERTIES-------------------------------
fprintf ('-----------------------------------------MASS PROPERTIES------------
---------------------------\n\n');

g = 9.801; % [m/s^2)

MTOW = input ('Airplane MTOW [Kgf] (600 kgf): ' );

fprintf ('Most Forward CG (~3.64m); Most Back CG (~3.92m)');
fprintf ('\n');
X_CG_fwd = input ('Airplane forward CG Position on X axix [m]: ' );
X_CG_aft = input ('Airplane rearward CG Position on X axix [m]: ' );
%Y_CG = :
%Z_CG = :

%I_xx = ;
%I_yy = ;
%I_zz = ;
fprintf ('-----------------------------------------------------------------------
---------------------------\n\n');
%--------------------------------------------------------------------------
```

```
%-------------------------LANDING GEAR POSITIONING-------------------------
fprintf ('-----------------------------------LANDING GEAR POSITIONING--------
---------------------------\n\n');

X_NLG = 0.493; % [m] Position of the Nose Landing Gear
X_MLG = 4.1; % [m] Position of the Main Landing Gear

B = X_MLG - X_NLG; % from [1; pg 267]
Nf = B - (X_MLG - X_CG_fwd);
Na = B - (X_MLG - X_CG_aft);
Mf = B - Nf;
Ma = B - Na;

MLG_LOADING_fwd = ((MTOW*(Nf/B))/MTOW)*100; % [%] % of Airplane Weight
suported by Main Landig Gear
MLG_LOADING_aft = ((MTOW*(Na/B))/MTOW)*100; % [%]
NLG_LOADING_fwd = ((MTOW*(Mf/B))/MTOW)*100; % [%] % of Airplane Weight
suported by Nose Landig Gear
NLG_LOADING_aft = ((MTOW*(Ma/B))/MTOW)*100; % [%]

fprintf ('\n');
fprintf ('Main Landig Gear FWD CG Airplane Weight Loading [Percent]: %g',
MLG_LOADING_fwd);
fprintf ('\n');
fprintf ('Main Landig Gear AFT CG Airplane Weight Loading [Percent]: %g',
MLG_LOADING_aft);
fprintf ('\n');
fprintf ('Nose Landig Gear FWD CG Airplane Weight Loading [Percent]: %g',
NLG_LOADING_fwd);
fprintf ('\n');
fprintf ('Nose Landig Gear AFT CG Airplane Weight Loading [Percent]: %g',
NLG_LOADING_aft);
fprintf ('\n\n');

fprintf ('-----------------------------------------------------------------
---------------------------\n\n');
%-------------------------------------------------------------------------

%-------------------------------TIRE SIZING-------------------------------
fprintf ('-----------------------------------------TIRE SIZING--------------
---------------------------\n\n');

%**Statitstical Approach**
fprintf ('***Statitstical Approach***\n\n');

    %**Main Leg**
    A_d = 5.1; % from [1; pg 266]
    B_d = 0.349;
    A_w = 2.3;
    B_w = 0.312;

    d_main = (A_d*((MTOW/2)^B_d))*1.3; % [cm] diameter for non prepared
runway; from [1; pg 267]
```

```
    w_main = (A_w*((MTOW/2)^B_w))*1.3; % [cm] widht for non prepared runway

    d_main_old = d_main*1.03; % [cm] diameter for aging; from [1; pg 269]
    w_main_old = w_main*1.04; % [cm] widht for aging

    fprintf ('Diameter for Main Tire Selection [cm]: %g', d_main);
    fprintf ('\n');
    fprintf ('Widht for Main Tire Selection [cm]: %g', w_main);
    fprintf ('\n\n');
    fprintf ('Diameter for Main Tire Fairing dimensioning [cm]: %g',
d_main_old);
    fprintf ('\n');
    fprintf ('Widht for Main Tire Fairing dimensioning [cm]: %g', w_main_old);
    fprintf ('\n\n');

    %**Nose Leg**
    d_nose = d_main*0.6; % [cm] diameter for non prepared runway; from [1; pg
267]
    w_nose = w_main*0.6; % [cm] widht for non prepared runway

    d_nose_old = d_nose*1.03; % [cm]
    w_nose_old = w_nose*1.04; % [cm]

    fprintf ('Diameter for Nose Tire Selection [cm]: %g', d_nose);
    fprintf ('\n');
    fprintf ('Widht for Nose Tire Selection [cm]: %g', w_nose);
    fprintf ('\n\n');
    fprintf ('Diameter for Nose Tire Fairing dimensioning [cm]: %g',
d_nose_old);
    fprintf ('\n');
    fprintf ('Widht for Nose Tire Fairing dimensioning [cm]: %g', w_nose_old);
    fprintf ('\n\n\n');

%**Loading Estimation**
fprintf ('***Loading Estimation***\n\n');

    %**Main Leg**
    if (MLG_LOADING_aft >= MLG_LOADING_fwd)

        W_main_max = (MTOW*(Na/B))/2; % [Kgf] maximum Load on each main tire
        W_main_max_lbs = W_main_max*2.204623; % [Lbs]
        W_main_min = (MTOW*(Nf/B))/2; % [Kgf] minimum Load on each main tire
        W_main_min_lbs = W_main_min*2.204623; % [Lbs]

    else
        W_main_max = (MTOW*(Nf/B))/2;
        W_main_max_lbs = W_main_max*2.204623;
        W_main_min = (MTOW*(Na/B))/2;
        W_main_min_lbs = W_main_min*2.204623;
    end

    fprintf ('Maximum Load on Main Gear Tire [Kgf]: %g', W_main_max);
    fprintf ('\n');
    fprintf ('Maximum Load on Main Gear Tire [Lbs]: %g', W_main_max_lbs);
```

```
    fprintf ('\n');
    fprintf ('Minimum Load on Main Gear Tire [Kgf]: %g', W_main_min);
    fprintf ('\n');
    fprintf ('Minimum Load on Main Gear Tire [Lbs]: %g', W_main_min_lbs);
    fprintf ('\n\n');

    %**Nose Leg**
    mi = 0.3; % standard brake friction coeficient
    a = 3.048; % [m/s^2] standard deceleration by brakes
    H = input ('Height between the CG and runway [m]: ' ); % [m] height
between the CG and runway

    if (NLG_LOADING_fwd >= NLG_LOADING_aft)

        W_nose_max = (MTOW*(Mf/B))/2; % [Kgf] maximum Load on nose tire
        W_nose_max_lbs = W_nose_max*2.204623; % [Lbs]
        W_nose_min = (MTOW*(Ma/B))/2; % [Kgf] minimum Load on nose tire
        W_nose_min_lbs = W_nose_min*2.204623; % [Lbs]
        W_nose_dyn = (a*H*W_nose_max)/(g*B); % [Kgf] Dynamic Braking Load on
nose tire
        W_nose_dyn_lbs = W_nose_dyn*2.204623; % [Lbs]

    else
        W_nose_max = (MTOW*(Ma/B))/2;
        W_nose_max_lbs = W_nose_max*2.204623;
        W_nose_min = (MTOW*(Mf/B))/2;
        W_nose_min_lbs = W_nose_min*2.204623;
        W_nose_dyn = (a*H*W_nose_max)/(g*B);
        W_nose_dyn_lbs = W_nose_dyn*2.204623;
    end

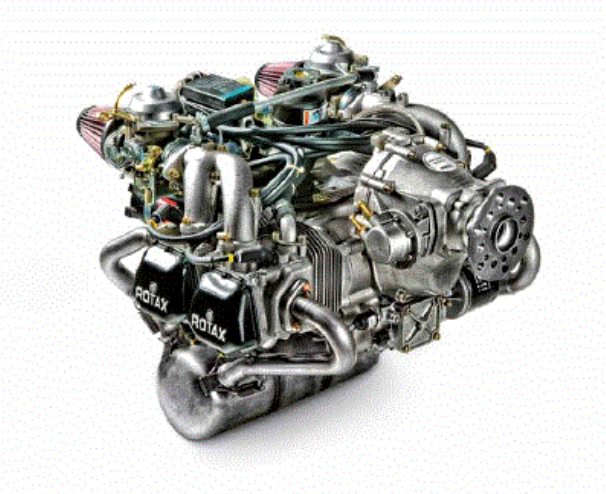
    fprintf ('Maximum Load on Nose Gear Tire [Kgf]: %g', W_nose_max);
    fprintf ('\n');
    fprintf ('Maximum Load on Nose Gear Tire [Lbs]: %g', W_nose_max_lbs);
    fprintf ('\n');
    fprintf ('Minimum Load on Nose Gear Tire [Kgf]: %g', W_nose_min);
    fprintf ('\n');
    fprintf ('Minimum Load on Nose Gear Tire [Lbs]: %g', W_nose_min_lbs);
    fprintf ('\n');
    fprintf ('Dynamic Braking Load on Nose Gear Tire [Kgf]: %g', W_nose_dyn);
    fprintf ('\n')
    fprintf ('Dynamic Braking Load on Nose Gear Tire [Lbs]: %g',
W_nose_dyn_lbs);
    fprintf ('\n\n\n')

fprintf ('-------------------------------------------------------------------
---------------------------\n\n');
%-------------------------------------------------------------------------
```

APPENDIX H

ENGINE TYPE 912 | 80 hp (UL/A/F)

ROTAX AIRCRAFT ENGINES



DESCRIPTION

- 4-cylinder
- 4-stroke liquid/air-cooled engine with opposed cylinders
- dry sump forced lubrication with separate oil tank, automatic adjustment by hydraulic valve tappet
- 2 carburetors
- mechanical fuel pump
- dual electronic ignition
- electric starter
- propeller speed reduction unit

FACTS

This series was BRP's first Rotax engine dedicated for aircraft application only. The Rotax 912 series is well regarded for its reliability and efficiency and is primarily targeted as the entry level engine in the light aviation industry. The 80 hp version of the Rotax 912 series offers a time between overhauls of 2.000 hours and is available as non-certified (Rotax 912 UL) as well as certified version according to FAR 33 (Rotax 912 F) and JAR 22 (Rotax 912 A).

ENGINE DATA

WEIGHT	kg	lb
engine with propeller speed reduction unit i=2.27 (opt. i=2.43)	55.4	122.0
overload clutch	1.7	3.7
exhaust system	4.0	8.8
external alternator	3.0	6.6
engine suspension frame	2.0	4.4
air guide hood	0.8	1.8
airbox	1.3	2.8

VERSION	PERFORMANCE			TORQUE			MAX RPM
	kW	ft. lb.	1/min	Nm	ft. lb.	1/min	1/min
912 UL[1]/F[2]/A[3]	59.6	80	5800	103	75.9	4800	5800

Limited for max. 5 min.

BORE		STROKE		DISPLACEMENT		FUEL
79.5 mm	3.13 in	61 mm	2.4 in	1211.2 cm³	73.91 cu. in.	min. MON 83 RON 91* min. AKI 87*

* leaded, unleaded, AVGAS 100LL or Ethanol 10

1) UL = non certified
2) F = certified acc. to FAR 33,
3) A = certified acc. to JAR 22

Picture: 912 UL - DCDI with options

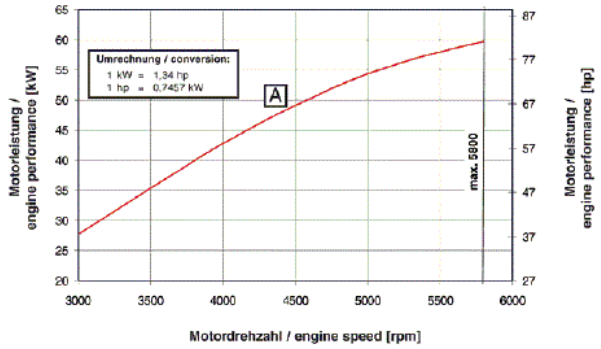
WWW.FLYROTAX.COM

® and TM are trademarks of BRP-Powertrain GmbH & Co. KG / © 2011 BRP-Powertrain GmbH & Co. KG / All rights reserved.

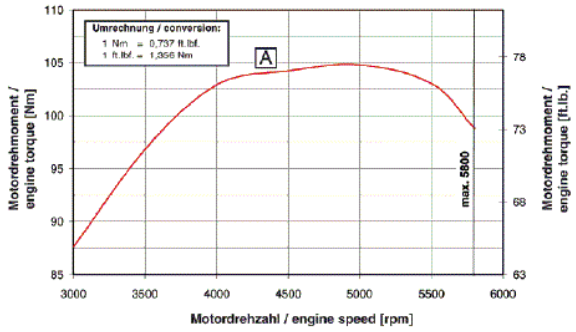
ENGINE TYPE 912 | 80 hp (UL/A/F)

ROTAX AIRCRAFT ENGINES

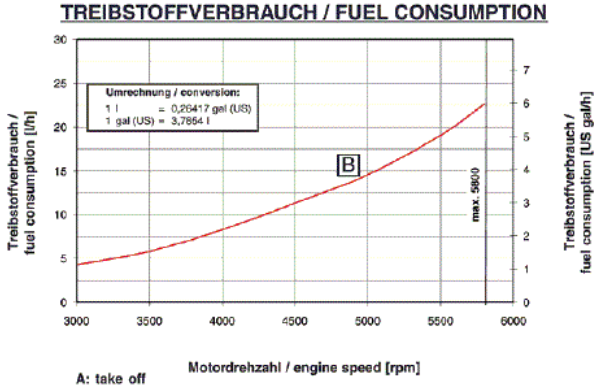
MOTORLEISTUNG / ENGINE PERFORMANCE



MOTORDREHMOMENT/ ENGINE TORQUE



TREIBSTOFFVERBRAUCH / FUEL CONSUMPTION



A: take off
B: propeller curve

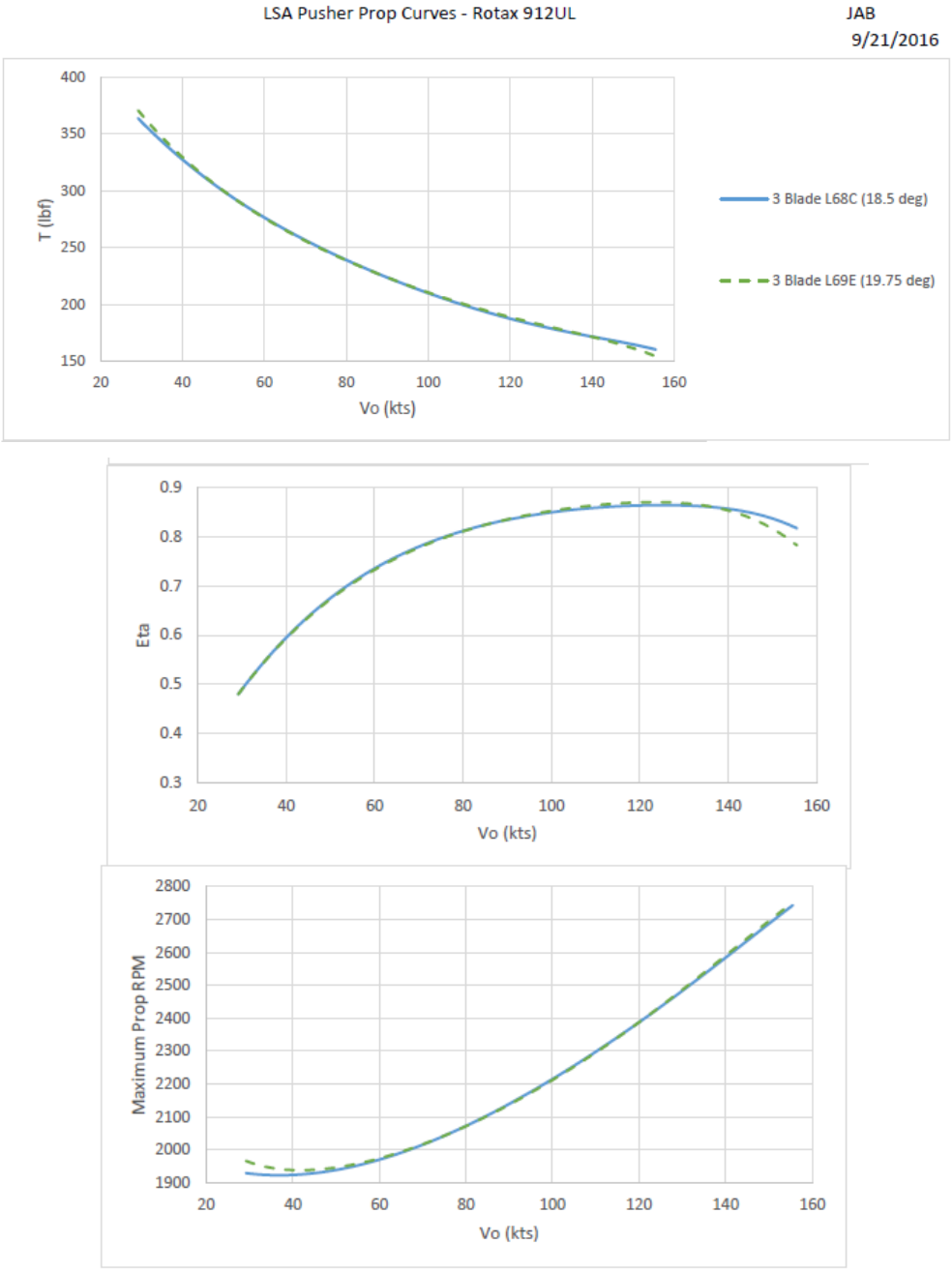
This engine is for use in experimental and ultralight uncertified aircraft only and only in circumstances in which an engine failure will not compromise safety.
Before operating the engine read operator's manual. Information is available from your local authorized ROTAX®-distributor.

BRP-Powertrain GmbH & Co. KG. BRP-Powertrain GmbH & Co. KG reserves the right at anytime to discontinue or change specifications, prices, designs, features, models or equipment without incurring obligation. Engine performance may vary depending on, among other things, general conditions, ambient temperature and altitude.

® and TM are trademarks of BRP-Powertrain GmbH & Co. KG / © 2011 BRP-Powertrain GmbH & Co. KG / All rights reserved.

APPENDIX I

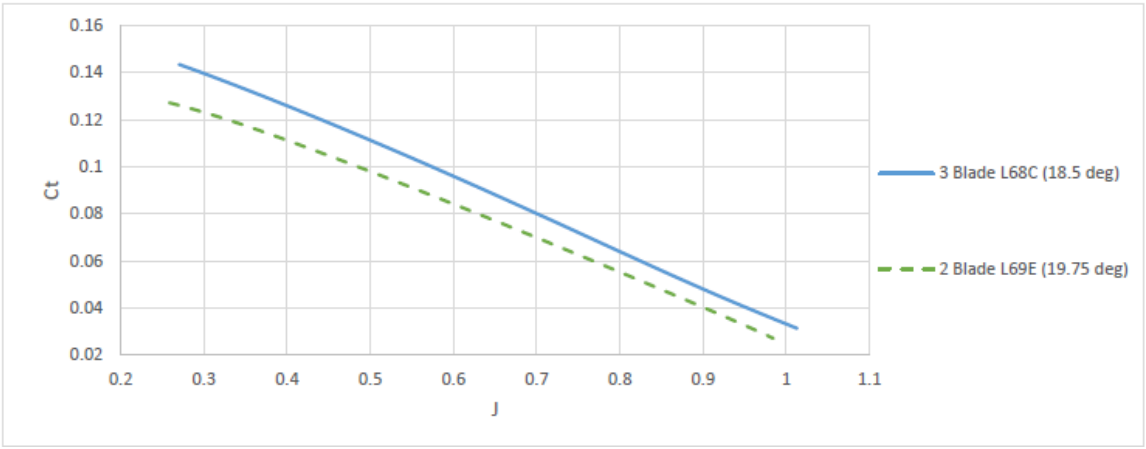
The blade angle shown on the charts is the beta angle of the section at 75% of the blade span. These technical data were gently provided by the Sensenich's design engineer Mr. Jon Bristol.

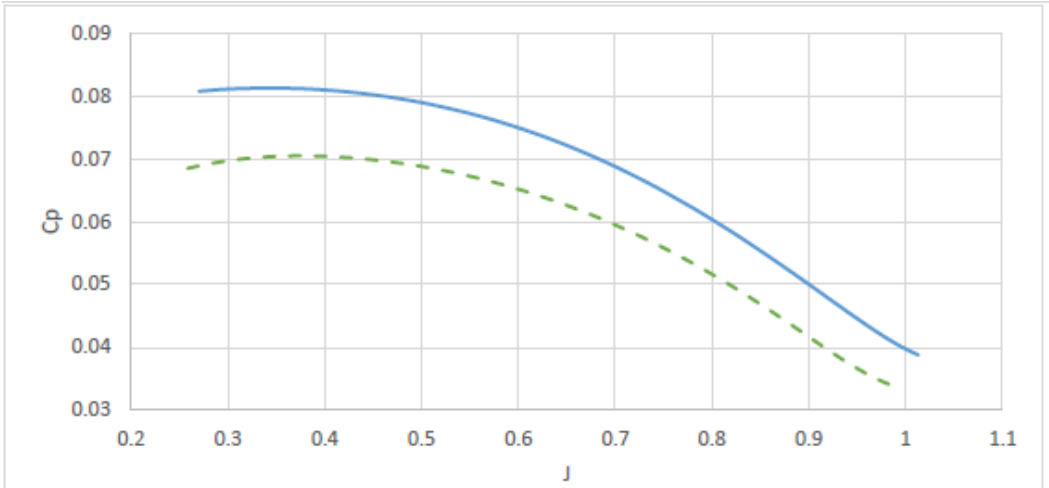


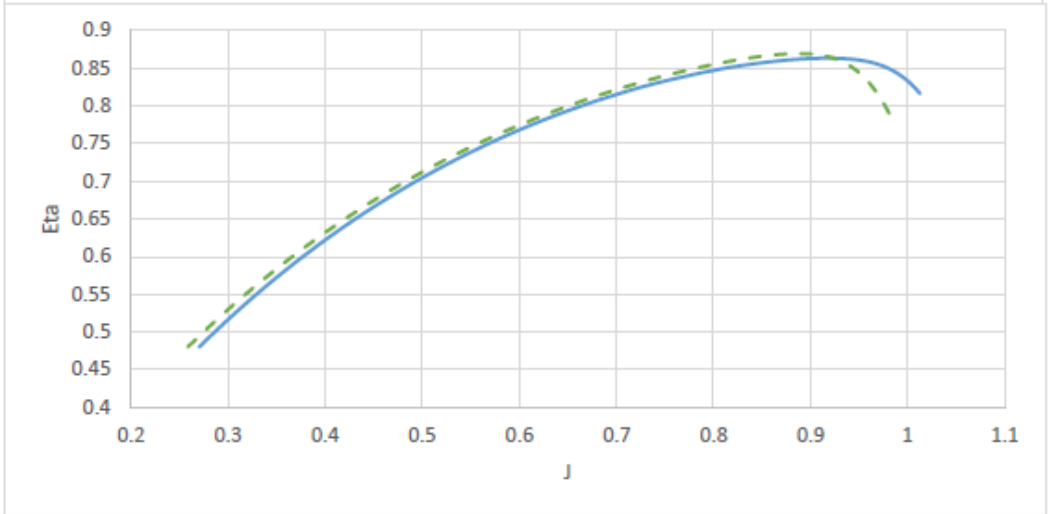
Props pitched for 80 HP @ 5800 Engine RPM at 120 kts

LSA Pusher Prop Curves

JAB
9/21/2016







Props pitched for 80 HP @ 5800 Engine RPM at 120 kts